Organoid based models to study the role of gut microbiota metabolites in post-weaning diarrhea

Bart van der Hee

Propositions

1. Establishing initial associations or correlations is an important goal in empirical research.

   (this thesis)
2. The wide-ranging effects of many microbial metabolites make it difficult to pinpoint their most important effects in humans and animals.

   (this thesis)
3. Space travel is crucial for human advancement and discovery of resources for sustainable living.
4. Pre-prints in science have revolutionized the publication and data dissemination process.
5. The urge to extract maximum biological significance from data leads researchers to over-analyse results.
6. Cognitive bias and social media activism discourage the pursuit of fundamental and groundbreaking scientific questions.
7. The best preparation for having a baby is doing research on piglet diarrhea.

Propositions belonging to the thesis, entitled

Organoid based models to study the role of gut microbiota metabolites in post-weaning diarrhea

Bart van der Hee
Wageningen, 28th of June 2023

Organoid based models to study the role of gut microbiota metabolites in post-weaning diarrhea

Bart van der Hee

Thesis committee

Promotors
Prof. Dr. J.M. Wells
Professor of Host-Microbe Interactomics
Wageningen University & Research

Prof. Dr. H. Smidt
Personal Chair at the Laboratory of Microbiology
Wageningen University & Research

Other members
Prof. Dr. J.M.J. Rebel, Wageningen University & Research
Prof. Dr. M. Bailey, University of Bristol, England
Dr. A.A. Schönherz, Aarhus University, Denmark
Dr. K. Schneeberger, Utrecht University

This research was conducted under the auspices of the Graduate School of Wageningen Institute of Animal Sciences (WIAS)

Organoid based models to study the role of gut microbiota metabolites in post-weaning diarrhea

Bart van der Hee

Thesis

Submitted in fulfilment of the requirements for the degree of doctor

at Wageningen University

by the authority of the Rector Magnificus,

Prof. Dr. A.P.J. Mol,

in the presence of the

Thesis Committee appointed by the Academic Board

to be defended in public

on Wednesday 28 June 2023

at 11:00 a.m. in the Omnia auditorium

Bart van der Hee

Organoid based models to study the role of gut microbiota metabolites in post-weaning diarrhea

372 pages

PhD thesis, Wageningen University & Research, Wageningen, The Netherlands (2023)

With references, with summary in English and Dutch

ISBN: 978-94-6447-708-5

DOI: 10.18174/630692

Pro aeterno vinculo meo

Table of contents

General introduction

Bart van der Hee[1,2]

[1] Host-Microbe Interactomics Group, Department of Animal Sciences, Wageningen University & Research, Wageningen, The Netherlands, [2] Laboratory of Microbiology, Wageningen University & Research, Wageningen, The Netherlands

General introduction to the thesis

Post-weaning diarrhea (PWD) is a common welfare problem in pig production, characterized by watery diarrhea and enteric bacterial infections, which could lead to reduced feed intake and mortality in piglets after weaning. The onset of PWD is associated with a broad range of factors, including major changes in the intestinal microbiome [1-4], the composition and quality of the diet [2, 4-8], stress [7-9], and infection by pathogenic microorganisms [3, 10]. At weaning, piglets are abruptly removed from the sow and given dry feed. This sudden change can lead to an imbalance in the microbiome, also referred to as dysbiosis, which may contribute to post-weaning diarrhea. Antibiotics are commonly used to control and treat PWD, but this increases the risk of antibiotic resistance and its spread to other pathogens [8, 11, 12]. Piglets are fed high protein (HP) diets to support their growth, but HP diets have been suggested to decrease fecal consistency and dry matter content, as well as to increase risk of PWD [1, 4, 6, 13].

Protein fermentation occurs when undigested protein reaches the colon and is fermented by colonic microbiota, resulting in metabolites that in relatively high concentrations negatively affect gut barrier function [1, 4]. The aim of the research described in this thesis was to determine whether there is a link between, microbiota, protein fermentation metabolites and piglet PWD under on farm conditions and secondly to gain a better understanding of the effects of protein fermentation metabolites on the intestinal epithelium using porcine intestinal organoid models.

The welfare and economic challenges of post-weaning diarrhea

Future meat consumption is estimated to increase by 76-100% between 2005 and mid-century [14], which amounts to 42% increase in pork consumption. Gastrointestinal (GI) infections are a major source of economic loss and welfare issues in the pig industry, particularly in the European Union [15]. To this end, particularly PWD and infections with enteropathogenic *E. coli* are a major burden [8, 16]. PWD often results in reduced growth rates, lower feed efficiency, and lower productivity, all of which can negatively affect profitability [8, 17, 18]. Antibiotics and zinc oxide (ZnO) are often used to control enteric infections resulting from PWD which has implications for the spread of antibiotic resistance and environmental burden in ZnO [17, 19]. Weaning of farmed piglets at a younger age (3-4 weeks) than would naturally occur (gradual weaning over 10-20 weeks) is considered a major factor contributing to PWD [8, 20, 21].

Weaning is typically accompanied by decreased feed and water intake, which can result in a temporary reduction in growth [1, 9, 13, 17 , 22, 23]. This is especially problematic for piglets, as it can take up to two weeks to reach their energy intake pre-weaning [23]. Stresses, such as overcrowding, inadequate ventilation, transportation, and social conflict via mixing with new piglets are known to increase intestinal permeability and cause inflammatory responses [24-26]. To address the problem of PWD, various post-weaning nutritional approaches have been tested. These include the use of organic acids [27, 28], which can improve animal health through the acidification of the GI tract and control of potentially pathogenic bacteria [28, 29], pro- and prebiotics that aid in the generation and persistence of beneficial metabolites [30, 31], or pre-weaning nutritional strategies, such as introducing feed before weaning to allow a more gradual transition from milk to solid feed [15, 19, 32].

Microbial colonization of the piglet intestine in early life

In the first few weeks of life the piglet gut microbiome rapidly develops over time and is affected by diet and weaning [33-35]. Microbial colonization of piglets is strongly influenced by exposure to microbiota of the sow during birth and post-partum as well as the farm environment itself [36]. Within 24 hours after birth, the GI tract of piglets is colonized by oxygen-tolerant bacteria, including Lactic Acid Bacteria (LAB), enterobacteria, and streptococci [36-40]. Between 1-5 days after birth bacteria such as *Bacteroides*, *Lactobacillus*, *Bifidobacterium*, and *Clostridium* colonize the GI tract [32, 38, 39], and by three weeks a stable microbiota composition is established mainly consisting of bacterial groups from the families *Enterobacteriaceae*, *Lachnospiraceae*, *Bacteroidaceae*, *Clostridiaceae*, and *Lactobacillaceae* [39, 41-43]. The development of the gut microbiota in early life can significantly impact gut health later. For example, a higher relative abundance of *Lachnospiraceae*, *Prevotellaceae*, *Ruminococcaceae*, and *Lactobacillaceae* during the nursing stage have been supposed as a signature composition linked to a decreased incidence of PWD in piglets [41-43].

Dietary modulation of the microbiome during weaning

The gut microbiota of weaned piglets is influenced by the levels and sources of dietary proteins and fibers [1, 40, 44, 45]. Nutritional interactions between gut microbiota and diet are important for supporting the GI tract's nutrient pool and a balanced microbial community. Administering multiple species of microbes to sows during gestation and lactation can also impact on the composition of the piglet microbiota and the concentration of short-chain fatty acids (SCFAs) in the feces of

piglets during the post-weaning phase [44, 45]. However, weaning stress can lead to reduced feed intake which limits nutrients for microbial survival and proliferation and SCFA production.

At weaning, piglets are abruptly switched from nursing to a diet that typically contains cereals and high concentrations of crude protein (CP) [36]. Some studies have shown weaning leads to a decrease in *Lactobacillus* and a temporary reduction of fecal microbiota diversity, while *Clostridium*, *Prevotella*, and facultative anaerobes like *Proteobacteriaceae* (including *E. coli*) tend to increase [35, 46, 47]. The different type and source of proteins and fibers in the diet can impact on the diversity and composition of the gut microbiota [48], with studies showing that enriched pectin diets and soybean meal increase *Prevotella* and decrease *Lactobacillus* [36, 37], while a fish protein source leads to a large expansion of the *Escherichia/Shigella* group [49]. These changes in the gut microbial ecosystem and loss of diversity during the initial stages of life can increase the risk of PWD.

The use of antibiotics in feed as growth promoters has been banned by the European Union since 2006 [12]. However, antibiotics are still widely used in the swine industry for therapeutic, prophylactic, and metaphylactic purposes including treatment of severe PWD. Studies in humans and mice have shown that administration of antibiotics increases the abundance of enteric pathogens such as *Salmonella*, *Clostridioides difficile*, and vancomycin-resistant *Enterococcus* [50-53]. Two major pathogens that impact the swine industry are *Salmonella enterica* serovar *Typhimurium* (*S. Typhimurium*) and Enterotoxigenic *Escherichia coli* (ETEC) [17, 21, 25, 38, 54].

The role of the microbiome in preventing inflammation and pathogen invasion

The microbiome is important for colonization resistance, a term used to describe competition with or direct inhibition of pathogens by the microbial community [55]. Certain members of the indigenous microbial community, called pathobionts, can increase inflammatory responses in the mucosa when the microbiome has been disturbed, for example, by antibiotic treatment. Rather than causing enteric epithelial invasion or systemic dissemination, overgrowth of these pathobiont microbes can lead to immune responses caused by secreted factors or mucosal adhesion. Mechanisms of colonization resistance against pathobionts and obligate pathogens include competition for limited nutrients and sites of epithelial adherence, as well as the production of antimicrobials and pH-altering SCFAs acetate, propionate, and butyrate [27, 50, 56, 57]. For example, certain intestinal bacteria produce SCFAs that can alter the local pH, prevent the growth of intestinal pathogens such as pathogenic

E. coli [57] and inhibit virulence of *S. enterica* [58]. Nutrient competition is also a key factor in supporting the stability of the microbial community. An example of this is that non-pathogenic strains of *E. coli* have been shown to compete with human pathogenic *E. coli* strains for consumption of critical carbohydrate metabolites in mice and calves [59-61]. However, this competition can be both exploitative, i.e., efficient nutrient competition, or interference based, i.e., sensing by-products of metabolism to induce inhibitory factors for the other bacteria [59, 62].

The transition to solid food and early life stress during weaning can lead to heightened inflammation in the intestine, which is exacerbated by enteric infections. The inflamed gut supplies an ideal environment for the expansion of *Enterobacteriaceae*, which is also seen in PWD and other inflammatory gut diseases in humans [54, 60, 63]. Intestinal inflammation triggers activation of epithelial enzymes Nox-1 and Duox2 producing reactive nitrogen and oxygen species, respectively [64]. Furthermore, neutrophils recruited by chemokine production generate abundant amounts of reactive oxygen species through their oxidative killing mechanisms. Inflammation also increases production of nitric oxide that in turn reacts with superoxide to form peroxynitrite ($ONOO^-$), which is then rapidly converted to nitrate (NO_3^-) [65]. Certain strains of *E. coli* including ETEC possess a nitrate reductase allowing them to grow through nitrate respiration [66]. This mechanism is absent in anaerobes belonging to the classes *Clostridia* or *Bacteroidia,* which partly explains the bloom of *E. coli* under inflammatory conditions [67, 68]. It also highlights a mechanism in which *E. coli* exploits host inflammation to compete with other species. These events can create a vicious circle of intestinal inflammation, proliferation of *E. coli* and persistent infections.

The *E. coli* pathotypes causing post-weaning diarrhea in pigs

Diarrhea in pigs can be caused by different pathotypes of *E. coli*, including enterotoxigenic *E. coli* (ETEC), enterohemorrhagic *E. coli* (EHEC) or shigatoxigenic *E. coli* (STEC), enteroaggregative *E. coli* (EAEC), enteropathogenic *E. coli* (EPEC), enteroinvasive *E. coli* (EIEC), and diffusely attached *E. coli.* Strains of ETEC are the most common cause of PWD in piglets and are currently responsible for around 50% of piglet deaths globally [8].

ETEC infections typically occur when the bacteria are ingested through contaminated feed or water [21, 54]. The first step in ETEC pathogenesis is the adherence of fimbriae to receptors on the microvilli of the small intestine [54]. Fimbriae are proteinaceous, filamentous adhesins that are involved in adhesion to host cells and

other functions, such as interactions with macrophages and biofilm formation [25, 54]. Several distinct types of fimbriae have been identified in ETEC, including F4, F5, F6, F18, and F41 (reviewed by [69]). F18 fimbriae are found on ETEC strains that cause diarrhea in post-weaning piglets, while F4 fimbriae are found on ETEC strains that cause both neonatal- and post-weaning diarrhea [70, 71]. A nucleotide polymorphism in the fucosyltransferase-1 (*FUT1*) gene [72, 73], confers resistance to infection with F18+ ETEC likely due to lack of adhesion and subsequent toxin secretion. When attached to the epithelium, ETEC secretes exotoxins, including heat-labile- (LT) and heat-stable exotoxins (ST).

ETEC secretes exotoxin causing inflammation and damage to the intestinal lining [74]. LT is an AB type toxin that binds to monocialotetrahexosyl-ganglioside (*GM1*) receptor through a pentamer of B chains which results in internalization and toxigenesis through the A chain (reviewed by [75]). Intracellularly, the A component elevates intracellular cyclic adenosine monophosphate (cAMP) which activates protein kinase A (PKA). Elevated cAMP levels then stimulate the activation of the cystic fibrosis transmembrane regulator (*CFTR*) channel leading to secretion of chloride ions and water from the enterocyte into the gut lumen [75].

The STa toxin binds to the guanylate cyclase C receptor and activates its intracellular catalytic domain, leading to the hydrolysis of guanosine triphosphate (GTP) and intracellular increase in the second messenger cyclic guanosine monophosphate (cGMP) that activates PKA-mediated chlorine secretion through CFTR [76, 77]. STb binds to sulfatide on the surface of intestinal epithelial cells and activates a GTP-binding regulatory protein, leading to an influx of extracellular calcium ions into the cell which activates calmodulin-dependent protein kinase II (CAMKII), which opens a calcium-activated chloride channel (CaCC), allowing for the secretion of chloride from the cell into the lumen [63, 74]. Thus, the activity of both LT and ST results in the secretion of fluids and electrolytes into the intestine due to osmotic deregulation leading to watery diarrhea.

The effects of dietary protein on the piglet gut microbiome

Fermentation of undigested dietary protein by the gut microbiota can vary depending on the amount of protein in the diet as well as the purity and quality of the protein source [1, 4, 78-81]. For example, soybean is a common protein source in pig feed, but it holds anti-nutritional factors that can interfere with the digestion and absorption of nutrients, and undigested soybean proteins can stimulate hypersensitivity in weanling piglets (reviewed by [82]). Lowering the CP level in the diet to reduce soybean content may help alleviate immune stress in weanling piglets.

However, many studies have shown that the level of dietary CP is more important than the protein source in altering the intestinal microbiome, particularly in weaned piglets, whose microbiome is more susceptible to change [1, 4, 6, 34, 35, 79, 81]. Results from studies on the effect of dietary CP on the microbiome have been inconsistent, with some showing an impact on certain bacterial populations, such as members of the *Clostridium* genus [83, 84], and others showing no significant changes [85, 86]; but these results might be different due to dietary composition differences. More recent studies using high-throughput sequencing techniques have indicated that reducing dietary CP by 3% decreases the relative abundance of *Lactobacillus* in the cecum and *Streptococcus* in the colon of growing pigs compared to HP diets [87]. These findings suggest that the intestinal microbiome may be influenced by different dietary CP levels, although the microbiome of adult pigs may be more stable and resistant to dietary changes than that of weaned piglets.

Increasing the level of CP in the diet can have complex and diverse effects on the richness and diversity of the microbiota in the intestines of pigs. Overall, higher protein levels can alter microbial richness and diversity [83, 86], although these effects may be dose- and site-dependent and may not always be beneficial. In terms of microbial composition, the effects of increasing CP levels are also complex and varied, with some studies finding an increase in certain types of bacteria (such as coliforms [88]) and others finding no change or a decrease [89-91]. At the phylum level, the effects of increasing CP levels are also varied, showing an increase in *Firmicutes* and a decrease in *Bacteroidetes* [86], while others have found no change or even an opposite effect [85, 92]. This underlines the discrepancy of different studies having different housing conditions, dietary compositions, and animal genetics.

To further elucidate these discrepancies, the catabolic activity of the microbiota, or the breakdown of protein into smaller molecules, could be assessed through the analysis of end-products or through microbial -omics techniques such as metatranscriptome sequencing or metaproteomics, addressing microbial community gene expression and protein production, respectively. For instance, overlapping and recurring end-products of protein fermentation in the gut of pigs include SCFAs, ammonia, branched chain fatty acids (BCFAs), hydrogen sulfide (H_2S), methanethiol, biogenic amines, and phenolic- and indolic compounds (reviewed by [1] and [4]). The specific end-products and the microbial genera involved can vary depending on the amino acid (AA) being fermented, but their biological implications might be shared.

Ammonia

The intestinal microbiota can produce ammonia through the deamination of AAs or the hydrolysis of urea [93]. Ammonia in the GI tract has various sources, some of which are unrelated to protein fermentation. However, research using stable isotope labelled valine and urea found that more than 70% of the ammonia in the ileal digesta of pigs is produced through the fermentation of dietary and endogenous protein by microbes, while about 30% comes from the hydrolysis of urea [94]. Studies have shown that ammonia levels increase along the length of the GI tract in piglets, being low in the stomach and high in the colon [95]. In almost all studies increasing the protein content of a pig's diet led to higher levels of ammonia in the digesta or feces [6, 81, 96, 97]. Similarly, in human studies, ammonia concentrations in feces increased with a higher intake of dietary protein [96, 97], and ammonia is usually around 13 mM [95] in the distal colon of pigs and can increase up to 21 mM when fed HP diets [90].

High ammonia concentrations (20 mM) have been found to be harmful to human colonic epithelial cells, potentially through the interference with colonocyte metabolism, the impairment of barrier function [98], and the promotion of inflammatory signals [4, 98]. In a study on rats, infusion of ammonium chloride (NH_4Cl) in isolated distal colon increased epithelial cell proliferation [99], which may contribute to GI disorders [1]. Another study in rats found that perfusion of the colon with NH_4Cl or ammonium acetate increased losses of epithelial cells and mucus, increased lymphocyte numbers in the lamina propria, and reduced intestinal health compared to perfusion with a control solution [100]. Ammonia has also been shown to decrease expression of the monocarboxylate transporter 1 (*MCT-1*, a transporter involved in butyrate uptake) in porcine colonic tissue and Caco-2 cells [101, 102], suggesting that increased luminal ammonia concentrations may decrease colonic butyrate uptake and energy supply to colonocytes [103, 104]. However, incubating isolated porcine colonic crypts with NH_4Cl for 4 hours did not decrease cell viability [105]. While ammonia may have negative effects on gut health, its role in PWD remains elusive.

Short and branched chain fatty acids

The digestion of protein by the gut microbiota of pigs can produce SCFAs and BCFAs as end products. SCFAs, including acetate, propionate, and butyrate, can be produced from the fermentation of various AAs including alanine, aspartate, glutamate, glycine, lysine, threonine, and serine [93]. However, SCFAs are mainly produced in the intestine through the breakdown of complex carbohydrates by certain species of bacteria (reviewed in [106] **Chapter 4**). SCFAs have been shown to impact host physiology and have potential health benefits. They can be absorbed by

epithelial cells in the intestine, enter the bloodstream, and reach the liver. They can provide a sizeable part of the caloric requirements for humans and other animals [107] and can be used as a dietary strategy for patients with short-bowel syndrome [108]. SCFAs also play a role in regulating nutrient and ion transporters in the colon, which can help alleviate diarrhea associated with short-bowel syndrome. There is ongoing research into the mechanisms by which SCFAs impact host physiology and the potential for using SCFAs in the prevention and treatment of human and animal diseases. BCFAs, including isobutyrate, isovalerate, and 2-methyl-butyrate, are produced specifically from the fermentation of branched chain amino acids (BCAAs) such as valine, leucine, and isoleucine [93]. The concentration of BCFAs in the intestine increases throughout the GI tract in piglets as the proteolytic activity of the microbiota increases [95]. BCFAs can be formed by multiple species from *Bacteroides*, *Propionibacterium*, *Streptococcus*, and *Clostridium*, e.g., through the Stickland reaction [109]. Studies have shown that individuals on an HP diet have higher fecal concentrations of isovalerate and isobutyrate, reflecting an increase in the fermentation of valine and leucine [110]. HP diets have also been linked to a shift from microbial carbohydrate to protein fermentation, as well as a reduction in beneficial butyrate-producing bacteria and lower levels of butyrate [110, 111]. Microbial BCFA production is greater when feces from individuals with IBD are compared to feces from healthy controls in an *in vitro* model of the proximal colon [112]. Although isobutyrate can serve as an energy source for colonocytes, butyrate is preferred by colonocytes [113]. Propionate, acetate, butyrate, and isobutyrate have all been shown to increase the expression of the Na+/H+ exchanger NHE3 in colon cells [114].

Hydrogen sulfide

H_2S is produced in the GI tract by fermentation of dietary sulfate or sulfur-containing AAs such as cysteine, methionine, cystine, and taurine [81, 115]. Increased sulfide in urine and feces have been positively correlated with dietary protein intake in humans [116]. In ulcerative colitis (UC) patients who are not receiving treatment, fecal concentrations of total sulfide are higher compared to healthy controls, indicating increased production of H_2S in UC patients [117]. Reducing dietary sulfur AAs has shown to improve UC symptoms in stool frequency [118]. Multiple studies have consistently shown that sodium hydrogen sulfide (NaSH) can inhibit cellular respiration and the oxidation of butyrate and glucose but does not affect cell viability due to adaptive responses of colonic cells [119-121]. Adaptive responses to H_2S have also been observed *in vivo*, with increased expression of the enzyme sulfide quinone reductase (SQR) [121], involved in H_2S detoxification, in the colon of rats fed an HP diet compared to those fed a normal-protein diet.

Studies on the effects of H_2S on cell proliferation show inconsistent results. Some studies reported an increase in proliferation rate following incubation with NaSH in rat small intestinal cells [122] and human mucosal biopsies from the rectum [123], whereas others reported a decrease in HT-29 $Glc^{-/+}$ cells [120]. The discrepancy in these results might be due to the physiological differences between the models, e.g., one having a mucus layer *in vivo* and the other not ([121]. Colorectal cancer-associated features hyperproliferation and reduced apoptosis of the epithelium, suggest a potential detrimental role for H_2S in gut health [124, 125]. Furthermore, H_2S may impact on gut health by breaking down the mucus layer and increasing mucus barrier permeability [126]. Sulfate-metabolizing bacteria belonging to the genus *Desulfovibrio*, can produce sulfide from the reduction of dietary sulfite, sulfate, and mucin-derived sulfated polysaccharides. Increased levels of sulfide and sulfide-producing bacteria have been observed in inflammatory bowel disease (IBD), and the sulfides reducing the mucus barrier may contribute to decreased barrier integrity (reviewed by [127]). In line with this concept, H_2S affects cytokine production, as continuous infusion of NaSH in the colon of rats increased gene expression of proinflammatory cytokine IL-6 and NO synthase [121]. However, likely due to the short duration of the experiment neutrophil infiltration in the distal colon was not affected. It has been hypothesized that concentrations of free sulfide and the metabolizing capacity of epithelial cells determines if their effects on colonic epithelium integrity are harmful [1].

Polyamines

Polyamines, which include putrescine, spermidine, and spermine, are naturally occurring compounds found in certain foods and produced by colonic bacteria (reviewed by [128, 129]). These compounds are crucial for normal mucosal development [130] and absorption in the small intestine of young piglets [131]. When arginine is converted by colonic bacteria, it forms citrulline and ornithine, which can then be converted into polyamines [93]. Piglets that were fed an HP diet had higher concentrations of putrescine and spermidine in the proximal colon [84]. However, putrescine was negatively related to the expression of MCT-1 in the colonic tissue of these piglets [101], suggesting a potential role in decreased energy supply to colon cells similar to ammonia. Histamine, which is produced by histidine fermentation [93, 132], was also increased in the proximal colon of piglets fed HP diets [84]. However, these piglets had increased histamine-degrading enzymes in their colonic tissue, indicating an adaptive response to excess histamine. When amines are converted to nitrosamines in the distal colon, it can potentially cause DNA damage and have carcinogenic effects [133]. Overall, HP diets increase the concentration of biogenic amines in the colon, but the impact of these amines on gut health is not yet fully understood.

Other metabolites

Phenol and indole compounds are produced by *Bacteroides*, clostridia, and bifidobacteria from aromatic AAs phenylalanine, tyrosine, and tryptophan [93]. They are generally absorbed by the colonic epithelium and detoxified by the colonic mucosa or liver with glucuronide and sulfate conjugation [134]. There is growing interest in physiological effects of certain indole derivatives, such as indole-3-aldehyde (I3A), indole-3-propionic acid (IPA), and indole-3-acetic acid (IAA) that are produced by gut bacteria from the breakdown of tryptophan [135]. These derivatives activate the aryl hydrocarbon receptor (AhR), a protein that helps regulate immune function in the intestine [135]. IPA in particular can also impact the intestinal barrier by binding to the Pregnane X Receptor (PXR) [136]. Studies have shown that higher intake of dietary fibers is associated with increased circulating levels of IPA in humans, [137], but research is needed to understand the impact of fibers on the production of these indole derivatives by gut bacteria [138]. p-Cresol, a phenol-derived metabolite produced by gut bacteria from L-tyrosine [139], is present at low levels in human and porcine feces [95]. Studies have shown that in *in vitro* experiments p-cresol can inhibit oxygen consumption in colonocytes [139] and increase the production of anion superoxide, a type of oxidant. These effects may result in the decrease of energy production in cells and impact on cellular physiology, potentially through the formation of peroxynitrite [66].

The effects of low-protein diets on pig production and gut health

In pig production, HP diets can lead to excesses of essential AAs and increased nitrogen excretion, which can lower the efficiency of nitrogen utilization and impair gut health through colonic fermentation [140]. The latest recommendations from the National Research Council (NRC, 2012 [141]) for standard nutrient requirements of swine do not include a specific requirement for CP, but a total nitrogen requirement which results in a CP requirement that is 2-4% lower than previous recommendations (1994, [142]). The CP content of typical diets for weaned piglets is between 21 and 25 %. Studies have shown that reducing CP can effectively lower the risk of problems with gut health such as PWD. Reducing CP by more than 2% below the NRC's 2012 recommendations may result in reduced weight gain due to limiting non-essential AAs [143]. Low protein (LP) diets supplemented with specific essential AAs have been shown to increase nitrogen utilization, reduce feed costs and nitrogen excretion, and improve gut health without negatively impacting growth performance [140, 144]. LP diets supplemented with free AAs can improve immune status and resistance to subclinical and clinical diseases, especially under stress conditions [143].

For example, threonine is important for mucin synthesis and maintaining gut barrier integrity, sulfur amino acids (methionine and cysteine) that are involved in the immune system, and tryptophan-derived metabolites have been associated with immune-regulating properties and can inhibit the production of pro-inflammatory molecules, and certain BCAAs leucine, isoleucine, and valine) can enhance immune function, improve gut barrier function, and reduce inflammation [80, 143, 145]. Finally, LP diets supplemented with AAs can improve the overall nutrient utilization efficiency, feed conversion ratio, and reduce nitrogen excretion [143, 144]. However, the use of LP diets can lead to fatter carcasses due to more dietary energy being available for fat deposition, but the adoption of the net energy system in dietary formulation can help achieve acceptable performance and meat quality. Decreasing the CP content by 3% or more also resulted in significantly reduced growth performance [140], even when supplemented with four crystalline AAs [140, 144, 146]. This effect was reverted by supplementing lowered CP diets with BCAAs, showing that BCAAs could be a limiting factor for growth performance in low CP diets [145, 147]. However, these studies were performed on piglets in their fattening or finishing stage [80, 145, 147]. Studies investigating lower CP levels in combination with AA supplementation at weaning show reduced growth performance and lower average daily gain in the first week after weaning [140]. These studies pose implications for finding a balance between reducing CP content and growth performance, which results in reluctance to adopt BCAA-supplemented low CP diets in practice.

The porcine GI tract

The porcine GI tract is composed of several specialized compartments. Anatomically, the stomach empties into the duodenum, a short section of the small intestine that contains Brunner's glands that produce bicarbonate [148]. This buffers the acidic contents from the stomach and activates intestinal enzymes by creating an alkaline environment [148]. The duodenum transitions into the jejunum at the duodenojejunal flexure. The jejunum is the largest section of the GI tract and is specialized in digestion and absorption of nutrients (reviewed by [149, 150]. The last section of the small intestine is the ileum and aids in the absorption of digested nutrients. The increasing concentration of Peyer's patches, localized immune compartments underneath the epithelium, indicate a more pronounced immune function and corresponds to an increased concentration of luminal bacteria. The ileum terminates into the large intestine at the ileocecal valve. The cecum is the most proximal compartment of the large intestine and is more prominent in pigs than in humans [149]. The cecum contains many bacteria that enzymatically break down plant materials and other carbohydrates undigested in the small intestine. This process is followed in the proximal section of the colon. The anatomy of the porcine colon is substantially different from that of humans, where pigs have a spiral colon

divided into downward centripetal (human equivalent to ascending and transverse colon) and upward centrifugal (human equivalent to descending colon) sections [150]. Its main function is reabsorption of water and transport of fermentation metabolites from the resident microbiota. The colon terminates into the rectum, the most distal section, and feces are passed as a semi-solid material.

The intestinal barrier is a multi-layered system that prevents the penetration of luminal microorganisms and allergens into the (sub)mucosa and is essential for maintaining the overall health of the GI tract. Components of the intestinal barrier include gastric acid and pancreatic juice, which help to degrade microorganisms and antigens in the lumen, as well as intestinal bacteria that produce antimicrobial substances to inhibit pathogen colonization. The microclimate close to the epithelium consists of a watery layer, glycocalyx, and mucus layer [151, 152], which prevent bacterial adhesion and contain antimicrobial peptides (AMPs) secreted by cells such as Paneth cells and enterocytes [153, 154].

Goblet cells: The role of mucins for mucus maintenance and defense

The glycocalyx consists of acidic mucopolysaccharides (glycosamino-glycans) and transmembrane glycoproteins [151, 152, 155]. These membrane-bound mucins are generally extended and heavily glycosylated and cover the microvilli of enterocytes. (Membrane) mucins are proteins that are characterized by a specific domain called the PTS domain, which is rich in Proline, Threonine and Serine residues. This domain is also O-glycosylated as the membrane mucin travels through the secretory pathway [156]. Parallel individual evolution of two functional mucin groups shows their biological importance, and both types are found on many mucosal surfaces [157]. For instance, next to membrane-bound mucins, gel-forming mucins from Goblet cells are critical in the intestine. Mucin-2 is the major secreted mucus in the GI tract, and its complete absence leads to spontaneous inflammation [158-160].

Several types of Goblet cells in the GI tract have been described with specialized functions, as canonical Goblet cells that regulate mucus biosynthesis and storage, non-canonical Goblet cells that regulate metabolic processes as ion transport and nutrient absorption, defense Goblet cells that produce AMPs, and inter-crypt Goblet cells that have a fast baseline mucus secretion (as reviewed by [155]). Mucin 2 is constitutively secreted throughout the intestine and expression is modulated by inflammatory signals, such as microbe-associated molecular patterns [154, 161, 162]. For instance, stimulating cells with proinflammatory cytokines [163, 164] and bacteria-derived lipopolysaccharide (LPS) [165] induces elevated expression of

mucins *in vitro*. Moreover, treating intestinal cancer cell lines with SCFA butyrate has shown an increase in Muc2 expression when treated with low doses *in vitro* (1 mM) [166, 167]. This stimulated mucin release is an immediate response to external stimuli and results in drastic secretory granule increase through hydration [168]. The oligosaccharide structures of mucins resemble those found on cell surfaces, and its constitutive secretion into the gut lumen possibly serves as adhesin decoy for pathogens (reviewed by [169]). Bacterial pathogens such as *Streptococcus pyogenes* [170], *Haemophilus influenzae* [171], *E. coli* [172], and *Campylobacter jejuni* [173], as well as rotaviruses [174] and enteroviruses [175], have evolved to bind to, or utilize host sialic acids and fucosylated oligosaccharides, which are abundant in secreted mucus.

Epithelial regeneration in the intestine

The GI tract could become compromised during weaning by decreasing the expression of proteins involved in energy metabolism and other cellular processes, leading to reduced proliferation of intestinal epithelial cells. Additionally, weaning stress can cause morphological and physiological changes such as villus atrophy and crypt hyperplasia, which can impair the digestive and absorptive capacity in weaned pigs [5, 18, 26, 176]. Disruption of these processes can greatly impact the digestion of HP diets and could lead to increased outflow of undigested protein into the colon [6, 18]. This then increases colonic proteolytic fermentation and favors protein-fermenting microorganisms to produce the previously described metabolites [81].

Homeostasis of epithelial regeneration and energy metabolism is vital, as intestinal epithelial cells undergo rapid turnover, with a lifespan of about 4 to 5 days. This high rate of turnover is a vital defense mechanism of the intestinal epithelium to shed infected or damaged cells [177-179]. These epithelial cells are produced by stem cells in the crypts and differentiate into several specialized types, including absorptive enterocytes, enteroendocrine cells, goblet cells, and Paneth cells (reviewed by [180]). These cells play important roles in maintaining the integrity of the intestine and aiding in recovery from tissue damage [181]. For instance, Paneth cells produce and secrete antimicrobial peptides like lysozyme and defensins, as well in supplying stem cell protection in the crypt bottom [154, 180]. Goblet cells secrete mucus that protects the mucosal surface, while M cells in the follicular epithelium of the Peyer's Patches are involved in the uptake of antigens. Beneath the epithelium, immune cells such as myeloid cell types and lymphocytes help to support intestinal homeostasis and protect the host against invading pathogens and subsequent inflammation (**Figure 1**).

Intestinal barrier function through tight junctions

The barriers that regulate permeability through the epithelial layer are formed by tight junction proteins located between epithelial cells. These intramembrane proteins, such as occludin and claudins, work together with cytoplasmic proteins like zonula occludens (ZO) to create a barrier between the luminal and basolateral compartments [182, 183]. This barrier controls the passive diffusion of ions and other small molecules through the paracellular pathway, acting as a filter to allow the transport of important nutrients, electrolytes, and water from the lumen of the intestine into circulation. Inflammation can significantly impact the integrity of the intestinal barrier [184], and pathogens can directly damage tight junctions using toxins or membrane adhesion as outlined above. Additionally, systemic inflammation can further impair barrier function and decrease the expression of tight junction proteins like occludin and claudin-1 [185]. Pro-inflammatory cytokines produced by immune cells, tumor necrosis factor alpha (TNF-α) and interferon gamma (IFNγ), can also play a role in the disruption of tight junctions and the impairment of barrier function. Early weaning and LPS injection showed detrimental effects on intestinal barrier function and increased immune responses in pigs, potentially through the alteration of mucosal immune responses and impaired nutrient digestibility. Three studies showed that higher dietary CP levels decrease expression of tight junction proteins occludin, ZO-3, claudin-1, -2 -3, and -7 in the small intestine and proximal colon and lead to a higher count of mucus-containing goblet cells in the proximal colon [83, 95, 186]. In addition, HP diets have been associated with increased expression of genes related to cell turnover and pro- and anti-inflammatory responses in the proximal colon of pigs [84], although it is unclear whether these increases are a result of increased permeability or a protective response to (potentially toxic) metabolites. Further indications that HP diets affect barrier function is the relation to longer villi and deeper crypts in the small intestine and a lower count of intraepithelial lymphocytes in the proximal colon of piglets. This could be related to the inefficient supply of ZO-proteins that are important mediators of collective cell migration and proliferation [187]. Increased levels of pro-inflammatory cytokines such as TNF-α, IL-1β, and IL-6 have been found in the colon of pigs fed HP diets, as well as increased activation of the transcription factor NF-kB in the ileum.

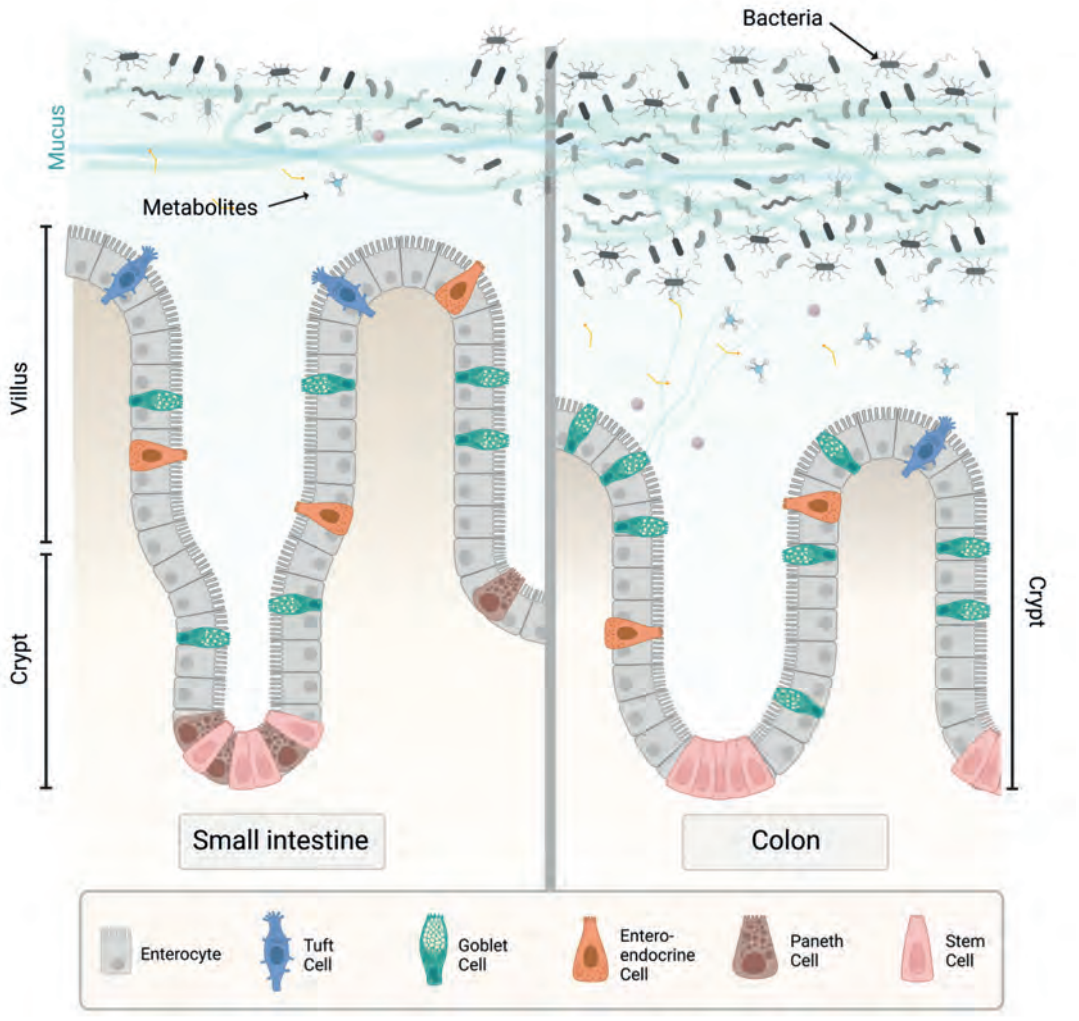

Figure 1. An overview of the structural morphology of the small intestine and colon. Stem cell replication in the crypt leads to the generation of rapidly amplifying progenitor cells that differentiate into mature enterocytes or secretory cells (goblet, enteroendocrine, Paneth, and tuft cells) as they move upwards to the epithelial surface. Cells at the top of the villus (small intestine) or crypt (colon) under apoptosis are extruded from the epithelium without loss of barrier function. Goblet cells in the intestine produce mucus, and Paneth cells produce antimicrobial factors and support stem cell maintenance in the bottom of the crypt. The number of bacteria increases along the intestinal tract and is highest in the colon. They produce numerous metabolites from their metabolism, which could interact with the host epithelium.

Antibodies in the intestine

The GI tract contains a substantial portion of the body's immune cells, located in the mucosa and submucosa. This area, known as the gut-associated lymphoid tissue (GALT), contains both isolated and aggregated lymphoid follicles, including Peyer's patches and mesenteric lymph nodes. The GALT is responsible for presenting antigens to the immune system and producing secretory antibodies, IgA and IgM, for defense against harmful substances (reviewed by [188]). The lamina propria serves as a compartment for the regulation of immune responses, particularly IgA production. The gut immune system in pigs reaches maturity at 7 weeks of age, whereas conventional weaning occurs between 3-4 weeks. Weaning-induced inflammation is often associated with oxidative stress, which can further disrupt the normal intestinal function. To maintain optimal growth and performance in pigs, the appropriate development of the intestinal immune system and a normal redox state are essential. Controlling pro-inflammatory cytokines may alleviate subsequent intestinal disorders caused by the stress of weaning.

Shaping of the microbiome by host factors

Bidirectional interaction between the host and microbiome also shapes microbiota composition. For instance, AMPs are innate immune peptides produced and secreted by most mucosal epithelial cells and some immune cells [50]. These peptides are particularly important in the GI tract, where they play a role in maintaining a healthy balance of the intestinal microbiome. There are several types of intestinal AMPs, including Paneth cell-derived alpha-defensins, lysozyme, phospholipase A2, and RNAses, enterocyte-derived beta-defensins and cathelicidins, and regenerating islet-derived protein (REG) III family, produced by Paneth cells and enterocytes) (reviewed in [189]). Some AMPs have broad-spectrum antimicrobial activity while others are more specific. For example, defensins and cathelicidins create pores that lead to cell lysis through attachment to negatively charged lipid membranes. On the other hand, C-type lectins target Gram-positive bacteria by binding to peptidoglycan that forms the cell wall of bacteria.

In summary, the relationship between the microbiota and the host is complex and has evolved to maximize benefits such as resistance to pathogens, metabolism, and immune development, while minimizing negative effects such as imbalanced over-representation of certain microbes, inflammation, and movement of microbes across epithelial cells. The host maintains balance by carefully controlling contact between the microbiota and the epithelial cells through mechanisms such as the mucus layer, AMPs, antibodies such as IgA, and microbial metabolites.

Modeling host epithelial responses with in vitro models

HP diets have been shown to significantly increase the microbial fermentation of protein, peptides, or AAs in the intestine, as indicated by increased concentrations of metabolites derived from microbial AA metabolism, particularly in the distal part of the intestine. However, the concentration of end-products in digesta or feces does not necessarily reflect microbial catabolic activity, as it depends on the rate of production and disappearance by processes such as absorption by enterocytes. *In vitro* studies can provide insight into microbial capabilities for protein fermentation, such as using fermentation models in the lab [190, 191], but the *in vivo* situation is more complex and involves multiple interactions with the host. SCFAs produced during (protein and carbohydrate) fermentation are thought to be beneficial for intestinal health, while increased colonic expression of genes involved in mucosal cell turnover and proinflammatory reactions have been associated with high concentrations of ammonia, biogenic amines, and other potential toxic metabolites induced by HP diets. The overall effects of protein fermentation on health can be studied in animal studies by increasing dietary protein levels but do not reflect the localized effects of metabolite exposure on the epithelial surface. Therefore, *in vitro* cell models are a good model to evaluate specific metabolite-epithelium interactions.

Protein fermentation metabolites

Several *in vitro* studies have been conducted on the effects of protein fermentation, in which cells, isolated colonic crypts or colon tissue were exposed to different potentially harmful metabolites. One metabolite studied was ammonia, which stimulated pyrimidine synthesis in gut epithelial cells. However, exposure of isolated pig colonic crypts to 50 mM NH_4Cl did not alter cell viability [105]. Exposure to p-cresol and phenol decreased the viability of colonic epithelial cells isolated from human biopsies and cell lines [98, 134]. Moreover, transepithelial resistance of Caco-2 cells was also found to decrease after incubation with these compounds, and permeability of endothelial cells was significantly increased after exposure to p-cresol [139, 192]. The toxic potential of H_2S has been extensively studied *in vitro*, and after exposure to NaSH, proliferation in non-transformed rat intestinal crypt cells was increased [121]. Furthermore, Attene-Ramos et al. found that H_2S affected vital cellular pathways at concentrations found in the lumen of the colon, causing genomic DNA damage in colonic cancer cells, preventing the oxidation of butyrate in colonocytes, and inhibit cellular respiration by acting as an inhibitor of cytochrome *c* oxidase [193].

The use of cell lines and the advent of intestinal stem cells

Recent studies on cancer or transformed cell lines have revealed several issues that may negatively impact the reproducibility of research results obtained. These issues include model misidentification, cross-contamination, and genetic aberrations [194]. To address these issues, methods such as short tandem repeat and single nucleotide polymorphism profiles have been proposed for authenticating cells [195]. Additionally, it is currently unknown to what extent genotypic variability in these cell lines may lead to variations in proteotype and phenotype when cultured in different laboratories [194, 196]. While there are some observations that suggest that many cell lines may be genomically unstable [197, 198], a recent report indicated that cancer cell lines undergo rapid genetic diversification due to positive clonal selection, which could lead to alterations in glycosylation patterns and general physiological responses [194, 199]. Thus, it is important to consider that reproducibility of research results may not always be guaranteed when using cell lines and could deviate due to biological complexities.

To overcome the issues of monotypic cell line models that could poorly reflect physiological conditions, there has been much interest in employing the self-replicative potential of stem cells. Recent advancements in stem cell biology have led to the successful cultivation of three-dimensional organ-like structures called organoids. These organoids, made up of functional living cells extracted from the stem-cell compartment in their resident tissue, have the ability to self-renew and organize spatially and can be obtained from normal or cancerous intestinal samples for long-term study. Organoids have been proven to be important tools in the fields of intestinal biology and cancer research, as they closely mimic the complex three-dimensional architecture of intestinal tissue and recapitulate the epithelial differentiation found *in vivo*. In the initial isolation method described by Sato et al. in 2009, isolated intestinal crypts were embedded in a collagen matrix (Matrigel) with growth factors, e.g., Wnt agonist R-spondin 1, epidermal growth factor (EGF), and Noggin that support stem cell replication and differentiation. This process allowed the development of crypt- or villous-like units containing all differentiated cell lineages [181, 200, 201]. Additional development of the model found that colonic crypt stem cells needed the addition of exogenous Wnt3A for long-term culture [202].

A favorable property of using piglet-specific stem-cell derived intestinal organoids is their intrinsic programming for functional recapitulation of the original tissue epithelium. For example, intestinal organoids have been used to investigate the physiology of electrolyte transport and membrane transporters such as NHE3, DRA,

CFTR, BLM, KCC1, and sodium potassium ATPase [203]. These are differentially expressed based on the tissue of origin, reflecting their *in vivo* function. For example, only organoids from the distal ileum expressed bile acid uptake transporters, whereas they did not express proximal small intestine associated GATA4 that define jejunal enterocytes [203, 204]. This means that the organoids resemble the important spatial patterning of intestinal functions, such as uptake, digestion, and barrier functioning. Disease modelling and host-microbe interactions using conventional cell models is hampered by the lack cell type-specific receptors or membrane mucins. Organoids allow physiological interactions between the epithelium and pathogens to be studied e.g., having a mucus barrier and epithelium-produced AMPs. Recent studies have shown successful replication of SARS-CoV-2 [205, 206] and *Cryptosporidium* [207] in intestinal organoids, which have previously only showed short-term infection mechanisms in cell lines [208, 209]. However, intestinal organoids also pose limitations that need to be addressed for their incorporation as physiological model of the intestine. The cellular recapitulation of organoids still does not fully mimic the intricate spatial crypt-villus structure, the importance of flow and nutrient diffusion, and complex composition of the luminal compartment. The results from organoid research should therefore carefully be interpreted and their function should be validated to *in vivo* systems.

Societal relevance of the thesis

Research into the effects of protein fermentation in piglets and its relation to post-weaning diarrhea is of great societal importance for several reasons. Firstly, post-weaning diarrhea (PWD) is a significant welfare issue for piglets as severe diarrhea leads to abdominal pain, discomfort, and death if left untreated. Understanding the associations between PWD and protein fermentation metabolites is important for the development of better strategies to prevent post-weaning health problems in piglets and has implications for humans. The use of experimental animals for biomedical or biotechnological research is currently under scrutiny, with the aim of greatly reducing animal experimentation by the end of the decade. Although the complexity of animals cannot be fully captured in cell models, the organoid models developed in this thesis could help **refine** animal experiments, **reduce** animal numbers by prescreening, and **replace** the use of animals for specific types of research questions. Moreover, organoids offer a more precise model compared to cell lines as they mimic the complex physiological and biochemical processes of the epithelium.

Thesis outline and aims

This thesis project is part of a larger consortium funded by the Dutch Research Council (NWO) and DSM. The consortium aims to investigate the contribution of protein fermentation in farm animal health and disease and aims to understand fundamental aspects of protein fermentation and intestinal health, with the goal of formulating prospects for "healthier animals through nutritional solutions" (HANS).

The thesis project has **four main aims**. The **first aim** is to examine the associations between piglet PWD, contributing factors before the onset of diarrhea, microbiota, and fermentation metabolites in practice (**Chapter 2**). The **second aim** is to develop and confirm the long-term culture stability of porcine intestinal organoids and their localized patterning between intestinal compartments (**Chapter 3**), as a model for studying the interaction between fermentation metabolites and the host epithelium (**Chapters 4 and 5**). The **third aim** is to specialize and extend the organoid model to be used for luminal interaction studies (**Chapters 6, 7, and 8**). Finally, the final **fourth aim** is to identify molecular effects of protein fermentation metabolites on the intestinal epithelium using scratch assays (**Chapter 9**).

Figure 2. Graphical overview of the thesis concept. This thesis consists of two main pillars. Primarily, we aim to identify the association between protein fermentation in piglets and their appearance in on-farm conditions. We will then aim to develop an intestinal model based on crypt-residing stem cells amenable for epithelium-metabolite interactions and their mechanistic effects *in vitro* to understand how they might contribute to intestinal pathology *in vivo*.

The thesis project aims to use a multidisciplinary approach, combining on-farm data, genetics, microbiology, and cell biology (**Figure 2**). We initially investigated the links between PWD, the intestinal microbiota, and fermentation metabolites and how they might interact with the piglet epithelium (**Chapter 2**). To study the effects on the piglet epithelium, we initially set up intestinal organoids from pigs and studied congruence of transcriptional programs over multiple passages (**Chapter 3** [210]).

The project further examined the effects of SCFAs on host physiology and epigenetics (**Chapters 4 and 5** [106]). As the 3-dimensional structure of intestinal organoids prohibited proper luminal exposure to metabolites, we optimized procedures for monolayer formation that retain heterotypic cellular differentiation (**Chapter 6** [211]) and explored the use of organoid models for evaluating feed-component interactions with the intestinal epithelium (**Chapter 7** [212]). We adapted procedures to use heterotypic organoid cells in wound repair assays (**Chapter 8**) and tested the effects of fermentation metabolites on epithelial renewal and barrier functioning (**Chapter 9**).

Finally, in **Chapter 10**, I provide a general discussion in the broader context of current literature and give an outlook on future research needs and opportunities for practical implementation of the knowledge generated by research described in this thesis.

Overall, **the thesis project aimed** to advance the scientific understanding of PWD and protein fermentation and to develop new tools and models for studying the interaction between protein fermentation metabolites and the intestinal epithelium.

References

1. Gilbert, M.S., et al., *Protein fermentation in the gut; implications for intestinal dysfunction in humans, pigs, and poultry.* Am J Physiol Gastrointest Liver Physiol, 2018. **315**(2): p. G159-G170.
2. Jayaraman, B. and C.M. Nyachoti, *Husbandry practices and gut health outcomes in weaned piglets: A review.* Anim Nutr, 2017. **3**(3): p. 205-211.
3. Nabuurs, M.J., F.G. van Zijderveld, and P.W. de Leeuw, *Clinical and microbiological field studies in The Netherlands of diarrhoea in pigs at weaning.* Res Vet Sci, 1993. **55**(1): p. 70-7.
4. Pieper, R., et al., *Health relevance of intestinal protein fermentation in young pigs.* Anim Health Res Rev, 2016. **17**(2): p. 137-147.
5. Hampson, D.J. and W.C. Smith, *Influence of creep feeding and dietary intake after weaning on malabsorption and occurrence of diarrhoea in the newly weaned pig.* Res Vet Sci, 1986. **41**(1): p. 63-9.
6. Heo, J.M., et al., *Effects of feeding low protein diets to piglets on plasma urea nitrogen, faecal ammonia nitrogen, the incidence of diarrhoea and performance after weaning.* Arch Anim Nutr, 2008. **62**(5): p. 343-58.
7. Lu, X., et al., *Growth Performance and Post-Weaning Diarrhea in Piglets Fed a Diet Supplemented with Probiotic Complexes.* J Microbiol Biotechnol, 2018. **28**(11): p. 1791-1799.
8. Rhouma, M., et al., *Post weaning diarrhea in pigs: risk factors and non-colistin-based control strategies.* Acta Vet Scand, 2017. **59**(1): p. 31.
9. Spencer, B.T. and P.G. Howell, *Some Husbandry Factors Influencing Weaning Stresses in Piglets.* Journal of the South African Veterinary Association-Tydskrif Van Die Suid-Afrikaanse Veterinere Vereniging, 1989. **60**(1): p. 62-64.
10. Heo, J.M., et al., *A between-experiment analysis of relationships linking dietary protein intake and post-weaning diarrhea in weanling pigs under conditions of experimental infection with an enterotoxigenic strain of Escherichia coli.* Anim Sci J, 2015. **86**(3): p. 286-93.
11. Barton, M.D., *Impact of antibiotic use in the swine industry.* Curr Opin Microbiol, 2014. **19**: p. 9-15.
12. European Centre for Disease, P., et al., *ECDC/EFSA/EMA second joint report on the integrated analysis of the consumption of antimicrobial agents and occurrence of antimicrobial resistance in bacteria from humans and food-producing animals: Joint Interagency Antimicrobial Consumption and Resistance Analysis (JIACRA) Report.* EFSA J, 2017. **15**(7): p. e04872.
13. Nyachoti, C.M., et al., *Performance responses and indicators of gastrointestinal health in early-weaned pigs fed low-protein amino acid-supplemented diets.* J Anim Sci, 2006. **84**(1): p. 125-34.
14. Tilman, D., et al., *Global food demand and the sustainable intensification of agriculture.* Proc Natl Acad Sci U S A, 2011. **108**(50): p. 20260-4.
15. Lalles, J.P., et al., *Nutritional management of gut health in pigs around weaning.* Proc Nutr Soc, 2007. **66**(2): p. 260-8.
16. Fairbrother, J.M., E. Nadeau, and C.L. Gyles, *Escherichia coli in postweaning diarrhea in pigs: an update on bacterial types, pathogenesis, and prevention strategies.* Anim Health Res Rev, 2005. **6**(1): p. 17-39.
17. Eriksen, E.O., et al., *Post-weaning diarrhea in pigs weaned without medicinal zinc: risk factors, pathogen dynamics, and association to growth rate.* Porcine Health Manag, 2021. **7**(1): p. 54.
18. Heo, J.M., et al., *Gastrointestinal health and function in weaned pigs: a review of feeding strategies to control post-weaning diarrhoea without using in-feed antimicrobial compounds.* J Anim Physiol Anim Nutr (Berl), 2013. **97**(2): p. 207-37.
19. Canibe, N., et al., *Review on Preventive Measures to Reduce Post-Weaning Diarrhoea in Piglets.* Animals (Basel), 2022. **12**(19).
20. Svensmark, B., et al., *Epidemiological studies of piglet diarrhoea in intensively managed Danish sow herds. II. Post-weaning diarrhoea.* Acta Vet Scand, 1989. **30**(1): p. 55-62.
21. Nabuurs, M.J., *Weaning piglets as a model for studying pathophysiology of diarrhea.* Vet Q, 1998. **20 Suppl 3**: p. S42-5.
22. Pluske, J.R., D.J. Hampson, and I.H. Williams, *Factors influencing the structure and function of the small intestine in the weaned pig: a review.* Livestock Production Science, 1997. **51**(1-3): p. 215-236.

23. Boudry, G., et al., *Weaning induces both transient and long-lasting modifications of absorptive, secretory, and barrier properties of piglet intestine.* J Nutr, 2004. **134**(9): p. 2256-62.
24. Hu, C.H., et al., *Early weaning increases intestinal permeability, alters expression of cytokine and tight junction proteins, and activates mitogen-activated protein kinases in pigs.* J Anim Sci, 2013. **91**(3): p. 1094-101.
25. McLamb, B.L., et al., *Early weaning stress in pigs impairs innate mucosal immune responses to enterotoxigenic E. coli challenge and exacerbates intestinal injury and clinical disease.* PLoS One, 2013. **8**(4): p. e59838.
26. Moeser, A.J., et al., *Gastrointestinal dysfunction induced by early weaning is attenuated by delayed weaning and mast cell blockade in pigs.* Am J Physiol Gastrointest Liver Physiol, 2007. **293**(2): p. G413-21.
27. Shin, R., M. Suzuki, and Y. Morishita, *Influence of intestinal anaerobes and organic acids on the growth of enterohaemorrhagic Escherichia coli O157:H7.* J Med Microbiol, 2002. **51**(3): p. 201-206.
28. Pluske, J.R., et al., *Impacts of feeding organic acid-based feed additives on diarrhea, performance, and fecal microbiome characteristics of pigs after weaning challenged with an enterotoxigenic strain of Escherichia coli.* Transl Anim Sci, 2021. **5**(4): p. txab212.
29. Tsiloyiannis, V.K., et al., *The effect of organic acids on the control of porcine post-weaning diarrhoea.* Res Vet Sci, 2001. **70**(3): p. 287-93.
30. Bron, P.A., P. van Baarlen, and M. Kleerebezem, *Emerging molecular insights into the interaction between probiotics and the host intestinal mucosa.* Nat Rev Microbiol, 2011. **10**(1): p. 66-78.
31. Su, W., et al., *The Role of Probiotics in Alleviating Postweaning Diarrhea in Piglets From the Perspective of Intestinal Barriers.* Front Cell Infect Microbiol, 2022. **12**: p. 883107.
32. Choudhury, R., et al., *Impact of early-life feeding on local intestinal microbiota and digestive system development in piglets.* Sci Rep, 2021. **11**(1): p. 4213.
33. Isaacson, R. and H.B. Kim, *The intestinal microbiome of the pig.* Anim Health Res Rev, 2012. **13**(1): p. 100-9.
34. Gresse, R., et al., *Gut Microbiota Dysbiosis in Postweaning Piglets: Understanding the Keys to Health.* Trends Microbiol, 2017. **25**(10): p. 851-873.
35. Guevarra, R.B., et al., *Piglet gut microbial shifts early in life: causes and effects.* J Anim Sci Biotechnol, 2019. **10**: p. 1.
36. Frese, S.A., et al., *Diet shapes the gut microbiome of pigs during nursing and weaning.* Microbiome, 2015. **3**: p. 28.
37. Tao, X., Z. Xu, and J. Wan, *Intestinal microbiota diversity and expression of pattern recognition receptors in newly weaned piglets.* Anaerobe, 2015. **32**: p. 51-56.
38. Konstantinov, S.R., et al., *Post-natal development of the porcine microbiota composition and activities.* Environ Microbiol, 2006. **8**(7): p. 1191-9.
39. Qi, R., et al., *Changes of Gut Microbiota and Its Correlation With Short Chain Fatty Acids and Bioamine in Piglets at the Early Growth Stage.* Front Vet Sci, 2020. **7**: p. 617259.
40. Inoue, R., et al., *Development of the intestinal microbiota in the piglet.* J Gen Appl Microbiol, 2005. **51**(4): p. 257-65.
41. Dou, S., et al., *Characterisation of Early-Life Fecal Microbiota in Susceptible and Healthy Pigs to Post-Weaning Diarrhoea.* PLoS One, 2017. **12**(1): p. e0169851.
42. Gaukroger, C.H., et al., *Changes in Faecal Microbiota Profiles Associated With Performance and Birthweight of Piglets.* Front Microbiol, 2020. **11**: p. 917.
43. Mach, N., et al., *Early-life establishment of the swine gut microbiome and impact on host phenotypes.* Environ Microbiol Rep, 2015. **7**(3): p. 554-69.
44. Liu, Y., *Fatty acids, inflammation and intestinal health in pigs.* J Anim Sci Biotechnol, 2015. **6**(1): p. 41.
45. Xiong, X., et al., *Nutritional Intervention for the Intestinal Development and Health of Weaned Pigs.* Front Vet Sci, 2019. **6**: p. 46.
46. Karasova, D., et al., *Development of piglet gut microbiota at the time of weaning influences development of postweaning diarrhea - A field study.* Res Vet Sci, 2021. **135**: p. 59-65.
47. Li, Y., et al., *Weaning Stress Perturbs Gut Microbiome and Its Metabolic Profile in Piglets.* Sci Rep, 2018. **8**(1): p. 18068.
48. Kuo, S.M., *The interplay between fiber and the intestinal microbiome in the inflammatory response.* Adv Nutr, 2013. **4**(1): p. 16-28.
49. Yang, Y., et al., *Glycation of fish protein impacts its fermentation metabolites and gut microbiota during in vitro human colonic fermentation.* Food Res Int, 2018. **113**: p. 189-196.

50. Kaiko, G.E. and T.S. Stappenbeck, *Host-microbe interactions shaping the gastrointestinal environment.* Trends Immunol, 2014. **35**(11): p. 538-48.
51. Brandl, K., et al., *Vancomycin-resistant enterococci exploit antibiotic-induced innate immune deficits.* Nature, 2008. **455**(7214): p. 804-7.
52. Brandt, L.J., et al., *Long-term follow-up of colonoscopic fecal microbiota transplant for recurrent Clostridium difficile infection.* Am J Gastroenterol, 2012. **107**(7): p. 1079-87.
53. Endt, K., et al., *The microbiota mediates pathogen clearance from the gut lumen after non-typhoidal Salmonella diarrhea.* PLoS Pathog, 2010. **6**(9): p. e1001097.
54. Nagy, B. and P.Z. Fekete, *Enterotoxigenic Escherichia coli in veterinary medicine.* Int J Med Microbiol, 2005. **295**(6-7): p. 443-54.
55. Buffie, C.G. and E.G. Pamer, *Microbiota-mediated colonization resistance against intestinal pathogens.* Nat Rev Immunol, 2013. **13**(11): p. 790-801.
56. Fukuda, S., et al., *Bifidobacteria can protect from enteropathogenic infection through production of acetate.* Nature, 2011. **469**(7331): p. 543-7.
57. Cherrington, C.A., et al., *Short-chain organic acids at ph 5.0 kill Escherichia coli and Salmonella spp. without causing membrane perturbation.* J Appl Bacteriol, 1991. **70**(2): p. 161-5.
58. Hung, C.C., et al., *The intestinal fatty acid propionate inhibits Salmonella invasion through the post-translational control of HilD.* Mol Microbiol, 2013. **87**(5): p. 1045-60.
59. Paquette, S.J., et al., *Competition among Escherichia coli Strains for Space and Resources.* Vet Sci, 2018. **5**(4).
60. Zhao, T., et al., *Pathogenicity of enterohemorrhagic Escherichia coli in neonatal calves and evaluation of fecal shedding by treatment with probiotic Escherichia coli.* J Food Prot, 2003. **66**(6): p. 924-30.
61. Fabich, A.J., et al., *Comparison of carbon nutrition for pathogenic and commensal Escherichia coli strains in the mouse intestine.* Infect Immun, 2008. **76**(3): p. 1143-52.
62. Majeed, H., et al., *Competitive interactions in Escherichia coli populations: the role of bacteriocins.* ISME J, 2011. **5**(1): p. 71-81.
63. Dubreuil, J.D., R.E. Isaacson, and D.M. Schifferli, *Animal Enterotoxigenic Escherichia coli.* EcoSal Plus, 2016. **7**(1).
64. El-Benna, J., P.M. Dang, and M.A. Gougerot-Pocidalo, *Role of the NADPH oxidase systems Nox and Duox in host defense and inflammation.* Expert Rev Clin Immunol, 2007. **3**(2): p. 111-5.
65. Singer, II, et al., *Expression of inducible nitric oxide synthase and nitrotyrosine in colonic epithelium in inflammatory bowel disease.* Gastroenterology, 1996. **111**(4): p. 871-85.
66. Bonnefoy, V. and J.A. Demoss, *Nitrate reductases in Escherichia coli.* Antonie Van Leeuwenhoek, 1994. **66**(1-3): p. 47-56.
67. Zeng, M.Y., N. Inohara, and G. Nunez, *Mechanisms of inflammation-driven bacterial dysbiosis in the gut.* Mucosal Immunol, 2017. **10**(1): p. 18-26.
68. Hughes, E.R., et al., *Microbial Respiration and Formate Oxidation as Metabolic Signatures of Inflammation-Associated Dysbiosis.* Cell Host Microbe, 2017. **21**(2): p. 208-219.
69. Gaastra, W. and A.M. Svennerholm, *Colonization factors of human enterotoxigenic Escherichia coli (ETEC).* Trends Microbiol, 1996. **4**(11): p. 444-52.
70. Garcia-Menino, I., et al., *Swine Enteric Colibacillosis in Spain: Pathogenic Potential of mcr-1 ST10 and ST131 E. coli Isolates.* Front Microbiol, 2018. **9**: p. 2659.
71. Wang, W., R.T. Zijlstra, and M.G. Ganzle, *Identification and quantification of virulence factors of enterotoxigenic Escherichia coli by high-resolution melting curve quantitative PCR.* BMC Microbiol, 2017. **17**(1): p. 114.
72. Bao, W.B., et al., *The effect of mutation at M307 in FUT1 gene on susceptibility of Escherichia coli F18 and gene expression in Sutai piglets.* Mol Biol Rep, 2012. **39**(3): p. 3131-6.
73. Meijerink, E., et al., *A DNA polymorphism influencing alpha(1,2)fucosyltransferase activity of the pig FUT1 enzyme determines susceptibility of small intestinal epithelium to Escherichia coli F18 adhesion.* Immunogenetics, 2000. **52**(1-2): p. 129-36.
74. Sack, D.A., et al., *Diarrhoea associated with heat-stable enterotoxin-producing strains of Escherichia coli.* Lancet, 1975. **2**(7928): p. 239-41.
75. Duan, Q., et al., *Review of Newly Identified Functions Associated With the Heat-Labile Toxin of Enterotoxigenic Escherichia coli.* Front Cell Infect Microbiol, 2019. **9**: p. 292.
76. Weiglmeier, P.R., P. Rosch, and H. Berkner, *Cure and curse: E. coli heat-stable enterotoxin and its receptor guanylyl cyclase C.* Toxins (Basel), 2010. **2**(9): p. 2213-29.

77. Gazzano, H., H.I. Wu, and S.A. Waldman, *Activation of particulate guanylate cyclase by Escherichia coli heat-stable enterotoxin is regulated by adenine nucleotides.* Infect Immun, 1991. **59**(4): p. 1552-7.
78. Kar, S.K., et al., *Dietary protein sources differentially affect microbiota, mTOR activity and transcription of mTOR signaling pathways in the small intestine.* PLoS One, 2017. **12**(11): p. e0188282.
79. Rocha, G.C., M.E. Duarte, and S.W. Kim, *Advances, Implications, and Limitations of Low-Crude-Protein Diets in Pig Production.* Animals (Basel), 2022. **12**(24).
80. Wang, Y., et al., *Advances in low-protein diets for swine.* J Anim Sci Biotechnol, 2018. **9**: p. 60.
81. Windey, K., V. De Preter, and K. Verbeke, *Relevance of protein fermentation to gut health.* Mol Nutr Food Res, 2012. **56**(1): p. 184-96.
82. Wang, T., et al., *Advances of research on glycinin and beta-conglycinin: a review of two major soybean allergenic proteins.* Crit Rev Food Sci Nutr, 2014. **54**(7): p. 850-62.
83. Chen, X., et al., *Moderate Dietary Protein Restriction Optimized Gut Microbiota and Mucosal Barrier in Growing Pig Model.* Front Cell Infect Microbiol, 2018. **8**: p. 246.
84. Pieper, R., et al., *Fermentable fiber ameliorates fermentable protein-induced changes in microbial ecology, but not the mucosal response, in the colon of piglets.* J Nutr, 2012. **142**(4): p. 661-7.
85. Zhang, C., et al., *Effect of early antibiotic administration on cecal bacterial communities and their metabolic profiles in pigs fed diets with different protein levels.* Anaerobe, 2016. **42**: p. 188-196.
86. Luo, Z., et al., *Effects of low dietary protein on the metabolites and microbial communities in the caecal digesta of piglets.* Arch Anim Nutr, 2015. **69**(3): p. 212-26.
87. Yu, D., W. Zhu, and S. Hang, *Effects of Long-Term Dietary Protein Restriction on Intestinal Morphology, Digestive Enzymes, Gut Hormones, and Colonic Microbiota in Pigs.* Animals (Basel), 2019. **9**(4).
88. Wellock, I.J., et al., *The effect of dietary protein supply on the performance and risk of post-weaning enteric disorders in newly weaned pigs.* Animal Science, 2006. **82**: p. 327-335.
89. Opapeju, F.O., et al., *Effect of dietary protein level on growth performance, indicators of enteric health, and gastrointestinal microbial ecology of weaned pigs induced with postweaning colibacillosis.* J Anim Sci, 2009. **87**(8): p. 2635-43.
90. Bikker, P., et al., *The effect of dietary protein and fermentable carbohydrates levels on growth performance and intestinal characteristics in newly weaned piglets.* J Anim Sci, 2006. **84**(12): p. 3337-45.
91. Wellock, I.J., et al., *Effects of dietary protein supply, weaning age and experimental enterotoxigenic Escherichia coli infection on newly weaned pigs: performance.* Animal, 2008. **2**(6): p. 825-33.
92. Zhou, L., et al., *Effects of the dietary protein level on the microbial composition and metabolomic profile in the hindgut of the pig.* Anaerobe, 2016. **38**: p. 61-69.
93. Smith, E.A. and G.T. Macfarlane, *Dissimilatory amino Acid metabolism in human colonic bacteria.* Anaerobe, 1997. **3**(5): p. 327-37.
94. Libao-Mercado, A.J., et al., *Dietary and endogenous amino acids are the main contributors to microbial protein in the upper gut of normally nourished pigs.* J Nutr, 2009. **139**(6): p. 1088-94.
95. Pieper, R., et al., *Interaction between dietary protein content and the source of carbohydrates along the gastrointestinal tract of weaned piglets.* Arch Anim Nutr, 2014. **68**(4): p. 263-80.
96. Geypens, B., et al., *Influence of dietary protein supplements on the formation of bacterial metabolites in the colon.* Gut, 1997. **41**(1): p. 70-6.
97. Cummings, J.H., et al., *The effect of meat protein and dietary fiber on colonic function and metabolism. II. Bacterial metabolites in feces and urine.* Am J Clin Nutr, 1979. **32**(10): p. 2094-101.
98. Hughes, R., et al., *Effect of colonic bacterial metabolites on Caco-2 cell paracellular permeability in vitro.* Nutr Cancer, 2008. **60**(2): p. 259-66.
99. Ichikawa, H. and T. Sakata, *Stimulation of epithelial cell proliferation of isolated distal colon of rats by continuous colonic infusion of ammonia or short-chain fatty acids is nonadditive.* J Nutr, 1998. **128**(5): p. 843-7.
100. Lin, H.C. and W.J. Visek, *Colon mucosal cell damage by ammonia in rats.* J Nutr, 1991. **121**(6): p. 887-93.

101. Villodre Tudela, C., et al., *Down-regulation of monocarboxylate transporter 1 (MCT1) gene expression in the colon of piglets is linked to bacterial protein fermentation and pro-inflammatory cytokine-mediated signalling.* Br J Nutr, 2015. **113**(4): p. 610-7.
102. Sepponen, K., et al., *Expression of CD147 and monocarboxylate transporters MCT1, MCT2 and MCT4 in porcine small intestine and colon.* Vet J, 2007. **174**(1): p. 122-8.
103. Roediger, W.E., *Role of anaerobic bacteria in the metabolic welfare of the colonic mucosa in man.* Gut, 1980. **21**(9): p. 793-8.
104. Cremin, J.D., Jr., M.D. Fitch, and S.E. Fleming, *Glucose alleviates ammonia-induced inhibition of short-chain fatty acid metabolism in rat colonic epithelial cells.* Am J Physiol Gastrointest Liver Physiol, 2003. **285**(1): p. G105-14.
105. Leschelle, X., et al., *Isolation of pig colonic crypts for cytotoxic assay of luminal compounds: effects of hydrogen sulfide, ammonia, and deoxycholic acid.* Cell Biol Toxicol, 2002. **18**(3): p. 193-203.
106. van der Hee, B. and J.M. Wells, *Microbial Regulation of Host Physiology by Short-chain Fatty Acids.* Trends Microbiol, 2021.
107. Bergman, E.N., *Energy contributions of volatile fatty acids from the gastrointestinal tract in various species.* Physiol Rev, 1990. **70**(2): p. 567-90.
108. Nordgaard, I., B.S. Hansen, and P.B. Mortensen, *Importance of colonic support for energy absorption as small-bowel failure proceeds.* Am J Clin Nutr, 1996. **64**(2): p. 222-31.
109. Macfarlane, S. and G.T. Macfarlane, *Proteolysis and Amino Acid Fermentation*, in *Human Colonic Bacteria: Role in Nutrition, Physiology and Pathology.* 1995, CRC Press.
110. Russell, W.R., et al., *High-protein, reduced-carbohydrate weight-loss diets promote metabolite profiles likely to be detrimental to colonic health.* Am J Clin Nutr, 2011. **93**(5): p. 1062-72.
111. Beaumont, M., et al., *Quantity and source of dietary protein influence metabolite production by gut microbiota and rectal mucosa gene expression: a randomized, parallel, double-blind trial in overweight humans.* Am J Clin Nutr, 2017. **106**(4): p. 1005-1019.
112. Vanholder, R., et al., *The uremic toxicity of indoxyl sulfate and p-cresyl sulfate: a systematic review.* J Am Soc Nephrol, 2014. **25**(9): p. 1897-907.
113. Jaskiewicz, J., et al., *Catabolism of isobutyrate by colonocytes.* Arch Biochem Biophys, 1996. **327**(2): p. 265-70.
114. Musch, M.W., et al., *SCFA increase intestinal Na absorption by induction of NHE3 in rat colon and human intestinal C2/bbe cells.* Am J Physiol Gastrointest Liver Physiol, 2001. **280**(4): p. G687-93.
115. Roediger, W.E. and W. Babidge, *Human colonocyte detoxification.* Gut, 1997. **41**(6): p. 731-4.
116. Magee, E.A., et al., *Contribution of dietary protein to sulfide production in the large intestine: an in vitro and a controlled feeding study in humans.* Am J Clin Nutr, 2000. **72**(6): p. 1488-94.
117. Pitcher, M.C., E.R. Beatty, and J.H. Cummings, *The contribution of sulphate reducing bacteria and 5-aminosalicylic acid to faecal sulphide in patients with ulcerative colitis.* Gut, 2000. **46**(1): p. 64-72.
118. Roediger, W.E., *Decreased sulphur aminoacid intake in ulcerative colitis.* Lancet, 1998. **351**(9115): p. 1555.
119. Moore, J.W., et al., *Hydrogen sulphide produces diminished fatty acid oxidation in the rat colon in vivo: implications for ulcerative colitis.* Aust N Z J Surg, 1997. **67**(5): p. 245-9.
120. Leschelle, X., et al., *Adaptative metabolic response of human colonic epithelial cells to the adverse effects of the luminal compound sulfide.* Biochim Biophys Acta, 2005. **1725**(2): p. 201-12.
121. Beaumont, M., et al., *Detrimental effects for colonocytes of an increased exposure to luminal hydrogen sulfide: The adaptive response.* Free Radic Biol Med, 2016. **93**: p. 155-64.
122. Deplancke, B. and H.R. Gaskins, *Hydrogen sulfide induces serum-independent cell cycle entry in nontransformed rat intestinal epithelial cells.* FASEB J, 2003. **17**(10): p. 1310-2.
123. Christl, S.U., et al., *Antagonistic effects of sulfide and butyrate on proliferation of colonic mucosa: a potential role for these agents in the pathogenesis of ulcerative colitis.* Dig Dis Sci, 1996. **41**(12): p. 2477-81.
124. Wong, W.M. and N.A. Wright, *Cell proliferation in gastrointestinal mucosa.* J Clin Pathol, 1999. **52**(5): p. 321-33.
125. Wong, R.S., *Apoptosis in cancer: from pathogenesis to treatment.* J Exp Clin Cancer Res, 2011. **30**(1): p. 87.

126. Ijssennagger, N., et al., *Gut microbiota facilitates dietary heme-induced epithelial hyperproliferation by opening the mucus barrier in colon.* Proc Natl Acad Sci U S A, 2015. **112**(32): p. 10038-43.
127. Ijssennagger, N., R. van der Meer, and S.W.C. van Mil, *Sulfide as a Mucus Barrier-Breaker in Inflammatory Bowel Disease?* Trends Mol Med, 2016. **22**(3): p. 190-199.
128. Bekebrede, A.F., et al., *The Molecular and Physiological Effects of Protein-Derived Polyamines in the Intestine.* Nutrients, 2020. **12**(1).
129. Larque, E., M. Sabater-Molina, and S. Zamora, *Biological significance of dietary polyamines.* Nutrition, 2007. **23**(1): p. 87-95.
130. Loser, C., et al., *Dietary polyamines are essential luminal growth factors for small intestinal and colonic mucosal growth and development.* Gut, 1999. **44**(1): p. 12-6.
131. Grant, A.L., et al., *Effects of dietary amines on small intestinal variables in neonatal pigs fed soy protein isolate.* J Anim Sci, 1990. **68**(2): p. 363-71.
132. Blachier, F., et al., *Effects of amino acid-derived luminal metabolites on the colonic epithelium and physiopathological consequences.* Amino Acids, 2007. **33**(4): p. 547-62.
133. Fahrer, J. and B. Kaina, *O6-methylguanine-DNA methyltransferase in the defense against N-nitroso compounds and colorectal cancer.* Carcinogenesis, 2013. **34**(11): p. 2435-42.
134. Pedersen, G., J. Brynskov, and T. Saermark, *Phenol toxicity and conjugation in human colonic epithelial cells.* Scand J Gastroenterol, 2002. **37**(1): p. 74-9.
135. Lamas, B., J.M. Natividad, and H. Sokol, *Aryl hydrocarbon receptor and intestinal immunity.* Mucosal Immunol, 2018. **11**(4): p. 1024-1038.
136. Venkatesh, M., et al., *Symbiotic bacterial metabolites regulate gastrointestinal barrier function via the xenobiotic sensor PXR and Toll-like receptor 4.* Immunity, 2014. **41**(2): p. 296-310.
137. Qi, Q., et al., *Host and gut microbial tryptophan metabolism and type 2 diabetes: an integrative analysis of host genetics, diet, gut microbiome and circulating metabolites in cohort studies.* Gut, 2022. **71**(6): p. 1095-1105.
138. Huang, Z., et al., *Distinct effects of fiber and colon segment on microbiota-derived indoles and short-chain fatty acids.* Food Chem, 2023. **398**: p. 133801.
139. Andriamihaja, M., et al., *The deleterious metabolic and genotoxic effects of the bacterial metabolite p-cresol on colonic epithelial cells.* Free Radic Biol Med, 2015. **85**: p. 219-27.
140. Spring, S., et al., *Effect of very low-protein diets supplemented with branched-chain amino acids on energy balance, plasma metabolomics and fecal microbiome of pigs.* Sci Rep, 2020. **10**(1): p. 15859.
141. Council, N.R., *Nutrient Requirements of Swine: Eleventh Revised Edition*. 2012: The National Academies Press.
142. Council, N.R., *Nutrient requirements of swine: Tenth revised edition*. 1994: National Academy Press.
143. Rodrigues, L.A., et al., *Formulating Diets for Improved Health Status of Pigs: Current Knowledge and Perspectives.* Animals (Basel), 2022. **12**(20).
144. Lee, J., et al., *Effects of dietary protein content and crystalline amino acid supplementation patterns on growth performance, intestinal histomorphology, and immune response in weaned pigs raised under different sanitary conditions.* J Anim Sci, 2022. **100**(10).
145. Zhang, S., et al., *Effects of dietary leucine supplementation in low crude protein diets on performance, nitrogen balance, whole-body protein turnover, carcass characteristics and meat quality of finishing pigs.* Anim Sci J, 2016. **87**(7): p. 911-20.
146. Roux, M.L., et al., *Maximizing the use of supplemental amino acids in corn-soybean meal diets for 20- to 45-kilogram pigs.* J Anim Sci, 2011. **89**(8): p. 2415-24.
147. Powell, S., et al., *Growth performance of 20- to 50-kilogram pigs fed low-crude-protein diets supplemented with histidine, cystine, glycine, glutamic acid, or arginine.* J Anim Sci, 2011. **89**(11): p. 3643-50.
148. Krause, W.J., *Brunner's glands: a structural, histochemical and pathological profile.* Prog Histochem Cytochem, 2000. **35**(4): p. 259-367.
149. Gonzalez, L.M., A.J. Moeser, and A.T. Blikslager, *Porcine models of digestive disease: the future of large animal translational research.* Transl Res, 2015. **166**(1): p. 12-27.
150. Yandza, T., et al., *The pig as a preclinical model for intestinal ischemia-reperfusion and transplantation studies.* J Surg Res, 2012. **178**(2): p. 807-19.
151. Pelaseyed, T., et al., *The mucus and mucins of the goblet cells and enterocytes provide the first defense line of the gastrointestinal tract and interact with the immune system.* Immunol Rev, 2014. **260**(1): p. 8-20.

152. Johansson, M.E., H. Sjovall, and G.C. Hansson, *The gastrointestinal mucus system in health and disease.* Nat Rev Gastroenterol Hepatol, 2013. **10**(6): p. 352-61.
153. Cash, H.L., et al., *Symbiotic bacteria direct expression of an intestinal bactericidal lectin.* Science, 2006. **313**(5790): p. 1126-30.
154. Wells, J.M., et al., *Epithelial crosstalk at the microbiota-mucosal interface.* Proc Natl Acad Sci U S A, 2011. **108 Suppl 1**(Suppl 1): p. 4607-14.
155. Gustafsson, J.K. and M.E.V. Johansson, *The role of goblet cells and mucus in intestinal homeostasis.* Nat Rev Gastroenterol Hepatol, 2022. **19**(12): p. 785-803.
156. Lang, T., G.C. Hansson, and T. Samuelsson, *Gel-forming mucins appeared early in metazoan evolution.* Proc Natl Acad Sci U S A, 2007. **104**(41): p. 16209-14.
157. Pajic, P., et al., *A mechanism of gene evolution generating mucin function.* Sci Adv, 2022. **8**(34): p. eabm8757.
158. Sovran, B., et al., *Identification of Commensal Species Positively Correlated with Early Stress Responses to a Compromised Mucus Barrier.* Inflamm Bowel Dis, 2016. **22**(4): p. 826-40.
159. Velcich, A., et al., *Colorectal cancer in mice genetically deficient in the mucin Muc2.* Science, 2002. **295**(5560): p. 1726-9.
160. Van der Sluis, M., et al., *Muc2-deficient mice spontaneously develop colitis, indicating that MUC2 is critical for colonic protection.* Gastroenterology, 2006. **131**(1): p. 117-29.
161. Caballero-Franco, C., et al., *The VSL#3 probiotic formula induces mucin gene expression and secretion in colonic epithelial cells.* Am J Physiol Gastrointest Liver Physiol, 2007. **292**(1): p. G315-22.
162. Dohrman, A., et al., *Mucin gene (MUC 2 and MUC 5AC) upregulation by Gram-positive and Gram-negative bacteria.* Biochim Biophys Acta, 1998. **1406**(3): p. 251-9.
163. Jarry, A., et al., *Direct secretory effect of interleukin-1 via type I receptors in human colonic mucous epithelial cells (HT29-C1.16E).* Gut, 1996. **38**(2): p. 240-2.
164. Enss, M.L., et al., *Proinflammatory cytokines trigger MUC gene expression and mucin release in the intestinal cancer cell line LS180.* Inflamm Res, 2000. **49**(4): p. 162-9.
165. Smirnova, M.G., et al., *LPS up-regulates mucin and cytokine mRNA expression and stimulates mucin and cytokine secretion in goblet cells.* Cell Immunol, 2003. **221**(1): p. 42-9.
166. Willemsen, L.E., et al., *Short chain fatty acids stimulate epithelial mucin 2 expression through differential effects on prostaglandin E(1) and E(2) production by intestinal myofibroblasts.* Gut, 2003. **52**(10): p. 1442-7.
167. Burger-van Paassen, N., et al., *The regulation of intestinal mucin MUC2 expression by short-chain fatty acids: implications for epithelial protection.* Biochem J, 2009. **420**(2): p. 211-9.
168. Tam, P.Y. and P. Verdugo, *Control of mucus hydration as a Donnan equilibrium process.* Nature, 1981. **292**(5821): p. 340-2.
169. Linden, S.K., et al., *Mucins in the mucosal barrier to infection.* Mucosal Immunol, 2008. **1**(3): p. 183-97.
170. Hytonen, J., S. Haataja, and J. Finne, *Streptococcus pyogenes glycoprotein-binding strepadhesin activity is mediated by a surface-associated carbohydrate-degrading enzyme, pullulanase.* Infect Immun, 2003. **71**(2): p. 784-93.
171. Bouchet, V., et al., *Host-derived sialic acid is incorporated into Haemophilus influenzae lipopolysaccharide and is a major virulence factor in experimental otitis media.* Proc Natl Acad Sci U S A, 2003. **100**(15): p. 8898-903.
172. Schwegmann, C., et al., *Comparison of the sialic acid binding activity of transmissible gastroenteritis coronavirus and E. coli K99.* Virus Res, 2001. **75**(1): p. 69-73.
173. McAuley, J.L., et al., *MUC1 cell surface mucin is a critical element of the mucosal barrier to infection.* J Clin Invest, 2007. **117**(8): p. 2313-24.
174. Willoughby, R.E., *Rotaviruses preferentially bind O-linked sialylglycoconjugates and sialomucins.* Glycobiology, 1993. **3**(5): p. 437-45.
175. Alexander, D.A. and K. Dimock, *Sialic acid functions in enterovirus 70 binding and infection.* J Virol, 2002. **76**(22): p. 11265-72.
176. Nabuurs, M.J., et al., *Villus height and crypt depth in weaned and unweaned pigs, reared under various circumstances in The Netherlands.* Res Vet Sci, 1993. **55**(1): p. 78-84.
177. Eisenhoffer, G.T., et al., *Crowding induces live cell extrusion to maintain homeostatic cell numbers in epithelia.* Nature, 2012. **484**(7395): p. 546-9.
178. Wells, J.M., et al., *Homeostasis of the gut barrier and potential biomarkers.* Am J Physiol Gastrointest Liver Physiol, 2017. **312**(3): p. G171-G193.

179. Gu, Y., et al., *Epithelial cell extrusion requires the sphingosine-1-phosphate receptor 2 pathway.* J Cell Biol, 2011. **193**(4): p. 667-76.
180. Clevers, H., *The intestinal crypt, a prototype stem cell compartment.* Cell, 2013. **154**(2): p. 274-84.
181. Barker, N., et al., *Identification of stem cells in small intestine and colon by marker gene Lgr5.* Nature, 2007. **449**(7165): p. 1003-U1.
182. Hartsock, A. and W.J. Nelson, *Adherens and tight junctions: structure, function and connections to the actin cytoskeleton.* Biochim Biophys Acta, 2008. **1778**(3): p. 660-9.
183. Ulluwishewa, D., et al., *Regulation of tight junction permeability by intestinal bacteria and dietary components.* J Nutr, 2011. **141**(5): p. 769-76.
184. McKay, D.M. and A.W. Baird, *Cytokine regulation of epithelial permeability and ion transport.* Gut, 1999. **44**(2): p. 283-9.
185. Poritz, L.S., et al., *Increase in the tight junction protein claudin-1 in intestinal inflammation.* Dig Dis Sci, 2011. **56**(10): p. 2802-9.
186. Hermes, R.G., et al., *Effect of dietary level of protein and fiber on the productive performance and health status of piglets.* J Anim Sci, 2009. **87**(11): p. 3569-77.
187. Skamrahl, M., et al., *Tight Junction ZO Proteins Maintain Tissue Fluidity, Ensuring Efficient Collective Cell Migration.* Adv Sci (Weinh), 2021. **8**(19): p. e2100478.
188. Butler, J.E., et al., *Antibody repertoire development in fetal and newborn piglets, III. Colonization of the gastrointestinal tract selectively diversifies the preimmune repertoire in mucosal lymphoid tissues.* Immunology, 2000. **100**(1): p. 119-30.
189. Salzman, N.H., M.A. Underwood, and C.L. Bevins, *Paneth cells, defensins, and the commensal microbiota: a hypothesis on intimate interplay at the intestinal mucosa.* Semin Immunol, 2007. **19**(2): p. 70-83.
190. Venema, K., *The TNO In Vitro Model of the Colon (TIM-2)*, in *The Impact of Food Bioactives on Health: in vitro and ex vivo models*, K. Verhoeckx, et al., Editors. 2015: Cham (CH). p. 293-304.
191. Van de Wiele, T., et al., *The Simulator of the Human Intestinal Microbial Ecosystem (SHIME((R)))*, in *The Impact of Food Bioactives on Health: in vitro and ex vivo models*, K. Verhoeckx, et al., Editors. 2015: Cham (CH). p. 305-17.
192. Cerini, C., et al., *P-cresol, a uremic retention solute, alters the endothelial barrier function in vitro.* Thromb Haemost, 2004. **92**(1): p. 140-50.
193. Attene-Ramos, M.S., et al., *Hydrogen sulfide induces direct radical-associated DNA damage.* Mol Cancer Res, 2007. **5**(5): p. 455-9.
194. Liu, Y., et al., *Multi-omic measurements of heterogeneity in HeLa cells across laboratories.* Nat Biotechnol, 2019. **37**(3): p. 314-322.
195. Yu, M., et al., *A resource for cell line authentication, annotation and quality control.* Nature, 2015. **520**(7547): p. 307-11.
196. Lorsch, J.R., F.S. Collins, and J. Lippincott-Schwartz, *Cell Biology. Fixing problems with cell lines.* Science, 2014. **346**(6216): p. 1452-3.
197. Frattini, A., et al., *High variability of genomic instability and gene expression profiling in different HeLa clones.* Sci Rep, 2015. **5**: p. 15377.
198. Muff, R., et al., *Genomic instability of osteosarcoma cell lines in culture: impact on the prediction of metastasis relevant genes.* PLoS One, 2015. **10**(5): p. e0125611.
199. Ben-David, U., et al., *Genetic and transcriptional evolution alters cancer cell line drug response.* Nature, 2018. **560**(7718): p. 325-330.
200. Sato, T., et al., *Single Lgr5 stem cells build crypt-villus structures in vitro without a mesenchymal niche.* Nature, 2009. **459**(7244): p. 262-5.
201. Sato, T., et al., *Paneth cells constitute the niche for Lgr5 stem cells in intestinal crypts.* Nature, 2011. **469**(7330): p. 415-8.
202. Sato, T., et al., *Long-term expansion of epithelial organoids from human colon, adenoma, adenocarcinoma, and Barrett's epithelium.* Gastroenterology, 2011. **141**(5): p. 1762-72.
203. Foulke-Abel, J., et al., *Human enteroids as an ex-vivo model of host-pathogen interactions in the gastrointestinal tract.* Exp Biol Med (Maywood), 2014. **239**(9): p. 1124-34.
204. Thompson, C.A., et al., *GATA4 Is Sufficient to Establish Jejunal Versus Ileal Identity in the Small Intestine.* Cell Mol Gastroenterol Hepatol, 2017. **3**(3): p. 422-446.
205. Qi, F., et al., *Single cell RNA sequencing of 13 human tissues identify cell types and receptors of human coronaviruses.* Biochem Biophys Res Commun, 2020. **526**(1): p. 135-140.
206. Lamers, M.M., et al., *SARS-CoV-2 productively infects human gut enterocytes.* Science, 2020. **369**(6499): p. 50-54.

207. Heo, I., et al., *Modelling Cryptosporidium infection in human small intestinal and lung organoids.* Nat Microbiol, 2018. **3**(7): p. 814-823.
208. Karanis, P., *The truth about in vitro culture of Cryptosporidium species.* Parasitology, 2018. **145**(7): p. 855-864.
209. Karanis, P. and H.M. Aldeyarbi, *Evolution of Cryptosporidium in vitro culture.* Int J Parasitol, 2011. **41**(12): p. 1231-42.
210. van der Hee, B., et al., *Congruence of Transcription Programs in Adult Stem Cell-Derived Jejunum Organoids and Original Tissue During Long-Term Culture.* Front Cell Dev Biol, 2020. **8**: p. 375.
211. van der Hee, B., et al., *Optimized procedures for generating an enhanced, near physiological 2D culture system from porcine intestinal organoids.* Stem Cell Res, 2018. **28**: p. 165-171.
212. Kar, S.K., et al., *Effects of undigested protein-rich ingredients on polarised small intestinal organoid monolayers.* J Anim Sci Biotechnol, 2020. **11**: p. 51.

Microbial Protein Fermentation and Fecal Metabolites in the Onset of Post-Weaning Diarrhea in Pigs

Bart van der Hee[1,2], Myrthe S. Gilbert[3], Walter J.J. Gerrits[3], Joanna C. Wolthuis[4], Arie K. Kies[5], Anja Taverne-Thiele[1], Ineke G.A.M. Heikamp-de Jong[2], Merlijn P. van Gaal[2], Edwin C.A. Stigter[4], Boudewijn M.T. Burgering[4], Saskia W.C. van Mil[4], Jerry M. Wells[1], Hauke Smidt[2]

[1] Host-Microbe Interactomics Group, Department of Animal Sciences, Wageningen University & Research, Wageningen, The Netherlands, [2] Laboratory of Microbiology, Wageningen University & Research, Wageningen, The Netherlands, [3] Animal Nutrition Group, Department of Animal Sciences, Wageningen University & Research, Wageningen, The Netherlands, [4] Center for Molecular Medicine, University Medical Center Utrecht and Utrecht University, The Netherlands, [5] DSM Nutritional Products, Animal Nutrition and Health, Kaiseraugst, Switzerland

Manuscript to be submitted

Abstract

Post-weaning diarrhea (PWD) is a common gastrointestinal disorder that affects piglets during the weaning process. It is caused by a combination of factors, including stress, changes in diet and the environment, and the presence of intestinal pathogens. Antibiotics have traditionally been used to control PWD, but the widespread use of these drugs has contributed to the development of antibiotic resistance. As a result, there has been increasing interest in using nutritional interventions as an alternative way to prevent PWD-related infections. Previous research has shown that increased levels of dietary crude protein (CP) are associated with PWD onset, and that reducing CP intake can alleviate diarrhea symptoms. It is thought that the inability to properly digest the changing dietary nutrients lead to the increased flow of undigested protein into the colon, where it is fermented by the resident microbiota. Some of the resulting metabolites may be detrimental to the host and contribute to intestinal barrier dysfunction and PWD. However, the relationship between PWD onset and protein fermentation in practice is not well understood. Therefore, we investigated the temporal associations between fecal microbiota development, fecal metabolites, and the morphological properties of the intestine in piglets during the weaning process from 4 separate farms. We found an increase of heat-stable toxin (ST)a and STb-expressing *E. coli* in piglets suffering from diarrhea at 4 days PW (n=52) compared to controls (n=28) in all 4 farms, and concurrent increase in the concentration of the protein fermentation metabolite ammonia. This suggests that commercially used dietary protein concentrations have an association between protein fermentation and PWD. There was a direct correlation between protein fermentation markers and relative abundance of proteolytic bacterial species in diarrheal animals, as well as an important contribution of fiber-fermentation associated tryptophan metabolism in control animals post weaning. However, most of the significant changes in these parameters were only observed at the point of diarrheal onset, suggesting that they are not exclusive contributors to PWD. These results do show an important link between PWD and microbially produced metabolites despite large individual variation, further reinforcing the multifactorial nature of the disorder.

Introduction

In pig production weaning commonly involves abrupt separation of piglets from the sow accompanied by dietary and environmental shifts. Weaning is often associated with a reduction and delay in feed intake, stress, maturation of the epithelial barrier and transport functions, changes in the immune system and shifts in the intestinal microbiota [1-3]. The stress that occurs due to separation from the sow and mixing with new pen mates is also considered to impact on barrier function, intestinal permeability, and the immune system [4-7]. The inability of piglets to properly respond to the changes in nutritional constituents and stress, owed to the early weaning at a premature developmental stage, has been linked to the onset of PWD [8, 9].

Because of abrupt weaning and stress there is an increased susceptibility to enteric infections by pathogens like enterotoxigenic *Escherichia coli* (ETEC), which necessitated the use of antibacterial drugs to decrease PWD incidence [10, 11]. Widespread use of antibiotics to control enteric infections, however, has led to increased antibiotic resistance [10] and regulatory restrictions for prophylactic use on farms. Nutritional interventions have been explored as an alternative to antibiotics to prevent occurrence of PWD-related infections [12, 13]. However, some of these approaches, like pre-weaning diets, are difficult to control at farm and animal level. Recent developments of vaccination with live attenuated ETEC have shown promising results on decreasing ETEC-related PWD but are currently not widely available [14].

Seminal studies have shown that increased levels of dietary crude protein (CP) elevate the risk of PWD onset and that its reduction alleviates diarrhea symptoms [15, 16]. It is thought that the underdevelopment of nutrient digestion leads to increased flow of undigested protein into the colon [16, 17]. In the colon, the long residence time and limited nutrient absorption facilitate increased protein fermentation by the resident microbiota and accumulation of metabolic end products, some of which may be detrimental to the host. For instance, *in vitro* studies have shown that hydrogen sulfide (H_2S) reduces colonic butyrate oxidation [18] and that ammonia (NH_3) down regulates expression of intestinal butyrate transporter monocarboxylate transport 1 (MCT1) [19]. The capacity to inhibit intestinal energy metabolism by these metabolites could adversely affect barrier function [20], and supports the notion that elevated levels of protein fermentation contribute to intestinal barrier dysfunction and PWD.

Increased dietary CP has been shown to increase relative abundance of pathogens in the genera *Escherichia*, *Campylobacter*, *Salmonella*, and *Fusobacterium* which could cause infectious diarrhea. Substrate availability drives functional metabolic selection of adaptable bacterial species. Increased levels of undigested protein that can serve as substrate for bacterial protein fermentation could be an intermediary effector in the progression of PWD by increased proliferation of colonic pathogens. However, the contribution of these protein fermenting pathogens to PWD has shown contradictory results in literature (reviewed by [21, 22]). Furthermore, studies showing PWD alleviation through CP reduction utilize levels not typically used in practice [16]. To get a better understanding of the role of protein fermentation under practical conditions, we investigated the temporal associations between fecal microbiota development, fecal metabolites, and morphological properties of the intestine. Our results show a direct correlation between protein fermentation markers NH_3 and branched-chain fatty acids (BCFAs) and proteolytic bacterial species in diarrheal animals, as well as an important distinction of fiber-fermentation associated tryptophan metabolism in animals with no diarrhea post weaning. However, most considerable changes in these parameters were only observed at the point of diarrheal onset and with a high individual animal variation, which suggests their non-exclusive contribution to PWD and reinforces the multifactorial nature of PWD onset.

Materials and methods

Animals and experimental setup

All experimental procedures were approved by the Animal Ethics Committee of Wageningen University. A total of 80 animals from four commercial pig farms (52 diarrhea, 28 control) were needed for the final diarrhea measurements as calculated by an initial pilot screening (**Supplementary methods, Figure 2**). Therefore, to prospectively secure that number, a total of 20 litters were sampled 14 days pre-weaning (Day -14 PW) and 2 days post weaning (Day 2 PW) per farm. The farms did not use antibiotics during the experiments to avoid effects on PWD or microbial composition. On each farm at day 4 PW, the animals were stratified to 7 control and 13 diarrhea animals for dissection on day 5 PW for intestinal morphology (see **Figure 1**). The diets of all piglets were according to the general farm practices of their respective farm and similar to all individual piglets on their corresponding farm.

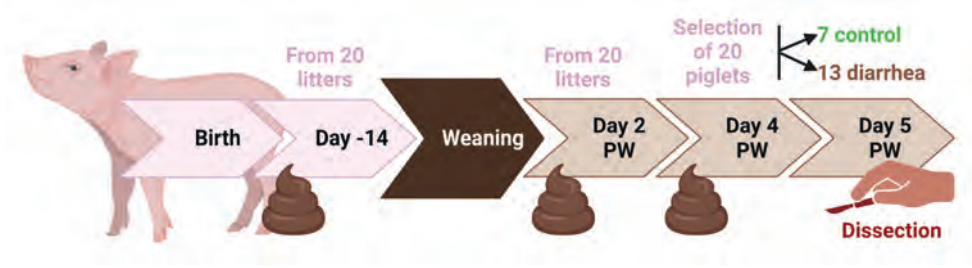

Figure 1. Timeline of sample selection pre- and post-weaning. At 14 days pre-weaning, 20 litters were sampled for feces per farm and prospectively sampled at day 2 and 4 post-weaning. 20 animals per farm with a corresponding diarrheal or control phenotype were then selected for microbiota analysis.

Fecal sampling

At day -14 PW and day 2 PW the fecal samples of all piglets were collected and directly stored in 100 ml containers at -20°C. The fecal samples were collected by gentle rectal stimulation with demi-H_2O pre-wetted swabs (Purflock, Puritan; day -14 PW) or manually (day 2 and 4 PW) and scored for consistency (from 1 (soft) to 5 (hard), see **Supplementary methods**). The pH and freeze-dry matter (FDM) content of the samples was measured as previously published [23]. The inclusion criteria for piglets in the diarrhea group (score 1-2) or control group (score 4-5) were determined on-farm and confirmed using FDM content (**Supplementary methods**).

Dissection and histology

After selection, the animals were dissected on-farm. Firstly, the animals were sedated via intramuscular injection of Zoletil + Xylazine (5:2 ratio, 1 mg/10 kg BW) and transferred to the dissection table. The piglets were then euthanized with Euthasol (20% pentobarbital, 24 mg/kg BW) in the ear vein and bled through the front left leg. The abdominal cavity was opened, and all intestinal segments were individually clamped to prevent digesta transit. Mid-jejunum, proximal colon, and distal colon sections were transferred to separate containers. To avoid fecal interference with histology, the sections were gently rinsed with demi-H_2O. Two 2 cm sections at 10 cm distances were taken for histology and fixed in tubes containing 4% paraformaldehyde (PFA). After overnight fixation at RT, the sections were placed into cassettes and washed with running water for 10 min. The cassettes were subsequently processed for automated paraffin embedding (Hisokinette) in gradual series of ethanol (70-100%) for dehydration and xylene. The sections were then fixed in paraffin blocks, cut using a microtome in 5 µm sections, and dried onto poly-l-lysine glass slides. Two sections (10 cm apart) of each intestinal location were then stained with hematoxylin and eosin following previous methods and tile-scanned on a microscope at 10x magnification (DM6, Leica). The images were then measured for crypt depth and villous height using LASX software (Leica) with 10 representative measurements per section per location. 10 measurements per section were sufficient for crypt depth and villous height estimation (see **Supplementary methods**).

Ammonia

The fecal samples were analyzed for ammonia as previously described [24, 25]. Briefly, water was added to the samples to release the ammonia and centrifuged at 2500 x *g* for 10 min. The supernatants were subsequently deproteinized with trichloroacetic acid (TCA, 10%) followed by centrifugation at 14,000 x *g* for 10 min. The ammonia was detected using Berthelot's reagent at 37°C for 30 min, and the colored product indolphenolblue measured on a spectrophotometer at 623 nm. A standard curve generated for different concentrations of ammonia was used for quantification.

Short Chain Fatty Acids

Feces were thawed and phosphoric acid was added at RT and shaken for 30 min. The samples were then centrifuged at 20,817 x *g* for 10 min, and the resulting supernatants were mixed with an internal standard (31.784 mM 2-methyl valeric acid). The mixture was centrifuged at 20,817 x *g* for 5 min and injected onto a gas chromatograph (GC, HIP-FFAP; 30 m x 0.32 mm x 0.25 µm, Agilent J&W, USA). The fatty acids were then separated, and short chain fatty acids (SCFAs) were detected using a flame ionization detector.

DNA extraction and 16S rRNA gene library preparation

The fecal samples were thawed on ice and processed for automated DNA extraction (Maxwell 16 Total RNA extraction kit customized for fecal DNA extraction, Promega, USA) as previously described [26]. 200 mg of each fecal sample was added to bead-beating tubes containing 700 µl Stool and Transport Recovery (STAR) solution (Roche Diagnostics, Switzerland), 0.5 g 0.1 mm zirconia beads and 5 2.5 mm glass beads and homogenized by repeated bead-beating (5.5 ms, 3 x 1 min, FastPrep; MP Biomedicals) at RT. The samples were incubated at 95°C for 15 min at 300 rpm, and then centrifuged at 15,000 x *g* for 5 min at 4°C. The supernatant was transferred into a clean 1.5 ml Eppendorf tube on ice and the remaining pellet was reprocessed with 300 µl STAR buffer. The resulting supernatants were subsequently pooled. In total, 250 µl supernatant was used for DNA extraction on the Maxwell 16 instrument, and DNA was eluted in 50 µl DNAse- and RNAse-free water (Promega). Total DNA concentrations were measured on a nanodrop spectrophotometer and Qubit (dsDNA BR DNA kit, Thermo-Fisher). Sequencing libraries for the V4 hypervariable 16S ribosomal RNA (rRNA) gene region was generated by PCR amplification with primers EMP-515F (5′-GTGYCAGCMGCCGCGGTAA-3′) and EMP-806R (5′-GGACTACNVGGGTWTCTAAT-3′) to which unique barcodes were added at the 5′-end. PCR-reactions contained 20 ng template DNA in a total volume of 50 µl master mix containing 1X HF buffer (Thermo-Fisher), 1 µl dNTP mix (10 mM, Roche

Diagnostics), both primers (200 nM), 1U Phusion hot-start II high fidelity DNA polymerase (Thermo-Fisher), and 36.5 µl DNAse- and RNAse-free water (Promega). PCR amplifications were performed in triplicate with an initial denaturation step for 30 s at 98°C, followed by 25 cycles of denaturation for 10 s at 98°C, annealing for 10 s at 56°C, elongation for 10 s at 72°C, followed by an extension for 7 min at 72°C. The resulting PCR-amplicon (approx. 290 bp) was verified for purity by gel electrophoresis (1% agarose, 20 min at 100V). The PCR products were then purified with the HighPrep PCR kit (Magbio genomics, USA), and total DNA concentrations were measured on Qubit (dsDNA BR kit, Thermo-Fisher). Libraries were prepared by pooling 200 ng DNA of each sample and concentrated to 20 µl total volume per library. The libraries also contained predetermined MOCK communities of known composition and DNAse- and RNAse-free water controls [27] and sequenced by Illumina Hiseq (Eurofins Genomics, Germany). The resulting reads were then processed as previously described using NGTax 2.0 for data filtering, de-multiplexing, and taxonomic assignment with SILVA v132 (amplicon sequence variants; ASV, [27]).

The biom and tree output files were then processed using R with the phyloseq [28] and microbiome packages [29]. The biom and tree files were merged into a phyloseq object and checked for total sample reads. The phyloseq data file was further processed with and without rarefying the data, and alpha and beta diversities were calculated for each sample and timepoint. Relative and total abundance files were exported and tested for differentially abundant ASV's with Deseq2 [30] using shrinkage estimation for dispersions and fold changes that focus on differential power and standard error rather than only abundance differences. The genus-level data of all timepoints were imported into Canoco (v. 5, [31]) with metadata, and ordination plots were generated with constrained partial redundancy analysis (p-RDA) and unconstrained principal component analysis (PCA) to plot sample- and group-specific variation. Explanatory variable percentages were calculated in constrained analysis with significance at $P < 0.05$ for simple and conditional effects. Composition plots were generated with the microbiome package [29], and the top 10 relative abundance groups were exported for order, family and genus. The relative abundance files were then tested for linear discriminant analysis with LEfSe [32] to determine differentially determining features between control and diarrhea groups with standard settings for alpha (0.05) and LDA threshold (2.0) with all-against-all multi-class analysis strategy. Functional prediction based on the 16S rRNA gene data was performed with Piphillin [33] with standard settings.

Total bacteria estimation and quantification of toxin DNA copy number

Copy numbers for total bacterial 16S rRNA genes (total bacteria) and pathogen-associated toxin encoding genes were measured in the day 4 PW fecal DNA samples. Total bacterial 16S rRNA genes was quantified by synthesizing a 16S rRNA gene fragment with known length as standard (**Supplementary methods**) and qPCR of all samples in quadruplicate with primers FW Bact1369: (5'CGGTGAATACGTTCYCGG 3') and RV Bact1492: (5'GGWTACCTTGTTACGACTT 3'). Total toxin copy numbers were also measured by qPCR using synthesized DNA fragments of genes that code for these specific toxins as standard. Genes encoding toxins of *Escherichia coli* (Heat stable protein a, STa; Heat stable protein b, STb; Heat labile protein, LT), *Salmonella enterica* subs*. enterica serovar Typhymurium* (invasin A, invA), *Campylobacter coli* (Cytolethal distending toxin, CDTcoli), *Campylobacter jejuni* (Cytolethal distending toxin, CDTjej), *Clostridium perfringens* (alpha toxin, αtox), and *Lawsonia intracellularis* (surface antigen A, LsaA) were measured in fecal DNA at day 4 PW using synthesized gene fragments as standards (gBlocks, IDT Technologies) and specific primers (**Supplementary methods**). The gene fragments were designed including flanking regions to ensure sequence-specific primer annealing. All samples were diluted to 1 ng/µl and qPCR was performed on a CFX384 in quadruplicate (Bio-rad). The master mix contained 5 µl SYBR green (SsoAdvanced Universal SYBR Green Supermix, containing dNTPs, Sso7d fusion polymerase, $MgCl_2$, SYBR Green I, and ROX normalization dyes), 0.4 µl primer mix (10 mM), and 2.6 µl RNAse- and DNAse-free water (Promega) per sample. Every reaction was performed using 2 µl template for a total reaction volume of 10 µl. The qPCR consisted of an initial denaturation step at 94°C for 10 min, followed by 34 cycles (20 s 94°C, 30 s 60°c, and 30 s 72°c). Amplicon specificity was checked using a melt curve, from 60-95°C with 0.5°C increments. Copy numbers were quantified using the standard curve in CFXMaestro (Bio-rad). The presence of Rotavirus type A was also assessed using immunochromatography strips (C-1001, Coris BioConcept, Belgium) on all fecal samples at day 4 PW.

Metagenome shotgun sequencing

In total 20 samples were selected for shotgun metagenomic sequencing (Novogene). The samples were selected based on their copy numbers for heat-stable protein a (STa) with five lowest and five highest for both groups stratified over all four farms. The genomic DNA was randomly fragmented using sonication and subsequently end repaired, A-tailed, and ligated with full-length Illumina sequencing index adapters. The samples were then processed for PCR amplification with P5 and indexed P7 oligos, and PCR products were then purified with an AMPure XP system. The libraries

were checked for size distribution by Bioanalyzer (Agilent 2100, Agilent Technologies, USA) and 150 bp paired-end sequenced (Illumina Novaseq 6000). The raw reads (6 Gb per sample) were checked for quality (FastQC, [34]) and trimmed for adapter and porcine genomic reads (sus scrofa 11.1, Ensembl [35]). Trimmed reads were then mapped to a customized reference database from microbial genomes in NCBI for taxonomic profiling and species identification. Antimicrobial resistance gene characterization was performed by mapping the trimmed reads to the Comprehensive Antimicrobial Resistance Database (CARD) [36]. Differential species data between control and diarrhea animals were visualized in a volcano plot with Volcanoser and used for top 10 bacterial species identification with Manhattan distance scores.

Metabolomics

The untargeted metabolomics was performed using Direct-Infusion high resolution Mass Spectrometry (DI-MS). For DI-MS, the feces samples were weighed (500 ± 3 mg) into 50 ml screw-cap tubes (polypropylene, Greiner) supplemented with 1-5 spoons of stainless-steel beads (0.9-2 mm, Next Advance, USA). Acetonitrile (1 ml per 150 mg feces) was added, and the samples were homogenized at 6°C with a Bullet Blender for 6 min (speed 8, model 50-DK, Next Advance). The tubes were subsequently removed and inspected visually for homogenization and re-homogenized if necessary following previous steps. The samples were then centrifuged for 3 min at 1000 *x g* to spin down solid particles (Hettich Rotanta 460R, The Netherlands) at 4°C. In total, 70 µl of extract supernatant was transferred to a 1.5 ml safe-lock tube (Eppendorf) and mixed with 70 µl 4x concentrated NSK AB internal standard solution and 60 µl 0.3% formic acid in double-distilled water. The tubes were then mixed by vortex and pulse centrifugation, and the content was subsequently filtered (0.2 µm). The filtrate was transferred to 96-well plates, sealed to avoid evaporation, and measured using DI-MS on an Advion TriVersa NanoMate (Advion, USA) with 5 µm ID chip-based infusion, and a Q-Exactive Plus MS (Thermo-Fisher, Germany). MS data was acquired in a scan range of 70-600 m/z. The system operated in a 140000-mass resolution in negative and positive ion mode for 1.5 min each at 1.6 kV. High mass accuracy mass calibration was performed before every experiment with internal lock masses. The raw data was subsequently converted into mzXML format with *MSConvert*. The data was filtered as previously described [37] and subjected to untargeted metabolomics analysis using *Metaboshiny* [38, 39].

The sample data was filtered for missing peaks >20% missing in all samples. The data was normalized by quantile adjustment and z-normalized per m/z value. Batch effect was corrected for farm and infusion using *WaveICA* [40], and missing samples

were appended using half-sample minimum with no outlier removal (**Supplementary methods**). The data was then tested for differences using t-tests and fold change (FC) and identified using the KEGG database with predefined adducts (**supplementary methods**). The identified metabolites were then submitted to the KEGG Pathway database for pathway estimation.

The targeted metabolomics was performed with Liquid Chromatography high resolution Mass Spectrometry (LC-MS). Sample derivatization was performed as previously described [41], with minor modifications. The amine- and hydroxyl-containing analytes were analyzed by adding 40 µl supernatant (from previous steps) to a 1.5 ml safe-lock tube (Eppendorf), supplemented with 40 µl internal standard solution (NSK-A in 70% acetonitrile) and 30 µl 250 mM carbonate buffer (pH 9.0). The samples were then mixed by vortex and supplemented with 50 µl fresh dansyl chloride (10 µM in acetonitrile). The samples were vortexed again for 5 s and incubated at 40°C for 45 min under constant agitation. A volume of 10 µl 250 mM sodium hydroxide was added, and the samples were vortexed and incubated at 40°C for an additional 10 min under constant agitation. After incubation, 10 µl 425 mM formic acid (in 50% acetonitrile) was added, vortexed for 5 s, and centrifuged at 17000 *x g* for 10 min at 4°C. A total volume of 80 µl was then transferred to an LC sample vial for further analysis.

Carboxyl-containing analytes were similarly handled as previously described steps, with some distinct differences. 40 µl sample supernatant was transferred to a 1.5 ml tube containing 40 µl internal standard (octanoic acid-D17 in acetonitrile) and 20 µl 500 mM trimethylamine solution in acetonitrile. The derivatization reaction was initiated by addition of 50 µl fresh dimethylaminophenacyl bromide (10 mg/ml in acetonitrile) and vortexed for 5 s. The samples were subsequently incubated at 85°C for 60 min under constant agitation and centrifuged at 17000 *x g* for 10 min at 4°C. A total volume of 80 µl supernatant was then added to LC sample vials for further analysis.

The derivatized analytes were quantified separately against standard solution standards using a Acquity HSS T3 column (2.1x100 mm, 1.8 µm, Waters, The Netherlands) operated with an Ultimate 3000 UHLPC coupled to an Q-Exactive HF (Thermo-Fisher, Germany). The Q-Exactive HF was operated at 120000 mass resolution in positive mode (2.5 kV) with a scan range of 80-1200 with high mass accuracy calibration before each experiment. The instrument settings were further optimized using derivatized glutamate and octanoic acid. The gradient was composed of 5% acetonitrile (containing 0.1% formic acid, eluent A) and acetonitrile (containing 0.1% formic acid, eluent B), starting from 0% with linear increase to 25% (B) in 1.5 min and to 99% (B) in the remaining 10.5 min. Regeneration of the column was performed at 99% (B) for 5 min and returned to 0% (B) in 0.1 min. The column

was then equilibrated at 0% (B) for 8 min prior to the next injection and all samples were stored at 4°C during the analysis. The column operated at 30°C and analysis was initiated upon injection of 5 µl sample. The quantified metabolites were then plotted using Graphpad and tested for group differences using a t-test after normality check.

Results

Samples from the prospective study on PWD were collected at 14 days pre-weaning (Day -14 PW), and 2- or 4-days post-weaning (Day 2 and 4 PW respectively) on four separate farms. It was estimated in a pilot experiment (**Supplementary methods**) that measurements of the protein fermentation marker ammonia (NH_3) varied by up to 2-fold in cases of PWD whereas they were more consistent in control animals without diarrhea. Therefore, on every farm 13 animals with diarrhea and 7 control animals were selected for sampling (total N = 80). The animals with diarrhea at day 4 PW did not differ in fecal consistency at day 2 PW compared to control animals (**Figure 2A**). Fecal samples from diarrheal animals had significantly decreased microbial richness (observed) and diversity (Shannon index) compared to control animals at day 4 PW (**Figure 2B, C**; p = 0.017 and 0.028 respectively). Furthermore, it was previously shown that decreased fecal consistency is related to lower microbial diversity [42]. In our data, fecal freeze dry matter and diversity (Shannon) did correlate significantly (r = 0.223, P = 0.047), but the relation was not as apparent when visualizing this (**Figure 2D**).

We then analyzed the microbial composition (16S rRNA gene, genus level) by sample ordination using constrained analysis (RDA), to elucidate the relation between grouping (control vs. diarrhea) and microbial composition. Grouping significantly contributed to explaining the observed variation in microbial composition at day 4 PW (**Figure 2E**; p=0.002), but not pre- and early post weaning (p=0.15 and 0.56 respectively). Next to the differences in microbial composition between diarrhea and control groups at day 4 PW, there were strong differences observed in microbial composition between pre- and post-weaning microbiomes based on unweighted Unifrac distance (**Supplementary figure 1**), indicating a strong temporal effect. Relative abundances of *Lactobacilliales* decreased post-weaning, whereas relative abundance of *Clostridiales* increased. As the fermentative capacity of these groups is dependent on diet, this is indicative of the shift from a milk diet to solid feed.

To identify bacterial taxa associated with control or diarrhea, partial least squares regression was performed using the 16S rRNA gene compositional data from all timepoints (**Figure 3A**). This showed significant association of *Ruminococcaceae* in animals with diarrhea at day -14 PW, while *Proteobacteria* and *Eubacterium* groups were higher in control animals pre-weaning (p < 0.05). Early post weaning, this

shifted to increased *Ruminococcus* and *Clostridia* in control animals, and increased *Alloprevotella* and *Parabacteroides* in diarrheal animals (**Figure 3A**). The largest differences in microbial composition were observed at day 4 PW, with a distinct increase in protein fermentation-associated groups in diarrhea animals, as *Gammaproteobacteria*, *Campylobacterales*, and *Verrucomicrobia*., most notably including corresponding lower taxa *Enterobacteriaceae*, *Campylobacter,* and *Akkermansiaceae*. On the other hand, groups that increased in control animals were carbohydrate fermentation-associated groups, such as *Ruminococcaceae*, *Christensenellaceae*, and *Clostridiaceae*, as well as the archaeal genus *Methanobrevibacter* (**Figure 3A**).

Temporal delineation of these specific microbial groups showed that pre-weaning *Proteobacteria* abundance was not significantly different (**Figure 3B**), but only increased at day 4 PW. The two main increased bacterial groups affiliated with the *Proteobacteria*, *Campylobacteraceae* and *Enterobacteriaceae,* both showed increased relative abundance in diarrheal animals at day 4 PW (**Figure 3B**; p = and respectively), whereas *Firmicutes*-affiliated *Ruminoccocaceae* were only increased in control animals at 2 days PW. Even though there was a large variation in relative abundance within and between control and diarrheal groups, there was a significant relation between pH levels and the relative abundance of *Proteobacteria* and *Ruminococcaceae* (**Figure 3D**), showing that increased pH was associated with increased Proteobacteria and decreased *Ruminococcaceae*. This alludes to their respective production of acidifying SCFAs or alkalizing protein fermentation metabolites. To further identify specific pathogens associated with both groups, we analyzed toxin-specific gene copy numbers for the cytolethal distending toxin (CDT) in *Campylobacter jejuni* and *C. coli* and the stable toxins STa and STb found in ETEC. We found a significant increase in CDT (**Figure 3E**) and heat-stable Sta and STb in the piglets with diarrhea, although the variation in each group was large indicating a non-exclusive contribution to diarrheal disease.

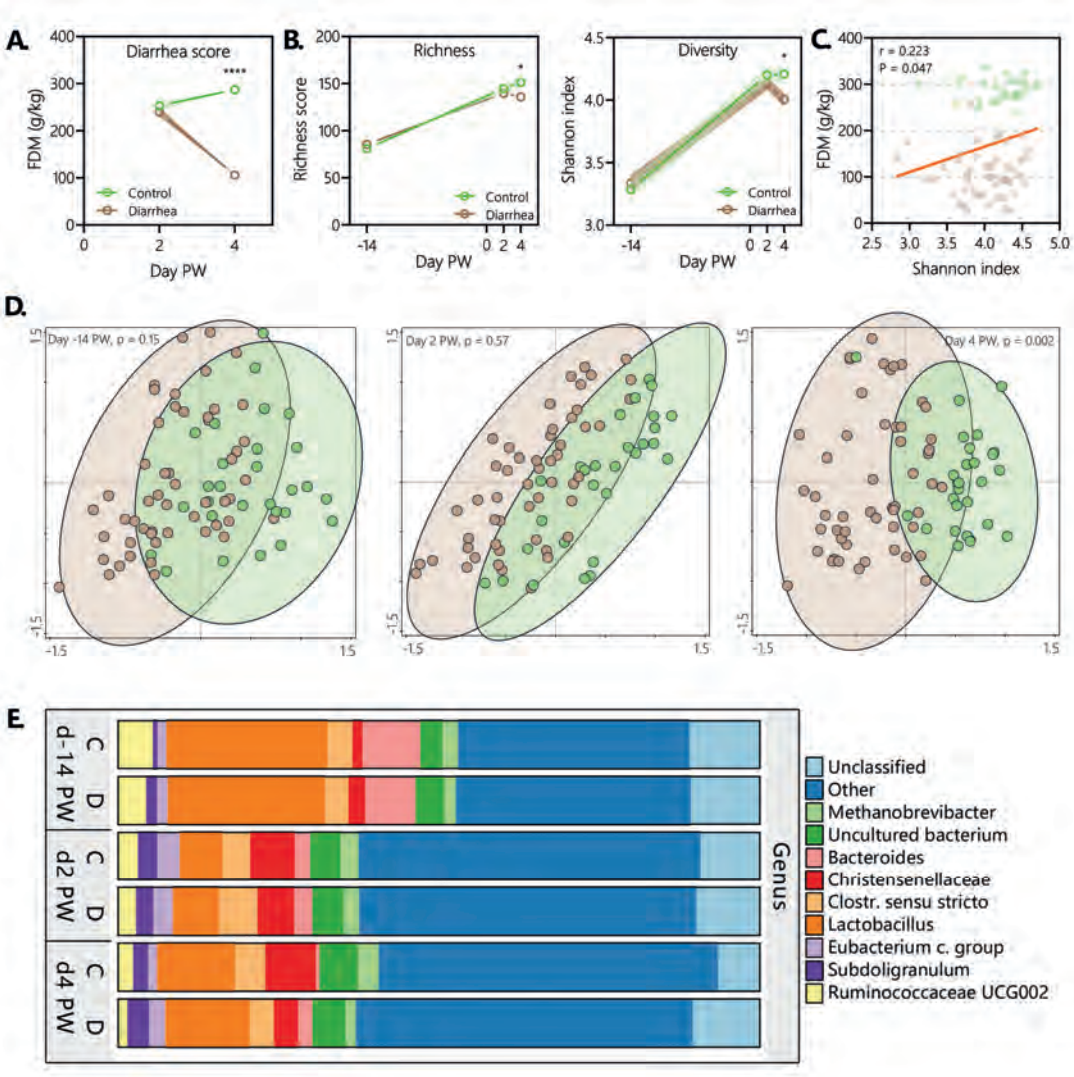

Figure 2. Temporal microbial colonization diversity and taxonomy around weaning. (A) Fecal freeze dry matter (FDM) content at 2- and 4-days post-weaning shows no diarrhea in both groups early post weaning (****; $p<0.001$). (B) Temporal ASV observed richness and alpha diversity (Shannon) of fecal microbiota at three timepoints of control (green) and diarrhea (brown) animals (*; $p<0.05$). (C) Correlation plot of Shannon index and fecal freeze-dry matter (in g/kg), orange line regression (p and r values in plot). (D) Ordination RDA plot of microbiota composition at day -14 PW, day 2 PW, and day 4 PW with grouping as observed at day 4 PW for control and diarrhea as predicted explanatory variables (circle areas indicate 95% confidence interval, and p-values represent RDA model significance and grouping). (E) Relative taxonomic composition of the 10 most abundant genus-level groups between control and diarrhea pre- and postweaning (day -14, 2, and 4).

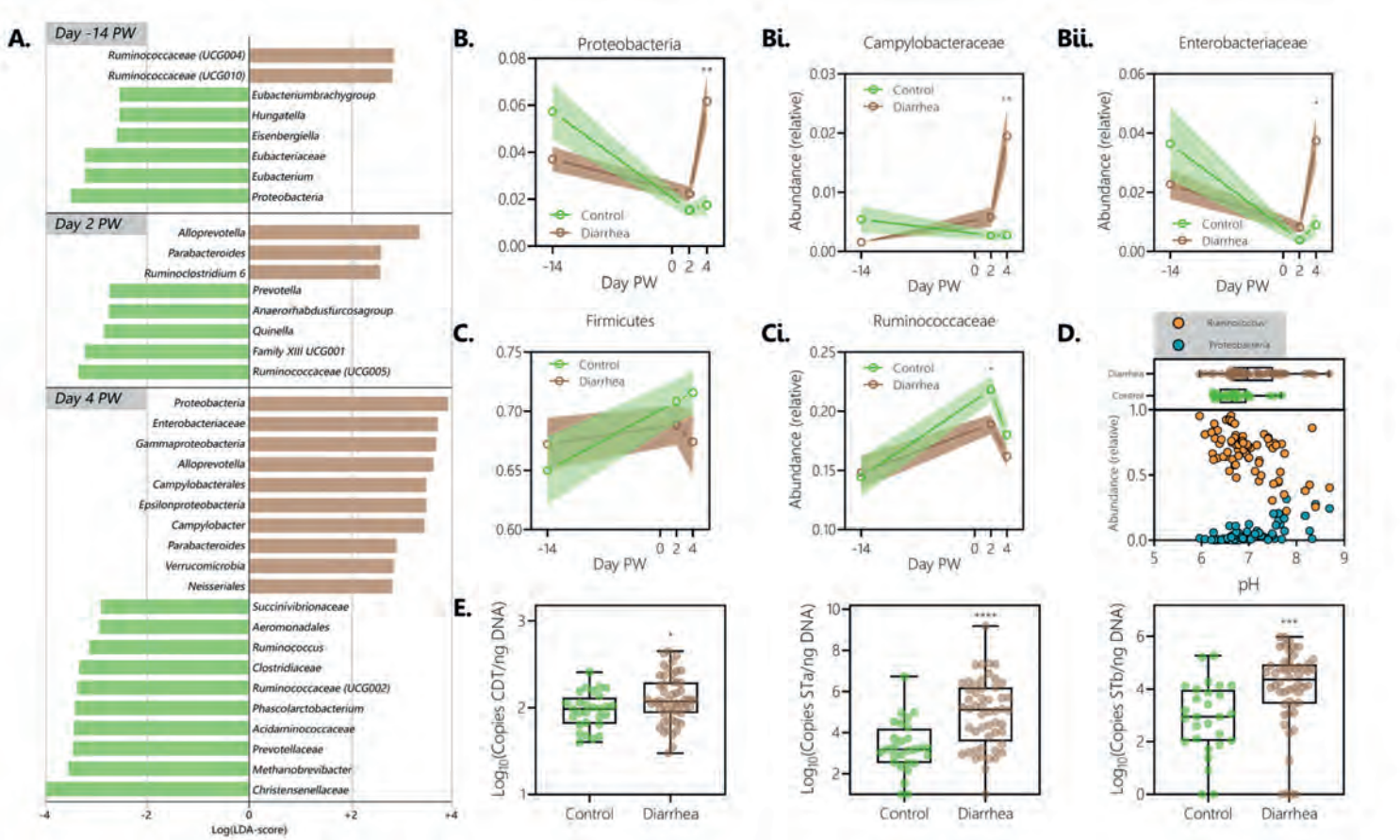

Figure 3. Analysis of microbial composition differences between control and diarrhea animals. (A) LEfsE plot showing the Log_{10} LDA scores for the bacterial groups (features) differentially abundant in control (green) or diarrhea (brown) groups at the different timepoints. (B) Relative abundance of *Proteobacteria* over time and corresponding families (Bi) *Campylobacteraceae* and (Bii) *Enterobacteriaceae*. (C) Relative abundance of phylum *Firmicutes* over time and (Ci) containing family *Ruminococcaceae*. (D) pH levels in fecal material from control or diarrhea piglets at day 4 PW (left), and their correlation to *Ruminoccus* or *Proteobacteria* (right). (E) Gene copy numbers for toxin genes from *Campylobacter coli* Cytolethal distending toxin (CDT) and Enterotoxigenic *Escherichia coli* Heat-stable enterotoxins A (STa) and B (STb). All data is shown as mean ± SEM for temporal relative abundance, or boxplots with 95% CI and all data points (* $p < 0.05$, ** $p < 0.01$, *** $p < 0.001$, **** $p < 0.0001$).

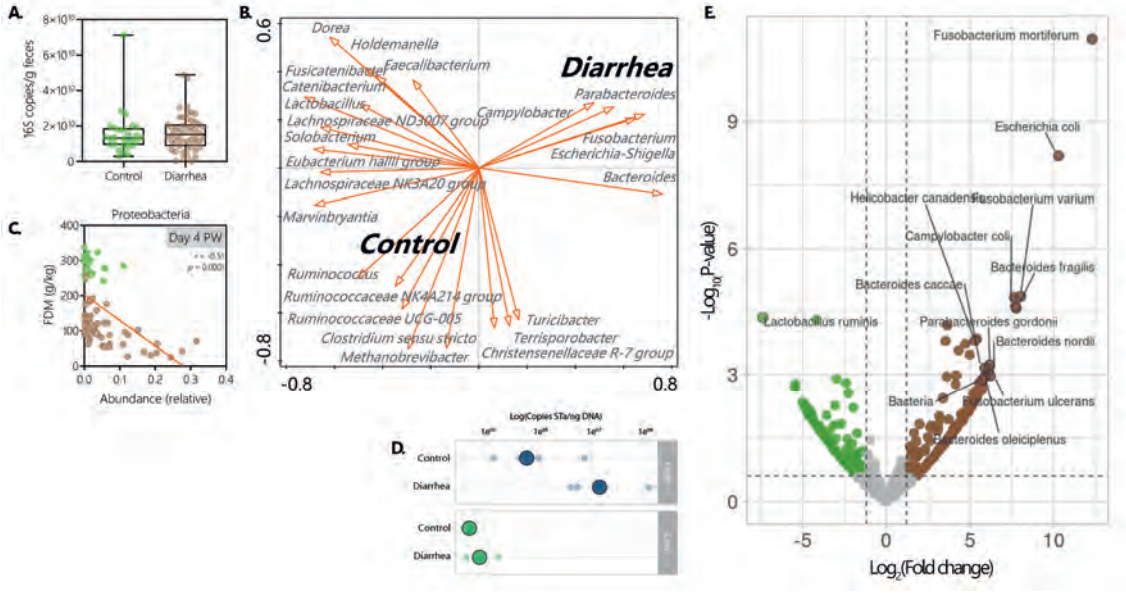

Figure 4. Characterization of contributing species to diarrhea based on 16S rRNA gene composition and metagenomic taxonomy data. (A) 16S rRNA gene copy numbers per gram of feces in control (green) and diarrhea (brown) animals based on wet weight at day 4 PW. PCR. (B) Redundancy analysis (RDA) ordination plot of 16S rRNA gene genus level data showing the relation of bacterial groups to piglet phenotype (control vs. diarrhea; arrows indicate bacterial direction and magnitude). (C) Correlation between relative abundance of *Proteobacteria* and fecal freeze-dry matter content (FDM) at day 4 PW (green indicates individual control animals and brown for diarrhea; orange line indicates regression; p and r values are included in the plot). (D) Sample selection of high and low Sta concentrations for diarrhea or control animals for metagenomic analysis. € Volcano plot of species-level metagenomics data with Log_2(Fold change) and significance threshold (>1.4 is P < 0.05), as well as the top 12 differential bacteria (Manhattan distance).

The number of bacterial 16S rRNA gene copies present in the fecal samples was not different between the control and diarrheal groups (**Figure 4A**), but the more liquid feces and shorter transit times associated with diarrhea suggests that the numbers of intestinal bacteria were in fact greater in diarrheal animals than controls. To further find associations between microbial composition and post-weaning groups, we performed constrained ordination analysis on the 16S rRNA gene compositional data at genus level with diarrhea and control as explanatory variables (RDA; **Figure 4B**). Here, we observed strong correlations with *Fusobacterium*, *Campylobacter*, *Bacteroides*, *Escherichia-Shigella*, and *Parabacteroides* in the diarrheal group. Furthermore, strong correlations with *Ruminococcus*, *Clostridium* sensu stricto, *Christensenellaceae* R7 and the archaeal genus *Methanobrevibacter* were observed in the control group (**Figure 4B**), corroborating the results from the partial least squares regression analysis (**Figure 3A**). Moreover, increased pathogenic load associated with increased toxin-encoding gene copy numbers of *C. coli* and *E. coli* showed large variation between animals in both groups (**Figure 3D**), but the

observed relation between fecal consistency (FDM) and relative abundance of *Proteobacteria* suggested that these bacteria are related to the observed diarrhea (**Figure 4C**). Therefore, to further characterize specific species associated with diarrhea or control, we generated subsets of samples for metagenomic analysis that contained high or low concentrations of STa copies (**Figure 4D**) in animals associated with a control or diarrheal phenotype stratified over all farms. Metagenomic analysis for species identification showed that multiple bacterial species associated with disease were significantly increased in diarrheal animals (**Figure 4E**). Most of these species consisted of expected subspecies of *Escherichia coli* (20k-fold increase in diarrhea), *Campylobacter coli* and *jejuni* (60-fold higher in diarrhea), but also *Bacteroides* spp. (6-fold higher in diarrhea), *Fusobacterium* spp. (40-fold higher in diarrhea), and *Streptococcus suis* (20-fold higher in diarrhea). Notably, the largest strain contributor to increased *E. coli* abundance was attributed to O139:H28, a strain of ETEC capable of small intestinal colonization by CFA pili (CS1 and CS3) adherence and subsequent heat-stable- and labile toxin production (**supplementary figure 9**). RDA analysis of the microbiota compositional data and metagenomic species identification showed a stronger contribution of fusobacterial species to diarrhea, and metagenomic sequence data linked this to *F. mortiferum*, *F. varium* and *F. ulcerans* (**Figure 4D**). Control animal feces contained more carbohydrate fermenting species, as *Lactobacillus ruminis* (1600-fold), *Clostridium* spp. (20-fold), *Treponema succinifaciens* (20-fold), and *Methanobrevibacter ruminantium* (46-fold).

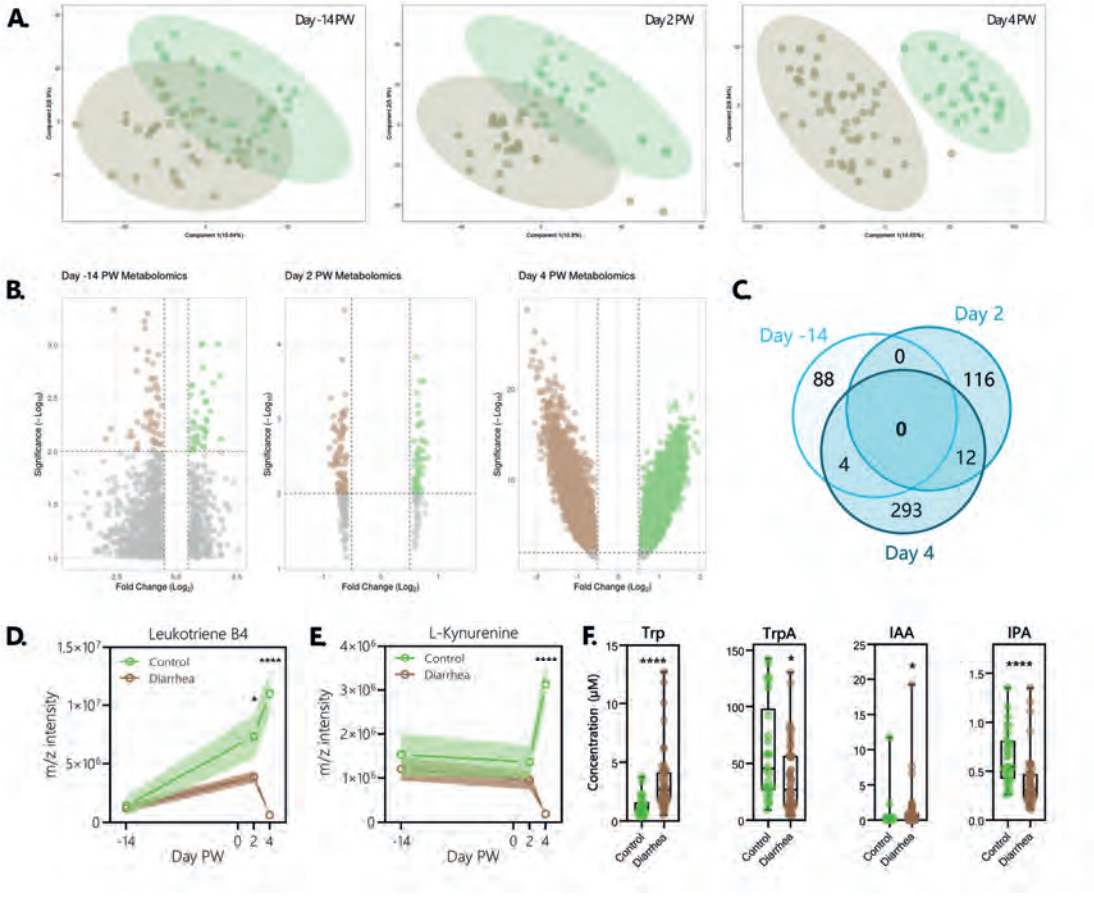

Figure 5. Fecal metabolites after weaning show greatest differences between control and diarrhea with a key role for tryptophan metabolism. (A) Partial least squares discriminant analysis of the untargeted metabolomics data for day -14 (left), day 2 (middle), and day 4 (right) PW for control (green) and diarrhea (brown) identified for day 4 PW (circle shows 95% CI). (B) volcano plots of differentially abundant metabolites (m/z values) selected for significance ($-Log_{10}(2)$) and fold change (FC, $Log_2(0.6)$) in control (green) or diarrhea (brown) piglets at day -14 (left), day 2 (middle), and day 4 (right) PW. (C) Venn diagram indicating overlapping m/z values that were significantly different in diarrhea or control animals from all three timepoints. (D) Cephalosporin C abundance identified by untargeted metabolomics over time (data is shown as mean m/z intensity ± SEM). (E) L-Kynurenine abundance identified by untargeted metabolomics over time between the two groups (mean ± SEM). (F) Fecal concentrations of tryptophan (Trp), tryptamine (TrpA), indoleacetic acid (IAA), and indolepropionic acid (IPA) measured by targeted metabolomics in control or diarrhea animals at day 4 PW (data is shown as boxplots and all data points). Significant differences between the two groups are identified per timepoint (* $p < 0.05$, ** $p < 0.01$, *** $p < 0.001$, **** $p < 0.0001$).

A total of 111,000 different m/z values were identified using direct infusion mass spectrometry (DIMS) in at least >20% of all samples. Significant differences between control and diarrhea were mainly observed at day 4 PW, but smaller differences were also observed at -14 and 2d PW (**Figure 5**). Fecal metabolomes at -14d PW showed no significant difference in their PLS-DA ordination between the two groups (**Figure 5A**) with most of the variance explained in PC1 (13.9%) and PC2 (8.2%). There was also no statistical difference in PLS-DA between control and diarrhea at day 2 PW (PC1: 16.6% and PC2: 10.7%; **Figure 5A**). In contrast, metabolomes of control and diarrheal animals did show a clear separation at day 4 PW (**Figure 5A**), indicating that the largest number of differential metabolites were present during diarrheal onset (PC1: 19.2% and PC2:12.2%; **Figure 5A**).

To decrease the large number of individually varying m/z values, we initially selected all FC data at a stringent significance level (log_2(FC) >2.0) and Manhattan distance scores before metabolite identification mapping. This approach resulted in 92 differential m/z values at -14d PW, 128 at 2d PW, and 309 at 4d PW (**Figure 5B**). Interestingly, we found that most of these highly differential metabolites were not shared among timepoints (**Figure 5C**). We then identified the metabolites corresponding to m/z values using KEGG and mapped for pathways to determine pathway-level effects. We found that all timepoints showed significant associations with secondary metabolite synthesis and metabolic pathways.

Upon analyzing the fecal metabolomes of diarrheal animals, we discovered several metabolites associated with the biosynthesis of antibiotics, with cephalosporin C being the most notably increased compound, which was found to be 2-fold higher before weaning (cephalosporin) (**Figure 5D**). Although these animals had not been treated with antibiotics before or during the experiment, our data suggests the presence of residual environmental compounds possibly resulting from increased bacterial pressure [43]. We also observed increased levels of antibiotic metabolites in diarrheal animals at day 2 and 4 PW, such as gentamicin C1 (1.5-fold at 2d PW) and quinolone antibiotic aurachin A (3-fold at day 4 PW). Furthermore, we found that metabolites from diarrheal animals mapped to multiple pathways associated with antibiotic synthesis, including macrolides, aminoglycoside, and glycopeptide antibiotics.

At day 4 PW in diarrheal animals, a three-fold increase in 6-Aminopenicillinate indicated breakdown of penicillin through penicillin G acylase (*pac*; EC 3.5.1.11 [44]), indicative of increased abundance of semi-synthetic penicillin in piglets with diarrhea. Additionally, we discovered a significantly higher prevalence of antimicrobial resistance (AMR) genes in the metagenomics data collected from piglets diagnosed with diarrhea (see **Supplementary figure 10**). This could be attributed to the fact that the host environment of diarrheal animals favors a

bacterial population carrying more AMR genes or the historic use of antibiotics in their farm practice.

Other key pathways determined from the metabolite composition show a 3-fold increase of indole-3-acetaldehyde (IAA) in diarrheal animals at 4d PW and a 3-fold increase of L-kynurenine in control animals (**Figure 5E**). These results point towards increased tryptophan metabolism in control animals, which we verified by targeted metabolomics for day 2 and 4 PW (**Figure 5F**). We observed increased concentrations of tryptophan in diarrheal animals ($p < 0.0001$), but also lower amounts of tryptamine than in control animals ($p = 0.013$). This might be due to the increased abundance of *Lactobacillus, Ruminococcus* and *Clostridium* in control animals compared to diarrheal animals, all of which contain species converting tryptophan to tryptamine through tryptophan (Trp) decarboxylase [45] (**Figure 5A**). Moreover, an increase in indole-3-propionic acid (IPA) was observed in control animals, which has been linked to increased mucosal homeostasis by decreasing inflammatory signals, e.g. Tumor necrosis factor alpha and increasing expression of tight junction (TJ)-coding proteins [46]. However, indole-3-acetic acid (IAA) was increased in diarrheal animals ($p = 0.022$) compared to control, which might indicate an increase in skatole concentrations [47]. After weaning, metabolite pathways in control animals were associated with elevated hormone secretion, neuronal signaling, and anti-inflammatory effects. For instance, there was pathway-predicted increase in arachidonic acid metabolism, consisting of elevated prostaglandins, leukotriene B4 and 15(S)-HETE. The observed increase in tryptophan metabolism could be linked to multiple of these metabolic pathways associated with hormone signaling in the intestine and signify a key role in mucosal homeostasis [48].

Fecal ammonia (NH_3) is a key metabolic indicator of protein fermentation in the gut, as it is a byproduct of amino acid deamination [49, 50]. We observed a significantly increased concentration of NH_3 in diarrheal animals at day 4 PW ($p < 0.01$), but not on day 2 PW (**Figure 6A**). Moreover, we observed a positive correlation between the relative abundance of *Proteobacteria* and ammonia concentration despite the large variation in ammonia concentration within both groups (**Figure 6B**). Correlating bacterial taxa with metabolites showed that there was a stronger positive correlation between pH and *Enterobacteriaceae* in diarrheal animals than control (**Figure 6C**). However, the relation between protein fermentation metabolites NH_3 and BCFAs was not different between control and diarrhea, indicating a general contribution of Proteobacteria abundance and protein fermentation metabolite concentrations irrespective of disease phenotype. More interestingly, there was a reverse correlation observed for distal colon crypt depth and *Campylobacter* groups (**Figure 6C**). We further observed a negative correlation between *Enterobacteriaceae* and jejunum villous height, indicating a small intestine-related effect of this group.

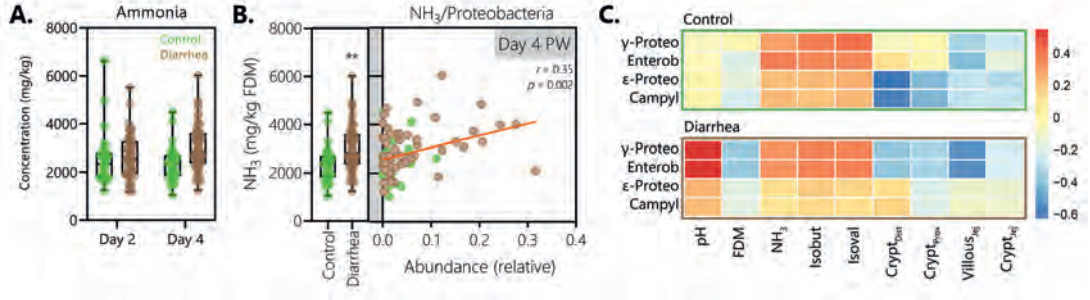

Figure 6. Protein fermentation is linked to relative abundance of proteobacterial groups irrespective of phenotype. (A) Ammonia (NH3) concentration in the fecal material of control (green box) and diarrhea (brown box) piglets at day 2 and 4 PW, (B) and their relation to the relative abundance of *Proteobacteria*. (C) Correlation analysis for bacterial groups and protein fermentation metabolites, fecal dry matter (FDM) or Intestinal morphology is measured as crypt depth of distal (Dist) and proximal (Prox) colon, crypt depth of the jejunum (Jej) and jejunum villous height (Jej). Correlation data of these parameters was performed with gamma (γ) and epsilon (ε) proteobacteria and families *Enterobacteriaceae* and *Campylobacteraceae*.

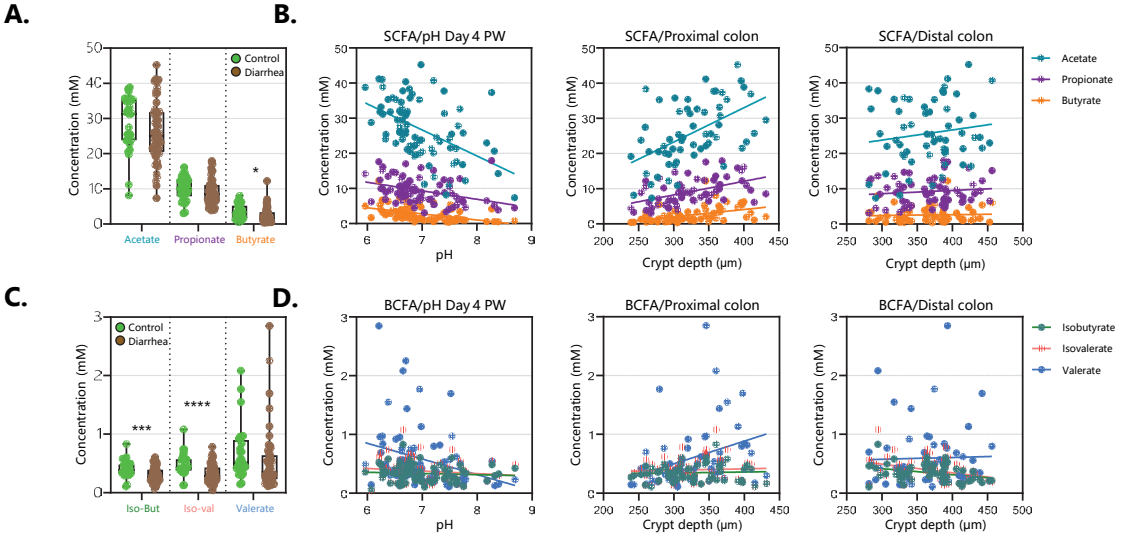

Figure 7. Relationships between microbially produced short-chain- and branched-chain fatty acids and intestinal morphology at day 4 PW. (a) Short-chain fatty acid concentrations in fecal material for control or diarrhea piglets in mM. (b) Correlation analysis between individual SCFA concentrations and pH (left), proximal colon crypt depth (middle), or distal colon crypt depth (right). (c) Branched-chain fatty acid concentration in fecal material for control or diarrhea piglets (Valerate included in graph of BCFA because of concentration range). (d) Correlation analysis with BCFA and pH (left), proximal colon crypt depth (middle), and distal colon crypt depth (right). Data is shown as boxplots with full data points and lines represent linear regression (* $p < 0.05$, *** $p < 0.001$, **** $p < 0.0001$).

Acetate was the most abundant SCFA in the piglet feces at day 4 PW, ranging from 8-39 mM/L (28.5 ± 7.9 mM) in control animals and 7-45 mM/L in diarrheal animals (26 ± 8.6 mM) (**Figure 7A**). Propionate was less abundant in control or diarrhea at 3-13 mM and 4-14 mM respectively. There were no differences observed for acetate or propionate between control and diarrhea animals at day 4 PW ($P = 0.221$ and 0.225 respectively). However, there was a small but significant difference in butyrate concentration between control and diarrhea animals ($p = 0.040$; control 3.5 ± 2.0 and diarrhea 2.5 ± 2.2 mM). The least abundant SCFA was valerate, the concentration of which was not significantly different between control and diarrhea animals (control 0.7 mM ± 0.5 and for diarrhea group 0.5 ± 0.5 mM). Even though most SCFAs were not different between groups there was a negative relation between fecal pH levels and SCFA concentrations (acetate $r = -0.503$, $p < 0.0001$, propionate $r = -0.386$, $p = 0.0004$, butyrate $r = -0.454$, $p < 0.0001$ and valerate $r = -0.301$, $p = 0.007$), which is likely due to the lowering of lumen pH by SCFAs (**Figure 7B**). Butyrate is an inhibitor of stem and progenitor cells, but the mammalian crypt architecture protects stem/progenitor cell proliferation through the transport and metabolism of butyrate by differentiated colonocytes [51]. In the colon we found a positive relationship between all SCFAs and proximal colon crypt depth ($r = 0.518$, 0.494, 0.437, and 0.348 for acetate, propionate, and butyrate respectively).

We found significantly higher fecal BCFA concentrations in control animals ($P < 0.001$) (**Figure 7C**). The observed concentrations were low (isobutyrate ranged from 0.07 to 0.73 mM and isovaleric acid from 0.04-0.95 mM), but they were consistent with previously reported values [52]. In contrast to SCFAs, BCFAs did not correlate to fecal pH, presumably due to their low concentration or alkaline-associated conditions in protein fermentation environments (**Figure 7D**). There was also no correlation of BCFA concentrations with proximal colon crypt depth, but we did find a negative correlation between both BCFAs and distal colon crypt depth (isobutyrate and isovalerate; $r = 0.329$ and 0.345 respectively).

Discussion

Bacterial proteolytic fermentation of undigested proteins has been implicated in post-weaning diarrhea in piglets (reviewed by [17, 22, 53]). Crude protein content in weaner diets has been optimized for lean muscle mass accretion in the fattening stages of growth but the post-weaning dietary shifts, the effectivity of its epithelial transport, and weaning-induced stress could lead to ineffective nutrient digestion and the subsequent production of microbial metabolites that could increase epithelial permeability. The aim of our study was to find associations between protein fermentation and its metabolites with microbiota, intestinal morphology, and PWD under practical conditions.

Intestinal transit time is a key factor in nutrient digestion and water reuptake, and metabolic potential of resident microbiota [42, 54]. Increased flow of undigested nutrients into the colon favors blooming of opportunistic resource utilizers [55] and rapid depletion of highly fermentable energy substrates like carbohydrates (saccharolytic fermentation) and subsequent shifts to generalist bacterial populations able to persist on residual nutrients like protein. It was previously shown that decreased transit time and increased stool consistency links to more diversified microbiota [42, 54], as was also shown in our data. However, the relation between fecal dry matter and diversity indices in our study was not as prominent as previously investigated. This could be attributed to the complexity of post-weaning diarrheal onset and tested timepoints at the point of diarrhea. Possibly, testing for a longer duration after weaning might reveal a more direct relation between these factors. There are contrasting results in literature stating that decreasing CP levels decreased microbial diversity or had no effects [56-58], but no associations were observed between diversity and fecal consistency. In our study, we did see a decrease in microbial diversity and richness in animals with diarrhea but not before the onset of diarrhea, suggesting rapid changes in microbial ecology as result of diarrhea.

Previous studies have established a relation between the incidence of diarrhea and abundance of proteolytic bacterial species such as *E. coli*. The microbial shift we observed at the onset of diarrhea at day 4 PW shows phylogenetically closely related groups, e.g., *Proteobacteria*. This can be attributed to individual species functional diversification of substrate utilization in the colon by increased substrate availability. Proteobacterial groups increased in the diarrheal groups generally consist of multiple protein fermentation-capable species, such as *Escherichia*, *Salmonella*, *Campylobacter*, *Fusobacterium*, and *Helicobacter* [59]. The PWD-associated increase we observed were mainly consisting of gamma- and epsilon-*Proteobacteria*. This shift was not observed at day 2 PW, indicating that there is a rapid onset of possibly pathogenic groups before or during diarrhea. Moreover, we showed an increase in enterotoxins associated with ETEC and *Campylobacter coli* and relative abundance

of these species with metagenomics. These bacteria have been implicated with diarrheal disease post weaning [60] and might play a large contribution to the disease phenotype we observed post-weaning, as well as production of protein fermentation metabolites. For instance, heat-stable protein enterotoxins (STa) of ETEC activates cyclic AMP-dependent protein kinase A that induces chloride (Cl^-) and bicarbonate (HCO_3^-) release into the gut lumen through the cystic fibrosis transmembrane conductance regulator (CFTR) [60]. Moreover, STb induces luminal liquid accumulation by interacting with GTP-binding regulatory protein Gαi and leads to calmodulin-dependent protein kinase II (CaMKII) activation of protein kinase C-induced activation of CFTR [60, 61].

Quantification of pathogen-related toxins, as well as microbial diversity markers and abundance levels, showed large animal-specific variation in our study. Previous studies also showed that incidence of diarrhea was only related to pathogens in 57% of tested piglets [62], and that only 50% of piglets inoculated with ETEC developed diarrhea [63]. However, further individual characterization of diarrhea- and control-associated microbiota at the species level by metagenomic sequencing further revealed other multiple bacterial species that were previously linked to piglet diarrheal disease, like *Fusobacterium mortiferum* [64, 65] and possibly enterotoxigenic strains of *Bacteroides fragilis* [66]. Interestingly, previous reviews have highlighted the interaction between proteobacteria and fusobacteria to cause colorectal disease through inflammatory processes [65]. Fusobacteria are highly acid-tolerant colonizers of the oral microbiota but can co-aggregate with other bacteria in the intestine. They generally increase pH levels through amino acid deamination into ammonia [65] and hydrogen sulfide by degradation of L-cysteine [67], which in turn can increase the opportunity for pathogenic proteobacteria to thrive [68].

We also observed an increased concentration of ammonia in animals with diarrhea, suggesting increased protein fermentation at day 4 PW. This difference was not observed at day 2 PW, indicating no preceding signs with respect to the etiology of diarrhea, similar to the bacterial shifts. Even though the group variation of the NH_3 concentrations was high, they correlated to the relative abundance of *Proteobacteria*, irrespective of the grouping. This indicates that relative *Proteobacteria* abundance plays a large role in fecal ammonia contents. There was, however, a stronger relation between *Proteobacteria* and intestinal pH in the diarrheal group, hinting towards the production of other alkaline compounds next to ammonia in animals with diarrhea. Perhaps this could be attributed to H_2S concentrations produced by *Fusobacterium* species only observed in diarrheal animals, but H_2S concentrations were not measured in this study. pH has previously been suggested as a marker of intestinal wellbeing, as increased pH levels have been shown to increase ETEC proliferation and predispose for PWD [69, 70], but this

observed relation might be a confounding consequence of proteolytic fermentation and simultaneous bacterial blooming as there were no differences observed in pH levels preceding the onset of PWD in our study.

The large inter-individual variation in data is also shown in metabolite composition. Even though 92 differential m/z values were identified pre-weaning, there were only singular pathways identifiable. Interestingly, at all three timepoints we observed pathways associated with antibiotic synthesis and antibiotic compounds. The animals were not treated for the duration of the experiment, but antibiotics like Cephalosporin C are generally used against *E. coli* and *Salmonella* infections [71]. The presence of this compound in our metabolomics data in pre-weaning piglets might indicate a residual effect, as it is not endogenously produced by the microbiota. Metagenome data mapping to the resistance database also indicated increased numbers of antimicrobial resistance genes. This might be related to an increase in multiple resistant bacteria and selective pressure from residual antibacterial drugs [72]. Nevertheless, at day 4 PW the metabolomics data showed the largest number of differentially expressed m/z values, indicative of a large difference in metabolome irrespective of farm. Further characterization of these metabolite differences could signify differentially expressed pathways in the microbiome and could be linked to differences in microbial metabolic functionality.

All timepoints contained differential metabolite pathways for tryptophan metabolism. Tryptophan metabolism, or catabolism by bacteria, produces indole derivatives and is associated with increased fiber fermentation [73, 74]. The higher concentrations of tryptophan in diarrheal animals might indicate less tryptophan catabolism. In line with lower tryptophan concentrations in control animals, there was a higher concentration of tryptamine in control animals, signifying increased tryptophan catabolism. Tryptamine is produced by *Firmicutes* and has strong effects on the microbial composition and host immunity. For instance, tryptamine acts as ligand for the aryl hydrocarbon receptor (AhR) [75, 76], which in turn induces interleukin-22 (IL-22) production by type 3 innate lymphoid cells (ILC3; [77, 78]). IL-22 is implicated in several processes, like epithelial cell proliferation through Notch signaling and upregulation of antimicrobial regulatory peptide Reg3b, a potent inhibitor of *E. coli* [79, 80]. Furthermore, an increase in IPA in control animals further corroborates a link to intestinal homeostasis, as this neuroprotective antioxidant has been shown to facilitate mucosal homeostasis and barrier functioning through the pregnane X receptor (PXR). After PXR binding this subsequently inhibits nuclear factor kappa B (NFkB)- mediated tumor necrosis factor α (TNFα) production [81] and increases mRNA expression of tight junction proteins [82]. Even though there are elevated levels of beneficial tryptophan-derived metabolites in control animals, based on the data presented here we cannot unambiguously conclude that they are protecting from the onset of sudden stress- and weaning-induced diarrhea.

Contrastingly, the increased concentration of IAA in diarrheal animals could also be linked to AhR-receptor activation but has also been implicated in cytotoxicity after oxidative carboxylation by plant peroxidases [83]. Moreover, IAA can be converted to skatole, which is abundant in pig feces[47], and might cause apoptosis of intestinal epithelial cells through p38 MAPK *in vitro* [84], and elevated levels of skatole are linked to increased apoptotic cells *in vivo* [85]. However, the difference between control and diarrhea animals was not as apparent as in IPA and Tryptamine contrasts. Shifts towards sufficient dietary fiber fermentation, as well as increased relative abundance of fiber fermenting bacterial groups in control animals, could underpin this functional microbial significance in post weaning piglet intestinal homeostasis.

Even though there was a higher relative abundance of fiber-fermenting bacterial groups in control animals, we did not observe relevant differences in SCFA levels. SCFAs are produced by anaerobic saccharolytic fermentation from non-digestible polysaccharides and consist of acetate, propionate, butyrate, and valerate [86]. They have been shown to impact host health and disease through metabolism [87], epigenetic modifications [88], immune regulation [89], and intestinal homeostasis [90]. Only butyrate was slightly elevated in control animals, but the objective difference between control and diarrhea might not impose biologically relevant differences. However, it was apparent that the levels of all SCFAs were directly related to the proximal colonic crypt depth. Recently, Kaiko et al (2016) have shown that butyrate, but not acetate or propionate, might induce crypt elongation [51] due to its inhibition of key cell-cycle genes through FoxO3 in crypt-residing stem cells. Interestingly, this relation was not found in the distal colon, possibly attributed to the biological location of SCFA production being more proximal. This hypothesis is corroborated by the relation found between BCFAs isovaleric acid and isobutyric acid with distal colon crypt depth, but not proximal, as fermentation of BCAA is thought to occur more distally.

Piglet PWD is an important contributor to decreased piglet welfare, and understanding its etiology could lead to more sustainable intervention methods. Our study signifies the relationship between PWD and the occurrence of proteolytic bacterial groups, like ETEC, and protein fermentation metabolites. Moreover, the incidence of pathogenic bacteria that produce or associate with protein fermentation metabolites are recurring culprits across all tested farms. The differences in microbial composition and diet utilization could be important factors to study further as key players in the onset of diarrhea on farms. Future research should include the role of stress during the weaning transition, as this could be a driver of microbiota changes and intestinal inflammation [8, 91, 92].

Supplementary Materials

Supplementary methods (Figures)

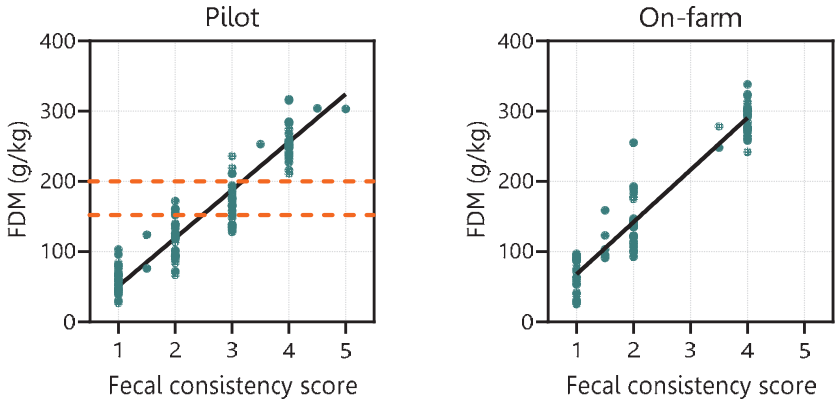

Supplementary methods Figure 1. Fecal scoring relates to freeze-dry matter content. Fecal scores were assigned when sampling during the (A) pilot and (B) on-farm experiments and were correlated to monitor proper phenotype selection.

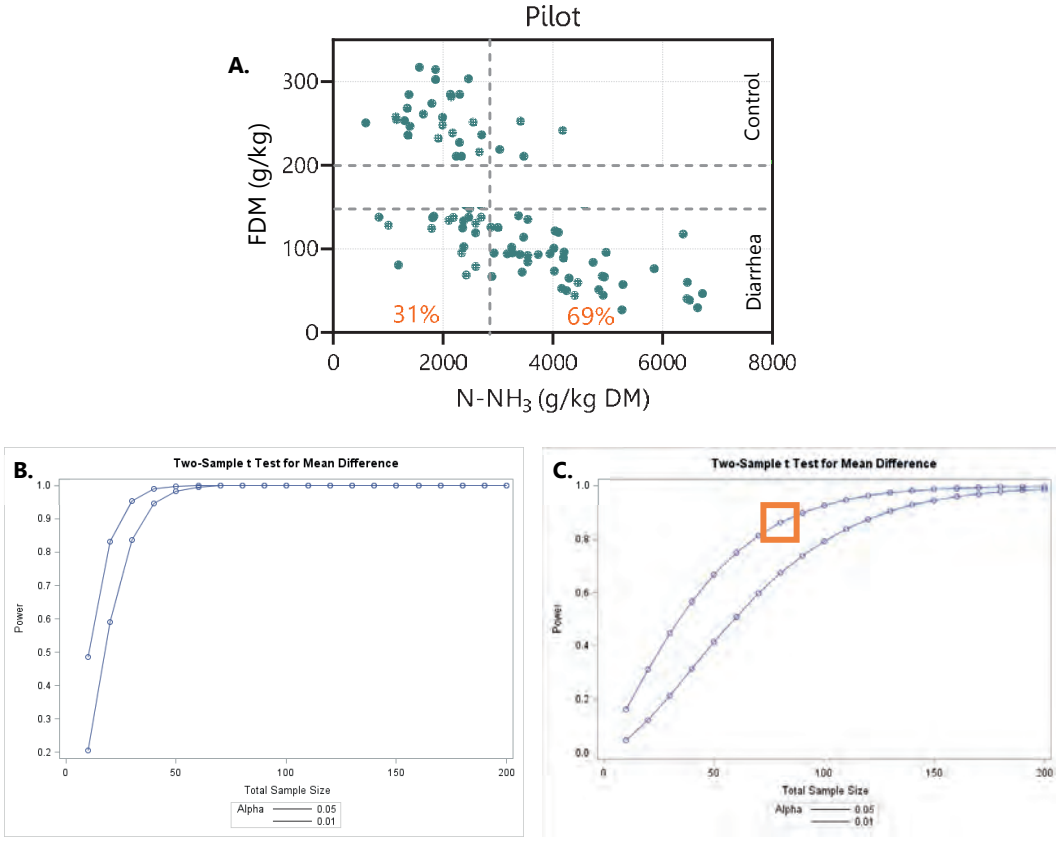

Supplementary methods Figure 2. Sample size estimation from pilot data. (A) The number of animals needed was calculated based on the variation in response variable (N-NH_3) as readout parameter of protein fermentation and its relation to fecal dry matter (FDM). The data was obtained from 9 separate farms (no farm effect observed). The first power analysis (B) was calculated based on the pilot N-NH_3 content in fecal samples (corrected for DM), whereas the (C) power calculation was also adjusted for the increased N-NH_3 variation observed in animals with lower fecal DM (DM < 150 g/kg) compared to control (DM > 200 g/kg) amounting to a mean standard deviation of 2 x pooled st. dev., resulting in an estimated 80 animals, of which 2/3 diarrhea (n = 52) and 1/3 control (n = 28), based on a necessary minimal group size of 8 animals per farm cross referenced to literature [57, 93].

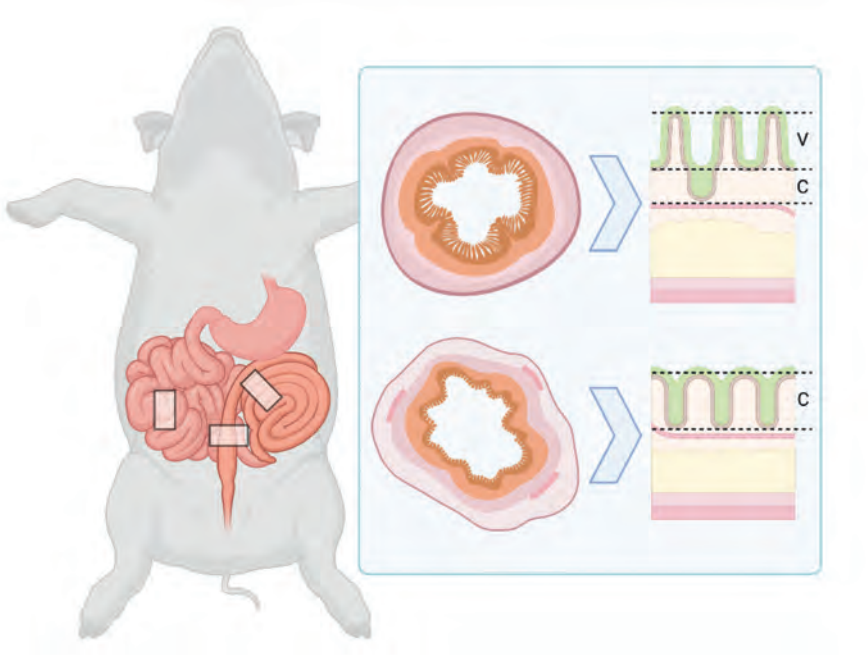

Supplementary methods figure 3. Overview of intestinal tissue selection. Intestinal tissue was obtained from the mid-jejunum and proximal- and distal colon (boxed selections) and cut as rings from two 10 cm-spaced sections. The rings were embedded upright, cut in transverse sections, and both rings adhered to poly-L-lysine slides. The sections were then stained using H & E and imaged as tile scan. The crypts (C) and their corresponding villi (V) were measured using LAS X software for downstream analysis.

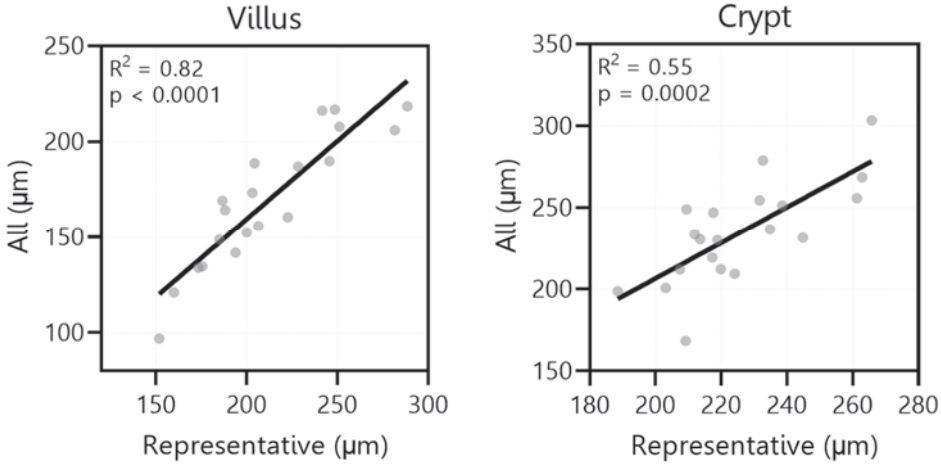

Supplementary methods Figure 4. Intestinal morphological measurements and correlation between methods. Morphological lengths of villi and crypts were measured for all (all) and representative (10 per image, 2 images per animal) to determine if 10 measurements would suffice per image.

Supplementary gene sequences (amplicons) with primer regions and *flanking regions*

Heat-stable protein A (STa)

*TCTGTATTATCTT***TCCCCTCTTTTAGTCAGTCAACTG**AATCACTTGACTCTTCAAAAGAG
AAAATTACATTAGAGACTAAAAAGTGTGATGTTGTAAAAAACAACAGTGAAAAAAAATC
AGAAAATATGAACAACACATTTTACTGCTGTGAACTTTGTTGTAAT**CCTGCCTGTGCTCC
ATGTTA***TTAAAAAGCATAG*

Heat-labile protein (LT)

*TCTCTATGTGCAT***ACGGAGCTCCCCAGTCTATT**ACAGAACTATGTTCGGAATCTCGCAA
CACACAAATATATACGATAAATGACAAGATACTATCATATACGGAATCGATGGCAGGCA
AAAGAGAAATGGTTATCATTA**CATTTAAGAGCGGCGCAACA***TTTCAGGTCGAAG*

Invasin A (invA)

*CCAGCTTTACGGT***TCCTTTGACGGTGCGATGAA**GTTTATCAAAGGTGACGCTATTGCC
GGCATCATTATTATCTTTGTGAACTTTATTGGCGGT**ATTTCGGTGGGGATGACTCG***CCA
TGGTATGGAT*

Lawsonia surface antigen A (LsaA)

*TTGTTTCTCGTGG***TGCTTATAAATTGCTCGCCGC**TATTGAAGCTTTTAAACTAGATTTTG
AAAATAAAGTTATTCTTGAT**ATCGGTGCATCAACAGGTGG***TTTTTCACAAGTT*

Cytolethal distending toxin, C. coli (CDTc)

*TGAAGTTTTTGTT***TTACCCCCTCCAACAGTTGC**TTCAAGACCTATTATAGGCATACGCAT
AGGCAATGATGCTTTTTTCAATATA**CACACTCTAGCAAGTGGGGG***AAATGACGCAGGA*

Cytolethal distending toxin, C. jejunu (CDTj)

*TGCAAGGCTCATC***CGCAGCCACAGAAAGCAAAT**GGAGTGTTAGTGTAAGACAACTTG
TAAGTGGAGCAAACCCCTTAGATATCTTAATGATACAAGAAGCAGGAACTTTACCAA**GA
ACAGCCACTCCAACAGGA***CGCCATGTGCAAC*

Alpha toxin (aTox)

*CATCCTGCTAATG***TTACTGCCGTTGATAGCGCA**GGACATGTTAAGTTTGAGACTTTTGC
AGAGGAAAGAAAAGAACAGTATAAAATAA**ACACAGCAGGTTGCAAAACT***AATGAGG
CTTTTT*

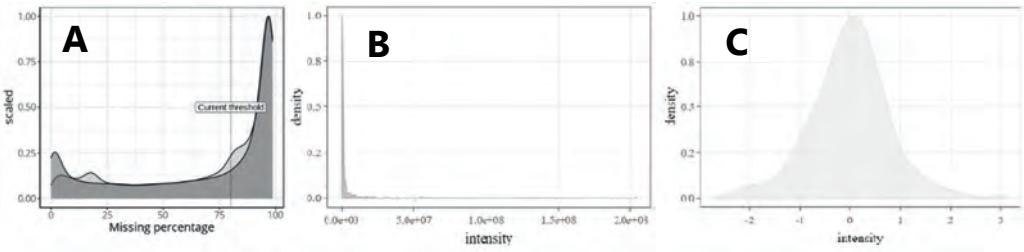

Supplementary methods Figure 5. Untargeted metabolomics data normalisation. Data was filtered for samples containing more than 20% missing peaks (A), and subjected to normalization (B) from old sample distribution to (C) Z-score normalized data.

Supplementary methods table 1. Adduct list used for the m/z compounds estimation.

Name	Ion mode	Charge	xM	AddAdd	RemAdd	AddEx	RemEx	Nelec	Rule
[M+3Na]3+	positive	3	1			Na3		-3	Nacc>2 AND Nch=0
[M+H+2Na]3+	positive	3	1			Na2H1		-3	Nacc>2 AND Nch=0
[M+2H+Na]3+	positive	3	1			Na1H2		-3	Nacc>2 AND Nch=0
[M+3H]3+	positive	3	1			H3		-3	Nacc>2 AND Nch=0
[2M+3H2O+2H]2+	positive	2	2			H8O3		-2	Nacc>1 AND Nch=0
[M+3ACN+2H]2+	positive	2	1			C6H11N3		-2	Nacc>1 AND Nch=0
[M+2ACN+2H]2+	positive	2	1			C4H8N2		-2	Nacc>1 AND Nch=0
[M+2Na]2+	positive	2	1			Na2		-2	Nacc>1 AND Nch=0
[M+CAN+2H]2+	positive	2	1			C2H5N1		-2	Nacc>1 AND Nch=0
[M+H+K]2+	positive	2	1			K1H1		-2	Nacc>1 AND Nch=0
[M+H+Na]2+	positive	2	1			Na1H1		-2	Nacc>1 AND Nch=0
[M+H+NH4]2+	positive	2	1			N1H5		-2	Nacc>1 AND Nch=0
[M+2H]2+	positive	2	1			H2		-2	Nacc>1 AND Nch=0
[M+2H-H2O-NH3]2+	positive	2	1		N1H2		O1H1	-2	Nnhh>0 AND Noh>0 AND Nch=0

[2M+CAN+Na]1+	positive	1	2		C2H3Na1N1		-1	Nacc>0 AND Nch=0
[2M+CAN+H]1+	positive	1	2		C2H4N1		-1	Nacc>0 AND Nch=0
[2M+K]1+	positive	1	2		K1		-1	Nacc>0 AND Nch=0
[2M+Na]1+	positive	1	2		Na1		-1	Nacc>0 AND Nch=0
[2M+NH4]1+	positive	1	2		N1H4		-1	Nacc>0 AND Nch=0
[2M+H]1+	positive	1	2		H1		-1	Nacc>0 AND Nch=0
[M+IsoProp+Na+H]1+	positive	1	1		C3H9O1Na1		-1	Nacc>0 AND Nch=0
[M+2ACN+H]1+	positive	1	1		C4H7N2		-1	Nacc>0 AND Nch=0
[M+DMSO+H]1+	positive	1	1		C2H6OS1		-1	Nacc>0 AND Nch=0
[M+2K-H]1+	positive	1	1		K2	H1	-1	Ndon>0 AND Nch=0
[M+CAN+Na]1+	positive	1	1		C2H3Na1N1		-1	Nacc>0 AND Nch=0
[M+IsoProp+H]1+	positive	1	1		C3H9O1		-1	Nacc>0 AND Nch=0
[M+2Na-H]1+	positive	1	1		Na2	H1	-1	Ndon>0 AND Nch=0
[M+CAN+H]1+	positive	1	1		C2H4N1		-1	Nacc>0 AND Nch=0
[M+K]1+	positive	1	1		K1		-1	Nacc>0 AND Nch=0
[M+H+CH3OH]1+	positive	1	1		C1H5O1		-1	Ndon>0 AND Nch=0
[M+Na]1+	positive	1	1		Na1		-1	Nacc>0 AND Nch=0
[M+NH4]1+	positive	1	1		N1H4		-1	Nacc>0 AND Nch=0
[M+H]1+	positive	1	1		H1		-1	Nacc>0 AND Nch=0
[M1+.]1+	positive	1	1				0	Nch=1
[M+H-NH3]1+	positive	1	1	N1H2			-1	Nnhh>0 AND Nch=0
[M+H-H2O]1+	positive	1	1	O1H1			-1	Noh>0 AND Nch=0
[M+H-FA]1+	positive	1	1	C1H1O2			-1	Ncooh>0

							AND Nch=0
[M+GLUC+H]1+	positive	1	1	C6H10O6	H1	-1	Ngluc>0 AND Nch=0
[3M-H]1-	negative	-1	3		H1	1	Ndon>0 AND Nch=0
[2M+Hac-H]1-	negative	-1	2	C2H3O2		1	Ndon>0 AND Nch=0
[2M+FA-H]1-	negative	-1	2	C1H1O2		1	Ndon>0 AND Nch=0
[2M+Na-2H]1-	negative	-1	2	Na1	H2	1	Ndon>1 AND Nacc>0 AND Nch=0
[2M-H]1-	negative	-1	2		H1	1	Ndon>0 AND Nch=0
[M+TFA-H]1-	negative	-1	1	C2O2F3		1	Ndon>0 AND Nch=0
[M+Br]1-	negative	-1	1	Br1		1	Nacc>0 AND Nch=0
[M+Hac-H]1-	negative	-1	1	C2H3O2		1	Ndon>0 AND Nch=0
[M+FA-H]1-	negative	-1	1	C1H1O2		1	Ndon>0 AND Nch=0
[M+K-2H]1-	negative	-1	1	K1	H2	1	Ndon>1 AND Nacc>0 AND Nch=0
[M+Cl]1-	negative	-1	1	Cl1		1	Nacc>0 AND Nch=0
[M+Na-2H]1-	negative	-1	1	Na1	H2	1	Ndon>1 AND Nacc>0 AND Nch=0
[M1-.]1-	negative	-1	1			0	Nch=-1
[M-H]1-	negative	-1	1		H1	1	Ndon>0 AND Nch=0
[M-2H]2-	negative	-2	1		H2	2	Ndon>1 AND Nch=0
[M-3H]3-	negative	-3	1		H3	3	Ndon>2 AND Nch=0
[M-H+GLUC]1-	negative	-1	1	C6H9O6	H2	1	Ngluc>0 AND Nch=0
[M+2K-D]1+	positive	1	1	K2	D1	-1	Ndon>0 AND Nch=0
[M+2Na-D]1+	positive	1	1	Na2	H1	-1	Ndon>0 AND Nch=0

[M+H-D2O]1+	positive	1	1	H1	O1D2			-1	Noh>0 AND Nch=0
[M+H-HDO]1+	positive	1	1	H1	O1D1H1			-1	Noh>0 AND Nch=0
[M+H-FA(D)]1+	positive	1	1		C1D1O2			-1	Ncooh>0 AND Nch=0
[3M-D]1-	negative	-1	3				D1	1	Ndon>0 AND Nch=0
[2M+Na-2D]1-	negative	-1	2			Na1	D2	1	Ndon>1 AND Nacc>0 AND Nch=0
[2M-D]1-	negative	-1	2				D1	1	Ndon>0 AND Nch=0
[M+K-2D]1-	negative	-1	1			K1	D2	1	Ndon>1 AND Nacc>0 AND Nch=0
[M+Na-2D]1-	negative	-1	1			Na1	D2	1	Ndon>1 AND Nacc>0 AND Nch=0
[M-D]1-	negative	-1	1				D1	1	Ndon>0 AND Nch=0
[M-2D]2-	negative	-2	1				D2	2	Ndon>1 AND Nch=0
[M-3D]3-	negative	-3	1				D3	3	Ndon>2 AND Nch=0
[M-H-H2O]1-	negative	-1	1		O1H2			1	Ndon>0 AND Nch=0 AND Noh>0

Supplementary figures

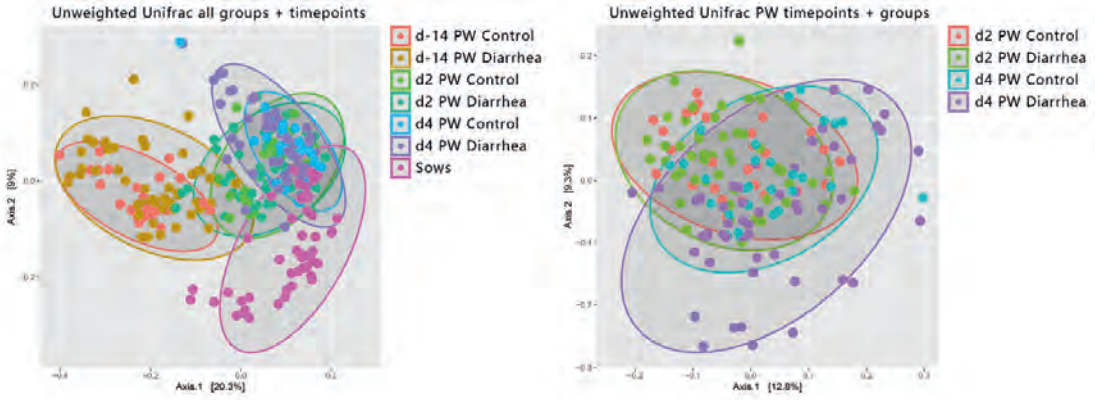

Supplementary figure 1. Unweighted Unifrac distances of genus-level microbial composition from all timepoints.

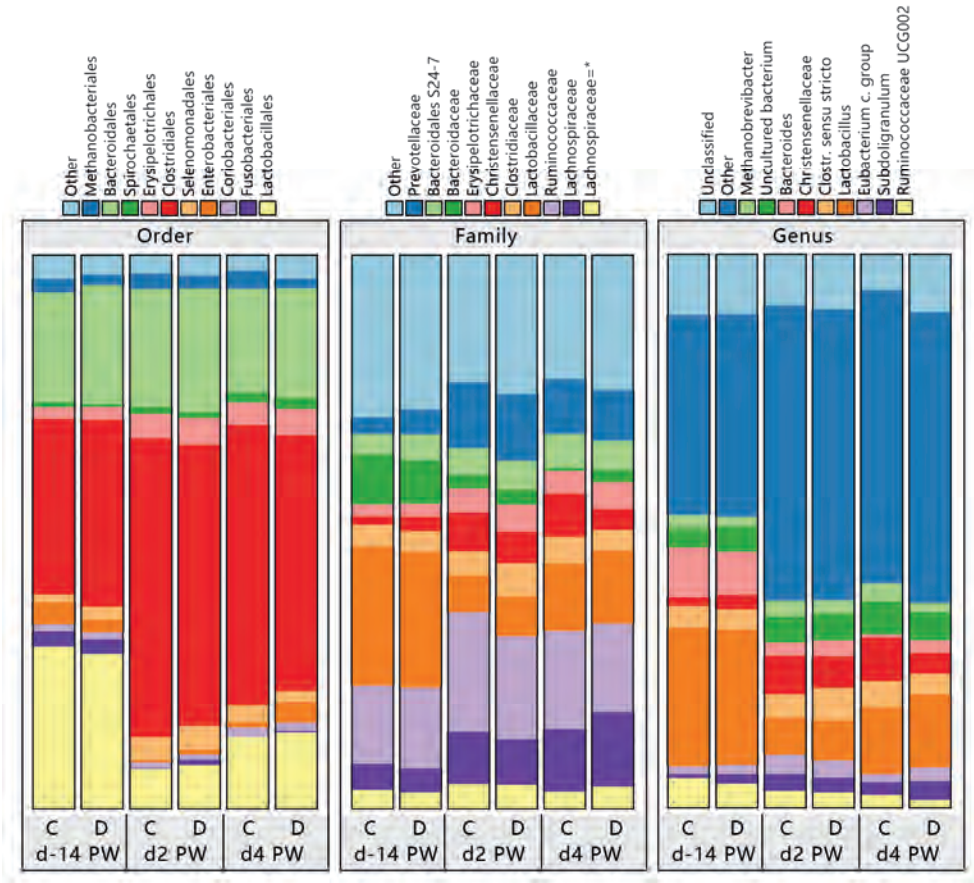

Supplementary figure 2. Taxonomic composition of the fecal microbiota for all timepoints and control or diarrhea at Order (left), Family (middle), and Genus (right) level (C: control, D: diarrhea, PW: Post weaning). Data is shown as relative abundance and top 10 most abundant per category.

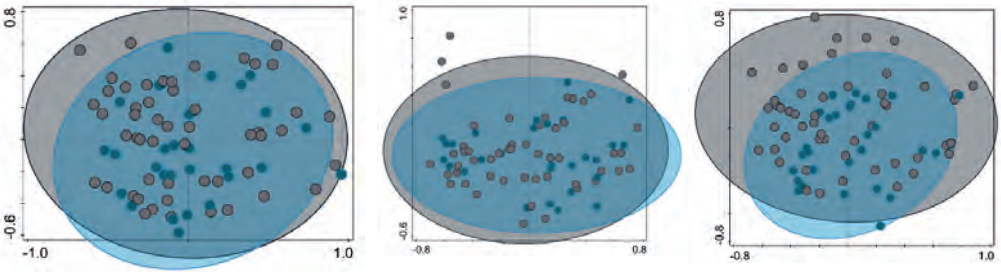

Supplementary figure 3. Principal coordinate (unconstrained PCA) plots for microbial composition at genus level for all animals identified as control (blue) or diarrhea (grey) at day 4 PW (left day -14, middle day 2, and right day 4 PW).

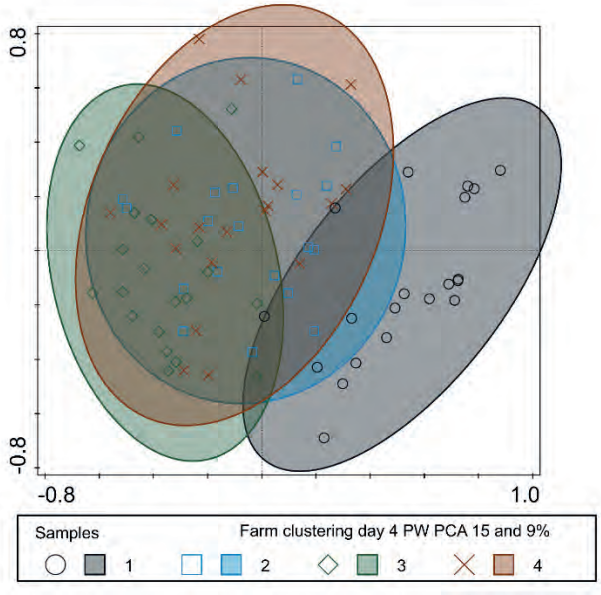

Supplementary figure 4. Principal component analysis on microbial composition for day 4 PW stratified per farm shows separation of farm 1.

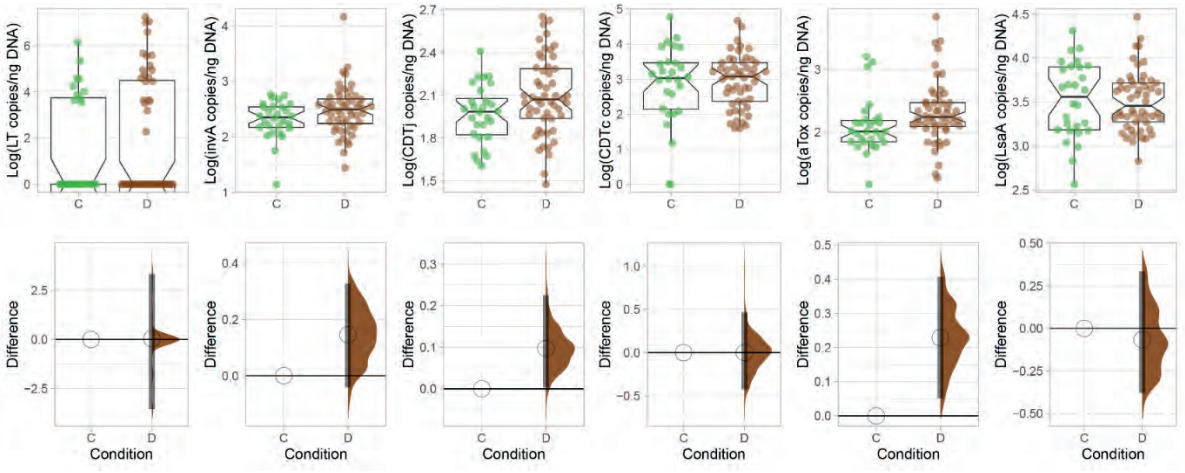

Supplementary Figure 5. Gene copy numbers for analyzed toxins in feces from day 4 PW. Total measured gene copy numbers for Labile toxin (LT), invasin A (invA), Cytolethal distending toxin (C. jejuni, CDTjej), Cytolethal distending toxin (*C. coli*, CDTc), alpha toxin (aTox), and *Lawsonia* surface antigen A (LssA), and their corresponding difference distribution plots with control as 0.0 reference.

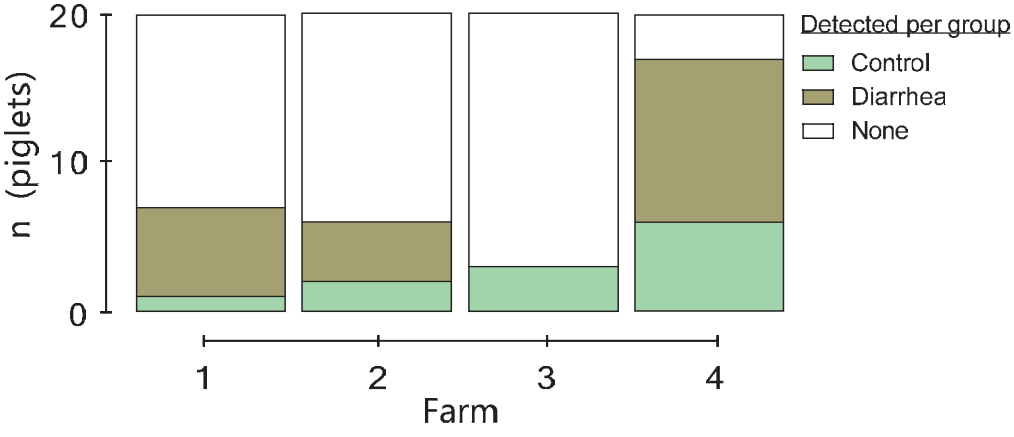

Supplementary figure 6. Rotavirus presence and association with control (green) or diarrhea (brown) per farm.

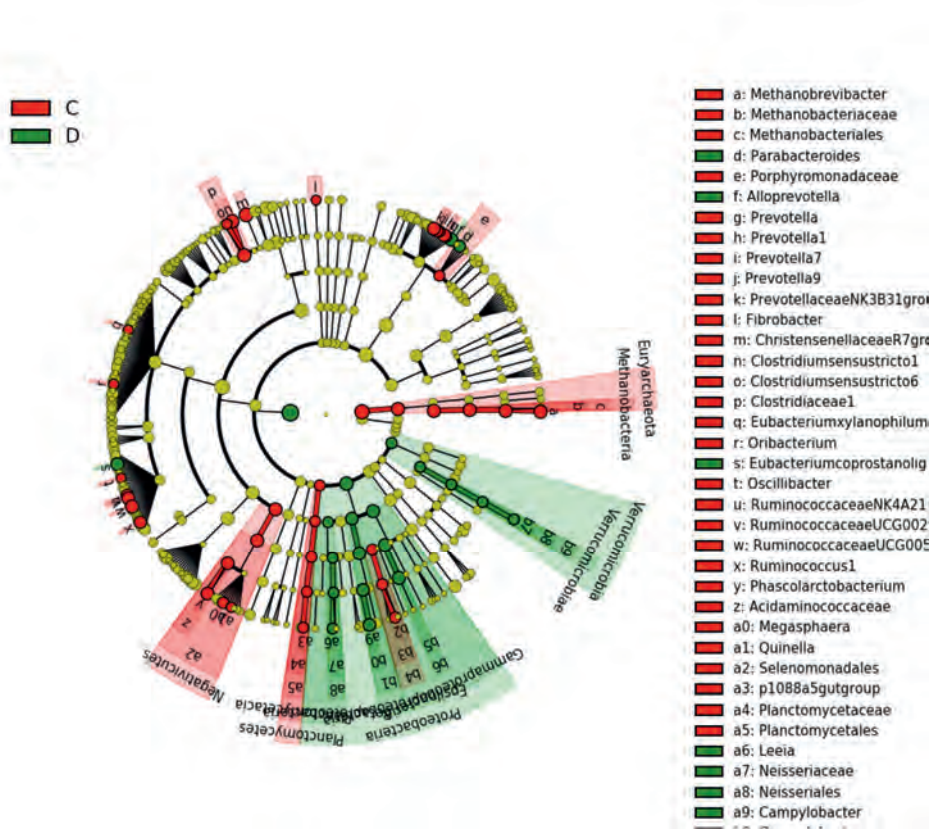

Supplementary figure 7. Lefse cladogram showing phylogenetic changes between control and diarrhea animals at day 4 PW.

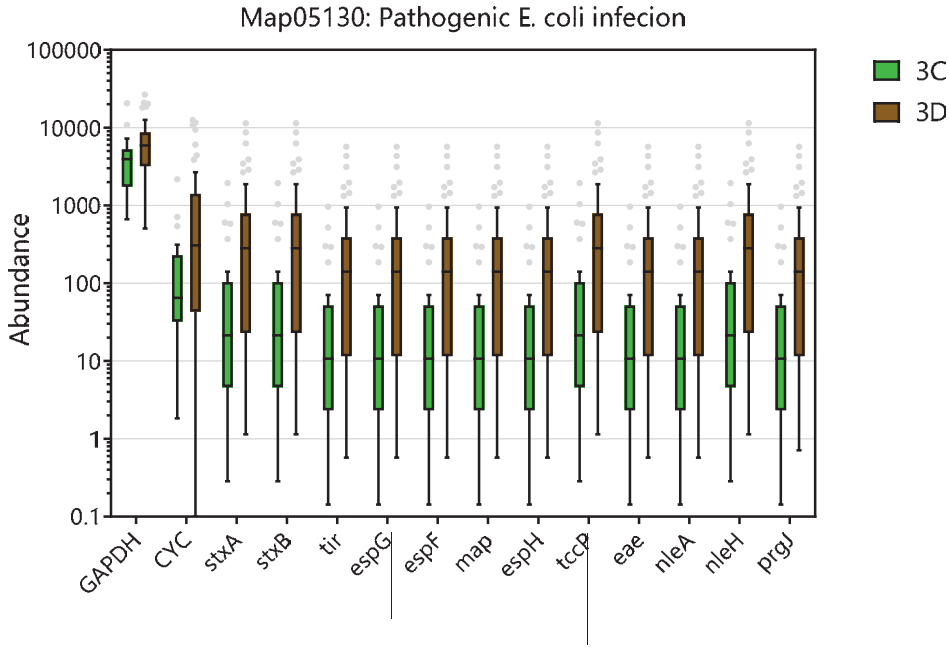

Supplementary figure 8. Predicted *Escherichia coli* infection pathway by Piphillin from 16S SSU rRNA data. The 16S data was submitted to Piphillin and normalized for copy numbers and mapped to known KEGG pathway identifiers. One pathway significantly increased was Map05130 (Pathogenic *E. coli* infection) with multiple pathogenic virulence factors increased in diarrhea.

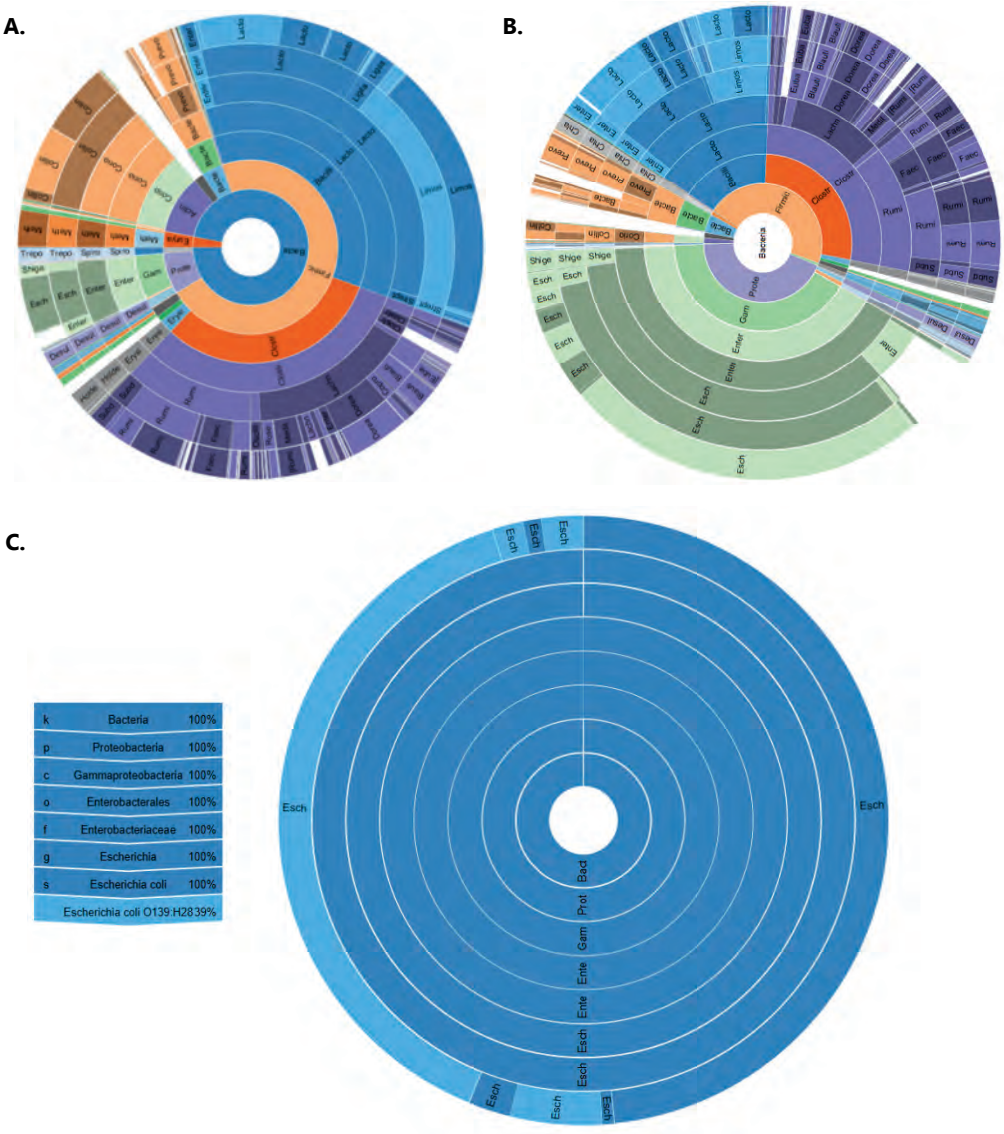

Supplementary figure 9. Leaf plots of relative bacterial taxonomy. (a) Composition of the microbiota for control (top) or diarrheal (bottom) animals as identified through metagenome sequencing. (b) *Escherichia coli* species contribution in diarrheal animals shows a large amount of E. coli)139:H28.

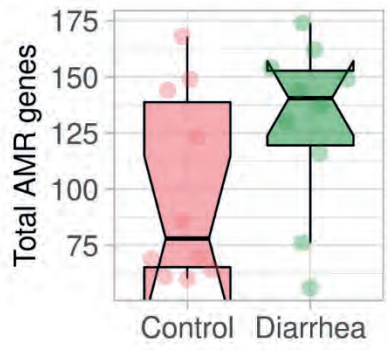

Supplementary figure 10. Total antimicrobial resistance (AMR) genes are present in the selected metagenome samples for control and diarrhea animals.

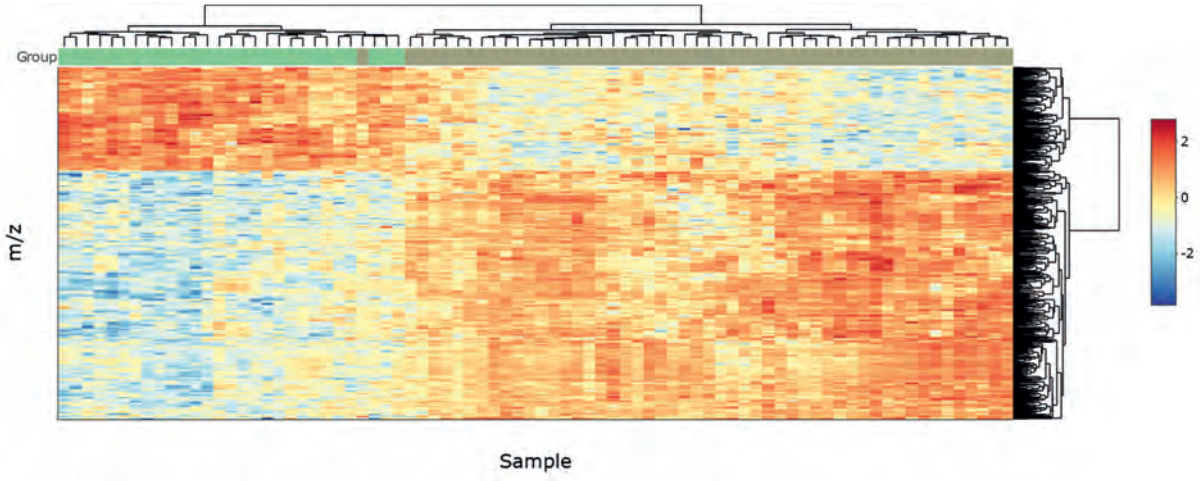

Supplementary figure 11. Top 100 differentially abundant m/z values.

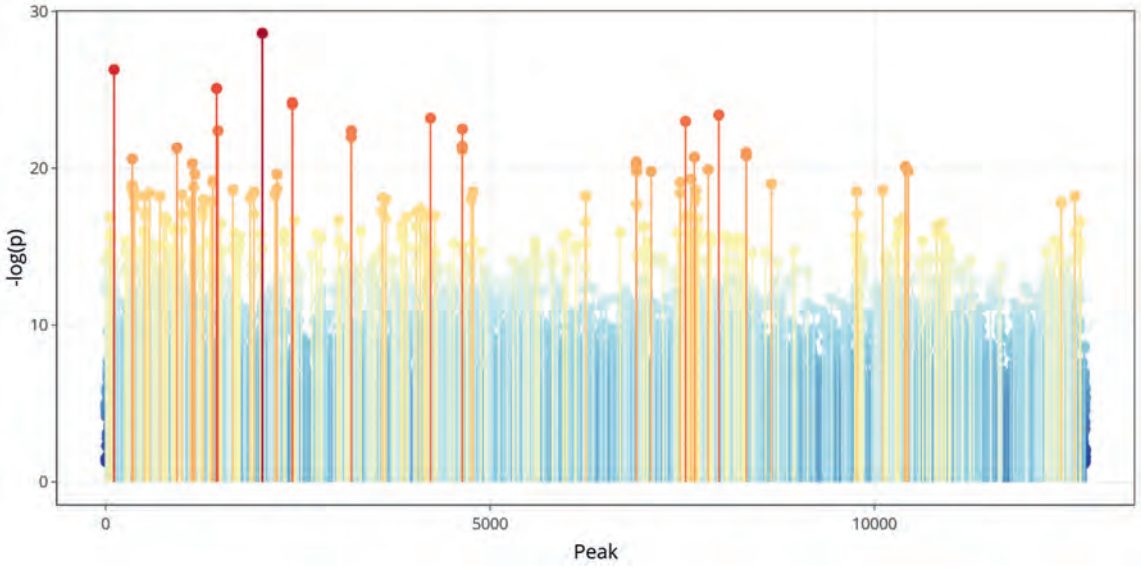

Supplementary figure 12. T-test plot of differentially abundant m/z values between control and diarrhea piglets at day 4 PW.

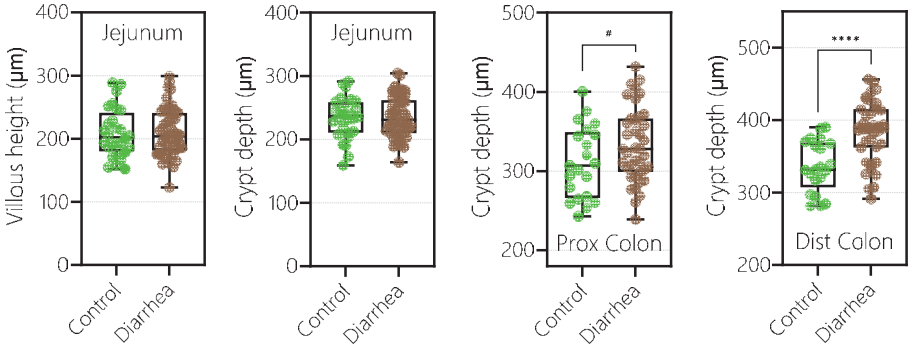

Supplementary figure 13. Morphological measurements of crypt and villi in jejunum and crypt between control and diarrhea animals at day 5 (dissection). The crypt and villi were measured as previously described and tested for group differences using a t-test after normality testing. * $p < 0.05$, **** $p < 0.0001$

References

1. Li, Y., et al., *Weaning Stress Perturbs Gut Microbiome and Its Metabolic Profile in Piglets.* Sci Rep, 2018. **8**(1): p. 18068.
2. Hu, C.H., et al., *Early weaning increases intestinal permeability, alters expression of cytokine and tight junction proteins, and activates mitogen-activated protein kinases in pigs.* J Anim Sci, 2013. **91**(3): p. 1094-101.
3. Boudry, G., et al., *Weaning induces both transient and long-lasting modifications of absorptive, secretory, and barrier properties of piglet intestine.* J Nutr, 2004. **134**(9): p. 2256-62.
4. Soderholm, J.D. and M.H. Perdue, *Stress and gastrointestinal tract. II. Stress and intestinal barrier function.* Am J Physiol Gastrointest Liver Physiol, 2001. **280**(1): p. G7-G13.
5. Moeser, A.J., et al., *Gastrointestinal dysfunction induced by early weaning is attenuated by delayed weaning and mast cell blockade in pigs.* Am J Physiol Gastrointest Liver Physiol, 2007. **293**(2): p. G413-21.
6. Spencer, B.T. and P.G. Howell, *Some Husbandry Factors Influencing Weaning Stresses in Piglets.* Journal of the South African Veterinary Association-Tydskrif Van Die Suid-Afrikaanse Veterinere Vereniging, 1989. **60**(1): p. 62-64.
7. Madec, F., et al., *Measurement of digestive disorders in the piglet at weaning and related risk factors.* Prev Vet Med, 1998. **35**(1): p. 53-72.
8. Moeser, A.J., C.S. Pohl, and M. Rajput, *Weaning stress and gastrointestinal barrier development: Implications for lifelong gut health in pigs.* Anim Nutr, 2017. **3**(4): p. 313-321.
9. van Beers-Schreurs, H.M.G. and E. Bruininx, *Nutritional management to prevent disorders in post-weaning pig health.* Nutrition and health of the gastrointestinal tract, 2002. **1**.
10. Rhouma, M., et al., *Post weaning diarrhea in pigs: risk factors and non-colistin-based control strategies.* Acta Vet Scand, 2017. **59**(1): p. 31.
11. Pluske, J.R., D.L. Turpin, and J.C. Kim, *Gastrointestinal tract (gut) health in the young pig.* Anim Nutr, 2018. **4**(2): p. 187-196.
12. Choudhury, R., et al., *Impact of early-life feeding on local intestinal microbiota and digestive system development in piglets.* Sci Rep, 2021. **11**(1): p. 4213.
13. Lv, Z., et al., *Effects of Dietary Fiber Type on Growth Performance, Serum Parameters and Fecal Microbiota Composition in Weaned and Growing-Finishing Pigs.* Animals (Basel), 2022. **12**(12).
14. Vangroenweghe, F., *Improved Piglet Performance and Reduced Mortality and Antimicrobial use Following Oral Vaccination with a Live Non-Pathogenic Escherichia coli F4/F18 Vaccine Against Post-Weaning Diarrhoea.* Austin J of Infectious Diseases, 2021. **8**(Special article - Diarrhea).
15. Heo, J.M., et al., *A between-experiment analysis of relationships linking dietary protein intake and post-weaning diarrhea in weanling pigs under conditions of experimental infection with an enterotoxigenic strain of Escherichia coli.* Anim Sci J, 2015. **86**(3): p. 286-93.
16. Heo, J.M., et al., *Effects of feeding low protein diets to piglets on plasma urea nitrogen, faecal ammonia nitrogen, the incidence of diarrhoea and performance after weaning.* Arch Anim Nutr, 2008. **62**(5): p. 343-58.
17. Pieper, R., et al., *Health relevance of intestinal protein fermentation in young pigs.* Anim Health Res Rev, 2016. **17**(2): p. 137-147.
18. Moore, J.W., et al., *Hydrogen sulphide produces diminished fatty acid oxidation in the rat colon in vivo: implications for ulcerative colitis.* Aust N Z J Surg, 1997. **67**(5): p. 245-9.
19. Villodre Tudela, C., et al., *Down-regulation of monocarboxylate transporter 1 (MCT1) gene expression in the colon of piglets is linked to bacterial protein fermentation and pro-inflammatory cytokine-mediated signalling.* Br J Nutr, 2015. **113**(4): p. 610-7.
20. JanssenDuijghuijsen, L.M., et al., *Mitochondrial ATP Depletion Disrupts Caco-2 Monolayer Integrity and Internalizes Claudin 7.* Front Physiol, 2017. **8**: p. 794.
21. Zhang, H., et al., *Impact of Fermentable Protein, by Feeding High Protein Diets, on Microbial Composition, Microbial Catabolic Activity, Gut Health and beyond in Pigs.* Microorganisms, 2020. **8**(11).
22. Gilbert, M.S., et al., *Protein fermentation in the gut; implications for intestinal dysfunction in humans, pigs, and poultry.* Am J Physiol Gastrointest Liver Physiol, 2018. **315**(2): p. G159-G170.
23. ISO, *6496: Animal Feeding Stuffs—Determination of Moisture and Other Volatile Matter Content.* 1999.
24. de Jonge, L. and S. van Laar, *DETERMINATION OF AMMONIA -N (NH3) CONTENT*

25. Searle, P.L., *The Berthelot or indophenol reaction and its use in the analytical chemistry of nitrogen. A review.* Analyst, 1984. **109.5**: p. 549-568.
26. de Vries, H., et al., *Impact of Yeast-Derived beta-Glucans on the Porcine Gut Microbiota and Immune System in Early Life.* Microorganisms, 2020. **8**(10).
27. Ramiro-Garcia, J., et al., *NG-Tax, a highly accurate and validated pipeline for analysis of 16S rRNA amplicons from complex biomes.* F1000Res, 2016. **5**: p. 1791.
28. McMurdie, P.J. and S. Holmes, *phyloseq: an R package for reproducible interactive analysis and graphics of microbiome census data.* PLoS One, 2013. **8**(4): p. e61217.
29. Lahti, L. and S. Shetty, *microbiome R package.* 2012-2019.
30. Love, M.I., W. Huber, and S. Anders, *Moderated estimation of fold change and dispersion for RNA-seq data with DESeq2.* Genome Biol, 2014. **15**(12): p. 550.
31. Braak, C. and P. Smilauer, *Canoco Reference Manual and User's Guide: Software for Ordination, version 5.* Microcomputer Power, 2012.
32. Segata, N., et al., *Metagenomic biomarker discovery and explanation.* Genome Biol, 2011. **12**(6): p. R60.
33. Narayan, N.R., et al., *Piphillin predicts metagenomic composition and dynamics from DADA2-corrected 16S rDNA sequences.* BMC Genomics, 2020. **21**(1): p. 56.
34. Andrews, S., *FastQC: a quality control tool for high throughput sequence data.* 2010(Babraham bioinformatics).
35. Warr, A., et al., *An improved pig reference genome sequence to enable pig genetics and genomics research.* Gigascience, 2020. **9**(6).
36. Alcock, B.P., et al., *CARD 2023: expanded curation, support for machine learning, and resistome prediction at the Comprehensive Antibiotic Resistance Database.* Nucleic Acids Res, 2023. **51**(D1): p. D690-D699.
37. Wolthuis, J.C., et al., *Multi-country metabolic signature discovery for chicken health classification.* Metabolomics, 2023. **19**(2): p. 9.
38. Chong, J. and J. Xia, *MetaboAnalystR: an R package for flexible and reproducible analysis of metabolomics data.* Bioinformatics, 2018. **34**(24): p. 4313-4314.
39. Wolthuis, J.C., et al., *MetaboShiny: interactive analysis and metabolite annotation of mass spectrometry-based metabolomics data.* Metabolomics, 2020. **16**(9): p. 99.
40. Deng, K., et al., *WaveICA: A novel algorithm to remove batch effects for large-scale untargeted metabolomics data based on wavelet analysis.* Anal Chim Acta, 2019. **1061**: p. 60-69.
41. Han, W. and L. Li, *Chemical Isotope Labeling LC-MS for Human Blood Metabolome Analysis.* Methods Mol Biol, 2018. **1730**: p. 213-225.
42. Vandeputte, D., et al., *Stool consistency is strongly associated with gut microbiota richness and composition, enterotypes and bacterial growth rates.* Gut, 2016. **65**(1): p. 57-62.
43. Versluis, D., et al., *Mining microbial metatranscriptomes for expression of antibiotic resistance genes under natural conditions.* Sci Rep, 2015. **5**: p. 11981.
44. Grigorenko, B.L., et al., *Catalytic Cycle of Penicillin Acylase from Escherichia coli: QM/MM Modeling of Chemical Transformations in the Enzyme Active Site upon Penicillin G Hydrolysis.* ACS Catalysis, 2014. **4**: p. 2521-2529.
45. Williams, B.B., et al., *Discovery and characterization of gut microbiota decarboxylases that can produce the neurotransmitter tryptamine.* Cell Host Microbe, 2014. **16**(4): p. 495-503.
46. Zhao, Z.H., et al., *Indole-3-propionic acid inhibits gut dysbiosis and endotoxin leakage to attenuate steatohepatitis in rats.* Exp Mol Med, 2019. **51**(9): p. 1-14.
47. Jensen, M.T., R.P. Cox, and B.B. Jensen, *3-Methylindole (skatole) and indole production by mixed populations of pig fecal bacteria.* Appl Environ Microbiol, 1995. **61**(8): p. 3180-4.
48. Martey, C.A., et al., *The aryl hydrocarbon receptor is a regulator of cigarette smoke induction of the cyclooxygenase and prostaglandin pathways in human lung fibroblasts.* Am J Physiol Lung Cell Mol Physiol, 2005. **289**(3): p. L391-9.
49. Macfarlane, S. and G.T. Macfarlane, *Proteolysis and Amino Acid Fermentation*, in *Human Colonic Bacteria: Role in Nutrition, Physiology and Pathology.* 1995, CRC Press.
50. Smith, E.A. and G.T. Macfarlane, *Dissimilatory amino Acid metabolism in human colonic bacteria.* Anaerobe, 1997. **3**(5): p. 327-37.
51. Kaiko, G.E., et al., *The Colonic Crypt Protects Stem Cells from Microbiota-Derived Metabolites.* Cell, 2016. **165**(7): p. 1708-1720.
52. Macfarlane, G.T., et al., *Estimation of short-chain fatty acid production from protein by human intestinal bacteria based on branched-chain fatty acid measurements.* FEMS Microbiology Letters, 1992. **101**(2): p. 81-88.

53. Windey, K., V. De Preter, and K. Verbeke, *Relevance of protein fermentation to gut health.* Mol Nutr Food Res, 2012. **56**(1): p. 184-96.
54. Muller, M., et al., *Distal colonic transit is linked to gut microbiota diversity and microbial fermentation in humans with slow colonic transit.* Am J Physiol Gastrointest Liver Physiol, 2020. **318**(2): p. G361-G369.
55. Vieira-Silva, S. and E.P. Rocha, *The systemic imprint of growth and its uses in ecological (meta)genomics.* PLoS Genet, 2010. **6**(1): p. e1000808.
56. Chen, X., et al., *Moderate Dietary Protein Restriction Optimized Gut Microbiota and Mucosal Barrier in Growing Pig Model.* Front Cell Infect Microbiol, 2018. **8**: p. 246.
57. Pieper, R., et al., *Fermentable fiber ameliorates fermentable protein-induced changes in microbial ecology, but not the mucosal response, in the colon of piglets.* J Nutr, 2012. **142**(4): p. 661-7.
58. Luo, Z., et al., *Effects of low dietary protein on the metabolites and microbial communities in the caecal digesta of piglets.* Arch Anim Nutr, 2015. **69**(3): p. 212-26.
59. Smith, E.A. and G.T. Macfarlane, *Enumeration of amino acid fermenting bacteria in the human large intestine: effects of pH and starch on peptide metabolism and dissimilation of amino acids.* FEMS Microbiology Ecology, 1998. **25**(4): p. 355-368.
60. Loos, M., et al., *Role of heat-stable enterotoxins in the induction of early immune responses in piglets after infection with enterotoxigenic Escherichia coli.* PLoS One, 2012. **7**(7): p. e41041.
61. Sack, D.A., et al., *Diarrhoea associated with heat-stable enterotoxin-producing strains of Escherichia coli.* Lancet, 1975. **2**(7928): p. 239-41.
62. Ruiz, V.L., et al., *Case-control study of pathogens involved in piglet diarrhea.* BMC Res Notes, 2016. **9**: p. 22.
63. Sinha, R., et al., *Resistance to ETEC F4/F18-mediated piglet diarrhoea: opening the gene black box.* Trop Anim Health Prod, 2019. **51**(6): p. 1307-1320.
64. Han, C., et al., *Diversity analysis of intestinal microflora between healthy and diarrheal neonatal piglets from the same litter in different regions.* Anaerobe, 2019. **55**: p. 136-141.
65. Allen-Vercoe, E. and C. Jobin, *Fusobacterium and Enterobacteriaceae: important players for CRC?* Immunol Lett, 2014. **162**(2 Pt A): p. 54-61.
66. Luo, Y., et al., *Dynamic Distribution of Gut Microbiota in Pigs at Different Growth Stages: Composition and Contribution.* Microbiol Spectr, 2022. **10**(3): p. e0068821.
67. Basic, A., et al., *The proteins of Fusobacterium spp. involved in hydrogen sulfide production from L-cysteine.* BMC Microbiol, 2017. **17**(1): p. 61.
68. Gonzales, L., et al., *Alkaline pH Is a signal for optimal production and secretion of the heat labile toxin, LT in enterotoxigenic Escherichia coli (ETEC).* PLoS One, 2013. **8**(9): p. e74069.
69. Smith, H.W. and J.E. Jones, *Observations on the Alimentary Tract and Its Bacterial Flora in Healthy and Diseased Pigs.* J Pathol Bacteriol, 1963. **86**: p. 387-412.
70. Nyachoti, C.M., et al., *Performance responses and indicators of gastrointestinal health in early-weaned pigs fed low-protein amino acid-supplemented diets.* J Anim Sci, 2006. **84**(1): p. 125-34.
71. Cameron-Veas, K., et al., *Shedding of cephalosporin resistant Escherichia coli in pigs from conventional farms after early treatment with antimicrobials.* Vet J, 2016. **211**: p. 21-5.
72. Katale, B.Z., et al., *Genetic diversity and risk factors for the transmission of antimicrobial resistance across human, animals and environmental compartments in East Africa: a review.* Antimicrob Resist Infect Control, 2020. **9**(1): p. 127.
73. Qi, Q., et al., *Host and gut microbial tryptophan metabolism and type 2 diabetes: an integrative analysis of host genetics, diet, gut microbiome and circulating metabolites in cohort studies.* Gut, 2022. **71**(6): p. 1095-1105.
74. Huang, Z., et al., *Distinct effects of fiber and colon segment on microbiota-derived indoles and short-chain fatty acids.* Food Chem, 2023. **398**: p. 133801.
75. Vikstrom Bergander, L., et al., *Tryptamine serves as a proligand of the AhR transcriptional pathway whose activation is dependent of monoamine oxidases.* Mol Endocrinol, 2012. **26**(9): p. 1542-51.
76. Sun, M., et al., *Tryptophan (Trp) modulates gut homeostasis via aryl hydrocarbon receptor (AhR).* Crit Rev Food Sci Nutr, 2020. **60**(10): p. 1760-1768.
77. Qiu, J. and L. Zhou, *Aryl hydrocarbon receptor promotes RORgammat(+) group 3 ILCs and controls intestinal immunity and inflammation.* Semin Immunopathol, 2013. **35**(6): p. 657-70.
78. Veldhoen, M., et al., *The aryl hydrocarbon receptor links TH17-cell-mediated autoimmunity to environmental toxins.* Nature, 2008. **453**(7191): p. 106-9.

79. Parks, O.B., et al., *Interleukin-22 Signaling in the Regulation of Intestinal Health and Disease.* Front Cell Dev Biol, 2015. **3**: p. 85.
80. Stelter, C., et al., *Salmonella-induced mucosal lectin RegIIIbeta kills competing gut microbiota.* PLoS One, 2011. **6**(6): p. e20749.
81. Zhou, C., et al., *Mutual repression between steroid and xenobiotic receptor and NF-kappaB signaling pathways links xenobiotic metabolism and inflammation.* J Clin Invest, 2006. **116**(8): p. 2280-2289.
82. Venkatesh, M., et al., *Symbiotic bacterial metabolites regulate gastrointestinal barrier function via the xenobiotic sensor PXR and Toll-like receptor 4.* Immunity, 2014. **41**(2): p. 296-310.
83. Folkes, L.K. and P. Wardman, *Oxidative activation of indole-3-acetic acids to cytotoxic species-a potential new role for plant auxins in cancer therapy.* Biochem Pharmacol, 2001. **61**(2): p. 129-36.
84. Kurata, K., et al., *Skatole regulates intestinal epithelial cellular functions through activating aryl hydrocarbon receptors and p38.* Biochem Biophys Res Commun, 2019. **510**(4): p. 649-655.
85. Claus, R., et al., *Effects of butyrate on apoptosis in the pig colon and its consequences for skatole formation and tissue accumulation.* J Anim Sci, 2003. **81**(1): p. 239-48.
86. van der Hee, B. and J.M. Wells, *Microbial Regulation of Host Physiology by Short-chain Fatty Acids.* Trends Microbiol, 2021.
87. Gao, Z., et al., *Butyrate improves insulin sensitivity and increases energy expenditure in mice.* Diabetes, 2009. **58**(7): p. 1509-17.
88. Krautkramer, K.A., et al., *Diet-Microbiota Interactions Mediate Global Epigenetic Programming in Multiple Host Tissues.* Mol Cell, 2016. **64**(5): p. 982-992.
89. Atarashi, K., et al., *Induction of colonic regulatory T cells by indigenous Clostridium species.* Science, 2011. **331**(6015): p. 337-41.
90. Singh, N., et al., *Activation of Gpr109a, receptor for niacin and the commensal metabolite butyrate, suppresses colonic inflammation and carcinogenesis.* Immunity, 2014. **40**(1): p. 128-39.
91. McLamb, B.L., et al., *Early weaning stress in pigs impairs innate mucosal immune responses to enterotoxigenic E. coli challenge and exacerbates intestinal injury and clinical disease.* PLoS One, 2013. **8**(4): p. e59838.
92. Pohl, C.S., et al., *Early weaning stress induces chronic functional diarrhea, intestinal barrier defects, and increased mast cell activity in a porcine model of early life adversity.* Neurogastroenterol Motil, 2017. **29**(11).
93. Dou, S., et al., *Characterisation of Early-Life Fecal Microbiota in Susceptible and Healthy Pigs to Post-Weaning Diarrhoea.* PLoS One, 2017. **12**(1): p. e0169851.

Congruence of Transcription Programs in Adult Stem Cell-Derived Jejunum Organoids and Original Tissue During Long-Term Culture

Bart van der Hee[1,2], Ole Madsen[3], Jacques Vervoort[4], Hauke Smidt[2] and Jerry M. Wells[1]

[1] Host-Microbe Interactomics Group, Department of Animal Sciences, Wageningen University & Research, Wageningen, Netherlands, [2] Laboratory of Microbiology, Wageningen University & Research, Wageningen, Netherlands, [3] Animal Breeding and Genomics, Department of Animal Sciences, Wageningen University & Research, Wageningen, Netherlands, [4] Laboratory of Biochemistry, Wageningen University & Research, Wageningen, Netherlands

Published chapter: van der Hee B, Madsen O, Vervoort J, Smidt H and Wells JM (2020) Congruence of Transcription Programs in Adult Stem Cell-Derived Jejunum Organoids and Original Tissue During Long-Term Culture. Front. Cell Dev. Biol. 8:375. *https://doi.org/10.3389/fcell.2020.00375*

Abstract

The emergence of intestinal organoids, as a stem cell-based self-renewable model system, has led to many studies on intestinal development and cell-cell signaling. However, potential issues regarding the phenotypic stability and reproducibility of the methodology during culture still needs to be addressed for different organoids. Here we investigated the transcriptomes of jejunum organoids derived from the same pig as well as batch-to-batch variation of organoids derived from different pigs over long-term passage. The set of genes expressed in organoids closely resembled that of the tissue of origin, including small intestine specific genes, for at least 17 passages. Minor differences in gene expression were observed between individual organoid cultures. In contrast, most small intestine-specific genes were not expressed in the jejunum cell line IPEC-J2, which also showed gene expression consistent with cancer phenotypes. We conclude that intestinal organoids provide a robust and stable model for translational research with clear advantages over transformed cells.

Keywords: intestinal organoids, porcine organoids, gastrointestinal, organoid stability, IPEC-J2

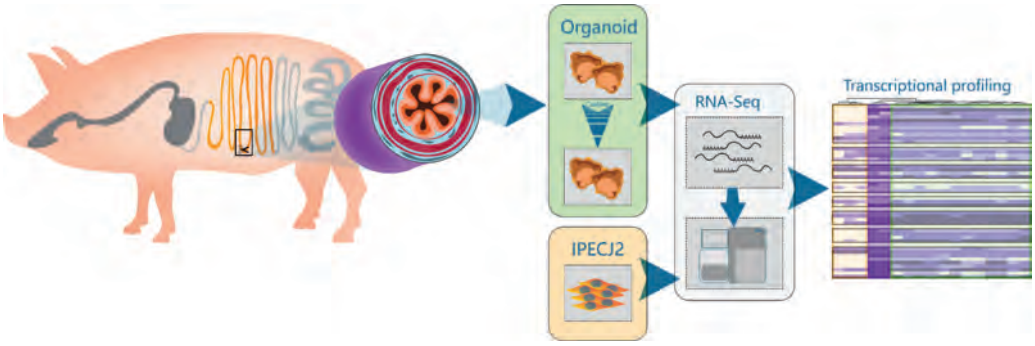

GRAPHICAL ABSTRACT. Porcine intestinal organoids show batch-independent homogeneity to their derived host and stability during long-term culture, as well as profound benefits over transformed cell cultures.

Introduction

The intestinal epithelium plays an essential role in the digestion and absorption of nutrients while also maintaining homeostasis with symbiotic microbiota [1-3]. The physical containment of microbes to the lumen and homeostasis of tolerance and immunity depends on the functions of different lineages of intestinal epithelial cells microbiota [1, 2]. For decades, scientists have exploited the replicative potential of immortalized intestinal cells as enterocyte models to study host-pathogen interactions and intestinal functions *in vitro*. Such monotypic cell models have led to important discoveries but have notable limitations. Immortalized cell lines can undergo significant genotypic alterations within a few passages *in vitro* which are potential threats to data reproducibility [4, 5 , 6]. Furthermore, cell lines often have altered pathway expression compared to primary cells [4]. Since 2009, when it was shown that intestinal adult leucine-rich repeat-containing G protein-coupled receptor 5 (LGR5+) stem cells [7] could be grown into organotypic cultures and propagated in 3D culture [8, 9], there has been much interest in employing intestinal organoids as advanced models. A distinct advantage of organoids is the development of a crypt-villus axis with a similar spatial organization of the heterotypic cell lineages found in the tissue of origin. Additionally, methods for generating polarized monolayers of organoids cells [10] have been optimized [11] to improve the versatility of the models, e.g., to study transport, and differential responses to luminal or basolateral stimulants. Another favorable property of organoids generated from adult intestinal stem cells is that they express specific functions associated with their original intestinal location [12]. This means that location-specific functions of different parts of the intestine are intrinsically programmed in adult stem cells.

In the future we can expect intestinal organoids to be increasingly adopted as intestinal models for humans and other mammals. However, there are some unresolved issues that need to be addressed to ensure reliability and reproducibility of results in this emerging field. As organoids contain different cell types there is potential for variability and problems with reproducibility which may compromise their application to phenotype individuals. To address this issue, we assessed the transcriptional stability of intestinal organoids differentiated from the same crypt batch and between organoids from different pigs (*Sus scrofa domesticus*) over long-term passage. Furthermore, we compared expressed genes and pathways in organoids, the original epithelial tissue from which the organoids were derived, and IPEC-J2, a porcine cell line derived from the jejunum. The results show that intestinal organoids derived from adult stem cells generally resemble the epithelial tissue of origin in terms of expressed genes and provide a reference for researchers wishing to investigate specific small intestinal functions not present in IPEC-J2.

Materials and Methods

Intestinal Organoid Generation

Jejunum tissue segments were obtained from control piglets used for another study, following guidelines of the animal ethics committee of Wageningen University. Two 5-week-old piglets were used for generating organoids following procedures previously described [11, 13]. Briefly, a 2 cm section of the mid-jejunum was dissected and placed in ice-cold PBS. After opening the sections longitudinally, jejunum segments were washed three times in ice-cold PBS and villi removed by carefully scraping with a scalpel. Small sections of the mucosa were cut from the muscle layer, divided into small cubes, and transferred into ice-cold PBS containing 30 mM EDTA and incubated with rotation at room temperature for 15 min. The PBS – EDTA was then replaced, and incubation continued for 10 min at 37°C. After washing in ice-cold DMEM supplemented with 5% penicillin/streptomycin (Gibco, Thermo Fisher Scientific), the crypts were dissociated by rigorous vortexing and passed through a 100 µm strainer into cold DMEM containing 5% fetal bovine serum (FBS, v/v). Crypts were pelleted by centrifugation at 300 × *g* for 5 min, and suspended in Matrigel (Basement Membrane, Growth factor reduced, REF 356231, Corning, Bedford, MA, United States). To improve surface tension, empty 24-well plates were preincubated overnight at 37°C. Seven drops of Matrigel containing crypts were placed in each well (approx. 35 µl per well) and inverted to polymerize at 37°C. After polymerization, 600 µl F12 cell culture medium (Gibco) was added, supplemented with 100 µg/ml primocin (Invivogen), 10 mM HEPES (HyClone), 1 × B-27 (Gibco), 1.25 mM *N*-acetylcysteine (Sigma), 50 ng/ml human epidermal growth factor (R&D systems), 15 nM gastrin, 10 mM nicotinamide, 10 µM p38 MAPK inhibitor (Sigma), 600 nM TGFβ receptor inhibitor A83-01, and conditioned media for recombinant Noggin (15% v/v), Spondin (15% v/v), and Wnt3A (30% v/v) provided by Dr. Kuo and Hubrecht Institute (Utrecht, Netherlands).

Organoids were passaged at a 1:5 ratio every 5 days using ice-cold DMEM by mechanical dissociation, centrifugation at 500 × *g* for 5 min, and plating in fresh Matrigel matrix droplets as previously described [11]. For measuring transport of amino acids (AAs), two-dimensional organoids were generated as previously described [11]. 3D organoids were dissociated into single cells by TrypLE digestion and seeded on Matrigel (0.5% v/v) precoated transwells (Falcon BD). After reaching confluence, the apical medium was replaced with DMEM (Gibco) and basolateral medium with HBSS (Gibco). After incubation, the basolateral AA composition was measured using triple quadrupole mass spectrometry (TQMS).

Culturing Methods and RNA Isolation

Directly after crypt isolation, organoid cultures were separated into three batches per animal and grown independently for 17 passages. Jejunum organoids were grown for 3 and 12 weeks (4– 17 passages) and extracted using ice-cold PBS. After washing twice in PBS, intact organoids were pelleted at 300 × g for 5 min and suspended in RLT lysis buffer and stored at −80°C prior to RNA isolation. Porcine jejunum epithelial cell line IPEC-J2 (ACC-701) was grown in DMEM F12 medium supplemented with 10% FBS and 5% penicillin/streptomycin (P/S, Gibco) in 75 cm^2 culture flasks. Data for one IPECJ2 (p67) transcriptome was kindly provided by Dr. Richard Crooijmans, via the Functional Annotation of ANimal Genomes (FAANG, BioSamples accession SAMEA4447551) [14]. For the analysis of the remaining two lines, IPEC-J2 at passage 87 and 91 were seeded at 5 × 10^4 cells/well in 24-well plates and grown to confluence within 48 h with reduced P/S (1%). The monolayers were subsequently left to differentiate for 5 days, lysed using RLT-buffer, and stored at −80°C prior to RNA isolation. For RNA extraction of tissue, 0.5 mg of whole jejunum cross section per animal was added to a gentleMACS M tube (Miltenyi Biotec, Germany) and dissociated in 2 ml RLT lysis buffer using a gentleMACS Dissociator for 30 s. Subsequently, 100 µl of homogenized tissue suspension was added to 500 µl fresh RLT buffer, homogenized using pipetting with a p200 pipette, and stored at −80°C until extraction. Total RNA was extracted using a RNeasy Mini Kit (Qiagen) following manufacturer's instructions including a 15 min on-column DNAse step. Preliminary tRNA concentrations, contamination and degradation were identified using Qubit (Thermo-Fisher) and gel-electrophoresis. The quantity and integrity of RNA was measured using a Bioanalyzer 2100 (Agilent).

RNA-Sequencing Procedures and Data Handling

A minimum of 1 µg total RNA in 50 µl was used for library preparation using the TruSeq RNA sample preparation kit (Illumina) following the manufacturer's protocol at Novogene. Briefly, total RNA samples were depleted for ribosomal RNA using the RiboZero kit and enriched for mRNA using oligo(dT) beads, fragmented, and synthesized into cDNA using mRNA template and hexamer primers. Custom second strand-synthesis buffer (Illumina), dNTP's, RNAse H and DNA Polymerase I were added for second strand synthesis initiation. Furthermore, following a series of terminal repair, cDNA library construction was completed with size selection and PCR enrichment. Samples were sequenced using an Illumina Hi-Seq 4000 (Novogene, Hong Kong) at 9 GB raw data/sample with 150 bp pairedend reads.

Raw sequencing reads were checked for quality using FastQC [v0.11.5; [15]] and trimmed using trimgalore for adaptors and quality [v0.4.4 [16]]. Only paired-end reads longer than 35 bp were included for further downstream analysis. Sequences were aligned against Ensembl *Sus scrofa* reference genome and annotation 11.1.91

[17] using Tophat [v2.1.1 [18]]. Transcriptomes were assembled with 5 bp intron overhang tolerance, merged, normalized, and analyzed using the Cufflinks package [v2.2.1 [18]]. Differential expression was analyzed with 0.01 false discovery rate (FDR) using cuffdiff with bias and weight correction and visualized in R using CummeRbund [v2.7.2 [18]]. Mapping analytics can be found in **Supplementary Table S1**. Fragments per kilobase million (FPKM) were calculated and log-transformed for downstream analysis. The sequencing data was also processed using CLC Genomics Workbench 11 (Qiagen) using identical reference genome, annotation and settings for identification of insertions/deletions, breakpoints, structural variants, and track generation. Output was filtered for genes <1 FPKM to establish expression.

Data Availability

All data are available for download through the gene expression omnibus under GEO accession number GSE146408. This data also contains the merged transcriptome file for cufflinks analysis and detailed analysis. The FPKM value data table is available at *https://www.frontiersin.org/articles/10.3389/fcell.2020.00375/full#supplementary-material*.

Functional Analysis and Pathway Expression

Differentially expressed genes were clustered by k-means into seven clusters using CummeRbund. Due to limited analysis methods for further downstream functional analysis in pig, databases for human genomes were used as a background. Differentially expressed genes were analyzed for functional enrichment and ontologies using the TOPPfun suite [19], and gene list enrichment and candidate prioritization were evaluated with a threshold <0.05 for *P*- and *Q*-value adjusted for FDR with the Benjamini-Hochberg procedure (B&H). Ingenuity Pathway Analysis (IPA, Qiagen) was used for determining overlapping networks of expressed genes between tissue and organoids, and overall expression of molecular and cellular development of organoids between time-points. Genes for elevated tissue-specific expression were acquired from the human protein atlas for specific mRNA transcription in the small intestine, and porcine orthologs were identified to determine tissue and group enriched genes [20].

Histological Analysis

Whole mount imaging was performed as previously described with small modifications [21]. Organoids grown in 8-well chambered slides (Millicell EZ slide, Merck) were fixed in 4% paraformaldehyde (PFA) for 2 h at RT. PFAfixed organoids were stained using FITC-conjugated UEA-1 antibody (1:250, FL-1061, Vector Laboratories, United States) for 2 h and counterstained with Hoechst (0.5 µg/ml, 33342, Thermo Fisher) for 10 min at room temperature. Z-stacks of whole organoids

were imaged on a confocal microscope (Zeiss). Immunohistochemical analysis for Mucin-2 was performed following procedures previously described [11, 22]. Organoids were retrieved from Matrigel using ice-cold PBS, pelleted, and fixed overnight using 1% PFA at 4°C. After pelleting, organoids were suspended in 2% agarose gel, dehydrated, and embedded in paraffin blocks. After cutting 5 µM-thick sections and subsequent drying on glass slides, sections were rehydrated, blocked in 5% normal goat serum, and stained using anti-MUC2 antibody (1:200, AB_1950958, GeneTex) overnight. After addition of secondary FITC-antibody (Thermo-Fisher), sections were counterstained using Hoechst and imaged using a DM6 microscope fitted with DFC365 camera at 40x magnification.

Results

Comparative Analysis of the Transcriptome of Organoids, Tissue, and a Cell Line Derived from the Porcine Jejunum

Jejunum tissue was isolated from two euthanized 5-weekold piglets for generating organoids and isolation of RNA from epithelial cells (**Figure 1A**). Triplicate batches of each organoid were separately cultured for 12 weeks by passaging approximately every 5 days. After 3- and 12-weeks continuous culture (4–17 passages) RNA was isolated from the organoids for RNA sequencing (**Figure 1A**). Within the first two passages after isolation, the organoids acquired a budding phenotype, which might be attributed to whole crypt isolation also containing transit amplifying cells in differentiation stages as opposed to basal culture after 2 weeks forming a more cyst-like phenotype. After 2 weeks of continuous culture the organoids formed spheroids (**Figure1B**) but maintained different cell lineages, as shown with UEA-1 staining for secretory cell lineages (**Figure 1C** and **Supplementary Figure S1**). Similarly, RNA was isolated from the porcine jejunum cell line IPEC-J2 at passage number 67, 87, and 91. RNA sequencing data was analyzed using a customized analysis pipeline and CLC genomics workbench 11. Multidimensional scaling showed the transcriptomes of the organoids clustered closely together, despite 12-weeks continuous passage and isolation from different pigs (**Figure 1D**). It was also evident that the transcriptomes of the tissue and organoid samples were most similar, not separating in the first dimension, whereas IPEC-J2 separated from tissue in both dimensions. A correlation matrix of transcriptomic data from all samples revealed the highest similarity for replicate samples of the same origin (**Figure 1E**).

The hierarchical clustering of gene expression (**Figure 1F**) further revealed that the transcriptome of organoids more closely resembled that of jejunum epithelial tissue than the IPEC-J2 cell line. The two tissue samples clustered under the same branch,

where organoids showed consistent homogenous expression derived from different pigs than between 3 and 12- week cultures of replicate samples of the same organoid batch. Furthermore, organoid transcriptomes showed better correlation to tissue (r = 0.77) than IPEC-J2 (r = 0.73), whereas between tissue and IPEC-J2 correlation is lower (r = 0.57) (**Supplementary Figure S2**).

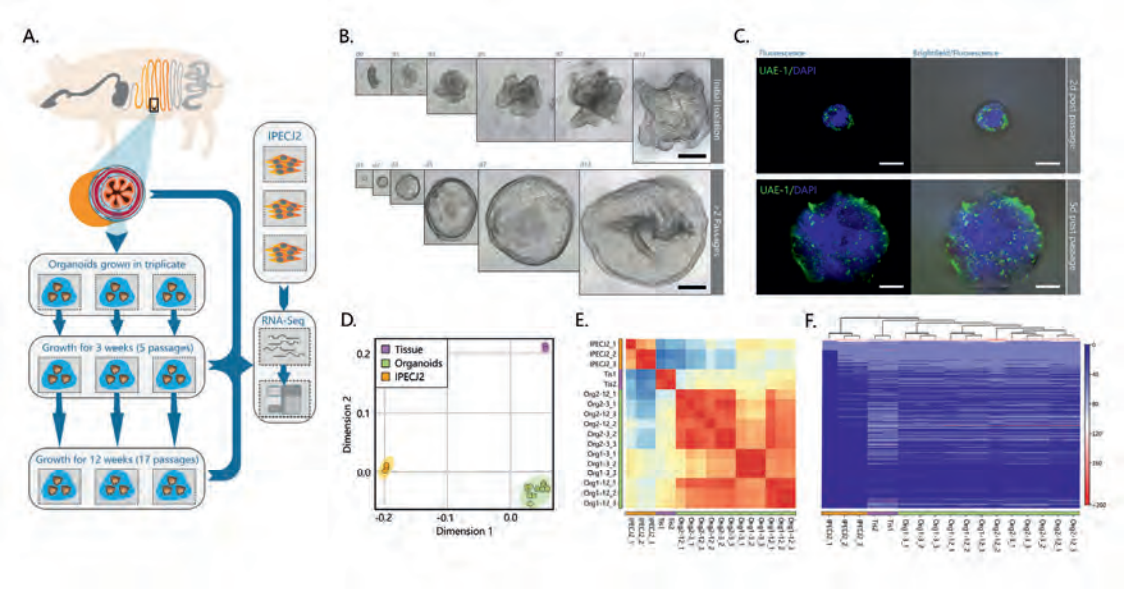

Figure 1. Porcine intestinal organoid culture and transcriptome sequencing overview. (A) graphical overview of the study design. Organoids were generated from the jejunum of two individual pigs, directly divided into triplicate organoid cultures per animal, and passaged for 12 weeks. Total RNA of tissue, organoids, and jejunum cell line IPEC-J2 was extracted and sequenced by RNA-seq. (B) Initially after isolation, intestinal crypts form budding organ-like structures in vitro. Within 2 weeks of passaging, organoids form more spheroid-resembling structures for the remainder of the experiment, indicating more long-term reproducibility after a short-term series of passaging. (C) After 12 weeks of growth, spheroids still retain secretory cell lineage differentiation early post-passaging (green: stained with UEA-1). (D) Multidimensional scaling of transcriptomic data showed separation of organoids, tissue and IPEC-J2, where organoids and tissue show separation in only one dimension. (E) Correlation matrix of all samples show high correlation among individual organoid batches, and strong correlation between tissue. (F) Heat map and hierarchical clustering of all expressed genes (>1 FPKM) in the dataset.

Organoid Transcriptomes Closely Resemble Gene Expression Signatures Associated with Their Tissue of Origin

Of the 24912 annotated genes in the pig genome, 11099 (44.6%) were not expressed in the dataset (<1 FPKM). All samples shared expression of 9117 genes, and a large set of genes was commonly expressed between organoids and tissue exclusively (1762 genes; **Figure 2A**). Genes associated with different overlapping areas of the Venn diagram were categorized by gene ontology using TOPPfun (**Supplementary File S2**).

However, the dataset for expressed genes in organoids still contained 1304 genes not annotated denoted with an unknown gene ID, and after conversion to human orthologs using g:profiler [23], only 121 of these unknown ID's with unknown function acquired a gene annotation. Nevertheless, after conversion most of the 1304 genes did contain a description (80.6%), but no gene ortholog name to identify specific function. It is therefore evident that further curation of the porcine ontology database is necessary to generate a more comprehensive reference genome for transcriptomics research.

The top clusters of all pathways, based on all expressed genes, in organoids are involved in basal molecular and cellular function as well as physiological system development, reflecting the interactions with extracellular factors and self-organization of organoid microanatomy (**Figure 2B**). Pathways of relevance for using organoid models in host-microbe interactions, such as homeostasis and innate immunity, were highly expressed. Cellular homeostatic signaling or activation pathways included integrin, mTOR, Sirtuin, PPARα, and RXRα, with typically more than 40% of genes in the annotation being expressed (**Figure 2C**). Immunity-pathways included important cytokine and cytokine receptor signaling pathways (e.g., *TNFR1, IL8, JAK/STAT, PKR*) and innate immune signaling (*NF-kB, ERK/MAPK, iNOS*).

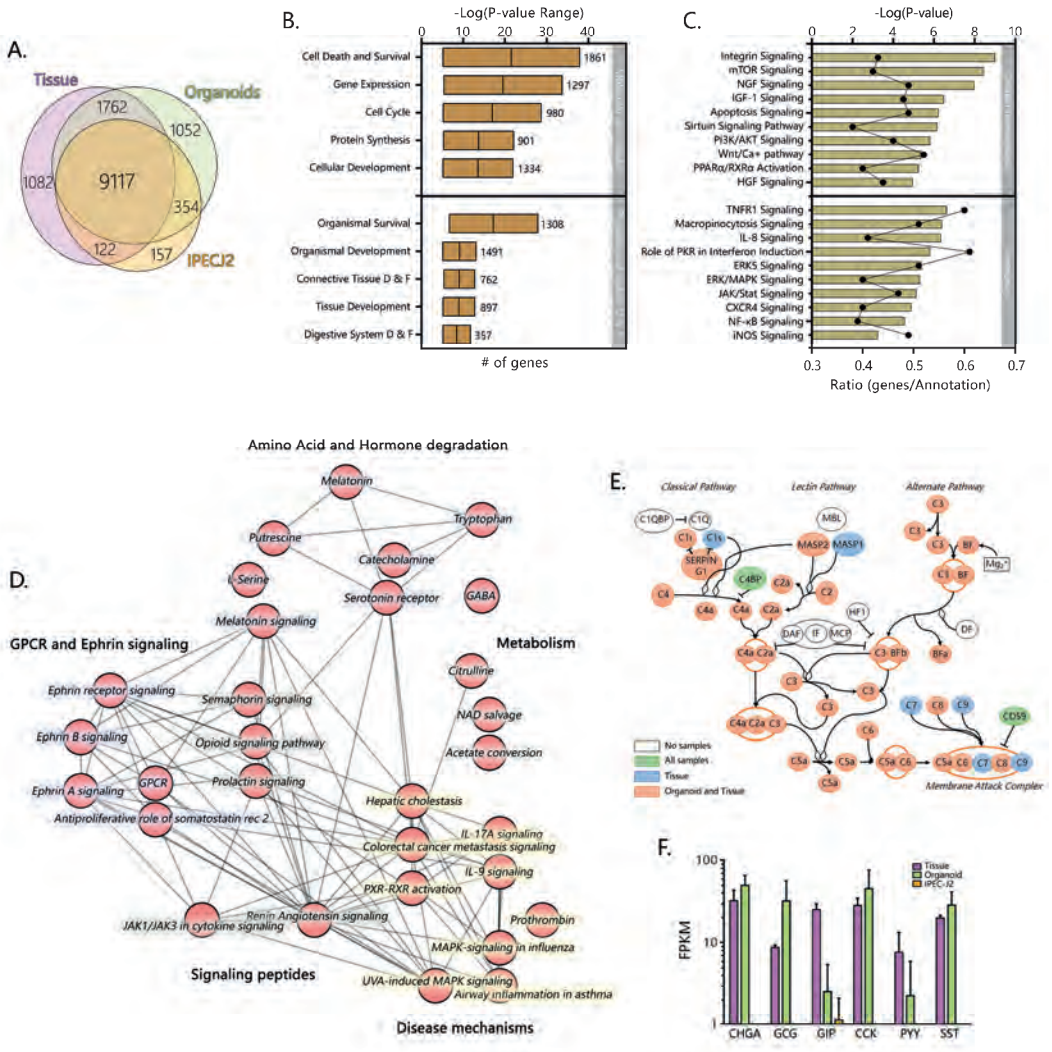

Figure 2. The transcriptome of jejunum organoids exhibits strong similarity to its derived tissue transcriptome, including a distinct group of overlapping genes not expressed in IPEC-J2. Averages of all expressed genes were compared between sample type and (A) can be viewed in the weighted Venn-diagram. All genes expressed in organoids after 12 weeks of culture were analyzed using Ingenuity pathway analysis. (B) Molecular, cellular, and physiological system development and function shows many genes involved in basic cellular and tissue specific processes. More than >400 pathways were expressed in the organoid RNA-seq dataset. (C) The top 10 cellular homeostasis and immunity related pathways; –logP values indicate statistical probability of pathway expression; ratio, indicates number of expressed genes divided by number of annotated genes in the pathway. Testing the RNA-seq dataset for overlapping genes revealed a set of 1762 genes exclusively expressed in tissue and organoids. (D) Top 30 connected canonical pathways of these 1762 genes from ingenuity pathway analysis, which showed subdivision into metabolic, disease, GPCR/Ephrin signaling, and small molecule degradation pathways. (E) Expression of genes involved in the complement pathway are expressed in organoids and tissue (Pink), Tissue only (Blue), organoids tissue and IPEC-J2 (Green), or not found to be expressed (White). (F) Expression patterns of genes involved in Enteroendocrine signaling [CHGA, Chromogranin A; GCG, Glucagon; GIP, Gastric inhibitory polypeptide; CCK, Cholecystokinin; PYY, Peptide YY; SST, Somatostatin; Purple, Tissue; Green, Organoid; Orange, IPEC-J2, data shown as Log(FPKM)].

Ingenuity pathway analysis of the 1762 expressed genes shared only between organoids and tissues revealed pathways associated with GPCR and Ephrin signaling, which is associated with processes such as cell migration and stem cell differentiation (**Figure 2D**). Pathways associated with the endocrine functions of cells were also identified including signaling via tryptophan derived melatonin and serotonin. Other pathways specific to organoids and tissue included pathways linked to cytokine, MAP-kinase and other signaling pathways, which are altered in various disease states. Genes encoding complement factors were also specifically expressed in tissue and organoids. Recent studies integrating intestinal transcriptomes deposited in public databases suggest that intestinal expression of complement pathways plays a homeostatic role, being upregulated by inflammatory challenges to control microbial invasion or colonization [24, 25]. From this data it is evident that many complement factors are expressed in organoids and tissue (**Figure 2E**). A key difference between IPEC-J2 and organoid or tissue was the specific expression of hormones associated with Enteroendocrine cells, such as *CCK* which induces secretion of digestive enzymes and *PYY*, a satiety hormone (**Figure 2F**).

Genes which are specific for the different cell lineages found in the small intestinal epithelium [26], were generally highly expressed in organoids (**Figure 3A**) but largely absent in IPEC-J2. Surprisingly IPEC-J2 lacked expression of some genes commonly associated with mature absorptive enterocytes, even though cultures of this cell line are reported to differentiate into functional epithelium [27]. Initially our dataset suggested lack of mucin 2 (*MUC2*) gene expression using Ensembl gene annotation. However, we identified a high number of RNA-seq reads from organoids and tissue mapping to the chromosomal locus associated with *MUC2* in the NCBI database (XM_021082584, Chromosome 2, bp 689,363–719,542) (**Figure 3B**). We verified the expression of *MUC2* in porcine organoids and tissue using histology confirming mucin production and secretion as described previously [11, 13]. The genes identified in the human protein atlas to be enriched in the small intestine (i.e., jejunum) [20, 28] were checked for expression in porcine jejunum tissue, jejunum and ileum organoids, and IPEC-J2 cells (**Supplementary File S3**). Most of the porcine orthologs (65% in tissue samples) were indeed expressed in epithelial tissue from the pig jejunum (**Figure 3C**). Moreover, between 74 and 86% of the porcine jejunum tissue-specific genes were also expressed in jejunum organoids, while this number was lower in ileum-derived organoids (52%). Furthermore, only 32% of small intestine-specific genes were expressed in IPECJ2 cells. Genes associated with general digestion (*SI*, *FABP1*), absorption (solute-carriers; *SLC*-genes), or immunity (*IL22RA1*) were exclusively expressed in the tissue and jejunum organoids. Some of the genes associated with secreted peptides for immunity and digestion were not expressed in organoids and IPEC-J2 (i.e., *MEP1A*, *MEP1B*, *AQP10*, *CCL11*). It was shown that the intestinal epithelium is intrinsically programmed to differentiate into location

specific organoid cultures [12]. To investigate this for our organoid lines, we identified overlapping and exclusively expressed genes between jejunum and ileum-derived organoids. Both organoid types shared a large set of genes (10601), but several genes were identified for jejunum (1685) or ileum (481) only (**Figure 3D**). These genes were subsequently analyzed for gene set function using and digestion (e.g., FABP1 and 2) (See **Supplementary File S4** TOPPfun. Jejunum exclusively expressed genes associated with output and gene lists). Ileum expressed genes associated with transmembrane transport, like solute-carrier transporters (SLC), with immune function, e.g., type 1 interferon responses by interferon alpha genes, as well as fucosyltransferase activity (FUT1 and FUT2).

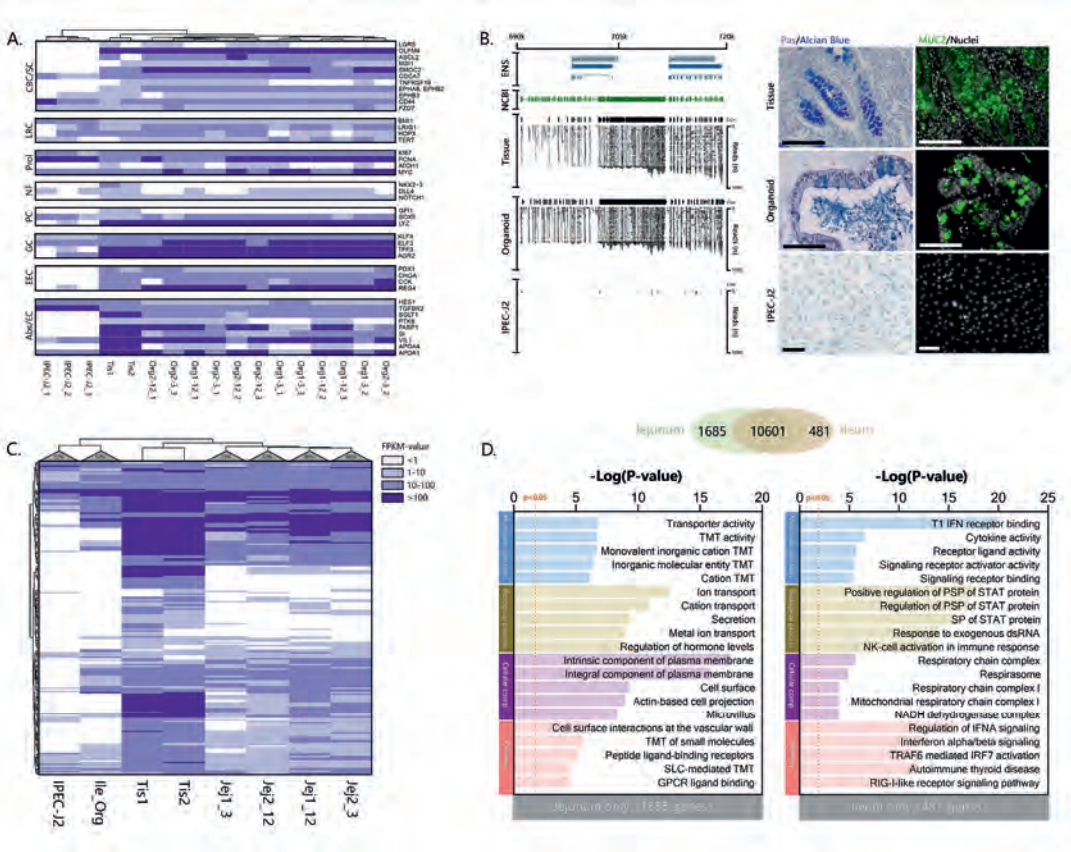

Figure 3. Organoids derived from adult intestinal stem cells show intrinsic programming to differentiate into different epithelial cell lineages and express small intestine-specific genes. (A) Cell type-specific transcripts for Crypt Base Columnar (CBC) and Stem cells, Label-retaining (LRC) +4 cells, Proliferation (Prol), Niche factors (NF), Paneth cells (PC), Goblet cells (GC), Enteroendocrine cells (EEC), and Absorptive cells or enterocytes (Abs/EC). (B) Overlaying the NCBI gene tracks of MUC2 NC_010444.4 on chromosome 2 at location 689363–719542bp (green area), shows identical overlap with the mapped reads and coverage (Cov) from organoid and tissue samples, but not in IPEC-J2 (ENS; Ensembl reference genome). To confirm MUC2 protein translation and subsequent mucus formation, Carnoy fixed tissue, organoid, and IPEC-J2 samples were stained with PAS/Alcian blue (left) and porcine anti-MUC2 (right; black and white size bars indicate 100 µm). (C) Most small intestine-specific genes identified in the human protein atlas are also expressed in porcine jejunum tissue and their derived organoids (>74%), whereas fewer are expressed in ileum organoids (52%). IPEC-J2 only expressed 32% of the small intestine-specific genes. (D) Organoid transcriptomes from jejunum and ileum were compared to identify differences in expressed genes, showing large overlap of genes (Venn), but also some differences. The different genes were analyzed using TOPPfun to identify putative differences in gene ontology and pathways (TMT, Transmembrane transport; PSP, Peptidyl-serine phosphorylation).

Cluster Analysis of Differentially Expressed Genes (DEGs)

Genes which were differentially expressed in tissue, organoids or IPEC-J2 ($P < 0.05$), were categorized by K means clustering and represented as biological processes and pathways (**Figures 4A–C**). The genes expressed only in tissue ($n = 141$) are mostly involved in immune pathways e.g., T cell and leukocyte functions, suggesting they might be due to presence of lamina propria immune cells in the tissue sample (**Figure 4A**). Genes related to extracellular matrix (ECM) or muscle contraction pathways were also differentially expressed in tissue compared to organoids and IPEC-J2. The cluster of genes expressed at higher levels in tissue and IPEC-J2 ($n = 52$) compared to organoids comprise of processes related to cell morphology, proliferation, movement, remodeling of the ECM as well as integrin and ECM signaling pathways (**Figure 4B**). Altered expression of some of these pathways has been reported in cancer [29, 30]. The low or absent expression of the ECM genes in organoids may be due to provision of Matrigel acting as a basement membrane substrate. Furthermore, there may be components present in the intestinal ECM capable of inducing cell integrin signaling which are not present in Matrigel. Clustering genes transcribed in significantly higher amounts in IPEC-J2 show gene-list enrichment in disease processes and pathways associated with cancer (**Figure 4D**). Furthermore, one of our IPEC-J2 cultures showed an insertion in the protein coding region and a large deletion in the splicing site of the adenomatous polyposis coli (*APC*) gene, which is a tumor suppressor often inactivated in colon cancer [31]. The cluster of genes with higher expression in organoids and tissue ($n = 299$) compared to IPEC-J2 involve nutrient transport and metabolic processes such as lipid digestion and transport, protein digestion and AA metabolism (**Figure 4C**). Examples include metabolism of tryptophan, arginine, proline, histidine, phenylalanine and transport of glucose, bile salts, fatty acids, lipids, and vitamins.

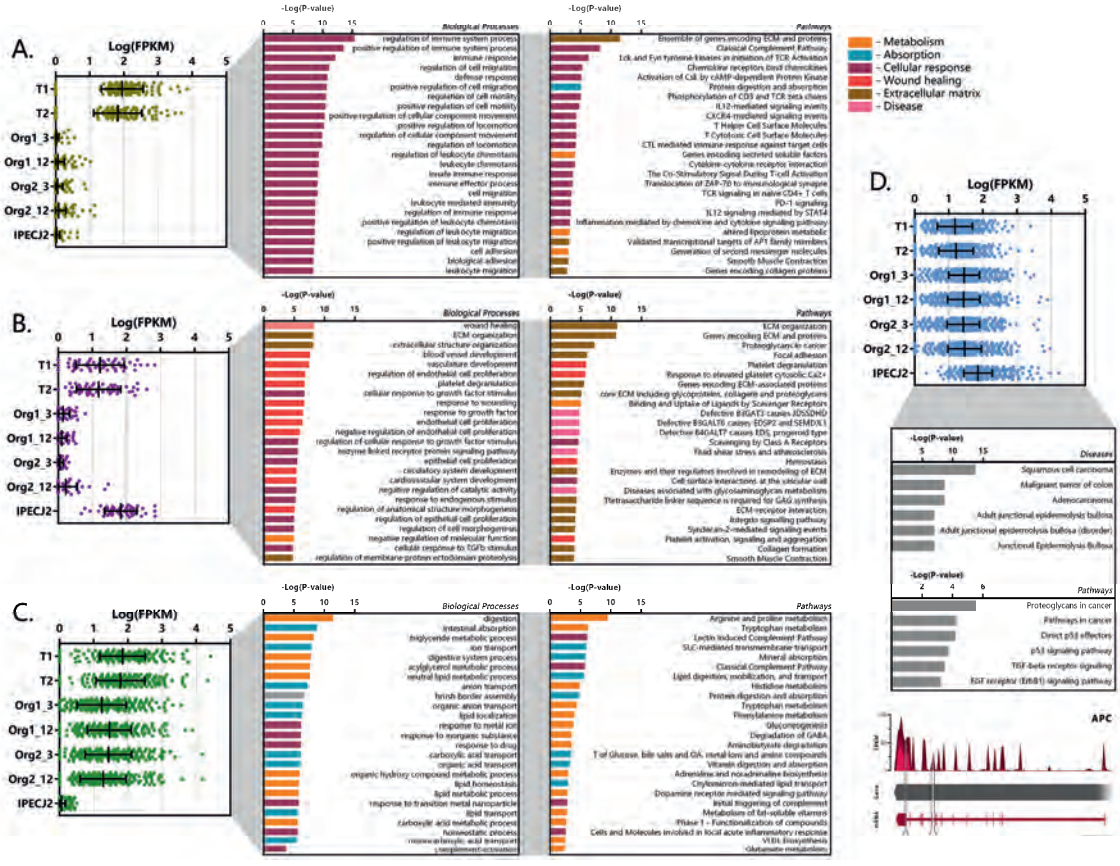

Figure 4. Cluster analysis of differentially expressed genes (DEGs). DEGs were clustered according to their expression pattern using k-means clustering, and subsequently analyzed for functional enrichment using TOPPfun. (A) Cluster of genes (n = 141) showing increased expression in tissue only and low expression in organoids and IPEC-J2. (B) Cluster of genes (n = 52) showing high expression in tissue and IPEC-J2, with low expression in organoids. (C) Cluster of genes (n = 299) with increased expression in tissue and organoids, with low expression in IPECJ-2 (data represented in Log(FPKM) or –Log(P-value), P and q < 0.05). (D) Cluster of genes (n = 841) expressed more highly in IPEC-J2 than tissue and organoids which were associated with diseases and pathways involved in tumor formation. A common mutation in colon cancer is inactivation of adenomatous polyposis coli (APC) gene where IPEC-J2 shows an insertion (217 bp, tandem duplication) in the protein coding region and splice site deletion (331 bp, cross mapped breakpoints; bottom).

Congruence of the Transcriptome in Individual Organoids During Passage

Comparison of transcriptomes of organoid cultures over time and between batches indicated high correlation in expression values (r = 0.906–0.910, **Figure 5A**). After long-term passage there were 199 genes in organoid 1 and 172 genes in organoid 2 which were significantly increased in expression (**Figure 5B**; n = 3 per group). All differentially expressed genes were distributed across nine common ontologies (**Figure 5B**) and consisted of only 1.93–3.67% of the annotated genes in each biological process. This included processes such as small molecule biosynthesis, organic acid metabolic processes and response to nutrient levels. Variation in expression of genes in organoid cultures over time may therefore be due to differences in nutrient abundance in culture medium, and replicative activity, rather than permanent loss or gain of functions. Long-term passage also resulted in differential down regulation of 78 and 137 genes in organoids 1 and 2, respectively (n = 3 per group, **Figure 5C**). The only common ontology found for these genes was small molecule biosynthetic process, which was also included in genes upregulated after long term passage (**Figure 5B**). This suggests that culture dependent conditions result in variation in a small percentage of genes in this ontology group, perhaps due to variation in number or activity of several cell types in low abundance. The heatmap in **Figure 5D** shows expression or fold change in genes that were commonly differentially expressed in organoids 1 and 2 after long-term passage. Although being significantly differentially regulated, a group of genes with significantly reduced fold change in expression after 12 weeks passage was seen to be overall reduced in transcript abundance (FPKM) and appeared to be involved in unrelated processes when tested for gene ontology. Differences between organoid 1 and 2 are likely to reflect individual variation and the most striking differences were for apolipoprotein A1 (*APOA1*), *ISG12*(A), and *ISG15*.

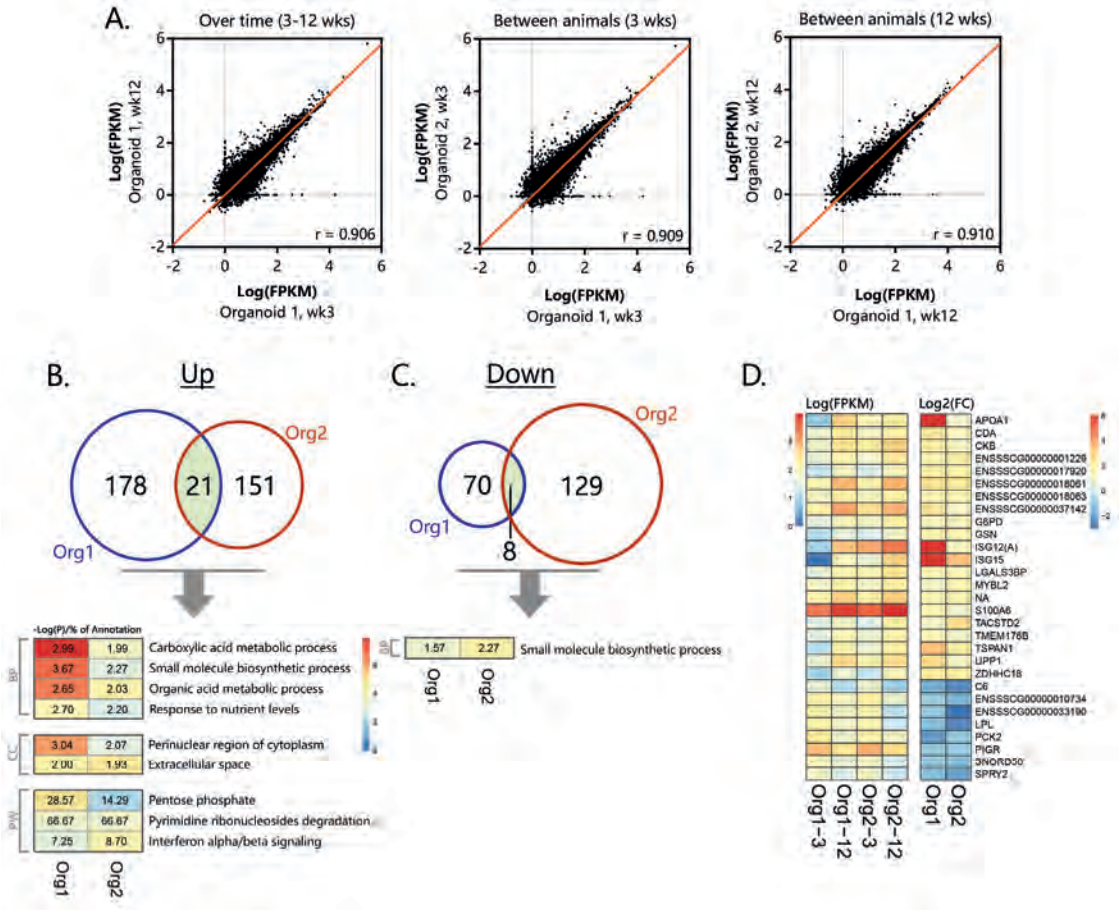

Figure 5. Differential gene- and pathway expression in organoids shows stable transcription over time. The two separate organoid cultures (n = 3 per group) were tested for expression differences between 3 and 12 weeks of culturing, (A) showing representative correlations over time within an organoid line and between different animals (n = 13813 genes with at least 1 sample >1 FPKM). Significant ($p < 0.05$) up- (B) and down-regulation (C) of genes and their corresponding overlapping pathways when tested individually using TOPPfun (overlapping area shows similar genes between organoid types, BP, Biological processes; CC, Cellular component; PW, Pathway). (D) Overlapping up- and down-regulated genes between 3 and 12 weeks of culturing in actual expression values [Log(FPKM)] and their corresponding fold change [Log2(FC)].

Small Molecule Transport by Intestinal Organoids

Determining cellular function by gene expression could result in biased interpretation. For this, functional assays can be used to determine cellular function *in vitro*. The luminal compartment of 3D organoids is in the center, preventing access for apical stimulation with compounds. Methods have been developed to inject compounds into organoids (**Supplementary Figure 3A**), but this temporarily disrupts the barrier, and injection of multiple organoids is laborious. We demonstrated basolateral efflux of compounds by adding celltracker red dye to 3D organoids and monitoring transport into the lumen (**Supplementary Figure 3B**). It was evident this was an active transport process, as the dye rapidly accumulated in the center of the organoids and was as inhibited by 200 nM zosuquidar, an inhibitor of the P-glycoprotein efflux pump, involved in multi-drug resistance. To make the apical side of the organoid epithelium more accessible for transport studies we generated 2-dimensional monolayers of polarized organoid cells that still retain their differentiated features [11] (schematic overview; **Figure 6A**). This allowed us to demonstrate the AA transport function of intestinal organoids (**Figure 6**). The individual AA's present in DMEM were transported across the intact monolayer in sufficient concentrations to be measured by TQMS (**Figure 6B**). We observed low variability in AA transport between replicates when the cell monolayers had TEER values >300 Ω/cm^2. To ensure integrity of the monolayers we used Transwell filters with *Trans*-epithelial electrical resistance (TEER) values between 750 and 850 Ω/cm^2 [32]. In addition to AA we showed that a variety of other molecules such as vitamin B5, choline, and epinephrine were transported from the apical to basolateral side. A high amount of niacinamide was measured in the basal compartment, which could be attributed to free NAD^+ [33]. Thus, polarized monolayers of small intestinal organoids provide a model for testing several compound transport mechanisms.

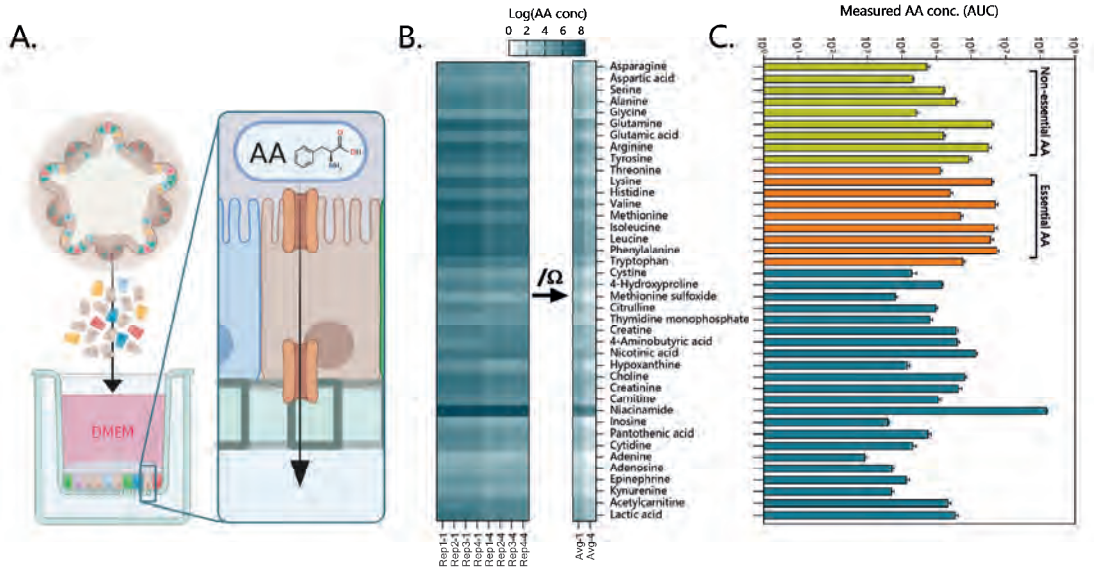

Figure 6. Functional amino acid transport assay using intestinal organoid monolayers. (A) 3-Dimensional organoids were dissociated into single cells and plated on Matrigel precoated (0.5% v/v) Transwell inserts. The monolayers were grown to confluence for 1 or 4 days and generated TEER values >750 Ω/cm2. The apical medium was replaced with DMEM and basolateral medium with HBSS. Amino acids (AA) and other molecules were measured in the basal compartment using TQMS. (B) AA concentrations (Log values) of individual amino acids and other molecules for 4 replicate Transwell inserts of ileum organoids. (C) AA concentrations in the basolateral compartment show increased transport of essential AA's (orange).

Discussion

(non-)Transformed and cancer cell lines commonly display aneuploidy and mutations affecting cellular physiology, which may further change during long-term passage. Intestinal organoids are considered an attractive alternative to cell lines, but there are no studies evaluating the variability of the transcriptome in different batches of organoids generated from the same crypts and the effect of long-term culture on genomic stability and the transcriptome.

In this study, we compared gene expression in the porcine jejunum cell line IPEC-J2, organoids derived from adult stem cells of the porcine jejunum and the intestinal tissue from which they were derived. The genes highly expressed in tissue, but not organoids or IPEC-J2, were mostly involved in immune cell, ECM or muscle contraction pathways. This is most likely due to the presence of elements of the (sub)mucosa, including lamina propria immune cells in the tissue sample. Porcine intestinal organoids possessed the different epithelial cell lineages found in tissue for at least 17 passages. An interesting observation in organoids was the high expression of *LYZ* which is often associated with Paneth cells. Until recently Paneth cells were considered to be absent in the porcine small intestine [34, 35]. Paneth cells facilitate regeneration of the intestinal mucosa after metaplasia and produce high amounts of *LYZ* in presence of intestinal disease or damage [36, 37].

The set of genes expressed in organoids closely resembled that of the tissue of origin, a characteristic reported for other types of organoids [38, 39]. Moreover, jejunum organoids expressed the majority of gene orthologs (>74%) that are specifically expressed in the human small intestine for at least 17 passages, showing that the adult stem cells retain small intestine-associated gene expression over long-term culture [12, 40]. Interestingly, fewer small intestine-specific genes were expressed in ileum-derived organoids (52%), indicating location-specific differences. We also noticed that ileum organoids expressed the fucosyltransferase-1 (FUT1) and FUT2 genes, which were absent in our jejunum organoid transcriptome. A polymorphism in these genes has been associated with decreased susceptibility to infection with specific pathogens [41], further highlighting the importance of selecting the correct tissue origin when studying specific host-pathogen interactions. Overall, the batch-to-batch variation in organoids from the same animal was low, which may have been aided by concurrent passage and consequently differentiation state. The functions of genes which significantly altered expression between organoids from different animals or different cultures suggests they arise from differences in abundance of nutrients in culture medium or replicative activity, rather than permanent loss or gain of functions.

The main described benefits of the jejunum cell line IPECJ2 are its non-cancerous origin and stability for more than 98 passages [27, 42]. However, we observed

multiple indications of increased expression of genes associated with cancer or tumors in IPEC-J2 (passage 67–91). For example, these included *ANXA1* and *CALD1* [43], as well as insertions and deletions in the tumor suppressor *APC* [31]. We conclude that porcine jejunum organoids more closely resemble jejunum tissue than IPEC-J2 and provide a robust model for gene expression studies for at least 12 weeks of culture. As such they provide an advanced model for mechanistic studies on host-microbe interactions and intestinal physiology [44]. Organoids are also likely to avoid changes in glycosylation patterns seen in cancer or (non-)transformed cell models, however, timepoints extending further than 3 months could still be investigated. Motivation not to do so in this study, was the assumption that researchers would utilize the model within the tested timeframe. The RNA-seq data provides a valuable resource for researchers to assess the suitability of intestinal organoids for studying specific pathways or biological processes, as well as providing a comprehensive transcriptional map of expressed genes in IPEC-J2, formerly mainly available from microarray studies.

Previous studies have shown that organoids express proteins involved in nutrient sensing, like fructose or glucose, as well as transport by several transporters, like GLUT5, SGLT1, or PEPT1 [45, 46]. We verified the ability of 3-dimensional organoids to transport small molecules into the lumen within a short amount of time. However, studying transport over the epithelial barrier requires apical stimulation with compounds. The spatial nature of 3-dimensional organoids prevents easy access to the apical surface but can be overcome by injection or monolayer formation. We have recently shown that apical stimulation of small intestinal organoids with various protein rich ingredients elicit specific metabolic responses, like altered lipid metabolism [47]. In that study, predicted putative pathways were verified using protein-detection assays, showing the ability to measure gene-predicted responses in organoids. Transport of AAs is an essential function of the small intestine, and by measuring individual AA concentrations in a monolayer Transwell system enabled us to identify the rate at which different AAs cross the epithelial barrier. In the future, such a model could be used to identify specific transporter genes and their activity using CRISPR-Cas9 gene editing methods or transport inhibitors [45, 48].

Pig organoids can be rapidly generated from left over slaughter material without requirement for ethical approval. Thus, they have potential to be used to identify new phenotypes and investigate the role of genetic polymorphisms in susceptibility to enteric infections or other production traits. Furthermore, porcine intestinal physiology is considered to closely resemble that of humans increasing the potential for translational *in vitro* studies. Moreover, recent progress in developing robust methods for generating 2D monolayers from 3D organoid cultures facilitates apical exposure to test substances and opens possibilities for studying epithelial transport [11, 49].

Data availability

The datasets generated for this study can be found in the Gene expression omnibus GSE146408.

Ethics statement

The animal study was reviewed by the Animal Ethics committee of Wageningen University and approved by the National Central Authority for Scientific Procedures on Animals (CCD) according to the legal and ethical requirements (No. AVD104002016515).

Supplementary material

The Supplementary Material for this article can be found online at: https://www.frontiersin.org/articles/10.3389/fcell.2020.00375/

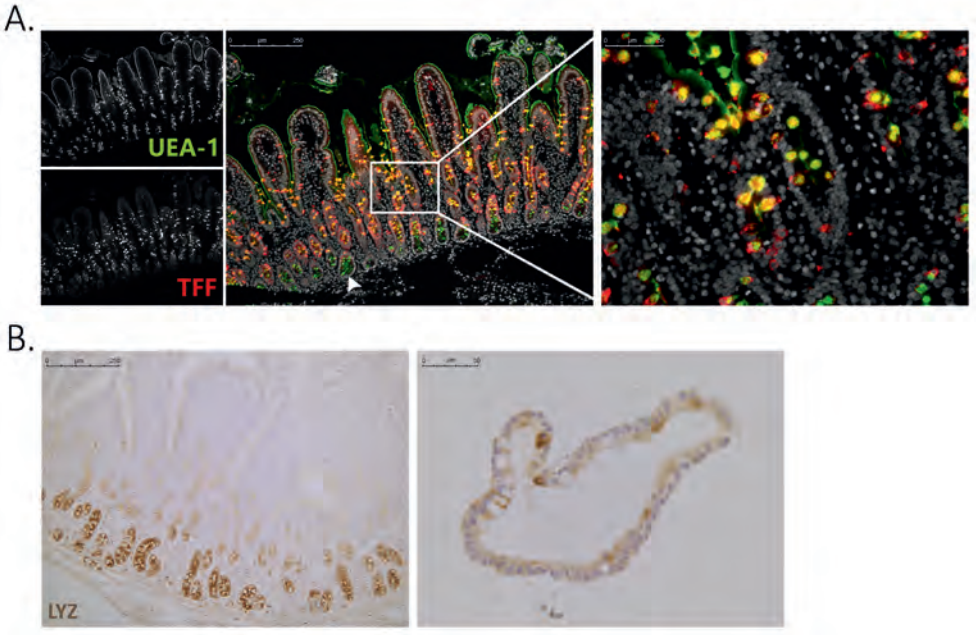

Supplementary Figure 1. Tissue and organoid staining for secretory lineages. (A) Double staining with UEA-1 (secretory cell lineage) and trefoil factor 3 (TFF3; goblet cell specific) shows overlapping staining, as well as staining deeper in the crypt. This indicates that UEA-1 stains for secretory cell lineages in the porcine small intestine (left: individual channels, middle: overlay, yellow is staining overlap, right: zoom panel of middle image. (B) Paneth cells have been identified in the porcine intestinal crypt by lysozyme staining (left), which recapitulates in their derived organoids (right).

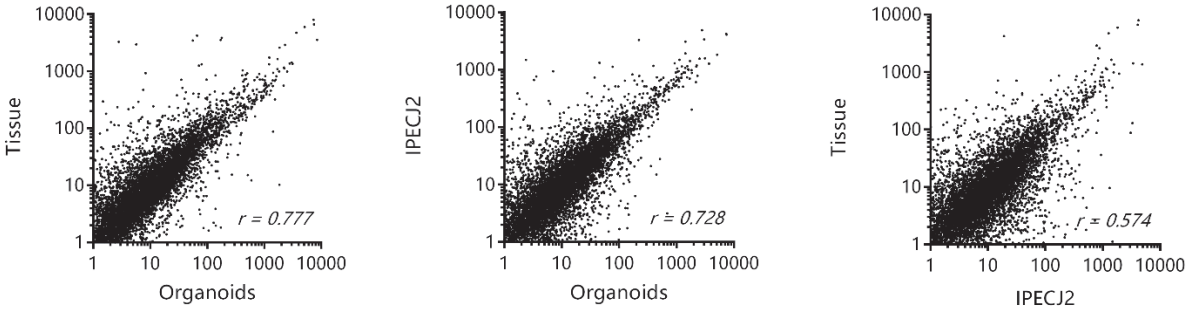

Supplementary Figure 2. Correlation plot of average FPKM per sample type. Organoids and tissue show strong correlation (r = 0.777), as well as between Organoids and IPEC-J2 (r = 0.728). The least amount of correlation was observed between Tissue and IPEC-J2 (r = 0.574)

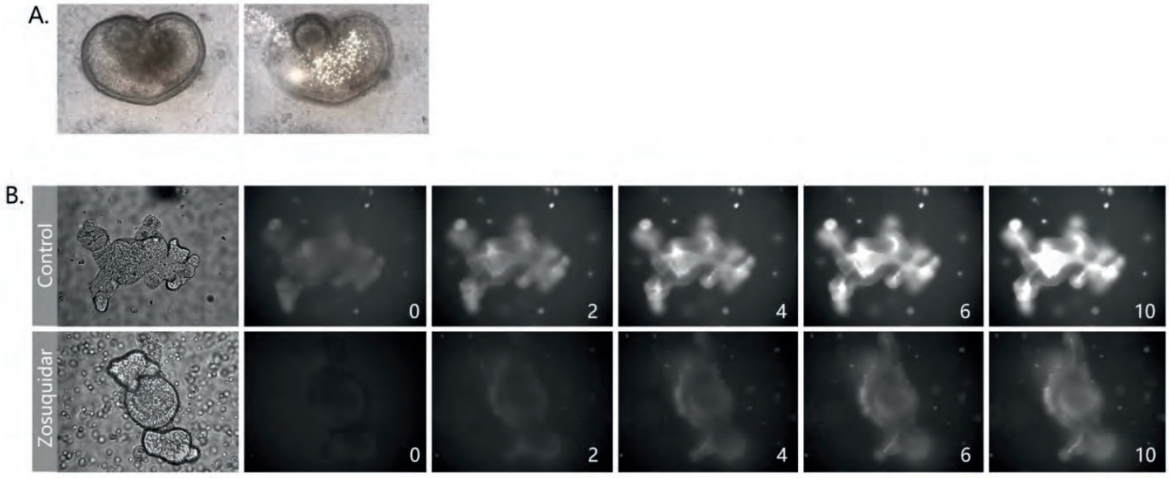

Supplementary Figure 3. Exposure of small compounds to intestinal organoids to study epithelial transport. (A) 3-dimensional organoids can be injected with compounds and substances such as GFP+ microbeads, to stimulate the luminal compartment. (B) Small compounds can be actively transported into the intestinal organoid lumen by addition of small compounds like celltracker red (CTR; control) and inhibited by using zosuquidar (200 nM) (time in minutes).

Supplementary Table 1. Summary of mapping RNA-seq data to reference genome Sus Scrofa 11.1.

	Mapped reads					
Sample	Left	Right	Overall mapping rate (%)	Pairs	Multiple alignments (%)	Concordant pair alignment (%)
Org1-3_1	2850198	2840118	98.7	2823464	2.2	98.7
Org1-3_2	2859471	2847581	98.6	2830605	2.2	97.6
Org1-3_3	2952697	2942165	98.7	2923881	2.1	97.7
Org1-12_1	3031397	3002603	97.4	2979507	2.4	96.0
Org1-12_2	2983917	2882268	98.5	2863455	2.5	97.4
Org1-12_3	2722083	2711853	98.5	2693562	2.6	97.3
Tissue 1	3030093	3019758	98.4	2998320	3.6	97.3
Org2-3_1	2728229	2717750	98.6	2700557	2.6	97.5
Org2-3_2	2705521	2696828	98.6	2679085	2.6	97.5
Org2-3_3	2697949	2732830	98.6	2671617	2.5	97.5
Org2-12_1	2228232	2222736	95.4	2208029	2.3	94.4
Org2-12_2	2252779	2245831	95.8	2231084	2.4	94.8
Org2-12_3	2359295	2333615	92.9	2315833	2.6	91.4
Tissue 2	2558842	2550033	98.4	2531447	3.3	97.2
IPEC-J2_1	3341302	3322134	98.7	3304568	1.8	96.7
IPEC-J2_2	3233204	3258153	98.1	3210559	2.0	96.8
IPEC-J2_3	2882496	2990369	94.8	2834108	2.1	91.3

References

1. van der Flier, L.G. and H. Clevers, *Stem Cells, Self-Renewal, and Differentiation in the Intestinal Epithelium.* Annual Review of Physiology, 2009. **71**: p. 241-260.
2. Wells, J.M., et al., *Epithelial crosstalk at the microbiota-mucosal interface.* Proceedings of the National Academy of Sciences of the United States of America, 2011. **108**: p. 4607-4614.
3. Bron, P.A., P. van Baarlen, and M. Kleerebezem, *Emerging molecular insights into the interaction between probiotics and the host intestinal mucosa.* Nature Reviews Microbiology, 2012. **10**(1): p. 66-U90.
4. Gillet, J.P., S. Varma, and M.M. Gottesman, *The clinical relevance of cancer cell lines.* J Natl Cancer Inst, 2013. **105**(7): p. 452-8.
5. Gisselsson, D., et al., *Clonal evolution through genetic bottlenecks and telomere attrition: Potential threats to in vitro data reproducibility.* Genes Chromosomes Cancer, 2018.
6. Liu, Y., et al., *Multi-omic measurements of heterogeneity in HeLa cells across laboratories.* Nat Biotechnol, 2019. **37**(3): p. 314-322.
7. Barker, N., et al., *Identification of stem cells in small intestine and colon by marker gene Lgr5.* Nature, 2007. **449**(7165): p. 1003-7.
8. Ootani, A., et al., *Sustained in vitro intestinal epithelial culture within a Wnt-dependent stem cell niche.* Nature Medicine, 2009. **15**(6): p. 1-U140.
9. Sato, T., et al., *Single Lgr5 stem cells build crypt-villus structures in vitro without a mesenchymal niche.* Nature, 2009. **459**(7244): p. 262-U147.
10. Moon, C., et al., *Development of a primary mouse intestinal epithelial cell monolayer culture system to evaluate factors that modulate IgA transcytosis.* Mucosal Immunology, 2014. **7**(4): p. 818-828.
11. van der Hee, B., et al., *Optimized procedures for generating an enhanced, near physiological 2D culture system from porcine intestinal organoids.* Stem Cell Research, 2018. **28**: p. 165-171.
12. Middendorp, S., et al., *Adult Stem Cells in the Small Intestine Are Intrinsically Programmed with Their Location-Specific Function.* Stem Cells, 2014. **32**(5): p. 1083-1091.
13. Sato, T., et al., *Long-term expansion of epithelial organoids from human colon, adenoma, adenocarcinoma, and Barrett's epithelium.* Gastroenterology, 2011. **141**(5): p. 1762-72.
14. Giuffra, E., C.K. Tuggle, and F.C. The, *Functional Annotation of Animal Genomes (FAANG): Current Achievements and Roadmap.* Annu Rev Anim Biosci, 2018.
15. Andrews, S. *FastQC: A quality control tool for high throughput sequence data*. 2017 [cited v0.11.5; Available from: http://www.bioinformatics.babraham.ac.uk/projects/fastqc/.
16. Krueger, F. *Trim galore: A wrapper around Cutadapt and FastQC to consistently apply adapter and quality trimming to FastQ files*. 2017 [cited v0.4.4; Available from: https://www.bioinformatics.babraham.ac.uk/projects/trim_galore/.
17. Zerbino, D.R., et al., *Ensembl 2018.* Nucleic Acids Res, 2018. **46**(D1): p. D754-D761.
18. Trapnell, C., et al., *Differential gene and transcript expression analysis of RNA-seq experiments with TopHat and Cufflinks.* Nat Protoc, 2012. **7**(3): p. 562-78.
19. Chen, J., et al., *ToppGene Suite for gene list enrichment analysis and candidate gene prioritization.* Nucleic Acids Res, 2009. **37**(Web Server issue): p. W305-11.
20. Fagerberg, L., et al., *Analysis of the human tissue-specific expression by genome-wide integration of transcriptomics and antibody-based proteomics.* Mol Cell Proteomics, 2014. **13**(2): p. 397-406.
21. Dow, L.E., et al., *Apc Restoration Promotes Cellular Differentiation and Reestablishes Crypt Homeostasis in Colorectal Cancer.* Cell, 2015. **161**(7): p. 1539-1552.
22. Loonen, L.M.P., et al., *REG3 gamma-deficient mice have altered mucus distribution and increased mucosal inflammatory responses to the microbiota and enteric pathogens in the ileum.* Mucosal Immunology, 2014. **7**(4): p. 939-947.
23. Reimand, J., et al., *g:Profiler-a web server for functional interpretation of gene lists (2016 update).* Nucleic Acids Res, 2016. **44**(W1): p. W83-9.
24. Sina, C., C. Kemper, and S. Derer, *The intestinal complement system in inflammatory bowel disease: Shaping intestinal barrier function.* Semin Immunol, 2018. **37**: p. 66-73.
25. Benis, N., et al., *High-level integration of murine intestinal transcriptomics data highlights the importance of the complement system in mucosal homeostasis.* Bmc Genomics, 2019. **20**(1).
26. Grun, D., et al., *Single-cell messenger RNA sequencing reveals rare intestinal cell types.* Nature, 2015. **525**(7568): p. 251-+.

27. Vergauwen, H., *The IPEC-J2 Cell Line*, in *The Impact of Food Bioactives on Health: in vitro and ex vivo models*, K. Verhoeckx, et al., Editors. 2015: Cham (CH). p. 125-134.
28. Berglund, L., et al., *A Genecentric Human Protein Atlas for Expression Profiles Based on Antibodies.* Molecular & Cellular Proteomics, 2008. **7**(10): p. 2019-2027.
29. Jorissen, R.N., et al., *Metastasis-Associated Gene Expression Changes Predict Poor Outcomes in Patients with Dukes Stage B and C Colorectal Cancer.* Clin Cancer Res, 2009. **15**(24): p. 7642-7651.
30. Viana, L.D., et al., *Relationship between the Expression of the Extracellular Matrix Genes SPARC, SPP1, FN1, ITGA5 and ITGAV and Clinicopathological Parameters of Tumor Progression and Colorectal Cancer Dissemination.* Oncology, 2013. **84**(2): p. 81-91.
31. Sakai, E., et al., *Combined Mutation of Apc, Kras, and Tgfbr2 Effectively Drives Metastasis of Intestinal Cancer.* Cancer Res, 2018. **78**(5): p. 1334-1346.
32. Srinivasan, B., et al., *TEER measurement techniques for in vitro barrier model systems.* J Lab Autom, 2015. **20**(2): p. 107-26.
33. Belenky, P., K.L. Bogan, and C. Brenner, *NAD+ metabolism in health and disease.* Trends Biochem Sci, 2007. **32**(1): p. 12-9.
34. Dekaney, C.M., F.W. Bazer, and L.A. Jaeger, *Mucosal morphogenesis and cytodifferentiation in fetal porcine small intestine.* Anatomical Record, 1997. **249**(4): p. 517-523.
35. Gonzalez, L.M., et al., *Cell Lineage Identification and Stem Cell Culture in a Porcine Model for the Study of Intestinal Epithelial Regeneration.* Plos One, 2013. **8**(6).
36. Brentnall, T.A., et al., *Proteins that underlie neoplastic progression of ulcerative colitis.* Proteomics Clinical Applications, 2009. **3**(11): p. 1326-1337.
37. Sarvestani, S.K., et al., *Cancer-predicting transcriptomic and epigenetic signatures revealed for ulcerative colitis in patient-derived epithelial organoids.* Oncotarget, 2018. **9**(47): p. 28717-28730.
38. Huch, M., et al., *Long-Term Culture of Genome-Stable Bipotent Stem Cells from Adult Human Liver.* Cell, 2015. **160**(1-2): p. 299-312.
39. Matano, M., et al., *Modeling colorectal cancer using CRISPR-Cas9-mediated engineering of human intestinal organoids.* Nature Medicine, 2015. **21**(3): p. 256-+.
40. Haber, A.L., et al., *A single-cell survey of the small intestinal epithelium.* Nature, 2017. **551**(7680): p. 333-+.
41. Meijerink, E., et al., *A DNA polymorphism influencing alpha(1,2)fucosyltransferase activity of the pig FUT1 enzyme determines susceptibility of small intestinal epithelium to Escherichia coli F18 adhesion.* Immunogenetics, 2000. **52**(1-2): p. 129-36.
42. Geens, M.M. and T.A. Niewold, *Optimizing culture conditions of a porcine epithelial cell line IPEC-J2 through a histological and physiological characterization.* Cytotechnology, 2011. **63**(4): p. 415-423.
43. De Marchi, T., et al., *Annexin-A1 and caldesmon are associated with resistance to tamoxifen in estrogen receptor positive recurrent breast cancer.* Oncotarget, 2016. **7**(3): p. 3098-3110.
44. Li, L., et al., *Porcine Intestinal Enteroids: a New Model for Studying Enteric Coronavirus PEDV Infection and the Host Innate Response.* J Virol, 2018.
45. Zietek, T., et al., *Intestinal organoids for assessing nutrient transport, sensing and incretin secretion.* Sci Rep, 2015. **5**: p. 16831.
46. Kishida, K., et al., *Nutrient sensing by absorptive and secretory progenies of small intestinal stem cells.* Am J Physiol Gastrointest Liver Physiol, 2017. **312**(6): p. G592-G605.
47. Kar, S.K., et al., *Effects of undigested protein-rich ingredients on polarised small intestinal organoid monolayers.* J Anim Sci Biotechnol, 2020. **11**: p. 51.
48. Schwank, G. and H. Clevers, *CRISPR/Cas9-Mediated Genome Editing of Mouse Small Intestinal Organoids.* Methods Mol Biol, 2016. **1422**: p. 3-11.
49. Wang, Y., et al., *Self-renewing Monolayer of Primary Colonic or Rectal Epithelial Cells.* Cell Mol Gastroenterol Hepatol, 2017. **4**(1): p. 165-182 e7.

Chapter 4

Microbial Regulation of Host Physiology by short-chain Fatty Acids

Bart van der Hee[1] and Jerry M. Wells[1]

[1]Host-Microbe Interactomics, Animal Sciences Group, Wageningen University, Wageningen, The Netherlands

Published chapter: van der Hee B, Wells JM (2021) Microbial Regulation of Host Physiology by Short-chain Fatty Acids. Trends in Microbiology. 29:8 special issue Regulation of Human Health by the Microbiota.
https://doi.org/10.1016/j.tim.2021.02.001

On the journal cover, volume 29, issue 8:

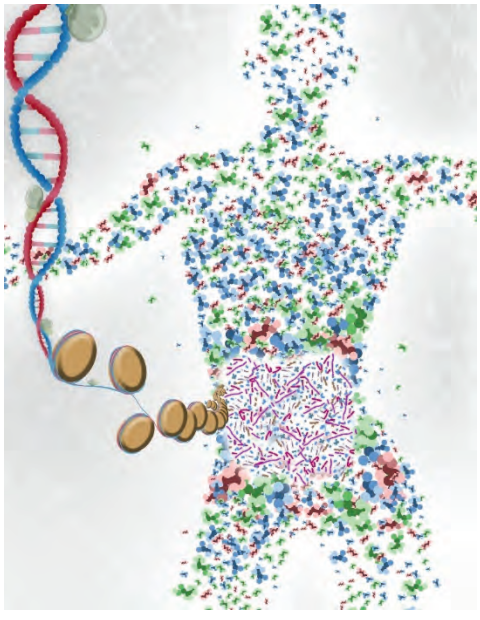

Abstract

Our ancestral diet consisted of much more nondigestible fiber than that of many societies today. Thus, from an evolutionary perspective the human genome and its physiological and nutritional requirements are not well aligned to modern dietary habits. Fiber reaching the colon is anaerobically fermented by the gut bacteria, which produce short-chain fatty acids (SCFAs) as metabolic by-products. SCFAs play a role in intestinal homeostasis, helping to explain why changes in the microbiota can contribute to the pathophysiology of human diseases. Recent research has shown that SCFAs can also have effects on tissues and organs beyond the gut, through their circulation in the blood. SCFAs not only signal through binding to cognate G-protein-coupled receptors on endocrine and immune cells in the body but also induce epigenetic changes in the genome through effects on the activity of histone acetylase and histone deacetylase enzymes. Furthermore, epigenetic imprinting likely occurs in utero, highlighting the importance of the maternal diet in early life. Here we review current understanding of how SCFAs impact on human and animal physiology and discuss the potential applications of SCFAs in the prevention and treatment of human diseases.

Highlights

Short chain fatty acids (SCFAs) contribute to intestinal homeostasis and the regulation of energy metabolism.

SCFAs circulating in the blood influence tissue-specific acetylation of histones 3 and 4 in a tissue-specific fashion.

Delivery of SCFAs to the colon, using specialized diets, prevents onset of diabetes in nonobese diabetic (NOD) mice.

During gestation, SCFAs can cause epigenetic imprinting in utero and protect against allergic airway disease.

SCFAs regulate the blood–brain barrier and neuroimmunoendocrine functions.

SCFAs Are the Main Players in the Interplay between Diet, Microbiota, and Health

SCFAs have fewer than six carbons in the aliphatic tail, and the most abundant in the intestine are acetate (C2), propionate (C3), and butyrate (C4). SCFAs are a metabolic by-product of microbial fermentation of complex polysaccharides not digested, or only partly digested, in the human small intestine. These nondigestible polysaccharides (NDPs) are found in plant cell walls and are further classified into soluble and non-soluble dietary fibers. The soluble NDPs are highly fermentable and typically generate greater quantities of SCFAs in the colon than do soluble fibers.

Currently there are three well characterized human SCFA-sensing G-protein-coupled receptors (GPCRs) which are differentially expressed on different sets of immune cells as well as epithelium and endocrine cells central to the regulation of metabolism (**Table 1**). Studies in GPCR-gene deficient mice have established the importance of SCFA signaling through these metabolite receptors in the control of inflammation and intestinal homeostasis but the functional roles of these receptors on different cell types is still not fully understood. Over the past century fiber intake by humans has decreased substantially as compared to the communities of populations eating traditional high-fiber diets [7]. This is especially the case in high-income countries where allergy, type 1 diabetes, inflammatory bowel disease (IBD), and autoimmune diseases have steadily increased over the past 60 years [8]. The importance of nondigestible fiber to health has recently been highlighted by a systematic review and meta-analyses of prospective studies and randomized controlled trials [9]. The results suggest a 15–30% decrease in all causes of cardiovascular-related mortality, type 2 diabetes, and colorectal cancer when comparing high- and low-fiber consumers [9].

SCFAs are now taking center stage as key players in the interactions with the host that impact on health and disease, especially given recent evidence for their capacity to modify the epigenome and effects on tissues and organs beyond the gut. Here we review the proposed mechanisms by which specific SCFAs may impact on host physiology and the in vivo evidence for their health benefits. Finally, we highlight the major findings and outstanding questions which will help to exploit SCFAs for the prevention and treatment of human diseases.

Table 1. Summary of Currently Recognized SCFA-binding GPCRs, Their Ligands, Associated G-protein-effector Mechanisms, and Likely Expression in Different Cell Types[a]

Receptor	Alternative	Carbons	Fatty acid	Transduction	Tissue	Cell type	Refs
GPCR41	FFAR3	C2-C5	Acetate, propionate, butyrate, formate	Gi/o, β-gastductin	Intestine, adipose tissue, spleen, immune cells, pancreas	Enteroendocrine L-cells, monocytes, neutrophils, mdDC, adipocytes,	[1]
GPCR43	FFAR2	C2-C5	Acetate, propionate, butyrate, formate, pentanoate	Gi/o, Gq, β-arrestin-2	Intestine, adipose tissue, skeletal muscle, immune cells, spleen, pancreas	Enteroendocrine L-cells, beta-cells, adipocytes, B/T-cells, myeloid cells, monocytes	[2,3]
GPCR109A	HCAR2, NIACR1	C4	Butyrate, niacin	Gi/o, β-arrestin-1	Immune cells, intestine (lumen), adipose tissue	Dendritic cells, macrophages, epithelial cells, mdDC, DC, macrophages, monocytes	[2,3]
OLFR78 (m), OR51E2 (h)	PSGR	C2-C3	Acetate, propionate	Gαs, unknown	Prostate, colon, lung	Enteroendocrine cells, prostate epithelium, airway smooth muscle cells, melanocytes	[4–6]

[a]Abbreviations: DC, dendritic cells; mdDC, monocyte-derived DC.

SCFAs – The What, the Where, and the How

Early studies in human cases of sudden death showed that SCFAs are produced in high amounts by the gut microbiota, reaching concentrations of around 13 ± 6 mmol/kg content in the terminal ileum and 80 ± 11 mmol/kg content in the descending colon [10]. In all parts of the colon acetate is at least twofold higher in concentration than propionate or butyrate. Measurements of acetate, propionate, and butyrate in the ascending colon, where most saccharolytic fermentation occurs, varies depending on the geographic origin of the cohort, but acetate typically accounts for about 60–75% of the total fecal SCFAs [11].

Nutritionally specialized bacteria in the phyla Firmicutes and Actinobacteria are considered to be important in initiating the degradation of NDPs [12]. The continued breakdown of complex carbohydrates is attributed to certain abundant species within the phylum Bacteroidetes (**Figure 1**). Acetate production is common to many bacterial groups in the phylum Bacteroidetes, one of the largest groups in the intestine [10]. Propionate is produced by a few dominant genera, including the cornerstone species *Akkermansia muciniphila* [13]. *Bacteroides vulgatus* and *Bacteroides thetaiotaomicron* are also producers of propionate through the succinate pathway [14]. *Coprococcus catus* has been reported to consume lactate and utilize the acrylate pathway for propionate production [14].

Butyrate can be synthesized through four different pathways: acetyl-CoA, glutamate, lysine, and succinate [12]. Butyrate is produced by clostridial clusters I, III, IV, XI, XIVa, XV, and XVI of obligate anaerobes, of which cluster XIVa and cluster IV bacteria, related to *Faecalibacterium prausnitzii*, are the most abundant groups in humans. Members of clostridial cluster IX are also propionate producers via the lactate pathway. Small amounts of other SCFAs are also produced in the gut, namely caproate, formate, and valerate. Valerate can be formed by elongation of propionate in the presence of methanol as an electron donor [15]. Caproate can be formed by butyrate or acetate, or directly from lactate as an electron donor [16]. However, there are metabolic links between different types of bacteria, for example acetate produced by Bacteroidetes species can be utilized by species of Firmicutes to produce butyrate.

SCFAs can be passively taken up by epithelial cells but in greater amounts by active transport via the monocarboxylate transporter 1 (MCT-1) and to a lesser extent the sodium-coupled monocarboxylate transporter 1 (SMCT-1) [17,18]. SCFAs, especially butyrate, can be metabolized by colonocytes, providing 60–70% of their energy supply [19]. The remaining SCFAs are transported out of the cell across the basolateral membrane via an unknown HCO_3^- exchanger, suggested to be monocarboxylate transporter (MCT) 4 or 5 [20]. In the mucosa, SCFAs can enter the blood capillaries and reach the liver via the portal vein. The liver clears a major part of propionate and butyrate from the portal circulation, but acetate can reach 200 μM in the venous serum of humans and pigs [18,21].

The rapid absorption of SCFAs, and their metabolism by intestinal epithelium and liver, means that they can make a substantial contribution to the caloric requirements of humans and other animals. In herbivorous ruminants, about 70% of the caloric requirement comes from SCFAs, and about 10% in omnivorous humans and pigs [23]. In patients with short-bowel syndrome (SBS), who lack a functional small intestine, NDPs have been used as a dietary strategy to overcome malabsorption

because the SCFAs produced by bacterial fermentation in the colon can provide up to 1000 kcal per day [24,25]. SCFAs are also important for stimulating sodium and water absorption in the colon through the regulation of nutrient and ion transporters which can also help against diarrhea associated with SBS [26].

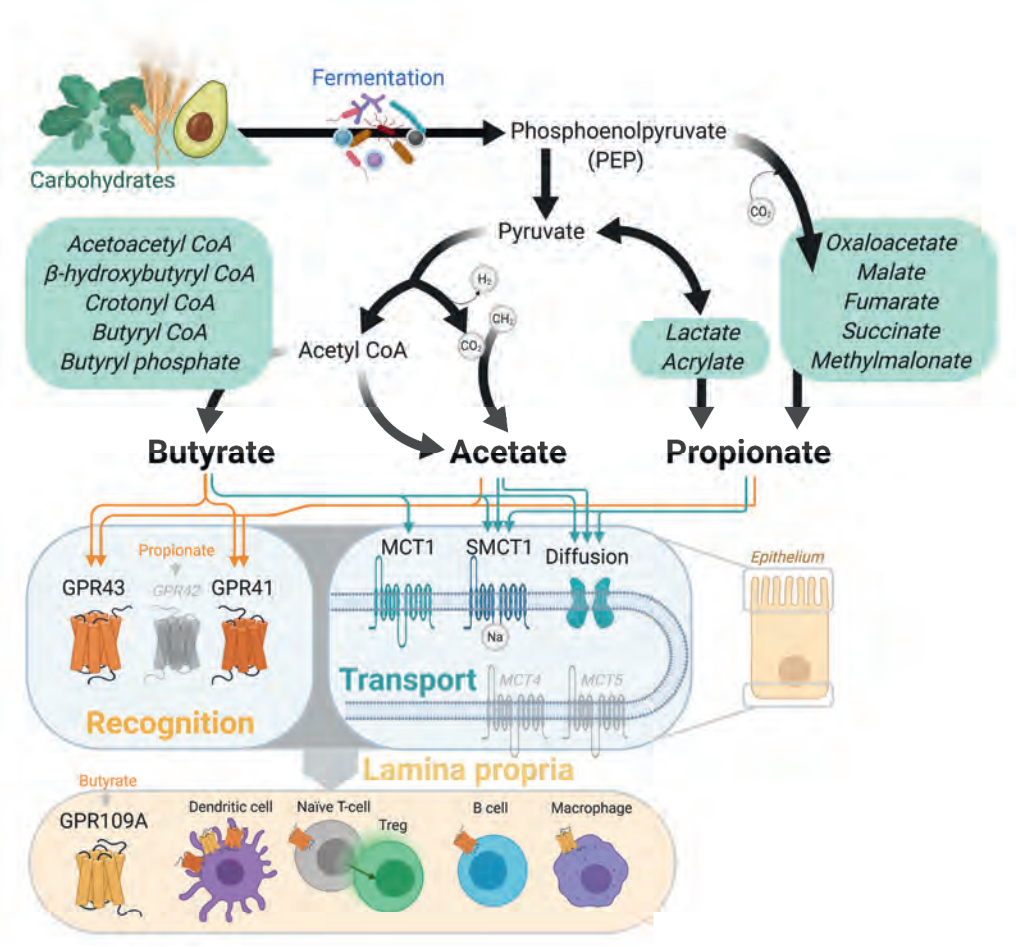

Figure 1. Gut Bacterial Pathways for Acetate, Propionate, and Butyrate Production by Fermentation of Nondigestible Fibers. Transporters MCT1 and SMCT1 take up short-chain fatty acids (SCFAs) from the lumen, and basolateral MCT4 and MCT5 are proposed to transport SCFAs out of the cell (light gray). SCFA receptors GPCR43 and 41 are expressed on intestinal epithelial cells and specific immune cells in the lamina propria and mucosal lymphoid tissue as indicated. GPCR42 (light gray) was a suspected pseudogene but was recently reclassified as a functioning gene, exhibiting sequence and copy number polymorphisms [22]. The figure was created using BioRender software. Abbreviation: Treg, T regulatory cell.

SCFA Signaling through Host GPCRs

Many common dietary metabolites are sensed by host GPCRs as a mechanism for the host to optimize responses and for survival with limiting nutrients (Figure 1 and Table 1). The same holds true for SCFAs which signal through three main GPCRs (Table 1). SCFA signaling through GPCRs on enteroendocrine cells, pancreatic cells and adipocytes plays an important role in the regulation of host metabolism [27–29] – for example, via butyrate- and propionate-stimulated secretion of glucagon-like peptide 1 (GLP-1) and the appetite-regulating hormone PYY in intestinal enteroendocrine cells [30–32]. Enteroendocrine cells also release GLP-2 in response to parenteral nutrition with butyrate, increasing plasma concentrations of GLP-2 [26,33]. GLP-2 increases the surface area of epithelial in the small intestinal by enhancing proliferation and inhibiting apoptosis in both humans and piglets [26,34]. GLP-2 also upregulates expression of the transporters for glucose, dipeptides, and amino acids in intestinal epithelial cells [35]. These effects of SCFAs most likely explain the intestinal enteropathy associated with starvation and the beneficial effects of prebiotic fiber on intestinal function.

GPCRs binding SCFAs are also expressed on intestinal enterocytes and other cell types in organs and tissues such as the liver, muscle, enteric neurons, and in immune cells – indicating the breadth of their potential interactions throughout the body [36,37]. GPCR41 is highly expressed on sympathetic neuronal ganglia – in particular, the superior cervical ganglion (SCG) which controls energy expenditure via neural and hormonal effects on glucose and fat metabolism. GPCR41 is most abundantly expressed on the SCG during embryonic (E13.5 and E15.5) and postnatal (P1) stages but also in the sympathetic nervous system (SNS) of adult mice and humans [38]. GPCR41$^{-/-}$ mice have no growth differences to wild-type (WT) mice or abnormalities in metabolic parameters and hormones, but during development the SCG volume is significantly smaller than it is in WT mice, indicating that GPCR41 may be involved in sympathetic nerve growth [38]. These authors found that propionate promotes GPCR41-mediated SNS activation whereas β-hydroxybutyrate, a major ketone body produced during starvation, depresses activation of sympathetic neuronal ganglia. These findings indicate that SCFAs and ketone bodies control energy balance by directly regulating GPCR41-mediated sympathetic activation.

Fatty acid signaling through GPCRs expressed on immune cells is also important in immune regulation. GPCR43-deficient mice have exacerbated or unresolving inflammation in experimentally induced models of colitis, arthritis, and asthma [39]. GRPR41 but not GRP43, was also shown to be necessary for the protective effect of propionate in an induced allergic airway disease mouse model [40]. In the colon mucosa, vitamin B3 or butyrate binding to GPCR109A on antigen-presenting cells (APCs) induces an anti-inflammatory expression program in colonic APCs, which, in

turn, induces differentiation of interleukin-10 (IL-10)-producing T regulatory cells (Tregs) [41].

SCFAs Modify the Host Epigenome

The epigenome describes the modifications to the genome that do not affect the DNA sequence but lead to altered gene expression. Epigenetic modifications include DNA methylation and histone modification which alter how the DNA is packaged into chromatin (**Box Figure 1**) [42,43].

Butyrate is often described as an inhibitor of histone deacetylase (HDAC) activity (Box 1) based on a report describing the accumulation of acetylated histones in butyrate-treated cancer cells [44]. Due to the Warburg effect, cancer cells undergo a metabolic shift to primarily aerobic glycolysis. Under these conditions, butyrate and propionate accumulate, resulting in decreased HDAC activity and altered histone acetylation. However, if cancer cells are grown in low glucose concentrations, then oxidative metabolism is increased, butyrate or propionate are oxidized to acetyl-CoA, and histone acetylation is not affected [45]. Thus, the epigenetic effects of butyrate exposure are strongly dependent on glucose metabolism and need to be considered when extrapolating results obtained in intestinal cancer cell lines to normal intestinal cells in vivo [45]. Indeed, many of the described effects of SCFAs on the epithelial barrier and integrity were performed in vitro using cancer or immortal intestinal cell lines (reviewed in [11,46]).

A role for SCFAs in histone modification of tissues in the body was definitively shown by the dietary supplementation of germ-free (GF) mice with microbially produced acetate, propionate, and butyrate. These SCFAs increased the acetylation of histone H4 and H3 in a tissue-specific fashion [47]. Moreover, this recapitulated much of the changes observed in chromatin states and gene expression due to microbial colonization, although the magnitude of the effects was less than in conventionally colonized mice [47]. Acetyl-CoA, an essential cofactor for histone acetyltransferase (HAT) enzymes, can be converted from acetate or formed from the oxidation of propionate or butyrate. An increase in the intracellular pool of acetyl-CoA can increase HAT activity. Additionally, butyrate is reported to inhibit histone deacetylases [48] potentially by binding to the Zn^{2+} in the catalytic site [49].

Butyrate-producing *Clostridium* promotes Treg Development in the Colon

Tregs expressing Foxp3 play an important role in regulating inflammation in the mucosa and were shown to be induced by colonization of the intestine by microbiota. GF mice have substantially lower numbers of Tregs in the colon mucosa, but this could be reversed by oral administration of the spore-forming component of the colonic bacteria, and in particular the spore-forming clusters IV and XIVa of the genus *Clostridium* [50,51]. The mechanism was linked to increased secretion of latent TGF-β by epithelial cells exposed to butyrate as well as upregulation of membrane metalloproteases involved in maturation of TGF-β. Treg induction was also shown to be independent of mucosal lymphoid tissue, suggesting that Treg differentiation from naïve T cells occurs in the lamina propria of the colonic mucosa [33]. Later, Furusawa et al. [51] showed that administration of 0.1 mM butyrate to peripheral naïve $CD4^+$ T cells promoted histone H3 acetylation of the Foxp3 gene promoter and intronic enhancers conserved in the noncoding region. These results were consistent with the earlier finding that in vivo administration of the HDAC inhibitor trichostatin A (TSA) leads to expansion of $Foxp3^+$ Tregs, increased suppressive activity of Tregs, and attenuation of colitis in mice [52]. More recently, Smith et al. showed that exposure of colonic Tregs to propionate induces a GPCR43-dependent decrease in expression of HDAC6 and HDAC9 [53]. Although Treg cells express multiple HDACs, HDAC9 is particularly important in regulating Foxp3-dependent suppression [52]. Moreover, butyrate exposure increases acetylation of several lysine residues in the forkhead domain of Foxp3 transcription factor that appear to be directly involved in optimal Treg function [54].

Box 1. Post-translational Modifications in the Histone Tails Enable Epigenetic Regulation

Chromatin comprises nucleosomes in which the DNA is wound around a central histone H3/H4 tetramer sandwiched between two histone H2A/H2B dimers. Adjacent nucleosomes are joined by a stretch of free linker DNA [92]. Further compaction is possible through the linking interaction of histone 1 proteins between nucleosomes. Condensed chromatin is generally limiting access of the transcription machinery to the DNA but can undergo relaxation in response to specific cellular and environmental signals to allow for DNA replication and transcription [93–95] (**Figure I**).

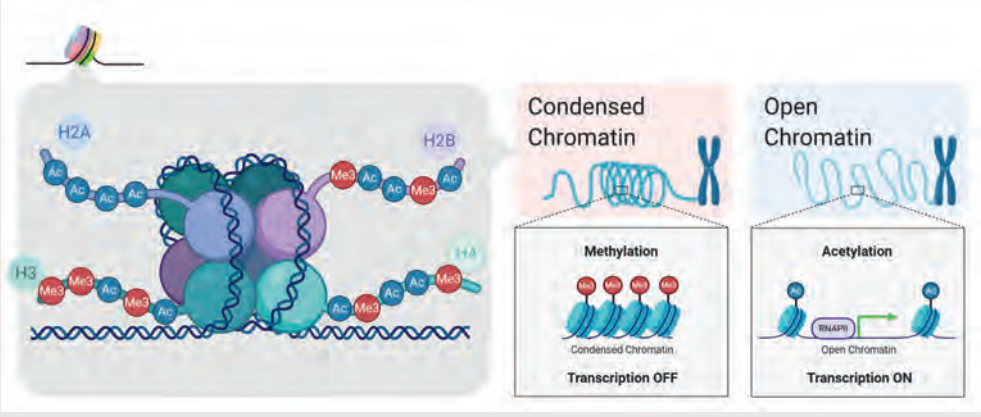

Figure I. Schematic Representation of DNA Wound Around a Central Histone H3/H4 Tetramer and Two Histone H2A/H2B Dimers. The accessible regions of histones that undergo post-translational modifications, such as acetylation and methylation, are depicted. The other panels depict the consequences of condensed or more open chromatic structures for gene transcription.

The accessible regions of histones, called histone tails, protrude from the nucleosome and undergo post-translational modifications (PTMs) such as acetylation, methylation, ubiquitination, and other modifications generating what is commonly referred to as 'the histone code'. The PTMs determine whether the chromatin is repressing or activating transcription. Acetylation of histone tails is carried out by histone acetyltransferase (HATs [43]) and reversed by histone deacetylases (HDACs). Acetylation of histone tails causes relaxation of chromatin through disruption of the DNA histone interaction, potentially activating transcription [96,97]. Conversely, removal of the acetyl groups by HDACs is considered to promote stronger histone–DNA associations. There are 18 known HDACs that are classified into four groups based on homologies and location. HDACs have also been shown to deacetylate more than 50 transcription factors and nonhistone targets, greatly extending their regulatory functions [98–100].

SCFAs Promote Intestinal Homeostasis

Butyrate and niacin signaling through receptor GPCR109a has been shown to confer anti-inflammatory properties in colonic macrophages and dendritic cells (DCs) [41], which are important for intestinal homeostasis [55]. In another study, using human monocyte-derived DCs, both butyrate and propionate strongly downregulated cytokine and chemokine gene expression in both immature and mature human monocyte-derived DCs, whereas only minor effects were seen with acetate [56]. In some studies, the anti-inflammatory effects of butyrate and propionate on macrophages and DCs were shown to be independent of GPCR receptors and or phenotypically reproduced by a pharmacological HDAC inhibitor [54,57].

Recently, butyrate – but not propionate or acetate – was shown to inhibit proliferation of stem/ progenitor cells in the intestinal crypt [58]. It was proposed that the crypt structure, gradient diffusion, and efficient metabolism of butyrate by mature enterocytes would limit its access to stem and progenitor cells near the bottom of the crypt (**Figure 2**). This may explain why colonocytes express high levels of butyrate-metabolizing enzymes compared to propionate-metabolizing enzymes. The transcription factor involved in inhibition of cell proliferation was identified as FoxO3, which regulates several key cell-cycle genes [58]. It is not known precisely how butyrate affects FoxO3, but the acetylation of several lysine residues of FoxO3 are known to affect its regulatory activity (Figure 2). It is further suggested that butyrate induces rapid differentiation processes, possibly linking intestinal crypt morphological development to stem cell protection [58,59].

Butyrate further affects intestinal barrier function by physiologic hypoxia restoration through hypoxia-inducible factor (HIF) depleting local O_2 concentrations, as well as a direct increase in the tight-junction-related proteins occludin and zonula occludens, and also downregulation of claudins 1 and 2 [60]. Several studies have reported that SCFAs increase the production of antimicrobial peptides (AMPs) by epithelial cells from pigs, rabbits, and humans [61,62]. In a clinical trial, cathelicidin (LL-37) was induced in human rectal epithelium of an intervention group given an enema containing sodium butyrate (80 mM), twice daily for 3 days compared to placebo [61]. Recently, Zhao et al. [3] identified that SCFAs regulate intestinal expression of antimicrobial REGIIIβ/γ and β-defensins through a GPCR43-dependent mechanism. Previous studies have also linked IL-22 production with activation of STAT3, indicating a relationship between antimicrobial regulation of the host microbiome through nutrient-sensing pathways [3,63], like the SCFA axis, thereby also altering the composition of the microbiological environment [3].

SCFAs Beyond the Gut

As mentioned previously, SCFAs transported across the intestine can enter the circulation and directly affect metabolism or the function of peripheral tissues. Although the liver clears a major part of SCFAs from the portal circulation, acetate reaches peripheral concentrations of 19–160 μmol/l compared with propionate (1–13 μmol/l) and butyrate (1–12 μmol/l) [65]. Recent evidence suggests that SCFAs are likely to play an important role in the etiology of several diseases, linking systemic effects with human diet and microbiota. The effects of butyrate on abundance of Tregs in the colon mucosa [63,64] and intestinal homeostasis are considered to be beneficial in several chronic diseases, including IBD [66]. Some major areas of therapeutic interest are outlined in more detail in the following text, and current knowledge of the effects of SCFAs on other organs and tissues, besides the gut, and also the developing fetus in utero, are summarized in **Figure 3**.

Type 1 Diabetes Mellitus

Genetic susceptibility plays a role in type 1 diabetes mellitus (T1D) but, as with other autoimmune and allergic diseases, there is compelling evidence of a role for environmental factors in the etiology of the disease [67]. Feeding specialized diets in the form of acetylated or butylated resistant starches, which release large amounts of the acetate or butyrate in the colon after bacterial fermentation, prevented onset of diabetes in nonobese diabetic (NOD) mice [68]. These results suggest that high-fiber diets and the microbiota might function cooperatively to reduce the risk of T1D in susceptible individuals. Interestingly, a combined acetate- and butyrate-yielding diet provided complete protection, which suggested that these SCFAs contribute to protection through distinct mechanisms [68]. The acetate-yielding diet alone altered the composition of B cell subsets in the spleen, whereas both diets decreased the frequency of autoreactive T cells in lymphoid tissues and reduced the expression of CD86 in IL-12-producing mature marginal-zone B cells, a subset implicated in the pathology of autoimmune disease [69]. In agreement with previous studies (discussed previously for the periphery) the butyrate-yielding diet increased the number and function of Tregs. The protection from diabetes provided by SCFAs probably also involves the engagement of metabolite-sensing GPCRs, such as GPCR43, on enteroendocrine-producing cells and pancreatic beta cells which play important roles in glucose tolerance [70].

Asthma

Recently, acetate administered in the drinking water to pregnant mice only during gestation was shown to protect the offspring in utero from induced allergic airway disease [71]. The mechanism of protection was linked to increased acetylation at the Foxp3 promoter and higher numbers of Tregs in the lung for at least 16 weeks after

birth. Addition of acetate to the drinking water strongly decreased expression of three genes in the fetal lung (Nppa, Ankrd1, and Pln). This was most likely mediated by acetylation of Foxp3 in the lung epithelial cells, which was bound in higher amounts to the Nppa promoter of fetuses from pregnant mice supplemented with acetate than in the control mice. Acetate still protected against allergic airway disease in GPCR43$^{-/-}$ mice, but a role for GPCR41, which also binds acetate, cannot be ruled out [72].

There is also indirect evidence that the effect of acetate on immune regulation in the lung can be translated to humans. SCFAs were measured in a cohort of pregnant women, and data were collected on visits to the general practitioner for infant cough or wheeze in the first year. Strikingly higher levels of serum acetate, but not propionate or butyrate, were significantly associated with fewer respiratory problems in the infants [71].

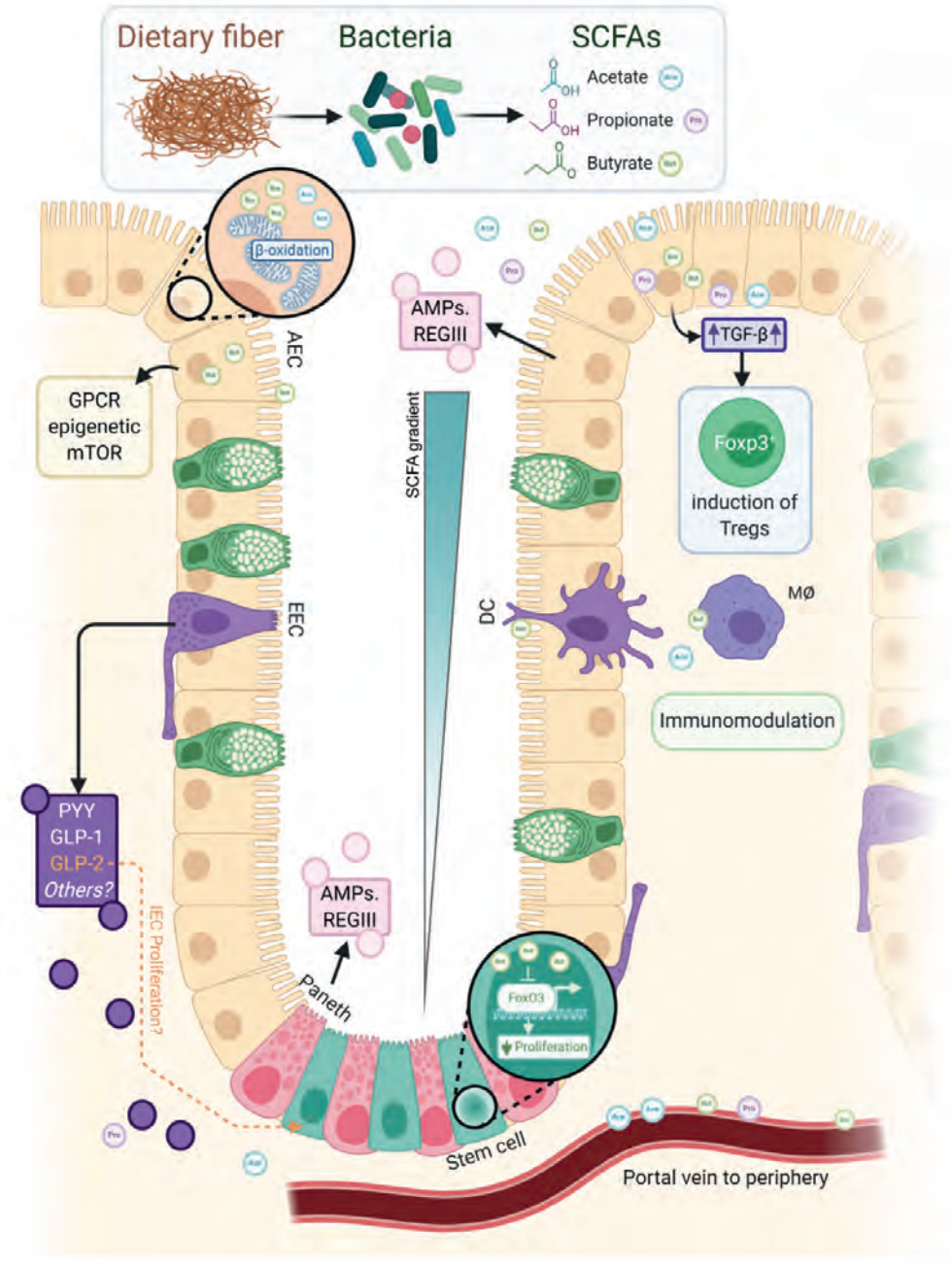

Figure 2. Interactions of Short-chain Fatty Acids (SCFAs) with the Colonic Epithelium by Binding to G-protein coupled Receptors (GPCRs), mTor-signaling, or Epigenetic Mechanisms. Butyrate can be metabolized by mature enterocytes via anaerobic β-oxidation providing an energy supply. This has been proposed as an evolutionary adaptation to reduce the concentration of butyrate in the intestinal crypt where it can inhibit proliferation of stem/progenitor cells [61]. Inhibition of stem cell replication is mediated through FoxO3, a transcription factor involved in inhibition of cell proliferation,

which is regulated by acetylation [61]. Butyrate induces expression of antimicrobial peptides (AMPs) and TGF-β in enterocytes [50,53]. Activated TGF-β promotes the development of inducible IL-10-producing T regulatory cells (Tregs) in the colon, which are important in controlling proliferation of effector T cells and suppressing inflammatory responses. Butyrate induces anti-inflammatory properties in colonic macrophages and dendritic cells (DCs) via GPCR109a [41,56,57]. In enteroendocrine cells, butyrate induces the release of appetite-regulating hormone PYY and glucagon-like peptide 1 (GLP-1) which can enter blood vessels and decrease blood glucose levels by stimulating the production of insulin [31,32]. Additionally, release of GLP2 induces crypt cell proliferation and inhibition of apoptosis, resulting in an increase in villous height and in the expansion of the absorptive mucosal surface in the small and large intestine [64].

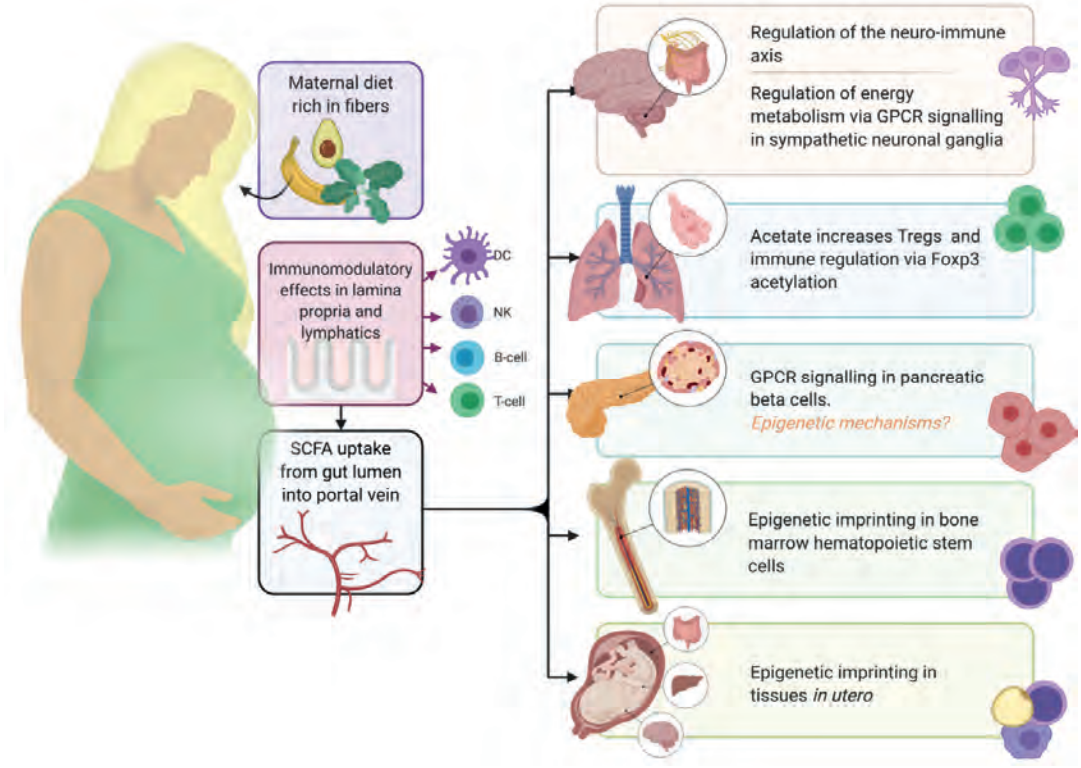

Figure 3. Effects of Short-chain Fatty Acids (SCFAs) on Organs and Tissues beyond the Gut, Including the Developing Fetus. Diets rich in nondigestible fiber increase microbial fermentation and the production of SCFAs in the colon, which promotes mucosal homeostasis through direct effects on intestinal epithelial cells and immune cells in the lamina propria (Figure 2). Hormones and transported SCFAs enter the blood vessels and, finally, the portal vein. Via the vascular system, SCFAs can influence energy homeostasis, endocrine and immune functions in different issues via G-protein-coupled receptor (GPCR)-dependent signaling, and epigenetic mechanisms, impacting on health and resilience to disease. SCFAs can also be found in the brain and cerebrospinal fluid (CSF) where they might influence growth and differentiation of neurones and synapses and inflammatory responses of brain glial cells.

Influence of SCFAs on the Blood–Brain Barrier and Neuro-immunoendocrine Function

There is growing interest in the role of the microbiota in the interconnected gut–brain axis, and here, SCFAs have already been implicated in the regulation of neuroimmune and neuroendocrine function [73]. The intestinal mucosa is innervated with a network of neurons regulating digestive processes that are influenced by secreted immune effector molecules [74]. The inner submucosal plexus, which is closer to the intestinal lumen, mainly innervates the mucosa and the muscularis mucosae and plays a sensory role, for example, in regulating blood flow in the intestine and epithelial functions. Thus, SCFAs transported across the gut could have direct roles on the activity of neurons, such as the vagal afferent nerves which play a key role in satiety, stress response, and mood (reviewed in [73]). Recently, oral supplementation of mice with acetate, propionate, and butyrate in the drinking water for 1 week gave protection from the subsequent effects of chronic psychosocial stress [75].

SCFAs entering into blood vessels can also be transported across the blood–brain barrier (BBB) into brain and CSF [76,77]. This might directly influence levels of neurotrophic factors that regulate growth and differentiation of neurons and synapses in the brain. Although the mechanisms remain unclear, SCFAs have already been shown to modulate learning and memory in a range of brain disorders [78–80] and to regulate neuropeptides that favor appetite suppression [14]. In addition, SCFAs play a role in the permeability of the BBB. The BBB of GF mice is more permeable to small molecules than is the case with conventional mice, and their recolonization with a complex microbiota or SCFA-producing bacteria restores the BBB integrity [81].

Antiviral Immunity

Another aspect of immunity which appears to be regulated by microbial SCFAs concerns the priming and function of natural killer (NK) cells in the tissues. Ganal et al. [82] compared nonmucosal-associated mononuclear phagocytes in GF and conventionally housed mice and revealed increased acetylation at the transcription start sites of proinflammatory genes such as interleukin 6 (IL-6) and interferon-beta-1 (Ifnb1) in conventional specific-pathogen-free (SPF) mice. These epigenomic modifications were associated with increased expression of IL-6 and IFN-1 in mononuclear phagocytes in response to microbial ligands and viral infection. Increased expression of these cytokines led to enhanced priming of NK cells residing at non-mucosal sites and more effective antiviral immunity [82].

Metabolic Disease, Obesity, and Type 2 Diabetes Mellitus

As mentioned previously, SCFA metabolism by the host can increase energy harvest from the diet – which might contribute to obesity depending on the total caloric intake. By contrast, several studies in rodents have shown that SCFAs can protect against obesity by increasing energy expenditure and appetite control (reviewed in [65]). Propionate can influence control of body weight via sympathetic nervous system activity, as mentioned previously [38]. Additionally, SCFAs decrease expression of PPARγ, resulting in increased oxidative metabolism in the liver and adipose tissue as well as reduced body fat accumulation, hepatic steatosis, and increased insulin sensitivity [83]. Results from a recent randomized clinical trial in type 2 diabetic patients indicated that SCFAs may be a promising strategy to treat pancreatic dysfunction in early-stage type I and type 2 diabetes in humans [84].

Based on studies in rodents, SCFAs are considered to have a beneficial rather than detrimental effect on host metabolism. However, there are conflicting results on the beneficial effects of SCFAs on glucose homeostasis in humans, and further well controlled long-term intervention studies are needed to confirm the beneficial role of SCFAs in metabolic disease [65].

New-generation Probiotics for Increasing SCFA Production

Numerous studies on the fecal microbiota of IBD patients report a decreased abundance of the Clostridium clusters IV and XIVa, which includes butyrate-producers such as *Faecalibacterium prausnitzii* and *Roseburia intestinalis* [85]. Given the relatively high abundance of *F. prausnitzii* in the fecal microbiota of healthy adults and the role of butyrate in intestinal homeostasis (discussed previously) there is much interest in using this human commensal as one of a new generation of probiotics for prevention and treatment of inflammatory diseases linked to the gut [86]. Moreover, the beneficial effects of *F. prausnitzii* may not be limited to butyrate production [86–88]. Similarly, administration of butyrate-producing *Clostridium tyrobutyricum* was shown to attenuate colitis in mice [89]. Additionally, *Clostridium butyricum* was demonstrated to have antidiabetic effects in mice [90] and neuroprotective effects in a mouse model of vascular dementia [80]. In the future we can expect more reports of interventions using prebiotics and probiotics to modulate gut microbiota to increase SCFA production and treat disease.

Concluding Remarks and Future Perspectives

Increasing evidence supports the notion that reduced intake of NDPs and production SCFAs by microbial fermentation in the colon lies behind the increasing incidence of diseases which have been steadily increasing in high-income countries over the past 50 years. However, the key to fully exploiting the opportunities for using SCFAs in disease prevention and treatment requires a better understanding of the mechanisms by which SCFAs exert their effects in the gut and other tissues and organs in the body. Furthermore, most research to date has focused on butyrate but, unlike acetate and propionate, it is typically present in undetectable or very low concentrations in the body. SCFAs appear to influence health through three principal mechanisms: (i) altering levels of HAT and HDAC activity, (ii) signaling by specific fatty acid sensing GPCRs, and (iii) anti-inflammatory mechanisms in the periphery and tissues due to the first two mechanisms. Unraveling the precise mechanisms by which SCFAs promote intestinal homeostasis, and protect from or ameliorate diseases, is further complicated by potentially broad effects of SCFAs on GPCR signaling, as well as epigenomic modifications. Moreover, we currently know little about the effects of SCFAs on the HAT- and HDAC-mediated post-translational modification of transcription factors, and how this alters their function, activity, and stability (see **Outstanding Questions**). The development of new tissue specific GPCR41 and/or GPCR43 knockout mice will help to elucidate the effects of SCFAs in the body. Studies in organoids or primary cells more closely mimicking the conditions in vivo can also give further insights into the activities of SCFAs, especially in combination with selective agonists and antagonists of SCFA-sensing receptors [91]. In the future, SCFA receptor-selective pharmacological drugs might open new possibilities for therapeutics, including applications in neurodegenerative diseases and behavior, by reinforcing BBB integrity, modulating neurotransmission, and influencing levels of neurotrophic factors.

Outstanding Questions

Can we discover selective agonists or antagonists, and produce cell-type specific knockouts of SCFA GPCRs, to elucidate the precise mechanisms by which microbially produced SCFAs impact on host physiology?

Can we devise studies on organoids, with sustained exposure to SCFAs at concentrations found in the body, to translate findings to humans and uncover the precise mechanisms?

What are the effects of circulating acetate and propionate on animal and human physiology?

How do SCFAs influence the acetylation and activity of transcription factors?

What are the effects of SCFAs on different HAT and HDAC activities in different organs and tissues?

Can we devise strategies to effectively increase SCFAs in the colon, and produce SCFA-receptor-selective pharmacological drugs, in order to explore the possibilities for disease prevention and treatment?

References

1. Brown, A.J. et al. (2003) The orphan G protein-coupled receptors GPR41 and GPR43 are activated by propionate and other short chain carboxylic acids. J. Biol. Chem. 278, 11312–11319
2. Thangaraju, M. et al. (2009) GPR109A is a G-protein-coupled receptor for the bacterial fermentation product butyrate and functions as a tumor suppressor in colon. Cancer Res. 69, 2826–2832
3. Zhao, Y. et al. (2018) GPR43 mediates microbiota metabolite SCFA regulation of antimicrobial peptide expression in intestinal epithelial cells via activation of mTOR and STAT3. Mucosal Immunol. 11, 752–762
4. Pluznick, J.L. et al. (2013) Olfactory receptor responding to gut microbiota-derived signals plays a role in renin secretion and blood pressure regulation. Proc. Natl. Acad. Sci. U. S. A. 110, 4410–4415
5. Fleischer, J. et al. (2015) Expression of odorant receptor Olfr78 in enteroendocrine cells of the colon. Cell Tissue Res. 361, 697–710
6. Aisenberg, W.H. et al. (2016) Defining an olfactory receptor function in airway smooth muscle cells. Sci. Rep. 6, 38231
7. Sonnenburg, E.D. and Sonnenburg, J.L. (2019) The ancestral and industrialized gut microbiota and implications for human health. Nat. Rev. Microbiol. 17, 383–390
8. Thorburn, A.N. et al. (2014) Diet, metabolites, and 'westernlifestyle' inflammatory diseases. Immunity 40, 833–842
9. Reynolds, A. et al. (2019) Carbohydrate quality and human health: a series of systematic reviews and meta-analyses. Lancet 393, 434–445
10. Cummings, J.H. et al. (1987) Short chain fatty acids in human large intestine, portal, hepatic and venous blood. Gut 28, 1221–1227
11. Parada Venegas, D. et al. (2019) Short chain fatty acids (SCFAs)-mediated gut epithelial and immune regulation and its relevance for inflammatory bowel diseases. Front. Immunol. 10, 277
12. Louis, P. and Flint, H.J. (2017) Formation of propionate and butyrate by the human colonic microbiota. Environ. Microbiol. 19, 29–41
13. Derrien, M. et al. (2004) Akkermansia muciniphila gen. nov., sp. nov., a human intestinal mucin-degrading bacterium. Int. J. Syst. Evol. Microbiol. 54, 1469–1476
14. Frost, G. et al. (2014) The short-chain fatty acid acetate reduces appetite via a central homeostatic mechanism. Nat. Commun. 5, 3611
15. de Smit, S.M. et al. (2019) Continuous n-valerate formation from propionate and methanol in an anaerobic chain elongation open-culture bioreactor. Biotechnol. Biofuels 12, 132
16. Zhu, X. et al. (2017) Production of high-concentration n-caproic acid from lactate through fermentation using a newly isolated Ruminococcaceae bacterium CPB6. Biotechnol. Biofuels 10, 102
17. Halestrap, A.P. and Meredith, D. (2004) The SLC16 gene family-from monocarboxylate transporters (MCTs) to aromatic amino acid transporters and beyond. Pflugers Arch. 447, 619–628
18. Sepponen, K. et al. (2007) Expression of CD147 and monocarboxylate transporters MCT1, MCT2 and MCT4 in porcine small intestine and colon. Vet. J. 174, 122–128
19. Clausen, M.R. and Mortensen, P.B. (1995) Kinetic studies on colonocyte metabolism of short chain fatty acids and glucose in ulcerative colitis. Gut 37, 684–689
20. den Besten, G. et al. (2013) The role of short-chain fatty acids in the interplay between diet, gut microbiota, and host energy metabolism. J. Lipid Res. 54, 2325–2340
21. Bloemen, J.G. et al. (2009) Short chain fatty acids exchange across the gut and liver in humans measured at surgery. Clin. Nutr. 28, 657–661
22. Puhl, H.L. et al. (2015) Human GPR42 is a transcribed multisite variant that exhibits copy number polymorphism and is functional when heterologously expressed. Sci. Rep. 5, 12880
23. Bergman, E.N. (1990) Energy contributions of volatile fatty acids from the gastrointestinal tract in various species. Physiol. Rev. 70, 567–590
24. Nordgaard, I. et al. (1996) Importance of colonic support for energy absorption as small-bowel failure proceeds. Am. J. Clin. Nutr. 64, 222–231
25. Parrish, C.R. and DiBaise, J.K. (2017) Managing the adult patient with short bowel syndrome. Gastroenterol. Hepatol. 13, 600–608

26. Tappenden, K.A. et al. (2003) Glucagon-like peptide-2 and short-chain fatty acids: a new twist to an old story. J. Nutr. 133, 3717–3720
27. Priyadarshini, M. et al. (2016) SCFA Receptors in pancreatic beta cells: novel diabetes targets? Trends Endocrinol. Metab. 27, 653–664
28. Ge, H. et al. (2008) Activation of G protein-coupled receptor 43 in adipocytes leads to inhibition of lipolysis and suppression of plasma free fatty acids. Endocrinology 149, 4519–4526
29. Gao, Z. et al. (2009) Butyrate improves insulin sensitivity and increases energy expenditure in mice. Diabetes 58, 1509–1517
30. Psichas, A. et al. (2015) The short chain fatty acid propionate stimulates GLP-1 and PYY secretion via free fatty acid receptor 2 in rodents. Int. J. Obes. 39, 424–429
31. Kaji, I. et al. (2014) Short-chain fatty acid receptor and its contribution to glucagon-like peptide-1 release. Digestion 89, 31–36
32. Chambers, E.S. et al. (2015) Effects of targeted delivery of propionate to the human colon on appetite regulation, body weight maintenance and adiposity in overweight adults. Gut 64, 1744–1754
33. Akiba, Y. et al. (2015) Short-chain fatty acid sensing in rat duodenum. J. Physiol. 593, 585–599
34. Jeppesen, P.B. (2012) Teduglutide, a novel glucagon-like peptide 2 analog, in the treatment of patients with short bowel syndrome. Ther. Adv. Gastroenterol. 5, 159–171
35. Sangild, P.T. et al. (2006) Glucagon-like peptide 2 stimulates intestinal nutrient absorption in parenterally fed newborn pigs. J. Pediatr. Gastroenterol. Nutr. 43, 160–167
36. Gelis, L. et al. (2016) Functional characterization of the odorant receptor 51E2 in human melanocytes. J. Biol. Chem. 291, 17772–17786
37. Priori, D. et al. (2015) The olfactory receptor OR51E1 is present along the gastrointestinal tract of pigs, co-localizes with enteroendocrine cells and is modulated by intestinal microbiota. PLoS One 10, e0129501
38. Kimura, I. et al. (2011) Short-chain fatty acids and ketones directly regulate sympathetic nervous system via G proteincoupled receptor 41 (GPR41). Proc. Natl. Acad. Sci. U. S. A. 108, 8030–8035
39. Maslowski, K.M. et al. (2009) Regulation of inflammatory responses by gut microbiota and chemoattractant receptor GPR43. Nature 461, 1282–1286
40. Trompette, A. et al. (2014) Gut microbiota metabolism of dietary fiber influences allergic airway disease and hematopoiesis. Nat. Med. 20, 159–166
41. Singh, N. et al. (2014) Activation of Gpr109a, receptor for niacin and the commensal metabolite butyrate, suppresses colonic inflammation and carcinogenesis. Immunity 40, 128–139
42. Lee, K.K. and Workman, J.L. (2007) Histone acetyltransferase complexes: one size doesn't fit all. Nat. Rev. Mol. Cell Biol. 8, 284–295
43. Roth, S.Y. et al. (2001) Histone acetyltransferases. Annu. Rev. Biochem. 70, 81–120
44. Riggs, M.G. et al. (1977) n-Butyrate causes histone modification in HeLa and Friend erythroleukaemia cells. Nature 268, 462–464
45. Donohoe, D.R. et al. (2012) The Warburg effect dictates the mechanism of butyrate-mediated histone acetylation and cell proliferation. Mol. Cell 48, 612–626
46. Tan, J. et al. (2014) The role of short-chain fatty acids in health and disease. Adv. Immunol. 121, 91–119
47. Krautkramer, K.A. et al. (2016) Diet-microbiota interactions mediate global epigenetic programming in multiple host tissues. Mol. Cell 64, 982–992
48. Vidali, G. et al. (1978) Butyrate suppression of histone deacetylation leads to accumulation of multiacetylated forms of histones H3 and H4 and increased DNase I sensitivity of the associated DNA sequences. Proc. Natl. Acad. Sci. U. S. A. 75, 2239–2243
49. Candido, E.P. et al. (1978) Sodium butyrate inhibits histone deacetylation in cultured cells. Cell 14, 105–113
50. Atarashi, K. et al. (2011) Induction of colonic regulatory T cells by indigenous Clostridium species. Science 331, 337–341
51. Furusawa, Y. et al. (2013) Commensal microbe-derived butyrate induces the differentiation of colonic regulatory T cells. Nature 504, 446–450
52. Tao, R. et al. (2007) Deacetylase inhibition promotes the generation and function of regulatory T cells. Nat. Med. 13, 1299–1307
53. Smith, P.M. et al. (2013) The microbial metabolites, short-chain fatty acids, regulate colonic Treg cell homeostasis. Science 341, 569–573
54. Arpaia, N. et al. (2013) Metabolites produced by commensal bacteria promote peripheral regulatory T-cell generation. Nature 504, 451–455

55. Wells, J.M. et al. (2011) Epithelial crosstalk at the microbiotamucosal interface. Proc. Natl. Acad. Sci. U. S. A. 108, 4607–4614
56. Nastasi, C. et al. (2015) The effect of short-chain fatty acids on human monocyte-derived dendritic cells. Sci. Rep. 5, 16148
57. Chang, P.V. et al. (2014) The microbial metabolite butyrate regulates intestinal macrophage function via histone deacetylase inhibition. Proc. Natl. Acad. Sci. U. S. A. 111, 2247–2252
58. Kaiko, G.E. et al. (2016) The colonic crypt protects stem cells from microbiota-derived metabolites. Cell 167, 1137
59. Sun, M. et al. (2018) Microbiota-derived short-chain fatty acids promote Th1 cell IL-10 production to maintain intestinal homeostasis. Nat. Commun. 9, 3555
60. Kelly, C.J. et al. (2015) Crosstalk between microbiota-derived short-chain fatty acids and intestinal epithelial HIF augments tissue barrier function. Cell Host Microbe 17, 662–671
61. Raqib, R. et al. (2006) Improved outcome in shigellosis associated with butyrate induction of an endogenous peptide antibiotic. Proc. Natl. Acad. Sci. U. S. A. 103, 9178–9183
62. Zeng, X. et al. (2013) Induction of porcine host defense peptide gene expression by short-chain fatty acids and their analogs. PLoS One 8, e72922
63. Sovran, B. et al. (2015) IL-22-STAT3 pathway plays a key role in the maintenance of ileal homeostasis in mice lacking secreted mucus barrier. Inflamm. Bowel Dis. 21, 531–542
64. Drucker, D.J. and Yusta, B. (2014) Physiology and pharmacology of the enteroendocrine hormone glucagon-like peptide-2. Annu. Rev. Physiol. 76, 561–583
65. Canfora, E.E. et al. (2015) Short-chain fatty acids in control of body weight and insulin sensitivity. Nat. Rev. Endocrinol. 11, 577–591
66. Parada Venegas, D. et al. (2019) Corrigendum: short chain fatty acids (SCFAs)-mediated gut epithelial and immune regulation and its relevance for inflammatory bowel diseases. Front. Immunol. 10, 1486
67. Okada, H. et al. (2010) The 'hygiene hypothesis' for autoimmune and allergic diseases: an update. Clin. Exp. Immunol. 160, 1–9
68. Marino, E. et al. (2017) Gut microbial metabolites limit the frequency of autoimmune T cells and protect against type 1 diabetes. Nat. Immunol. 18, 552–562
69. Brummel, R. et al. (2006) Higher-order CpG-DNA stimulation reveals distinct activation requirements for marginal zone and follicular B cells in lupus mice. Eur. J. Immunol. 36, 1951–1962
70. Tang, C. et al. (2015) Loss of FFA2 and FFA3 increases insulin secretion and improves glucose tolerance in type 2 diabetes. Nat. Med. 21, 173–177
71. Thorburn, A.N. et al. (2015) Evidence that asthma is a developmental origin disease influenced by maternal diet and bacterial metabolites. Nat. Commun. 6, 7320
72. Hudson, B.D. et al. (2012) Extracellular ionic locks determine variation in constitutive activity and ligand potency between species orthologs of the free fatty acid receptors FFA2 and FFA3. J. Biol. Chem. 287, 41195–41209
73. Silva, Y.P. et al. (2020) The role of short-chain fatty acids from gut microbiota in gut–brain communication. Front. Endocrinol. (Lausanne) 11, 25
74. Chesne, J. et al. (2019) Neuro-immune regulation of mucosal physiology. Mucosal Immunol. 12, 10–20
75. van de Wouw, M. et al. (2018) Short-chain fatty acids: microbial metabolites that alleviate stress-induced brain-gut axis alterations. J. Physiol. 596, 4923–4944
76. Vijay, N. and Morris, M.E. (2014) Role of monocarboxylate transporters in drug delivery to the brain. Curr. Pharm. Des. 20, 1487–1498
77. Bachmann, C. et al. (1979) Short chain fatty acids in plasma and brain: quantitative determination by gas chromatography. Clin. Chim. Acta 92, 153–159
78. Intlekofer, K.A. et al. (2013) Exercise and sodium butyrate transform a subthreshold learning event into long-term memory via a brain-derived neurotrophic factor-dependent mechanism. Neuropsychopharmacology 38, 2027–2034
79. Barichello, T. et al. (2015) Sodium butyrate prevents memory impairment by re-establishing BDNF and GDNF expression in experimental pneumococcal meningitis. Mol. Neurobiol. 52, 734–740
80. Liu, J. et al. (2015) Neuroprotective effects of Clostridium butyricum against vascular dementia in mice via metabolic butyrate. Biomed. Res. Int. 2015, 412946
81. Braniste, V. et al. (2014) The gut microbiota influences blood–brain barrier permeability in mice. Sci. Transl. Med. 6, 263ra158

82. Ganal, S.C. et al. (2012) Priming of natural killer cells by nonmucosal mononuclear phagocytes requires instructive signals from commensal microbiota. Immunity 37, 171–186
83. den Besten, G. et al. (2015) Short-chain fatty acids protect against high-fat diet-induced obesity via a PPARgammadependent switch from lipogenesis to fat oxidation. Diabetes 64, 2398–2408
84. Zhao, L. et al. (2018) Gut bacteria selectively promoted by dietary fibers alleviate type 2 diabetes. Science 359, 1151–1156
85. Miquel, S. et al. (2013) Faecalibacterium prausnitzii and human intestinal health. Curr. Opin. Microbiol. 16, 255–261
86. Martin, R. et al. (2018) Searching for the bacterial effector: the example of the multi-skilled commensal bacterium Faecalibacterium prausnitzii. Front. Microbiol. 9, 346
87. Rossi, O. et al. (2015) Faecalibacterium prausnitzii strain HTF-F and its extracellular polymeric matrix attenuate clinical parameters in DSS-induced colitis. PLoS One 10, e0123013
88. Quevrain, E. et al. (2016) Identification of an anti-inflammatory protein from Faecalibacterium prausnitzii, a commensal bacterium deficient in Crohn's disease. Gut 65, 415–425
89. Hudcovic, T. et al. (2012) Protective effect of Clostridium tyrobutyricum in acute dextran sodium sulphate-induced colitis: differential regulation of tumour necrosis factor-alpha and interleukin-18 in BALB/c and severe combined immunodefihttp://refhub.elsevier.com/S0966-842X(21)00035-4/rf0445ciency mice. Clin. Exp. Immunol. 167, 356–365
90. Jia, L. et al. (2017) Anti-diabetic effects of Clostridium butyricum CGMCC0313.1 through promoting the growth of gut butyrate-producing bacteria in type 2 diabetic mice. Sci. Rep. 7, 7046
91. Bolognini, D. et al. (2016) The pharmacology and function of receptors for short-chain fatty acids. Mol. Pharmacol. 89, 388–398
92. Felsenfeld, G. and Groudine, M. (2003) Controlling the double helix. Nature 421, 448–453
93. Grunstein, M. (1997) Histone acetylation in chromatin structure and transcription. Nature 389, 349–352
94. Arrowsmith, C.H. et al. (2012) Epigenetic protein families: a new frontier for drug discovery. Nat. Rev. Drug Discov. 11, 384–400
95. Berger, S.L. et al. (2009) An operational definition of epigenetics. Genes Dev. 23, 781–783
96. Chen, J. et al. (2001) The relation of histone acetylation/ deacetylation and DNA methylation. Sheng Li Ke Xue Jin Zhan 32, 362–364
97. Berger, S.L. (2007) The complex language of chromatin regulation during transcription. Nature 447, 407–412
98. Choudhary, C. et al. (2009) Lysine acetylation targets protein complexes and co-regulates major cellular functions. Science 325, 834–840
99. Sun, H. et al. (2013) Epigenetics of the depressed brain: role of histone acetylation and methylation. Neuropsychopharmacology 38, 124–137
100. You, S.H. et al. (2010) The interaction between nuclear receptor corepressor and histone deacetylase 3 regulates both positive and negative thyroid hormone action in vivo. Mol. Endocrinol. 24, 1359–1367

Exploring the Transcriptional Effects of Acetate and Butyrate on Gene Expression in 3D Porcine Ileal Organoid Cultures

Nuning Winaris*[1,2], Bart van der Hee*[1,3], Ellen Kranenbarg[1], Hauke Smidt[3], Jerry M. Wells[1]

[1]Host-Microbe Interactomics Group, Department of Animal Science, Wageningen University & Research, Wageningen, The Netherlands, [2]Master Program in Biomedical Sciences, Faculty of Medicine, Universitas Brawijaya, Malang, Indonesia, [3]Laboratory of Microbiology, Department of Agrotechnology and Food Sciences, Wageningen University & Research, Wageningen, The Netherlands

***These authors contributed equally**

Manuscript to be submitted

Abstract

Short-chain fatty acids (SCFAs), such as butyrate, acetate, and propionate, have been reported to reduce the risk of gastrointestinal disorders. A previous study reported that incubation of ileum organoids with bacterial culture supernatant of *Akkermansia muciniphila* and *Faecalibacterium prausnitzii* (which contained different SCFAs), as well as individual SCFAs affected the expression of metabolic cellular growth and cell survival pathways. However, these results are difficult to interpret because of the mixture of SCFAs and other metabolites present in the bacterial culture supernatants. Furthermore, the combined concentration of SCFAs used was high, and possible toxicity was not assessed. In this study we aimed to investigate the effects of non-toxic concentrations of acetate and butyrate on gene expression in 3D organoid cultures in order to gain more insight into their transcriptional effects on epithelial functions. Porcine 3D ileal organoids were exposed to non-toxic concentrations of butyrate and acetate for 5 h or buffer control, and RNA was purified for RNA sequencing. Differentially expressed genes and pathways were identified using various bioinformatic and biostatistic tools. Butyrate treatment induced the largest set of differentially expressed genes (DEG) compared to acetate. The top canonical pathways activated by acetate treatment mostly associated with cellular processes-related pathways, whereas butyrate evoked many cell-cycle related pathways. Moreover, butyrate was predicted to reduce cell proliferation through inhibition of histone deacetylase 3 (HDAC3). In contrast, the effect of acetate on histone 3 acetylation is still unclear. These results revealed that acetate and butyrate regulate different intestinal epithelial functions.

Keywords: porcine ileal organoids, transcriptomics, epithelial function

Introduction

Commensal bacteria in the gut produce short-chain fatty acids (SCFAs), such as butyrate, acetate, and propionate, which have been demonstrated to reduce the risk of gastrointestinal disorders [1, 2]. Total SCFA concentrations in the terminal ileum are estimated to be 13 ± 6 mmol/kg content but much higher in the caecum (131 ± 9 mmol/kg content) and descending colon (80 ± 11 mmol/kg content) [3, 4]. In all parts of the colon acetate was found to be at least 2-fold higher in concentration than propionate or butyrate. A study on individuals in sudden death cases revealed that in the ascending colon, where most saccharolytic fermentation occurs, the concentrations of acetate, propionate and butyrate in mmol/kg content were found to be 63.4 ± 6.8, 26.7 ± 4.0 and 24.5± 4.2 respectively [3].

SCFA can be passively taken up by epithelial cells but in greater amounts by active transport via monocarboxylate transporter 1 (MCT-1) and SMCT-1 [5]. Most butyrate is oxidized and used as fuel for colonocytes, deriving 60–70% of their energy supply from SCFA oxidation [6]. The remaining SCFA are transported out of the cell across the basolateral membrane via an unknown HCO_3^- exchanger, monocarboxylate transporter (MCT) 4 or 5 [5, 7]. Here SCFA can enter the blood vessels and circulation via the portal vein [6]. The liver clears a major part of propionate and butyrate from the portal circulation, but acetate can reach 200 μM in venous serum of humans and pigs [8].

SCFAs can also interact with G-protein-couple receptors GPR41 and GPR43 on intestinal epithelial cells, which is important for immune homeostasis in the intestine [9]. SCFAs have been reported to induce the expression of vitamin A–converting enzyme RALDH1 in intestinal epithelial cells *in vivo* and *in vitro*, which has been linked to increased numbers of intestinal regulatory T cells and a higher production of luminal IgA [10, 11]. SCFAs have also been reported to down-regulate LPS-stimulated IL-8 secretion in different intestinal cancer cell lines [10]. Butyrate has been reported to maintain and/or increase transepithelial electrical resistance (TEER) in human intestinal cell lines Caco-2 and T84, through induction of genes encoding tight-junction (TJ) components and protein reassembly regulated by transcription factors Signal Transducer and Activator of Transcription 3 (STAT3) and Specificity Protein 1 (SP1) [12-15].

Lukovac *et al.* (2014) reported that 3 hours incubation of ileum organoids with bacterial culture supernatant of *Akkermansia muciniphila* (containing 3.65 mM acetate and 7.14 mM propionate), *Faecalibacterium prausnitzii* (1.51 mM acetate, 5.51 mM formate, 7.06 mM propionate, and 8.03 mM butyrate), as well as 5 mM of individual SCFAs led to altered expression of metabolic cellular growth and cell

survival pathways [1]. These results are difficult to interpret because of the mixture of SCFAs and other metabolites present in the bacterial culture supernatants. Furthermore, the combined concentration of SCFAs is high and possible toxicity was not assessed. Recently, Kaiko et al., showed that 1 mM butyrate inhibits proliferation of intestinal stem cells and that higher concentrations 1-3 mM cause stem cell apoptosis [16].

The aim of this study was to investigate the effects of non-toxic concentrations of acetate and butyrate on gene expression in 3D organoid cultures to gain more insight into their transcriptional effects on epithelial functions. Porcine 3D ileal organoids were exposed to non-toxic concentrations of butyrate and acetate for 5 hours or buffer control, and RNA was purified for RNA sequencing. Differentially expressed genes and pathways were identified using bioinformatic and biostatistic tools.

Materials and Methods

Porcine Ileum 3D organoids culture

Ileum organoids were generated from intestinal tissue of two 5-month-old slaughter pigs, according to the procedure described by Sato and colleagues [17, 18]. Porcine ileal organoids were grown in basal culture medium that was refreshed every two days (BCM: DMEM/F12 (Gibco), supplemented with 100 µg/ml primocin (Invivogen), 10 mM HEPES (HyClone), 1 × B-27 (Gibco), 1.25 mM N-acetylcysteine (Sigma-Aldrich), 50 ng/ml human epidermal growth factor (R&D systems), 15 nM gastrin, 10 mM nicotinamide, 10 µM p38 MAPK inhibitor (Sigma-Aldrich), 600 nM TGFβ receptor inhibitor A83-01, and conditioned media for recombinant Noggin (15% v/v), Spondin (15% v/v), and Wnt3A (30% v/v) (provided by Dr Kuo and the Hubrecht Institute). Organoids were passaged by enzymatic dissociation at a 1:5 ratio every 5 days using TrypLE Express (Thermo Fisher) and plating in fresh Matrigel matrix droplets (Basement Membrane, Growth factor reduced, REF 356231, Corning).

Viability test different concentration of SCFAs

The 3-dimensional organoids were cultured in single 5 µl Matrigel droplets in 24-well plates (9 replicates per treatment) for 5 days. Organoids were stimulated for 5 hours with non-toxic concentrations of butyrate (1 mM) and acetate (2.5 mM). The Cell Proliferation Reagent WST-1 (Sigma-aldrich) was added to the well after 5 hours incubation. Absorbance was then measured using a Spectramax M5 microplate reader (Molecular Devices) at 450/690 nm.

SCFA exposure and RNA isolation from 3D organoids

Initially the potential toxicity of acetate and butyrate exposure to 3D organoids was tested using Cell Proliferation Reagent WST-1 (Sigma-aldrich) to determine which concentrations to use for the transcriptomics study. Triplicate wells containing 3D ileum organoids in Matrigel were incubated with 2.5 mM acetate, 1 mM butyrate or medium control for 5 hours at 37°C. After incubation, the medium was removed and 1 ml ice-cold DMEM/F12 was added to each well, the organoid suspension transferred to 15 ml tubes on ice (Falcon) and then centrifuged 5 min at 300 x g at 4°C to recover the organoids. The supernatant was then carefully removed, and lysis buffer (Qiagen) was added to lyse the organoids. Total RNA was extracted immediately according to the manufacturer's recommended protocol (RNEasy mini-kit, Qiagen). Total RNA concentrations were measured using a Qubit 4 Fluorometer (Invitrogen) and RNA quality (230/260 and 260/280 ratios) was checked with a DeNovix spectrophotometer.

mRNA sequencing and transcriptomic analysis

Library preparations were performed using total RNA extracted from acetate, butyrate, or medium-treated organoids and then sequenced on an Illumina sequencing system by Novogene (Hong Kong). The sequencing reads were checked for quality using CLC Genomic Workbench (QIAGEN) and FastQC [19] and mapped to the *Sus scrofa* 11.1 reference genome (Ensembl, [20], see **Supplementary Table S1**), and processed as previously described [21] for further downstream analysis.

Differentially expressed genes (DEGs) were identified using CLC with a probability (P) value < 0.05 and false discovery rate (FDR) < 0.05 for determination of significant differences. Gene ontology and pathway integration of DEGs were analysed using Ingenuity pathway analysis (IPA). To utilise the IPA database, unknown *Sus scrofa* identifiers were re-annotated to their human homologues using g:profiler [22]. A schematic diagram of this experimental setup is shown in **Figure 1.**

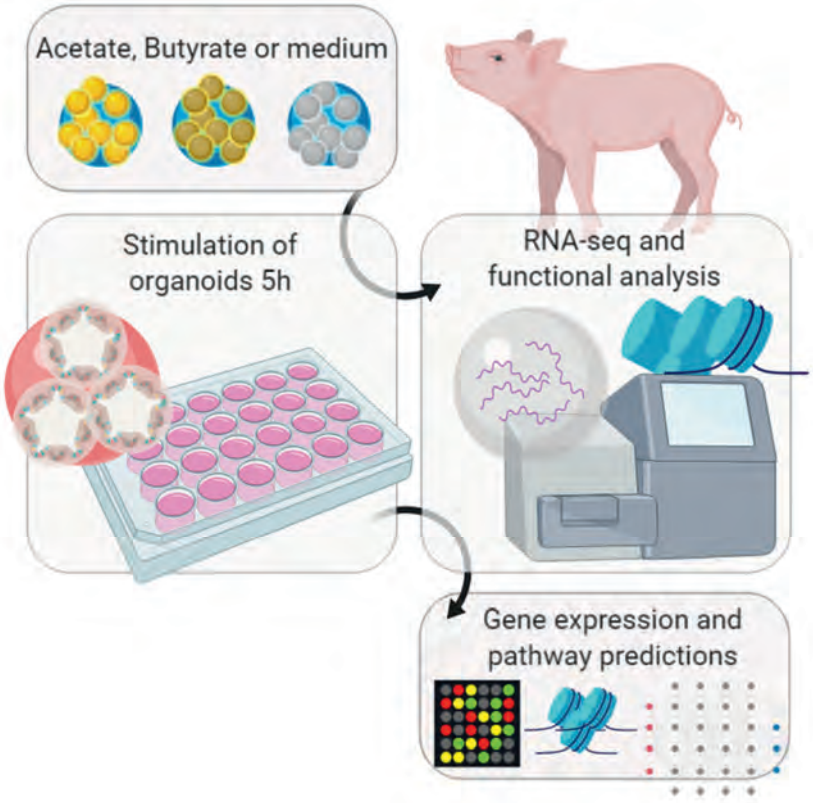

Figure 1. Schematic diagram of experimental setup. Ileum organoids were incubated with acetate, butyrate or medium control for 5 hours, followed by RNA extraction and library preparation. RNA sequencing was then performed, and the results were analysed using various bioinformatic and biostatistical tools.

Extraction and detection of histone H3 total acetylation

The same batch of 3D ileum organoid culture was also used for extraction and detection of histone H3 acetylation. Histones were extracted from organoids using a Histone Extraction Kit (ab113476, Abcam) according to manufacturer's protocol. Extracted histones were then aliquoted and stored at -80 °C for further use. Total concentrations of histone proteins were determined using the Bradford protein assay with Coomassie Protein Assay Reagent (Thermo Scientific). 2 µg protein was used for histone H3 acetylation detection with a fluorometric-based assay using Histone H3 Total Acetylation Detection Fast Kit (ab131581, Abcam).

Results and Discussion

Viability of organoids exposed to acetate and butyrate

Organoids were incubated with acetate (2.5 mM) or butyrate (1 mM) or buffer alone as a control to evaluate their potential toxicity. The viability assay measures conversion of the WST-1 dye into a coloured product by mitochondrial dehydrogenase enzymes. Microscopic examination suggested the large variability in WST-1 conversion between replicates was due to different numbers of organoids per well and thus total cell numbers. Stimulating organoids with non-toxic concentrations of SCFA did not show profound effects on the ability to convert WST-1 to formazan compared to the medium control **(Figure 2)**.

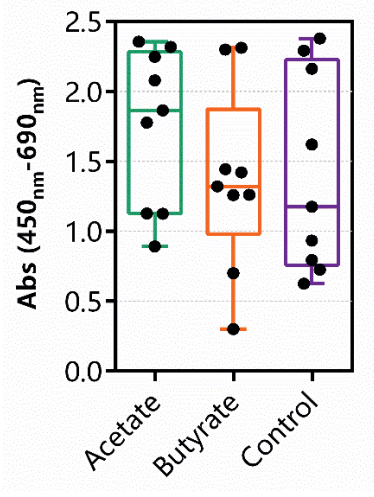

Figure 2. WST-1 assay for cell viability of 3D organoids incubated for 5 hours with 2.5 mM acetate, 1 mM butyrate or buffer control. Error bars represent Min to Max, n = 9 per group.

Differentially expressed genes induced by SCFAs acetate and butyrate

A projection scatter plot of principal component analysis (PCA) showed that organoid samples treated with acetate mainly clustered together, with one being close to the untreated (control) samples, indicating low variation between the two groups. Moreover, the close scatter of this acetate sample was also not due to major differences in the number of reads or mapping efficiency. In contrast, organoids treated with butyrate were clustered furthest away from the control and acetate group **(Figure 3A)**. An expression correlation matrix showed good correlation between replicates of the butyrate-treated organoids and replicates of the untreated

organoid samples. Higher variation was evident in expression profiles of the acetate-treated organoid samples **(Figure 3B)**. The DEGs (log2 cut off 1.5-fold change and $p < 0.05$) induced by butyrate or acetate exposure of organoids compared to untreated organoid controls are shown in Volcano plots **(Figure 3C)**. Butyrate-treatment induced the largest set of DEGs when $p < 0.05$ (9776 genes, 4841 up/4935 down), whereas acetate had significantly less DEGs (1492 genes, 661 up/831 down). DEG expression values are visualized for acetate (**Figure 3D**) and butyrate (**Figure 3E**). Both treatments had a substantial amount of DEGs in common (1173, **Figure 3F-left**), but heatmap clustering shows the same sample variability observed in the projection scatter plot for acetate (**Figure 3F-right**). Moreover, when the data was adjusted for FDR < 0.05, the amount of DEGs by butyrate slightly decreased (8989 genes, 4400 up/4589 down), whereas DEG numbers in acetate-treated organoids dropped substantially (17 genes, 13 up, down).

Ingenuity Pathway Analysis (IPA) of differentially expressed genes

IPA analysis was used to generate a list of the top canonical pathways (**Figure 4**), predicted upstream regulators, and biological functions. This is a tool which categorises genes with significantly altered expression according to their molecular and cellular functions (**Table 1**). For both acetate and butyrate, the top regulated molecular and cellular functions were Cell Death and Survival, Cellular Assembly and Organization, and Cellular Function and Maintenance (**Table 1**). Functions regulated only by butyrate were Gene Expression and Cell Cycle and those only affected by acetate were Cellular Movement and Cellular Development.

IPA listed 57 significantly regulated canonical pathways ($p < 0.05$, threshold of 1.3) because of butyrate exposure and 51 because of acetate treatment. The top pathways regulated by acetate were Sirtuin Signalling Pathway, a complex pathway involved in many cellular processes including apoptosis and inflammation, and Signalling by Rho Family GTPases, a pathway related to cell-to-cell movement (**Figure 4A**). The top canonical pathway regulated by butyrate was High Mobility Group Box 1 (*HMGB1*) Signalling Pathway. The high-mobility group box-1 (HMGB1) protein is a DNA-binding nuclear protein, present in almost all eukaryotic cells that can activate a series of signalling components, including mitogen-activated protein kinases (MAPKs) and AKT, which play an important role in proliferation and inflammation [23]. This top pathway may be linked to many other cell cycle and cancer pathways regulated by butyrate (**Figure 4B**). Cell stress related pathways such as the unfolded protein response, autophagy and Nuclear Factor Erythroid 2-related Factor 2 (NRF2)-mediated oxidative stress pathway were regulated by butyrate but not acetate.

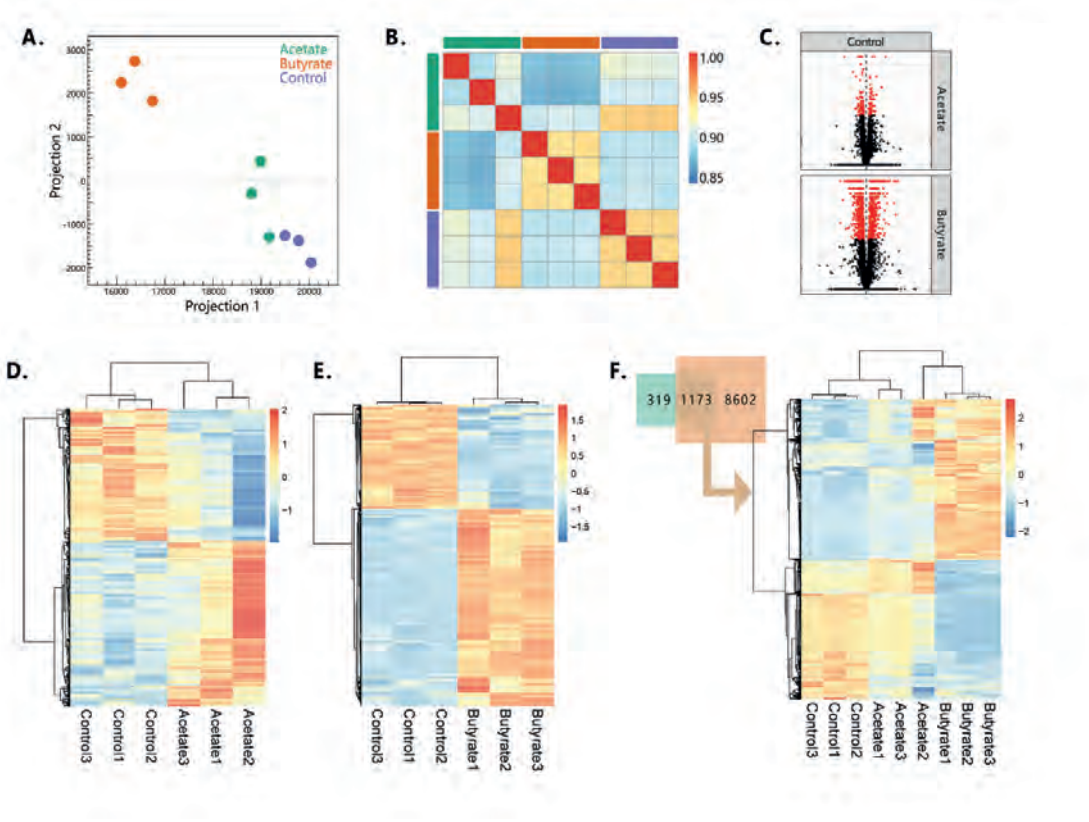

Figure 3 (A-F). Organoid transcriptome differences when treated with acetate or butyrate compared to control. (A) Projection scatter plot of principal component analysis clustering organoids treated with acetate, butyrate, or medium control. (B) Expression correlation matrix for organoids treated with acetate, butyrate, or medium control shows strong separation of butyrate, and variable expression patterns in acetate treated samples. (C) Volcano plots showing the comparison of differentially expressed genes induced by acetate and butyrate (data shown as FC (x-axis) and -Log_{10}(P-value), red color: $p < 0.05$). Heat maps showing clustering dendrograms of differentially expressed genes when treated with Acetate (D) or Butyrate (E) when p-value < 0.05. (F) All DEGs from control were compared between acetate and butyrate and showed 1173 overlapping genes and were visualized in a heatmap to show actual expression values (right).

Table 1. IPA analysis of Molecular and Cellular Functions affected by SCFA exposure.

Comparison	Molecular and Cellular Functions
Acetate vs. control	Cell Death and Survival, Cellular Movement, Cellular Assembly and Organization, Cellular Function and Maintenance, Cellular Development
Butyrate vs. control	Gene Expression, Cell Death and Survival, Cell Cycle, Cellular Assembly and Organization, Cellular Function and Maintenance

Some of the top canonical pathways were examined in more detail to give more insights into the genes induced by acetate and butyrate treatment (**Table 2-6**). Acetate was predicted to upregulate the Sirtuin signalling pathway, including 3 genes which could have epigenetic effects, namely *H1F0*, *SIRT6* and *KAT2A*. Histone H1F0 is one of the main chromatin proteins which plays an important role in organizing eukaryotic DNA into a compact structure (**Table 2 and Supplementary Figure 1**). Histone H1F0 is devoid of enzymatic activity and binds nucleosomes without apparent DNA sequence specificity leading to changes in the architecture of chromatin [24]. *SIRT6*, which was upregulated, encodes an NAD^+-dependent deacetylase of histones and regulating multiple processes including DNA stability and repair [25]. *KAT2A*, a gene encoding a lysine acetyltransferase with demonstrated activity on histone variant H2A.Z, was downregulated. Posttranslational modifications such as acetylation and ubiquitination of H2A.Z, as well as its specific binding partners, is a central player in the control of gene expression [26]. These findings could explain why acetate has such a broad effect on many different types of pathways.

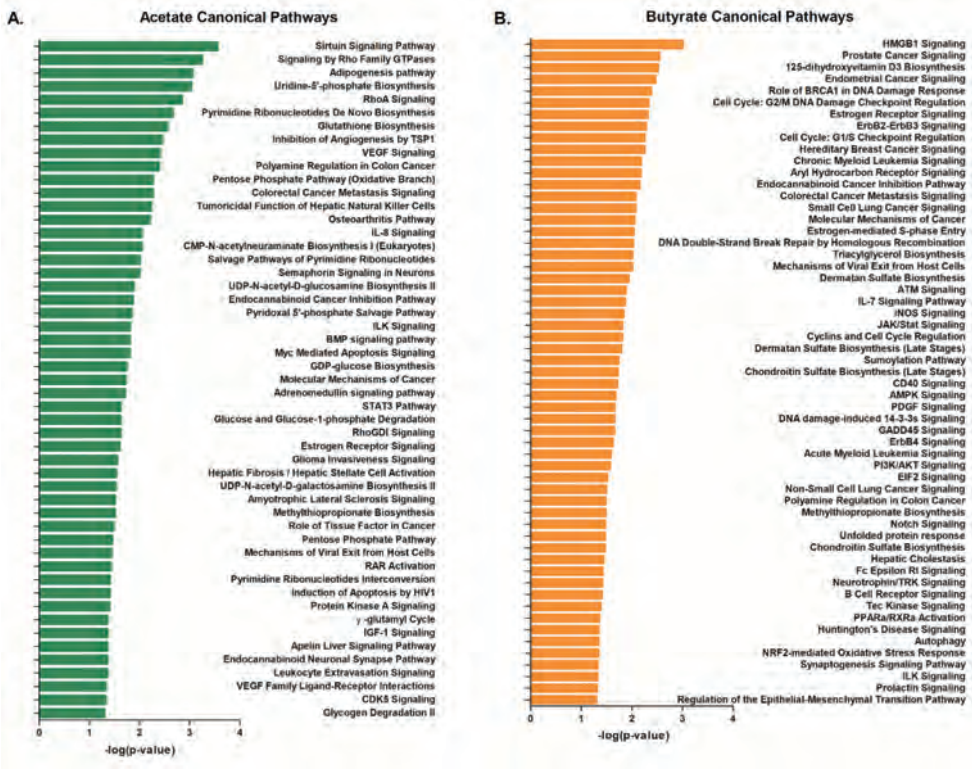

Figure 4 (A-B). Ingenuity Pathway Analysis (IPA). The top canonical pathways expressed in ileum organoids as a result of acetate and butyrate exposure for 5 hours. **(A)** Top canonical pathways activated by 2.5 mM acetate exposure. **(B)** Top canonical pathways activated by 1 mM butyrate exposure.

The second top canonical pathway, predicted to be upregulated by acetate, was the Rho Family GTPases signaling pathway in which *ACTA1* and *ACTC1*, were highly upregulated (**Table 3**). The reasons for this are not clear but may indicate remodeling of the actin cytoskeleton. Butyrate was predicted to regulate cell cycle-related pathways e.g., by downregulating cyclin genes *CCNB2* in the G2/M DNA Damage Checkpoint pathway and *CCND1* (**Table 5**) as well as *CCNE2* in the G1/S Checkpoint pathway which controls the cell cycle. Additionally, *HDAC3* which is inhibited by butyrate was upregulated. Histone deacetylase 3 (HDAC3) directly interacts with and deacetylates cyclin A in the G1/S Checkpoint pathway (**Table 6**). Given that deacetylated cyclin A promotes cell proliferation butyrate inhibition of HDAC3 deacetylation activity is predicted to reduce cell proliferation.

Several genes involved in the regulation of HMGB1 Signaling Pathway were downregulated by butyrate including *TLR4* (-2.744) that encodes an innate receptor to which HMGB1 released from cells has been reported to bind and the RELA subunit of NF-κB (-1.531). (**Table 5**). However, expression of SERPINE1, a protein regulated by nuclear HMGB1, was increased more than 16-fold. Like the histones, HMGB1 is an important chromatin protein. In the nucleus HMGB1 interacts with nucleosomes,

transcription factors, and histones, thereby organising DNA and regulating transcription [27, 28]. The presence of HMGB1 in the nucleus depends on post-translational acetylation [28]. It is therefore possible that butyrate inhibits deacetylation of HMGB1 possibly through HDAC3, increasing the concentration of HMGB1 in the nucleus and upregulating *SERPINE1*.

Expression2Kinases (X2K) was used to identify upstream regulators likely responsible for observed patterns in genome-wide gene expression induced by acetate and butyrate. The inferred networks of transcription factors, proteins and kinases predicted to regulate the expression of the inputted gene lists are indicated in **Figure 5**.

The top 10 predicted transcription factors and kinases (log2 cut off 1.5 and p-value < 0.05) that were up- or downregulated as a result of acetate and butyrate exposure are shown in **Table 7**. Implicated in the transcriptomic response to butyrate were transcription factors GATA1 and RELA which are known substrates for HDAC3. Some of the other transcription factors listed in **Table 7** may be unidentified substrates for post-translational modification enzymes identified in the acetate or butyrate induced transcriptome (such as *KAT2A*, *SIRT6* or *HDAC3*).

Table 2. Regulation of Sirtuin signaling pathway (acetate vs. control).

Symbol	Entrez Gene Name	Type(s)	Expr Fold Change
ATG3	autophagy related 3	enzyme	1.122
ATG12	autophagy related 12	other	1.119
BAX	BCL2 associated X, apoptosis regulator	transporter	1.133
EPAS1	endothelial PAS domain protein 1	transcription regulator	1.263
GABARAPL1	GABA type A receptor associated protein like 1	other	1.259
H1F0	H1 histone family member 0	other	1.24
HIF1A	hypoxia inducible factor 1 subunit alpha	transcription regulator	1.164
KAT2A	lysine acetyltransferase 2A	enzyme	-1.19
MT-ND1	NADH dehydrogenase, subunit 1 (complex I)	enzyme	-1.232
MT-ND2	MTND2	enzyme	-1.201
MYC	MYC proto-oncogene, bHLH transcription factor	transcription regulator	-1.192
NAMPT	nicotinamide phosphoribosyltransferase	cytokine	1.412
NDUFB7	NADH:ubiquinone oxidoreductase subunit B7	enzyme	-1.124
NDUFS4	NADH:ubiquinone oxidoreductase subunit S4	enzyme	1.28
NEDD4	neural precursor cell expressed, developmentally down-regulated 4, E3 ubiquitin protein ligase	enzyme	1.27
NQO1	NAD(P)H quinone dehydrogenase 1	enzyme	1.318
PCK1	phosphoenolpyruvate carboxykinase 1	kinase	1.534
PFKFB3	6-phosphofructo-2-kinasefructose-2,6-biphosphatase 3	kinase	1.378
PPARG	peroxisome proliferator activated receptor gamma	ligand-dependent nuclear recepto	1.185
SIRT6	sirtuin 6	enzyme	1.226
TIMM10	translocase of inner mitochondrial membrane 10	transporter	-1.145

Table 3. Regulation of signaling by Rho Family GTPases (acetate vs. control).

Symbol	Entrez Gene Name	Type(s)	Expr Fold Change
ACTA1	actin alpha 1, skeletal muscle	other	3.855
ACTC1	actin alpha cardiac muscle 1	enzyme	19.68
ARHGEF4	Rho guanine nucleotide exchange factor 4	other	1.506
CDC42EP1	CDC42 effector protein 1	other	-1.196
CDC42EP5	CDC42 effector protein 5	other	-2.151
CDH17	cadherin 17	transporter	1.296
GNAI1	G protein subunit alpha i1	enzyme	1.122
GNG7	G protein subunit gamma 7	enzyme	1.433
LIMK2	LIM domain kinase 2	kinase	-1.133
MAPK10	mitogen-activated protein kinase 10	kinase	-3.067
MSN	moesin	other	1.147
NEDD4	neural precursor cell expressed, developmentally down-regulated 4, E3 ubiquitin protein ligase	enzyme	1.27
PKN1	protein kinase N1	kinase	1.118
RHOQ	ras homolog family member Q	enzyme	1.21
RHOV	ras homolog family member V	enzyme	1.202
ROCK2	Rho associated coiled-coil containing protein kinase 2	kinase	1.145
SEPT10	septin 10	transcription regulator	1.131
VIM	vimentin	other	-1.306

Table 4. Regulation of HMGB1 Signaling pathway (butyrate vs. control).

Symbol	Entrez Gene Name	Type(s)	Expr Fold Change
CD70	CD70 molecule	cytokine	-2.279
CLCF1	cardiotrophin like cytokine factor 1	cytokine	-2.372
CSF2	colony stimulating factor 2	cytokine	-4.834
ICAM1	intercellular adhesion molecule 1	transmembrane receptor	-2.054
IFNGR1	interferon gamma receptor 1	transmembrane receptor	1.549
IL1R1	interleukin 1 receptor type 1	transmembrane receptor	-1.928
MAP2K7	mitogen-activated protein kinase kinase 7	kinase	-2.703
PIK3C2A	phosphatidylinositol-4-phosphate 3-kinase catalytic subunit type 2 alpha	kinase	2.078
RELA	RELA proto-oncogene, NF-kB subunit	transcription regulator	-1.531
RHOD	ras homolog family member D	enzyme	2.021
RHOV	ras homolog family member V	enzyme	1.556
SERPINE1	serpin family E member 1	other	16.558
TLR4	toll like receptor 4	transmembrane receptor	-2.744
TNFSF9	TNF superfamily member 9	cytokine	-1.738

Table 5. Regulation of Cell Cycle: G2/M DNA Damage Checkpoint pathway (butyrate vs. control).

Symbol	Entrez Gene Name	Type(s)	Expr Fold Change
ABL1	ABL proto-oncogene 1, non-receptor tyrosine kinase	kinase	-1.595
CCNB2	cyclin B2	other	-1.586
CKS1B	CDC28 protein kinase regulatory subunit 1B	kinase	1.852
PLK1	polo like kinase 1	kinase	-2.035
PTPMT1	protein tyrosine phosphatase, mitochondrial 1	phosphatase	-1.675
YWHAG	tyrosine 3-monooxygenasetryptophan 5-monooxygenase activation protein gamma	other	2.531

Table 6. Regulation of Cell Cycle: G1/S Checkpoint pathway (butyrate vs. control).

Symbol	Entrez Gene Name	Type(s)	Expr Fold Change
ABL1	ABL proto-oncogene 1, non-receptor tyrosine kinase	kinase	-1.595
CCND1	cyclin D1	transcription regulator	-2.265
CCNE2	cyclin E2	other	-3.382
CDKN2D	cyclin dependent kinase inhibitor 2D	transcription regulator	2.533
E2F8	E2F transcription factor 8	transcription regulator	-2.433
HDAC3	histone deacetylase 3	transcription regulator	1.644
MYC	MYC proto-oncogene, bHLH transcription factor	transcription regulator	-7.166

Table 7. Transcription factor and kinase enrichment analysis based on differentially expressed gene lists. Genes with a minimal fold change of log2 (1.5) and p-value < 0.05 were analyzed for transcription factor (TFEA) and kinase (KEA) enrichment using X2K. Shown are the top 10 regulated factors when organoids were stimulated with acetate or butyrate. Gold color indicates p-value > 0.05.

Acetate (2.5 mM)

Down in acetate		**Down in acetate**	
TFEA	***p-value***	***KEA***	***p-value***
REST	6.68E-09	CDK1	1.28E-23
SUZ12	1.11E-08	CSNK2A1	1.79E-21
REST	2.23E-08	CDK2	1.43E-18
TP53	0.01585	MAPK14	2.34E-18
SMAD4	0.01754	CDK4	6.22E-17
EZH2	0.02395	GSK3B	7.88E-17
AR	0.06142	MAPK1	2.55E-16
EZH2	0.06994	HIPK2	8.00E-15
TRIM28	0.07271	ATM	2.03E-14
SALL4	0.08036	MAPK3	5.57E-13
Up in acetate		**Up in acetate**	
TFEA	***p-value***	***KEA***	***p-value***
SMC3	0.02308	MAPK3	1.15E-11
RAD21	0.02891	CDK1	2.19E-10
GATA1	0.03991	MAPK1	9.87E-09
VDR	0.07167	ERK2	2.17E-08
CTCF	0.08494	ERK1	3.41E-08
ZC3H11A	0.1182	CSNK2A1	4.28E-08
REST	0.1206	CK2ALPHA	1.07E-07
GATA2	0.1692	GSK3B	1.43E-07
SUZ12	0.2168	MAPK14	6.51E-07
PPARD	0.2428	HIPK2	1.42E-06

Butyrate (1 mM)

Down in Butyrate		**Down in Butyrate**	
TFEA	***p-value***	***KEA***	***p-value***
UBTF	0.000122	MAPK1	6.01E-19
SUZ12	0.000174	MAPK14	4.36E-16
ZBTB7A	0.000189	CSNK2A1	1.04E-14
RELA	0.000895	CK2ALPHA	1.24E-14
CTCF	0.00516	CDK1	4.73E-14
TCF3	0.01002	CDK2	5.24E-14
FOXA2	0.01791	MAPK3	1.47E-13
YY1	0.02933	GSK3B	5.31E-13
HDAC2	0.03932	MAPK8	8.49E-13
E2F6	0.05342	ERK1	7.44E-10
Up in butyrate		**Up in butyrate**	
TFEA	***p-value***	***KEA***	***p-value***
SUZ12	5.80E-14	HIPK2	1.08E-09
REST	1.91E-08	CDK1	2.36E-09
REST	1.13E-06	CK2ALPHA	4.77E-09
EZH2	9.88E-05	CSNK2A1	5.66E-09
SUZ12	0.00033	GSK3B	1.00E-07
RAD21	0.001882	MAPK3	7.34E-07
SMC3	0.002604	CDK2	1.3E-06
EZH2	0.003035	MAPK14	3.87E-06
CTCF	0.00419	AKT1	6.39E-06
GATA1	0.007389	ATM	2.12E-05

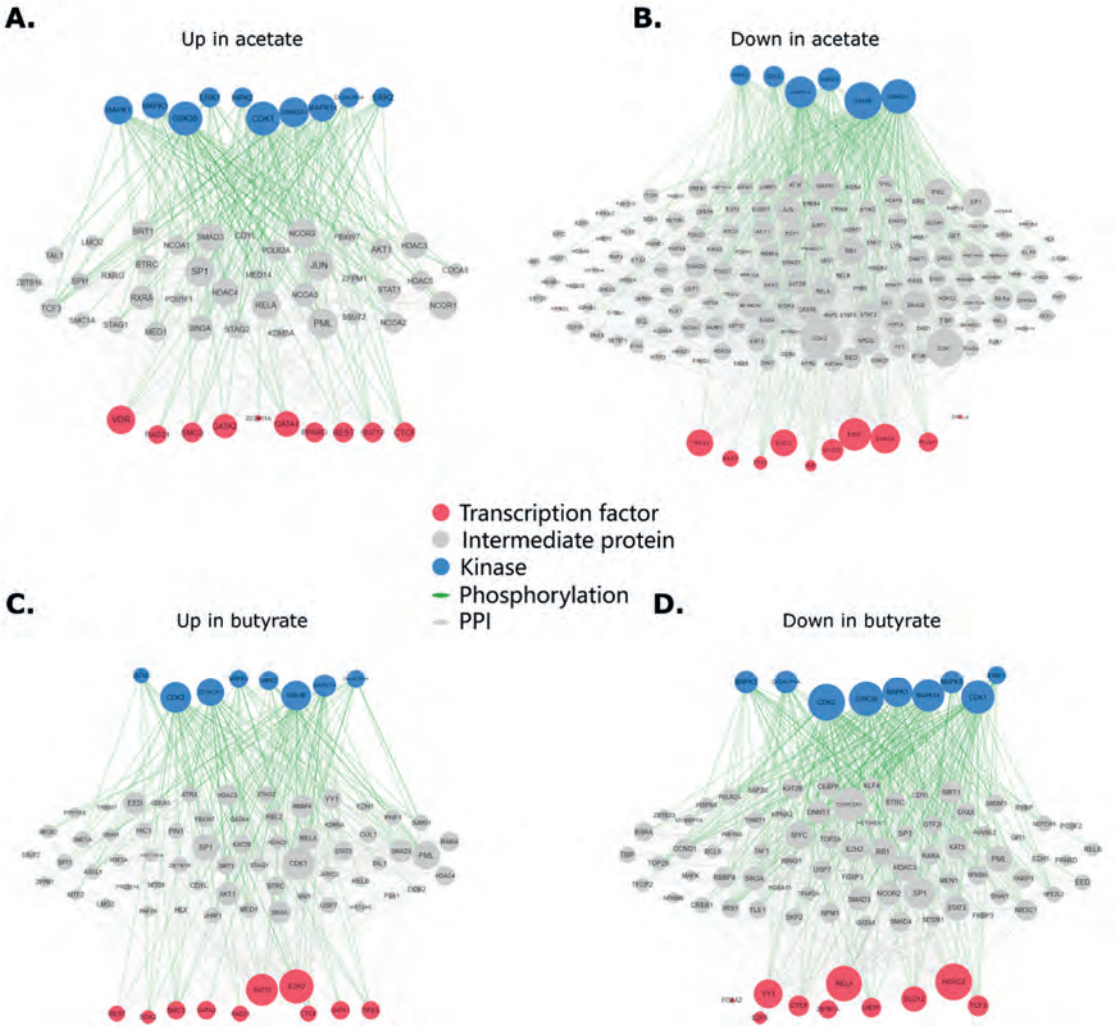

Figure 5 (A-D). X2K network analysis based on differentially expressed gene lists. Genes with a minimal fold change of log2 (1.5) and p-value < 0.05 were analysed for transcription factor (TFEA) and kinase (KEA) enrichment using X2K. Shown are interactions between transcription factors, intermediate proteins and kinases when organoids were stimulated with acetate or butyrate.

Epigenetic Effect of SCFAs in Ileum Organoids

As butyrate is a known inhibitor of Class I histone deacetylases (including histone 3 deacetylase), and the IPA analysis suggested acetate exposure may have epigenetic effects via acetylation of at least two histones, we measured total histone 3 acetylation in organoids 5 hours after SCFA incubation. The percentage of total histone H3 acetylation increased in organoids exposed to butyrate and acetate compared to control **(Figure 6)**. Although we observed a tendency for higher histone H3 acetylation in SCFA-treated organoids, these were not statistically different from control ($p > 0.05$) due to high variation among the treatment samples **(Figure 6)**. This is most likely due to the variation we observed in the number of organoids per well.

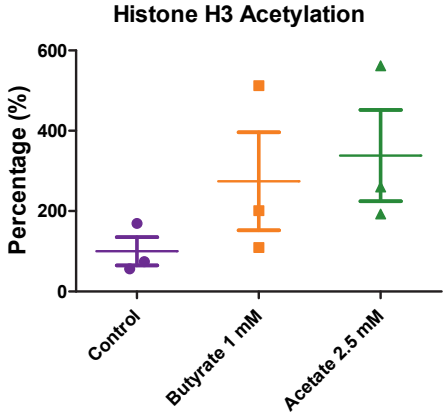

Figure 6. Percentage of histone H3 acetylation measured from ileum organoids as a result of 5 hours acetate (2.5 mM) or butyrate (1 mM) exposure. Results are shown as mean ± SEM, n = 3.

Conclusion

The top canonical pathway predicted to be upregulated by acetate was the Sirtuin Signaling Pathway, which contains a group of proteins regulating a wide range of cellular processes such as transcription, apoptosis, and inflammation, mainly by deacetylase activity [29]. Three of the regulated genes in this pathway are known to induce epigenetic effects, i.e., *H1F0*, *SIRT6* and *KAT2A*. The Sirtuin pathway is also known to suppress histone deacetylation of pro-inflammatory cytokines and transcription factors which lead to suppression of inflammation [30]. This underlying mechanism may explain an anti-inflammatory effect of acetate on immune cells. Acetate exposure increased histone 3 acetylation in organoids, although this was not significant due to the high variability, which we hypothesized to be due to variation in the number of organoids in replicate wells. The second top canonical pathway regulated by acetate was the Rho Family GTPases signaling pathway. This pathway has been shown to regulate many aspects of intracellular actin dynamics including organelle development, cytoskeletal dynamics, cell movement, and other common cellular functions. The cellular effects arising from regulation of this pathway are still to be elucidated but might involve proliferation and epithelial remodeling.

Butyrate, a known HDAC3 inhibitor had a much stronger effect on the transcriptome than acetate, presumably through epigenetic mechanisms affecting chromatin as well as acetylation of protein substrates for HDAC3. Consistent with this hypothesis we observed regulation of GATA1 and RELA transcription factors which are known substrates for HDAC3. Our results with butyrate are difficult to compare to a previous study by Lukovac *et al.* (2014) as they used 5-fold higher concentrations of butyrate [1]. Besides, our preliminary data suggest that butyrate may have some toxicity at 5 mM.

The finding that acetate significantly alters gene expression in intestinal organoids has major implications for understanding the impact of this bacterial metabolite on intestinal function *in vivo* and warrants further study. In future experiments we aim to investigate transcriptional and functional effects of longer periods of exposure to acetate on both the colon and ileum. Polarized monolayers of organoids cells [18] will also be used to reduce variability between replicates for biochemical and cellular assays.

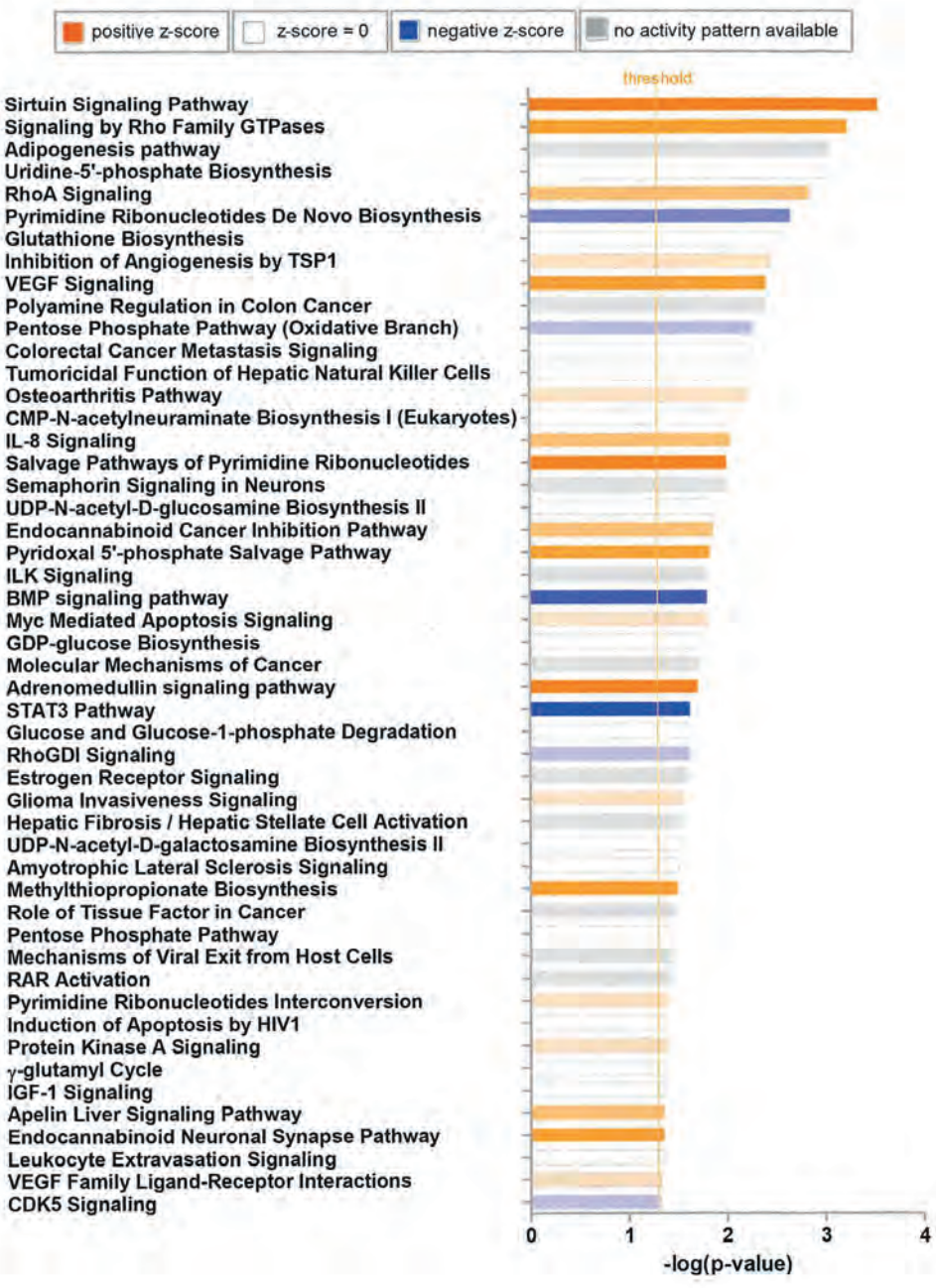

Supplementary Figure S1. IPA analysis. Regulation of canonical pathways induced by acetate

Supplementary Table S1:

Unidentified identifiers for differentially expressed genes, after conversion using G:Profiler ($p < 0.05$, log2 fold change > 1.5) when treated with acetate (first two tables), or butyrate (last two tables).

Acetate Down-regulated:

Unidentified gene identifiers	Chromosome	Region	Max group mean	Log_2 fold change	Fold change	P-value	FDR p-value	Bonferroni	description
ENSSSCG00000001455	7	complement(78856611..78857570)	0.087626	4.691947	25.97672	0.043819	0.76843	1	MHC class II histocompatibility antigen SLA-DRB1 [Source:NCBI gene;Acc:100153386]
ENSSSCG00000002608	6	49895083..49931417	0.017089	1.862174	3.63555	0.023372	0.634052	1	olfactory receptor 11H12-like [Source:NCBI gene;Acc:100523076]
ENSSSCG00000003045	1	complement(22383978 0..224125540)	0.020633	3.291713	9.792744	0.019553	0.60590 2	1	ATPase Na+/K+ transporting subunit alpha 3 [Source:NCBI gene;Acc:100329126]
ENSSSCG00000005257	3	complement(41482260..41487800)	0.073242	3.29759	9.832715	0.014336	0.58157	1	transient receptor potential cation channel subfamily M member 3 [Source:NCBI gene;Acc:100157158]
ENSSSCG00000007978	3	complement(63205017..63486666)	0.033534	3.297161	9.829796	0.01457	0.58157	1	hemoglobin subunit alpha [Source:NCBI gene;Acc:110259958]
ENSSSCG00000008250	X	complement(103325989..103327383)	0.073483	4.978641	31.52972	0.033238	0.70593 9	1	catenin alpha 2 [Source:NCBI gene;Acc:100525337]
ENSSSCG00000012645	2	125663425..125719312	0.056149	2.129775	4.376491	0.019106	0.60133 9	1	DDB1- and CUL4-associated factor 12-like protein 2 [Source:NCBI gene;Acc:100521308]
ENSSSCG00000014233	15	44066193..44407632	0.020337	3.375226	10.37634	0.000991	0.20909 3	1	zinc finger protein 474 [Source:NCBI gene;Acc:100525452]

ENSSSCG00000026701	2	142505136..142527509	0.017363	2.817662	7.05018 9	0.012764	0.563445	1	phosphoethanolamine/phosphocholine phosphatase [Source:NCBI gene;Acc:100621753]
ENSSSCG00000029442	X	74463059..74968349	0.015905	5.414098	42.63889	0.020078	0.611464	1	protocadherin alpha-7 [Source:NCBI gene;Acc:102160218]
ENSSSCG00000029771	7	complement(20849712..20850023)	0.278108	2.91826	7.559337	0.046899	0.784094	1	protocadherin 11 X-linked [Source:NCBI gene;Acc:414736]
ENSSSCG00000032640	1	complement(261228701..261256850)	7.210892	1.801106	3.484872	7.52E-09	6.07E-05	0.000182	histone H4 [Source:NCBI gene;Acc:110261675]
ENSSSCG00000034749	Y	complement(4680259..4704188)	0.809013	8.173292	288.6728	0.001712	0.256098	1	None
ENSSSCG00000036341	14	48943274..49010871	0.014467	5.100439	34.30718	0.029502	0.678111	1	G protein-coupled receptor 143 [Source:NCBI gene;Acc:100624736]
ENSSSCG00000037214	Y	4758466..4783794	0.385653	8.348846	326.0267	0.000463	0.135131	1	None
ENSSSCG00000037429	5	40454911..40455240	0.543074	5.748079	53.74576	0.013422	0.568602	1	shroom family member 2 [Source:NCBI gene;Acc:100522965]
ENSSSCG00000038998	9	complement(113438776..113439696)	0.102813	4.845724	28.75466	0.038452	0.746439	1	None
ENSSSCG00000039428	9	complement(10541283..10542795)	0.126706	5.777227	54.84266	0.022205	0.628374	1	olfactory receptor 2A1/2A42-like [Source:NCBI gene;Acc:100525599]
ENSSSCG00000039803	6	84257809..84258372	0.241407	2.800299	6.965846	0.032305	0.698315	1	None
ENSSSCG00000040871	6	complement(47986147..47997228)	0.023288	3.296744	9.826951	0.013909	0.575445	1	None
ENSSSCG00000001455	7	complement(24868656..24914037)	0.032137	4.845676	28.75371	0.037054	0.734167	1	MHC class II histocompatibility antigen SLA-DRB1 [Source:NCBI gene;Acc:100153386]
Acetate Up-regulated:									

Unidentified gene identifiers	Chromosome	Region	Max group mean	Log_2 fold change	Fold change	P-value	FDR p-value	Bonferroni	description
ENSSSCG00000007642	3	7856701..7876040	0.038981	-1.99864	-3.99622	0.015348	0.588801	1	alpha-2-glycoprotein 1, zinc-binding [Source:NCBI gene;Acc:100519648]
ENSSSCG00000031997	8	51576485..51579375	0.093432	-1.64501	-3.12751	0.030982	0.693806	1	None
ENSSSCG00000033190	18	complement(42062327..42076551)	0.118997	-2.28557	-4.87557	0.005998	0.442082	1	aquaporin 1 (Colton blood group) [Source:NCBI gene;Acc:407773]
ENSSSCG00000038035	6	81509567..81519072	0.080799	-5.08129	-33.8549	0.041018	0.757013	1	elongation factor 1-alpha, somatic form-like [Source:NCBI gene;Acc:100620900]
ENSSSCG00000039584	13	112751265..112753925	0.498275	-1.83928	-3.57832	0.04004	0.751363	1	None
Butyrate down-regulated:									
Unidentified gene identifiers	**Chromosome**	**Region**	**Max group mean**	**Log_2 fold change**	**Fold change**	**P-value**	**FDR p-value**	**Bonferroni**	**description**
ENSSSCG00000001441	7	24274149..24286960	10.10294	2.259787	4.789207	0	0	0	butyrophilin-like protein 1 [Source:NCBI gene;Acc:100512174]
ENSSSCG00000002348	7	96984542..96990397	3.133309	1.600909	3.033344	0	0	0	acyl-CoA thioesterase 6 [Source:NCBI gene;Acc:100152868]
ENSSSCG00000002877	6	44243314..44357540	2.546945	2.171006	4.503372	0	0	0	zinc finger protein 181 [Source:NCBI gene;Acc:100513473]
ENSSSCG00000002900	6	45184684..45195058	1.893706	1.57515	2.979664	2.66E-15	2.47E-14	6.46E-11	proline and serine rich 3 [Source:NCBI gene;Acc:106504209]
ENSSSCG00000003243	6	complement(58137569..58152660)	0.671589	1.567878	2.964683	2.18E-10	1.45E-09	5.29E-06	zinc finger protein 432 [Source:NCBI

									gene;Acc:100624217]
ENSSSCG00000003839	6	155800840..155894915	6.409979	2.766972	6.806777	0	0	0	phospholipid phosphatase 3 [Source:NCBI gene;Acc:100512419]
ENSSSCG00000004246	1	43171887..43198297	1.930329	1.504333	2.836936	2.62E-11	1.88E-10	6.36E-07	None
ENSSSCG00000005398	1	complement(24303515 4..243039581)	2.955452	2.007342	4.020407	0	0	0	acyl-coenzyme A amino acid N-acyltransferase 2-like [Source:NCBI gene;Acc:110255172]
ENSSSCG00000007454	17	complement(49258553..49337793)	20.84095	1.732559	3.323167	0	0	0	zinc finger MYND-type containing 8 [Source:NCBI gene;Acc:100155989]
ENSSSCG00000007964	3	38934599..38951526	0.045851	3.337304	10.10715	0.000153	0.000586	1	MEFV, pyrin innate immunity regulator [Source:NCBI gene;Acc:100517333]
ENSSSCG00000008722	8	complement(2842123..3005466)	0.915487	1.944108	3.847999	0	0	0	SH3 domain and tetratricopeptide repeats 1 [Source:NCBI gene;Acc:100737944]
ENSSSCG00000008954	8	70141611..70149557	47.37662	3.997348	15.97062	0	0	0	None
ENSSSCG00000008965	8	complement(70645057..70697907)	0.402263	1.840185	3.580559	2.57E-11	1.84E-10	6.23E-07	betacellulin [Source:NCBI gene;Acc:100505411]
ENSSSCG00000008981	8	71940500..71988112	1.613645	2.627846	6.181024	0	0	0	starch binding domain 1 [Source:NCBI gene;Acc:100522745]
ENSSSCG00000009627	14	6853069..6857835	0.529099	2.225142	4.67557	2.18E-09	1.34E-08	5.29E-05	None
ENSSSCG00000010839	10	complement(11797572..11835322)	0.274257	1.953918	3.874252	0.000356	0.001301	1	None
ENSSSCG00000011531	13	60915098..60925744	2.513689	1.803202	3.48994	0	0	0	histone-lysine N-methyltransferase SETMAR [Source:NCBI gene;Acc:100514009]

ENSSSCG00000012392	X	57374316..57374891	0.585	1.584	2.999	0.00513	0.01583	1	None
ENSSSCG00000012812	X	125452699..125461489	0.454	1.714	3.281	0.00481	0.01493	1	None
ENSSSCG00000014672	9	complement(4174294..4188413)	0.729	1.818	3.527	1.38E-12	1.09E-11	3.35E-08	tripartite motif-containing protein 34 [Source:NCBI gene;Acc:100738479]
ENSSSCG00000016091	15	complement(104071283..104099195)	1.846	1.751	3.367	0	0	0	potassium channel tetramerization domain containing 18 [Source:NCBI gene;Acc:100523334]
ENSSSCG00000020988	6	53718935..53726017	4.979	2.012	4.034	0	0	0	zinc finger protein 114 [Source:NCBI gene;Acc:106510560]
ENSSSCG00000021322	X	20221414..20275192	5.041	2.699	6.494	0	0	0	zinc finger protein X-linked [Source:NCBI gene;Acc:397294]
ENSSSCG00000021414	2	142875088..142877496	0.093	4.183	18.16	0.00125	0.00428	1	protocadherin beta-17-like [Source:NCBI gene;Acc:100739498]
ENSSSCG00000021656	13	complement(135864539..136156061)	0.097	1.511	2.850	0.00147	0.00496	1	None
ENSSSCG00000022083	5	84986748..85148983	0.071	1.738	3.336	0.00793	0.02364	1	ankyrin repeat and sterile alpha motif domain containing 1B [Source:NCBI gene;Acc:100513089]
ENSSSCG00000022361	8	complement(118815752..118867551)	0.190	1.922	3.789	0.00621	0.01887	1	B cell scaffold protein with ankyrin repeats 1 [Source:NCBI gene;Acc:100525061]
ENSSSCG00000022466	3	25239062..25245917	1.682	1.738	3.337	5.75E-09	3.42E-08	0.000139	ERI1 exoribonuclease family member 2 [Source:NCBI gene;Acc:100526162]
ENSSSCG00000023403	10	24340150..24454427	1.894	1.624	3.083	0	0	0	leucine rich repeat containing G protein-coupled receptor 6 [Source:NCBI gene;Acc:100511400]

ENSSSCG00000023596	14	complement(60998430..61030598)	0.24894	1.522822	2.873525	3.66E-08	2.04E-07	0.000888	zinc finger protein 33B [Source:NCBI gene;Acc:100738050]
ENSSSCG00000026960	1	115219883..115345923	0.973047	1.801084	3.484819	0	0	0	zinc finger protein 280D [Source:NCBI gene;Acc:100513772]
ENSSSCG00000027790	13	complement(99745467..99786519)	11.52014	1.591401	3.013419	0	0	0	NACHT, LRR and PYD domains-containing protein 1a-like [Source:NCBI gene;Acc:100514323]
ENSSSCG00000028195	15	complement(32547059..32592851)	4.64195	1.654713	3.148605	0	0	0	glutamate rich 1 [Source:NCBI gene;Acc:100620858]
ENSSSCG00000028345	14	complement(60884782..60905183)	1.717285	2.337342	5.053708	0	0	0	zinc finger protein 33B [Source:NCBI gene;Acc:100627762]
ENSSSCG00000028635	3	complement(11841991..12026009)	4.124334	1.505013	2.838273	0	0	0	general transcription factor II-I repeat domain-containing protein 2 [Source:NCBI gene;Acc:100620992]
ENSSSCG00000030901	7	24323772..24334955	1.698269	2.229322	4.689135	1.11E-15	1.06E-14	2.69E-11	None
ENSSSCG00000031121	9	125300365..125337850	5.169511	1.843687	3.589262	0	0	0	tRNA splicing endonuclease subunit 15 [Source:NCBI gene;Acc:100516387]
ENSSSCG00000031589	14	complement(60794333..60861636)	0.121477	2.574617	5.957126	2.80E-06	1.30E-05	0.067911	zinc finger protein 37A [Source:NCBI gene;Acc:100152623]
ENSSSCG00000031644	1	complement(16272696..16275341)	0.281772	2.394624	5.258402	0.012145	0.035056	1	None
ENSSSCG00000031849	X	complement(58941164..58947059)	0.200587	2.234131	4.704793	0.000889	0.003095	1	None
ENSSSCG00000031979	9	complement(12442414..12451687)	30.20611	1.733256	3.324774	0	0	0	potassium channel tetramerization domain containing 14 [Source:NCBI gene;Acc:110255405]
ENSSSCG00000032190	8	131976014..131998159	0.123657	3.323573	10.01141	0.016175	0.045649	1	chromosome 8 C4orf36 homolog [Source:NCBI

									gene;Acc:10062741 7]
ENSSSCG00000032450	12	complement(44271412..44289645)	5.799669	1.798666	3.478985	0	0	0	LYR motif containing 9 [Source:NCBI gene;Acc:10062335 9]
ENSSSCG00000032594	6	complement(59239779..59254652)	1.923512	1.637583	3.111441	0	0	0	uncharacterized LOC110261048 [Source:NCBI gene;Acc:11026104 8]
ENSSSCG00000032969	6	58189335..58201899	0.073252	2.759967	6.773809	4.53E-05	0.000185	1	zinc finger protein 84-like [Source:NCBI gene;Acc:10051716 1]
ENSSSCG00000033366	3	68539848..68545430	0.899941	1.6344	3.104584	2.55E-15	2.38E-14	6.19E-11	polycomb group ring finger 1 [Source:NCBI gene;Acc:10051463 6]
ENSSSCG00000033434	11	complement(5317557..5333839)	0.211417	1.622565	3.07922	0.017354	0.048706	1	None
ENSSSCG00000033464	8	67304325..67305962	0.773683	1.811015	3.508891	1.33E-08	7.67E-08	0.000321	None
ENSSSCG00000034074	3	25246175..25247353	0.149594	3.057302	8.324146	0.005772	0.017654	1	None
ENSSSCG00000034540	6	complement(57089528..57129251)	0.222625	1.903916	3.742277	1.03E-10	7.02E-10	2.48E-06	protein ZNF738-like [Source:NCBI gene;Acc:10215890 6]
ENSSSCG00000034555	5	62106284..62124604	0.035526	3.851751	14.43752	0.003833	0.012059	1	killer cell lectin-like receptor subfamily B member 1B allele B [Source:NCBI gene;Acc:10052049 1]
ENSSSCG00000034610	5	30188571..30332703	10.35819	1.922448	3.790658	0	0	0	high mobility group AT-hook 2 [Source:NCBI gene;Acc:10051320 6]
ENSSSCG00000035073	9	92843230..92925360	0.072339	1.677332	3.198358	0.005915	0.018046	1	multidrug resistance protein 1 [Source:NCBI gene;Acc:10052245 5]
ENSSSCG00000035649	2	complement(44315662..44366880)	1.284465	1.509634	2.847378	4.67E-12	3.54E-11	1.13E-07	calcitonin-related polypeptide beta [Source:NCBI gene;Acc:396563]
ENSSSCG00000035650	2	57245386..57271405	4.916321	2.580477	5.981373	0	0	0	tripartite motif containing 52 [Source:NCBI

									gene;Acc:100626428]
ENSSSCG00000036078	15	62264268..62416294	0.068189	2.378608	5.200347	0.001072	0.003698	1	None
ENSSSCG00000037214	14	48943274..49010871	0.014467	3.204037	9.215336	0.017755	0.049705	1	None
ENSSSCG00000037324	17	32594220..32597054	2.923211	1.751889	3.367992	0	0	0	None
ENSSSCG00000037571	6	62205215..62215077	0.290109	2.009528	4.026504	0.007039	0.021184	1	None
ENSSSCG00000038171	1	complement(24297861 5..243050442)	1.784049	2.34527	5.081554	0	0	0	acyl-coenzyme A amino acid N-acyltransferase 2 [Source:NCBI gene;Acc:100515185]
ENSSSCG00000038260	5	79281586..79288705	2.115734	2.101582	4.291798	0	0	0	None
ENSSSCG00000038998	5	40454911..40455240	0.543074	5.744827	53.62475	0.017735	0.049666	1	None
ENSSSCG00000039084	1	43258485..43265580	1.149191	1.81073	3.508199	1.59E-11	1.16E-10	3.86E-07	None
ENSSSCG00000039368	10	25738231..25789518	3.065736	1.587984	3.006289	0	0	0	solute carrier family 35 member D2 [Source:NCBI gene;Acc:100514312]
ENSSSCG00000039443	1	104157073..104170987	5.279409	2.535015	5.795831	0	0	0	dynactin-associated protein [Source:NCBI gene;Acc:106508962]
ENSSSCG00000039531	4	122648447..122792723	0.19121	1.576465	2.982382	1.95E-05	8.28E-05	0.471621	None
ENSSSCG00000039688	3	114503150..114508440	1.878528	1.881314	3.684104	0	0	0	None
ENSSSCG00000039695	3	111564931..111570490	0.808278	1.883438	3.689533	0	0	0	coiled-coil domain containing 121 [Source:NCBI gene;Acc:100520301]
ENSSSCG00000040032	5	99297125..99298088	0.610097	2.381957	5.212433	1.74E-05	7.45E-05	0.422134	None
ENSSSCG00000040169	15	133014490..133032001	0.165151	2.257485	4.781573	3.44E-07	1.75E-06	0.008329	None

ENSSSCG00000040187	2	complement(66650447..66711337)	3.162135	1.585142	3.000373	0	0	0	zinc finger protein 791-like [Source:NCBI gene;Acc:106508100]
Butyrate up-regulated:									
Unidentified gene identifiers	**Chromosome**	**Region**	**Max group mean**	**Log$_2$ fold change**	**Fold change**	**P-value**	**FDR p-value**	**Bonferroni**	**description**
ENSSSCG00000000148	5	complement(11509336..11543032)	0.078966	-4.31043	-19.8413	7.93E-08	4.27E-07	0.00192	apolipoprotein L3-like [Source:NCBI gene;Acc:106510284]
ENSSSCG00000000483	5	complement(32644709..32673639)	9.033349	-1.61586	-3.06494	0	0	0	Mdm1 nuclear protein [Source:NCBI gene;Acc:100625194]
ENSSSCG00000001859	7	55806636..55807790	17.71863	-2.17471	-4.51495	0	0	0	GDP-D-glucose phosphorylase 1 [Source:NCBI gene;Acc:100156697]
ENSSSCG00000001931	7	61033831..61078507	0.746044	-2.25341	-4.76808	1.13E-13	9.50E-13	2.74E-09	GRAM domain containing 2A [Source:NCBI gene;Acc:100158151]
ENSSSCG00000002140	7	78470339..78480705	0.048015	-1.71585	-3.2849	0.00401	0.012581	1	kelch like family member 33 [Source:NCBI gene;Acc:100154698]
ENSSSCG00000003045	6	49895083..49931417	0.052636	-1.59844	-3.02816	0.001342	0.004561	1	ATPase Na+/K+ transporting subunit alpha 3 [Source:NCBI gene;Acc:100329126]
ENSSSCG00000004081	1	13715672..14042954	0.050566	-1.62093	-3.07573	0.012872	0.037031	1	None
ENSSSCG00000004572	1	109825438..109827175	0.463051	-2.74718	-6.71405	1.76E-06	8.34E-06	0.042553	C2 calcium dependent domain containing 4B [Source:NCBI gene;Acc:100738739]
ENSSSCG00000004598	1	complement(114287627..114386473)	10.51405	-3.13879	-8.80785	0	0	0	myocardial zonula adherens protein [Source:NCBI gene;Acc:100154487]

ENSSSCG00000005738	1	complement(27277684..27282418)	5.590601	-1.53392	-2.90633	0	0	0	ral guanine nucleotide dissociation stimulator [Source:NCBI gene;Acc:100513970]
ENSSSCG00000006719	4	complement(101563728..101573906)	0.21562	-1.89681	-3.7239	1.05E-05	4.60E-05	0.25402	hydroxy-delta-5-steroid dehydrogenase, 3 beta- and steroid delta-isomerase 1 [Source:NCBI gene;Acc:445539]
ENSSSCG00000007665	3	8494530..8497318	0.344692	-1.92525	-3.79804	3.41E-06	1.57E-05	0.082751	insulin receptor substrate 1-like [Source:NCBI gene;Acc:100515824]
ENSSSCG00000010064	14	complement(49801161..49807602)	0.278076	-1.60527	-3.04252	0.003885	0.012214	1	glutathione S-transferase theta-1 [Source:NCBI gene;Acc:100153094]
ENSSSCG00000010609	14	complement(115133419..115172417)	0.777489	-1.90235	-3.73822	2.22E-06	1.04E-05	0.053827	None
ENSSSCG00000011291	13	complement(26253910..26265856)	0.102737	-3.21809	-9.30557	0.002215	0.007271	1	None
ENSSSCG00000012832	X	complement(487572..513928)	0.057418	-2.45544	-5.48481	2.23E-05	9.42E-05	0.540889	matrix-remodeling-associated protein 5 [Source:NCBI gene;Acc:100519997]
ENSSSCG00000014079	2	complement(84142287..84219767)	0.043474	-2.15566	-4.45862	0.006845	0.020646	1	None
ENSSSCG00000014993	9	33917370..34033888	0.492114	-1.52881	-2.88548	0.000204	0.000767	1	None
ENSSSCG00000016224	15	124565318..124566979	0.249336	-1.96887	-3.91446	0.000483	0.001738	1	None
ENSSSCG00000016401	15	complement(139610625..139665202)	0.48637	-2.59058	-6.02339	0	0	0	kinesin family member 1A [Source:NCBI gene;Acc:100517246]
ENSSSCG00000020838	5	17585590..17591134	3.792191	-3.99826	-15.9807	0	0	0	keratin, type II cuticular Hb6-like [Source:NCBI gene;Acc:100621639]
ENSSSCG00000023127	6	12421018..12426270	0.253263	-3.97688	-15.7456	0.005931	0.018091	1	chymotrypsinogen B2 [Source:NCBI

									gene;Acc:10062164 2]
ENSSSCG00000023156	3	68618571..68624344	1.103944	-2.87495	-7.3358	0	0	0	chromosome 3 C2orf81 homolog [Source:NCBI gene;Acc:10051378 8]
ENSSSCG00000023812	3	complement(60064302..60114275)	1.120152	-1.63507	-3.10602	2.08E-08	1.18E-07	0.000504	None
ENSSSCG00000024281	6	47613763..47614785	2.453724	-1.52515	-2.87816	0.001877	0.006225	1	galectin-7-like [Source:NCBI gene;Acc:1102609 83]
ENSSSCG00000024500	13	complement(207195537..207204827)	8.71256	-1.52216	-2.87221	0	0	0	cilia and flagella associated protein 410 [Source:NCBI gene;Acc:1006218 58]
ENSSSCG00000024588	2	complement(75538359..75542331)	1.503294	-2.50217	-5.66538	0	0	0	TLE family member 6, subcortical maternal complex member [Source:NCBI gene;Acc:1006235 64]
ENSSSCG00000025655	1	239209387..239251317	0.089355	-2.60818	-6.09734	0.000199	0.000751	1	None
ENSSSCG00000026512	2	complement(44042923..44049006)	1.442448	-2.15108	-4.44075	4.00E-15	3.67E-14	9.69E-11	calcitonin-related polypeptide beta [Source:NCBI gene;Acc:1001244 07]
ENSSSCG00000026701	12	complement(25441225..25449239)	0.30059	-2.2688	-4.81921	4.24E-07	2.13E-06	0.01027	phosphoethanolamine/phosphocholine phosphatase [Source:NCBI gene;Acc:1006217 53]
ENSSSCG00000027025	13	complement(122391783..122392670)	0.278075	-1.68221	-3.20919	0.011322	0.03284	1	transmembrane epididymal protein 1A-like [Source:NCBI gene;Acc:1021662 40]
ENSSSCG00000027232	1	complement(137199072..137297207)	0.036581	-6.07089	-67.2234	0.014205	0.040575	1	family with sequence similarity 169 member B [Source:NCBI gene;Acc:1006235 31]
ENSSSCG00000027890	3	complement(9821272..9847024)	4.425769	-2.31755	-4.98487	0	0	0	RAS p21 protein activator 4B [Source:NCBI gene;Acc:1006241 52]

ENSSSCG00000028062	X	complement(83597179..83599213)	0.176445	-1.72002	-3.2944	0.01714	0.048131	1	transcription elongation factor A protein-like 3 [Source:NCBI gene;Acc:100621480]
ENSSSCG00000029321	4	complement(86166016..86170278)	0.692635	-1.60705	-3.04627	0.000246	0.000918	1	None
ENSSSCG00000031706	2	complement(47045931..47120943)	5.448767	-2.48678	-5.60527	0	0	0	None
ENSSSCG00000032309	18	54431140..54470801	0.26549	-1.99772	-3.99369	0.000311	0.001147	1	None
ENSSSCG00000032949	1	complement(108730293..108763353)	2.806953	-2.59111	-6.02562	0	0	0	aph-1 homolog B, gamma-secretase subunit [Source:NCBI gene;Acc:100624829]
ENSSSCG00000033090	2	complement(75547473..75550616)	0.737417	-3.05569	-8.31486	7.00E-10	4.48E-09	1.70E-05	None
ENSSSCG00000033235	5	complement(17571162..17579963)	1.695502	-3.30351	-9.87316	0	0	0	keratin, type II microfibrillar, component 7C-like [Source:NCBI gene;Acc:100621844]
ENSSSCG00000033787	14	51624286..51644457	2.269769	-2.54226	-5.82503	0	0	0	proline dehydrogenase 1, mitochondrial [Source:NCBI gene;Acc:110256626]
ENSSSCG00000033864	15	complement(139646918..139674853)	0.086949	-2.95163	-7.73623	0.002008	0.006638	1	None
ENSSSCG00000033937	9	33721060..33770390	0.28009	-2.33926	-5.06044	1.84E-08	1.05E-07	0.000446	None
ENSSSCG00000034069	1	complement(147939952..147963552)	0.134243	-3.50927	-11.3866	0.001112	0.003825	1	None
ENSSSCG00000034702	17	54557574..54559861	0.076348	-2.49974	-5.65582	0.006387	0.019357	1	None
ENSSSCG00000034739	9	complement(109740516..109809999)	0.930081	-2.70246	-6.50911	0	0	0	None
ENSSSCG00000035224	12	25426079..25444517	0.227096	-2.71166	-6.55074	1.57E-09	9.73E-09	3.79E-05	ABI gene family member 3 [Source:NCBI gene;Acc:100621521]

ENSSSCG00000035256	3	17978746..17985101	1.006683	-3.11521	-8.66508	0	0	0	sialophorin [Source:NCBI gene;Acc:100623653]
ENSSSCG00000035577	5	9361818..9417874	0.122788	-2.57612	-5.96332	0.000322	0.001185	1	None
ENSSSCG00000035617	9	complement(119858969..119896385)	2.357047	-1.50066	-2.82973	0	0	0	quinone oxidoreductase-like protein 2 [Source:NCBI gene;Acc:106505010]
ENSSSCG00000036305	6	65255823..65259126	5.982891	-2.45618	-5.48762	0	0	0	small integral membrane protein 1 (Vel blood group) [Source:NCBI gene;Acc:100625759]
ENSSSCG00000036748	3	complement(46071315..46081668)	0.555556	-1.62857	-3.09206	1.23E-05	5.37E-05	0.2989	zinc finger protein 2 [Source:NCBI gene;Acc:100521785]
ENSSSCG00000036884	4	93651708..93676153	0.055236	-3.23232	-9.39775	9.01E-06	3.99E-05	0.218304	None
ENSSSCG00000036948	10	23628938..23663545	0.031994	-2.01628	-4.04 54	0.000217 3	0.00715	1	immunoglobulin-like and fibronectin type III domain containing 1 [Source:NCBI gene;Acc:102167611]
ENSSSCG00000037391	18	55943496..55955067	0.91873	-1.50784	-2.84383	1.52E-11	1.11E-10	3.68E-07	zinc finger protein 775 [Source:NCBI gene;Acc:110257534]
ENSSSCG00000037466	6	55781905..55824239	0.076417	-2.19607	-4.58228	0.001031	0.032041	1	sialic acid-binding Ig-like lectin 5 [Source:NCBI gene;Acc:100515551]
ENSSSCG00000037566	6	complement(88704599..88712853)	1.655641	-2.28145	-4.86168	0	0	0	myotubularin-related protein 9 [Source:NCBI gene;Acc:106510645]
ENSSSCG00000037796	9	130915700..130919520	0.17613	-2.36287	-5.14394	1.88E-05	8.02E-05	0.45623	None
ENSSSCG00000037879	6	complement(47588661..47591122)	11.87566	-1.76334	-3.39483	1.27E-10	8.66E-10	3.09E-06	galectin 7 [Source:NCBI gene;Acc:100217394]
ENSSSCG00000037941	5	complement(41172539..41424734)	0.037533	-2.56272	-5.90822	0.000983 2	0.02883 7	1	None

ENSSSCG00000038009	6	62528293..62548163	0.038016	-2.83117	-7.11649	0.001926	0.00638	1	zinc finger protein 850-like [Source:NCBI gene;Acc:100737912]
ENSSSCG00000038036	1	complement(26189630 8..261945723)	0.064743	-3.73058	-13.2744	2.69E-05	0.000113	0.653046	None
ENSSSCG00000038112	2	complement(7028909..7033883)	0.163503	-4.34168	-20.2757	5.03E-07	2.51E-06	0.012191	speedy/RINGO cell cycle regulator family member C [Source:NCBI gene;Acc:100518768]
ENSSSCG00000038331	2	59545870..59557993	0.105821	-1.85996	-3.62997	0.001173	0.004019	1	IQ motif containing N [Source:NCBI gene;Acc:110259318]
ENSSSCG00000038606	1	103906316..103921908	0.429038	-3.43464	-10.8126	8.15E-13	6.53E-12	1.97E-08	uncharacterized LOC102160380 [Source:NCBI gene;Acc:102160380]
ENSSSCG00000038684	3	complement(59957461..59991512)	0.168026	-2.52093	-5.73951	0.000896	0.003121	1	None
ENSSSCG00000039926	Y	complement(6512528..6524995)	0.051039	-2.81884	-7.05595	0.000939	0.003262	1	matrix-remodeling-associated protein 5-like [Source:NCBI gene;Acc:110257935]
ENSSSCG00000040260	3	complement(7581544..7623302)	1.106706	-1.78548	-3.44733	0	0	0	transmembrane protein 238-like [Source:NCBI gene;Acc:110259862]
ENSSSCG00000040412	3	complement(28815796..28816799)	0.17301	-2.94198	-7.68464	0.010749	0.031288	1	None
ENSSSCG00000040467	15	48784307..48835517	0.132044	-1.68154	-3.20769	0.000172	0.000655	1	None
ENSSSCG00000040753	17	complement(47884368..47888879)	0.145138	-6.67593	-102.248	0.007085	0.021304	1	WAP four-disulfide core domain 10A-like [Source:NCBI gene;Acc:100302697]
ENSSSCG00000040837	10	complement(68578573..68621321)	2.789626	-2.35021	-5.09898	0	0	0	None
ENSSSCG00000040885	7	complement(23822741..23825399)	1.248746	-2.10547	-4.30339	3.89E-15	3.57E-14	9.42E-11	sperm acrosome membrane-associated protein 4-like [Source:NCBI

									gene;Acc:110261493]
ENSSSCG00000040909	6	167973089..167974427	0.203166	-6.33325	-80.6303	0.014357	0.040963	1	None
ENSSSCG00000040925	6	4660531..4668003	0.28297 6	-3.0928	-8.53152	8.47E-12	6.30E-11	2.05E-07	None

References

1. Lukovac, S., et al., *Differential modulation by Akkermansia muciniphila and Faecalibacterium prausnitzii of host peripheral lipid metabolism and histone acetylation in mouse gut organoids.* mBio, 2014. **5**(4): p. e01438-14.
2. Parada Venegas, D., et al., *Short Chain Fatty Acids (SCFAs)-Mediated Gut Epithelial and Immune Regulation and Its Relevance for Inflammatory Bowel Diseases.* Frontiers in Immunology, 2019. **10**: p. 277.
3. Cummings, J.H., et al., *Short chain fatty acids in human large intestine, portal, hepatic and venous blood.* Gut, 1987. **28**(10): p. 1221-1227.
4. Pomare, E.W., W.J. Branch, and J.H. Cummings, *Carbohydrate fermentation in the human colon and its relation to acetate concentrations in venous blood.* The Journal of clinical investigation, 1985. **75**(5): p. 1448-1454.
5. den Besten, G., et al., *The role of short-chain fatty acids in the interplay between diet, gut microbiota, and host energy metabolism.* Journal of lipid research, 2013. **54**(9): p. 2325-2340.
6. Clausen, M.R. and P.B. Mortensen, *Kinetic studies on colonocyte metabolism of short chain fatty acids and glucose in ulcerative colitis.* Gut, 1995. **37**(5): p. 684-689.
7. Ritzhaupt, A., et al., *Identification and characterization of a monocarboxylate transporter (MCT1) in pig and human colon: its potential to transport l-lactate as well as butyrate*. The Journal of Physiology, 1998. **513**(3): p. 719-732.
8. Bloemen, J.G., et al., *Short chain fatty acids exchange across the gut and liver in humans measured at surgery.* Clinical Nutrition, 2009. **28**(6): p. 657-661.
9. Kim, M.H., et al., *Short-Chain Fatty Acids Activate GPR41 and GPR43 on Intestinal Epithelial Cells to Promote Inflammatory Responses in Mice.* Gastroenterology, 2013. **145**(2): p. 396-406.e10.
10. Asarat, M., et al., *Short-Chain Fatty Acids Regulate Secretion of IL-8 from Human Intestinal Epithelial Cell Lines in vitro.* Immunological Investigations, 2015. **44**(7): p. 678-693.
11. Goverse, G., et al., *Diet-Derived Short Chain Fatty Acids Stimulate Intestinal Epithelial Cells To Induce Mucosal Tolerogenic Dendritic Cells.* The Journal of Immunology, 2017. **198**(5): p. 2172.
12. Miao, W., et al., *Sodium Butyrate Promotes Reassembly of Tight Junctions in Caco-2 Monolayers Involving Inhibition of MLCK/MLC2 Pathway and Phosphorylation of PKCβ2.* International journal of molecular sciences, 2016. **17**(10): p. 1696.
13. Peng, L., et al., *Butyrate enhances the intestinal barrier by facilitating tight junction assembly via activation of AMP-activated protein kinase in Caco-2 cell monolayers.* The Journal of nutrition, 2009. **139**(9): p. 1619-1625.
14. Valenzano, M.C., et al., *Remodeling of Tight Junctions and Enhancement of Barrier Integrity of the CACO-2 Intestinal Epithelial Cell Layer by Micronutrients.* PloS one, 2015. **10**(7): p. e0133926-e0133926.
15. Zheng, L., et al., *Microbial-Derived Butyrate Promotes Epithelial Barrier Function through IL-10 Receptor-Dependent Repression of Claudin-2.* Journal of immunology (Baltimore, Md. : 1950), 2017. **199**(8): p. 2976-2984.
16. Kaiko, G.E., et al., *The Colonic Crypt Protects Stem Cells from Microbiota-Derived Metabolites.* Cell, 2016. **165**(7): p. 1708-1720.
17. Sato, T., et al., *Long-term Expansion of Epithelial Organoids From Human Colon, Adenoma, Adenocarcinoma, and Barrett's Epithelium.* Gastroenterology, 2011. **141**(5): p. 1762-1772.
18. van der Hee, B., et al., *Optimized procedures for generating an enhanced, near physiological 2D culture system from porcine intestinal organoids.* Stem Cell Research, 2018. **28**: p. 165-171.
19. Andrews, S. *FastQC: A quality control tool for high throughput sequence data*. 2017; v0.11.5:[Available from: http://www.bioinformatics.babraham.ac.uk/projects/fastqc/.
20. Zerbino, D.R., et al., *Ensembl 2018.* Nucleic Acids Research, 2017. **46**(D1): p. D754-D761.
21. van der Hee, B., et al., *Congruence of location-specific transcriptional programs in intestinal organoids during long-term culture.* bioRxiv, 2019: p. 600940.
22. Reimand, J., et al., *g:Profiler-a web server for functional interpretation of gene lists (2016 update).* Nucleic acids research, 2016. **44**(W1): p. W83-W89.
23. Sorci, G., et al., *RAGE in tissue homeostasis, repair and regeneration.* Biochimica et Biophysica Acta (BBA) - Molecular Cell Research, 2013. **1833**(1): p. 101-109.
24. Chikhirzhina, E., T. Starkova, and A. Polyanichko, *The Role of Linker Histones in Chromatin Structural Organization. 1. H1 Family Histones.* Biophysics, 2018. **63**(6): p. 858-865.
25. Vitiello, M., et al., *Multiple pathways of SIRT6 at the crossroads in the control of longevity, cancer, and cardiovascular diseases.* Ageing Research Reviews, 2017. **35**: p. 301-311.

26. Giaimo, B.D., et al., *The histone variant H2A.Z in gene regulation.* Epigenetics & Chromatin, 2019. **12**(1): p. 37.
27. Bianchi, M.E. and A. Agresti, *HMG proteins: dynamic players in gene regulation and differentiation.* Current Opinion in Genetics & Development, 2005. **15**(5): p. 496-506.
28. Klune, J.R., et al., *HMGB1: endogenous danger signaling.* Molecular medicine (Cambridge, Mass.), 2008. **14**(7-8): p. 476-484.
29. Preyat, N. and O. Leo, *Sirtuin deacylases: a molecular link between metabolism and immunity.* Journal of Leukocyte Biology, 2013. **93**(5): p. 669-680.
30. Mendes, K.L., D.d.F. Lelis, and S.H.S. Santos, *Nuclear sirtuins and inflammatory signaling pathways.* Cytokine & Growth Factor Reviews, 2017. **38**: p. 98-105.

Optimized procedures for generating an enhanced, near physiological 2D culture system from porcine intestinal organoids

Bart van der Hee[1,2], Linda M.P. Loonen[1], Nico Taverne[1], Anja J.J. Taverne-Thiele[1], Hauke Smidt[2], Jerry M. Wells[1]

[1]Host-Microbe Interactomics, Animal Sciences Group, Wageningen University, De Elst 1, Wageningen, The Netherlands, [2] Molecular Ecology, Laboratory of Microbiology, Wageningen University, Stippeneng 4, Wageningen, The Netherlands

Published chapter: van der Hee B, Loonen LMP, Taverne N, Taverne-Thiele JJ, Smidt H, Wells JM (2018) Optimized procedures for generating an enhanced, near physiological 2D culture system from porcine intestinal organoids. Stem Cell Res. 28 *https://doi.org/10.1016/j.scr.2018.02.013*

Abstract

An important practical limitation of the three-dimensional geometry of stem-cell derived intestinal organoids is that it prevents easy access to the apical epithelium for testing food components, microorganisms, bioactive and toxic compounds. To this end, we here report on a new robust method for generating confluent intestinal cell monolayers from single-cell suspensions of enzymatically-dissociated porcine organoids using modified culture conditions. With this method, cell seeding densities can be standardised, overcoming problems with methods based on mechanical dissociation of organoids. Confluent monolayers formed tight junctions with high transepithelial electrical resistance in three days and could be used in experiments for up to two weeks. Multilineage differentiation of ileal stem cells was demonstrated by immunohistochemistry and RT-qPCR of cell-specific transcripts, also unequivocally confirming the controversial existence of Paneth-like cells in the porcine small intestine. The method described here is useful to standardize primary epithelial monolayer formation from intestinal organoids and allows rapid and robust studies of intestinal physiology.

Keywords: Porcine, Organoids, Monolayer, Intestinal Epithelium

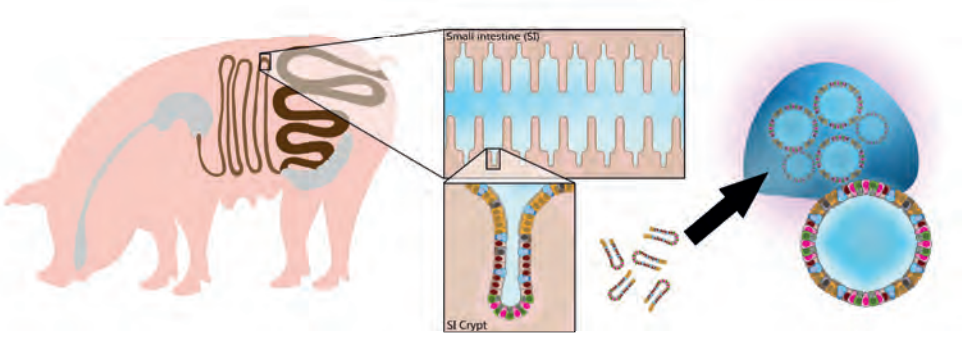

Isolated intestinal crypts form self-renewing organ-like structures (3D organoids) when embedded in Matrigel, with the addition of WNT3A, Noggin, and Spondin in F12 culture medium (BCM)

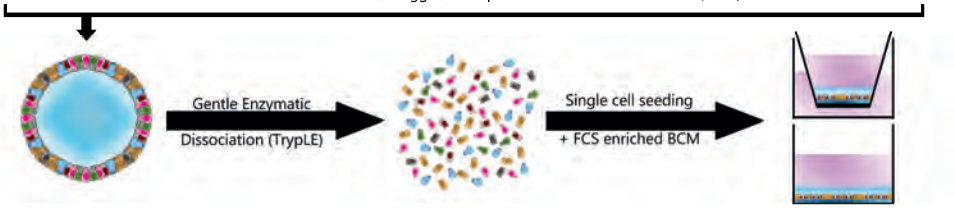

5-day-old organoids can be enzymatically dissociated into single cells and plated on matrigel precoated (0.5%) plates or transwells, with the addition of 20% FBS in the culture medium and form a 2D organoid monolayer

Highlights

•Rapid establishment of 3-D and 2-D cultures of porcine intestinal organoids

•Generation of a robust in vitro organoid model for physiological studies

•Monolayers contain multilineage cell populations

•Organoid model to facilitate luminal exposure to substances

• Existence of Paneth-like cells demonstrated in pig ileum

Introduction

Adult stem-cell derived organoids have already proven to be powerful experimental models of mammalian biology, advancing our understanding of the cellular mechanisms that drive epithelial tissue development and the role of microenvironmental factors in normal development and disease. Additionally, organoid technology enables disease phenotyping and the testing of therapeutic approaches on patient-derived cells. Adult stem cell-derived intestinal organoids are capable of self-renewal and differentiation into intestine-like structures in a 3D matrix [1, 2], which is crucial for obtaining a spatial organisation of heterogeneous tissue-specific cells resembling real-life cell lineage composition and functionality.

One practical limitation of the 3D geometry of intestinal organoids is that it prevents access to the apical epithelium for treatments with food components, microorganisms, bioactive and (toxic) compounds, unless they are small enough to pass through tight junctions or transported into cells. Although for some applications, physiological responses can be quantified in individual organoids by microscopy after microinjection of substances into the lumen [3], this can be challenging due to heterogeneity in organoid size and problems of synchronous exposure and variability in injected volumes. Furthermore, the lumen of 3D organoids accumulates debris from cell turnover which may bind or sterically hinder interaction of injected substances with the apical membranes. To overcome these problems, methods have been reported for generating short-term cultures of polarised cell monolayers derived from mechanically dissociated organoid cultures [4-6]. However, in our hands this method often leads to slower growth, increased variability between wells, and appearance of 3D organoid structures on the surface of the cell monolayer.

Cultures of polarised intestinal cell monolayers are important not only for ease of access to the apical surface but also because transepithelial permeability and responses to food and microorganisms can be measured in a more standardised way (i.e. using similar numbers of cells and trans-epithelial resistance measurements). To exploit the benefits of two-dimensional cultures, the aim of this study was to develop a robust and reproducible method for generating a confluent monolayer of porcine intestinal organoids based on enzymatic dissociation into single cells, rather than mechanical disruption and fragment seeding. Our hypothesis was that such a method would enable the seeding density and time of culture to be standardised, thereby increasing efficiency, and reducing experimental variation. Indeed, our method rapidly generates organoid-derived cell monolayers within three days after seeding, for pharmacological or transport studies. Additionally, the growth of organoid cells on a planar surface facilitated whole cell cytochemistry due to

increased cellular resolution. As an example of the application of this new method we monitored cellular development and re-examined the controversial existence of Paneth-like cells in the porcine small intestine [7, 8].

Materials and methods

Ileum organoid culture

Ileum organoids were generated from intestinal tissue of two 5month-old slaughter pigs, according to the procedure described by Sato and colleagues [9] with minor modifications (see Supplementary methods SM1.1). Porcine ileal organoids were grown in basal culture medium that was refreshed every two days (BCM: DMEM/F12 (Gibco), supplemented with 100 µg/ml primocin (Invivogen), 10 mM HEPES (HyClone), 1 × B-27 (Gibco), 1.25 mM Nacetylcysteine (Sigma), 50 ng/ml human epidermal growth factor (R&D systems), 15 nM gastrin, 10 mM nicotinamide, 10 µM p38 MAPK inhibitor (Sigma), 600 nM TGFβ receptor inhibitor A83-01, and conditioned media for recombinant Noggin (15% v/v), Spondin (15% v/v), and Wnt3A (30% v/v) provided by Dr Kuo and the Hubrecht Institute). Organoids were passaged at a 1:5 ratio every 5 days by mechanical dissociation and plating in fresh Matrigel matrix droplets (Basement Membrane, Growth factor reduced, REF 356231, Corning, Bedford, MA, USA).

Two-dimensional monolayers

Spherical ileum organoids were recovered from Matrigel after 5 days growth by addition of ice-cold DMEM/F12 medium, transferred into 15 ml tubes followed by centrifugation at 250 ×g for 5 min. The pellet of organoids was incubated in TrypLE Express dissociation medium (Gibco) for 10 min at 37 °C and dissociated by repeated pipetting to obtain a single cell suspension (see supplementary methods SM1.2 for images). Four volumes of BCM, enhanced with 20% (v/v) FBS (E-BCM) was added to the single cell suspension and centrifuged at 900 ×g for 5 min. Cell pellets were resuspended in E-BCM, counted manually using a Bürker chamber and seeded at 78,125 cells/cm^2 in pre-coated culture plates or Transwells. The pre-coating procedure involved incubation with 0.5% (v/v) Matrigel in F12 medium at 37 °C for 1 h after which the liquid was removed, and the plates were air-dried for 10 min. After 3 days incubation at 37 °C (5% CO_2) the cell monolayers reached confluence and were used for experiments.

Transepithelial electrical resistance (TER)

Spheroids at 5 days after passage were recovered from Matrigel and dissociated into single cells as described in Section 2.2. Transwell inserts were coated in the apical

chamber as described in Section 2.2. Single cells were seeded at a density of 2.5 × 10^4 cells/well in 24-well transparent transwell inserts (0.33 cm^2, Falcon, BD), and incubated with 400 µl apical, and 800 µl basolateral E-BCM with or without 10 µm ROCK inhibitor (Y27632, Tocris Biotechne, United Kingdom). For transepithelial electrical resistance (TER) measurements, six transwell inserts per group were placed in a Cellzscope apparatus (Nanoanalytics, Münster, Germany) 2 h after seeding, containing 500 µl basolateral BCM. ROCK inhibitor was removed after 24 h postseeding, and medium was refreshed in all wells using E-BCM. TER of the forming monolayers was measured over 72 h post-seeding as previously described (Karczewski et al., 2010).

Permeability measurements of the cell monolayer

To follow epithelial permeability to small molecules, stationary TER monolayers were apically treated with 0.5 mg/ml 0.4 kDa FITC, 4 kDa or 40 kDa FITC-Dextran (Thermo-Fisher). Controls contained transwells without a monolayer. At 5, 10, 30, 60, 120 and 240 min, 50 µl of basolateral medium was measured on FITC-dextran contents using fluorescence on a Spectramax M5 (Molecular Devices, Sunnyvale, CA, USA) with 490 nm excitation and 530 nm emission.

Monolayer formation using ROCK inhibitor

To visualize the impact of seeding density and ROCK inhibitor on monolayer formation, cells were treated with or without ROCK inhibitor for 24 h [4], two-fold dilution series from 10 × 10^4 to 1.25 × 10^4 cells/well, and subsequently grown for 72 h. After 72 h, cell monolayers were fixed in 1% paraformaldehyde (PFA), and nuclei were stained (Hoechst) for 20 min. Images of cell monolayers were acquired using a high-content, high-throughput microscope (BD Pathway HT 855, BD Biosciences). Images were stitched in 4 × 5 image grids using Attovision software, and slightly adjusted for brightness and contrast to show nuclei in ImageJ. For growth videos, serial dilutions of cell suspensions were plated in pre-coated 96-well culture plates (Corning), placed in an oCelloscope (BioSense Solutions, Denmark) 2 h after seeding, and migration and proliferation was imaged every hour for 70 h.

Cell lineage identification of porcine tissue and 2D-monolayers

Confluent cell monolayers or ileal tissue were fixed with 1% PFA, Carnoy's or 4% PFA, respectively, for 1 h at room temperature. Tissues and monolayers were prepared for incubation with antibodies to identify different cell types present (Table 1 and *supplementary methods*).

Table 1. List of antibodies used for cell identification. Stem cells (SOX9), proliferative (PCNA), enteroendocrine (Chromogranin A), goblet cell (Mucin-2), Enterocyte (Villin), Paneth (Lysozyme), and TJ proteins Occludin and Zonula-occludens 1 (ZO-1).

ANTIBODY	PRODUCT NUMBER	SUPPLIER	ANTIGEN RETRIEVAL (TISSUE)	CLONALITY	ANTIBODY ID
SOX9	AB5535	Merck-Millipore	No	Polyclonal	AB_2239761
PCNA	MAB424R	Merck-Millipore	No	Polyclonal	AB_95107
CHROMOGRANIN-A	20086	Immunostar	No	Polyclonal	AB_10717642
MUCIN-2	GTX100664	GeneTex	No	Polyclonal	AB_1950958
VILLIN	SC-58897	Santa Cruz	Yes	Monoclonal	AB_2304475
LYSOZYME	A0099	Dako	Yes	Polyclonal	AB_2341230
OCCLUDIN	71-1500	Thermo-Fisher	No	Polyclonal	AB_88065
ZO-1	33-9100	Thermo-Fisher	No	Monoclonal	AB_87181

Transmission electron microscopy

Preparation of tissue and staining was performed as previously described [10]. Briefly, confluent monolayers were fixed overnight in Karnovsky's fixative (1% glutaraldehyde, 3% formol, in 0.2M PBS at pH 7.2). Fixed monolayers were washed in ice-cold 0.1M sodium-cacodylate buffer (containing 0.075% Ruthenium red) and treated with 1% osmium tetroxide (in H_2O). After a graded series of dehydration steps in ethanol, samples were treated with epoxypropane and epon, and subsequently embedded in epon overnight at 60 ^{o}C. All following procedures were executed as previously described, and images were captured using a JEM-1400 Flash TEM (JEOL Ltd, Japan).

RT-qPCR for cell specific transcripts

Total RNA was extracted from spheroids and 3-day old monolayers using a Qiagen mini-kit following manufacturer's instructions, including an on-column DNase treatment (Cat No.: 74104 and 79254). cDNA was generated from 1 µg total RNA using the QScript cDNA synthesis kit (Quantabio), and qPCR was performed using a Rotorgene-Q2 Plex (Qiagen) for cell-specific transcripts with 7 µl SYBR green (Qiagen), 0.25 µl RNAse free water, 1.75 µl primer mix (5 mM desalted forward and reverse in H2O), and 5 µl template cDNA following methods previously described (Loonen et al. 2014). Relative expression values were calculated using GAPDH and β-Actin as endogenous controls, using the delta Ct method previously described [11] using individual amplification values.

Table 2. Primers for cell-specific transcripts to identify or follow cell type differentiation in porcine intestinal organoids. LGR5 for stem cells, PCNA for proliferating cells, MUC2 for goblet cells, CGA for enteroendocrine cells, SGLT1 for mature enterocytes, LYZ1, FZD5 and EPHB2 for Paneth cells, and GAPDH and B-ACTIN for endogenous controls. All primer sequences are given in 5′ – 3′ direction (AT: Annealing temperature).

Gene	***Forward***	***Reverse***	***AT (°C)***	***Size (bp)***	***Ref***
LGR5	CCT-TGG-CCC-TGA-ACA-AAA-TA	ATT-TCT-TTC-CCA-GGG-AGT-GG	60	110	[12]
PCNA	TAC-GCT-AAG-GGC-AGA-AGA-TAA-TGC	TGA-GAT-CTC-GGC-ATA-TAC-GTG	60	192	[13]
MUC2	GGC-TGC-TCA-TTG-AGA-GGA-GT	ATG-TTC-CCG-AAC-TCC-AAG-G	60	249	[12]
CGA	GAC-CTC-GCT-CTC-CAA-GGA-GCC-A	TGT-GCG-CCT-GGG-CGT-TTC-TT	60	332	[12]
SGLT1	GCA-GCT-GTC-TTC-CTA-CTT-GC	GCA-AAC-TCG-GTA-ATC-ATA-CGG	60	113	[12]
LYZ1	GGT-CTA-TGA-TCG-GTG-CGA-GT	AAC-TGC-TTT-GGG-TGT-CTT-GC	60	220	[12]
FZD5	CTG-TGG-TCT-GTG-CTG-TGC-TT	TAG-TGG-ATG-TGG-CTG-TGC-TC	62	200	This study
EPHB2	CGC-TTT-CTG-GAG-GAC-GAT-AC	CCT-GCT-CTA-TGG-CGT-TGA-TT	62	220	This study
GAPDH	ATC-CTG-GGC-TAC-ACT-GAG-GAC	AAG-TGG-TCG-TTG-AGG-GCA-ATG	60	108	[12]
B-ACTIN	CAC-GCC-ATC-CTG-CGT-CTG-GA	AGC-ACC-GTG-TTG-GCG-TAG-AG	63	380	[14]

Results

Development of a method for growing 2D organoid cultures

Growth of 3D porcine intestinal organoids has been previously described [12], although a follow up study by the same authors highlighted the fact they were not long-lived and limited to about ten passages [15]. In our study, the conditions described resulted in formation of spheroids within 3–5 days and appearance of mature cryptile morphology by day 7 to 10 without restrictions of the Hayflick limit or replicative potential (Fig. 1A). In the medium of Khalil et al., stem cells may not be adequately maintained due to absence or limiting amounts of growth factors, while our medium allowed 3D organoid cultures to be passaged for at least several months (Fig. 1A). Using our 3D culture method, stem/progenitor cells were observed at the bottom of crypts (by immunofluorescent histology), where they are normally maintained by asymmetric division. This is unaffected by long-term passage of organoids, indicating that stem cells are not lost in our 3D culture system. Confluent monolayers were generated by disruption of 5-day old spheroids into a single cell suspension that was plated on Matrigel coated Transwells or tissue culture plates in E-BCM (Fig. 1B–C; Supplementary video S1). Although previous studies on mouse and human 2D organoid culture employed gelatine or collagen-based coatings we found Matrigel to be suitable [4-6, 16]. We observed that the seeding density in 96-well plates (0.33 cm^2/well) affected the capacity to generate monolayers, with an optimal density of 1.5 to 2.5 × 10^4 cells per well considering growth kinetics and efficient use of cells (Fig. 1D). At lower and higher cell densities, confluent monolayers were not obtained at three days. Although confluency was reached with higher seeding densities within 24–30 h post-seeding, this was lost after 50 h (Supplementary videos S2-S3). ROCK inhibitor was used in previous studies on 2D organoid cultures to inhibit caspase-dependent pathways of apoptosis. However, in our hands use of ROCK inhibitor slowed growth and formation of confluent monolayers in the 3-day incubation and was not necessary for overall cell survival (Fig. 1E).

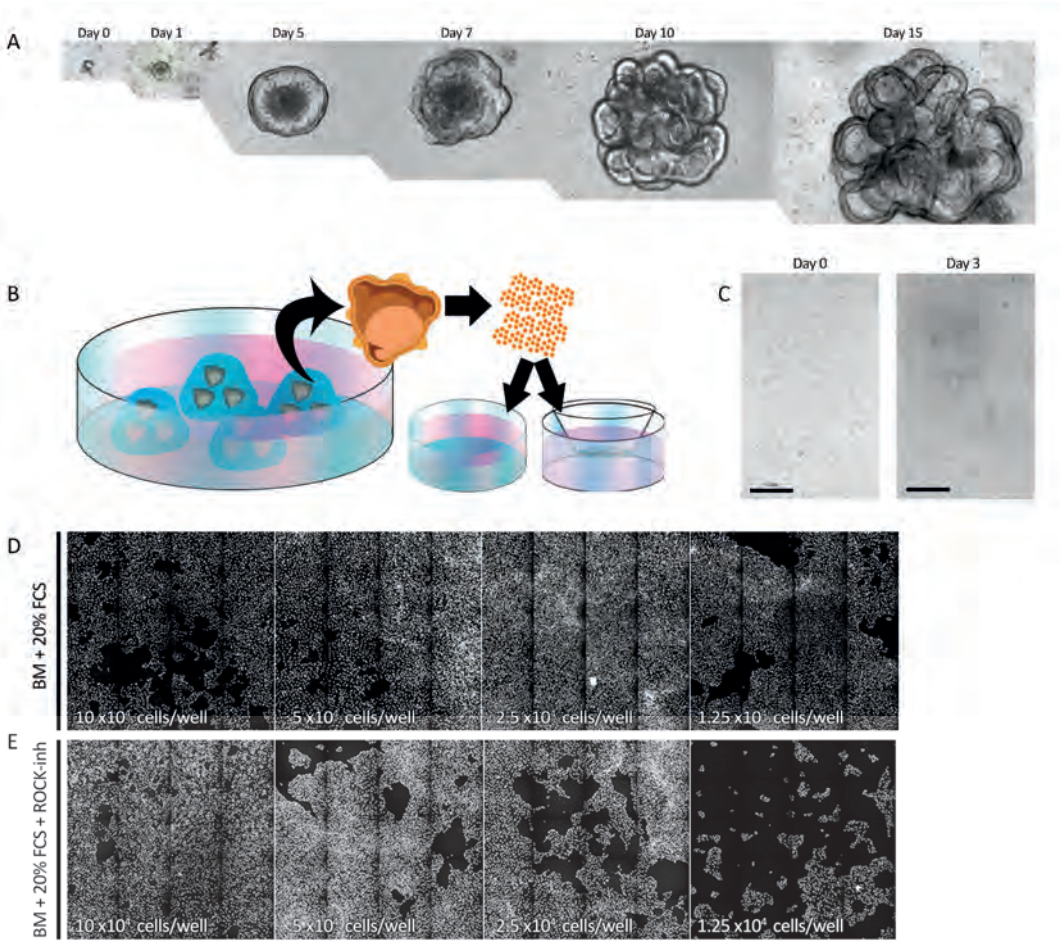

Figure 1. Growing 3D intestinal organoids from porcine ileal crypts and monolayer formation. (A) Time course of organoid development from isolated intestinal crypts. After crypt isolation, small spheroids form 1 day after culture in Matrigel, mature over time and form crypt-like structures after 7 days. (B) Graphical representation of 3-dimensional organoid isolation and plating of single cells for monolayer formation. 3D spheroids can be isolated from Matrigel droplets, enzymatically dissociated into single-cells, and plated on pre-coated plates or Transwells. (C) After single cell plating, cells attach within 1 day and grow into a confluent monolayer within 3 days (black bar = 50 µm). Single cells at different seeding densities (white text), incubated in the absence (D) or presence (E) of 10 µM ROCK inhibitor for 24 h, were grown for 3 days in 96-well plates (0.33 cm2/well), and imaged in a 4 × 5 grid using a BD Pathway.

Confluent 2D organoid cultures form cellular junctions resulting in high TER values

After 3 days culture the confluent organoid monolayers reproducibly gave a TER value between 1032 and 1120 Ω/cm^2, whereas addition of ROCK inhibitor led to loss of TER over time, resulting in values between 206 and 253 Ω/cm^2 (Fig. 2A). The TER could be maintained for 12–15 d when medium was replenished daily (Supplementary Fig. 1). The permeability of confluent organoid monolayers to fluorescein-conjugated dextran of different molecular weight was investigated in the Transwell system using a fluorimeter. Paracellular permeability for fluorescent dextrin was highly reproducible between wells and showed size dependent flux across the epithelial monolayers (Fig. 2B). Formation of tight-junctions was confirmed by staining for occludin and ZO-1 (Fig. 2C and Supplementary Fig. 2). TEM micrographs revealed the presence of paracellular adherens and desmosome junctions (Fig. 2D).

Multilineage differentiation of porcine 2D organoid cultures

Immunohistochemical methods were used to show that the differentiated cell lineages found in the tissue of origin were also present in 2D organoid cultures. Sox9, a transcription factor and recognized marker of stem/progenitor cells, revealed these cells in tissue crypts and throughout the 2D monolayers (Fig. 3A and B). Proliferating cells staining positive for proliferating cell nuclear antigen (PCNA) were similarly distributed throughout the 2D monolayers. The homogeneous distribution of stem cells in the monolayers confirms successful stem cell maintenance in the 3D organoids. Additionally, goblet cells (MUC2 positive) and enteroendocrine cells (Chromogranin A-positive) were identified in both tissue and 2D monolayers (Fig. 3X, Y, K, and Supplementary Fig. 3). Large numbers of villin-positive cells in villus tips and throughout the 2D monolayer indicated the presence of mature absorptive enterocytes. Moreover, microvilli, which are characteristic of mature enterocytes, were seen on the apical membrane of cells in the 2D monolayers using immunohistochemistry (Fig. 3J) and TEM (Fig. 3K). Measurements of relative expression of cell lineage-specific transcripts in 2D and 3D organoid cultures supported the histochemical evidence for presence of different epithelial cell types (Fig. 3L). The RTqPCR data suggested that 2D cultures may contain more stem cells and goblet cells than 3D organoids.

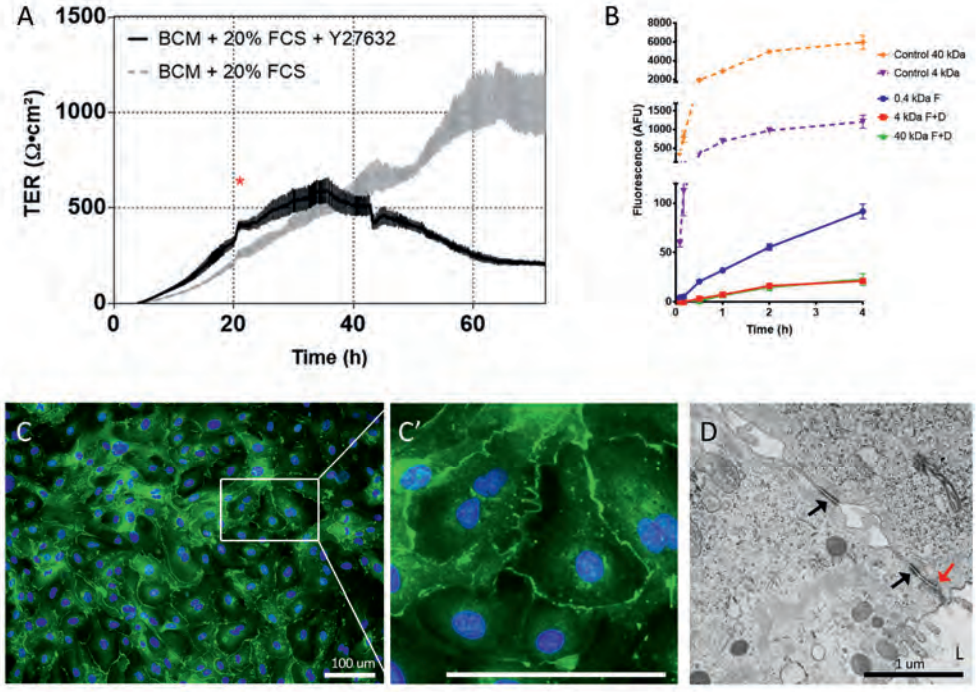

Figure 2. Tight junction formation of the epithelial monolayer. (A) Transepithelial electrical resistance (TER) was measured for 72 h post-seeding (Grey line = Non-treated, Black line = Treated 24 h with ROCK inhibitor, n = 6 per group, error bars = SEM, red star = medium replacement). (B) Transport of 0.4 kDa, 4 kDa, and 40 kDa FITC-Dextran across the confluent monolayer over time (n = 4 per group, data is shown ± SEM, controls were inserts without monolayer). (C) Occludin staining (green) in cell monolayers after 3 days growth in 96-well plates shows tight junction formation (C' = Insert of C showing enlarged picture, white bars = 100 µm). (D) TEM pictures of tight junctions (red arrow), adherens junction and desmosomes (black arrows) (L = luminal side, black bar = 1 µm).

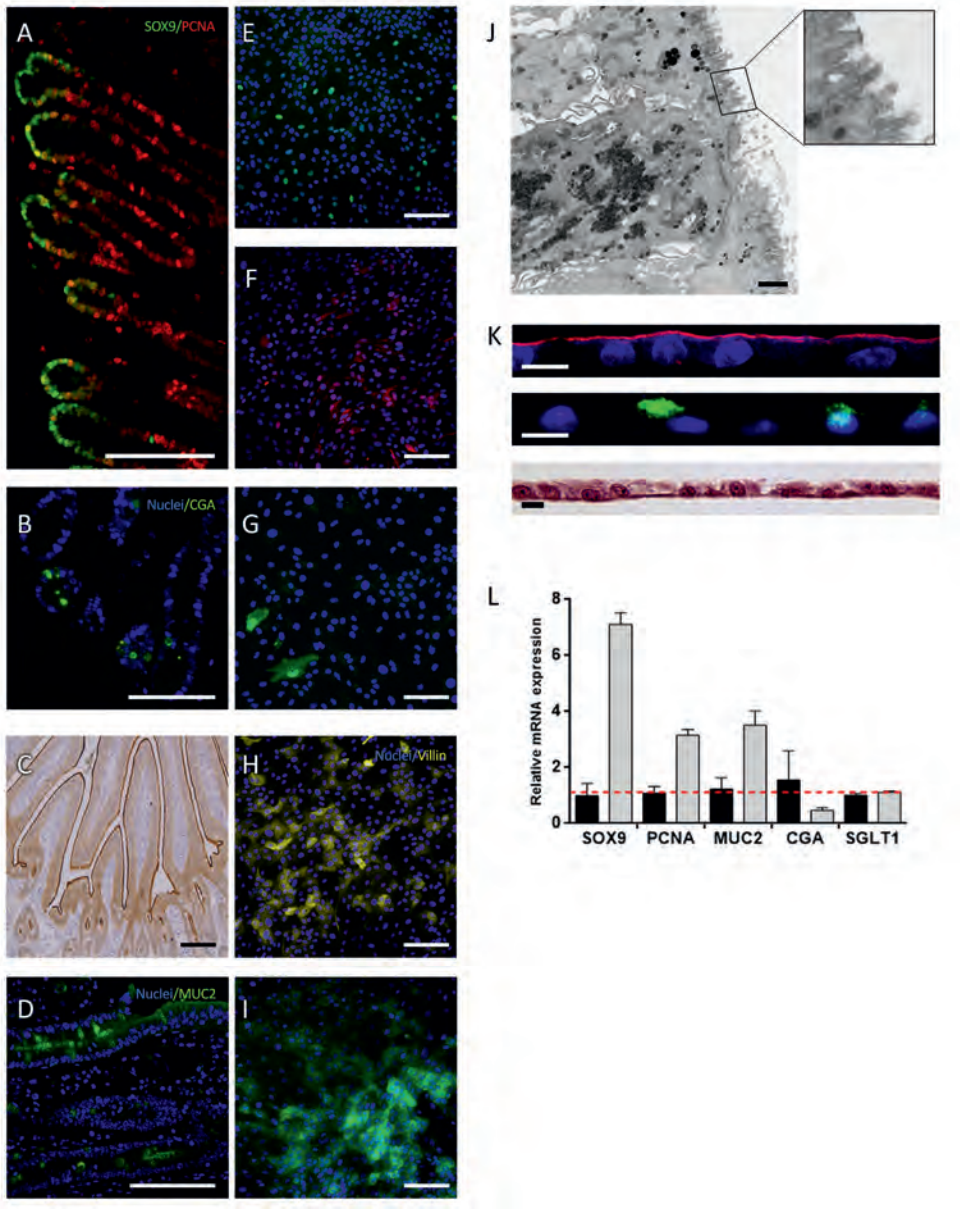

Figure 3. Identification of different cell lineages in organoid monolayers. Staining for specific cell lineages in porcine tissue with antibodies for: (A) SOX9, stem/progenitor cells and PCNA, proliferating cells; (B) Enteroendocrine (CGA); (C) Mature enterocytes (VIL1); (D) Goblet cells (MUC2). The same cell types found in tissue were seen in monolayers after three days culture; progenitor SOX9 (E), proliferative PCNA (F), enteroendocrine CGA (G), mature enterocytes VIL1 (H); and goblet cells MUC2 (I). (J) TEM showing apical microvilli on the cell monolayers. (K) Transwell grown monolayers were immunostained with VIL1 (red) or MUC2 (green) or stained with H&E to show cell differentiation. (L) Relative mRNA expression of cell specific transcripts to show maturation of the cell monolayer between 3D (black) and three-day-old monolayers (grey). Data is shown as mean ± SEM, n = 4 per group, red line = 1.

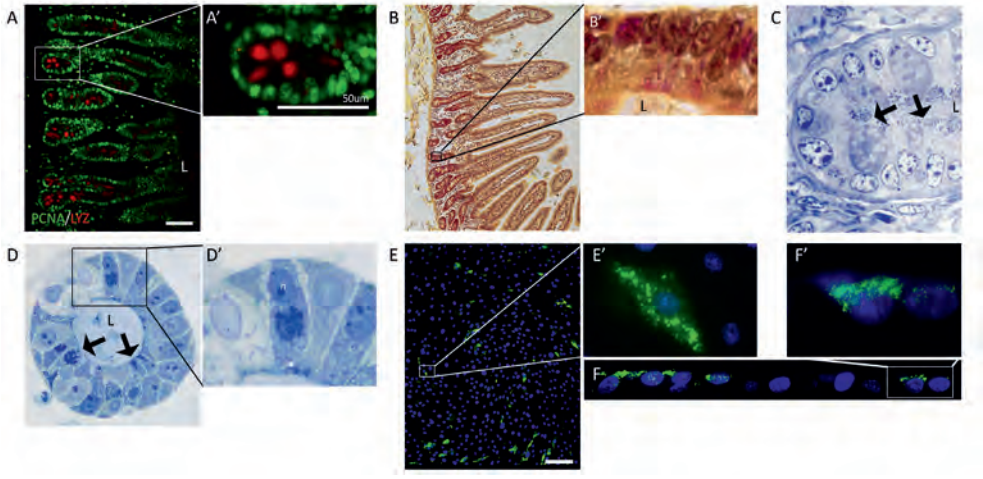

Figure 4. Paneth cell identification in porcine intestinal development. Ileal tissue was stained for lysozyme (A-A') or phloxine-tartrazine (B-B') to show apical granules in the intestinal crypt. (C) TEM image of ileal crypt to show apical granular cells (black arrows). (D) 3D organoid showing cells containing apical granules (D' and black arrows). Growing monolayers from ileal tissue stained with lysozyme (E-E') and transwells (F-F') showing apical granules. L: indicates luminal side of tissue or organoid.

Identification of Paneth cells in porcine small intestine and organoid cultures

The existence of Paneth cells in the porcine small intestine is controversial, but here we showed lysozyme-positive and phloxine-tartrazine staining at the bottom of the crypts (Fig. 4A-B). Moreover, secretory-like granules found in Paneth cells were detected using TEM in tissue (Fig. 4C and Supplementary Fig. 4A) and 3D organoids (Fig. 4D). In 2D organoid cultures lysozyme-positive cells were detected throughout the monolayer (Fig. 4E) and at higher magnification lysosome staining appeared speckled, suggesting its location within apical secretory granules (Fig. 4E–F). To substantiate differentiation to Paneth cells, expression of genes encoding Lysozyme 1 (LYZ1), Frizzled 5 (FZD5) and Ephrin-beta receptor 2 (EPHB2) was measured by RT-qPCR (Supplementary Fig. 4B-C). Overall, these results demonstrate that the Paneth cell lineage is also present in the porcine small intestine and that adult stem cells from the ileum can differentiate into this cell type in primary epithelial culture.

Discussion

Here, we report on the development of a robust method for generating confluent organoid cell monolayers from porcine 3D intestinal organoid cultures in three days. Previously described methods for generating 2D intestinal organoid cultures are based on seeding of organoid fragments into tissue culture plates or Transwells following mechanical disruption, and partial enzymatic dissociation [4-6, 17]. Here we used complete enzymatic dissociation of organoids to generate cell suspensions, allowing us to accurately count cells and optimize the seeding density to give reproducible results. None of the previous studies used completely dissociated suspensions of organoid cells, presumably to minimize anoikis or epithelial cell detachment-induced apoptosis [18].

To prevent anoikis, the previously described methods used ROCK inhibitor during the first 24h after dissociation, which is reported to block caspase-dependent apoptotic pathways [19, 20]. However, we found that adding ROCK inhibitor to single-cell dissociated porcine organoids resulted in reduced growth over time. Moreover, adding ROCK inhibitor led to a maximal TER value of about 500 Ω/cm^2 after culturing for about 30 h, which then decreased to 253 Ω/cm^2 by 60 h. This is consistent with previous findings that were obtained in calcium switch assays showing that ROCK is necessary for the assembly of tight and adherens junctions. Upon calcium repletion, occludin, zonula occludens 1, and E-cadherin failed to redistribute to the intercellular junctions; assembly of the apical F-actin cytoskeleton was prevented, and barrier function failed to recover in the presence of ROCK inhibitor [21]. We concluded therefore that ROCK inhibitor has similar detrimental effects on the assembly of tight junctions and intercellular permeability when growing porcine monolayers for trans-epithelial studies when growing 3 days. Another difference to previous studies is that we used an enhanced basal culture medium (E-BCM) containing a higher percentage of serum (20% v/v). This may have helped to reduce apoptosis due to the increased concentration of anti-apoptotic growth factors.

It is difficult to estimate the number of cells seeded into 2D culture using previously reported methods because organoid fragments were used. In the method of Moon et al. (2014), seeding density was estimated to be about 5×10^5 cells per well, which resulted in about 50% loss of cells at the end of the culture period [4]. In our model, enzymatically dissociated single cells seeded at 1×10^5 per well showed no significant increase in cell number after 3 days, whereas 2.5×10^4 cells per well resulted in a 6–8-fold increase in total cell number (data not shown). Thus, seeding densities, which are difficult to estimate for not fully dissociated organoid fragments, appear to be critical to prevent cell loss and to generate confluent monolayers. These

findings may explain results of recent studies, which failed to generate confluent monolayers using the previously described fragment seeding methods [6]. In our studies, we have employed a trypsin-like alternative from fungal-derived protease (TrypLE Express) which has similar dissociation kinetics to trypsin but induces lower cell toxicity and retains extracellular proteins. Other 'gentle' dissociation methods may also be considered [22].

Using our method, the porcine organoid monolayers grown in Transwell devices generated a TER of about 1000 Ω/cm^2, which is comparable to the porcine cell line IPECJ2 [23]. Staining for occludin and ZO-1 revealed the presence of tight junction complexes between adjacent cells across the entire monolayer. Previously described methods reported TER values of 400 Ω/cm^2 in human-derived, and 400–3000 Ω/cm^2 in mouse-derived monolayers [4, 5, 17]. Our model gave a low standard error between samples (CV = 2.96%), showing that it is a robust and reproducible system at least for intestinal tissue.

Plating porcine intestinal organoids as single-cells initiated multilineage differentiation without the need for previously described differentiation medium or γ-secretase-inhibitor (DAPT; [4, 5]). However, asymmetric division of stem cells is crucial to maintain self-renewal of the cell monolayer and the homogenous distribution observed in our staining confirms successful stem cell maintenance. Increased relative abundance of the Sox9 mRNA in 2D culture might indicate higher self-renewal of stem cells due to a faster growth rate when compared to 3D cultures (as suggested by [6]). Multilineage differentiation allowed us to follow rapid stem cell differentiation on a planar surface, including the development of classical Paneth cells, the existence of which has been debated in pigs [7, 8, 24]. In other species, Paneth cells have been shown to be important in stem cell regulation and maintenance [25, 26].

Cross-species comparisons of Paneth cell characteristics have identified lysozyme staining as an important marker [25, 27]. A recent study failed to detect lysozyme-positive cells or lysozyme encoding gene transcripts in porcine tissue and organoids derived from different intestinal locations. Nevertheless, the authors showed the presence of cells containing apically located secretory vesicles in porcine intestinal crypts, which they concluded might be Paneth-like cells [12]. In contrast to other studies we detected Paneth cells in crypts of ileum tissue and in organoid crypts using antibodies to lysozyme and the classical histological method for staining Paneth cells with phloxinetartrazine. Previously attempts to stain lysosome positive cells may have failed due to use of different antibodies to lysozyme. Furthermore, Paneth cell granules differ in electron density and morphology between different animal species [28], and may have been difficult to observe in previous studies. Using

our 2D model, we showed supranuclear staining of lysozyme containing granules after growth for 3 days. To validate the existence of Paneth cells in our organoid cultures we demonstrated expression of genes coding for LYZ1, EPHB2, and FZD5, which are important transcriptional markers for Paneth cell differentiation [29]. Furthermore, we showed TEM pictures of granules inside tissue crypt cells with similar morphology as human Paneth cells. This finding further strengthens the pig as a translational model for human intestinal physiology [30, 31]. To fully determine if Paneth cells constitute niche support for stem cells in the porcine intestine as shown in mice [25], more research is needed.

A key advantage of our porcine 2D model is easy access to the apical surface and reproducible, rapid formation of confluent monolayers with a high TER for investigating drug or nutrient transport and permeability functions. Moreover, the monolayers contain cell lineages present in the tissue of origin, creating a near physiological model for studies on innate immunity, infection and disease associated polymorphisms through gene editing [4, 5, 32, 33]. An advantage of the 3D intestinal organoid culture is the reproduction of the spatial morphology of a differentiated epithelium which is needed to study mechanisms involved in self-organization of tissue and development. Cultures of polarized cell monolayers on the other hand allow easy access to the apical surface and facilitate transport studies. This is important for studies on cell signaling and cellular responses because many receptors are differentially expressed on the apical and basolateral membranes, including transporters, Toll-like receptors (TLRs) and cytokine receptors [34-36]. Different cellular transcriptional responses have been reported for polarized intestinal monolayers stimulated apically or basolateral with agonists of TLR9 [37]. Furthermore, the direction of the stimulus leading to a cellular response can lead to polarized secretion of effector molecules such as chemokines [34, 38] which can be more easily studied using polarized cell monolayers.

Supplementary information
Supplementary data to this article can be found online at
https://doi.org/10.1016/j.scr.2018.02.013

Supplementary methods

SM1.1 Generating intestinal spheroids from porcine ileal tissue

Following dissection of ileal tissue, intestinal sections were opened longitudinally, washed by emersion in ice-cold PBS, and the villi removed by gentle scrapping of the mucosa with a glass slide. The remaining tissue was washed 5 times in ice-cold PBS using a vortex mixer and then incubated for 30 minutes at 4 °C in 2 mM EDTA chelation buffer. After 3 washes in ice-cold PBS, a scalpel was used to remove intestinal crypts, which were recovered by passing through a 70 µm strainer into fresh PBS containing 5% (v/v) FBS at 4 °C. The suspension was centrifuged at 300 x g for 5 minutes to separate the crypts from single cells. The total number of crypts was calculated by microscopic counting, and crypts were pelleted by centrifugation and resuspended in Matrigel at 100 crypts/25 µl. Matrigel was then diluted 0.5 volumes with basic culture medium, and dispensed as small hemispherical droplets in 24-well plates. Plates were then inverted and incubated at 37 oC for 15 minutes to promote polymerization of Matrigel, and then 600 µl basic culture medium was added per well.

SM1.2 Extended methods for monolayer formation

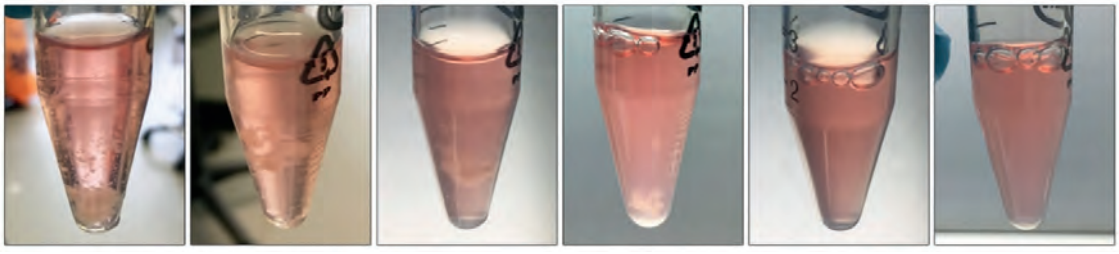

Figure SM1. After isolation from Matrigel, organoids were pelleted at 250 x g for 5 min. Supernatant was aspirated, and 2 mL TrypLE dissociation reagent was added (Gibco). The pellet was gently resuspended (first image) and placed in a water bath at 37 oC. After a few minutes, the mixture formed a clump and was dissociated using repetitive pipetting with a 200 µl pipet tip (last two images) providing a single-cell suspension within 10 minutes.

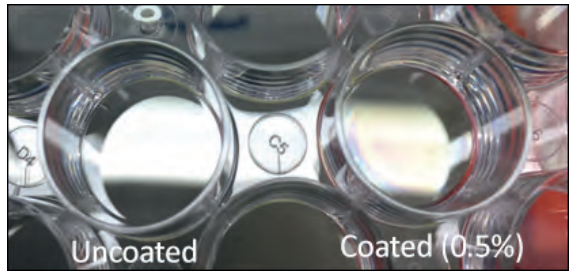

Figure SM2. Coating of the wells generated a small film of Matrigel. 0.5% (v/v) Matrigel was added to ice-cold DMEM/F12 medium and added to 96-well tissue culture plates (Corning) or Transwell inserts (BD Falcon). The plates were incubated at 37 oC for 1 hour, and medium was aspirated. After aspiration, the plates were placed in the fume-hood without a lid to dry for 10 minutes, prior to seeding with a single-cell suspension.

SM2 Histological analysis of tissue and monolayers

Staining procedures were carried out following previously described methods with minor changes (Loonen et al. 2014). Confluent cell monolayers were fixed in 1% paraformaldehyde (PFA) for 1h at room temperature and permeabilized by washing three times in TBS-t buffer containing 8.8 g/L NaCl, 6.06 g/L Tris-base, and 0.02% triton X-100 at pH 7.4. Paraffin-embedded sections of ileum tissue fixed with Carnoy's or 4% (w/v) PFA were dried onto poly-L-lysine-coated glass slides and permeabilized by washing in TBS-t buffer as described above. The ileum tissue sections were subsequently incubated at 95 °C in 10 mM citrate buffer (pH 6.0) for 10 min to facilitate antigen retrieval. Cross reaction of endogenous immunoglobulins was blocked with 5% (v/v) normal goat or donkey serum for 30 min at room temperature (RT) and subsequently incubated with primary antibody overnight at 4 °C (see supplementary table 1 for antibody list). Slides were washed three times in TBS-t at RT and incubated with Alexa fluor 488 or Cy3 (Thermo-Fisher) for 60 min. Nuclei were stained with Hoechst for 30 minutes at RT. Confluent monolayers were imaged using a Leica DMi8 inverted microscope and DFC3000 G camera, and tissue sections were captured using a Leica DM6 microscope and DFC365 FX camera. Monolayers grown on Transwell inserts were fixed in 1% PFA or Carnoy's fixative for 20 minutes. Transwell inserts were gently removed using a scalpel and processed in 1.5 ml tubes (Eppendorf). After a series of dehydration steps, the inserts were vertically embedded in paraffin. Sections (5 µm thick) were processed and stained as previously described above.

Tissue sections were also stained for Paneth cells using Lendrum's phloxine-tartrazine. Following graded series of xylene and ethanol, nuclei were stained with Mayer's hematoxylin. After washing in running tap water for 5 minutes, the sections

were submerged in solution A (0.5 g Phloxine B, 0.5 g calcium chloride, 100 mL distilled water) for 10 minutes. Sections were subsequently rinsed in tap water, and 2-ethoxy ethanol (cellosolve) to remove water residue. Then the sections were placed in solution B (100 ml cellosolve and tartrazine to saturation) for 10 minutes until the tissue became yellow. The slides were then rinsed thoroughly with absolute ethanol, dehydrated to xylene, and embedded using depex.

Supplementary figures

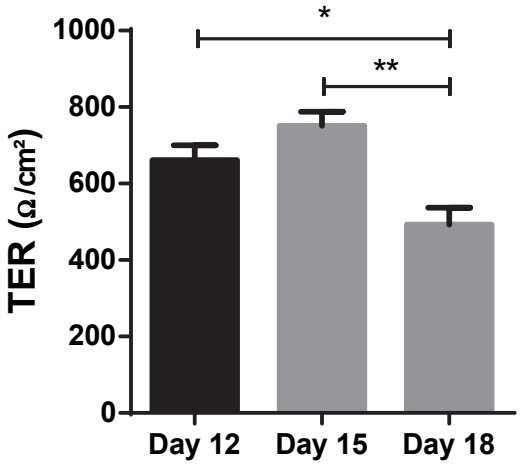

Supplementary figure 1. TEER is maintained for at least 15 days, when apical E-BCM is refreshed daily, and basolateral E-BCM every 2 days. Enzymatically dissociated single cells were seeded at 2.5 x 104 cells per well and grown for 2 weeks. At day 12 and 15, TER was measured using a volt-ohm meter (Millicell-ERS, Millipore), and resistance in Ω/cm2 was calculated using transwell size (0.33 cm2, n = 12 transwells). Significance of observed differences between days was tested using One-way ANOVA with Tukey multiple comparisons (Graphpad Prism 6.0, ** P < 0.01, * P < 0.05).

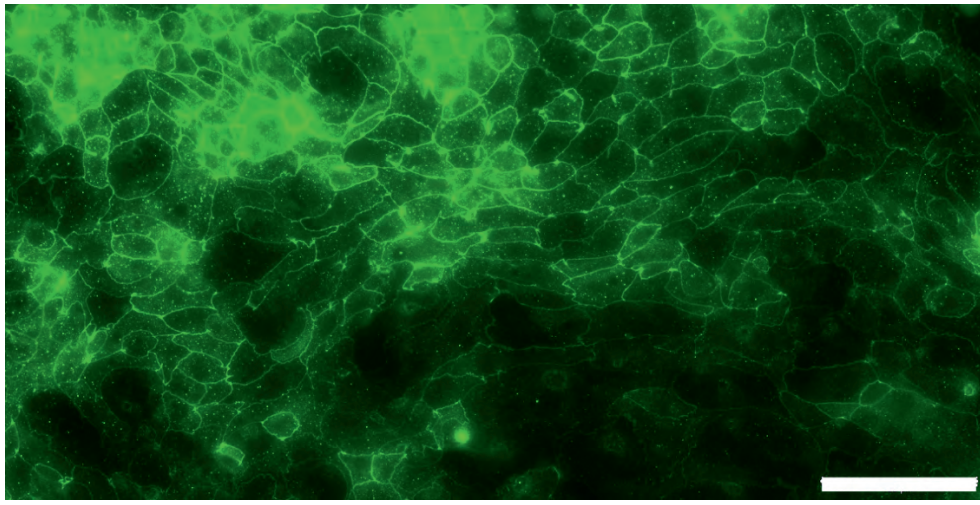

Supplementary figure 2. Zonula-occludens 1 (ZO-1) staining (green) in cell monolayers after 3 days of growth to show tight junction formation (white bar = 100 µm). Cells were grown as a monolayer for 3 days and fixed in 1% PFA for 24 h at RT. Slides were washed in TBS-t buffer, and stained with ZO-1 antibody at 1:100, containing 1% normal donkey serum in TBS-t buffer overnight at 4 oC. The slides were then washed and counterstained using 1:200 donkey anti-mouse Cy3. Subsequently, the slides were imaged using protocols described in SM2.

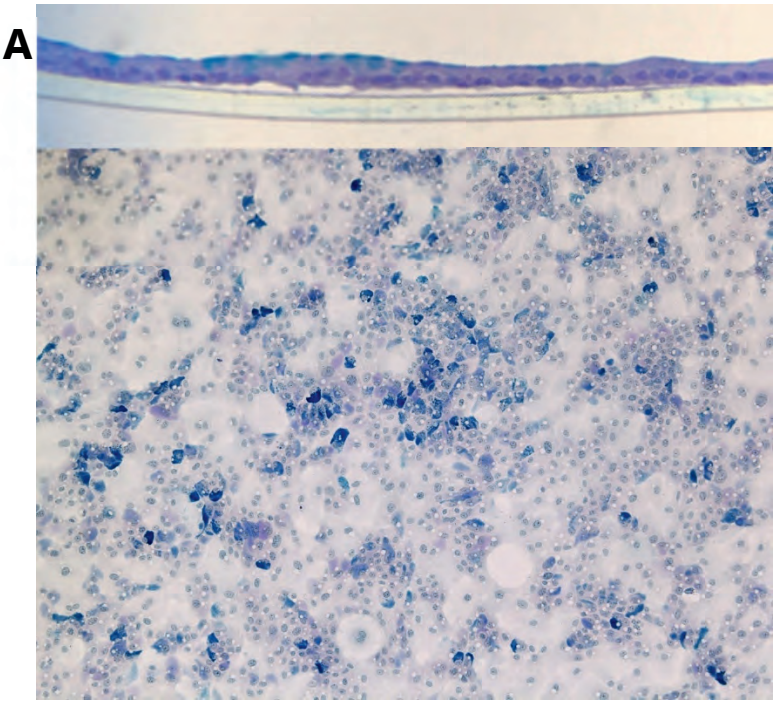

Supplementary figure 3. Pas/Alcian blue staining of mucus-containing goblet cells from cell monolayers grown for 3 days (dark blue shows acidic mucus, purple shows neutral mucus on top picture). Cell monolayers were grown in plates (A) or Transwells (B), were fixed in Carnoy's fixative for 1h at room temperature, and subsequently incubated in Alcian blue for 20 minutes. After washing, the slides were transferred to 0.5% periodic acid for 10 min, rinsed with distilled water, and incubated in Schiff's reagent for 40 min. Schiff was washed with three freshly made SO2 water steps (5% K2S2O5, 5% 1N HCl, in distilled water) and counterstained in Mayer's hematoxylin for 15 sec. Sections were then rinsed for 10 minutes, dehydrated, and embedded in depex.

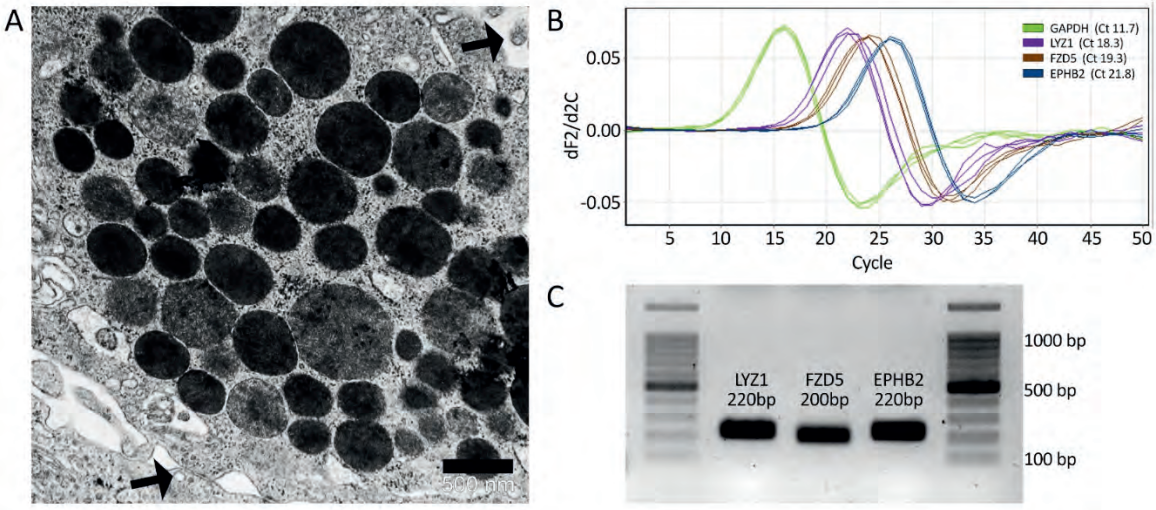

Supplementary figure 4. Paneth cell like characteristics were found at the cellular and molecular levels. (A) Transmission electron microscopic image of supranuclear vesicles in porcine ileal tissue. Large, electron dense granular structures were observed apically showing Paneth-cell like characteristics (black arrows = cellular junctions, black line = 500 nm). (B) RT-qPCR on Paneth cell differentiation markers shows expression in 3-day old monolayers (GAPDH = Glyceraldehyde 3-phosphate dehydrogenase, Ct 11.7; LYZ1 = Lysozyme 1, Ct 18.3; FZD5 = Frizzled 5, Ct 19.3; EPHB2 = Ephrin type-B receptor 2, Ct 21.8). qPCR was performed on 20x diluted cDNA, every line representing biological replicates (n = 3, average Ct is shown). (C) PCR amplicons show sizes predetermined at primer design. Amplicon size was determined for PCR product on 1.6% agarose gel, for 45 minutes at 90V to check non-specific amplification and specificity of primers (imaged on GelDoc (BD Biosciences), 100bp ladder shown on both sides).

References supplementary methods

- Benga, L., R. Goethe, M. Rohde, and P. Valentin-Weigand. 2004. 'Non-encapsulated strains reveal novel insights in invasion and survival of Streptococcus suis in epithelial cells', Cell Microbiol, 6: 867-81.
- Gonzalez, L. M., I. Williamson, J. A. Piedrahita, A. T. Blikslager, and S. T. Magness. 2013. 'Cell lineage identification and stem cell culture in a porcine model for the study of intestinal epithelial regeneration', PLoS One, 8: e66465.
- Krishna, V. D., E. Roach, N. A. Zaidman, A. Panoskaltsis-Mortari, J. H. Rotschafer, S. M. O'Grady, and M. C. Cheeran. 2015. 'Differential Induction of Type I and Type III Interferons by Swine and Human Origin H1N1 Influenza A Viruses in Porcine Airway Epithelial Cells', PLoS One, 10: e0138704.
- Loonen, L. M., E. H. Stolte, M. T. Jaklofsky, M. Meijerink, J. Dekker, P. van Baarlen, and J. M. Wells. 2014. 'REG3gamma-deficient mice have altered mucus distribution and increased mucosal inflammatory responses to the microbiota and enteric pathogens in the ileum', Mucosal Immunol, 7: 939-47.
- Schmittgen, T. D., and K. J. Livak. 2008. 'Analyzing real-time PCR data by the comparative C(T) method', Nat Protoc, 3: 1101-8.
- Spurr, A. R. 1969. 'A low-viscosity epoxy resin embedding medium for electron microscopy', J Ultrastruct Res, 26: 31-43.
- Willing, B. P., and A. G. Van Kessel. 2007. 'Enterocyte proliferation and apoptosis in the caudal small intestine is influenced by the composition of colonizing commensal bacteria in the neonatal gnotobiotic pig', J Anim Sci, 85: 3256-66.

References

1. Ootani, A., et al., *Sustained in vitro intestinal epithelial culture within a Wnt-dependent stem cell niche.* Nat Med, 2009. **15**(6): p. 701-6.
2. Sato, T., et al., *Single Lgr5 stem cells build crypt-villus structures in vitro without a mesenchymal niche.* Nature, 2009. **459**(7244): p. 262-5.
3. Wilson, S.S., et al., *A small intestinal organoid model of non-invasive enteric pathogen-epithelial cell interactions.* Mucosal Immunol, 2015. **8**(2): p. 352-61.
4. Moon, C., et al., *Development of a primary mouse intestinal epithelial cell monolayer culture system to evaluate factors that modulate IgA transcytosis.* Mucosal Immunol, 2014. **7**(4): p. 818-28.
5. VanDussen, K.L., et al., *Development of an enhanced human gastrointestinal epithelial culture system to facilitate patient-based assays.* Gut, 2015. **64**(6): p. 911-20.
6. Wang, Y., et al., *Self-renewing Monolayer of Primary Colonic or Rectal Epithelial Cells.* Cell Mol Gastroenterol Hepatol, 2017. **4**(1): p. 165-182 e7.
7. Dekaney, C.M., F.W. Bazer, and L.A. Jaeger, *Mucosal morphogenesis and cytodifferentiation in fetal porcine small intestine.* Anat Rec, 1997. **249**(4): p. 517-23.
8. Myer, M.S., *The presence of Paneth cells confirmed in the pig.* Onderstepoort J Vet Res, 1982. **49**(2): p. 131-2.
9. Sato, T., et al., *Long-term expansion of epithelial organoids from human colon, adenoma, adenocarcinoma, and Barrett's epithelium.* Gastroenterology, 2011. **141**(5): p. 1762-72.
10. Benga, L., et al., *Non-encapsulated strains reveal novel insights in invasion and survival of Streptococcus suis in epithelial cells.* Cell Microbiol, 2004. **6**(9): p. 867-81.
11. Schmittgen, T.D. and K.J. Livak, *Analyzing real-time PCR data by the comparative C(T) method.* Nat Protoc, 2008. **3**(6): p. 1101-8.
12. Gonzalez, L.M., et al., *Cell lineage identification and stem cell culture in a porcine model for the study of intestinal epithelial regeneration.* PLoS One, 2013. **8**(6): p. e66465.
13. Willing, B.P. and A.G. Van Kessel, *Enterocyte proliferation and apoptosis in the caudal small intestine is influenced by the composition of colonizing commensal bacteria in the neonatal gnotobiotic pig.* J Anim Sci, 2007. **85**(12): p. 3256-66.
14. Krishna, V.D., et al., *Differential Induction of Type I and Type III Interferons by Swine and Human Origin H1N1 Influenza A Viruses in Porcine Airway Epithelial Cells.* PLoS One, 2015. **10**(9): p. e0138704.
15. Khalil, H.A., et al., *A novel culture system for adult porcine intestinal crypts.* Cell Tissue Res, 2016. **365**(1): p. 123-34.
16. Scott, A., et al., *Long-term renewable human intestinal epithelial stem cells as monolayers: A potential for clinical use.* J Pediatr Surg, 2016. **51**(6): p. 995-1000.
17. Fernando, E.H., et al., *A simple, cost-effective method for generating murine colonic 3D enteroids and 2D monolayers for studies of primary epithelial cell function.* Am J Physiol Gastrointest Liver Physiol, 2017. **313**(5): p. G467-G475.
18. Hofmann, C., et al., *Cell-cell contacts prevent anoikis in primary human colonic epithelial cells.* Gastroenterology, 2007. **132**(2): p. 587-600.
19. Koyanagi, M., et al., *Inhibition of the Rho/ROCK pathway reduces apoptosis during transplantation of embryonic stem cell-derived neural precursors.* J Neurosci Res, 2008. **86**(2): p. 270-80.
20. Watanabe, K., et al., *A ROCK inhibitor permits survival of dissociated human embryonic stem cells.* Nat Biotechnol, 2007. **25**(6): p. 681-6.
21. Hirase, T., et al., *Regulation of tight junction permeability and occludin phosphorylation by Rhoa-p160ROCK-dependent and -independent mechanisms.* J Biol Chem, 2001. **276**(13): p. 10423-31.
22. Bajpai, R., et al., *Efficient propagation of single cells Accutase-dissociated human embryonic stem cells.* Mol Reprod Dev, 2008. **75**(5): p. 818-27.
23. Brown, D.R. and L.D. Price, *Characterization of Salmonella enterica serovar Typhimurium DT104 invasion in an epithelial cell line (IPEC J2) from porcine small intestine.* Vet Microbiol, 2007. **120**(3-4): p. 328-33.
24. Obremski, K., et al., *Morphology and ultrastructure of small intestine mucosa in gilts with zearalenone mycotoxicosis.* Pol J Vet Sci, 2005. **8**(4): p. 301-7.
25. Sato, T., et al., *Paneth cells constitute the niche for Lgr5 stem cells in intestinal crypts.* Nature, 2011. **469**(7330): p. 415-8.

26. van Es, J.H. and H. Clevers, *Paneth cells.* Curr Biol, 2014. **24**(12): p. R547-R548.
27. Farin, H.F., J.H. Van Es, and H. Clevers, *Redundant sources of Wnt regulate intestinal stem cells and promote formation of Paneth cells.* Gastroenterology, 2012. **143**(6): p. 1518-1529 e7.
28. Satoh, Y., et al., *Ultrastructure of Paneth cells in the intestine of various mammals.* J Electron Microsc Tech, 1990. **16**(1): p. 69-80.
29. Wang, D., et al., *Paneth cell marker expression in intestinal villi and colon crypts characterizes dietary induced risk for mouse sporadic intestinal cancer.* Proc Natl Acad Sci U S A, 2011. **108**(25): p. 10272-7.
30. Gonzalez, L.M., A.J. Moeser, and A.T. Blikslager, *Porcine models of digestive disease: the future of large animal translational research.* Transl Res, 2015. **166**(1): p. 12-27.
31. Swindle, M.M. and A.C. Smith, *Comparative anatomy and physiology of the pig.* Scandinavian Journal of Laboratory Animal Science, 1998. **25**: p. 11-21.
32. In, J., et al., *Enterohemorrhagic Escherichia coli reduce mucus and intermicrovillar bridges in human stem cell-derived colonoids.* Cell Mol Gastroenterol Hepatol, 2016. **2**(1): p. 48-62 e3.
33. Vogel, G.F., et al., *Disrupted apical exocytosis of cargo vesicles causes enteropathy in FHL5 patients with Munc18-2 mutations.* JCI Insight, 2017. **2**(14).
34. Rossi, O., et al., *Vectorial secretion of interleukin-8 mediates autocrine signalling in intestinal epithelial cells via apically located CXCR1.* BMC Res Notes, 2013. **6**: p. 431.
35. Rossi, O., P. van Baarlen, and J.M. Wells, *Host-recognition of pathogens and commensals in the mammalian intestine.* Curr Top Microbiol Immunol, 2013. **358**: p. 291-321.
36. Yang, C.C., et al., *Chemokine receptor CCR6 transduces signals that activate p130Cas and alter cAMP-stimulated ion transport in human intestinal epithelial cells.* Am J Physiol Cell Physiol, 2005. **288**(2): p. C321-8.
37. Lee, J., et al., *Maintenance of colonic homeostasis by distinctive apical TLR9 signalling in intestinal epithelial cells.* Nat Cell Biol, 2006. **8**(12): p. 1327-36.
38. Nakagawa, M., et al., *Effect of various lipid emulsions on total parenteral nutrition-induced hepatosteatosis in rats.* JPEN J Parenter Enteral Nutr, 1991. **15**(2): p. 137-43.

Effects of undigested protein-rich ingredients on polarized small intestinal organoid monolayers

Soumya K. Kar*[1], Bart van der Hee*[1,2], Linda M.P. Loonen[1], Nico Taverne[1], Johanna J. Taverne-Thiele[1], Dirkjan Schokker[3], Mari A. Smits[1, 3], Alfons J.M. Jansman[3], Jerry M. Wells[1]

[1] Host Microbe Interactomics Group, Wageningen University & Research, De Elst 1, 6708WD, Wageningen, The Netherlands. [2] Laboratory of Microbiology, Wageningen University & Research, Stippeneng 4, 6708WE, Wageningen, The Netherlands [3] Wageningen Livestock Research, Wageningen University & Research, Wageningen, The Netherlands

*These authors contributed equally to this work.

Published chapter: Kar, S.K., van der Hee, B., Loonen, L.M.P. *et al.* (2020) Effects of undigested protein-rich ingredients on polarised small intestinal organoid monolayers. J Animal Sci Biotechnol. 11, 51. *https://doi.org/10.1186/s40104-020-00443-4*

Abstract

Here, we describe the use of monolayers of intestinal epithelial cells derived from intestinal organoids and transcriptomics to investigate the direct effects of dietary protein sources on epithelial function. Mechanically dissociated 3D organoids of mouse duodenum were used to generate a polarized epithelium containing all cell types found in the tissue of origin. The organoid-derived cell monolayers were exposed to 4% *w/v* of 'undigested (non-hydrolyzed)-soluble' fraction of protein sources used as feed ingredients (soybean meal (SBM) and casein), or alternative protein sources (spray dried plasma protein, and yellow meal worm), or controls for 6 hours prior to RNA isolation and transcriptomics. All protein sources altered the expression of unique biological processes in the epithelial cells. Exposure of intestinal organoids to SBM downregulated expression of retinol and retinoid metabolic processes as well as cholesterol and lipid biosynthetic pathways, consistent with the reported hypotriglyceridemic effect of soy protein *in vivo*. These findings support the use of intestinal organoids as models to evaluate complex interactions between dietary ingredients and the intestinal epithelium and highlights some unique host effects of alternative protein sources in animal feed and potentially human food.

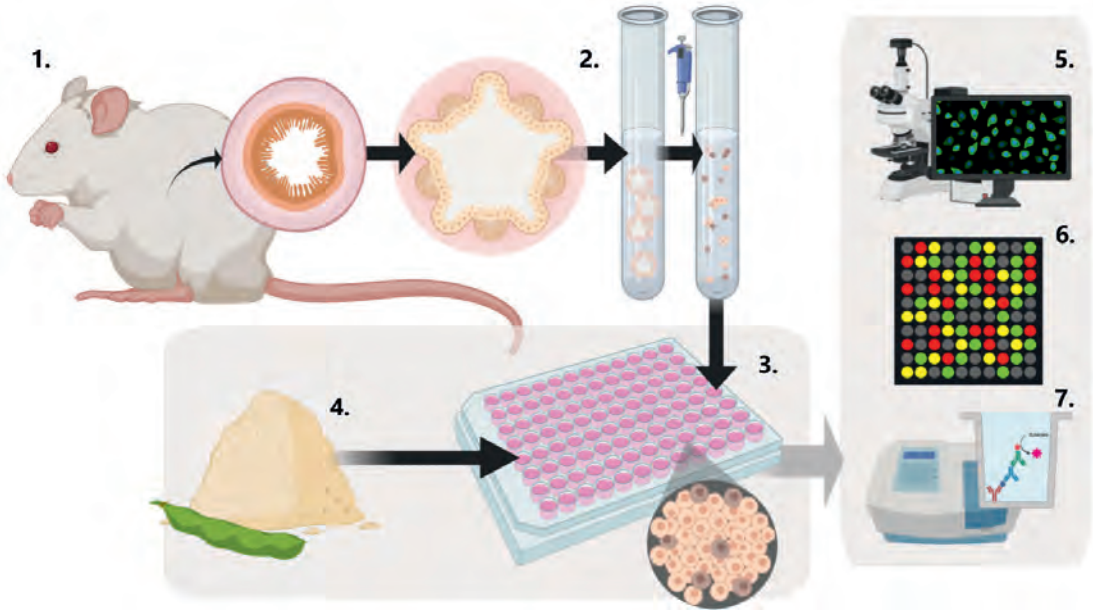

Graphical abstract: Schematic representation of the study. 3-dimensional organoids were generated from mouse duodenum (1). The organoids were subsequently dissociated into single cells (2) and grown as 2-dimensional polarized monolayers (3). Polarized monolayers of organoid cells were exposed to different protein sources (CAS, SBM, SDPP, YMW, or medium control (MC)) for 6 h (4) and further processed for imaging (5) gene expression (6), and biochemical assays (7), to investigate the effects of undigested protein sources on the duodenal epithelium.

Introduction

Currently, there is much interest in alternative sources of protein for animal feed, driven by the expected growth in the human population and increasing demand for animal protein. Moreover, cheaper sources of feed protein are being explored to sustain increased animal production. Alternative sources of protein include insect larvae and blood plasma. Little is known, however, about their potential non-nutritional effects on the host [1]. *In vitro* models commonly used to study intestinal responses to luminal factors include intestinal cell lines, primary cells, or tissue explants. However, cancer or transformed cell lines usually display aneuploidy, altered glycosylation patterns, and genetic mutations and deletions. Moreover, primary intestinal cells or explants are short-lived, making them less physiologically relevant for translational research [2-4].

To overcome these issues, we used three-dimensional (3D) organoid cultures from isolated crypts of the duodenum [5, 6]. Intestinal organoids can be generated within 2 weeks, maintained for > 2 years in culture or cryopreserved, and when differentiated contain all the epithelial cell lineages found at the location of origin [7, 8]. Recently, we and others have described methods for growing polarised monolayers of 3D organoid cells on semipermeable membrane supports, enabling apical exposure to luminal factors [9-11]. These two-dimensional (2D) organoid monolayers contain all the differentiated cell types found in the intestine and include many characteristics of intact, polarized epithelium, including barrier integrity and a secreted mucus layer [9, 10, 12].

Here we report on the effects of different undigested (non-hydrolysed soluble fractions) of different protein sources on the transcriptome of duodenal organoids. We performed our study in duodenum organoids, as it is likely this specific location will be the primary site of undigested protein exposure *in vivo*. Soybean meal (SBM) protein and other protein sources being considered for animal feed such as milk casein (CAS), spray-dried plasma protein from porcine blood (SDPP), and ground freeze-dried yellow mealworm larvae (YMW) were applied to the apical surface of 2D organoid for 6 hours after which RNA was isolated for transcriptomics using mouse gene microarrays. Potential effects of protein sources on cell viability and metabolism were measured, to control for unwanted side effects of the treatments such as apoptosis. Biochemical assays were used to validate production of triglyceride (TG) and phosphatidylcholine (PC), two pathways predicted to be activated by the different protein sources.

Materials and Methods

2D organoids and imaging

All protocols were approved by the animal ethics board of Wageningen University & Research, The Netherlands (2013023.f). Three nine-week-old wild type C57BL/6J female mice were purchased from Harlan Sprague Dawley Inc. (Horst, the Netherlands) and kept in the animal facility of Wageningen University & Research (12:12 h reversed light/dark cycle, 20 ± 2°C). The mice were housed together in a specific pathogen-free environment with *ad libitum* access to a standard diet (AIN-93M) and water. Mice were euthanized and dissected to remove the duodenum and the crypts isolated for generating organoids as previously described with minor modifications [7, 8] and grown in basal culture medium (W-ENR: DMEM/F12 medium enriched with 50 ng/mL mouse Epidermal growth factor (mEGF), 10 mM Hepes (Invitrogen, the Netherlands), 1 x B-27 supplement (ThermoFisher scientific, The Netherlands), and recombinant Noggin (15% v/v), WNT3A (30% v/v, Hubrecht Institute, Utrecht, Netherlands [7]), and R-Spondin (15% v/v, Stanford university, Palo Alto, USA [5]) (Method S1). To facilitate access to the apical surface of epithelial cells, we generated 2D monolayers of cells from dissociated 3D organoids. The organoids were extracted from the plate by adding 1 ml/well ice-cold DMEM F12 containing 1% *v/v* penicillin/streptomycin and disrupted using a p200 pipette for 40 consecutive passages and centrifuged at 250 x *g* for 5 min at 4 °C. The resulting pellet was suspended in TrypLE dissociation reagent, incubated for 10 minutes to receive a single-cell suspension. The cells were centrifuged at 750 x g for 5 min, resuspended in W-ENR at room temperature and plated at 25,000 cells per well in a 96-well culture plate, pre-coated with 0.5% Matrigel matrix as previously described [9, 10]. To confirm the presence of secretory cell lineages, the organoid monolayers were grown to confluence on 96-well plates, fixed in 1% paraformaldehyde (PFA), and subsequently visualised in histology sections with a fluorescent phalloidin conjugate (cell membranes, 1:100, A12379, Thermo-Fisher), Ki-67 (proliferating cells, 1:200, ab66155, Abcam), UEA-1 (secretory cell lineages, 1:100, FITC-conjugated, FL-1061, Vector Laboratories), and MUC2 (1:200, sc-515031, Santa Cruz Biotechnology) as previously described [9].

Protein treatments, RNA isolation, transcriptomics, and biological pathway analysis in 2D organoids

Finely powdered SBM (*glycine max*, Research diet services, The Netherlands), CAS (Bos taurus, Fronterra, Auckland, New Zealand), SDPP (*Sus scrofa*, Darling Ingredients, The Netherlands), and YMW (*Tenebrio molitor*, Kreca, The Netherlands) (see [19]) were added to DMEM F12 media (40 mg/ml) and homogenised using a vortex mixer and 2 cycles of 1 min with a 15 min interval. The homogenate was then allowed to settle at room temperature. Finally, the homogenate was centrifuged at 10,000 x *g* for 1 min to remove insoluble material, diluted to 400 µg/ml, and 1:10 of supernatant was added to the apical compartment of 2D organoid monolayers in W-ENR (resulting in 40 µg/ml protein; 4% w/v). After 6 h incubation at 37 °C RNA was isolated from protein-treated or medium control (DMEM-F12 only; MC) organoid monolayers for generating cDNA (Method S2). The labelled cDNA was hybridized to mouse gene 1.1 ST array (Affymetrix, Thermo Fisher Scientific, CA, USA) microarray plate and the results analysed essentially as previously described [13, 14] (Method S2). Genes differentially expressed in organoids exposed to protein sources compared to MC were identified for biological pathway analysis using GeneAnalytics (LifeMap Sciences, Inc. a subsidiary of BioTime, Inc., USA) [15]. The resulting microarray data is available in the Gene Expression Omnibus from NCBI with accession number GSE98051. Microarray results were confirmed by RT-qPCR on a selected set of differentially expressed genes (Method S3 and Table S1).

The potential effects of organoid exposure to different protein sources on cell viability and metabolism were measured using the CellTiterGlo 2.0 ATP-luminescence assay (G9241, Promega). After 6h incubation with different protein sources, the cells were lysed using the CellTiter Glo reagent (1:1 *v/v*) and ATP quantified by luminescence in a Spectramax M5 (Molecular Devices, Sunnyvale, CA, USA).

Biochemical analysis of triglyceride and phosphatidylcholine

Two compounds, triglyceride (TG) and phosphatidylcholine (PC), were measured in the organoid culture supernatant for each mouse organoid line (n = 3 biological replicates) exposed to undigested (non-hydrolysed) protein sources using commercial detection kits (n = 2 per biological replicate, ab65336, and ab83377, Abcam). Samples and standards were prepared and measured according to the manufacturer's instructions.

Results and Discussion

Multi-cell lineage composition of 2D organoid monolayers

Two-dimensional (2D) organoid cultures from murine small intestine were generated to investigate the effects of different dietary protein sources by image analysis, transcriptomics, and biochemical assays (**Figure 1**). To verify that our 2D monolayers of organoid cells contained heterotypic epithelial cell lineages as previously reported [8], we performed histological and transcriptomic analyses. Our 2D monolayers indeed contained secretory Paneth cells, and mucus-positive goblet cells as shown by immunohistochemical staining (**Supplementary Figure S1**), which is consistent with expression values for *Lyz* and *Muc2* transcripts in the microarray data (Figure S2). Similarly, the genome-wide transcriptomics data revealed expression of other genes associated with specific cell lineages of intestinal epithelium including columnar base cells (CBC), and enteroendocrine cells (EEC) (**Supplementary Figure S2**).

Different undigested sources of dietary protein have distinct biological effects on organoids

Organoid monolayers were exposed to different undigested protein sources (4% w/v, SBM, CAS, SDPP, and YMW) or DMEM as a MC for 6 h. Testing the effects of the treatments on cellular metabolism or survival, an ATP assay was performed. A statistically significant decline in cell ATP (<5% compared to medium control) was observed after exposure to SBM, CAS, and YMW (**Supplementary Figure S1B**), which could be caused by treatment-induced changes in energy metabolism or metabolic activity. However, biologically we do not expect this to have detrimental physiological consequences on the organoid monolayers.

Principal Component Analysis (PCA) of transcriptomics data suggest separation of the treatments (95% CI) from the medium control-treated samples (PC1: 72.5% variance, **Supplementary Figure S3**). Analysis of the microarray data revealed that many genes were significantly (P < 0.05 and fold change > 1.5) differentially expressed in 2D intestinal organoids following exposure to different protein sources for 6 h (Table 1).

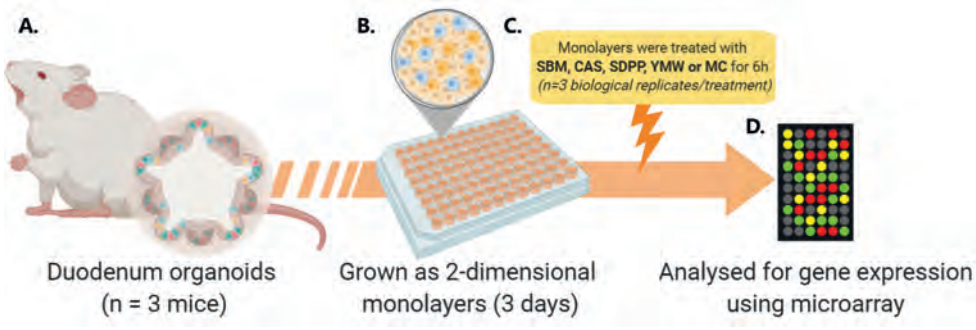

Figure 1. Experimental overview of the study. (A) Duodenum organoids were generated from 3 individual mice and separately cultured in Matrigel. (B) 3-dimensional organoids were single-cell dissociated by pipetting and TrypLE enzymatic digestion, plated in Matrigel coated 96-well plates, and grown until confluence for 3 days. (C) After confluence the monolayers were treated for 6 hours with 4% w/v soybean meal (SBM), casein (CAS), spray-dried plasma protein (SDPP), yellow mealworm (YMW), or medium control (MC). (D) After 6 hours, the monolayers were lysed and processed for gene expression profiling by microarray.

Table 1. Overview of differentially expressed (P < 0.05) genes along with the number of related GO-biological processes in 2D organoids exposed to undigested protein sources compared to medium control (MC).

Treatment	Regulation	Differentially expressed genes [a]		GO biological processes [b]
CAS	Up	417	823	26
	Down	406		
SBM	Up	340	796	27
	Down	456		
SDPP	Up	262	379	40
	Down	117		
YMW	Up	391	824	20
	Down	433		

[a] P < 0.05 and log Fold Change > |1.5|

[b] Analysed by GeneAnalytics; pathway analysis significance using a corrected P-value of < 0.05.

Abbreviations used: CAS, Casein, SBM, soybean meal, SDPP, spray dried plasma protein; YMW, yellow meal worm.

Several of these differentially regulated genes were verified to have altered expression by RT-qPCR, showing a strong correlation (r = 0.8) to the microarray expression (Table S1). Using GeneAnalytics, the genes were matched to GO-biological processes (Table 2). Strikingly, several unique biological processes were influenced by each of the protein sources, while only one biological process was commonly regulated by all treatments (Figure S4). For CAS, SBM, SDPP and YMW, the number of uniquely modulated GO-biological processes compared to control were 5, 8, 24 and 11, respectively. The biological process upregulated by all protein ingredients compared to MC, was cell proliferation, indicating altered rates of cell turnover. CAS exposure to 2D organoids significantly downregulated expression of genes related to glutathione- metabolic and glutathione-derivative biosynthetic processes. Glutathione is a tripeptide, ubiquitously distributed in living cells and plays an important role in the intracellular defense mechanism against oxidative stress [16, 17]. It is known that glutathione metabolism is important for the antioxidant and detoxifying action of the intestine [18]. This suggests that CAS has detoxifying or anti-oxidative (functional) properties reducing the requirement for glutathione.

Exposure of organoids to SDPP upregulated several biological pathways associated with processes of cell migration and movement, including 'wound healing', 'cytokinesis' 'mitotic spindle midzone assembly', and is consistent with the upregulation of 'DNA-templated transcription', 'initiation', and 'nucleosome assembly'. Additionally, the upregulation of angiogenesis could be related to cell apoptosis and altered expression of membrane metalloproteases and connective tissue growth factors involved in epithelial repair processes. Overall, these findings suggest increased cell turnover reflected in the upregulation of apoptosis and replication processes. The background of this observation is unclear but may involve reconstituted serum factors from SDPP (porcine origin) and warrants further investigation.

YMW exposure down regulated biological processes involved in lipid metabolism such as 'steroid metabolic process', 'cholesterol biosynthesis process' 'very-long chain fatty acid metabolic process' and 'isoprenoid biosynthesis'. Isoprenoids are needed for biosynthesis of sterols such as cholesterol, which is vital for membrane structure. The effects of YMW are most likely to be due to the relatively high residual fat content (total fat, dry matter basis: 270 g/Kg) of this protein source [19].

Table 2. Uniquely regulated GO-biological processes of 2D organoids exposed to various protein sources. List of biological processes as analyzed in GeneAnalytics using the differentially expressed genes compared to medium control (MC).

Sl No.	Biological processes modulated in treatments compared to MC	Putative regulation of biological process
	CAS	
1	Glutathione Metabolic Process	Down
2	Notochord Development	Up
3	Microtubule-based Movement	Up
4	Glutathione Derivative Biosynthetic Process	Down
5	Cellular Detoxification of Nitrogen Compound	Down
	SBM	
1	Phosphatidylcholine Biosynthetic Process	Down
2	Triglyceride Homeostasis	Down
3	Drug Metabolic Process	Down
4	Type I Interferon Signaling Pathway	Up
5	Retinol Metabolic Process	Down
6	Hexose Transport	Down
7	Lipoprotein Metabolic Process	Down
8	Retinoid Metabolic Process	Down
	SDPP	
1	Nucleosome Assembly	Up
2	Positive Regulation of Apoptotic Process	Up
3	Positive Regulation of Cell Migration	Up
4	Response to Wounding	Up
5	Wound Healing, Spreading of Cells	Up
6	Negative Regulation of Cell Cycle	Up
7	DNA Replication-independent Nucleosome Assembly	Up
8	Cellular Response to Organic Cyclic Compound	Up
9	Angiogenesis	Up
10	Telomere Organization	Up
11	Response to Virus	Up
12	Cytokinesis	Up
13	DNA Replication-dependent Nucleosome Assembly	Up
14	DNA-templated Transcription, Initiation	Up
15	Response to Hypoxia	Up
16	Positive Regulation of Fever Generation	Up
17	Mitotic Spindle Midzone Assembly	Up

18	Platelet Degranulation	Up
19	Positive Regulation of Cytokinesis	Up
20	Chromatin Silencing at RDNA	Up
21	Protein Stabilization	Up
22	Protein Localization to Kinetochore	Up
23	Omega-hydroxylase P450 Pathway	Up
24	Positive Regulation of Protein Localization to Nucleus	Up
	YMW	
1	Cholesterol Biosynthetic Process	Down
2	Steroid Metabolic Process	Down
3	Response to Drug	Down
4	Oxidation-reduction Process	Up
5	Transmembrane Transport	Down
6	Isoprenoid Biosynthetic Process	Down
7	Very Long-chain Fatty Acid Metabolic Process	Down
8	CDP-choline Pathway	Down
9	Long-chain Fatty Acid Metabolic Process	Down
10	Steroid Hormone Mediated Signaling Pathway	Down
11	Response to Gamma Radiation	Up

[a]Analyzed by GeneAnalytics; pathway analysis significance at corrected *P*-value < 0.05
[b] $P < 0.05$ and log Fold Change > |1.5|
Abbreviations used: CAS is Casein, SBM, soybean meal, SDPP, spray dried plasma protein; YMW, yellow meal worm; MC, medium control.

Soybean meal is a common protein ingredient of animal feed and down-regulated biological processes involved in triglyceride (TAG) and phosphatidylcholine (PC) biosynthesis as well as pathways associated with retinoid and retinol metabolism (Table 2). This is consistent with *in vivo* studies showing soy protein intake to be hypotriglyceridemic in rats, having cholesterol lowering effects and reducing lipid deposition in liver [20-22].

Intestinal organoids produce and secrete chylomicrons [23], large triglyceride-rich lipoprotein particles enveloped by phospholipids, which are used for the transport of dietary fat and fat-soluble vitamins. Recently, van Rijn and colleagues showed that intestinal organoids secrete chylomicrons upon stimulation with fatty acids and measured the intracellular formation of lipid droplets [24]. To investigate whether SBM incubated organoids secreted lower amounts of these molecules we measured their concentration in the culture medium (Figure S5). Interestingly, supernatants from SBM-treated monolayers had lower amounts of TAG and PC than the other protein treatments but were not different from MC. However, transcriptional down-

regulation of these pathways was predicted from microarray data of SBM treated cells compared to the MC. This result could be explained by the presence of a minimal TAG and PC amount in the normal culture supernatant. Moreover, higher amounts of TAG and PC were found in supernatants of organoids treated with ingredients containing higher fat content than SBM (See [19]).

The hypotriglyceridemic effect of soy protein was recently shown to be due to suppression of retinoic acid receptor expression in liver of rats fed soybean protein but not casein protein in their diet [25]. This is consistent with reports that administration of retinoids in cancer treatments are associated with hypertriglyceridemia via their interaction with retinoid receptors [26-28]. Taken together, these observations suggest that a component in SBM also negatively regulates retinoid and retinol biosynthesis as well as cholesterol and lipid biosynthetic pathways through down regulation of retinoic acid receptors in the intestinal epithelium.

In the present study we observe only part of the bio-functionality of the protein ingredients. The soluble constituents in the undigested (non-hydrolysed) soluble fraction of the protein ingredients are likely responsible for the observed effects in the present study. It can either be proteins or naturally present peptides or likely non-protein constituents that are responsible for the observed effects. However *in vivo* we can expect additional effects of the digested protein sources, in particular on metabolism. Moreover, the kinetics of protein digestion in the gastrointestinal tract differs substantially among the protein sources, especially to SBM and SDPP [29].

Conclusion

Collectively, our results indicate a direct diet-host interaction of the 'undigested (non-hydrolysed)-soluble fraction' of different protein sources and demonstrates that organoid monolayers are useful models to evaluate complex interaction between feed or food ingredients and the intestinal epithelium. Our transcriptome results for SBM and CAS, protein sources for which extensive studies have been performed *in vivo*, reflected those shown in animal studies. Our study suggests that a 2D intestinal organoid model can predict some effects also seen *in vivo* and might help to predict host-feed interactions.

Less studied protein sources such as SDPP and YMW also had significant effects on epithelial gene expression. For SDPP the main pathways affected indicate a possible stress response or stimulation of epithelial regeneration, for example, through increased cell turn-over [30]. Future studies can be focused on verifying the biological processes altered by SDPP and YMW in 2D intestinal organoid models, as

well as fractionation of the protein sources to identify bio-molecular component(s) responsible for their effects or pre-hydrolysed fractions of other food/feed ingredients. Additionally, species-specific advances in organoid cultivation could be used to identify molecular responses of various host-species or tissue types [9, 11].

List of abbreviations:

SBM, soybean meal; **CAS,** casein; **SDPP,** spray dried plasma protein; **YMW,** yellow meal worm; MC, Medium Control, **3D,** three-dimensional; **2D,** two-dimensional; **PBS,** phosphate-buffered saline solution; **TBS-T,** tris-buffered saline-tween 20**; DMEM,** dulbecco's modified Eagle medium; mEGF, mouse Epidermal Growth Factor; EDTA, Ethylenediaminetetraacetic acid; IMBT, Intensity based moderated T-statistic; FC, Fold change; Muc2, Mucin-2; Lyz, Lysozyme; UEA-1, Ulex Europaeus Agglutinin 1; CBC, Columnar Base Cell; SC, Stem cell; EEC, Enteroendocrine cells; HKG, Miscellaneous genes; ATP, Adenosine triphosphate; **GO,** gene ontology; **RT-qPCR,** quantitative reverse transcription PCR; AIN, American Institute of Nutrition. TG, Triglyceride; PC, Phosphatidylcholine; PCA, Principal Component Analysis.

Ethics approval

All procedures were approved by the Wageningen Animal Ethics Committee (Wageningen, The Netherlands; accession number 2013023.f) and carried out according to the guidelines of the European Council Directive 86/609/EEC dated November 1986.

Availability of data and materials

The microarray data resulted from this study is available in the Gene Expression Omnibus of NCBI with the accession number GSE98051.

Supplementary Materials and Methods

Method S1. Description of crypt isolation and culture of 3D organoids

A two-centimeter section of the duodenum was isolated and opened longitudinally. Duodenal segments were washed in ice-cold phosphate-buffered saline solution (PBS) until the supernatant was clear. Subsequently, the tissue was incubated in PBS containing 2mM ethylenediaminetetraacetic acid (EDTA) for 30 minutes on ice. Intestinal villi were gently removed using a glass slide, the remaining tissue was sectioned into smaller pieces, and washed with ice-cold PBS. After precipitation of the tissue fragments, PBS containing EDTA was removed and resulting fragments were thoroughly suspended in advanced Dulbecco's modified Eagle medium (DMEM/F12, ThermoFisher scientific, the Netherlands) containing 1% *v/v* penicillin/streptomycin (PenStrep, Sigma-Aldrich, the Netherlands). Supernatant containing the crypts was filtered through a 70 µm cell strainer and centrifuged at 200 x *g* for 3 minutes at 4 °C. The pellet was suspended in Matrigel matrix (growth factor reduced, phenol red free, BD biosciences, the Netherlands) and plated at a density of 40-100 crypts per 50µl in a 24-well culture plate (Corning, the Netherlands) for 3D growth of the organoids. After inverted polymerization of the matrix at 37 ºC with 5% CO_2 for 20 minutes, 600 µl/well W-ENR was added. After seeding, the culture medium was initially replaced after 24h and subsequently every 72h. Organoids were sub-cultured and passaged 1:5 every 8-10 days by mechanical disruption and seeded in fresh Matrigel matrix.

Method S2. RNA isolation, transcriptome, and biological pathway analysis

After incubation, the wells were washed with 200 µl PBS at room temperature. Total RNA was isolated using the RNeasy Mini kit (Qiagen, The Netherlands), with a 15-minute on-column DNase treatment (RNAse free DNAse kit, Qiagen). RNA purity and integrity were verified using spectrophotometry (NanoDrop Technologies, USA) and Bioanalyzer (Agilent, USA). The RNA was only used to generate cDNA and perform microarray hybridization when there was no evidence of RNA degradation (RNA Integrity Number > 8). The labelling, hybridization of individual samples on Affymetrix GeneChip mouse gene 1.1 ST arrays (Affymetrix, USA), scanning, quality control and normalization of the resulting datasets was performed as described previously [1]. The resulting data is available in the Gene Expression Omnibus from NCBI with the accession number GSE98051. Differentially expressed probe sets were identified using linear models, applying moderated T-statistics that implemented

empirical Bayes regularization of standard errors [2]. A Bayesian hierarchical model was used to define an intensity based moderated T-statistic (IMBT) [3]. Only genes with a fold-change (FC) of at least 1.5 (up or down) and *P*-value < 0.05 were considered significantly different. Biological interaction networks among regulated genes activated in response to protein ingredients from different sources were identified using "GeneAnalytics" (LifeMap Sciences, Inc. a subsidiary of BioTime, Inc., USA). GeneAnalytics [15] automatically integrates gene-centric data from ~125 web sources, including genomic, transcriptomic, proteomic, genetic, clinical and functional information to identify Gene Ontology (GO) terms related to their gene sets, providing information about the molecular functions and biological roles of the genes of interest. The annotation of mice genes was performed for the subsequent functional analysis. Our GeneAnalytics analyses compared differentially regulated genes in the 2D organoids exposed to treatments compared to medium control (MC). The input was all differentially regulated genes (*P*-value < 0.05 and FC > 1.5) in the 2D organoids with/without exposure to the treatments. Here, the GO biological processes were retrieved from GeneAnalytics analysis with a high or medium score (*P*-value <0.05).

Method S3. RT-qPCR

The cDNA was generated from 1 microgram of total RNA by reverse transcription using a qScript cDNA synthesis kit (Quantabio, USA) according to manufacturer's instructions and diluted 1:20. Primers were designed using Primer3 software [4-5], and purchased from Eurogentec (Oligo center, Belgium). RT-qPCR was performed using the Rotor-gene SYBR green PCR kit (Qiagen, the Netherlands) with primers specified in Table S1. Expression levels were measured in triplicate assays per sample using the Rotor-gene Q2plex real-time cycler (Qiagen). *18S* and *beta-Actin* acted as endogenous control genes and relative expression was calculated using individual amplification values, following methods described in [6]. RT-qPCR data are presented as mean ± standard error of the mean (SEM). Statistical analysis was performed by one-way analysis of variance (ANOVA) followed by Dunnet's multiple comparisons test (Treatments vs medium control) using GraphPad prism version 5.03 (GraphPad Software, San Diego, California, USA). *P*-values < 0.05 were considered statistically significant.

Supplementary references for methods

1. Sovran B, Loonen LMP, Lu P, Hugenholtz F, Belzer C, Stolte EH, et al. IL-22-STAT3 Pathway Plays a Key Role in the Maintenance of Ileal Homeostasis in Mice Lacking Secreted Mucus Barrier. Inflammatory Bowel Diseases. 2015;21(3):531-42.
2. Storey J, Tibshirani R. Statistical significance for genomewide studies. Proc Natl Acad Sci USA. 2003;100.
3. Sartor MA, Tomlinson CR, Wesselkamper SC, Sivaganesan S, Leikauf GD, Medvedovic M. Intensity-based hierarchical Bayes method improves testing for differentially expressed genes in microarray experiments. Bmc Bioinformatics. 2006;7.
4. Koressaar T, Remm M. Enhancements and modifications of primer design program Primer3. Bioinformatics. 2007;23(10):1289-91.
5. Untergasser A, Nijveen H, Rao X, Bisseling T, Geurts R, Leunissen JAM. Primer3Plus, an enhanced web interface to Primer3. Nucleic Acids Research. 2007;35:W71-W4.
6. Schmittgen TD, Livak KJ. Analyzing real-time PCR data by the comparative C-T method. Nat Protoc. 2008;3(6):1101-8.

Supplementary Tables and Figures

Table S1. RT-qPCR primer sequences and fold-change results (average ± SEM, n = 3 per treatment) for microarray validation of significantly regulated genes in protein-treated organoids compared to medium control.

Gene	Primer forward	Primer reverse	°C*	Micro-array	qPCR	ρ
Stxbp1	ATTTTCATCCTTGGGGGTGT	AAGTCGGGGTGTCTCAGGT	60	4.23	4.57 ± 1.75	0.80
TNFsf13b	TGCCTTGGAGGAGAAAGAGA	CCAGCCGAGTAGCAGGAA	60	2.13	2.19 ± 0.83	
Gm41	CCTGTCCTGTTTGCTGCTCT	CTCCTTTCTCTCCTGCCTTG	61	1.95	6.32 ± 2.33	
Cyp1a1	CAGAAGGTGATGGCAGAGGT	GGTAACGGAGGACAGGAATG	60	1.92	7.00 ± 0.15	
Olfr1162	TGGAAAGAAATGTGAGTGTGG	TGATGGTTGAGTAGCAGAAGTC	59	-1.82	-1.20 ± 0.23	
Lims2	GCGGATTCTGTGGTGAATTT	CTTGAACATGAGGGGCTGTT	60	-2.38	-1.41 ± 0.21	

* Annealing Temperature, ᵖcorrelation coefficient

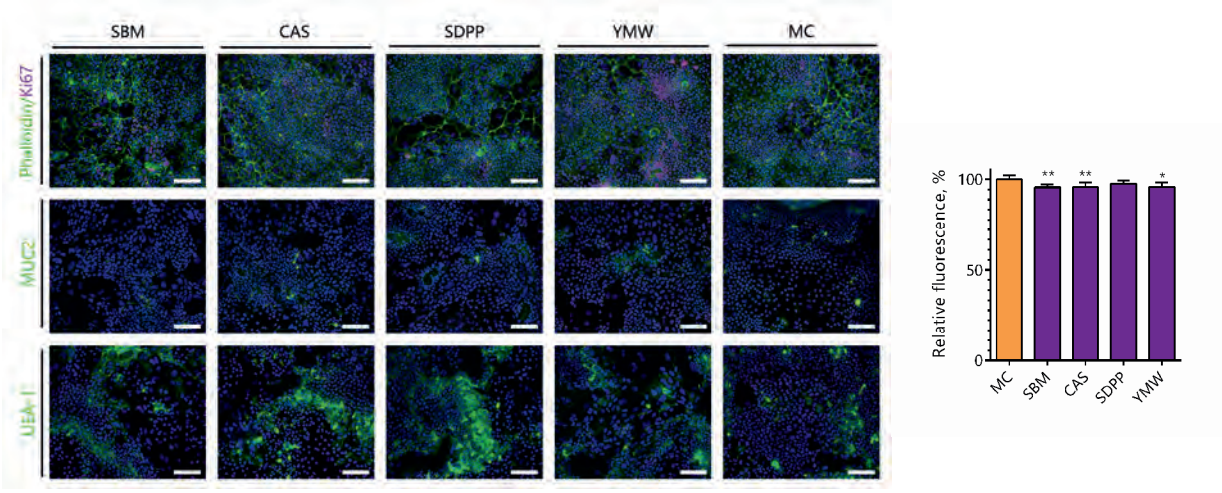

Figure S1. Organoid monolayers differentiate into polarized epithelium containing multiple cell types irrespective of treatment. (A) Staining of organoid monolayers to test for cellular morphology and proliferation (top), and secretory cell lineages, goblet (middle; MUC2) and Paneth (bottom; UEA-1) cells, when treated with various protein sources. (B) Cell ATP assay of organoids exposed to various protein sources relative to medium control (average % ± SD, n = 6 per treatment, * $P < 0.05$, ** $P < 0.01$). MC, medium control; SBM, soybean meal; CAS, casein; SDPP, spray dried plasma protein; YMW, yellow meal worm.

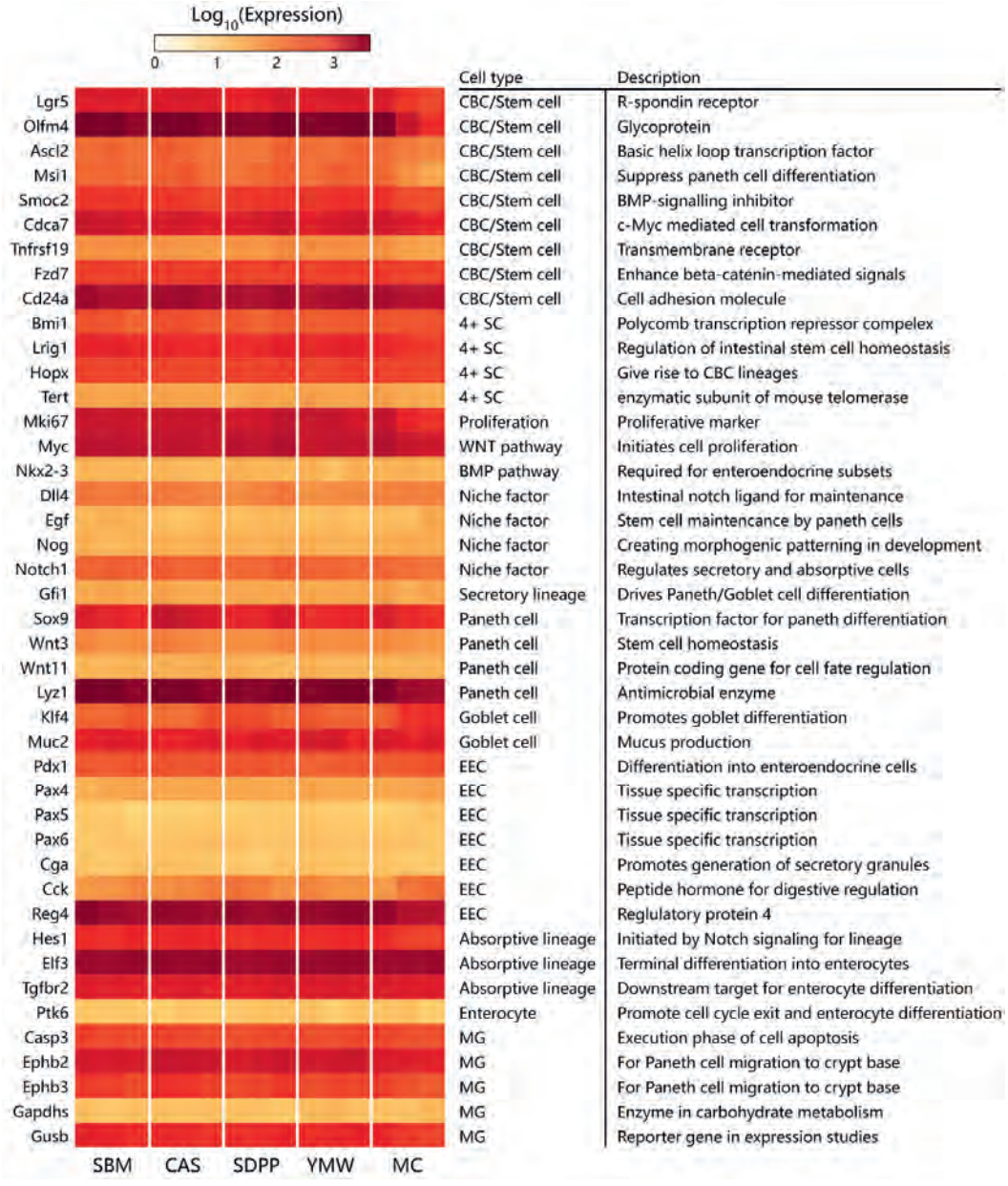

	Cell type	Description
Lgr5	CBC/Stem cell	R-spondin receptor
Olfm4	CBC/Stem cell	Glycoprotein
Ascl2	CBC/Stem cell	Basic helix loop transcription factor
Msi1	CBC/Stem cell	Suppress paneth cell differentiation
Smoc2	CBC/Stem cell	BMP-signalling inhibitor
Cdca7	CBC/Stem cell	c-Myc mediated cell transformation
Tnfrsf19	CBC/Stem cell	Transmembrane receptor
Fzd7	CBC/Stem cell	Enhance beta-catenin-mediated signals
Cd24a	CBC/Stem cell	Cell adhesion molecule
Bmi1	4+ SC	Polycomb transcription repressor compelex
Lrig1	4+ SC	Regulation of intestinal stem cell homeostasis
Hopx	4+ SC	Give rise to CBC lineages
Tert	4+ SC	enzymatic subunit of mouse telomerase
Mki67	Proliferation	Proliferative marker
Myc	WNT pathway	Initiates cell proliferation
Nkx2-3	BMP pathway	Required for enteroendocrine subsets
Dll4	Niche factor	Intestinal notch ligand for maintenance
Egf	Niche factor	Stem cell maintencance by paneth cells
Nog	Niche factor	Creating morphogenic patterning in development
Notch1	Niche factor	Regulates secretory and absorptive cells
Gfi1	Secretory lineage	Drives Paneth/Goblet cell differentiation
Sox9	Paneth cell	Transcription factor for paneth differentiation
Wnt3	Paneth cell	Stem cell homeostasis
Wnt11	Paneth cell	Protein coding gene for cell fate regulation
Lyz1	Paneth cell	Antimicrobial enzyme
Klf4	Goblet cell	Promotes goblet differentiation
Muc2	Goblet cell	Mucus production
Pdx1	EEC	Differentiation into enteroendocrine cells
Pax4	EEC	Tissue specific transcription
Pax5	EEC	Tissue specific transcription
Pax6	EEC	Tissue specific transcription
Cga	EEC	Promotes generation of secretory granules
Cck	EEC	Peptide hormone for digestive regulation
Reg4	EEC	Reglulatory protein 4
Hes1	Absorptive lineage	Initiated by Notch signaling for lineage
Elf3	Absorptive lineage	Terminal differentiation into enterocytes
Tgfbr2	Absorptive lineage	Downstream target for enterocyte differentiation
Ptk6	Enterocyte	Promote cell cycle exit and enterocyte differentiation
Casp3	MG	Execution phase of cell apoptosis
Ephb2	MG	For Paneth cell migration to crypt base
Ephb3	MG	For Paneth cell migration to crypt base
Gapdhs	MG	Enzyme in carbohydrate metabolism
Gusb	MG	Reporter gene in expression studies

Figure S2. Organoid monolayers stimulated with various protein sources still maintained cell type-specific differentiation markers. Heatmap showing $\log_{10}$(expression) values of cell-specific genes in the dataset for crypt base columnar (CBC)/stem cells, label-retaining cells (+4 SC), niche cells, Paneth cells, goblet cells, enteroendocrine cells (EEC), absorptive enterocytes, and miscellaneous genes (MG).

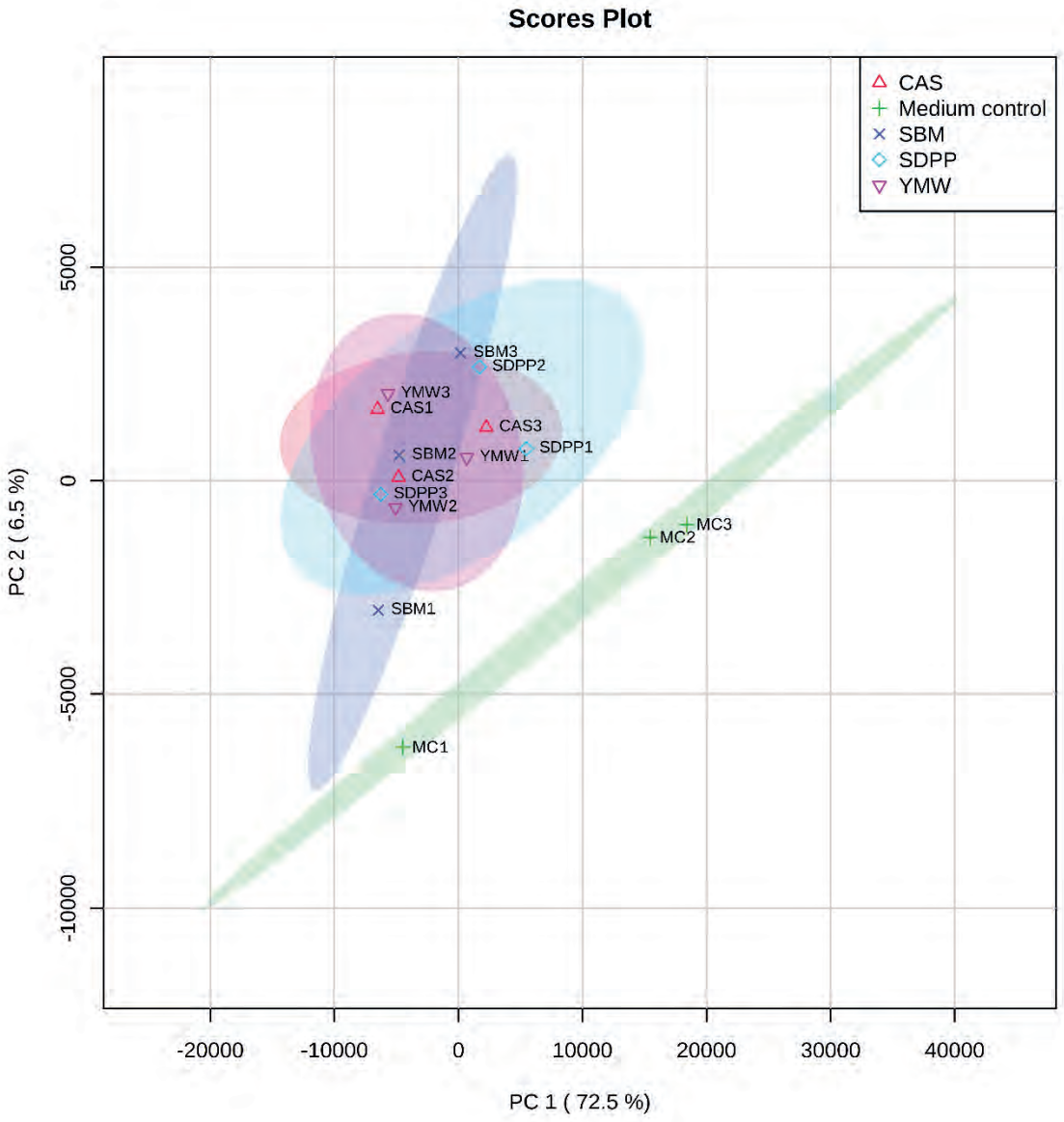

Figure S3. PCA score plot based on genome-wide transcriptomic response measured by microarray of 2D organoids stimulated with different protein source. Colored spherical areas display 95% confidence region of respective experimental diets. Each dot represents a batch culture of organoids. MC, medium control; CAS, Casein; SBM, Soybean meal; SDPP, Spray dried plasma protein; YMW, Yellow meal worm.

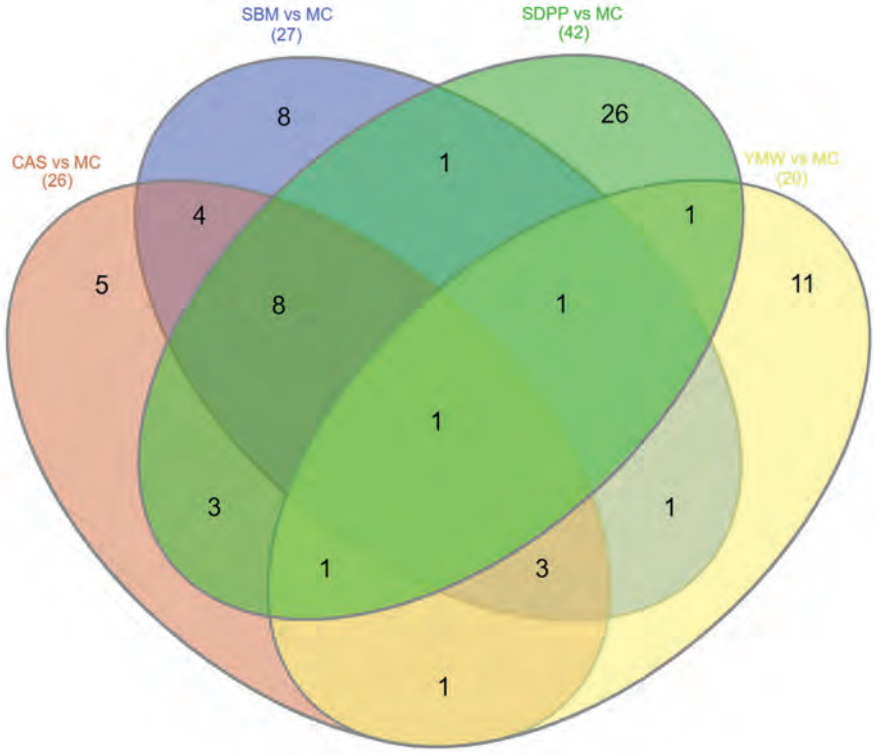

Figure S4. Overview of non-overlapped and overlapped significant GO-biological processes modulated by protein ingredients from different sources compared to medium control, based on functional analysis results using GeneAnalytics. CAS, casein; SBM, soybean meal; SDPP, spray dried plasma protein; YMW, yellow meal worm; MC, Medium control.

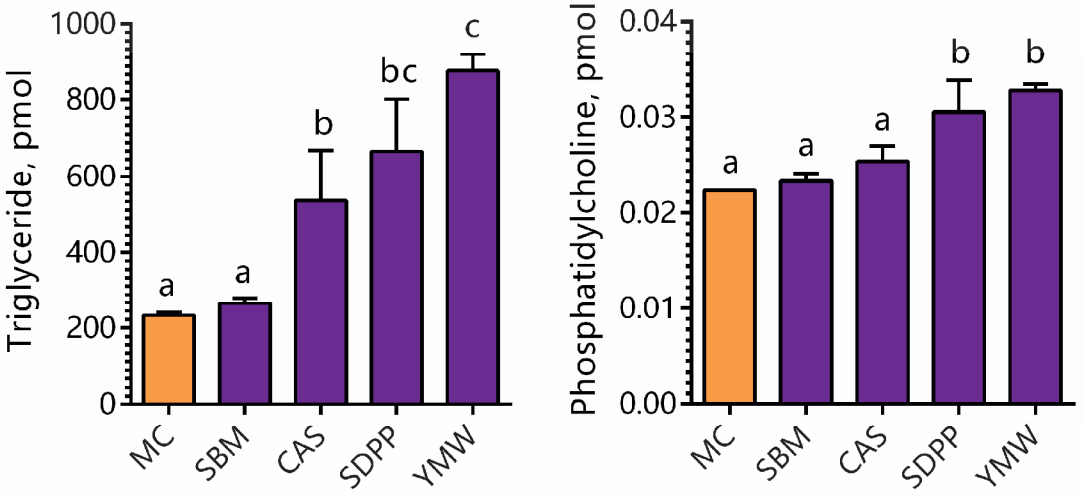

Figure S5. Triglyceride (A) and phosphatidylcholine (B) content in supernatant of organoid monolayers stimulated for 6 h with various protein sources. Letters indicate similarity or significant differences using One-way ANOVA (concentrations given in pmol, average ± SEM, n = 6 monolayers per treatment derived from 3 mice, $P < 0.05$).

References

1. Jahan-Mihan, A., et al., Dietary Proteins as Determinants of Metabolic and Physiologic Functions of the Gastrointestinal Tract. Nutrients, 2011. **3**(5): p. 574-603.
2. Kosti, I., et al., Cross-tissue Analysis of Gene and Protein Expression in Normal and Cancer Tissues. Scientific Reports, 2016. **6**.
3. Liu, Y.S., et al., Multi-omic measurements of heterogeneity in HeLa cells across laboratories. Nature Biotechnology, 2019. **37**(3): p. 314-+.
4. Randall, K.J., J. Turton, and J.R. Foster, Explant culture of gastrointestinal tissue: a review of methods and applications. Cell Biology and Toxicology, 2011. **27**(4): p. 267-284.
5. Ootani, A., et al., Sustained in vitro intestinal epithelial culture within a Wnt-dependent stem cell niche. Nature Medicine, 2009. **15**(6): p. 1-U140.
6. Sato, T., et al., Single Lgr5 stem cells build crypt-villus structures in vitro without a mesenchymal niche. Nature, 2009. **459**(7244): p. 262-U147.
7. Sato, T., et al., Long-term Expansion of Epithelial Organoids From Human Colon, Adenoma, Adenocarcinoma, and Barrett's Epithelium. Gastroenterology, 2011. **141**(5): p. 1762-1772.
8. van der Hee, B., et al., Congruence of location-specific transcriptional programs in intestinal organoids during long-term culture. bioRxiv, 2019: p. 600940.
9. van der Hee, B., et al., Optimized procedures for generating an enhanced, near physiological 2D culture system from porcine intestinal organoids. Stem Cell Research, 2018. **28**: p. 165-171.
10. VanDussen, K.L., et al., Development of an enhanced human gastrointestinal epithelial culture system to facilitate patient-based assays. Gut, 2015. **64**(6): p. 911-920.
11. Vogel, G.F., et al., Disrupted apical exocytosis of cargo vesicles causes enteropathy in FHL5 patients with Munc18-2 mutations. Jci Insight, 2017. **2**(14).
12. Wang, Y.L., et al., Self-renewing Monolayer of Primary Colonic or Rectal Epithelial Cells. Cellular and Molecular Gastroenterology and Hepatology, 2017. **4**(1): p. 165-+.
13. Rossi, O., et al., Vectorial secretion of interleukin-8 mediates autocrine signalling in intestinal epithelial cells via apically located CXCR1. BMC Res Notes, 2013. **6**: p. 431.
14. Sovran, B., et al., Identification of Commensal Species Positively Correlated with Early Stress Responses to a Compromised Mucus Barrier. Inflammatory Bowel Diseases, 2016. **22**(4): p. 826-840.
15. Ben-Ari Fuchs, S., et al., GeneAnalytics: An Integrative Gene Set Analysis Tool for Next Generation Sequencing, RNAseq and Microarray Data. Omics-a Journal of Integrative Biology, 2016. **20**(3): p. 139-151.
16. Couto, N., J. Wood, and J. Barber, The role of glutathione reductase and related enzymes on cellular redox homoeostasis network. Free Radical Biology and Medicine, 2016. **95**: p. 27-42.
17. Diaz-Vivancos, P., et al., Glutathione - linking cell proliferation to oxidative stress. Free Radical Biology and Medicine, 2015. **89**: p. 1154-1164.
18. Iantomasi, T., et al., Glutathione transport system in human small intestine epithelial cells. Biochimica Et Biophysica Acta-Biomembranes, 1997. **1330**(2): p. 274-283.
19. Kar, S.K., et al., Protein, peptide, amino acid composition, and potential functional properties of existing and novel dietary protein sources for monogastrics. Journal of Animal Science, 2016. **94**: p. 30-39.
20. Ascencio, C., et al., Soy protein affects serum insulin and hepatic SREBP-1 mRNA and reduces fatty liver in rats. Journal of Nutrition, 2004. **134**(3): p. 522-529.
21. Lin, Y.G., et al., Soy protein enhances the cholesterol-lowering effect of plant sterol esters in cholesterol-fed hamsters. Journal of Nutrition, 2004. **134**(1): p. 143-148.
22. Moriyama, T., et al., Soybean beta-conglycinin diet suppresses serum triglyceride levels in normal and genetically obese mice by induction of beta-oxidation, downregulation of fatty acid synthase, and inhibition of triglyceride absorption. Bioscience Biotechnology and Biochemistry, 2004. **68**(2): p. 352-359.
23. Luchoomun, J. and M.M. Hussain, Assembly and secretion of chylomicrons by differentiated Caco-2 cells - Nascent triglycerides and preformed phospholipids are preferentially used for lipoprotein assembly. Journal of Biological Chemistry, 1999. **274**(28): p. 19565-19572.
24. van Rijn, J.M., M. van Hoesel, and S. Middendorp, A Fluorescence-based Assay for Characterization and Quantification of Lipid Droplet Formation in Human Intestinal Organoids. J Vis Exp, 2019(152).
25. Torre-Villalvazo, I., et al., Soy protein ameliorates metabolic abnormalities in liver and adipose tissue of rats fed a high fat diet. Journal of Nutrition, 2008. **138**(3): p. 462-468.
26. Radcliffe, J.D., V.L. Imrhan, and A.N. Hsueh, The use of soy protein isolate to reduce the severity of 13-cis retinoic acid-induced hypertriglyceridemia. Cancer Detection and Prevention, 1998. **22**(6): p. 526-532.
27. Standeven, A.M., et al., Retinoid-induced hypertriglyceridemia in rats is mediated by retinoic acid receptors. Fundamental and Applied Toxicology, 1996. **33**(2): p. 264-271.

28. Xiao, C.W., et al., Dietary soy protein isolate modifies hepatic retinoic acid receptor-beta proteins and inhibits their DNA binding activity in rats. Journal of Nutrition, 2007. **137**(1): p. 1-6.
29. Chen, H., Protein digestion kinetics in pigs and poultry. 2017, Wageningen University: Wageningen.
30. Tarnawski, A.S. and A. Ahluwalia, Molecular Mechanisms of Epithelial Regeneration and Neovascularization During Healing of Gastric and Esophageal Ulcers. Current Medicinal Chemistry, 2012. **19**(1): p. 16-27.

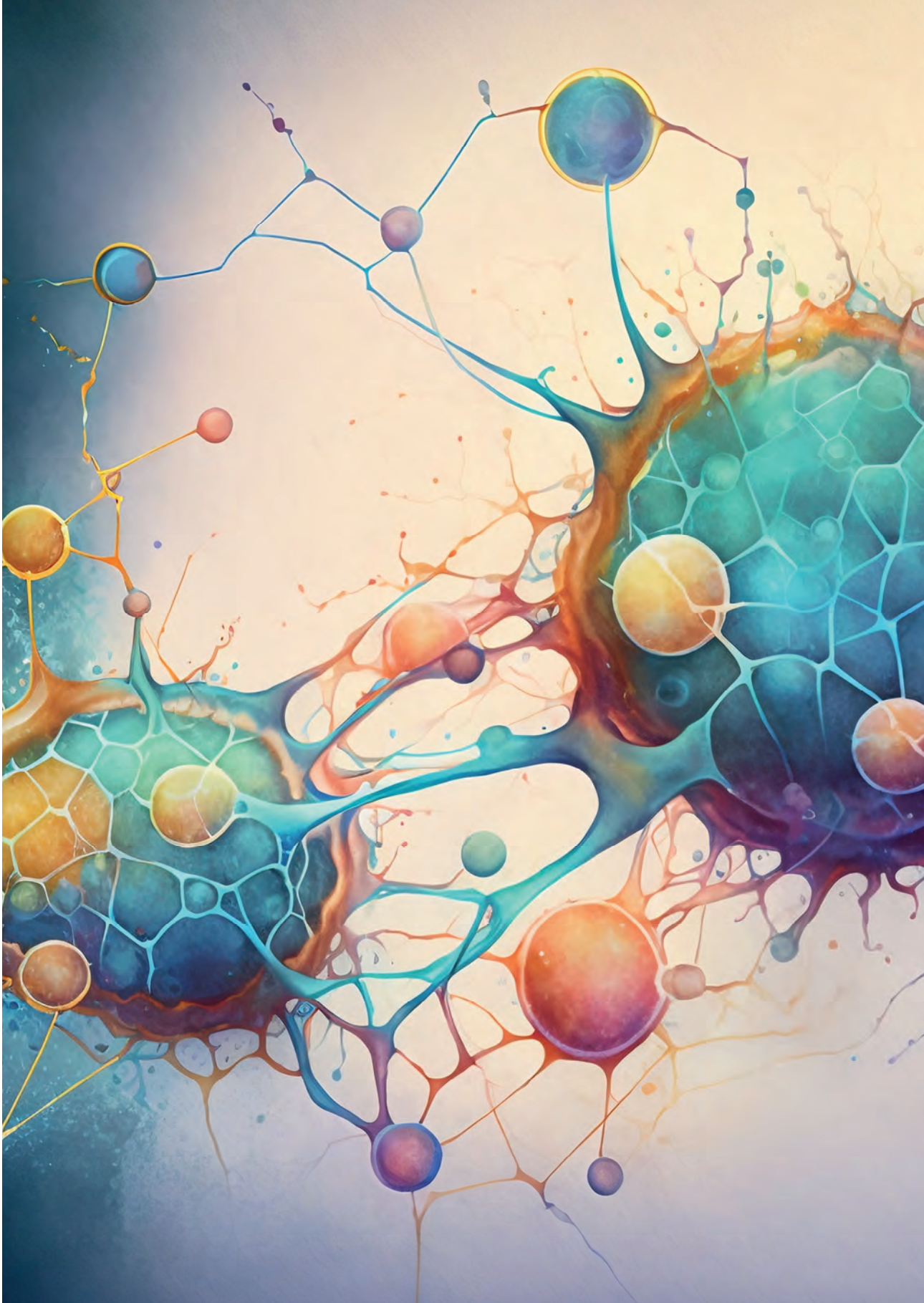

High-Throughput Scratch Assay for Quantifying Re-Epithelialization Kinetics of Stem Cell-Derived Organoid Monolayers and Cell Lines

Marcela M. Fernandez-Gutierrez*[1,2], Bart van der Hee*[1,3], Peter P.J. Roosjen[4], David B.H. van Zessen[5], Nico Taverne[1], Peter van Baarlen[1], Andrew P. Stubbs[5], Hauke Smidt[3], Jerry M. Wells[1], Michiel Kleerebezem[1,2]

[1]Host-Microbe Interactomics, Department of Animal Sciences, Wageningen University & Research, De Elst 1, 6708 WD, Wageningen, The Netherlands. [2] TI Food and Nutrition, Nieuwe Kanaal 9-A, 6709 PA, Wageningen, The Netherlands. [3]Laboratory of Microbiology, Wageningen University & Research, Stippeneng 4, 6708WE, Wageningen, The Netherlands. [4]Laboratory of Geo-Information Science and Remote Sensing, Wageningen University & Research, Droevendaalsesteeg 3, 6708 PB, Wageningen, The Netherlands. [5]Department of Bioinformatics, Erasmus University Medical Centre, Wytemaweg 80, 3015 CN, Rotterdam, The Netherlands.

***These authors contributed equally.**

Manuscript to be submitted

Abstract

An *in vitro* scratch test is an appealing approach to investigate the control and procedures of epithelial cell growth and movement associated with wound healing. It is done by making a scratch in a complete cell layer and subsequently observing the epithelization of the "injury" by capturing images over time. Despite the advancements to the method in recent years, high-throughput screenings often require the integration of various image analysis and data extraction software tools. We have created a high-throughput image-based scratch test for diverse cell models, such as intestinal organoids and cell lines, in combination with an automated processing pipeline which utilizes a mathematical model to explain re-epithelialization kinetics. This pipeline was embedded in Galaxy (KREAP), providing an open-source web-based platform to facilitate scientists from different backgrounds to conduct reproducible and quantitative repair data analyses in less than 45 minutes.

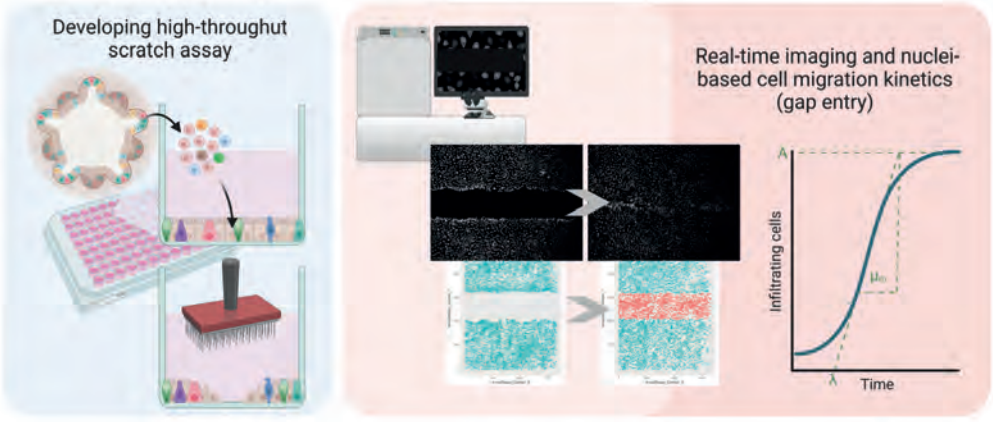

Introduction

Most tissue epithelia are lined with a rapidly self-renewing layer of cells, for protection, sensing, secretion, and selective absorption. However, most models testing interactions with compounds use static confluent layers of transformed or cancer cell lines, which do not closely mimic spatial kinetics and epithelia containing multiple cell types, including stem and progenitor cells. To embrace increasing use of stem cell technologies, we developed methods to grow planar monolayers of intestinal organoid cells [4] and adapted growth protocols to make them suitable for scratch assays.

In vitro scratch tests have been commonly used to examine the effects of bioactive elements on cell movement and expansion [7-13]. These assessments are usually conducted in multi-well plates and involve the manual insertion of a scratch in an epithelial cell monolayer with a sterile pipette tip, razor blade, scraper, or needle. The residual epithelial cells will then spread and proliferate into the scratched area until cell-cell contacts are re-established [14, 15].

In order to standardize and amplify the output, considerable progressions have been made in the *in vitro* wounding instruments and methods, comprising the use of hand-directed pin or pipette tip arrays, robotically powered scratching-pin gadgets, chemically provoked wounds, and laser ablation [6, 16]. Moreover, the tests have changed from inspecting images taken manually at fixed-time points to the application of automated fluorescent microscopy that observes live cells expressing fluorescent markers [14]. Similarly, manual measurement of the scratched region has been replaced by the implementation of automated image segmentation algorithms that help with the examination of high-throughput screenings [18].

Despite all these improvements, data analysis has been usually limited to the calculation of wound closure [18, 19], disregarding the kinetic information inherent to the healing process. In addition, effective processing, and quantification of high-throughput image-based assays involves the integration of multiple image analysis and data extraction software tools that often require computer programming skills and/or a commercial license, increasing total experimental costs [2].

In this protocol we present the procedure of a high-throughput scratch assay using high-content microscopy and a mathematical model that quantifies the kinetics of epithelial wound repair in individual wells. This enables the calculation of biologically relevant parameters, as well as methods to visualize spatial-temporal cell trajectories. The assay can be used for screening chemical compounds, bacterial suspensions [2],

and other bioactive substances for their effect on re-epithelialization kinetics. Furthermore, we developed the Kinetic Re-Epithelialization Analysis Pipeline (KREAP) that was implemented in Galaxy, providing an end-to-end workflow that integrates different validated tools for reproducible image analysis, cell enumeration, re-epithelialization modelling, and HTML reporting [20]. KREAP is available for download and use as a virtual machine for both large and small-scale laboratories (http://gigadb.org/dataset/100472).

Development of the protocol: Quantification of re-epithelialization kinetics

To quantify the re-epithelialization kinetics of intestinal organoid monolayers (porcine colon) and other cell lines exposed to different bacterial suspensions or compounds using our standardized scratch assay, we developed an automated image segmentation pipeline using CellProfiler 2.2.0 (http://www.cellprofiler.org/) that identifies and records the location of each cell within the well over time [2].

The number of cells moving into the scratched area over time can be represented by a sigmoidal curve. We then used a modified form of the Gompertz function [21] to quantify the kinetics of wound repair. This Gompertz function consists of three biologically measurable parameters: lag time (λ parameter, in minutes), repair rate (μ_m parameter, cells/minute), and maximum number of infiltrating cells (A parameter, in cells). The maximum number of cells (A) corresponds to the maximum carrying capacity of the scratch and mimics population dynamics for wound repair.

This function was fitted through the number of infiltrating cells over time by a nonlinear least squares regression using the Levenberg-Marquardt algorithm [22]. This reduces the sum of the squares of the errors between the modelled and measured data points iteratively. This allows researchers to obtain excellent and accurate fits, characterized by a goodness of fit (R^2) with values close to one and low root-mean-square errors (RMSE) (**Figure 1**).

Experimental design

Selection of suitable cell models. For automated microscopy, it is preferable to select a cell model that grows in a single layer of cells, rather than in multilayers. Furthermore, it is important to evaluate the expression of relevant receptors (e.g., Toll-like receptors, epidermal growth factor receptor, etc.) in the candidate cell line as well as its responsiveness to chemical stimuli. The addition of Intestinal organoids could provide a more physiologically relevant model of tissue epithelium than

conventional cell lines [23], but the spatial morphology of three-dimensional intestinal organoids limits access to the apical surface or epithelium. Therefore, dissociation into single cells and plating on tissue culture plates enables heterotypic cellular differentiation within a brief period and formation of polarized monolayers for scratch assays [4, 24, 25].

Controls. Titration curves of the controls must be done on each cell line to determine the optimal concentrations resulting in a large dynamic range between the positive and negative controls (Supplementary Fig. 1 and Box 1). A non-treated or medium control should be included as a reference to determine whether the screened substances have a stimulating or attenuating effect on re-epithelialization kinetics.

Z' factor calculation. The overall quality of each assay can be assessed by calculation of the Z' factor [17] defined by the means and variability of the positive and negative controls (**Box 1**).

Limitations

The modified Gompertz function was implemented to describe growth curves. Therefore, if the growth curves resulting from a particular treatment do not resemble a sigmoidal curve, the modified Gompertz function cannot be used to calculate the kinetic parameters. For instance, when a treatment severely inhibits re-epithelialization where only a few cells migrate into the scratched area during the assay. However, the KREAP "Data-Modelling" tool flags the wells from which the parameter values were not successfully retrieved, and the user can then manually examine the curves resulting from the measured data points over time as well as the image segmentation output (also see [20]). Moreover, the carrying capacity of the cell population or cell death-inducing treatments may affect the plateau of the growth curve, leading to a reduction in the number of infiltrating cells towards the end of the assay and lower R^2 values (< 0.9). Adverse effects of compounds or cell overcrowding can be identified by inspecting the curves generated by the KREAP tool and identifying the measured and modelled growth curves. R^2 values lower than 0.9 are also flagged by KREAP to alert the user to examine the re-epithelialization curves. Next to modelling, a limitation of using organoid monolayers is that the intestinal physiological nature (i.e., crypt/villous structures) is not recapitulated on a planar sheet of cells, resulting in direct contact of compounds with cells that are physiologically not exposed to xeno- or exobiotics (e.g., stem cells and Paneth cells residing at the crypt base). Furthermore, the cells need to be scratched before fully

developing, as adherens- and tight junction formation might result in irregular scratches. However, differentiation before plating resulted in fully differentiated cell lineages and tight junction formation [4] simultaneously which did not inhibit scratching in this case.

Box 1. Assay Quality Assessment

Positive controls included human epidermal growth factor (hEGF) and transforming growth factor α (hTGFα), which both bind to the epidermal growth factor receptor (EGFR) and act as mitogenic and cell motility factors [1]. Specific inhibitors of p38 mitogen-activated protein kinase (SB203580) and MEK1/2 (U0126) can be used both separately or in combination to suppress wound repair by blocking the activation of cell migration [3] and proliferation [5, 6] pathways, respectively (**Supplementary Fig. 2)**.

Calculation of the Z′ factor can be used to assess the overall quality of each independent run. The Z′ factor [17] is based on the ratio between the variability of the controls (i.e., standard deviation, σ) and the absolute difference between the means (μ) of the positive and negative controls. The difference between the controls defines the dynamic range of the assay signal. The Z′ factor can be calculated using the following equation:

$$Z' = 1 - \frac{(3\sigma_{c+} + 3\sigma_{c-})}{|\mu_{c+} - \mu_{c-}|}$$

If the Z′ factor values are negative it generally indicates that the assay conditions are not optimal and cannot be used to generate useful data. Values between 0 and 0.5 indicate that the separation band between the controls is small, whereas values between 0.5 and 1 indicate a large dynamic range and a likely successful assay.

Materials

Reagents

- Intestinal organoids from a location and species of interest
- Epithelial cell lines. Here we provide the protocol for the following cell lines: Ca9-22 (gingival cells obtained from the National Institute of Biomedical Innovation JCRB Cell Bank, cat. no. JCRB0625), HO-1-N-1 (oral mucosa cells obtained from the National Institute of Biomedical Innovation JCRB Cell Bank, cat. no. JCRB0831), and HaCat (skin keratinocytes obtained from AddexBio, cat. no. T0020001)
  ! CAUTION. The cell models should be routinely checked to ensure that they are authentic and not cross-contaminated (e.g., using short-tandem repeat analysis) or infected with mycoplasma (PCR-based detection).
- Cell culture medium, e.g., Dulbecco's Modified Eagle Medium (DMEM), DMEM/F12 (1:1) or Keratinocyte-Serum Free Medium (SFM) Gibco, cat. no. 61965-026, 31331-028, 17005-034)
- Heat inactivated fetal calf serum (FCS) (Gibco, cat. no. 10500)
- Penicillin-Streptomycin 100X (Sigma, P0781-20ML)
- Recombinant murine Noggin, human R-spondin 1, human WNT3A, or conditioned media from Noggin (15% v/v), R-Spondin (15% v/v), and WNT3A (30% v/v)-producing cells [26, 27]
- Primocin (500x, 50mg/ml, Invitrogen ant-pm-xx)
- HEPES buffer (Sigma-Aldrich)
- B-27 supplement (50x, Gibco 17504-044)
- N-acetylcysteine (Sigma-Aldrich
- Glutamax (Gibco, 35050-061)
- Gastrin (
- Nicotinamide (
- TGF-β receptor inhibitor (A83-01)
- TrypLE Express [- Phenol red] (Gibco, 12604-013)
- 0.25% Trypsin EDTA (1x) (Gibco, 25200-056)
- Sterile phosphate-buffered saline (PBS) (Gibco, 18912-014)
- CellTracker™ Red CMTPX (Molecular Probes, cat no. C34552) (optional)
- Hoechst 33342 (Molecular Probes, cat no. H1399)
  ! CAUTION. Hoechst stains are known mutagens and should be handled with care.
- Human transforming growth factor α (hTGFα; R&D Systems, cat. no. 239-A-100)
- Human epidermal growth factor (hEGF, Gibco, cat. no. PHG0311)

- Inhibitor of p38 (SB203580; Cell Signaling Technology, cat. no. 5633)
- Inhibitor of MEK1/2 (U0126, Cell Signaling Technology, cat. no. 9903)
  ! CAUTION. The MEK1/2 inhibitor (U0126) may cause irritation to eyes, skin, and mucous membranes.

Equipment

- 75 cm^2 cell culture flasks (Corning Incorporated, cat. no. 430641U)
- Tissue culture-treated 24-well plates (Corning Incorporated, cat. no. CLS3527)
- Tissue culture-treated 96-well plates (BD Falcon, cat. no. 353219)
- Tissue culture-treated 96-well plates with flat bottom (Corning Incorporated, cat. no. 3599)
- Tissue culture-treated 96-well plates with round bottom (Corning Incorporated, cat. no. 3799)
- Multichannel pipette, 8-channel, 100 µl (Eppendorf Research Plus, cat. no. 3122000035)
- Disposable serological pipette 5 ml, 10 ml and 25 ml (Corning Incorporated, cat. no. 4051, 4101, and 4251)
- Reagent Reservoir 50 ml (Corning Incorporated, cat. no. 4870)
- Pipette 10 µl, 200 µl and 1 ml (Eppendorf Research Plus, cat. no. 3120000020, 3120000054, and 3120000062)
- Filter sterile tips 10 µl, 200 µl and 1 ml (Corning Incorporated, 4807, 4823, and 4809)
- Tips for multichannel pipette 2-200 µl (Eppendorf, cat. no. 0030073.428)
- Counting chamber (Brand, cat. no. 719520)
- HTSScratcher (Peira, https://www.peira.be/platforms/oncology-platforms)
- Laminar flow cabinet
- Laboratory vacuum pump
- Inverted microscope, e.g., Zeiss, Axiovert 40CFL
- Automated fluorescent microscope with controlled temperature and atmosphere, e.g., BD Pathway 855 Bioimaging System or similar
- Humidified tissue culture incubator (Thermo-Scientific, Forma Direct Heat CO_2 Incubator)
- KREAP (Kinetic Re-epithelialization Analysis Pipeline) virtual machine (**http://gigadb.org/dataset/100472**)

Reagent Setup

Organoid culture medium. Maintenance and expansion medium (EM) for 3D organoids (W-ENR) is prepared by supplementing DMEM-F12 with 100 µg/ml primocin, 10 mM HEPES, B-27 supplement (1x), 1.25 mM N-acetylcysteine, Glutamax (1x), 50 ng/ml hEGF, 15 nM gastrin, 10 µM p38 MAPK inhibitor, 600 nM TGFβ receptor inhibitor, and 100 ng/ml recombinant murine Noggin, 500 ng/ml human R-spondin 1, 100 ng/ml recombinant human WNT3A, or conditioned medium from Noggin (15% v/v), R-Spondin (15% v/v), and WNT3A (30%v/v) producing cell lines. The differentiation medium (DM) which is added to a single suspension of cells from organoids prior to seeding is based on EM but lacks WNT3A, p38 MAPK inhibitor, and nicotinamide. All media can be stored for 3 months (-20 ºC) or 2 weeks (4 ºC) but avoid freeze-thaw cycles as this negatively affects the activity of the growth factors.

Growth media cell lines. Add penicillin-streptomycin to the cell culture media to a final concentration of 1x and the inactivated FCS to a final concentration of 10% (v/v). Store at 4ºC.

Hoechst 33342 stock solution (10 mg/ml) and working solution (1 mg/ml). To prepare the stock solution, dissolve 100 mg lyophilized dye in 10 ml dimethyl sulfoxide (DMSO). Divide the stock solution into aliquots to avoid repeated freeze-thaw cycles. Store at -20ºC protected from light. This solution is stable for at least one year according to the manufacturer. To prepare the working solution, add 100 µl of the stock solution into 900 µl PBS and store at 2-6 ºC for a maximum of three months.

CellTracker™ Red CMTPX stock solution (100 µM). Dissolve 50 µg lyophilized dye in 730 µl DMSO. Divide the solution into aliquots to avoid repeated freeze-thaw cycles. Store at -20ºC protected from light. This solution is stable for at least three months. Lyophilized dye is stable for at least one year according to the manufacturer.

hTGFα stock solution (10 µg/ml). Reconstitute 100 µg hTGFα in 1 ml 10 mM filter-sterilized acetic acid. Add this solution into 9 ml DMEM to obtain the stock solution. Divide into aliquots and store at -20ºC to avoid repeated freeze-thaw cycles. According to the manufacturer, this solution is stable for at least three months.

hEGF stock solution (10 µg/ml). Reconstitute 100 µg hEGF in 1 ml sterile PBS. Add this solution into 9 ml DMEM containing heat inactivated FCS to obtain the stock solution. Divide into aliquots and store at -20ºC to avoid repeated freeze-thaw cycles. According to the manufacturer, this solution is stable for one year.

SB203580 stock solution (10 mM). Reconstitute 5 mg of lyophilized inhibitor in 1.32 ml DMSO. Divide into aliquots and store at -20ºC to avoid repeated freeze-thaw cycles.

U0126 stock solution (10 mM). Reconstitute 5 mg of lyophilized inhibitor in 1.32 ml DMSO. Divide into aliquots and store at -20ºC to avoid repeated freeze-thaw cycles.

Equipment Setup

Fluorescence Microscope. Hoechst 33342 and CellTracker™ Red CMTPX images should be acquired using an excitation filter of 350 nm and 577 nm, respectively. Bright-field images serve as visual control for cell morphology and vitality. The microscope should be programmed to acquire fluorescent and bright-field images of the same field of each well every 20-30 minutes (recommended, but the time intervals can be adjusted according to the user's needs and cell line) using a 4x objective (40x magnification).

Procedure

Rapid isolation of intestinal crypts for organoid culture

TIMING 2 hours, depending on sample number

1. Place the required number of 24-well plates in a 37 °C incubator overnight. CRITICAL STEP. The high humidity reduces the net flow of evaporating water molecules lowering the surface tension and making Matrigel drop formation easier.
2. Extract intestinal tissue and open longitudinally using surgical scissors
3. Remove the muscle layer from the lamina propria by lifting the epithelium with tweezers and carefully snipping between the two layers
4. Dissect the lamina propria and epithelium into small sections (± 25 mm^2) and place them into a 50 mL tube containing 12 mL ice-cold PBS.

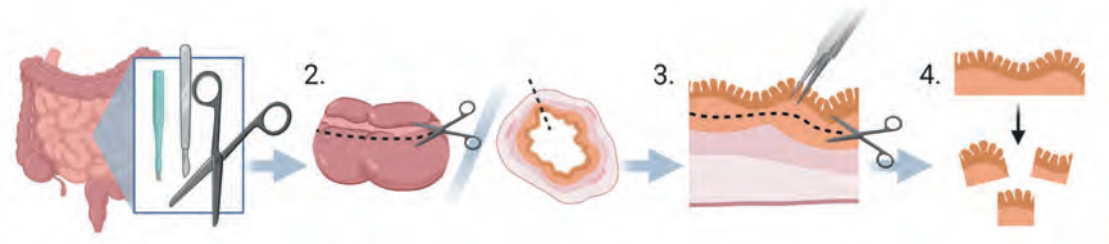

5. Vortex at maximum speed for 10 seconds to remove fecal material and mucus.
6. Precipitate the tissue fragments and discard the PBS.
7. Repeat steps 5-6 an additional 2 times with 12 mL of fresh ice-cold PBS every time.
8. Remove PBS and add 6 mL ice-cold PBS supplemented with 30 mM EDTA.

9. Agitate using an orbital shaker for 15 minutes at room temperature.
10. Refresh the PBS/EDTA mixture with prewarmed (37 °C) PBS/EDTA (30 mM) and incubate at 37 °C for 10 minutes
11. Remove PBS/EDTA and add 30 mL ice-cold DMEM (+penicillin/streptomycin) to wash away any residual chelating compounds from steps 8 to 10.
12. Take out the tissue fragments and gently scrape the luminal side with the back of a scalpel or glass slide. **CRITICAL STEP** Make sure to not put too much pressure while scrapping, as this will also scrape off the lamina propria.
13. Add all scraped material to a 15 mL tube containing 10 mL ice-cold DMEM (+ 1% pen/strep) and suspend by vortexing at maximum speed for 10 seconds.
14. Place a 100 µm cell strainer over a 50 mL tube and filter the suspension**.** **CRITICAL STEP** Large crypts or debris clog the filter. If yields are low, pour an additional 30 mL ice-cold DMEM over the filter to increase the recovery of crypts.
15. Count the number of crypts in the suspension using a counting chamber.
16. Centrifuge the tube at 300 x g for 5 minutes at 4 °C.
17. Resuspend the crypts in 1 mL/300 crypts ice-cold Matrigel and create small droplets on the pre-incubated 24-well plate (6 droplets per well).
18. Invert the plate and polymerize the Matrigel at 37 °C for 10 minutes. **CRITICAL STEP** The Matrigel can be diluted 1.5 times using PBS to allow less rigid extracellular matrix formation. This increases polymerization time, so check full gel-formation by tapping lightly while tilting the plate and ensure the droplets stay in place.
19. Overlay the droplets with 600 ul W-ENR medium per well and incubate at 37 °C at 5% CO_2.
20. Monitor successful organoid formation by checking small sphere formation within 2 days and refresh the medium every 2 days with prewarmed (37 °C) W-ENR.

Passaging of intestinal organoid cultures for maintenance and expansion

TIMING 1h

21. Passage the organoids every 5 days.
22. Remove the growth medium and add 1 mL ice-cold DMEM (+ pen/strep).
23. Agitate by repeated pipetting (p1000) to dissolve the Matrigel and transfer to a 15 mL tube on ice.
24. Pellet the organoids by centrifugation at 300 x g for 5 minutes at 4 °C.
25. Remove the supernatant and add 1 mL prewarmed (37 °C) TrypLE dissociation reagent and incubate for 5 minutes in a water bath (37 °C). **CRITICAL STEP** Ensure that the organoids do not fully dissociate into single

cell suspensions. Small clumps of 5-10 cells are optimal for regeneration of organoids

26. Stop the reaction by adding 4 volumes of ice-cold DMEM and centrifuge at 300 x g for 5 minutes at 4 °C.
27. Discard the supernatant and suspend the pellet in fresh Matrigel.
28. Plate and culture following steps 17 to 20.
29. Organoids can be frozen using standard cell-freezing methods when cultured for more than one week. **CRITICAL STEP** To optimize revival of the organoids, we advise freezing them when they are small spheroids, e.g., 2 days post-passage in a mixture of DMEM supplemented with high-grade FCS (20-50% v/v) and DMSO (10% v/v)

Procedures for generating monolayers

TIMING 3 days

30. Culture 3-dimensional intestinal organoids in DM for 3 days to generate a heterotypic cell culture. **? TROUBLESHOOTING**
31. Add 200 µl pre-warmed (37 °C) DMEM to a black-walled 96-well plate (BD Falcon, cat. no. 353219) and incubate for 1 hour at 37 °C.
32. Aspirate the medium and add 1 mL ice-cold DMEM to each well to solubilize the Matrigel and release the organoids.
33. Add the suspension to a 15-mL tube (Falcon) and centrifuge at 250 x g for 5 minutes at 4 °C.
34. Discard the supernatant and add 1 mL pre-warmed (37 °C) TrypLE dissociation reagent to the tube.
35. Agitate the pellet by repeated pipetting with a p200 pipette to suspend the organoids and place immediately in a 37 °C water bath for 5 minutes.
36. Agitate the suspension by repeated pipetting with a p200 pipette 30 times and incubate for another 5 minutes in the water bath (37 °C).
37. Generate a homogenous suspension by repeated pipetting with a p200 pipette until no clumps are present, add 4 volumes of ice-cold DMEM and centrifuge at 750 x g for 5 minutes at 4 °C **CRITICAL STEP** At this stage, check the suspension for complete single-cell dissociation before stopping the enzymatic reaction. If clumps are present, re-incubate for 2 minutes and agitate by repeated pipetting using a p200 pipette before adding DMEM. **? TROUBLESHOOTING**
38. Resuspend the pellet in 1 mL prewarmed DM (37 °C) and count cells using a counting chamber.
39. Aspirate the medium from the 96-well plate and place in the fume hood until all wells are dry (remove lid to allow evaporation).

40. Adjust the suspension to 1 x 10^6 cell per mL and add 200 µl cell suspension to each well.
41. Grow the monolayer to confluence over 24 hours and proceed with step 11. **CRITICAL STEP** The cell seeding density should be optimized for each type of organoid to ensure a confluent monolayer is formed in 24h. **? TROUBLESHOOTING**

Cell culturing and seeding of cell lines

TIMING 3-7 days depending on the cell line

1. Grow low-passage epithelial cells to 70-80% confluence in 75 cm^2 tissue culture flasks. Ca9-22 and HaCat cells should be grown in DMEM supplemented with 10% FCS, 100 U/ml penicillin and 100 µg/ml streptomycin. HO-1-N-1 cells should be cultured in DMEM/F12 (1:1) supplemented with 10% FCS, 100 U/ml penicillin and 100 µg/ml streptomycin. **CRITICAL STEP** Always wear gloves when handling cells and work in a laminar flow cabinet. The cell culture environment should be kept clean, i.e. in absence of bacteria, molds and mycoplasma.
2. Discard the growth culture media and wash the cells with 6 ml PBS.
3. Discard the PBS and add 2 ml trypsin/EDTA and incubate at 37ºC for 3-5 minutes.
4. **CRITICAL STEP** Verify complete detachment of the cells under an inverted microscope.
5. Add 8 ml of supplemented growth media into the flask and gently resuspend the cells by gently pipetting up and down.
6. Take an aliquot of the cell suspension and determine the cell counts using a counting chamber. Dilute the cell suspensions in the corresponding growth media. The Ca9-22 cell suspension should be diluted to obtain 3.5 x 10^5 cells/ml; whereas HO-1-N-1 and HaCat cell suspensions should be diluted to obtain 3.0 x 10^5 cells/ml.
7. **CRITICAL STEP** The number of cells required to form an intact monolayer within the standard timeframe depends on the cell type and thus, should be pre-determined for each cell line.
8. Mix the cell suspension gently and add the suspension into a reagent reservoir.
9. Using a multichannel pipette, add 100 µl of the cell suspension into each well of a 96-well plate with flat bottom (BD Falcon; recommended for imaging using the BD Pathway 855 Bioimaging System).
10. Incubate for 16 hours in a humidified incubator at 37ºC with 5% CO_2.

Cell starvation

TIMING 2 hours (might vary for other cell lines)

1. Replace the growth media by 100 µl starvation media (i.e. FCS-free media) by aspiration of the culture medium without disturbing the cell monolayers. HaCat cells should be starved in keratinocyte serum-free medium (SFM). Starvation of Ca9-22 cells should be performed in FCS-free DMEM/F12, whereas HO-1-N-1 cells should be starved in FCS-free DMEM. SFM is not recommended when using Ca9-22 or HO-1-N-1 cells as it was shown to promote significant cell migration and proliferation in our setup that restricted the detection of exogenously added stimulatory compounds.
2. **CRITICAL STEP** The duration and the media used during starvation needs to be optimized for each cell line. FCS deprivation should minimize cell migration and proliferation without inducing apoptosis or cell detachment. **? TROUBLESHOOTING**
3. Incubate the cells (Ca9-22, HO-1-N-1 or HaCat cells) for 2 hours in a humidified incubator at 37ºC with 5% CO_2.

Preparation of master plate with treatment and control samples

TIMING 1.5 hours

4. Prepare the necessary assay treatments. An example of bacterial preparations is provided in **Box 2.** Initial screenings can be performed in duplicates, but refined studies should be carried out with at least three technical replicates in two or more independent experiments.
5. **CRITICAL STEP** All treatments should be diluted in the starvation media.
6. Prepare the positive and negative controls as indicated in **Table 1**.
7. **CRITICAL STEP** Optimal concentrations of the controls should be determined by performing a titration for the target cell lines (**Supplementary Fig. 1**) and should result in a large dynamic range between the positive and negative controls (**Box 1**). **? TROUBLESHOOTING**
8. Prepare a master plate by adding 120 µl of each sample into the corresponding well.
9. **CRITICAL STEP.** Exclude outer wells to avoid any possible edge-specific artifacts, e.g., due to evaporation of the medium. It is also recommended to add the treatments into the wells in a randomized manner.

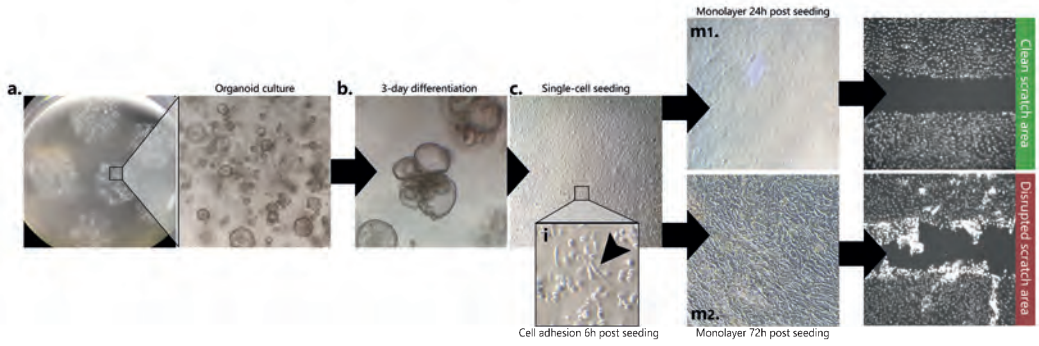

Figure 1. Generating intestinal organoid monolayers for re-epithelialization assays. (a) organoids can be grown in 3-dimensional morphology long-term from a tissue location of choice and differentiated (b) with differentiation medium for 3 days into a heterotypic cell culture. (c) After single-cell dissociation, cells are seeded in 96-well plates and cell adhesion occurs within 6 hours (i). After 24 h the cells reach confluence and are ready for the scratch assay (m1). Longer incubations lead to irregular scratches (m2)

Box 2. Preparation of bacterial suspensions

High-throughput screening of viable bacteria [2] often require preparation of 15% glycerol stocks at a specific growth stage prior to the experiment.

Preparation of 15% (v/v) glycerol stocks

1. Culture the bacterial strains until the desired growth stage (e.g., early stationary stage) under the required atmospheric conditions.
2. Take 700 µl of the bacterial suspension into a cryovial (Corning Incorporated, cat. no. 430488) and add 300 µl glycerol 50% (final concentration 15%).
3. Store at -80°C until used.

Preparation of bacterial suspensions for screening

1. Thaw the bacterial suspensions completely by placing them at room temperature.
2. Pellet the bacteria by centrifugation (4,000 x g, 7 minutes at room temperature).
3. Remove the spent media and resuspend the bacteria in 700 µl starvation media.
4. Dilute the bacterial suspension in starvation media until the required multiplicity of infection (MOI) is obtained in 100 µl of the bacterial suspension. For example, to obtain a MOI of 10 with an epithelial density of 3.5×10^4 cells per well, prepare a bacterial suspension containing 3.5×10^6 bacterial cells per ml and add 100 µl to each well.

Table 1. Working concentrations of positive and negative controls. Preparation of the controls for the target cell models. The indicated volumes are sufficient for 10 replicates (100 µl each).

Cell model	hTGFα	hEGF	p38, MEK1/2 inhibitors
Porcine colonoid	Add 2 µl hTGF (10 µg/ml) into 998 µl DM to a concentration of 20 ng/ml		Add 0.1 µl of each inhibitor (10 mM) into 999 µl DM for a final concentration of 1 µM
Ca9-22	Add 2 µl hTGF (10 µg/ml) into 998 µl starvation media to a concentration of 20 ng/ml. Add 200 µl hTGF (20 ng/ml) into 800 µl starvation media to a final concentration of 4 ng/ml.	Add 2 µl hEGF (10 µg/ml) into 998 µl starvation media to a concentration of 20 ng/ml. Add 300 µl hEGF (20 ng/ml) into 700 µl starvation media to a final concentration of 6 ng/ml.	Add 1 µl of each inhibitor (10 mM) into 998 µl starvation media for a final concentration of 10 µM each.
HO-1-N-1	Add 2 µl hTGF (10 µg/ml) into 998 µl starvation media to a concentration of 20 ng/ml. Add 500 µl hTGF (20 ng/ml) into 500 µl starvation media to a final concentration of 10 ng/ml.	Add 2 µl hEGF (10 µg/ml) into 998 µl starvation media to a concentration of 20 ng/ml. Add 500 µl hEGF (20 ng/ml) into 500 µl starvation media to a final concentration of 10 ng/ml.	
HaCat	Add 2 µl hTGF (10 µg/ml) into 998 µl starvation media to a concentration of 20 ng/ml. Add 500 µl hTGF (20 ng/ml) into 500 µl starvation media to a final concentration of 10 ng/ml.	Add 2 µl hEGF (10 µg/ml) into 998 µl starvation media to a concentration of 20 ng/ml. Add 250 µl hEGF (20 ng/ml) into 750 µl starvation media to a final concentration of 5 ng/ml.	

Fluorescent labelling with live-compatible dyes

TIMING 25 minutes

1. Prepare a solution of starvation (cell lines) or DM (organoids) media with fluorescent dyes. Add 10 µl of Hoechst 33342 working solution and optionally 100 µl of CellTracker™ Red CMTPX stock solution into 5 ml medium to obtain a final concentration of 2 µg/ml and 2 µM, respectively.
2. **CRITICAL STEP** Nuclear labelling with Hoechst 33342 stain is needed for accurate image segmentation and feature extraction with the automated image analysis pipeline. Furthermore, labelling of cellular cytoplasm with CellTracker™ Red CMTPX can be performed to visualize cell morphological features. The concentrations of these dyes may need to be adjusted depending on the selected cell model, session duration, and intensity. When using different cell models, check that addition of dyes at the desired

concentration does not result in adverse effects in re-epithelialization kinetics.

? TROUBLESHOOTING

3. Add the labelling solution into a reagent reservoir and carefully aspirate the starvation media from the cells using a vacuum pump without disturbing the cell monolayer.
4. Add 50 µl of the solution to each of the wells and incubate at 37°C with 5% CO_2 for 20 minutes.

Scratch assay and imaging

TIMING 5-16 hours depending on the cell model

5. After incubation with labelling solution for 20 minutes a scratch can be performed in the cell monolayers of each well using the HTSScratcher, which assures equally sized and reproducible scratches. Place the plate on the platform, slide the plate under the 96-pin array, press the array towards the bottom of the wells, and slide the array from left to right 3 times. Release pressure from the array and remove the plate from the platform.
6. **CRITICAL STEP** Rinse the array with water followed by ethanol before and after each experiment. Monitor the organoid monolayer for a well scratched surface, if the scratch shows tearing the monolayer growth period should be optimized (**Fig. 1**)

   ? TROUBLESHOOTING
7. Carefully aspirate the liquid from each well using the vacuum pump and wash the cells with 100 µl PBS. Repeat this step one or two times to remove all detached cells and debris.
8. Aspirate the PBS and immediately transfer 100 µl (optimize per assay duration) of each pre-diluted treatment from the master plate to their corresponding well in the assay plate using a multichannel pipette.
9. **CRITICAL STEP** Add 100-200 µl PBS in the outer wells to avoid differential evaporation of the samples. **? TROUBLESHOOTING**
10. Start image acquisition. Depending on the cell growth rate, we recommend programming the microscope to acquire images every 20 minutes for 5 hours. For slow-growing cells, imaging intervals can be adjusted to 60 minutes for 14-16 hours.
11. **CRITICAL STEP** The duration of the assay may vary depending on the cell model and can be determined by the time required for the positive control to achieve wound closure.

Image and data Analysis

TIMING 45 minutes

1. The virtual machine (VM) can be downloaded containing the Kinetic Re-Epithelialization Analysis Pipeline (KREAP) toolbox [20] as well as the VM player for your operating system via:
   http://gigadb.org/dataset/100472
2. Import the VM into the player following the step-by-step instructions provided in the manual on the website.
3. Create an .txt index file and a compressed plate folder containing the acquired images organized in separate folders for each well. Indications on how to create these files are provided at:

   https://erasmusmc-bioinformatics.github.io/KREAP/file_formats

4. Upload the compressed folder and index file into the Galaxy history via the "Get data" tool.
5. **CRITICAL STEP** Set the compressed folder's type to .zip in the upload menu. Run the KREAP Image Analysis tool to perform automated image segmentation (**Figure 2c**). The results are reported in an HTML format, can be downloaded, and stored locally [20]. A manual is provided at: **? TROUBLESHOOTING**
   https://erasmusmc-bioinformatics.github.io/KREAP/use_kreap_analysis
6. Run the KREAP Data-Modeling tool to quantify re-epithelialization kinetics (**Figure 1**). The results are reported in an HTML format, can be downloaded, and stored locally [20]. A manual is provided at:
   https://erasmusmc-bioinformatics.github.io/KREAP/use_kreap_modeling
7. **CRUCIAL STEP** Remember to set the time interval (min) between images in the index file. **? TROUBLESHOOTING**

Overall Timing

Organoid cultures

Step 1, isolating (2h) and growing intestinal organoids: 7-14 days after isolating crypts.

Step 2, differentiation of organoids: 3 days.

Step 3, generating single cell suspensions from 3D organoids: 40 minutes depending on the number of wells chosen (to extract organoids) and the time for enzymatic dissociation.

Step 4, seeding cells in 96-well plate: 20 minutes including cell counting and plating.

Step 5, growing a confluent monolayer: 24 hours after seeding onto tissue culture plates.

Cell culturing and seeding of cells

Step 1, growing cells to 70-80% confluence in 75 cm^2 tissue culture flasks: 3-7 days depending on starting point and doubling time.

Step 2-7, seeding cells in 96-well plates: ~15 minutes.

Step 8, growing of cells into a cell monolayer: 16 hours (overnight).

Cell starvation

Step 9-10, cell starvation: 2 hours (might vary depending on the cell line).

Preparation of master plate (can be done in parallel with cell starvation)

Steps 11-13, preparation of master plate with treatment and control samples: 1.5 hours.

Fluorescent labelling (last 20 minutes of cell starvation)

Steps 14-16, labelling of cells with fluorescent dyes: 25 minutes.

Scratch assay and imaging

Step 17, performing scratches in the cell monolayers: less than 1 minute.

Step 18-19, washing cells with PBS and addition of treatments into assay plate: ~5-7 minutes.

Step 20, image acquisition: 5-16 hours (may vary depending on the cell line).

Image and data analysis

Step 21, downloading and importing the KREAP toolbox into the VM player: ~1 hour (only required once).

Step 22-23, creating and uploading input files for analysis with the KREAP toolbox: ~15 minutes.

Step 24, performing automated image analysis of a 96-well plate: ~30 minutes.

Step 25, determining re-epithelialization kinetics: less than 1 minute.

? TROUBLESHOOTING Troubleshooting advice is found in **Table 2**.

Table 2. Troubleshooting.

Step	Problem	Possible solution
1	Differentiation process does not work	The differentiation protocol should be adapted for varied species or tissue types. Ensure or optimize this process accordingly and verify using staining or qPCR (cell-type specific).
8	Cells are not fully dissociated after long TrypLE incubation	Some residual Matrigel or DMEM interferes with the enzymatic reaction. If the problem persists after careful separation of the pellet and residual components, add a washing step with ice-cold sterile D-PBS, and centrifuge at 500 x g for 5 min at 4ºC before TrypLE treatment.
12	Cells do not show attachment within 6 hours post-seeding	By adding and removing prewarmed DMEM in the 96-well plate, the surface tension should be eliminated. Some organoid models are sensitive to tissue-culture treated plates and should be precoated with a small amount of extracellular matrix, e.g., 0.5% v/v Matrigel or collagen. It should be noted that this could interfere with cells entering the scratched area, due to valley formation. Test this first by creating wells with or without coating and monitoring regrowth after scratching.
12	There is a high number of apoptotic cells in the suspension	This can be attributed to longer handling times during isolation and a sensitive cell population to detachment. To inhibit unwanted cell death, add 10 µM Rho/ROCK-inhibitor (Y-27632) to all the media in steps 3-12. However, inhibiting the caspase 3-induced apoptotic processes might affect normal cellular behavior, so effects should be tested with other molecular methods like qPCR or staining to verify functionality.
12	Cells are not confluent after 24 hours post seeding	Optimize the seeding density of the organoid model used for the assay. Some need higher numbers of cells (cell-cell contact) or lower (crowded space) to optimally attach and grow. Sometimes cells have a slow doubling time, so protocol should be adapted. Try avoiding longer incubation times than 24 hours, as intestinal organoids rapidly generate functional tight junctions (24-72 hours) causing difficulties in proper scratching.
9	Cells look healthy but are not confluent after overnight incubation.	Increase the seeding density or the time of incubation.
12	No significant difference between the controls (positive and negative) and untreated cells.	This can result from higher than optimal seeding densities. Decrease the seeding density. Also verify the expiration date and storage conditions of the reagents and replace them if necessary. Avoid repeated freeze-thaw cycles by storing the reagents in aliquots.
14	Dim or patchy fluorescence.	Dim cells can result from incubation with the labelling solution too briefly. Incubate the cells with the dyes for

		at least 20 minutes. If the problem persists, increase the concentration of the dye or the exposure time. Patchy staining can result from precipitation of the dye after thawing. Homogenize the dyes stock solutions before preparing the labelling solution. Verify the expiration date and storage conditions of the reagents.
14	Nuclei lose fluorescence rapidly after staining	Some cell models contain specific ATP-binding cassette transporter proteins that actively pump stains out of the cytoplasm. Also, rapidly dividing cells lose fluorescence due to dilution of the Hoechst reagent; a solution could be to repeat staining at specific intervals with small concentrations of dye, (N.B. without interfering with the assay plate positioning to avoid image shifting).
17	Some cell monolayers were left intact with the HTSScratcher.	Verify that the pins in the array are clean and move smoothly up and down. Assure the pins are touching the bottom of the wells when the array is pressed towards the plate.
19	High standard deviation between replicates.	This can result from uneven sample suspensions. Assure all sample preparations are homogenized. When transferring the samples from the master plate into the assay plate, pipette the treatment solution/suspensions up and down with the multichannel pipette.
24	Image analysis pipeline is not performing optimal image segmentation.	Adjust image segmentation settings in the index file. The illumination correction parameter (pixel_block_size) should be set in a range between 10-20 pixels. Nuclei size typically ranges between 4 (object_size_min) and 15 (object_size_max) pixels.
24	Some replicates show a higher lag-time than anticipated	Make sure that the scratched area does not contain any debris, as this interferes with the gap-estimation of the software. If so, discard the replicate as this cannot be rectified.
25	The estimation of the kinetic parameter values for a treatment are overestimated.	This can happen when the re-epithelialization growth curve does not reach the plateau phase. It is advised to extend the timeframe of the assay.

Anticipated results

Representative growth curves for each of the target cell models generated with the measured and modelled number of infiltrating cells over time upon treatment with the positive (i.e., hTGFα and hEGF) and negative (i.e. p38 and MEK1/2 inhibitors) controls at the recommended concentrations are provided in **Figure 1**. Similarly, to HaCat cells, colon-derived organoid monolayers are not optimally growing without hEGF in the culture medium, as nontreated organoids showed no proper re-epithelialization. Only when adding hEGF the cells recovered the wounded area and showed an essential growth factor for the rest of the experimental model.

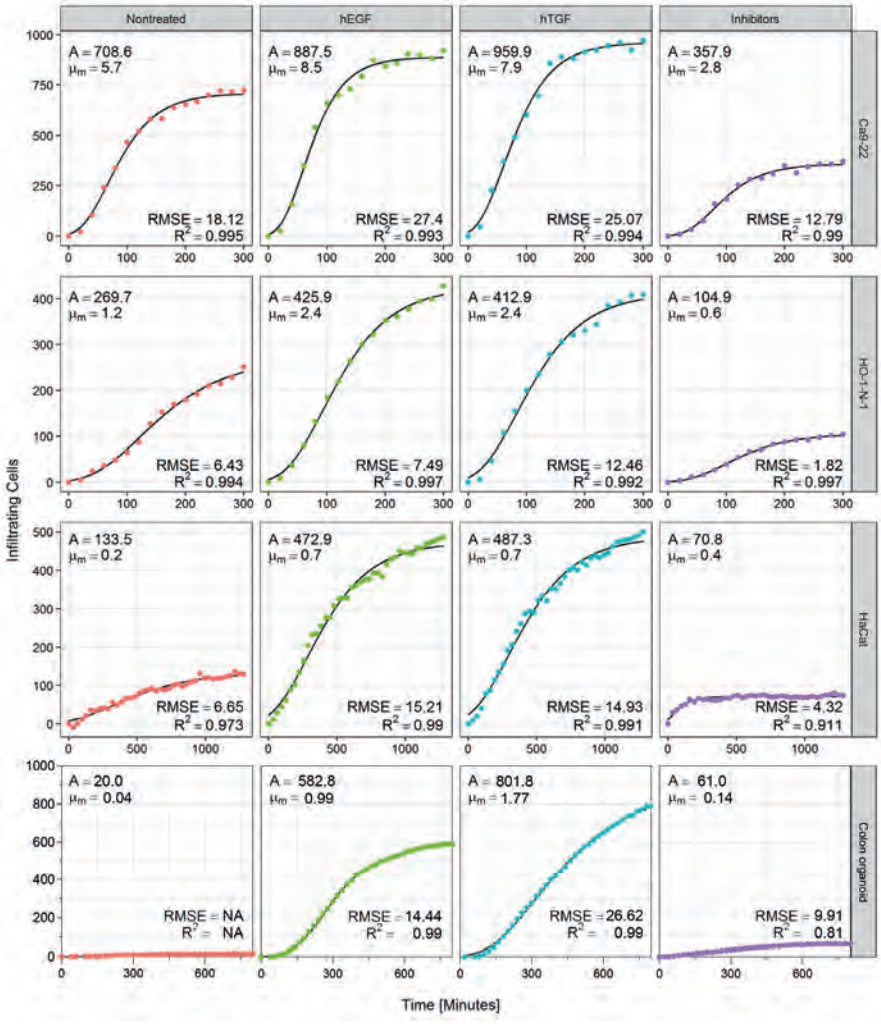

Figure 1. Enumeration of infiltrating cells. The modified Gompertz model (black line) was fitted through the measured data points (colored dots, colored area shows SEM, n > 9) to estimate the repair rate (μ_m) and the maximum number of cells inside the scratched area at the plateau of the growth curve (A). Goodness of fit (R^2). Root-mean-square error (RMSE). As organoid monolayers were not viable without hEGF, positive and negative control medium always contained EGF.

As an example, we employed this protocol to analyze the influence of *Lactobacillus rhamnosus* GG (LGG) and *Porphyromonas gingivalis* (W83) on re-epithelialization of gingival cells. Ca9-22 cells were exposed to three dosages (MOI 5, 50 and 500) of these bacteria and the re-epithelialization kinetics were determined using the KREAP toolbox. Addition of LGG at the intermediate dosage tested led to an increased repair rate (P = 0.03) (**Figure 2a**) and a significantly higher number of cells inside the scratched area as compared to the non-treated control (**Figure 2b, c**). However, higher dosages of LGG resulted in reduced re-epithelialization. This could be attributed to the acidification of the media (down to pH 5) by LGG fermentation products, leading to cell death and suppressed wound closure, which was clearly reflected by the modeled A parameter (i.e., maximum number of cells) (**Figure 2b)**. In contrast, we obtained a clear negative dosage effect upon exposure of gingival cells to increasing dosages of *P. gingivalis* (**Figure 2a, b**). At the higher dosage tested, *P. gingivalis* led to reduced migration of cells into the scratched area, resulting in a significantly lower number of infiltrated cells ($P < 0.001$) as illustrated by the A parameter (**Figure 2b, c**). Nonetheless, we also showed that the repair rate (μ_m) was not significantly influenced by any of the *P. gingivalis* preparations (**Figure 2a**). After introduction of the scratch in the cell monolayer, the cells were not immediately affected by the presence of *P. gingivalis* (MOI 500) and started to migrate into the scratched area to restore cell-cell contacts. However, during the experiment migration of cells into the scratched area eventually ceased, resulting in an unresolved wound (**Figure 2c**) and a low A parameter value.

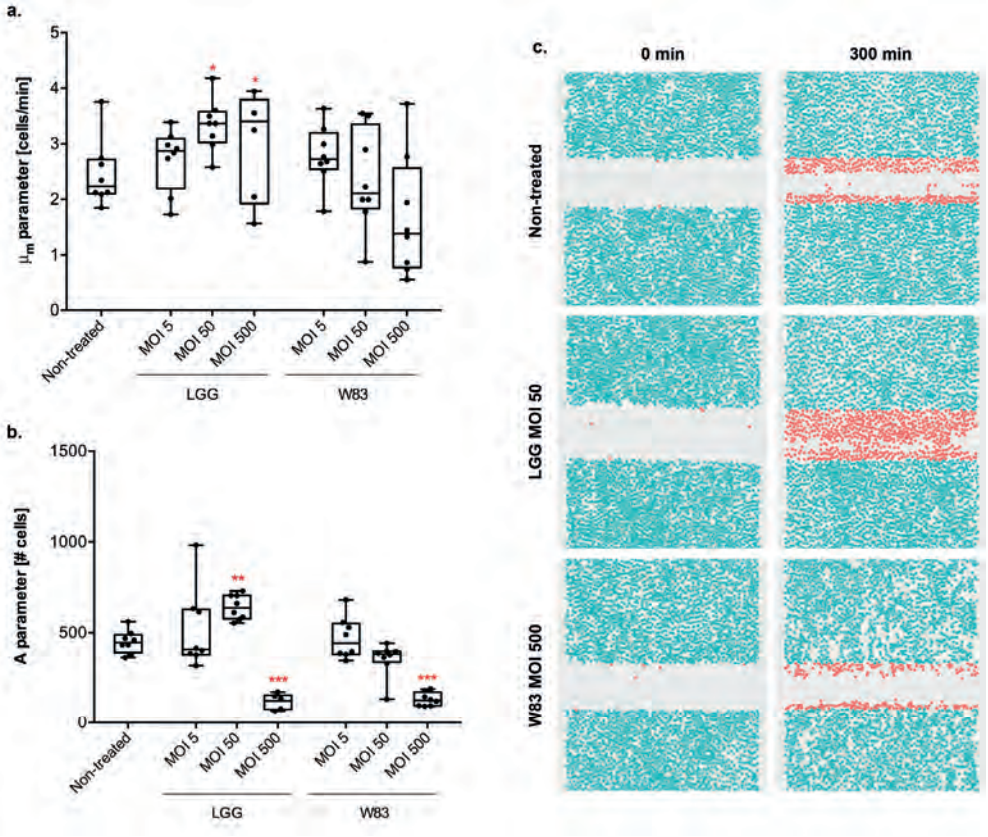

Figure 2. Re-epithelialization kinetics of gingival cells upon exposure to bacterial preparations. (a) Repair rate represented by the μ_m parameter. (b) Maximum number of cells inside the scratched area represented by the A parameter. Bacterial suspensions were added at an MOI of 5, 50 and 500. The non-treated control consisted of FCS-free DMEM. Significant differences from the non-treated control were assessed by a one-way ANOVA (n ≥ 5; *, $P < 0.05$; **, $P < 0.01$; ***, $P < 0.0001$). (c) Image segmentation output at the start of the experiment (0 min) and after 5 hours (300 min) of incubation with LGG (MOI 50) and *P. gingivalis* W83 (MOI 500) in comparison with the non-treated control.

Supplementary Figures

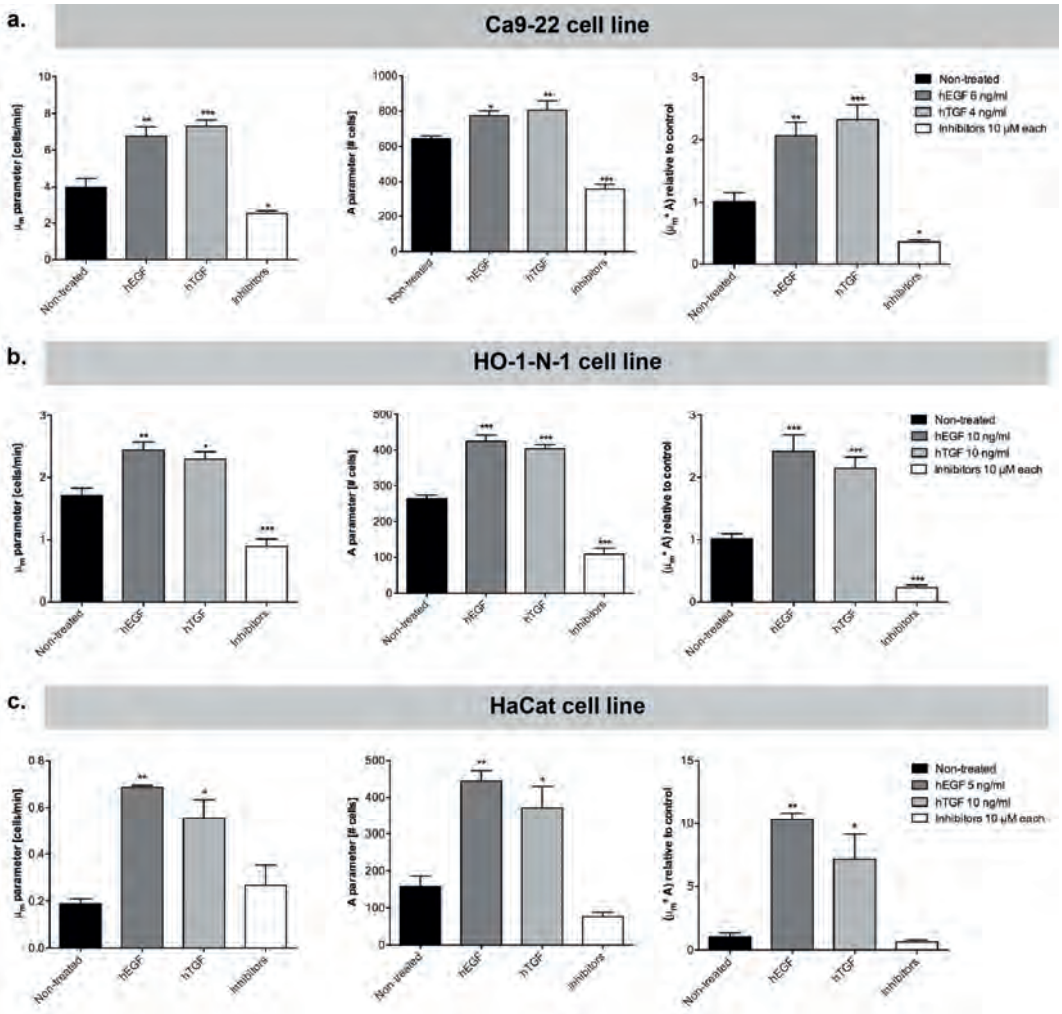

Figure S1. Optimal control concentrations on each target cell line. Human transforming growth factor α (hTGF) and human epidermal growth factor (hEGF) were used as positive controls. Inhibitors of p38 and MEK1/2 were used in combination as negative control. The repair rate is represented by the μ_m parameter, whereas the A parameter represents the maximum number of cells inside the scratched area. The overall re-epithelialization performance (μ_m*A) was calculated relative to the non-treated control. (a) Ca9-22 gingival cell line. (b) HO-1-N-1 buccal cell line. (c) HaCat keratinocyte cell line. Significant differences from the non-treated control were assessed by a one-way ANOVA using a Dunnett's test for multiple comparisons (n ≥ 3; *, $P < 0.05$; **, $P < 0.01$; ***, $P < 0.0001$).

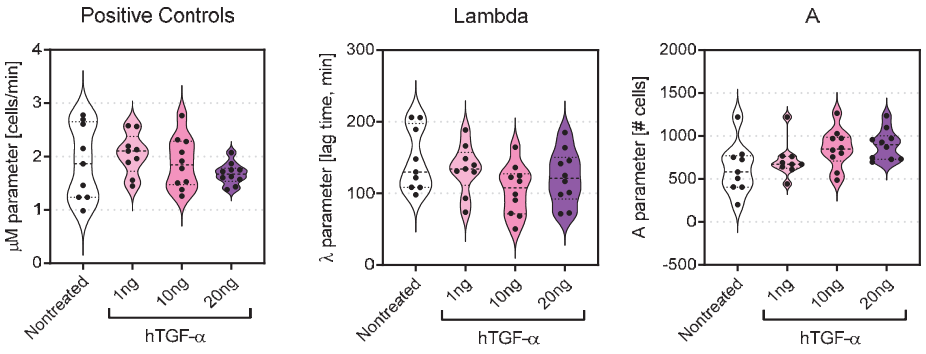

Figure S2. Differentiating effects of conventional culture medium containing different concentrations of hTGFα in colonic organoid monolayers. The reliance of intestinal organoids on human Epidermal Growht Factor (hEGF) means that only hTGFα remains as positive stimulant of re-epithelialization. We therefore tested various concentrations to optimize the minimum amount necessary to provoke a difference in regrowth. Although addition of TGFα did not show very apparent benefits to the three measured parameters, we did observe decreased well variability between replicates when stimulated with 20 ng/ml TGFα on cell infiltration per minute and total cell infiltration. This indicates that 20 ng/ml is an effective positive control as it permits better optimal regrowth.

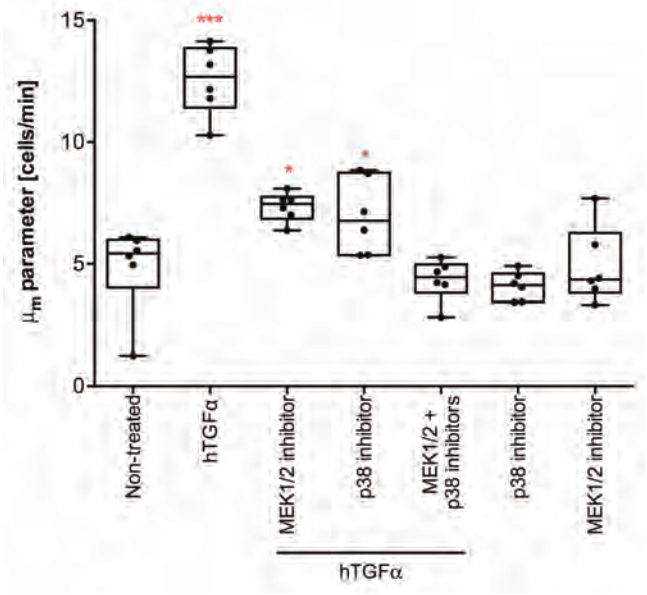

Figure S3. Human transforming growth factor α (hTGFα) promotes re-epithelialization through p38 and MEK1/2 activation. Stimulation of Ca9-22 cells with hTGFα in combination with either inhibitor reduced the repair rate (μ_m parameter) to an intermediate level. Addition of hTGFα in combination with both inhibitors decreased the repair rate to the level of the non-treated control, indicating that hTGFα can promote both migration and proliferation through activation of p38 and MEK1/2, respectively. Significant differences from the non-treated control were assessed by a one-way ANOVA using a Dunnett's test for multiple comparisons (n = 6; *, $P < 0.05$; ***, $P < 0.0001$).

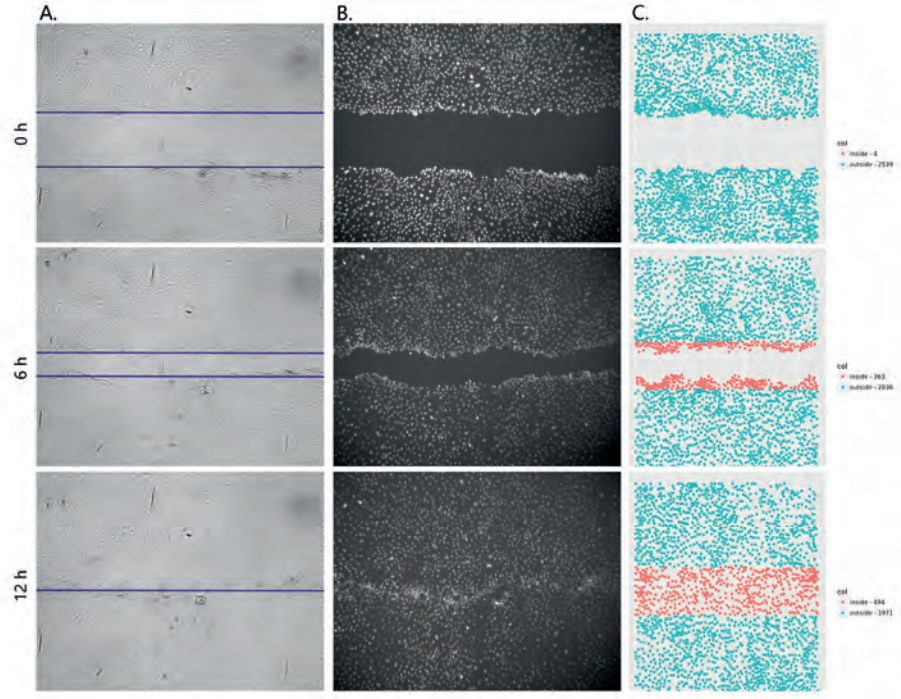

Figure S4. Visual representation of re-epithelialization tracking. (a) Current models exist of brightfield gap estimation and regrowth, but this does not include intricate cellular movement into wounding areas. (b) staining nuclei and perform live tracking on automated microscope devices enable more granular control over cellular movement, (c) which can be converted to wounding kinetics to estimate more accurate re-epithelialization of scratched areas.

References

1. Ebner, R. and R. Derynck, *Epidermal growth factor and transforming growth factor-alpha: differential intracellular routing and processing of ligand-receptor complexes.* Cell Regulation, 1991. **2**(8): p. 599-612.
2. Fernandez-Gutierrez, M.M., et al., *Streptococcus salivarius MS-oral-D6 promotes gingival re-epithelialization in vitro through a secreted serine protease.* Scientific Reports, 2017. **7**(1): p. 11100.
3. Huang, C., K. Jacobson, and M.D. Schaller, *MAP kinases and cell migration.* Journal of Cell Science, 2004. **117**(20): p. 4619-4628.
4. van der Hee, B., et al., *Optimized procedures for generating an enhanced, near physiological 2D culture system from porcine intestinal organoids.* Stem Cell Res, 2018. **28**: p. 165-171.
5. Zhang, W. and H.T. Liu, *MAPK signal pathways in the regulation of cell proliferation in mammalian cells.* Cell Res, 2002. **12**(1): p. 9-18.
6. Simpson, K.J., et al., *Identification of genes that regulate epithelial cell migration using an siRNA screening approach.* Nat Cell Biol, 2008. **10**(9): p. 1027-1038.
7. Oudhoff, M.J., et al., *Histatins are the major wound-closure stimulating factors in human saliva as identified in a cell culture assay.* FASEB J, 2008. **22**(11): p. 3805-12.
8. Oudhoff, M.J., et al., *Histatins enhance wound closure with oral and non-oral cells.* Journal of Dental Research, 2009. **88**(9): p. 846-850.
9. Laheij, A.M., et al., *The influence of oral bacteria on epithelial cell migration in vitro.* Mediators Inflamm, 2013. **2013**: p. 154532.
10. Bhattacharya, R., et al., *Effect of bacteria on the wound healing behavior of oral epithelial cells.* PLoS ONE, 2014. **9**(2).
11. Yue, P.Y.K., et al., *A Simplified Method for Quantifying Cell Migration/Wound Healing in 96-Well Plates.* Journal of Biomolecular Screening, 2010. **15**(4): p. 427-433.
12. Bürk, R.R., *A Factor from a Transformed Cell Line That Affects Cell Migration.* Proceedings of the National Academy of Sciences, 1973. **70**(2): p. 369-372.
13. Coomber, B.L. and A.I. Gotlieb, *In vitro endothelial wound repair. Interaction of cell migration and proliferation.* Arteriosclerosis, 1990. **10**(2): p. 215-22.
14. Liang, C.C., A.Y. Park, and J.L. Guan, *In vitro scratch assay: a convenient and inexpensive method for analysis of cell migration in vitro.* Nat Protoc, 2007. **2**(2): p. 329-33.
15. Riahi, R., et al., *Advances in Wound-Healing Assays for Probing Collective Cell Migration.* Journal of Laboratory Automation, 2012. **17**(1): p. 59-65.
16. Yarrow, J.C., et al., *A high-throughput cell migration assay using scratch wound healing, a comparison of image-based readout methods.* BMC Biotechnol, 2004. **4**: p. 21.
17. Zhang, J.-H., T.D.Y. Chung, and K.R. Oldenburg, *A Simple Statistical Parameter for Use in Evaluation and Validation of High Throughput Screening Assays.* Journal of Biomolecular Screening, 1999. **4**(2): p. 67-73.
18. Geback, T., et al., *TScratch: a novel and simple software tool for automated analysis of monolayer wound healing assays.* Biotechniques, 2009. **46**(4): p. 265-74.
19. Zordan, M.D., et al., *A high throughput, interactive imaging, bright-field wound healing assay.* Cytometry A, 2011. **79**(3): p. 227-32.
20. Fernandez-Gutierrez, M.M., et al., *KREAP: An automated Galaxy Platform to Quantify Re-epithelialization Kinetics.* GigaScience, 2017.
21. Zwietering, M.H., et al., *Modeling of the Bacterial Growth Curve.* Applied and Environmental Microbiology, 1990. **56**(6): p. 1875-1881.
22. Elzhov, T.V., et al., *minpack.lm: R Interface to the Levenberg-Marquardt Nonlinear Least-squares Algorithm Found in MINPACK, Plus Support for Bounds. R package version 1.2-1. https://CRAN.R-project.org/package=minpack.lm.* 2016.
23. van der Hee, B., et al., *Congruence of Transcription Programs in Adult Stem Cell-Derived Jejunum Organoids and Original Tissue During Long-Term Culture.* Front Cell Dev Biol, 2020. **8**: p. 375.
24. Hinman, S.S., et al., *In vitro generation of self-renewing human intestinal epithelia over planar and shaped collagen hydrogels.* Nat Protoc, 2021. **16**(1): p. 352-382.
25. Anzai, S., et al., *TGF-beta promotes fetal gene expression and cell migration velocity in a wound repair model of untransformed intestinal epithelial cells.* Biochem Biophys Res Commun, 2020. **524**(3): p. 533-541.
26. Sato, T., et al., *Single Lgr5 stem cells build crypt-villus structures in vitro without a mesenchymal niche.* Nature, 2009. **459**(7244): p. 262-5.

27. Ootani, A., et al., *Sustained in vitro intestinal epithelial culture within a Wnt-dependent stem cell niche.* Nat Med, 2009. **15**(6): p. 701-6.

Effects of Protein Fermentation Metabolites NH_3 and H_2S on Wound Repair Kinematics and Cell Junctions in Colon Organoid Monolayers

Bart van der Hee[1,2], Myrthe S. Gilbert[3], Marcela M. Fernandez-Gutierrez[1], Maria H. van Triest[4], Walter J.J. Gerrits[3], Nico Taverne[1], Boudewijn M.T. Burgering[4], Arie K. Kies[5], Linda M.P. Loonen[1], Michiel Kleerebezem[1], Hauke Smidt[2], Jerry M. Wells[1]

[1] Host-Microbe Interactomics Group, Department of Animal Sciences, Wageningen University & Research, Wageningen, The Netherlands, [2] Laboratory of Microbiology, Wageningen University & Research, Wageningen, The Netherlands, [3] Animal Nutrition Group, Department of Animal Sciences, Wageningen University & Research, Wageningen, The Netherlands, [4] Center for Molecular Medicine, University Medical Center Utrecht and Utrecht University, The Netherlands, [5] DSM Nutritional Products, Animal Nutrition and Health, Kaiseraugst, Switzerland

Manuscript to be submitted

Abstract

The intestinal epithelium acts as a physical barrier between the luminal content and the lamina propria and is vital for nutrient transport. The intestinal microbiota can produce harmful metabolites which at high concentrations can damage and reduce the effectiveness of the epithelial barrier. Epithelial wound healing is a process in which epithelial cell proliferation and migration rapidly reseal damaged epithelium to limit inflammatory responses to the microbiota. To take account of stem and progenitor cell replication we established methods for using colon organoid monolayers to study wound-repair kinematics. Epithelial monolayers exposed to 5 mM H_2S, or ammonia resulted in reduced wound-healing and aberrant cell movement. The transcriptome of H_2S or ammonia treated epithelial cells revealed downregulation of various biological pathways, including stress signaling, mitochondria-associated autophagy, and epithelial barrier capacity-related pathways. H_2S exposure led to dose-dependent decline in transepithelial electrical resistance (TEER), indicating increased leakiness due to impaired tight junction function. Moreover, H_2S treatment upregulated the endoplasmic reticulum stress pathway and genes associated with oxidative stress. We verified the effects on oxidative capacity and found that H_2S significantly reduced the oxidative capacity of cells that could lead to decreased barrier function. By including kinematic analysis in wound healing assays, we also showed that gut metabolites have specific effects on epithelial cell locomotion.

Introduction

In the intestine a single layer of epithelial cells provides a physical barrier between the luminal content and the lamina propria, while also passively and actively transporting nutrients [1]. Under certain dietary or disease conditions the microbiota may produce metabolites at concentrations which are cytotoxic leading to impairment of the epithelial barrier [2]. Epithelial wound healing is the process by which the epithelial barrier is rapidly resealed, which is driven by proliferation and migration [3], to mitigate further harmful effects.

Several dietary and microbiota derived metabolites have been shown to influence intestinal physiological and immunological responses in health and diseases. One important group of metabolites affecting host physiology are the short chain fatty acids (SCFAs) containing 1 to 4 carbons, present as butyrate, propionate and acetate in the intestinal tract [4]. Undigested complex carbohydrates reaching the proximal colon are fermented by the resident microbiota to SCFA. Notably, butyrate serves as an important energy substrate for colonocytes and thereby contributes to barrier function [4, 5].

Undigested protein reaching the colon can also be digested and metabolized by the gut microbiota as an energy source. Numerous metabolites produced from the metabolism of several amino acids participate in various physiological functions related to host health and diseases. Specific microbial metabolites of tryptophan are agonists of the aryl-hydrocarbon receptor (AhR) which is involved in the regulation of diverse cellular processes such as cell proliferation, metabolism, and immune development and regulation [6]. Conversely, metabolism of the sulfur-containing amino acids methionine, (homo)cysteine, and taurine increases luminal concentrations of hydrogen sulfide (H_2S) above 5 mM. H_2S concentrations greater than 1 mM were reported to have toxic effects on the colonic epithelium [7-9]. Conversely a low concentration of H_2S (100 µM) has been demonstrated to enhance growth and proliferation of intestinal epithelial cell lines, via the activation of the EGFR/ERK/MMP-2 and PI3K/Akt pathways [10]. H_2S also promotes angiogenesis which is crucial in the early stage of wound healing in tissues [11], but this effect is reversed at increased concentrations (800-1000 µM, [10]).

Protein fermentation in the colon increases luminal ammonia concentrations because of deamination of amino acids [12], which has been associated with diarrheal onset in piglets post weaning (**Chapter 2**, and [13, 14]). Ammonia has been shown to inhibit the PI3K/Akt and mTOR axis, decreasing cell proliferation and causing cell apoptosis at low mM concentrations [15]. Moreover, elevated levels of ammonia can decrease butyrate uptake by colonocytes due to inhibition of monocarboxylate transporter 1 and thereby compromise its utilization as an energy

source [16, 17], which is critical for maintaining cell barrier and expression of tight junction protein claudin 7 [18, 19] that restricts the paracellular diffusion of luminal compounds [1].

Epithelial wound healing is commonly modelled *in vitro* using scratched monolayers of cancer-derived cell lines, and measuring the gap closure rates from the leading edge [20, 21]. However, cancer-derived cell lines consist of monotypic cell populations that exhibit genetic aberrations that may affect many aspects of cellular physiology, such as metabolism, survival, and replication [22]. Therefore, epithelial wound healing models are needed that more closely mimic the role of stem and progenitor cell replication *in vivo*. Purified intestinal stem cells or isolated intestinal crypts have been used to develop intestinal organoids that mimic the functional, structural, and biological complexity of the intestinal segment from which they are derived [23, 24]. Previously, we have discussed key considerations for performing reliable experiments with organoids and described the stability of transcriptional pathways in intestinal organoids in long term culture [25]. Additionally, we described an optimized procedure for generating porcine 2D epithelial monolayers from 3D organoids that recapitulate many of the properties of the intestinal epithelium (Figure 1A) [26]. Combined with wound healing assays, such models would enable the investigation of gut lumen constituents (e.g., microbiome members or their metabolites) on cellular physiology and epithelial renewal.

To better understand the effects of ammonia and H_2S on epithelial repair we studied the direct effects of these metabolites at concentrations found in piglets using a 2D colon organoid-based wound healing model. The model allows the study of the early stages of restitution and re-epithelialization ([21, 27] and **Chapter 8**) and includes the quantitative measurement of wound-repair kinetics, migration dynamics and individual cell movement. The effects of ammonia and H_2S were further characterized by analyzing transcriptional responses and measurements of barrier function in 2D colonic organoids. Our results demonstrate that both ammonia and sulfide inhibit the regenerative capacity of the epithelium, and that the highest levels of H_2S observed in the piglet lumen induces mitochondrial perturbance and the unfolded protein stress response (UPR).

Materials and Methods

Organoid development

Colonic tissue was obtained from 4-week-old control piglets used for different study approved by the ethical committee of Wageningen University. Colonic organoids were derived from the crypts using methods described in [25, 26]. Culture medium was changed every other day and the organoids were sub-cultured every 5 days and passaged as spherical structures by mechanical dissociation in pre-warmed TrypLE and plating in Matrigel GFR BME. Organoid differentiation was initiated by reducing the total concentration of conditioned media components WNT3A and R-Spondin to 5% to decrease stem cell numbers and increase cell differentiation.

Two-dimensional organoid models

The colon organoids were extracted from the wells by repeated pipetting with ice-cold DMEM-F12 (Gibco) containing 1% P/S (v/v) and transferred to a 15 ml conical tube. The organoids were pelleted at 500 x g for 5 min and the supernatant removed. The cells were then dissociated as previously described and seeded into wells without Matrigel coating (see previous methods [26]) to prevent adverse effects on re-epithelialization kinetics and cell adhesion and proliferation. Cell adhesion was monitored for 6 hours after seeding. The differentiation medium was replaced daily to remove cellular debris with pre-warmed media.

Scratch assay development, automated imaging, and image analysis

After seeding (2.5 x 10^4 cells/wells) on tissue culture-treated plates, the cells were grown to confluency in 24h post-seeding. The redBCM was removed prior to the scratch experiments, and 30 min before scratching the nuclei were stained with cell-permeable Hoechst solution (2 µg/ml, 33342 20 mM, Thermo Fisher). The monolayers were subsequently scratched using a 96-pronged HTS-scratcher (Peira, Belgium) with three repeated alternating motions and visually inspected on an inverted microscope (Zeiss) for evenness of the scratches (±0.3 x 2 mm). The wells were then washed twice with prewarmed D-PBS to remove cellular debris and then 200 µl redBCM at 37 °C containing dilutions of metabolites was added to the inner 60 wells of the plate. Human transforming growth factor alpha (hTGFα, R&D systems) was used as positive control (4 ng/ml) for motogenic activity. As a negative control, we added 1 µM p38 mitogen-activated protein kinase (MAPK) inhibitor (SB203580, Cell Signaling Technology) and 1 µM MEK1/2 inhibitor (U0126, Cell Signaling Technology) as migration and proliferation inhibitors All treatments were diluted in D-PBS (Gibco). Ammonia (as 5 mM NH_3 or 5 mM NH_4Cl), hydrogen sulfide (as 5 mM

Na_2S or 5 mM NaSH), BCFAs isobutyrate, isovalerate (both 1 mM), and SCFAs acetate (2.5 mM), butyrate (1 mM), and valerate (1 mM) were used as treatments.

Single cell tracking and analysis

After treatment, the plates were placed in a high content bioimager (BD Pathway 855, BD Biosciences, USA) at 37 ºC and 5% CO_2. The cell layers were imaged using brightfield microscopy, and the nuclei were imaged at 350 nm (Hoechst) every 20 minutes for the duration of the experiment (±17h) at a predefined location and z-height to follow re-epithelialization kinetics (4x magnification). Time series images were then analyzed as previously described using the KREAP analysis pipeline (https://erasmusmc-bioinformatics.github.io/KREAP/). Sequential images were uploaded in the Galaxy pipeline per well and the number of infiltrating cells were assessed for nonlinear least squares regression analysis of a modified Gompertz function [21]. The analysis software calculates the closure rate (μ_m) of infiltrating cells per minute, the lag time of repair (λ), and total infiltrating cell numbers (A).

Cell nuclei migration kinetics were visualized using pseudo-coloration of hyperstacks. The sequential images were opened in FIJI (ImageJ, [28]) and then converted to stacks (Image>Stacks>Images to stacks). It is important to open the images in sequential order to prevent non-linear stacking. The stacks were then converted to hyperstacks (Image>Hyperstacks>Stack to hyperstack) and pseudo-colored using temporal color code (Image>Hyperstacks>Temporal-color code, color fire [28]) for directionality visualization. Displacement kinetics were then analyzed by nuclear tracking in FIJI (Plugins>Tracking>TrackMate, [29]). The stacks were analyzed using standard calibration settings (which can be adapted to image scale if necessary) and nuclei were detected using the Laplacian of Gaussian filter (LoG) detector in Fourier space. This allowed for quadratic fitting for sub-pixel localization. Within the LoG detector, the estimated blob diameter and threshold needed to be adapted to fit the most optimal number of nuclei (**Figure S1**) and was then computed with sub-pixel localization. Initial thresholding was not used in our experiments, as this removed a large fraction of grey or faded nuclei from the analysis (±30%). The tracked nuclei were then viewed as HyperStack displayer to overlay tracked dots on the images stack and the nuclei were tracked using a Linear motion LAP tracker. This tracker uses the Kalman filter for the next nucleus location prediction moving in a constant velocity vector and is beneficial for bridging gaps where necessary. The Linear motion LAP tracker needs to be set specifically for the images and we set the initial search radius to 0.1 and the next search radius to 0.2 with a maximum frame gap of 2. The tracks were then displayed as displacement distance and data for y-location, displacement, velocity, and imaging duration were calculated and exported by plotted features of links and tracks.

RNA-sequencing and analysis

For transcriptomic analysis, cell monolayers were grown to confluency within 24h as previously described and treated with control (D-PBS), 5 mM ammonia (NH_3), and 5 mM hydrogen sulfide precursor sodium sulfide (Na_2S) for 5h. The cells were then washed with prewarmed D-PBS, lysed using RLT buffer and placed on ice for immediate extraction using the RNeasy mini kit (ID:74104, Qiagen) with on-column DNAse (ID: 79254, Qiagen) following manufacturer's instructions. The extracted RNA was then eluted in 30 µl RNAse- and DNAse-free water (Promega) and concentration measured using Qubit (RNA HS assay kit, Thermo-Fisher). The RNA was then normalized to 250 ng/µl and stored at -80 °C.

RNA library preparation was performed using the TruSeq RNA sample kit as previously described [25] at Novogene. The samples were depleted for ribosomal RNA using the RiboZero kit and enriched for mRNA with oligo(dT) beads. The RNA was subsequently fragmented and synthesized into cDNA using mRNA template and hexamer primers. Second strand synthesis initiation was performed with the addition of second strand synthesis buffer (Illumina), dNTP's, RNAse H, and DNA polymerase I and following a series of terminal repair the cDNA library construction was completed by size selection and PCR enrichment. The libraries were then paired-end sequenced on a Illumina Hi-Seq 4000 (at Novogene, Hong Kong) at 9 GB raw data (±55million reads) per sample with 150 bp length. The raw data was then checked for quality using FastQC (v0.11.5, [30]) and trimmed for quality, polyA, and adapter using trim-galore (v0.4.4, [31]). The trimmed reads were then mapped to *sus scrofa* (Ensembl, v 11.1.91, [32]) using TopHat (v2.1.1, [33]) and analyzed in R using the Cufflinks package (v2.1.1, [33]). Differential gene expression was analyzed with false discovery rate (FDR) p-value < 0.05 and visualized using pheatmap and volcanoser [34]. Genes expressed with >1 RPKM were considered to be expressed. Figures display z-score normalized values for range optimization or RPKM values. Biological functions were analyzed by gene set enrichment analysis using Gene Ontology (GO, [35]), Reactome [36], and Kyoto Encyclopedia of Genes and Genomes (KEGG) pathway mapper [35] and differentially tested from control (expressed as p value and gene set).

Histological analysis

Colon tissue was fixed in 4% paraformaldehyde (PFA) or Canoy's fixative solution overnight at 4 °C and embedded in paraffin as previously described [25]. 3D organoids were grown in Matrigel and transferred into a 1.5ml Eppendorf tube. The organoids were subsequently embedded in low-melting agar and fixed with 1% PFA or Carnoy's fixative solution overnight at 4 °C and embedded in paraffin. Sections of tissue and 3D organoids were cut as 5 µm sections and adhered to poly-L-lysine

slides. Prior to staining, the slides were rehydrated, and antigen retrieval was performed in sodium citrate buffer (10 mM sodium citrate, 0.05% Tween 20, pH 6.0) at 95 °C for 10 min. Cell monolayers were grown to confluency within 24h from differentiated 3D organoids on non-Matrigel coated tissue culture-treated 96-well plates or transwells and fixed in 1% PFA or Carnoy's fixative overnight at 4 °C. The slides, plates, and transwells were washed with tris-buffered saline (TBS) solution with triton (6.06 g/L Tris, 8.8 g/L NaCl, 0.02% triton X-100 at pH 7.4) three times and blocked using 5% (in TBS-t) normal goat serum (Thermo-Fisher) for 30 min at RT. The samples were then incubated with antibodies for Trefoil factor 3 (TFF3), villin (VIL; AB_2304475, Santa-Cruz), zonula occludens 1 (ZO-1; AB_87181, Thermo-Fisher) and beta-catenin (bCAT) for 1h at RT, and subsequently washed three times with TBS-t. The antibodies were visualized with a goat anti-rabbit or goat anti-mouse secondary antibody (Alexa Fluor 555), washed, and mounted using DAPI-containing solution (Thermo-Fisher). The slides containing tissue, 3D colon organoids, and transwell colon monolayers were then imaged on a fluorescent microscope (Leica DM6) using a 10x, 40x, or 100x objective. To visualize mucus production and goblet cells, transwells were fixed in Carnoy's fixative and stained using PAS/Alcian blue with methods previously described [25, 26].

TEER assay and permeability

Epithelial integrity was measured using trans-epithelial electrical resistance (TEER). Differentiated colon organoid monolayers were grown in non-Matrigel coated permeable transwell inserts as previously described and placed in a 24-well Cellzscope apparatus to measure electric impedance (Nanoanalytics, Germany). The cell monolayers were acclimatized in the apparatus for 24h at 37 °C with 5% CO_2 before treatment. The cells were subsequently treated with ammonia (2.5 or 5 mM NH_3), sulfide (2.5 or 5 mM Na_2S) or control (D-PBS) and TEER was monitored over time at 37 °C. After 18h exposure, the transwells were placed in a 24-well plate holder and media was refreshed with prewarmed redBCM. Permeability was then assessed by addition of 0.4, 4, or 40 kDa FITC-labeled dextrans (2 mg/ml in redBCM; Thermo-Fisher) to the apical compartment. After 1h incubation, 100 µl of the basolateral compartment was placed in black-wall 96-well plates and measured for fluorescence on a Spectramax M5 (Molecular Devices, USA) with 490 nm excitation and 530 nm emission.

Cell viability and ATP assay

Measuring cellular viability using formazan-based compounds showed significant background reaction to the sulfide-based compounds in our assays (**Figure S3**). We therefore chose to measure the available ATP using luminescence-based compounds. The Cell Titer Glo 2.0 assay (Promega) was used to quantify the amount

of available ATP in the colon organoid monolayers. The colon monolayers were grown from differentiated 3D colon organoids to confluency in 24h as described above in black-wall tissue culture treated 96-well plates at 37 °C with 5% CO_2. The colon monolayers were subsequently treated with 5 mM NH_3 (ammonia), NH_4Cl (ammonium chloride), Na_2S (sodium sulfide), NaSH (sodium hydrosulfide), 1 µg/ml lipopolysaccharide (LPS), or control (D-PBS) in 100 µl redBCM for 5h. After incubation, the plate medium was replaced with redBCM and placed at RT for 30 min to acclimatize. Then 100 µl Cell titer Glo 2.0 reagent was added to each well, and the plate was shaken at 250 rpm for 2 min and incubated at RT an additional 10 min. Luminescence was measured on a Spectramax M5 plate reader (Molecular Devices, USA), and data was normalized as relative percentual difference from control-treated wells.

Mitochondrial stress test experiments

Oxygen consumption rate (OCR) of colon organoid monolayers was measured on a Seahorse Bioscience XFe24 extracellular flux analyzer in pmol O_2 per min. Differentiated 3D colon organoids were dissociated and plated on XF24 cell culture microplates (Agilent) at 2.5 x 10^4 cells per well and grown to confluency overnight. The cells were then treated with 5 mM NH_3, Na_2S, or control for 5h. 1h prior to the assay, the treatments were replaced with prewarmed differentiation medium and incubated at 37 °C. The cells were then subjected to a mitochondrial stress test following methods previously described [37]. The culture medium was replaced with prewarmed Seahorse DMEM containing 0.5 mM pyruvate, 2.5 mM glutamine, and 17.5 mM glucose. The stress test was performed using interval injections of 5 µM oligomycin (18 minutes), 4.5 µM FCCP (45 minutes), and 5 µM of rotenone and antimycin A (68 minutes, all Sigma-Aldrich). After injection, the mixture was homogenized for 4 min and measured for 2 min. Basal respiration was calculated by subtracting the initial OCR from the non-mitochondrial oxygen consumption (after rotenone/antimycin A). Maximum respiration, or spare capacity, was measured by subtracting the OCR after FCCP from non-mitochondrial oxygen consumption and basal respiration respectively. The ATP-linked respiration (or projected ATP) was calculated by subtracting the basal respiration from the OCR after oligomycin injection (**Figure S4**).

Results

Optimizing monolayer culture conditions for scratch assays

Long-term culture and self-renewal of adult stem cell derived intestinal organoids depends on reconstituting the stem cell niche in a laminin rich extracellular matrix (**Figure 1a-b**) [23]. To generate monolayers for the scratch assay, we utilized a differentiation and cell dissociation method to generate confluent multi-lineage epithelial cell monolayers (**Figure 1c-d**). Plating differentiated 3D organoids enabled formation of an intact polarized monolayer (**Figure 1e** inserts), but when grown for longer than 7 days, surface protrusions appear due to detachment of sections the epithelium from the surface (**Figure 1f**). Epithelial polarity was confirmed by staining of villin on the apical surface, and apically oriented tight junction protein zonula occludens-1 (ZO-1) and cell adhesion beta-catenin (βCAT). The presence of mature mucus-producing goblet cells was shown by positive staining with lectin-binding Ulex Europaeus agglutinin-1 (UEA-1) and antibody to trefoil factor 3 (TFF3) (**Figure 1g**). Differentiation of 2-dimensional colon organoids was verified by mapping the transcriptome of 2D monolayers to a single cell sequencing database for colon [38] to identify the cell type-specific transcripts expressed in our dataset (**Figure 1h**). This comparative transcriptome analysis confirmed the presence of multiple cell types commonly found in the colon.

For wound-healing assays organoids were grown in Matrigel and differentiated for 3 days prior to monolayer seeding (**Figure 1i**). It was found to be crucial to differentiate the 3D organoids before generating a clean scratch (insert **m2**) otherwise cells lifted off the surface at the edge (**insert m1**). As previously described for cell lines [39], epidermal growth factor (EGF) was critical for re-epithelialization (**Figure 1j**). The addition of TGFα was not required for initiation but increased the number of infiltrating cells moving into the gap area. Finally, the addition of p38-MAPK-inhibitor and MEK1/2-inhibitor halted gap re-epithelialization, confirming the critical role of these pathways in cell mobilization in these wound healing assays [21](**Figure 1j**).

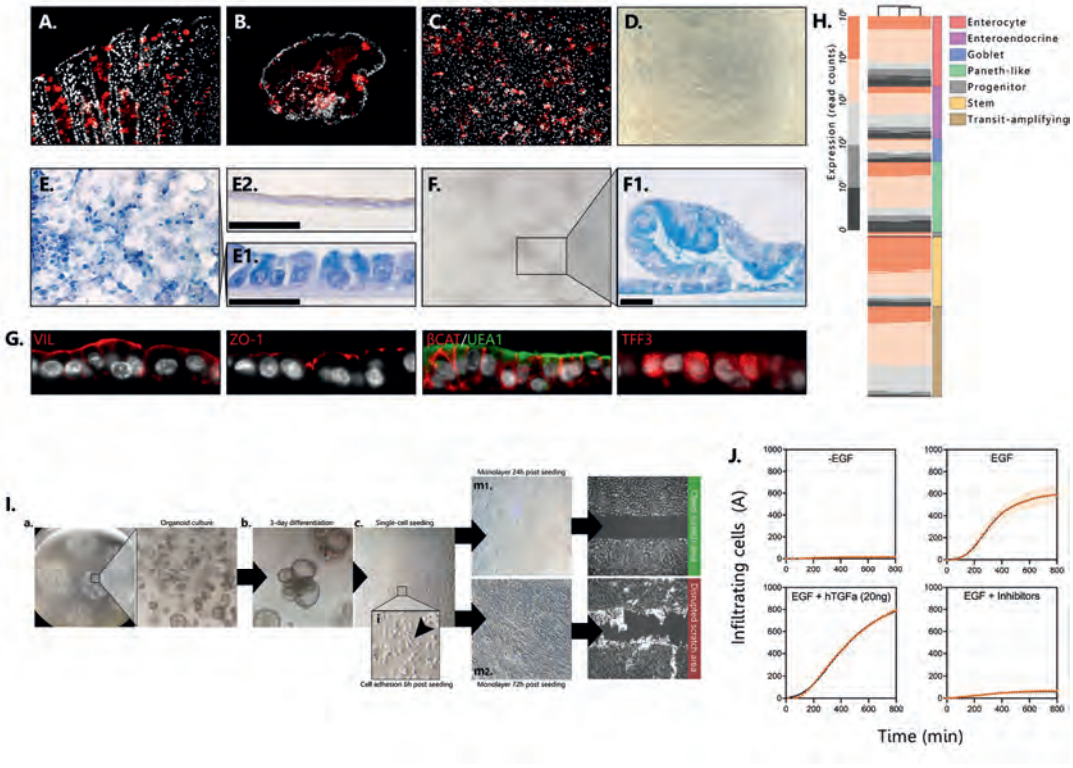

Figure 1. Porcine colonic organoids mimic epithelial cell type differentiation and can be used for wound assays. (a) Porcine colon crypt stem cells can be isolated and grown in (b) three-dimensional structures containing mucus-secreting goblet cells (Trefoil factor 3, red; nuclei, white). (c) Organoid monolayers on flat-bottom plates generate a confluent layer of cells (d). (e) Differentiated monolayers show increased columnar development (e2) compared to non-differentiated monolayers (e1). (f) Colon monolayers can form ridges when grown for longer than 7 days resembling protruding 3D organoid growth. (g) Differentiated colon monolayers stained for brush border microvilli (VIL, villin), intestinal tight junctions (ZO1, zonula occludens 1; βCAT, beta-catenin), and mucus (UEA1, Ulex Europaeus agglutinin 1; TFF3, trefoil-factor 3). (h) Transcriptome expression profile for cell type-specific gene transcripts in colon organoid monolayers. (i) Scratch assay protocol overview using 3D differentiated seeding (m1) and in-plate differentiated (m2) colon monolayers. (j) Epidermal growth factor, (EGF) is necessary for re-epithelialization and is enhanced by human Transforming growth factor alpha, (hTGFa). Re-epithelialization is prevented by p38 MAPK- and MEK1/2-inhibitors.

Effects of fermentation metabolites on wound healing kinetics in colon organoid monolayers

To investigate the effects of fermentation metabolites on wound healing kinetics, we performed scratch assays on colon organoid monolayers to quantify re-epithelialization when treated with physiologically relevant concentrations of gut metabolites (**Figure 2a** and **Figure S5**). The protein fermentation metabolites ammonia (5 mM NH_3) and sulfide (5 mM H_2S-precursor Na_2S) significantly decreased cellular infiltration into the gap preventing repair within 24 h (Figure S6). Negative effects on re-epithelialization were also found with isovalerate and valerate, whereas SCFAs isobutyrate, butyrate, and acetate did not significantly inhibit general wound healing kinetics (**Figure 2a**). The negative effect of the protein fermentation metabolites was evident from the increased lag time and decreased gap closure rates relative to control (**Figure 2b**). Sulfide and ammonia doubled the lag period prior to initiation of cell migration and halved the rate of gap closure. There was a noticeable difference in gap closure rate between sulfide-treated monolayers, where cells treated with NaSH showed less reduction (-32 ± 3.2%) compared to control than Na_2S (-75 ± 5.3%). Moreover, gap closure rate was also impaired by all other compounds, most notably butyrate (62 ± 5.8%), which accelerated gap closure initiation, as apparent from the decreased lag time compared to the control (**Figure 2b**).

Recently, Kaiko et. al (2016) demonstrated that butyrate suppresses intestinal stem cell and progenitor cell proliferation *in vitro* and *in vivo* [40]. It is odd that we observed a decreased lag time (faster repair start) in monolayers treated with butyrate, while also having a decreased gap closure rate. It could be that the cells utilize the initial increase of butyrate for oxidation enhance mitochondrial oxidation [41, 42] but overtime the intracellular accumulation of butyrate leads to inhibition of biological pathways linked to stem and progenitor proliferation in the crypt [40], thereby reducing the gap repair rate.

Wound repair in the epithelium relies on coordinated cellular crosstalk and collective migratory capacity [43, 44]. Cellular directionality and migration patterns are not considered when measuring gap infiltration using KREAP although this information can help to better understand the effects of different metabolites on the overall wound healing process. To visualize cellular migration-directionality, we used FIJI to temporally pseudo-color individual cell nuclei during the re-epithelialization experiments (**Figure 2c**). For the medium-treated control, gap closure occurred after approximately 15h and the cell kinetics show collective movement into the gap consistent with the cellular displacement plot (**Figure 2d**). Although gap closure was incomplete at the end of the assay period (15 h) in the metabolite treated samples

there were substantial changes in cell displacement (**Figure 2d**). In the ammonia-treated monolayers cell movements tended to occur close to the gap and were of shorter duration compared to those observed for the control (**Figure 2c and d**). The effect of sulfide treatment on gap closure was different from the effect of ammonia and was characterized by cell movements occurring in only randomly distributed, localized areas and lacking directionality towards the gap (**Figure 2c**). This effect was also apparent from the y-location displacement data, with larger displacement observed in the peripheral areas (**Figure 2d**).

Shared pathways downregulated in Ammonia and Sulfide treated colon organoid monolayers

Transcriptomics was used to further investigate the pathways which might be involved in the effects of ammonia and sulfide on cellular migration kinetics. Principal component analysis of RNA-sequencing data from ammonia, sulfide, or control-treated monolayers showed dimensional separation of treated samples (**Figure 3a**). All samples shared a substantial proportion of their expressed genes (10,404 >1 RPKM) (**Figure 3b**). Most differentially expressed genes were detected in sulfide-treated colon monolayers (2738 genes vs control, FDR $p < 0.05$) compared to (1242 genes vs control, FDR $p < 0.05$) after ammonia treatment (**Figure 3c** and **d**). A large proportion of the treatment associated DEGs (Differentially Expressed Genes) were overlapping between sulfide and ammonia treatments.

Pathways that were common to sulfide and ammonia treatment versus the untreated control are shown in (**Figure S7**). These pathways included stress signaling (e.g., stress activated p53 and MAPK kinase signaling), mitochondria-associated autophagy, and FoxO signaling (**Figure 3e**). Moreover, both treatments significantly reduced tight junction, focal adhesion, and extracellular matrix remodeling pathways. Pathways specifically upregulated by ammonia treatment were associated with bioprocessing of monosaccharides, which may reflect increased glucose oxidation in the presence of ammonia.

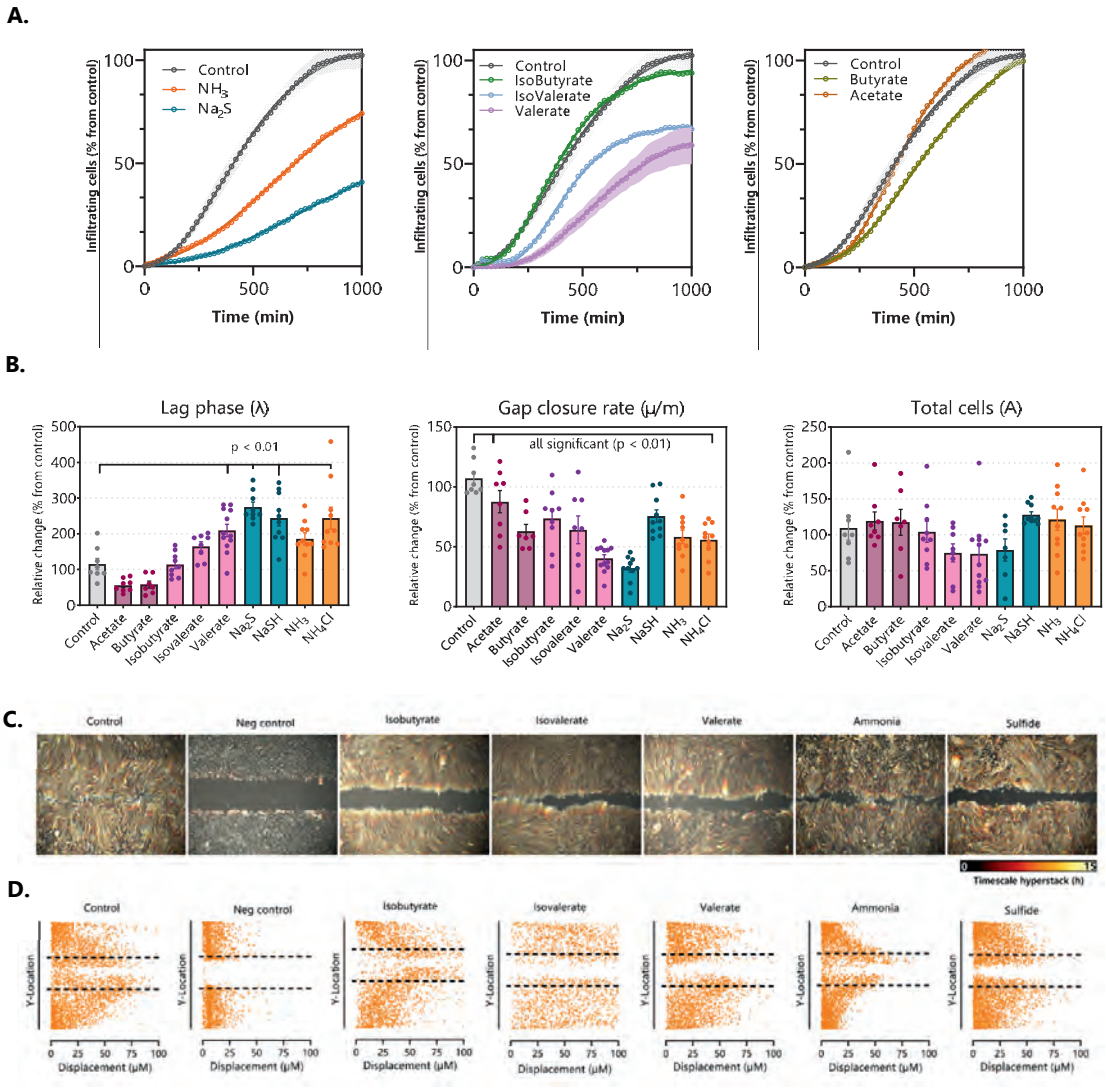

Figure 2. Effects of protein fermentation metabolites on colon organoid monolayer re-epithelialization. (a) Sigmoidal re-epithelialization curves enumerating cells infiltrating the gap over time (NH_3, ammonia; Na_2S, sodium sulfide; n>10 replicates per compound, error bands display ±SEM at every timepoint) measured for 1000 minutes. (b) Re-epithelialization kinetics were estimated by calculating the lag phase (λ), gap closure rate (μ/m), and total cell infiltration (A) (all data are shown as relative % compared to the medium control). (c) Nuclei kinetic hyperstacks were pseudo-colored per timepoint to visualize cell trajectories over time for 15h. (d) Dotted lines represent the gap area and individual cell displacements are plotted on the y-axis for each treatment.

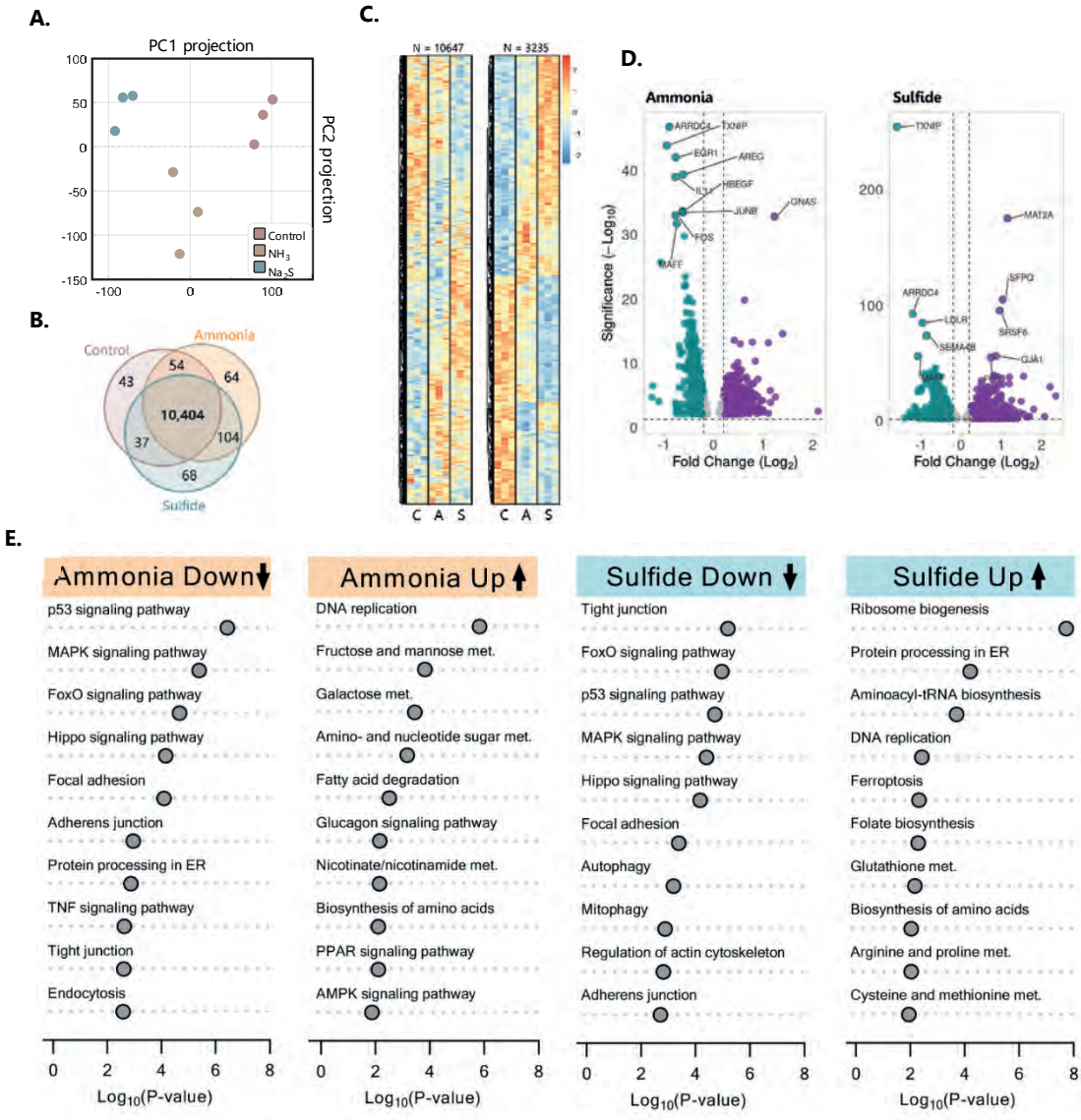

Figure 3. Transcriptional effects of ammonia and sulfide on colon monolayers. (a) Principal component plot of transcriptomics data showing dimensional separation of treatments and control. (b) Expressed transcriptome overlap and exclusivity between all treatments (>1 FPKM). (c) Heatmaps showing expression patterns for all genes (left columns) and only differentially expressed genes (right column) (C, control; A, ammonia; S, sulfide). Data is represented as z-score values. Blue represents lower expression and red higher expression compared to control. (d) Volcano plots representing the significantly differentially expressed genes compared to control in colon monolayers exposed to ammonia (left) of sulfide (right) and the top 10 different genes based on their relative differences expressed as Manhattan distance scores (DEG $p < 0.05$, FC > 2, green represents down-regulated genes and purple up-regulated genes). (e) Top 10 differential pathways for the down- and up-regulated genes for colon organoid monolayers treated with ammonia (orange) or sulfide, (blue) compared to control ($Log_{10}(P_{adj})$).

Effects of Sulfide on intestinal epithelial tight junctions and barrier integrity

Intestinal epithelial tight junctions play a key role in regulating the paracellular permeability of small molecules [1]. Moreover, tight junctions and focal adhesions to the ECM play important roles in regulating cell proliferation, migration, and re-epithelialization (**Figure 4a-b**)[45-48]. Analysis of wound healing kinetics in sulfide-treated monolayers revealed the formation of gaps appearing and reforming in the monolayer (**Figure 4c**). We hypothesized that this effect was due to improper functioning of the junctions and focal adhesions, which was supported by downregulated pathways associated with cellular motility (ECM-receptor interaction, actin cytoskeleton, focal adhesion) and barrier capacity (tight- and adherens junctions) in sulfide and ammonia-treated monolayers (**Figure 4d**). More in-depth analysis of the tight junction pathway revealed that the largest set of down-regulated genes was associated with sulfide-treated monolayers (**Figure 4e**), encompassing tight junction-associated claudins 1, 7 and 4, as well as tight junction protein 2 (*TJP2*) and cingulin (*CGN*). Moreover, decreased focal adhesion for both ammonia and sulfide-treated monolayers is associated with reduced expression of Integrin Subunit-alpha (*ITGA1*) and -beta (*ITGB1*) and vinculin (*VCL*; **Figure S9**) which play key-roles in cell motility [49, 50].

To confirm the effect of sulfide on cell junctions predicted by transcriptomics, we measured transepithelial electrical resistance (TEER) in organoid cell monolayers treated with sulfide (**Figure 4f**). Exposure to sulfide showed a dose-dependent decline in TEER relative to untreated monolayers. Complete loss of the barrier integrity was not observed, which was verified using a dextran diffusion assay. Small dextran molecules (0.4 kDa) can diffuse across the barrier upon partial loss of integrity, whereas larger dextran molecules (4 and 40 kDa) only diffuse to the basolateral compartment upon more substantial barrier loss. The latter was not observed in our experiments (**Figure 4f**) indicating that the monolayers had increased permeability, most probably due to the detrimental effects of sulfide on tight junction function.

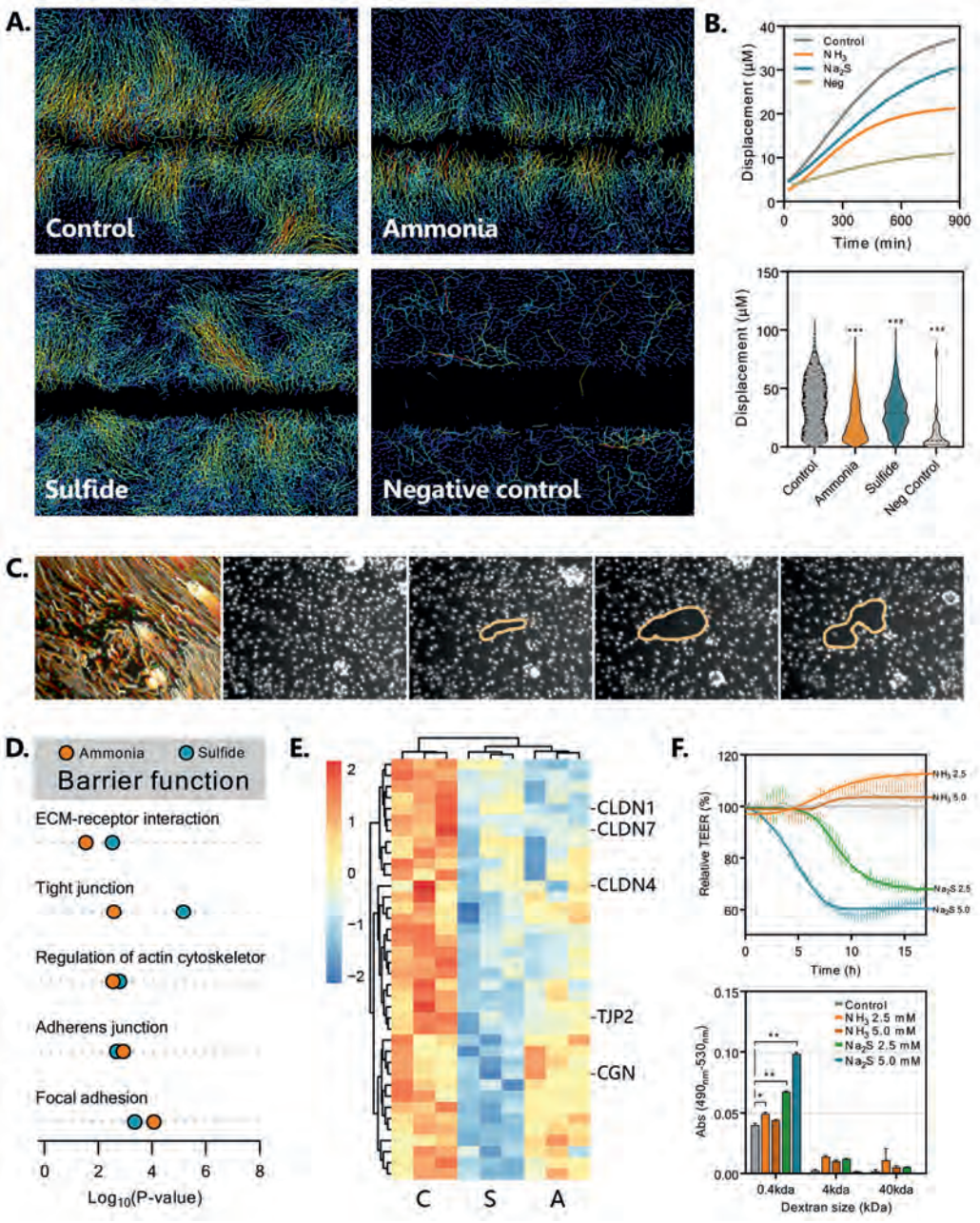

Figure 4. Sulfide directly affects cell-cell and cell-matrix junctions (barrier function) in colon organoid monolayers. (a) Nuclei displacement plots depicting cellular traveling and path length (blue is low, red is high displacement). (b) Temporal nuclei displacement curves depicting the average travelled distance for each timepoint (top) and total quantified displacement volcano plots per treatment (bottom). (c) timeseries of gap formation during sulfide treatment of colon organoid monolayers. (d) Intestinal barrier related pathways significantly down regulated by sulfide and ammonia treatments. (e) Heatmap of the tight junction pathway and corresponding z-score normalized gene expression for monolayers treated with ammonia (A), sulfide (S), or control (C, n=3 replicates per treatment) and selected genes denoted (CLDN, Claudin; TJP2, tight junction protein 2; CGN, cingulin). (f) Transepithelial electrical resistance (TEER)

was measured in response to sulfide (2.5, green; and 5.0 mM/L, blue) or ammonia (2.5, orange; or 5.0 mM/L, brown) relative to the control (grey, ±SEM). (e) Transport of 0.4 kDa, 4 kDa, and 40 kDa FITS-labeled Dextran across the monolayer at 15h (* $p < 0.05$, ** $p < 0.01$).

Sulfide treatment triggers the UPR and impairs mitochondrial function in colonic monolayers

Notably, sulfide-treated monolayers upregulated the expression of protein processing in the endoplasmic reticulum (ER) and autophagy pathways, which have been associated with compromised tight junction function [51]. To further corroborate this, we investigated which genes were up-regulated by sulfide associated with the "protein-processing in ER" pathway (**Figure 5a**), revealing that many of these genes also participate in the unfolded protein response (UPR) pathway, including activating transcription factor 6 beta (*ATF6B*), wolframin ER transmembrane glycoprotein (*WSF1*), DnaJ heat shock protein family (Hsp40) member C3 (*DNAJC3*), mitochondria apoptosis related BCL2 antagonist/killer-1 (*BAK1*). The production of oxygen radicals (ROS) has been associated with altered redox status and ER stress, which is consistent with sulfide treatment increasing expression of genes encoding antioxidant enzymes like superoxide dismutase 2 (*SOD2*) and peroxiredoxin 1 (*PRDX1*) (**Figure 5b**). Elevated expression of antioxidant enzymes has been previously associated with mitochondrial stress caused by H_2S-mediated inhibition of mitochondrial complex IV [9]. Therefore, we anticipated that oxidative phosphorylation would be impaired in sulfide-treated monolayers, which would lead to reduced availability of ATP. Indeed, colon organoid monolayers treated with sulfide for 5 h showed a significant decrease in available ATP (**Figure 5c**).

To further characterize the effects of sulfide on cellular respiration, the oxygen consumption rate (OCR) was measured in sulfide or ammonia-treated and control wells (**Figure 5d**). Initially, basal oxygen consumption rate determination showed that baseline respiratory capacity was impaired by Na_2S (**Figure 5e**). Moreover, uncoupling mitochondrial respiration with FCCP showed that also the maximal respiration rate of the cells was negatively affected by Na_2S treatment, indicating overall impaired respiratory capacity of the mitochondria. The reduction in mitochondrial respiration measured by the ATP-assay was confirmed in the oxygen consumption rate assay, which predicted a similar reduction of ATP production in colonic monolayers upon sulfide-treatment (**Figure 5e**). Importantly, the sulfide-treated cells did not display a noticeable decrease in cellular viability or abundance of mitochondria by histology (**Figure 5f**). Based on the critical role of mitochondrial functioning in colonic cells, and stem cells, we hypothesized that the detrimental effects of Na_2S on mitochondrial oxidative phosphorylation and ATP production would deregulate intestinal homeostasis by FoxO signaling. The FoxO-signaling

pathway was significantly down-regulated by sulfide treatment (**Figure 5g**), with *FoxO3* being the most significantly down-regulated gene (**Figure 5h**). In animals, FOXO3 promotes tissue regeneration, autophagy, and the growth of stem cells [52, 53].

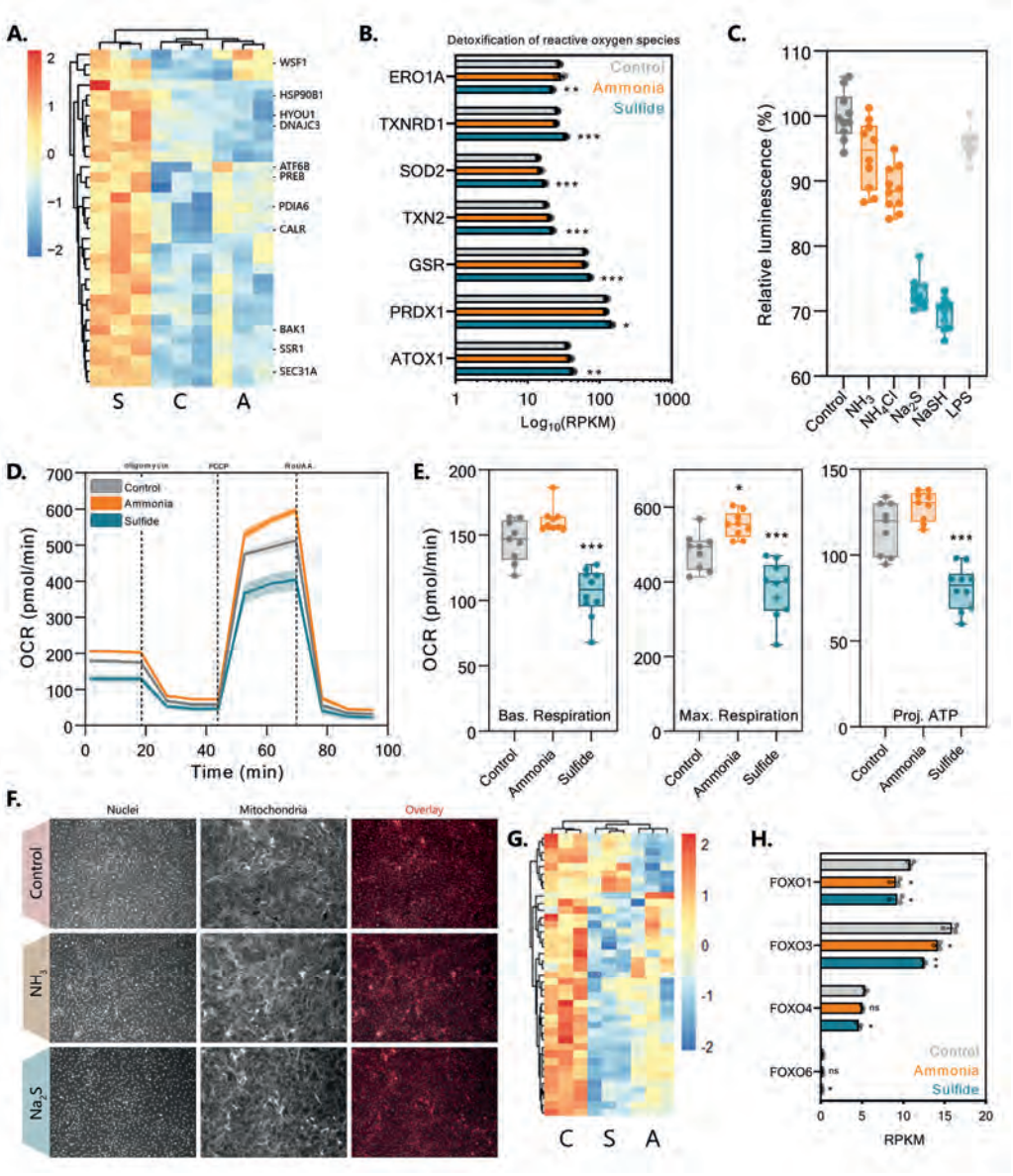

Figure 5. Sulfide reduces oxidative capacity in colon organoid monolayers. (a) Heatmap showing expression z-score values for the pathway "Protein Processing in the Endoplasmic Reticulum" with genes denoted to overlap with the Unfolded Protein Response (UPR) for colon organoid monolayers treated with sulfide (S), ammonia (A), or control (C) for 5h. (b) Expression values for genes differentially expressed in the Detoxification of reactive oxygen species pathway (values as Log10(RPKM), * $p < 0.05$, ** $p < 0.01$, *** $p < 0.001$). (c) Cell viability assay that measures available ATP (CellTiter-Glo assay) to estimate oxidative capacity after treatment with ammonia (NH_3, ammonia; NH_4Cl, ammonium chloride) or hydrogen sulfide precursors (Na_2S, sodium sulfide; NaSH, sodium hydrosulfide). (d) Oxygen consumption rate curves for ammonia (NH_3), sulfide (Na_2S), or control treated monolayers and their respective mitochondrial functioning during the mitochondrial stress test (data shown as mean ± SEM). (e) Derived mitochondrial capacity for basal respiration (left), maximal respiratory capability (middle), and projected ATP production (right) based on the Seahorse OCR mitochondrial stress test from ammonia, sulfide, or control treated colon organoid monolayers (5h exposure, treatments were removed 1h prior to the assay; data shown as

range, * $p < 0.05$, *** $p < 0.001$). (f) Representative images of colon organoid monolayers after the Seahorse experiment for nuclei (left) and mitochondria (middle). (g) Heatmap of z-score normalized expression values for the FOXO signaling pathway after 5h treatment with control (C), ammonia (A), or sulfide (S). (h) Gene expression RPKM values for FOXO genes 1, 3, 4, and 6 after 5h treatment with control, ammonia, or sulfide (* $p < 0.05$, ** $p < 0.01$).

Discussion

Renewal and restitution are vital for the maintenance of the physical barrier function of the intestinal epithelium [43] but can be compromised by protein fermentation metabolites ammonia and hydrogen sulfide (H_2S). Among bacterial metabolites, hydrogen sulfide has received increasing attention. Sulfide is normally oxidized by cells to oxidize thiosulfate generating ATP and providing energy for the cells [54]. However, when extracellular concentration in the colon increases above 50 µM the oxidative capacity of the cell is insufficient [10] and H_2S inhibits the mitochondrial respiratory chain as we confirmed in Figure 5.

Other studies have indicated that monolayer TEER formation development initiates after multiple days due to spontaneous differentiation [55]. However, introducing a standardized scratch in differentiated monolayers led to lifting or 'tearing' of the monolayers, resulting in poorly defined scratch areas. This problem was overcome by differentiating the organoids prior to dissociation and seeding. The confluent monolayers had TEER values of 1000 ± 62 Ω within 24h similar to other 2D models like Caco2, IPECJ2, and organoids [56-58]. Moreover, the polarization of the epithelial monolayer was confirmed by the immunohistological detection of tight junction ZO-1 proteins in the apical region of the paracellular space and villin expression predominantly at the apical surface of the cells.

Sulfide inhibits gap closure rates and barrier integrity

Treatment with sulfide affected the directionality and collective movement of cells towards the gap or 'wound' scratched in the confluent monolayer. However, in some areas of the monolayer the displacement/migration of cells was large and similar to the controls. At low concentrations (10–100 µM) sulfide has been shown to increase cell proliferation through the EGFR/ERK/MMP-2 pathways necessary for wound healing and the PTEN/AKT pathway but at higher concentrations (>1 mM) proliferation is inhibited [10]. At the sulfide concentrations used in our assay (5 mM), inhibition of cell displacement was anticipated, but our results showed this effect to be patchy (Figure 4). The reasons for this remain unclear, but we speculate this could relate to the thickness of the mucus layer in different parts of the monolayer, which could affect the interaction with the epithelial cells due to reaction of sulfide with disulfide bonds in the mucus [59, 60].

There was a distinct inhibitory effect of sulfide on gap closure rates as well as barrier integrity in our study. We observed that sulfide decreased expression of tight junction associated genes and caused a lowering of TEER and increased permeability of smaller-sized dextran molecules, indicative of a partial loss of barrier function (Figure 4). The downregulation of claudin-7 expression, and reduced mitochondrial activity observed upon sulfide-treatment is in agreement with the observation that loss of sufficient ATP production in the intestine leads to decreased barrier integrity through internalization of Claudin-7 [5, 18]. Moreover, other studies have indicated that increased ROS production leads to altered expression and localization of tight junction proteins [61, 62], agreeing with the significant impairment of tight junction function and the upregulation of oxidative stress associated enzymes upon sulfide exposure in our study (see also below). In addition, the decrease in integrin signaling is consistent with the observed reduction of cellular motility. Notably, recent studies have shown that hydrogen sulfide at endogenous concentrations (200-500 μM) attenuated injury-induced barrier loss in Caco2 cells, which was tentatively associated with inhibition of NF-kB signaling [63]. However, the concentrations produced in the intestinal lumen substantially exceed endogenous hydrogen sulfide production [9, 64]. Our results showed that 5 mM hydrogen sulfide inhibits cellular migration and wound healing, which is in agreement with studies on epithelial cell lines [65, 66]. A recent study exposing epithelial cell lines (Caco2, and IEC6) to slow H_2S-releasing molecule (GYY4137) was shown to arrest cell proliferation for a prolonged period (48h) leading to wound healing inhibition via MEK1/2 [65]. These effects of sulfide on MEK1/2 are in agreement with our decreased expression of focal adhesion-related genes and significant down-regulation of MEK1 (**Figure S8**), although we still observed a high displacement and velocity of cell migration after sulfide treatment. The difference between our results and those obtained with epithelial cell lines may be due to differences in cell type heterogeneity and the loss of barrier function in colon organoid monolayers that could cause loss of directionality and aberrant migration patterns.

Sulfide exposure leads to decreased MAPK-signaling and mitochondrial respiration

Our data suggests that reduced gap closure rate in sulfide treated organoid monolayers is linked to down regulation of MAPK-signaling (**Figure S9**). Decreased activation of the classical MAP kinase pathway through decreased growth factor signaling upon the exposure to sulfide or ammonia is likely to contribute to lower proliferation and differentiation through c-FOS [67]. Moreover, both treatments show reduced MAPK pathway expression and decreased *TXNIP*, likely associated with decreased expression of FOXO1 and 3, and likely implicated in intracellular ROS levels [68, 69]. Moreover, increased gene expression of thioredoxin reductase 1

(*TXNRD1*) and other antioxidant enzymes, as well as increased expression of the ferroptosis pathway are in line with increased oxidative stress of sulfide-treated colon organoid monolayers. Increased genes expressed in the ferroptosis pathway also point towards accumulation of lipid reactive oxygen species [9]. Low levels of sulfide (500 µM) are also known to play a role in combating oxidative stress through the direct scavenging of reactive oxygen species and/or the upregulation of cellular antioxidant defense mechanisms via FOXO1 through the PEN/AKT pathway [68, 70], although that pathway appears to be slightly downregulated in our assays but might not affect signaling functionality (**Figure 5**). It has been suggested that low levels of hydrogen sulfide promote FOXO regulation through increased expression of SIRT1 [71]. Increased levels of hydrogen sulfide were shown to directly inhibit *cytochrome c* oxidase functioning within mitochondrial complex IV, leading to mitochondrial stress and reduced ATP production [9, 72] which would ultimately lead to increased ROS production. This is supported by our finding that sulfide treated organoid monolayers had reduced levels of ATP production, and mitochondrial respiratory capacity (Figures 5). Importantly, we could demonstrate that these effects do not correlate with reduced cell viability or mitochondrial presence due to the treatment. Sulfide increased the expression of functions associated with Protein processing in ER, many of which have been implicated in unfolded protein ER-stress, which has also been shown to be activated by increased ROS activity [73]. Eventually, deregulated, and erroneous protein folding can affect a plethora of cellular functions and could also lead to cell apoptosis [73, 74].

Recent work showed that physiologically relevant levels of hydrogen sulfide induced autophagy in colon cell lines by increased phosphorylation of AMPK and decreased mTOR signaling, resulting in decreased cell proliferation [66, 75]. However, our transcriptome analyses suggest that mito-toxic levels of hydrogen sulfide induce downregulation of both autophagy and the AMPK pathway. Colon organoid proliferation is regulated by self-replication of the colon stem cells, and thus relies on mitochondrial respiration capacity and cellular energy levels [37, 76]. FOXO genes are known regulators of the cell cycle, apoptosis, mitochondrial functioning, and autophagy [69, 77], and compromised FOXO-signaling leads to decreased homeostasis of mitochondrial respiration and increased oxidative stress in intestinal stem cells [37, 78]. Our results indicated decreased expression of FOXO3 in sulfide-exposed colon monolayers, coinciding with increased expression of functions involved in ROS clearance, which supports a previous study showing that reduced FOXO3 expression is associated with mitochondrial dysfunction in intestinal organoids [37]. Taken together, these results lead us to propose that a physiologically relevant concentration of hydrogen sulfide in piglet gut reduce respiratory capacity of the mitochondria through inhibition of complex IV cytochrome c oxidase leading to reduced ATP production, increased ROS stress due

to compromised FOXO3 regulation, and unfolded-protein associated ER-stress, which ultimately leads to a reduction in epithelial wound repair and barrier capacity.

Ammonia reduces gap closure at levels lower than physiologically observed

Ammonia severely inhibits cAMP-regulated Cl^- transport [79] at concentrations exceeding 10 mM, but induces oxidative stress and apoptosis at 40 mM in IPECJ2 cells [80]. At the latter concentration, epithelial barrier-loss was also observed, but this could very well be attributed to the induction of apoptosis combined with the reduced tight junction expression. In the present study we used 5 mM ammonia exposure and only confirmed the decreased tight junction gene expression, but not the detrimental effects on barrier function or mitochondrial respiration observed when using concentrations exceeding 15 mM [62]. We also looked at its effects on wound healing, revealing reduced cellular displacement and a lack of directionality of migration compared to control, which may be attributed to reduced TGFβ signaling [81, 82] and/or down-regulation of genes associated with RhoA signaling leading to inhibited motility [83]. However, our RNA-sequencing data points towards increased expression of genes involved in cell cycle regulation. The concomitant increase of expression of genes involved in monosaccharide metabolism is in line with increased expression of fatty acid metabolism associated genes, like fatty acid synthase (*FASN*), in ammonia-treated colon organoid monolayers. Luminal concentrations of ammonia are estimated to exceed 15 mM in the proximal colon of piglets fed high protein diets [84]. In our study the small effects of ammonia on colon organoid monolayers might be explained by using only 5 mM.

Concluding remarks

Scratch assays of colon organoid monolayers provide a novel method for investigating epithelium-metabolite interactions and understanding the impact of microbiome-derived metabolic products on intestinal epithelia. Our results highlight the complex pathways involved in cell migration and the importance of tissue-specific heterotypic cell populations in epithelial wound healing. The development of innovative strategies for monitoring high-throughput cellular behavior and compound interactions will provide new insights into the physiological consequences of these interactions.

Supplementary information

Supplementary methods

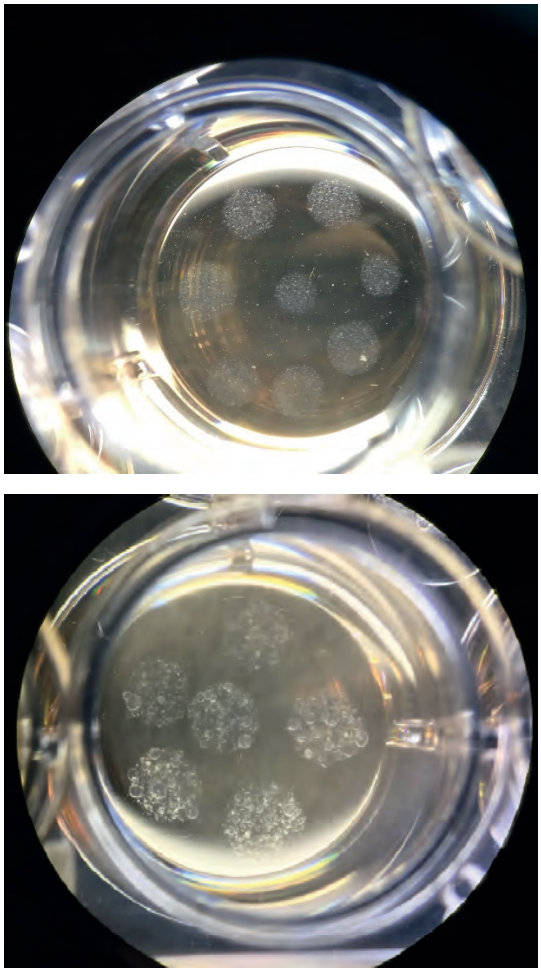

Supplementary methods figure 1. Plating single cells in Matrigel droplets (a) results in a rapid formation of spherical organoids within 5-7 days (b).

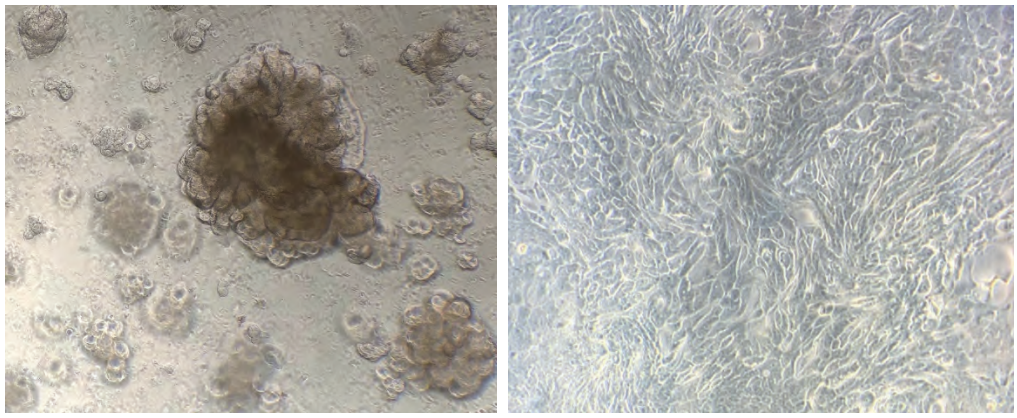

Supplementary methods figure 2. Differentiation of the organoids (by removal of WNT3A or culture in ODM) results in (left) a more globular structure compared to the spherical morphology in OGM. (right) Plating these complex organoids after single-cell processing results in a monolayer overnight (at 75 x 10^4 cells/cm^2) showing visible cell junctions.

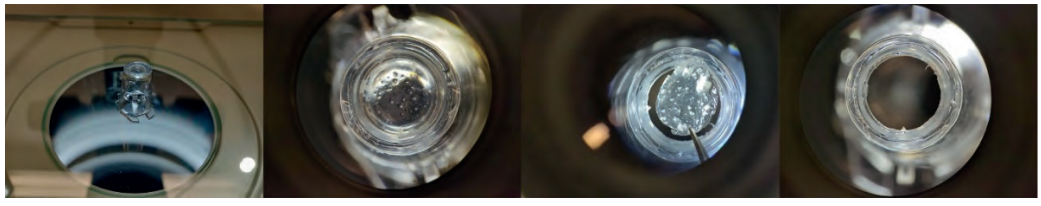

Supplementary methods figure 3. The monolayers grown on transwells were cut from the plastic support ring (a) and placed in a 1.5ml Eppendorf tube containing 1% PFA (b). After overnight fixation at 4°C, the monolayers were processed for embedding by transferring to a gradient of ethanol and xylene, and ultimately embedded upright in paraffin blocks.

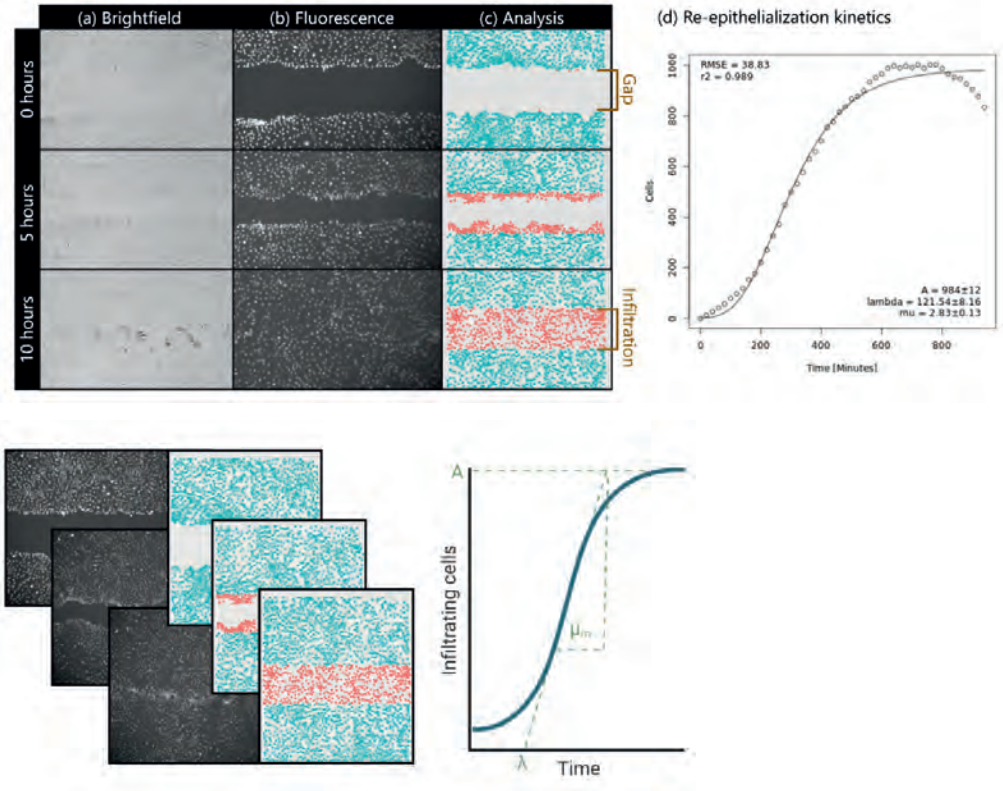

Supplementary methods figure 4. The nuclei image data is processed by the KREAP galaxy pipeline and identifies the gapped area. All nuclei outside the gapped area are denoted in blue, and cells entering the predefined area are marked red. The increase in gap infiltration by cells is then plotted and modelled into a Gompertz function that simultaneously calculates lag time (λ), cell infiltration per minute (μ_m), and total cell number (A), see detailed methods in chapter 8.

Supplementary figures

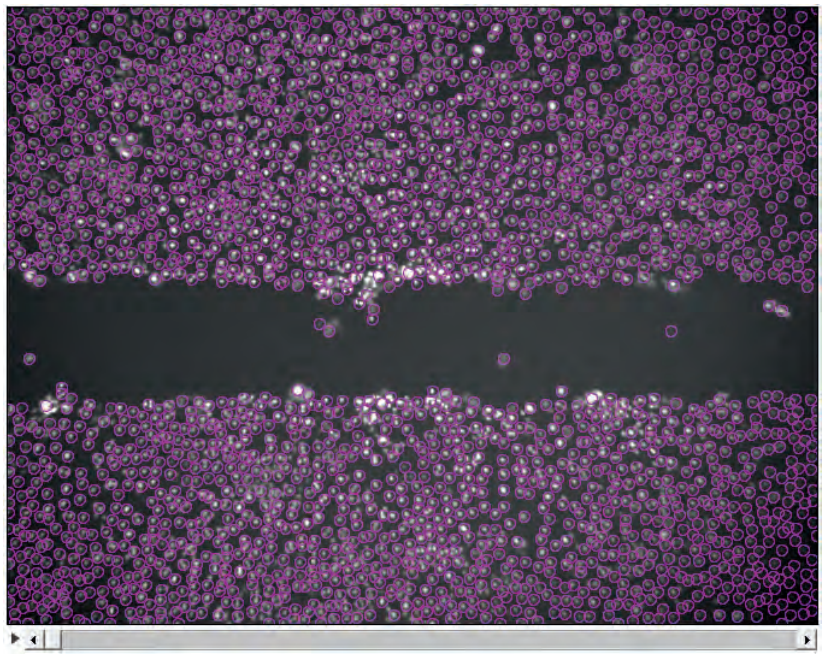

Supplementary figure 1. Nuclei identification in TrackMate with thresholding for cell tracking. Cells were identified by adjusting the LoG detector threshold to prevent missing cells or misidentifying background noise as cell nuclei. This should be adjusted for different experiments to increase reliability of nuclear tracking.

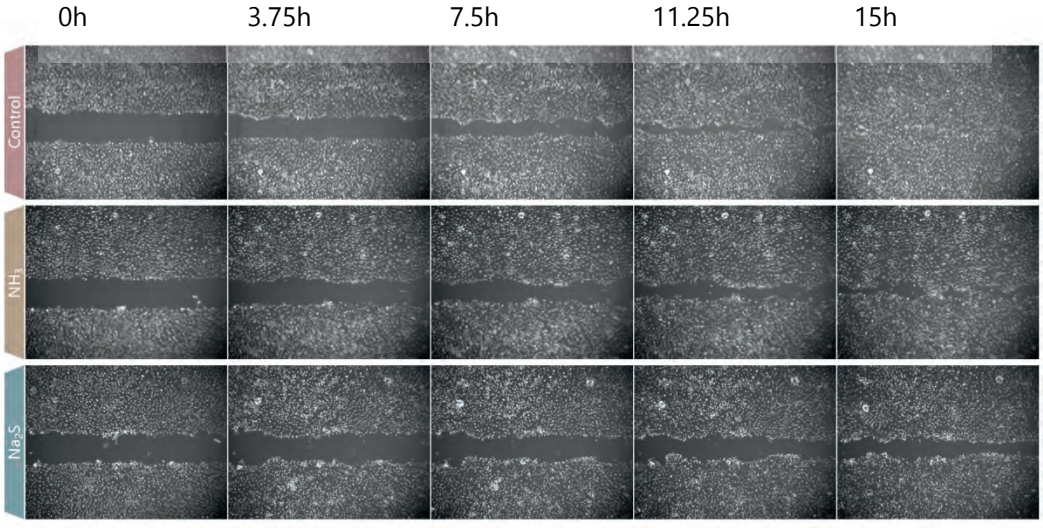

Supplementary figure 2. Time-series images of re-epithelialization when treated. Monolayers treated with ammonia (middle), or sulfide (bottom) show reduced closure rates when compared to control.

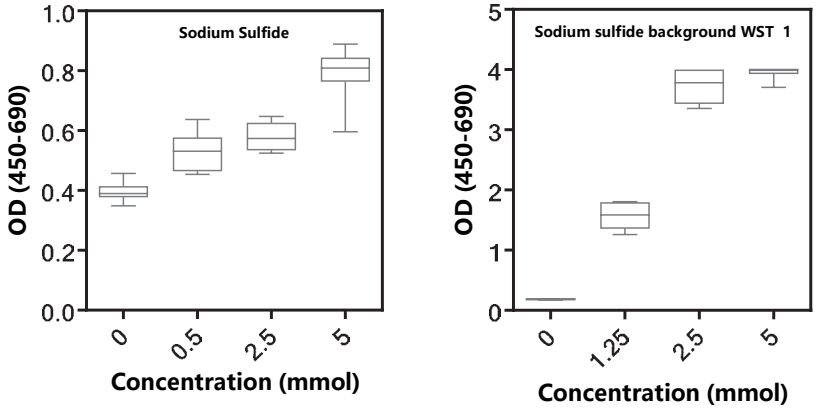

Supplementary figure 3. Determining cell viability using WST-1 is not effective when treating with sulfide-containing compounds. WST-1 was found to react with residual sodium sulfide in the treated wells after washing the monolayer with D-PBS (a). When adding dilutions of sodium sulfide to a clean plate and mixed with sodium sulfide, the WST-1 reacts within 5 minutes (b).

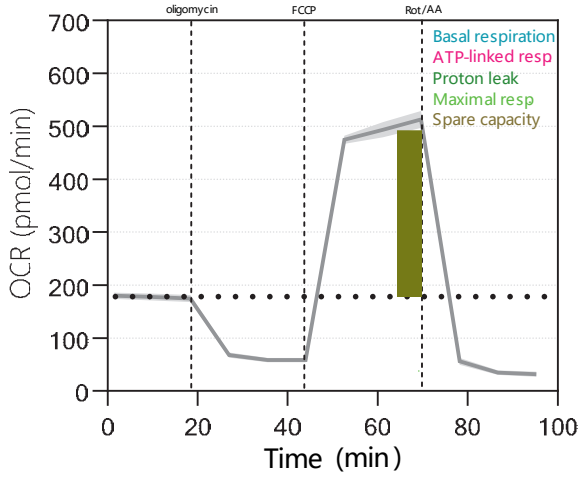

Supplementary figure 4. Mitochondrial stress test calculations for cellular metabolism. Oxygen consumption rates (OCR) were measured in organoid monolayers in response to luminal metabolites. Basal respiration (blue) was first measured and is calculated by subtracting the initial OCR rate from non-mitochondrial respiration (orange). After addition of oligomycin, the ATP-linked respiration (purple) was calculated by the difference between basal respiration and resulting OCR values. The difference between ATP-linked respiration and basal respiration indicates proton leak (dark green). By adding FCCP, the cells exert maximal respiratory capacity (light green) and gives the spare oxidative capacity (brown) of the cells.

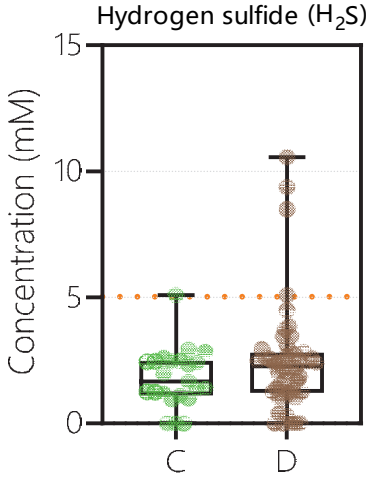

Supplementary figure 5. Luminal concentration of Hydrogen sulfide (H_2S) in piglets with diarrhea (D) or non-diarrheic control group (C) 4 days after weaning. The selection of relevant H_2S concentration was based on the maximum value observed in control animals (C) in relation to diarrhea (D) animals at 4 days post-weaning in a previous study (at 5 mM orange dotted line; data are shown as boxplots with all data points, mean and 95% CI).

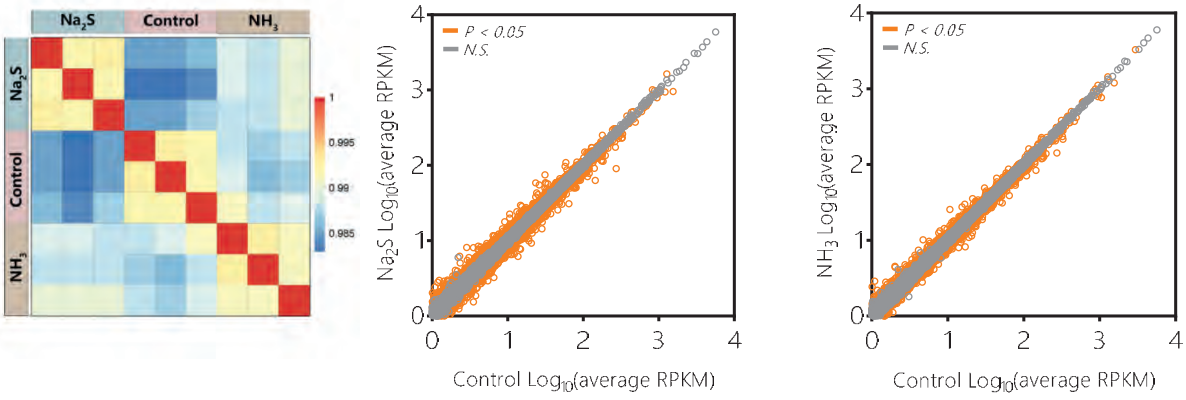

Supplementary figure 6. Transcriptome correlations of all samples and individual sample variation in colon organoid monolayers treated with 5 mM ammonia or sodium sulfide.

Supplementary table 1. RNA-sequencing reads mapping information.

FPKM Interval	Na_2S_1	Na_2S_2	Na_2S_3	Con_1	Con_2	Con_3	NH_3_1	NH_3_2	NH_3_3
0~1	20911 (65.54 %)	20891 (65.47 %)	20891 (65.47 %)	20972 (65.73 %)	21011 (65.85 %)	20915 (65.55 %)	20903 (65.51 %)	20860 (65.38 %)	20907 (65.52 %)
1~3	2020 (6.33%)	2024 (6.34%)	2037 (6.38%)	2009 (6.30%)	1966 (6.16%)	2053 (6.43%)	1997 (6.26%)	2075 (6.50%)	2004 (6.28%)
3~15	5107 (16.01 %)	5143 (16.12 %)	5127 (16.07 %)	5002 (15.68 %)	4984 (15.62 %)	5058 (15.85 %)	5125 (16.06 %)	5112 (16.02 %)	5158 (16.17 %)
15~60	2956 (9.26%)	2937 (9.20%)	2943 (9.22%)	2984 (9.35%)	2984 (9.35%)	2958 (9.27%)	2950 (9.25%)	2925 (9.17%)	2915 (9.14%)
>60	914 (2.86%)	913 (2.86%)	910 (2.85%)	941 (2.95%)	963 (3.02%)	924 (2.90%)	933 (2.92%)	936 (2.93%)	924 (2.90%)

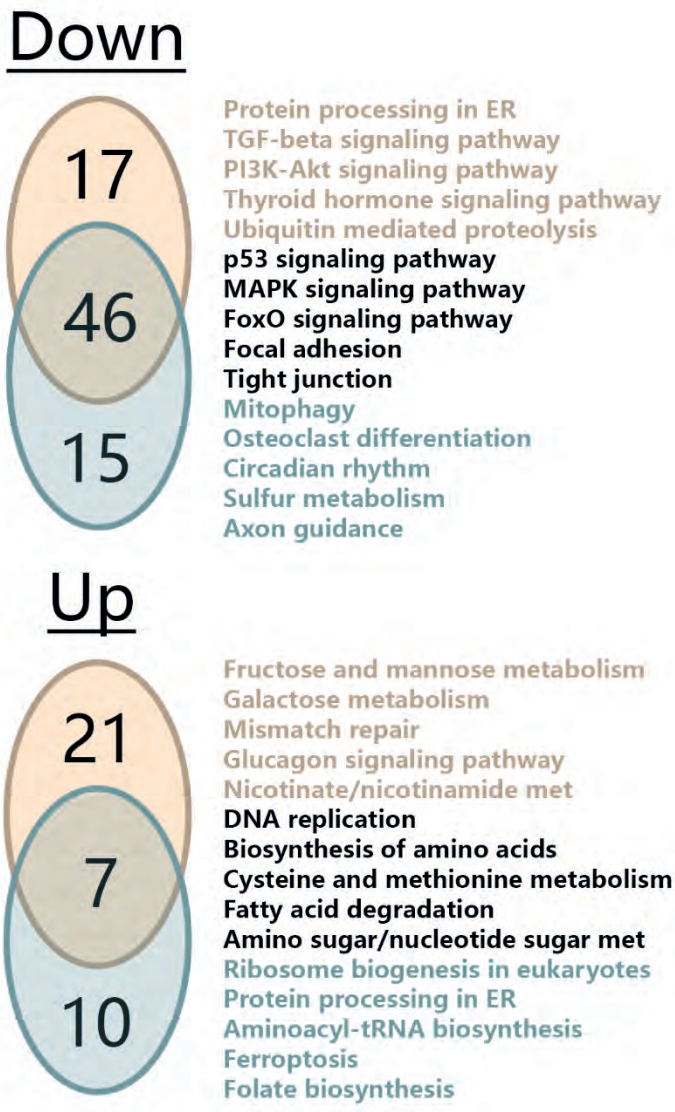

Supplementary figure 7. Overlapping differentially expressed pathways between treated colon monolayers. Colon organoid monolayers were treated with 5 mM ammonia (brown) or sulfide (blue), and the number of differentially expressed pathways were checked for mutual overlap. The top 5 distinct and overlapping pathways for each treatment are shown on the right in their corresponding coloring.

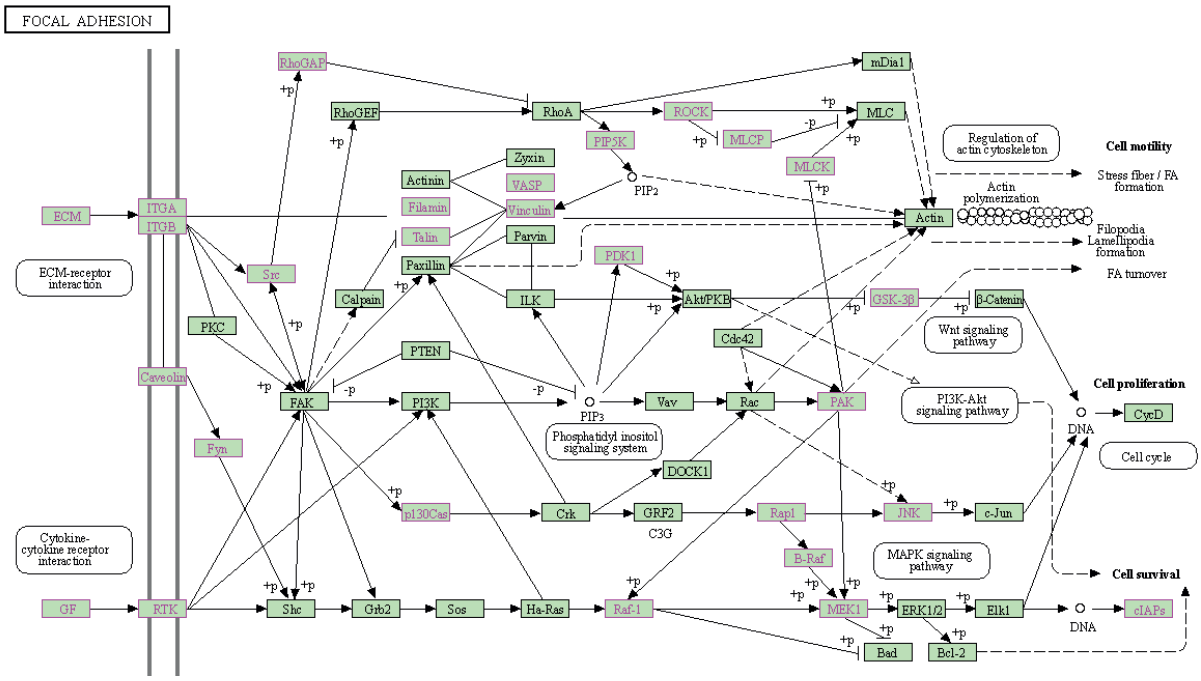

Supplementary figure 8. Focal adhesion pathway significantly downregulated by sulfide and ammonia. Genes with decreased expression by sulfide or ammonia-treated colon organoid monolayers compared to control were mapped to Kegg Pathway (hsa04510: Focal adhesion, genes down-regulated are pink). Most genes down-regulated by both treatments compared to control signal for cell motility via ECM-receptor interaction and cell survival through the MAPK-signaling pathway.

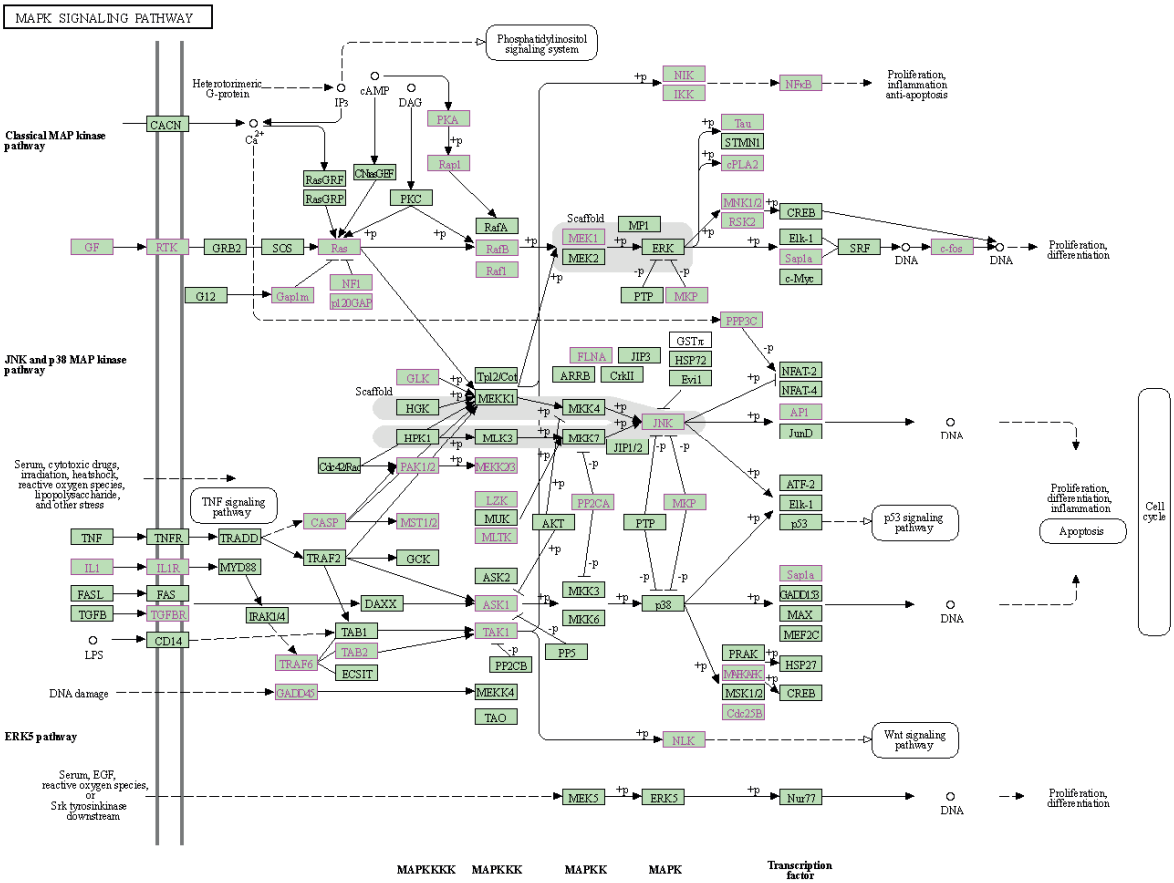

Supplementary figure 9. MAPK-signaling pathway significantly down-regulated by sulfide and ammonia-treated monolayers. Genes with decreased expression by sulfide or ammonia-treated colon organoid monolayers compared to control were mapped to Kegg Pathway for MAPK signaling (Pink are genes significantly down regulated, green is not differentially expressed).

References

1. Wells, J.M., et al., *Homeostasis of the gut barrier and potential biomarkers.* Am J Physiol Gastrointest Liver Physiol, 2017. **312**(3): p. G171-G193.
2. Iyer, N. and S.C. Corr, *Gut Microbial Metabolite-Mediated Regulation of the Intestinal Barrier in the Pathogenesis of Inflammatory Bowel Disease.* Nutrients, 2021. **13**(12).
3. Sturm, A. and A.U. Dignass, *Epithelial restitution and wound healing in inflammatory bowel disease.* World J Gastroenterol, 2008. **14**(3): p. 348-53.
4. van der Hee, B. and J.M. Wells, *Microbial Regulation of Host Physiology by Short-chain Fatty Acids.* Trends Microbiol, 2021. **29**(8): p. 700-712.
5. Donohoe, D.R., et al., *The microbiome and butyrate regulate energy metabolism and autophagy in the mammalian colon.* Cell Metab, 2011. **13**(5): p. 517-26.
6. Roager, H.M. and T.R. Licht, *Microbial tryptophan catabolites in health and disease.* Nat Commun, 2018. **9**(1): p. 3294.
7. Magee, E.A., et al., *Contribution of dietary protein to sulfide production in the large intestine: an in vitro and a controlled feeding study in humans.* Am J Clin Nutr, 2000. **72**(6): p. 1488-94.
8. Leschelle, X., et al., *Isolation of pig colonic crypts for cytotoxic assay of luminal compounds: effects of hydrogen sulfide, ammonia, and deoxycholic acid.* Cell Biol Toxicol, 2002. **18**(3): p. 193-203.
9. Beaumont, M., et al., *Detrimental effects for colonocytes of an increased exposure to luminal hydrogen sulfide: The adaptive response.* Free Radic Biol Med, 2016. **93**: p. 155-64.
10. Wu, D., et al., *Hydrogen sulfide acts as a double-edged sword in human hepatocellular carcinoma cells through EGFR/ERK/MMP-2 and PTEN/AKT signaling pathways.* Sci Rep, 2017. **7**(1): p. 5134.
11. Jiang, W., et al., *H(2)S promotes developmental brain angiogenesis via the NOS/NO pathway in zebrafish.* Stroke Vasc Neurol, 2021. **6**(2): p. 244-251.
12. Smith, E.A. and G.T. Macfarlane, *Dissimilatory amino Acid metabolism in human colonic bacteria.* Anaerobe, 1997. **3**(5): p. 327-37.
13. Heo, J.M., et al., *Effects of feeding low protein diets to piglets on plasma urea nitrogen, faecal ammonia nitrogen, the incidence of diarrhoea and performance after weaning.* Arch Anim Nutr, 2008. **62**(5): p. 343-58.
14. Windey, K., V. De Preter, and K. Verbeke, *Relevance of protein fermentation to gut health.* Mol Nutr Food Res, 2012. **56**(1): p. 184-96.
15. Feng, L., et al., *Inhibition of PI3K/Akt/mTOR pathway by ammonium chloride induced apoptosis and autophagy in MAC-T cell.* Res Vet Sci, 2021. **136**: p. 622-630.
16. Villodre Tudela, C., et al., *Down-regulation of monocarboxylate transporter 1 (MCT1) gene expression in the colon of piglets is linked to bacterial protein fermentation and pro-inflammatory cytokine-mediated signalling.* Br J Nutr, 2015. **113**(4): p. 610-7.
17. Thibault, R., et al., *Down-regulation of the monocarboxylate transporter 1 is involved in butyrate deficiency during intestinal inflammation.* Gastroenterology, 2007. **133**(6): p. 1916-27.
18. JanssenDuijghuijsen, L.M., et al., *Mitochondrial ATP Depletion Disrupts Caco-2 Monolayer Integrity and Internalizes Claudin 7.* Front Physiol, 2017. **8**: p. 794.
19. Hou, J., et al., *Study of claudin function by RNA interference.* J Biol Chem, 2006. **281**(47): p. 36117-23.
20. Liang, C.C., A.Y. Park, and J.L. Guan, *In vitro scratch assay: a convenient and inexpensive method for analysis of cell migration in vitro.* Nat Protoc, 2007. **2**(2): p. 329-33.
21. Fernandez-Gutierrez, M.M., et al., *KREAP: an automated Galaxy platform to quantify in vitro re-epithelialization kinetics.* Gigascience, 2018. **7**(7).
22. Liu, Y., et al., *Multi-omic measurements of heterogeneity in HeLa cells across laboratories.* Nat Biotechnol, 2019. **37**(3): p. 314-322.
23. Sato, T., et al., *Single Lgr5 stem cells build crypt-villus structures in vitro without a mesenchymal niche.* Nature, 2009. **459**(7244): p. 262-5.
24. Sato, T., et al., *Long-term expansion of epithelial organoids from human colon, adenoma, adenocarcinoma, and Barrett's epithelium.* Gastroenterology, 2011. **141**(5): p. 1762-72.
25. van der Hee, B., et al., *Congruence of Transcription Programs in Adult Stem Cell-Derived Jejunum Organoids and Original Tissue During Long-Term Culture.* Front Cell Dev Biol, 2020. **8**: p. 375.

26. van der Hee, B., et al., *Optimized procedures for generating an enhanced, near physiological 2D culture system from porcine intestinal organoids.* Stem Cell Res, 2018. **28**: p. 165-171.
27. Fernandez-Gutierrez, M.M., et al., *High-Throughput Screening Model to Quantify Re-Epithelialization Kinetics.* Protocol Exchange (Preprint), 2019.
28. Schindelin, J., et al., *Fiji: an open-source platform for biological-image analysis.* Nat Methods, 2012. **9**(7): p. 676-82.
29. Tinevez, J.Y., et al., *TrackMate: An open and extensible platform for single-particle tracking.* Methods, 2017. **115**: p. 80-90.
30. Andrews, S., *FastQC: a quality control tool for high throughput sequence data.* Babraham Bioinformatics, 2010. **1**.
31. Krueger, F., *Trim Galore: A Wrapper Around Cutadapt and FastQC to Consistently Apply Adapter and Quality Trimming to FastQ.* Babraham Bioinformatics, 2017. **1**.
32. Cunningham, F., et al., *Ensembl 2022.* Nucleic Acids Res, 2022. **50**(D1): p. D988-D995.
33. Trapnell, C., et al., *Differential gene and transcript expression analysis of RNA-seq experiments with TopHat and Cufflinks.* Nat Protoc, 2012. **7**(3): p. 562-78.
34. Goedhart, J. and M.S. Luijsterburg, *VolcaNoseR is a web app for creating, exploring, labeling and sharing volcano plots.* Sci Rep, 2020. **10**(1): p. 20560.
35. Kanehisa, M., et al., *KEGG for taxonomy-based analysis of pathways and genomes.* Nucleic Acids Res, 2022.
36. Gillespie, M., et al., *The reactome pathway knowledgebase 2022.* Nucleic Acids Res, 2022. **50**(D1): p. D687-D692.
37. Ludikhuize, M.C., et al., *Mitochondria Define Intestinal Stem Cell Differentiation Downstream of a FOXO/Notch Axis.* Cell Metab, 2020. **32**(5): p. 889-900 e7.
38. Wang, Y., et al., *Single-cell transcriptome analysis reveals differential nutrient absorption functions in human intestine.* J Exp Med, 2020. **217**(2).
39. Andasari, V., et al., *Computational model of wound healing: EGF secreted by fibroblasts promotes delayed re-epithelialization of epithelial keratinocytes.* Integr Biol (Camb), 2018. **10**(10): p. 605-634.
40. Kaiko, G.E., et al., *The Colonic Crypt Protects Stem Cells from Microbiota-Derived Metabolites.* Cell, 2016. **165**(7): p. 1708-1720.
41. Liu, J., et al., *Beneficial effects of butyrate in intestinal injury.* J Pediatr Surg, 2020. **55**(6): p. 1088-1093.
42. Ma, X., et al., *Butyrate promotes the recovering of intestinal wound healing through its positive effect on the tight junctions.* J Anim Sci, 2012. **90 Suppl 4**: p. 266-8.
43. Iizuka, M. and S. Konno, *Wound healing of intestinal epithelial cells.* World J Gastroenterol, 2011. **17**(17): p. 2161-71.
44. Sommer, K., et al., *Intestinal Mucosal Wound Healing and Barrier Integrity in IBD-Crosstalk and Trafficking of Cellular Players.* Front Med (Lausanne), 2021. **8**: p. 643973.
45. Mishra, Y.G. and B. Manavathi, *Focal adhesion dynamics in cellular function and disease.* Cell Signal, 2021. **85**: p. 110046.
46. Gates, R.E., et al., *Potential role for focal adhesion kinase in migrating and proliferating keratinocytes near epidermal wounds and in culture.* Cell Growth Differ, 1994. **5**(8): p. 891-9.
47. Campbell, H.K., J.L. Maiers, and K.A. DeMali, *Interplay between tight junctions & adherens junctions.* Exp Cell Res, 2017. **358**(1): p. 39-44.
48. Webb, P.G., M.A. Spillman, and H.K. Baumgartner, *Claudins play a role in normal and tumor cell motility.* BMC Cell Biol, 2013. **14**: p. 19.
49. Benoit, Y.D., et al., *RGD-Dependent Epithelial Cell-Matrix Interactions in the Human Intestinal Crypt.* J Signal Transduct, 2012. **2012**: p. 248759.
50. Le Clainche, C., et al., *Vinculin is a dually regulated actin filament barbed end-capping and side-binding protein.* J Biol Chem, 2010. **285**(30): p. 23420-32.
51. Li, B., et al., *Intestinal epithelial tight junctions and permeability can be rescued through the regulation of endoplasmic reticulum stress by amniotic fluid stem cells during necrotizing enterocolitis.* FASEB J, 2021. **35**(1): p. e21265.
52. Warr, M.R., et al., *FOXO3A directs a protective autophagy program in haematopoietic stem cells.* Nature, 2013. **494**(7437): p. 323-7.
53. Audesse, A.J., et al., *FOXO3 directly regulates an autophagy network to functionally regulate proteostasis in adult neural stem cells.* PLoS Genet, 2019. **15**(4): p. e1008097.

54. Hildebrandt, T.M. and M.K. Grieshaber, *Three enzymatic activities catalyze the oxidation of sulfide to thiosulfate in mammalian and invertebrate mitochondria.* FEBS J, 2008. **275**(13): p. 3352-61.
55. Kozuka, K., et al., *Development and Characterization of a Human and Mouse Intestinal Epithelial Cell Monolayer Platform.* Stem Cell Reports, 2017. **9**(6): p. 1976-1990.
56. Takenaka, T., et al., *Human small intestinal epithelial cells differentiated from adult intestinal stem cells as a novel system for predicting oral drug absorption in humans.* Drug Metab Dispos, 2014. **42**(11): p. 1947-54.
57. Wang, J., et al., *Caprylic acid and nonanoic acid upregulate endogenous host defense peptides to enhance intestinal epithelial immunological barrier function via histone deacetylase inhibition.* Int Immunopharmacol, 2018. **65**: p. 303-311.
58. Jelinsky, S.A., et al., *Molecular and Functional Characterization of Human Intestinal Organoids and Monolayers for Modeling Epithelial Barrier.* Inflamm Bowel Dis, 2023. **29**(2): p. 195-206.
59. Liu, L., et al., *Mucus layer modeling of human colonoids during infection with enteroaggragative E. coli.* Sci Rep, 2020. **10**(1): p. 10533.
60. Ijssennagger, N., R. van der Meer, and S.W.C. van Mil, *Sulfide as a Mucus Barrier-Breaker in Inflammatory Bowel Disease?* Trends Mol Med, 2016. **22**(3): p. 190-199.
61. Basuroy, S., et al., *MAPK interacts with occludin and mediates EGF-induced prevention of tight junction disruption by hydrogen peroxide.* Biochem J, 2006. **393**(Pt 1): p. 69-77.
62. Yokoo, K., Y. Yamamoto, and T. Suzuki, *Ammonia impairs tight junction barriers by inducing mitochondrial dysfunction in Caco-2 cells.* FASEB J, 2021. **35**(11): p. e21854.
63. Chen, S.W., et al., *Protective effect of hydrogen sulfide on TNF-alpha and IFN-gamma-induced injury of intestinal epithelial barrier function in Caco-2 monolayers.* Inflamm Res, 2015. **64**(10): p. 789-97.
64. Rowan, F.E., et al., *Sulphate-reducing bacteria and hydrogen sulphide in the aetiology of ulcerative colitis.* Br J Surg, 2009. **96**(2): p. 151-8.
65. Xu, W., et al., *Hydrogen sulfide suppresses the proliferation of intestinal epithelial cells through cell cycle arrest.* Arch Biochem Biophys, 2021. **712**: p. 109044.
66. Wu, Y.C., et al., *Hydrogen sulfide lowers proliferation and induces protective autophagy in colon epithelial cells.* PLoS One, 2012. **7**(5): p. e37572.
67. Wang, Q., et al., *Involvement of c-Fos in cell proliferation, migration, and invasion in osteosarcoma cells accompanied by altered expression of Wnt2 and Fzd9.* PLoS One, 2017. **12**(6): p. e0180558.
68. Akasaki, Y., et al., *FoxO transcription factors support oxidative stress resistance in human chondrocytes.* Arthritis Rheumatol, 2014. **66**(12): p. 3349-58.
69. Ludikhuize, M.C. and M.J. Rodriguez Colman, *Metabolic Regulation of Stem Cells and Differentiation: A Forkhead Box O Transcription Factor Perspective.* Antioxid Redox Signal, 2021. **34**(13): p. 1004-1024.
70. Klotz, L.O., et al., *Redox regulation of FoxO transcription factors.* Redox Biol, 2015. **6**: p. 51-72.
71. Zhu, L., et al., *Protective effect of hydrogen sulfide on endothelial cells through Sirt1-FoxO1-mediated autophagy.* Ann Transl Med, 2020. **8**(23): p. 1586.
72. Nicholls, P., et al., *Sulfide inhibition of and metabolism by cytochrome c oxidase.* Biochem Soc Trans, 2013. **41**(5): p. 1312-6.
73. Ma, X., et al., *Intestinal Epithelial Cell Endoplasmic Reticulum Stress and Inflammatory Bowel Disease Pathogenesis: An Update Review.* Front Immunol, 2017. **8**: p. 1271.
74. Fribley, A., K. Zhang, and R.J. Kaufman, *Regulation of apoptosis by the unfolded protein response.* Methods Mol Biol, 2009. **559**: p. 191-204.
75. Mihaylova, M.M. and R.J. Shaw, *The AMPK signalling pathway coordinates cell growth, autophagy and metabolism.* Nat Cell Biol, 2011. **13**(9): p. 1016-23.
76. Rodriguez-Colman, M.J., et al., *Interplay between metabolic identities in the intestinal crypt supports stem cell function.* Nature, 2017. **543**(7645): p. 424-427.
77. Eijkelenboom, A. and B.M. Burgering, *FOXOs: signalling integrators for homeostasis maintenance.* Nat Rev Mol Cell Biol, 2013. **14**(2): p. 83-97.
78. Rimmele, P., et al., *Mitochondrial metabolism in hematopoietic stem cells requires functional FOXO3.* EMBO Rep, 2015. **16**(9): p. 1164-76.
79. Prasad, M., et al., *Ammonia inhibits cAMP-regulated intestinal Cl- transport. Asymmetric effects of apical and basolateral exposure and implications for epithelial barrier function.* J Clin Invest, 1995. **96**(5): p. 2142-51.

80. Huang, Y., et al., *Ammonia-induced excess ROS causes impairment and apoptosis in porcine IPEC-J2 intestinal epithelial cells.* Ecotoxicol Environ Saf, 2022. **243**: p. 114006.
81. Anzai, S., et al., *TGF-beta promotes fetal gene expression and cell migration velocity in a wound repair model of untransformed intestinal epithelial cells.* Biochem Biophys Res Commun, 2020. **524**(3): p. 533-541.
82. Amento, E.P. and L.S. Beck, *TGF-beta and wound healing.* Ciba Found Symp, 1991. **157**: p. 115-23; discussion 123-9.
83. Ray, R.M., et al., *RhoA inactivation inhibits cell migration but does not mediate the effects of polyamine depletion.* Gastroenterology, 2002. **123**(1): p. 196-205.
84. Pieper, R., et al., *Interaction between dietary protein content and the source of carbohydrates along the gastrointestinal tract of weaned piglets.* Arch Anim Nutr, 2014. **68**(4): p. 263-80.

General discussion

Bart van der Hee[1,2]

[1] Host-Microbe Interactomics Group, Department of Animal Sciences, Wageningen University & Research, Wageningen, The Netherlands, [2] Laboratory of Microbiology, Wageningen University & Research, Wageningen, The Netherlands

General discussion

Post-weaning diarrhea (PWD) is a widespread problem in pig production and associated with increased abundance of enterotoxigenic *E. coli* (ETEC [1, 2]). Antibiotics are commonly used to control and treat PWD, but the spread of antibiotic resistance in animal and human pathogens has brought more attention to antibiotic use [3, 4]. Piglets are often fed high-protein diets to support rapid growth, but this has been linked to decreased fecal consistency and an increased risk of PWD [5, 6].

Stresses due to abrupt weaning can lead to an imbalance in the microbiome and increased protein fermentation [6-8] metabolites, which can directly affect the gut mucosa [9] by targeting barrier function and inflammation [6-9]. With the research described in this thesis, we aimed to understand if protein fermentation metabolites are associated with piglet PWD under on-farm conditions and investigate the effects these metabolites have on the intestine using porcine intestinal organoids. To this end, this thesis focused on further developing the organoid model in the context of epithelial-metabolite interactions.

Protein fermentation and PWD in piglets

Bacterial fermentation of proteins has been linked to PWD in piglets. The crude protein (CP) content of weaner diets is often optimized for muscle mass accretion, but changes in diet and stress can lead to digestive issues in the small intestine [10]. This increases substrate availability in the colon and subsequent fermentation by the resident microbiota that produce potentially harmful metabolites. It has been suggested that these metabolites can increase the permeability of the intestine [11, 12]. The **first aim** was to investigate the relationship between protein fermentation and its metabolites, microbiota, and PWD in practical conditions. In **chapter 2** we found that animals with diarrhea had higher concentrations of protein fermentation metabolites. As these animals all received the same diets during the experiment on their respective farms, the protein fermentation markers ammonia and BCFAs (Branched Chain Fatty Acids) increased in animals with diarrhea were not necessarily associated with an increased level of dietary CP but more likely increased undigested protein flow into the colon. The observed rapid change in microbial composition between day 2 and 4 post-weaning (PW) signified an ecological shift more associated with a bloom in pathogens in the diarrheal animals. This suggests that the increased concentrations of protein fermentation markers in diarrheal animals are linked to diarrheal onset. Whether these fermentation metabolites themselves are causal remains elusive, but the increase in toxin-producing *E. coli* (ETEC) and other protein fermentation-associated pathogens like *Fusobacterium* spp. are most likely important players in diarrhea post-weaning.

Recently it was shown that low sanitary housing conditions [13, 14] reduce protein digestion in the small [15] intestine and impact on colonic microbiota composition with decreased relative abundance of carbohydrate fermenting groups like *Lachnospiraceae* [16], which is in line with our own results at day 4 post-weaning (**Chapter 2**, **Figure 3B**). Furthermore, the authors also showed lower serum levels of metabolites produced by the microbiota that are important for health, e.g., vitamin B3 [16]. These studies on sanitary conditions collectively showed that there is an increased risk of protein fermentation in the colon related to hygiene and suggested a direct link between dietary protein and microbiota shifts. Preliminary results from a study we performed recently evaluating the effects of sanitary conditions and fermentable protein indicated that both microbial pressure and fermentation can contribute separately to diarrheal onset post-weaning. The temporal diarrhea patterns that occurred in animals exposed to different sanitary conditions and fermentable protein levels could be grouped into two distinctly different patterns (**Figure 1**). This suggests that the multifactorial induction of diarrhea associated with protein fermentation is more likely linked to increased abundance of protein fermenting species rather than environmental hygiene and showed persistent problems of the gastrointestinal (GI) tract for the complete duration of the experiment. However, the weekly recurrence of diarrhea in piglets under low sanitary conditions might elicit an initial diarrheal response and restoration period. This might be related to PW overeating [17], while the secondary relapse might be associated with a more transient pathogenic shift. These results highlight the importance of colonic protein fermentation and its relation to intestinal disturbance as it shows a more prominent diarrhea pattern than low sanitary conditions alone.

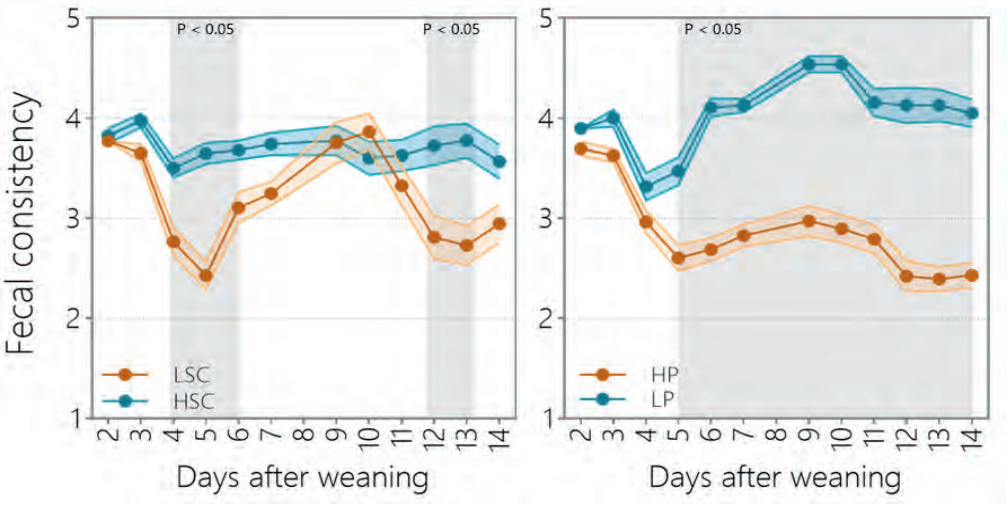

Figure 1. The effects of sanitary conditions or fermentable protein on diarrhea in piglets post-weaning. In a cross-over study, we studied the effects of high- or low fermentable protein (HP and LP), and high- and low sanitary (HSC and LSC) conditions on the onset of PWD in piglets. The effects seen on PWD in all groups did not show an interaction effect, which allowed us to combine groupings to visualize fecal consistency patterns. In the low sanitary conditions (LSC), a significant decrease in fecal consistency was observed from days 4-6 and days 12-13 post-weaning, whereas the piglets receiving high fermentable protein (HP) had diarrhea onset from day 5-14 post-weaning (n = 40 piglets per group, divided over 5 batches).

Alterations in the microbiota composition during PWD

Post-weaning adaptation of the microbiota to utilize available feed substrates has previously been shown vital for the weaning transition. Pre-weaning microbiota is functionally specialized for sow milk digestion and fermentation (**Chapter 2**) with a relatively low microbial diversity (**Chapter 2**, **Figure 1**). Even though pre-weaner (creep feed) diets are often used to stimulate colonization by PW microbial communities to prevent onset of PWD, the observed feed intake variation pre-weaning might compromise transient microbiota adaptation around the weaning transition [18-21]. Compositional changes in microbiota PW have been previously reported [18, 22-24], with some bacteria associated with predisposition to diarrhea [25]. Although the variation between animals was large the relative abundance of *Proteobacteria* was higher in control piglets than in diarrheal piglets pre-weaning (**Chapter 2**, **Figure 2A**). There are several factors that could explain the absence of disease in these piglets given the known pathogenic members of the *Proteobacteria*. One protective factor might be the presence of pathogen-binding immunoglobulin-G (IgG) in sow colostrum- and milk [26]. In pigs, antibodies in the colostrum pass across the intestinal wall in the first 48 hours and enter the blood circulation and

provide protection against systemic infection by pathogen binding, immune activation of the complement system and toxin neutralization. When the piglet matures, there is increased production of IgA, which mainly coats mucosal surfaces and provides a barrier to enteric infections[27]. Individual differences with respect to the transition to weaning and decrease in maternal antibodies could be a differentiating factor in PWD and ETEC resistance [28, 29]. As markers for this, antibodies could be measured in feces and serum in future experiments [27, 30].

The shift of the microbial composition and abundance of pathogen-associated species was prominent at day 4 PW in diarrheal animals (**Chapter 2**, **Figure 2**). The most pronounced difference was the increased concentration of ETEC heat stable toxin A (STa) in diarrheal animals. As ETEC is commonly associated with diarrheal disease in piglets PW, it was not surprising to find elevated levels in our diarrheal group irrespective of farm. However, co-occurrence of other species that increased in relative abundance, like *Fusobacterium mortiferum* and *F. nucleatum,* also points towards a larger role of microbial composition association with PWD. *Fusobacterium* spp. play a prominent role in the developing piglet gut microbiome as early colonizers [18].

In the control animals, we deduced that there might be increased fermentation of fibers, e.g., by increased relative abundance of *Ruminococcus* and *Clostridium* spp., which could be a factor in intestinal homeostasis. Fermentable carbohydrates in piglet diets can affect the composition and activity of the intestinal microbiota [31], possibly reducing protein fermentation in the GI tract. Fermentable carbohydrates that have been studied for this purpose include non-starch polysaccharides (such as cellulose, hemicellulose, and pectin), resistant starches, and nondigestible oligosaccharides. The inclusion of these fermentable carbohydrates in pig diets has been shown to increase the number of lactobacilli in the small intestine and enhance the stability and diversity of the bacterial community in the porcine colon [31], potentially suppressing pathogenic proteolytic bacteria. Supplementation of newly weaned piglets with nondigestible oligosaccharides was found to decrease total aerobes and enterococci in the ileum, while reducing potentially pathogenic *E. coli* [32]. Even though there was increased relative abundance of fiber fermenting groups in the control animals on-farm (**Chapter 2**), we did not observe elevated levels of short chain fatty acids (SCFAs) compared to diarrhea at day 4 PW. However, the SCFA concentrations did correlate to proximal colon morphology, but not distal, verifying the location-dependent fermentation by anaerobic bacteria [33]. This significantly positive relation between crypt depth and SCFA concentrations is most likely initiated by metabolite interactions with crypt elongation due to biological toxicity of butyrate to stem cells (discussed more in depth below in the section on organoid-SCFA experiments).

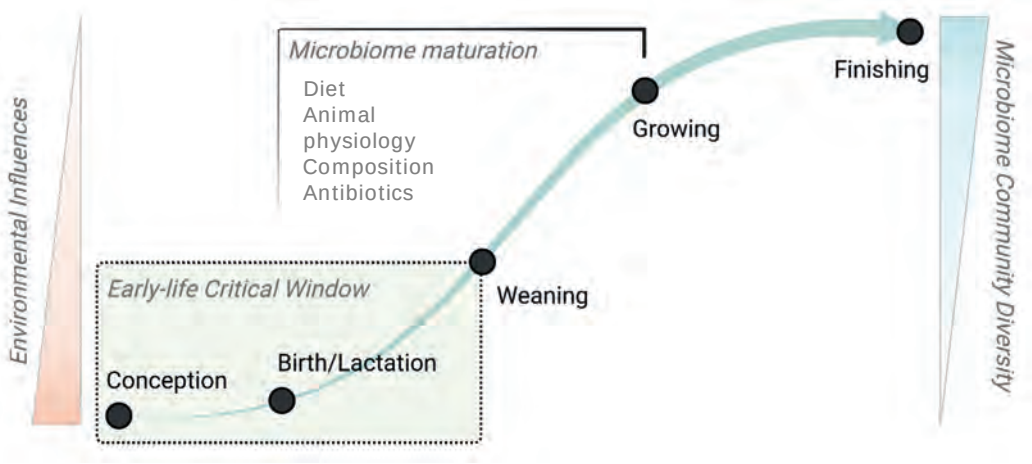

Figure 2. The gut microbiome of piglets undergoes rapid compositional succession in early life. It has been proposed that the early life microbiome plays a vital and prominent role in the developmental origins of health and disease [34] and their involvement in disease predisposition. After conception and birth, the intestinal microbiome colonization is most susceptible to environmental influences, and it has been hypothesized that this offers a critical window of opportunity (and threat) for influencing microbial composition. The composition of the microbiota has further been implicated in immune system maturation, which is critical at the point of weaning as the piglet diet shifts from highly digestible milk to solid feed. The lactation phase offers milk oligosaccharides as key energy source but also contains many bacteria that help shape the microbial composition. The weaning transition poses a large strain on the intestinal microbiome by altering dietary source, differences in the exposure to environmental microorganisms, and stress. After weaning, the microbial community diversifies more, depending on several factors [35]. Diet plays an influential role in the microbial composition due to nutrient availability for the resident microbiota. Moreover, the initial composition of the microbiota is important as it influences the general composition and nutrient utilization of opportunistic microbes. Therefore, adjusting the microbial community more transiently to a more favorable composition around the weaning period offers a more robust microbiota establishment.

Development of porcine intestinal organoids for metabolite interaction studies

Recent studies have highlighted that perturbation of the intestinal barrier could lead to increased inflammation and subsequent disease onset [8, 11, 36]. Localized or systemically originating responses can be difficult to disentangle and understand with respect to the mechanisms of how they affect the barrier. This thesis' **second aim** was therefore to develop a comprehensive model based on intestinal organoids that would let us study the interaction between microbially produced metabolites and the epithelium (**Chapters 3, 5, 7** and **9**). Conventional cell lines often lack piglet-specific genes that are commonly associated with disease receptors. For instance, fucosyltransferase-1 (*FUT1*), a gene that has been linked to disease resistance from F18^{+} ETEC [37, 38], is not expressed in the porcine jejunum cell line IPEC-J2 (**Chapter**

3). This gene was also absent in our jejunum organoids but was expressed in the ileum organoids (**Chapter 3**, **Figure 3D**). Furthermore, essential genes associated with digestion (sucrase isomaltase; *SI*, fatty acid binding protein 1; *FABP1*) were exclusively expressed in the organoid model and not IPEC-J2 (**Chapter 3**, **Figure 3C**). Moreover, a recent study highlighted the aberrant genetic properties of IPEC-J2 with heteroploidy of various chromosomes [39], whereas a comparison with the transcriptome of our jejunum organoids showed the organoids to be more stable. This location-specific expression and general transcriptome results highlight the importance of model selection for disease interaction studies and the characterization of expressed receptors.

Exploring the effects of SCFAs butyrate and acetate on organoids

As alluded to previously in this discussion, the fermentation of nondigestible fiber may play an important role in intestinal homeostasis and immunity by SCFAs. The large quantities produced by the resident microbiota and rapid metabolism by intestinal epithelial cells signify the importance of SCFAs in energy necessity (**Chapter 4**). Recent studies have shown that 1.0-2.0 mM butyrate reduces inflammatory signaling through interleukin-8 and TLR4 in IPEC-J2 cells [40, 41], as well as decreased proinflammatory cytokines and mast cell degranulation in weaned piglets [42, 43]. A study by Lukovac *et al.* (2014) described the effects of individual and mixed SCFAs derived from *Akkermansia muciniphila* and *Faecalibacterium prausnitzii* on ileum organoids [44]. Their results show altered expression of pathways associated with cellular growth and survival, but more interestingly also genes associated with histone deacetylation (HDAC). Recent papers have shown the importance of intestinal butyrate in suppressing intestinal infection and the upregulation of antimicrobial peptides in pigs and mice, most likely through histone deacetylases [44-47] Dietary inclusion of sodium butyrate has also been implicated in decreased PWD and increased barrier functionality in piglets [48-50] and shows promising results as dietary modulator of intestinal disease.

In **Chapter 5** we utilized luminally relevant concentrations of butyrate and acetate based on concentrations observed in the field study (**Chapter 2**), namely 1 mM butyrate and 2.5 mM acetate. As it has been stated that butyrate concentrations exceeding 1 mM have toxic effects in organoids [33], we initially verified that no toxicity was elicited by these concentrations in the ileum organoids. Moreover, at these concentrations the effects of acetate and butyrate on histone deacetylase 3 (HDAC3) were comparable to previous studies [44, 51]. However, one limitation of this model is that the spatial morphology of the organoids does not mimic the diffusion gradient of the *in vivo* small intestinal (macro)villus and colonic crypt

structures [52]. It has been shown that the absence of SCFAs from the crypt bottom is essential for stem cell maintenance and survival as it inhibits key cell-cycle genes through FoxO3 [33]. In another study, the effectiveness of the butyrate induced HDAC inhibitor (HDACi) was found to be closely linked to the Warburg effect [53], which is a high glucose environment under culture conditions. When cells were stimulated but the Warburg effect was prevented, histone 3 ac (H3ac) was not inhibited, and cell proliferation increased [53]. The increased HDACi observed in the presence of the Warburg effect points to glucose saturation, resulting in an increase in cellular accumulation of butyrate acting as HDACi. The nutrient environment of the organoid model is less glucose rich than conventional cell lines; this still increases the likelihood for the Warburg effect (**Chapter 4**) that further affects intracellular butyrate accumulation and subsequent effects on HDACi activity (**Figure 3**). This suggests that the effects seen on histone acetylation might be related to histone actyltransferases (HAT) instead. These observations, especially the effects of butyrate on stem cell replication, suggests that the effects of butyrate may vary along the crypt-villous axis or in different glucose states, with more HDACi apically and increased HAT activity basolaterally in the *in vivo* intestinal lumen. To determine the more precise epigenetic effects of both butyrate and acetate through HDAC activity could be followed up by experiments that also investigate HAT activity under low glucose environments. Moreover, this includes using different tissue types, e.g., colon, and apical stimulation of the organoids.

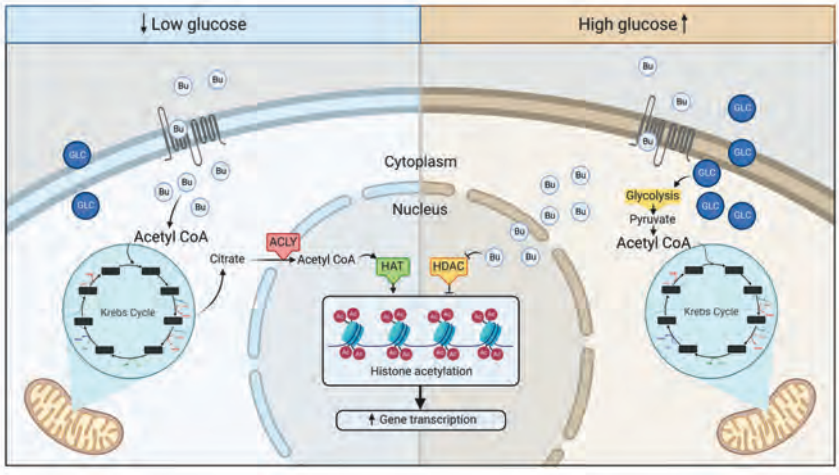

Figure 3. Utilization of butyrate by colonic epithelial cells under normal (left) or high glucose (right) environments react differently. Under normal conditions, cells prefer metabolism of butyrate in the TCA cycle, producing substrates for histone acyltransferases. In tumor state, or high glucose environments, the Warburg effect prefers glucose as energy source, increasing intracellular butyrate, favoring histone deacetylase inhibition (adapted from [53]).

The physiological relevance of organoid models

2D intestinal organoid model for luminal compound stimulation

Our initial organoid experimentation to test effects of microbial metabolites were performed using 3-dimensional (3D) organoids (**Chapters 3 and 5**). However, the polarized intestinal epithelium vectorially expresses surface receptors and signaling molecules [54, 55]. This means that stimulating basolateral oriented organoids with luminal compounds poses a physiological discrepancy in responses. In **Chapter 6**, we optimized procedures for a 2-dimensional (2D) model that still recapitulates the cellular heterogeneity of intestinal organoids while also providing luminal access for compound stimulation without the need for injection into the 3D organoid lumen. Other 2D models of intestinal organoids have also been developed for other animal species [52, 56-58], which generate various rates of cell confluency with functional tight junction barriers and multilineage differentiation. TEER (Transepithelial Electrical Resistance) values were monitored during 2D organoid formation and observed values (1000 Ω/cm^2) were slightly higher than those measured *ex vivo* using Ussing chambers (300-400 Ω/cm^2 [59]). However, other studies measuring TEER in organoid monolayers also show variable results, with some reporting lower values more in line with physiological intestinal epithelium and others more in line with values found in our experiments. This may be due to laboratory specific differences in measuring TEER values due to differences in cell layer uniformity, measurement apparatus [60], cell passage number [61], medium composition [62], temperature fluctuations [63], cell origin [64], etc. Moreover, shear stress due to medium replacements is also a key factor that influences tight junction expression in endothelial [65, 66] and epithelial [67, 68] cell models. Depending on medium replacement incidence, this could affect the barrier formation in our model due to cell layer agitation. Furthermore, we also observed that prolonged culture on 2D culture promoted localized detachment and rising of the epithelium (**Chapter 9, Figure 1**), which can have large effects on TEER values and should be avoided.

We showed that the 2D monolayer model can be used to study dietary ingredient interactions with the small intestinal epithelium (**Chapter 7**). In this study we investigated the non-nutritional effects of novel sources of dietary protein on the pig epithelial transcriptome. In this assay the novel protein sources were applied without digestion, allowing the effects of intact glycans, lipids, and proteins to be measured [69, 70]. The effects of soybean meal on the intestinal epithelium have been studied in other species [71, 72] or models [73], but mainly focused on its effects on barrier functioning and survival. Our study found that soybean meal decreased the expression of hypotriglyceridemic and retinoid receptors. This finding

supports existing evidence in the liver [74, 75], which suggests that a constituent of soy protein negatively regulates the biosynthetic pathways of cholesterol and lipids in the small intestinal epithelium. The results from **Chapter 7** demonstrated that intestinal organoid monolayer models are a valuable reductionist model for studying the effects of dietary components including metabolites on the intestinal epithelium.

Mimicking epithelial wound healing with intestinal organoids

The ability to rapidly repair damaged epithelium and restore barrier functions due to infection and excessive inflammation, toxicity, trauma, and acute mesenteric ischemia is vital for intestinal homeostasis [76-78]. Conventional cell models utilize confluent and static monolayers that no longer migrate or proliferate due to contact inhibition. However, these do not mimic the complex cell-cell interactions needed for epithelial regeneration, migration, and wound healing. Therefore, we optimized the use of intestinal organoid monolayers in a wound healing assay that mimics cell migration during wound healing *in vivo* (**Chapter 8**). Initially we needed to optimize the adhesion and confluence properties of the organoids, as they generally need Matrigel pre-coated surfaces. We observed that if Matrigel is absent and differentiation was performed in 3D prior to seeding, the cells adhered within six hours and generated a confluent monolayer overnight (**Chapter 9**, **Figure 1I**), amenable for scratch assays.

The re-epithelialization model developed in **Chapter 8** monitors cell migration into a scratched area and has the advantage that it allows to monitor individual cell kinetics. The model is sensitive when using cytotoxic compounds that severely hamper the sigmoidal regrowth curve as well as intricate cellular movement outside the software-identified scratch area. The videos of cellular movement in **Chapter 6** show that the cell population in 2D organoids is highly mobile (see online video material at [79]). This mobility could potentially reduce the effectiveness of the nuclei-based analysis by causing collective movement of cells into and out of the scratched area, resulting in false-positive measurements that could alter conclusions about re-epithelialization. To address this issue, we supplemented the re-epithelialization curves with cell kinetics tracking of the entire image, which provided increased resolution of migratory behavior (**Chapter 9**, **Figure 2C**) on nuclei displacement and velocity over time. Another study also implemented individual cell movement analysis with manual tracking in Fiji image software [80], but this manual tracing of trajectory tracks is not feasible for a 96-well, high nuclei density assay. Therefore, we opted to use automated tracking using Trackmate [81], which was developed for automated identification of individual nucleus migration in a large population of cells. The automated tracking feature is most effective if the interval

between images is short enough to avoid misidentification of the anticipated trajectory. In following experiments, we could use the differentiated heterogeneity of the organoid cell population to also track individual cell types during wound healing, by labeling with cell-specific markers and implementing these in newly developed overlap trackers [82, 83].

Individual protein fermentation metabolites affected epithelial repair substantially (**Chapter 9**, **Figure 2A**). However, tracking the locomotion of all cells in the image showed distinct characteristics in the response to all tested compounds, reinforcing the importance of more thoroughly investigating their effects on cell migration. Although previous studies showed a reduction in wound healing capacity by hydrogen sulfide *in vitro*, our cell displacement data suggest an effect of this metabolite on cell directionality during migration that leads to impaired wound healing (**Chapter 9**, **Figure 4**). This could be attributed to its observed effects on barrier functioning, focal adhesion, and integrin signaling (**Chapter 9**, **Figure 4B**). Cells in an epithelium generally rely on collective migration and synchronized directionality for wound healing when contact inhibition is broken [84]. This is achieved through adherens junctions [85], cadherins, and integrins, which interact for movement. Cells are also signaled to move by mechanosensing, and the (focal) adhesion and adherens junctions sense these changing physical properties to react to conformational change [86, 87]. The RNA-sequencing data and loss of cell directionality in hydrogen sulfide-treated monolayers showed a loss of junctional complexes vital for collective migration, including Tight junction expression, actin cytoskeleton remodeling, adherens junction expression, and focal adhesion. This was further corroborated by a loss of barrier integrity and increased small compound permeability in our transwell assays (**Chapter 9**, **Figure 5E**). Moreover, it seems that hydrogen sulfide therefore acts as a chemokinetic compound that elicits loss of cellular directionality by inhibiting junction functionality (**Figure 4**). Interestingly, slow-releasing sulfide donor GYY4137 has shown beneficial effects on LPS- or TNFα/IFNɣ-induced barrier injury by reconstituting altered TJ (Tight Junction) localization *in vitro* and *in vivo* [88-90]. The difference could be in the acute release of high hydrogen sulfide concentrations in our experiments using Na_2S or NaHS as donors.

Intestinal bioenergetics are essential for cellular functioning, but epithelial energy metabolism is a complex interaction with available substrate from arterial or luminal origin [91, 92]. Maintaining epithelial renewal, and concomitant nutrient absorption requires high metabolic activity [92, 93]. Moreover, progenitor cells in the intestine contain many mitochondria to sustain energy necessities [94, 95]. The negative effects of hydrogen sulfide on ATP production and oxidative phosphorylation could be vital in the loss of barrier functioning. For instance, recent observations indicated that decreased energy metabolism results in membrane-to-cytoplasm redistribution

of claudin-7 (CLDN7) and decreased barrier integrity [96, 97]. Our data also showed decreased expression of claudin genes, e.g. *CLDN7* (**Chapter 9**, **Figure 4C**), which could link decreased metabolic activity to pathophysiological barrier functioning in our assays. It has already been shown that hydrogen sulfide at elevated levels inhibits cytochrome c oxidase functioning of complex IV, leading to decreased ATP production and increased mitochondrial stress [98, 99]. Our data further showed increased mitochondrial stress as seen by elevated gene expression of oxygen radical scavengers like Superoxide dismutase 2 (*SOD2*), Thioredoxin reductase 1 (*TXNRD1*), and mitochondrial thioredoxin (*TXN2*). More interestingly, we also observed decreased expression of genes related to FOXO signaling in hydrogen sulfide-treated monolayers, especially *FOXO3* (**Chapter 9**, **Figure 5G**). Recent studies have indicated the importance of *FOXO3* in stem cell maintenance and mitochondrial functioning [100-102], highlighting a key role of FOXO signaling in intestinal homeostasis. Reduced nutrient availability at weaning and increased levels of protein fermentation metabolites could lead to reduced energy availability and subsequent ineffective epithelial regeneration [93, 103, 104].

Essential processes like protein folding in the endoplasmic reticulum (ER) are stressed by hydrogen sulfide (**Chapter 9**, **Figure 5A**). Correct ER functioning is vital for highly metabolic cells such as intestinal stem cells [94, 95, 105]. Nutrient deficiency has been implicated in the unfolded protein response (UPR) [106], which is a defense mechanism to prevent misfolded proteins and restore ER homeostasis [107, 108]. Prolonged UPR and ER stress can result in severe metabolic dysfunction and increase apoptotic signaling pathways [107, 109]. The link we and others, using different models, found between hydrogen sulfide treated colon monolayers and molecular defense responses as the UPR and reduced energy metabolism could be vital for understanding the molecular interaction of individual protein fermentation metabolites and intestinal homeostasis. Moreover, understanding the individual effects of metabolites on the intestinal epithelium could provide future opportunities for testing key genes and proteins from *in vivo* studies to correlate protein fermentation metabolites with physiological responses.

In the future, a combination of several metabolites could be important to evaluate synergistic effects on the intestinal epithelium. The compounds tested in this thesis showed individual responses, but physiologically they are rarely exclusively present. Moreover, complex (bidirectional) interactions between the immune system and other tissues are not captured in the organoid model. Methods to overcome this could be generating coculture models, e.g. addition of immune cells [110, 111], morphological organization, e.g. adding crypt structures [52, 112, 113] or combining different tissue sections in connected chips [68, 114] and treatments using filtered fecal digesta, fecal water, or luminally measured concentrations in combination with microbial cultures [67]. For instance, organoid crypt arrays have been developed to

generate chemical gradients along the crypt axis [52, 112, 113] to mimic the spatial organization of the intestinal epithelium more closely. However, a limiting factor is that these collagen scaffolds are non-renewing systems and are degraded by epithelium-produced metalloproteases. Refining these systems is necessary for physiologically relevant results and should still be cross referenced with *in vivo* epithelial responses for validation. Another factor not considered in this thesis is long-duration exposure and its transient effects on cells. Even though the onset of protein fermentation and possibly resulting diarrhea is a very acute problem, it would be interesting to see if consecutive stimulation with beneficial metabolites, like SCFAs, in combination with protein fermentation metabolites could reinstate metabolic homeostasis. Combining this with the results obtained from the on-farm study described in **Chapter 2** could provide piglet specific data to identify personalized PWD predisposition compounds. Moreover, this would also provide a more insightful combination of compounds found in the intestinal lumen that interact with the epithelium. Clustering metabolite, microbiota, and physiological parameters, for instance using multi-omics factor analysis, would then generate compound combinations that could be tested in our organoid models.

During this thesis, we mainly focused on the contribution protein fermentation markers have with the onset of PWD. However, multiple studies have identified individual stressors that are associated with diarrhea and highlight separate causes for PWD, like hygienic conditions [115], environmental factors such as housing [115, 116], genetic and immune predisposition [115, 117], infectious pathogens, dietary changes [118, 119], microbiota composition, preweaning health status [9], and stress [120] (**Figure 4**). With this final section of my discussion on PWD and fermentation metabolites, I would like to emphasize that the multifactorial nature of piglet PWD can be related to any combination of these associated causes. The complexity of these contributors to PWD and the variable effects they could have on individual animals highlights that single solutions to individual contributors are challenging for preventing PWD. However, timely intervention before or after weaning to avoid or decrease the incidence of diarrhea is important to decrease the welfare burden on these young animals. From the research described in this thesis, we do see the importance of intestinal barrier function and future research could focus on finding ways to support its function throughout weaning and the importance of the intestinal microbiota. The further restrictions on (prophylactic) antibiotics and medicinal zinc use are needed due to their unsustainable characteristics [121, 122], but also consequently creates additional challenges in finding solutions to PWD.

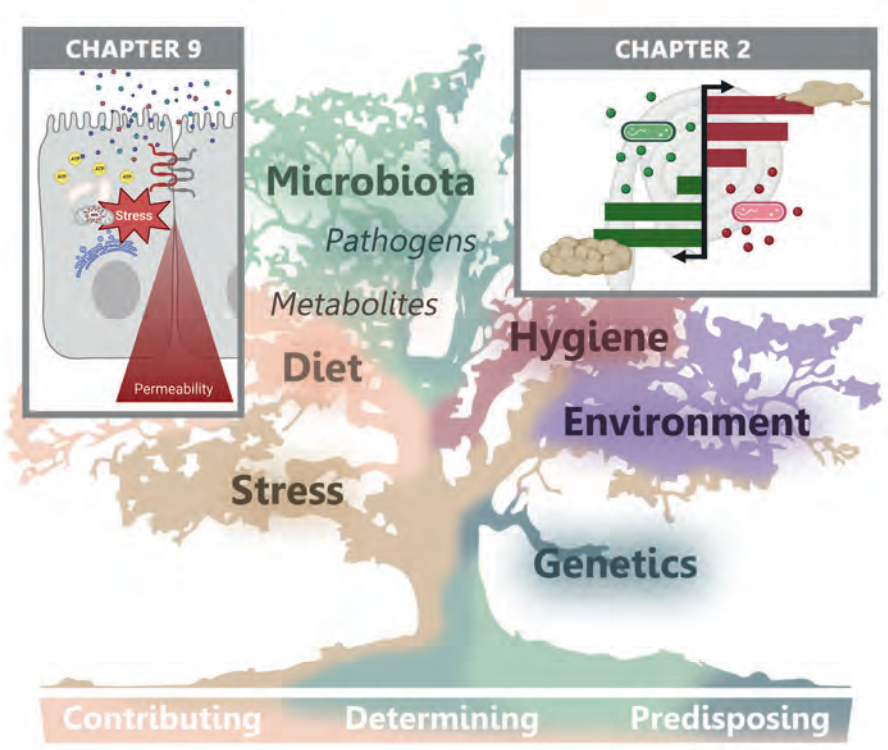

Figure 4. Factors that contribute to the onset of PWD in piglets.

Recent developments in the use of fecal microbiota transplantation (FMT) have shown promising results on alleviating PWD by stimulating the growth and persistence of beneficial microbiota. For instance, treating weaned piglets with an FMT from healthy weaned piglets significantly decreased the abundance of pathogenic *E. coli* [123]. Moreover, another study using FMT discovered that bacteriocin gassericin A produced by *Lactobacillus gasseri* and *L. frumenti* prevented the onset of PWD in piglets [124]. It has been suggested by studies that probiotics, e.g., *L. frumenti*, have the capacity to support intestinal barrier functioning [125] and proposed reduction of PWD by promoting fatty acid β-oxidation in the liver of piglets [126]. These results indicate that the use of probiotics [127], or even prebiotics that stimulate the proliferation and persistence of these species, could be an interesting research topic to pursue. This would also include studying the role of feed additives that stimulate the persistence of beneficial microbial species and how these functional foods can provide desired effects on intestinal health. Studies could further develop different feed additives that stimulate a beneficial microbial population that produces metabolites assisting in improving intestinal barrier function or systemic piglet resilience [128, 129]. Furthermore, the intestinal organoid models developed in this thesis could provide a platform to test the (non-)nutritional effects of pro- and prebiotics or their catabolic byproducts and streamline the discovery of effective PWD reducers.

Current and future improvements to intestinal organoid models

Organoid cells are typically cultured in biologically derived matrices that mimic the natural extracellular matrix (ECM). These are mainly composed of Matrigel [130, 131], ECM-components like collagen [132], or synthetic hydrogels [133]. Matrigel is similar to basement membrane and is composed of various proteins and growth factors, but its heterogeneous and poorly defined composition limits its ability to provide precise biochemical and biophysical cues for improving organoid culture [133]. Alternative matrices with defined compositions [133, 134], such as recombinant collagen or fibrin, or synthetic hydrogels, have been explored as substitutes for Matrigel [133-135]. Synthetic hydrogels offer the possibility to independently manipulate biochemical and biophysical matrix properties to control organoid features and enhance functionality [133, 136]. However, the growth of organoids in synthetic matrices is less efficient compared to Matrigel-cultured organoids possibly attributed to biochemical cues and poses a need to develop a better matrix for organoid culture.

Nutrient supply and waste removal, which depend on diffusion in 3D organoids (reviewed by [137, 138]), can become less efficient as organoids grow into larger tissue structures [137]. This can lead to problems such as necrosis within the inner core of organoids due to nutrient inaccessibility [138]. Bioreactors that shake, spin, or continuously stir the organoids can help improve mass transfer and minimize shear stress, and semipermeable microfluidic chips have also been developed to promote long-term organoid culture [139, 140]. Providing topographical cues, such as the topography of the substrate on which the organoids are grown, can also affect stem cell fate by modulating cell area, shape, and cell-cell interactions. This has been demonstrated using intestinal organoids grown on soft hydrogels [135, 141]. It is also important to consider how to mimic shear effects under flow that occur in the intestine [142-144] because this may influence secreted waste removal and mechano-transduction for cell differentiation [68, 110, 143].

Concluding remarks

This thesis is aimed at studying the associations of protein fermentation metabolites to piglet PWD and further evaluate their effects in optimized intestinal *in vitro* models. The tools we developed for pig organoids could provide a more intricate screening model for direct metabolite-epithelium interactions and mechanistic impact discovery. Moreover, our on-farm study highlights the multifactorial nature of PWD, but also shows that increased abundance of pathogens after weaning still plays a significant role in PWD. The development and adaptation of our organoid model also shows its use for compound testing in multiple settings, e.g., in spatially oriented 3D, static high throughput 2D monolayers, and regenerative wound healing scratch assays. These models can be used to gain knowledge of feed- or metabolite interactions with host-specific tissues before *in vivo* testing. As our metabolite-organoid interaction data suggests that metabolites can have profound effects on epithelial homeostasis we further hypothesize that animal-derived organoids can be a great tool in further discovery of beneficial or detrimental nutrients and metabolites.

References

1. Fairbrother, J.M., E. Nadeau, and C.L. Gyles, *Escherichia coli in postweaning diarrhea in pigs: an update on bacterial types, pathogenesis, and prevention strategies.* Anim Health Res Rev, 2005. **6**(1): p. 17-39.
2. Nagy, B. and P.Z. Fekete, *Enterotoxigenic Escherichia coli in veterinary medicine.* Int J Med Microbiol, 2005. **295**(6-7): p. 443-54.
3. Madec, J.Y., et al., *Extended-spectrum beta-lactamase/AmpC- and carbapenemase-producing Enterobacteriaceae in animals: a threat for humans?* Clin Microbiol Infect, 2017. **23**(11): p. 826-833.
4. European Centre for Disease, P., et al., *ECDC/EFSA/EMA second joint report on the integrated analysis of the consumption of antimicrobial agents and occurrence of antimicrobial resistance in bacteria from humans and food-producing animals: Joint Interagency Antimicrobial Consumption and Resistance Analysis (JIACRA) Report.* EFSA J, 2017. **15**(7): p. e04872.
5. Windey, K., V. De Preter, and K. Verbeke, *Relevance of protein fermentation to gut health.* Mol Nutr Food Res, 2012. **56**(1): p. 184-96.
6. Heo, J.M., et al., *Effects of feeding low protein diets to piglets on plasma urea nitrogen, faecal ammonia nitrogen, the incidence of diarrhoea and performance after weaning.* Arch Anim Nutr, 2008. **62**(5): p. 343-58.
7. Gilbert, M.S., et al., *Protein fermentation in the gut; implications for intestinal dysfunction in humans, pigs, and poultry.* Am J Physiol Gastrointest Liver Physiol, 2018. **315**(2): p. G159-G170.
8. Pieper, R., et al., *Health relevance of intestinal protein fermentation in young pigs.* Anim Health Res Rev, 2016. **17**(2): p. 137-147.
9. Madec, F., et al., *Measurement of digestive disorders in the piglet at weaning and related risk factors.* Prev Vet Med, 1998. **35**(1): p. 53-72.
10. Pluske, J.R., D.J. Hampson, and I.H. Williams, *Factors influencing the structure and function of the small intestine in the weaned pig: a review.* Livestock Production Science, 1997. **51**(1-3): p. 215-236.
11. Hughes, R., et al., *Effect of colonic bacterial metabolites on Caco-2 cell paracellular permeability in vitro.* Nutr Cancer, 2008. **60**(2): p. 259-66.
12. Salzman, A.L., et al., *Nitric oxide dilates tight junctions and depletes ATP in cultured Caco-2BBe intestinal epithelial monolayers.* Am J Physiol, 1995. **268**(2 Pt 1): p. G361-73.
13. Jayaraman, B. and C.M. Nyachoti, *Husbandry practices and gut health outcomes in weaned piglets: A review.* Anim Nutr, 2017. **3**(3): p. 205-211.
14. Spencer, B.T. and P.G. Howell, *Some Husbandry Factors Influencing Weaning Stresses in Piglets.* Journal of the South African Veterinary Association-Tydskrif Van Die Suid-Afrikaanse Veterinere Vereniging, 1989. **60**(1): p. 62-64.
15. van der Meer, Y., A.J.M. Jansman, and W.J.J. Gerrits, *Low sanitary conditions increase energy expenditure for maintenance and decrease incremental protein efficiency in growing pigs.* Animal, 2020. **14**(9): p. 1811-1820.
16. te Pas, M.F.W., et al., *Sanitary Conditions Affect the Colonic Microbiome and the Colonic and Systemic Metabolome of Female Pigs.* Frontiers in Veterinary Science, 2020. **7**.
17. Hampson, D.J. and W.C. Smith, *Influence of creep feeding and dietary intake after weaning on malabsorption and occurrence of diarrhoea in the newly weaned pig.* Res Vet Sci, 1986. **41**(1): p. 63-9.
18. Choudhury, R., et al., *Impact of early-life feeding on local intestinal microbiota and digestive system development in piglets.* Sci Rep, 2021. **11**(1): p. 4213.
19. Heo, P.S., et al., *Effects of different creep feed types on pre-weaning and post-weaning performance and gut development.* Asian-Australas J Anim Sci, 2018. **31**(12): p. 1956-1962.
20. Pajor, E.A., D. Fraser, and D. Kramer, *Consumption of solid food by suckling pigs: individual variation and relation to weight gain.* Applied Animal Behaviour Science, 1991. **32**(2-3): p. 139-155.
21. van Beers-Schreurs, H.M.G. and E. Bruininx, *Nutritional management to prevent disorders in post-weaning pig health.* Nutrition and health of the gastrointestinal tract, 2002. **1**.
22. Dou, S., et al., *Characterisation of Early-Life Fecal Microbiota in Susceptible and Healthy Pigs to Post-Weaning Diarrhoea.* PLoS One, 2017. **12**(1): p. e0169851.
23. Gaukroger, C.H., et al., *Changes in Faecal Microbiota Profiles Associated With Performance and Birthweight of Piglets.* Front Microbiol, 2020. **11**: p. 917.

24. Inoue, R., et al., *Development of the intestinal microbiota in the piglet.* J Gen Appl Microbiol, 2005. **51**(4): p. 257-65.
25. Karasova, D., et al., *Development of piglet gut microbiota at the time of weaning influences development of postweaning diarrhea - A field study.* Res Vet Sci, 2021. **135**: p. 59-65.
26. Noblet, J., et al., *Energy metabolism in pregnant sows and newborn pigs.* J Anim Sci, 1997. **75**(10): p. 2708-14.
27. Levast, B., et al., *Development of gut immunoglobulin A production in piglet in response to innate and environmental factors.* Dev Comp Immunol, 2014. **44**(1): p. 235-44.
28. Steinsland, H., et al., *Protection from natural infections with enterotoxigenic Escherichia coli: longitudinal study.* Lancet, 2003. **362**(9380): p. 286-91.
29. Chakraborty, S., et al., *Characterization of Mucosal Immune Responses to Enterotoxigenic Escherichia coli Vaccine Antigens in a Human Challenge Model: Response Profiles after Primary Infection and Homologous Rechallenge with Strain H10407.* Clin Vaccine Immunol, 2016. **23**(1): p. 55-64.
30. Laird, T.J., et al., *Porcine enterotoxigenic Escherichia coli: Antimicrobial resistance and development of microbial-based alternative control strategies.* Vet Microbiol, 2021. **258**: p. 109117.
31. Rist, V.T., et al., *Impact of dietary protein on microbiota composition and activity in the gastrointestinal tract of piglets in relation to gut health: a review.* Animal, 2013. **7**(7): p. 1067-78.
32. Luo, Y., et al., *Dietary supplementation of fructo-oligosaccharides alleviates enterotoxigenic E. coli-induced disruption of intestinal epithelium in a weaned piglet model.* Br J Nutr, 2022. **128**(8): p. 1526-1534.
33. Kaiko, G.E., et al., *The Colonic Crypt Protects Stem Cells from Microbiota-Derived Metabolites.* Cell, 2016. **165**(7): p. 1708-1720.
34. Stiemsma, L.T. and K.B. Michels, *The Role of the Microbiome in the Developmental Origins of Health and Disease.* Pediatrics, 2018. **141**(4).
35. Wang, X., et al., *Longitudinal investigation of the swine gut microbiome from birth to market reveals stage and growth performance associated bacteria.* Microbiome, 2019. **7**(1): p. 109.
36. Gresse, R., et al., *Gut Microbiota Dysbiosis in Postweaning Piglets: Understanding the Keys to Health.* Trends Microbiol, 2017. **25**(10): p. 851-873.
37. Meijerink, E., et al., *A DNA polymorphism influencing alpha(1,2)fucosyltransferase activity of the pig FUT1 enzyme determines susceptibility of small intestinal epithelium to Escherichia coli F18 adhesion.* Immunogenetics, 2000. **52**(1-2): p. 129-36.
38. Bao, W.B., et al., *The effect of mutation at M307 in FUT1 gene on susceptibility of Escherichia coli F18 and gene expression in Sutai piglets.* Mol Biol Rep, 2012. **39**(3): p. 3131-6.
39. de Vos, J., et al., *Detailed molecular and epigenetic characterization of the pig IPEC-J2 and chicken SL-29 cell lines.* iScience, 2023. **26**(3): p. 106252.
40. Yan, H. and K.M. Ajuwon, *Butyrate modifies intestinal barrier function in IPEC-J2 cells through a selective upregulation of tight junction proteins and activation of the Akt signaling pathway.* PLoS One, 2017. **12**(6): p. e0179586.
41. Farkas, O., et al., *Effects of Lactobacillus plantarum 2142 and sodium n-butyrate in lipopolysaccharide-triggered inflammation: comparison of a porcine intestinal epithelial cell line and primary hepatocyte monocultures with a porcine enterohepatic co-culture system.* J Anim Sci, 2014. **92**(9): p. 3835-45.
42. Grilli, E., et al., *Butyrate modulates inflammatory cytokines and tight junctions components along the gut of weaned pigs.* Journal of Animal Science, 2016. **94**(3): p. 433-436.
43. Wang, C.C., et al., *Sodium butyrate enhances intestinal integrity, inhibits mast cell activation, inflammatory mediator production and JNK signaling pathway in weaned pigs.* Innate Immun, 2018. **24**(1): p. 40-46.
44. Lukovac, S., et al., *Differential modulation by Akkermansia muciniphila and Faecalibacterium prausnitzii of host peripheral lipid metabolism and histone acetylation in mouse gut organoids.* mBio, 2014. **5**(4).
45. Chromek, M., I. Arvidsson, and D. Karpman, *The antimicrobial peptide cathelicidin protects mice from Escherichia coli O157:H7-mediated disease.* PLoS One, 2012. **7**(10): p. e46476.
46. Takahashi, M., et al., *The effect of probiotic treatment with Clostridium butyricum on enterohemorrhagic Escherichia coli O157:H7 infection in mice.* FEMS Immunol Med Microbiol, 2004. **41**(3): p. 219-26.

47. Xiong, H., et al., *Butyrate upregulates endogenous host defense peptides to enhance disease resistance in piglets via histone deacetylase inhibition.* Sci Rep, 2016. **6**: p. 27070.
48. Tappenden, K.A., et al., *Glucagon-like peptide-2 and short-chain fatty acids: a new twist to an old story.* J Nutr, 2003. **133**(11): p. 3717-20.
49. Pohl, C.S., et al., *Early weaning stress induces chronic functional diarrhea, intestinal barrier defects, and increased mast cell activity in a porcine model of early life adversity.* Neurogastroenterol Motil, 2017. **29**(11).
50. Huang, C., et al., *Dietary Sodium Butyrate Decreases Postweaning Diarrhea by Modulating Intestinal Permeability and Changing the Bacterial Communities in Weaned Piglets.* J Nutr, 2015. **145**(12): p. 2774-80.
51. Waldecker, M., et al., *Inhibition of histone-deacetylase activity by short-chain fatty acids and some polyphenol metabolites formed in the colon.* J Nutr Biochem, 2008. **19**(9): p. 587-93.
52. Wang, Y., et al., *Bioengineered Systems and Designer Matrices That Recapitulate the Intestinal Stem Cell Niche.* Cell Mol Gastroenterol Hepatol, 2018. **5**(3): p. 440-453 e1.
53. Donohoe, D.R., et al., *The Warburg effect dictates the mechanism of butyrate-mediated histone acetylation and cell proliferation.* Mol Cell, 2012. **48**(4): p. 612-26.
54. Rossi, O., et al., *Vectorial secretion of interleukin-8 mediates autocrine signalling in intestinal epithelial cells via apically located CXCR1.* BMC Res Notes, 2013. **6**: p. 431.
55. Kayisoglu, O., et al., *Location-specific cell identity rather than exposure to GI microbiota defines many innate immune signalling cascades in the gut epithelium.* Gut, 2021. **70**(4): p. 687-697.
56. Jelinsky, S.A., et al., *Molecular and Functional Characterization of Human Intestinal Organoids and Monolayers for Modeling Epithelial Barrier.* Inflamm Bowel Dis, 2023. **29**(2): p. 195-206.
57. Kozuka, K., et al., *Development and Characterization of a Human and Mouse Intestinal Epithelial Cell Monolayer Platform.* Stem Cell Reports, 2017. **9**(6): p. 1976-1990.
58. Moon, C., et al., *Development of a primary mouse intestinal epithelial cell monolayer culture system to evaluate factors that modulate IgA transcytosis.* Mucosal Immunol, 2014. **7**(4): p. 818-28.
59. Fleischer, D., *Biological Transport Phenomena in the Gastrointestinal Tract: Cellular Mechanisms*. Transport Processes in Pharmaceutical Systems. Vol. 1. 1999: CRC Press.
60. Zhang, G. and R. Zhu, *Effect of Parasitic Capacitance on Impedance Measurement and Model Extraction.* Electroanalysis, 2010. **22**(3): p. 351-358.
61. Lu, S., et al., *Transport properties are not altered across Caco-2 cells with heightened TEER despite underlying physiological and ultrastructural changes.* J Pharm Sci, 1996. **85**(3): p. 270-3.
62. Ferruzza, S., et al., *Serum-reduced and serum-free media for differentiation of Caco-2 cells.* ALTEX, 2013. **30**(2): p. 159-68.
63. Matter, K. and M.S. Balda, *Functional analysis of tight junctions.* Methods, 2003. **30**(3): p. 228-34.
64. Kauffman, A.L., et al., *Alternative functional in vitro models of human intestinal epithelia.* Front Pharmacol, 2013. **4**: p. 79.
65. Galbraith, C.G., R. Skalak, and S. Chien, *Shear stress induces spatial reorganization of the endothelial cell cytoskeleton.* Cell Motil Cytoskeleton, 1998. **40**(4): p. 317-30.
66. Siddharthan, V., et al., *Human astrocytes/astrocyte-conditioned medium and shear stress enhance the barrier properties of human brain microvascular endothelial cells.* Brain Res, 2007. **1147**: p. 39-50.
67. Jalili-Firoozinezhad, S., et al., *A complex human gut microbiome cultured in an anaerobic intestine-on-a-chip.* Nat Biomed Eng, 2019. **3**(7): p. 520-531.
68. Kasendra, M., et al., *Development of a primary human Small Intestine-on-a-Chip using biopsy-derived organoids.* Sci Rep, 2018. **8**(1): p. 2871.
69. Kar, S.K., et al., *Dietary protein sources differentially affect microbiota, mTOR activity and transcription of mTOR signaling pathways in the small intestine.* PLoS One, 2017. **12**(11): p. e0188282.
70. Kar, S.K., et al., *Effects of undigested protein-rich ingredients on polarised small intestinal organoid monolayers.* J Anim Sci Biotechnol, 2020. **11**: p. 51.
71. Miao, S., et al., *Dietary soybean meal affects intestinal homoeostasis by altering the microbiota, morphology and inflammatory cytokine gene expression in northern snakehead.* Sci Rep, 2018. **8**(1): p. 113.

72. Solis, C.J., et al., *Intestinal Inflammation Induced by Soybean Meal Ingestion Increases Intestinal Permeability and Neutrophil Turnover Independently of Microbiota in Zebrafish.* Front Immunol, 2020. **11**: p. 1330.
73. Zhu, Q., et al., *Effects of soybean extract on morphology and survival of Caco-2, SW620, and HT-29 cells.* Nutr Cancer, 2002. **42**(1): p. 131-40.
74. Lin, Y., et al., *Soy protein enhances the cholesterol-lowering effect of plant sterol esters in cholesterol-fed hamsters.* J Nutr, 2004. **134**(1): p. 143-8.
75. Ascencio, C., et al., *Soy protein affects serum insulin and hepatic SREBP-1 mRNA and reduces fatty liver in rats.* J Nutr, 2004. **134**(3): p. 522-9.
76. Rath, E. and D. Haller, *Intestinal epithelial cell metabolism at the interface of microbial dysbiosis and tissue injury.* Mucosal Immunol, 2022. **15**(4): p. 595-604.
77. Peterson, L.W. and D. Artis, *Intestinal epithelial cells: regulators of barrier function and immune homeostasis.* Nat Rev Immunol, 2014. **14**(3): p. 141-53.
78. Turner, J.R., *Intestinal mucosal barrier function in health and disease.* Nat Rev Immunol, 2009. **9**(11): p. 799-809.
79. van der Hee, B., et al., *Optimized procedures for generating an enhanced, near physiological 2D culture system from porcine intestinal organoids.* Stem Cell Res, 2018. **28**: p. 165-171.
80. Pijuan, J., et al., *In vitro Cell Migration, Invasion, and Adhesion Assays: From Cell Imaging to Data Analysis.* Front Cell Dev Biol, 2019. **7**: p. 107.
81. Fazeli, E., et al., *Automated cell tracking using StarDist and TrackMate.* F1000Res, 2020. **9**: p. 1279.
82. Oost, K.C., et al., *Specific Labeling of Stem Cell Activity in Human Colorectal Organoids Using an ASCL2-Responsive Minigene.* Cell Rep, 2018. **22**(6): p. 1600-1614.
83. Ershov, D., et al., *TrackMate 7: integrating state-of-the-art segmentation algorithms into tracking pipelines.* Nat Methods, 2022. **19**(7): p. 829-832.
84. Molinie, N. and A. Gautreau, *Directional Collective Migration in Wound Healing Assays.* Methods Mol Biol, 2018. **1749**: p. 11-19.
85. Shapiro, L. and W.I. Weis, *Structure and biochemistry of cadherins and catenins.* Cold Spring Harb Perspect Biol, 2009. **1**(3): p. a003053.
86. Das, T., et al., *A molecular mechanotransduction pathway regulates collective migration of epithelial cells.* Nat Cell Biol, 2015. **17**(3): p. 276-87.
87. Mayya, C., et al., *Mechanisms of Collective Cell Migration in Wound Healing: Physiology and Disease*. Wound Healing Research. Vol. 1. 2021: Springer.
88. Chen, Z., et al., *GYY4137 Attenuates Sodium Deoxycholate-Induced Intestinal Barrier Injury Both In Vitro and In Vivo.* Biomed Res Int, 2019. **2019**: p. 5752323.
89. Cui, W., et al., *GYY4137 protected the integrity of the blood-brain barrier via activation of the Nrf2/ARE pathway in mice with sepsis.* FASEB J, 2021. **35**(7): p. e21710.
90. Chen, S., et al., *GYY4137 ameliorates intestinal barrier injury in a mouse model of endotoxemia.* Biochem Pharmacol, 2016. **118**: p. 59-67.
91. van der Schoor, S.R., et al., *The pattern of intestinal substrate oxidation is altered by protein restriction in pigs.* Gastroenterology, 2001. **121**(5): p. 1167-75.
92. Van Der Schoor, S.R., et al., *The high metabolic cost of a functional gut.* Gastroenterology, 2002. **123**(6): p. 1931-40.
93. Yang, H., et al., *Energy metabolism in intestinal epithelial cells during maturation along the crypt-villus axis.* Sci Rep, 2016. **6**: p. 31917.
94. Ludikhuize, M.C., et al., *Mitochondria Define Intestinal Stem Cell Differentiation Downstream of a FOXO/Notch Axis.* Cell Metab, 2020. **32**(5): p. 889-900 e7.
95. Rodriguez-Colman, M.J., et al., *Interplay between metabolic identities in the intestinal crypt supports stem cell function.* Nature, 2017. **543**(7645): p. 424-427.
96. Hou, J., et al., *Study of claudin function by RNA interference.* J Biol Chem, 2006. **281**(47): p. 36117-23.
97. JanssenDuijghuijsen, L.M., et al., *Mitochondrial ATP Depletion Disrupts Caco-2 Monolayer Integrity and Internalizes Claudin 7.* Front Physiol, 2017. **8**: p. 794.
98. Andriamihaja, M., et al., *The deleterious metabolic and genotoxic effects of the bacterial metabolite p-cresol on colonic epithelial cells.* Free Radic Biol Med, 2015. **85**: p. 219-27.
99. Beaumont, M., et al., *Detrimental effects for colonocytes of an increased exposure to luminal hydrogen sulfide: The adaptive response.* Free Radic Biol Med, 2016. **93**: p. 155-64.
100. Yeo, H., et al., *FoxO3 coordinates metabolic pathways to maintain redox balance in neural stem cells.* EMBO J, 2013. **32**(19): p. 2589-602.

101. Sancho, R., C.A. Cremona, and A. Behrens, *Stem cell and progenitor fate in the mammalian intestine: Notch and lateral inhibition in homeostasis and disease.* EMBO Rep, 2015. **16**(5): p. 571-81.
102. Ludikhuize, M.C. and M.J. Rodriguez Colman, *Metabolic Regulation of Stem Cells and Differentiation: A Forkhead Box O Transcription Factor Perspective.* Antioxid Redox Signal, 2021. **34**(13): p. 1004-1024.
103. Borisova, M.A., et al., *Mucin-2 knockout is a model of intercellular junction defects, mitochondrial damage and ATP depletion in the intestinal epithelium.* Sci Rep, 2020. **10**(1): p. 21135.
104. Bekebrede, A.F., et al., *Functional metabolic capacity of pig colonocytes is differentially modulated by fermentable fibre and poorly digestible protein.* Animal, 2022. **16**(11): p. 100625.
105. Schwarz, D.S. and M.D. Blower, *The endoplasmic reticulum: structure, function and response to cellular signaling.* Cell Mol Life Sci, 2016. **73**(1): p. 79-94.
106. Ma, X., et al., *Intestinal Epithelial Cell Endoplasmic Reticulum Stress and Inflammatory Bowel Disease Pathogenesis: An Update Review.* Front Immunol, 2017. **8**: p. 1271.
107. Hetz, C., *The unfolded protein response: controlling cell fate decisions under ER stress and beyond.* Nat Rev Mol Cell Biol, 2012. **13**(2): p. 89-102.
108. Walter, P. and D. Ron, *The unfolded protein response: from stress pathway to homeostatic regulation.* Science, 2011. **334**(6059): p. 1081-6.
109. Fribley, A., K. Zhang, and R.J. Kaufman, *Regulation of apoptosis by the unfolded protein response.* Methods Mol Biol, 2009. **559**: p. 191-204.
110. Beaurivage, C., et al., *Development of a human primary gut-on-a-chip to model inflammatory processes.* Sci Rep, 2020. **10**(1): p. 21475.
111. Schreurs, R., et al., *In vitro co-culture of human intestinal organoids and lamina propria-derived CD4(+) T cells.* STAR Protoc, 2021. **2**(2): p. 100519.
112. Wang, Y., et al., *Formation of Human Colonic Crypt Array by Application of Chemical Gradients Across a Shaped Epithelial Monolayer.* Cell Mol Gastroenterol Hepatol, 2018. **5**(2): p. 113-130.
113. Nikolaev, M., et al., *Homeostatic mini-intestines through scaffold-guided organoid morphogenesis.* Nature, 2020. **585**(7826): p. 574-578.
114. Bhatia, S.N. and D.E. Ingber, *Microfluidic organs-on-chips.* Nat Biotechnol, 2014. **32**(8): p. 760-72.
115. Inman, C.F., et al., *Rearing environment affects development of the immune system in neonates.* Clin Exp Immunol, 2010. **160**(3): p. 431-9.
116. Whittemore, C.T. and I. Kyriazakis, *Environmental management of pigs* Whittemore's Science and Practice of Pig Production, 3rd Edition. Vol. 1. 2006: Wiley.
117. McLamb, B.L., et al., *Early weaning stress in pigs impairs innate mucosal immune responses to enterotoxigenic E. coli challenge and exacerbates intestinal injury and clinical disease.* PLoS One, 2013. **8**(4): p. e59838.
118. Le Dividich, J. and B. Seve, *Effects of underfeeding during the weaning period on growth, metabolism, and hormonal adjustments in the piglet.* Domest Anim Endocrinol, 2000. **19**(2): p. 63-74.
119. Heo, J.M., et al., *Gastrointestinal health and function in weaned pigs: a review of feeding strategies to control post-weaning diarrhoea without using in-feed antimicrobial compounds.* J Anim Physiol Anim Nutr (Berl), 2013. **97**(2): p. 207-37.
120. Campbell, J.M., J.D. Crenshaw, and J. Polo, *The biological stress of early weaned piglets.* J Anim Sci Biotechnol, 2013. **4**(1): p. 19.
121. Eriksen, E.O., et al., *Post-weaning diarrhea in pigs weaned without medicinal zinc: risk factors, pathogen dynamics, and association to growth rate.* Porcine Health Manag, 2021. **7**(1): p. 54.
122. Hojberg, O., et al., *Influence of dietary zinc oxide and copper sulfate on the gastrointestinal ecosystem in newly weaned piglets.* Appl Environ Microbiol, 2005. **71**(5): p. 2267-77.
123. Nowland, T.L., et al., *A Single Faecal Microbiota Transplantation Altered the Microbiota of Weaned Pigs.* Life (Basel), 2020. **10**(9).
124. Hu, J., et al., *A Microbiota-Derived Bacteriocin Targets the Host to Confer Diarrhea Resistance in Early-Weaned Piglets.* Cell Host Microbe, 2018. **24**(6): p. 817-832 e8.
125. Hu, J., et al., *Lactobacillus frumenti Facilitates Intestinal Epithelial Barrier Function Maintenance in Early-Weaned Piglets.* Front Microbiol, 2018. **9**: p. 897.
126. Wang, Z., et al., *Lactobacillus frumenti mediates energy production via fatty acid beta-oxidation in the liver of early-weaned piglets.* J Anim Sci Biotechnol, 2019. **10**: p. 95.

28. Xiao, C.W., et al., Dietary soy protein isolate modifies hepatic retinoic acid receptor-beta proteins and inhibits their DNA binding activity in rats. Journal of Nutrition, 2007. **137**(1): p. 1-6.
29. Chen, H., Protein digestion kinetics in pigs and poultry. 2017, Wageningen University: Wageningen.
30. Tarnawski, A.S. and A. Ahluwalia, Molecular Mechanisms of Epithelial Regeneration and Neovascularization During Healing of Gastric and Esophageal Ulcers. Current Medicinal Chemistry, 2012. **19**(1): p. 16-27.

Appendices

Thesis Summary

This project was part of a larger consortium funded by the Dutch Research Council (NWO) and DSM, investigating the contribution of protein fermentation in farm animal health and disease. The main aim of the consortium was to understand fundamental aspects of protein fermentation and intestinal health and formulate prospects into 'healthier animals through nutritional solutions' (HANS). There is a general belief that protein fermentation metabolites negatively affect intestinal integrity. This thesis aims to elucidate the links between post weaning diarrhea (PWD) and fermentation metabolites and investigate the direct interactions these have on the piglet epithelium.

The **first aim** of this thesis was to examine the associations between PWD, its contributing factors before the onset of diarrhea, microbiota, and fermentation metabolites. To relate this to conditions found in practice in **Chapter 2**, we sampled piglets prospectively on four separate farms before and after weaning. Earlier studies investigated the effect of feeding high or low crude protein diets on the concentration of protein fermentation metabolites, but we investigated whether the concentration of protein fermentation metabolites and varied across farms in piglets receiving typical feed formulations and correlated with occurrence of PWD. At the point of diarrhea, an increase in protein fermentation metabolites was observed, underlining the strong associative links to PWD. Microbiota profiling, metagenomic sequencing and qPCR on fecal DNA showed the presence of Enterotoxigenic *Escherichia coli* (ETEC) in many piglets with PWD but the observed large interindividual variation could be due to a multifactorial cause of PWD onset. The results also indicate that protein fermentation is likely carried out by pathogenic bacteria, e.g., ETEC and *Fusobacterium spp*.

To gain a better understanding of the effects of protein fermentation metabolites on the colonic epithelium we established an adult stem cell organoid-based model that mimics the spatial and heterotypic cellular composition of the intestinal epithelium than cancer cell lines. Our **second aim** was to validate the robustness of the model before using it by evaluating the long-term culture stability of biological pathway expression in porcine intestinal organoids and the maintenance of segment specific gene expression. In **Chapter 3**, we found that jejunum organoids resemble their host epithelium gene expression patterns and are stable for at least 17 passages. Moreover, we also showed that the intrinsically problematic cancer-like mutations found in IPEC-J2, a jejunal cell line of piglets considered to be non- cancerous, are not observed in jejunum organoids. Moreover, the localized expression of digestion genes compared to ileum indicates the importance of tissue selection for subsequent experimentation.

In **Chapter 4** we wrote a review on the effects of short chain fatty acids (SCFAs) on host physiology highlighting its multifaceted role in signaling through GPCR and effects on the epigenome. Based on this we were interested to identify the effects of SCFAs in the distal ileum organoids, the first intestinal segment where SCFAs are produced. Therefore, in **Chapter 5** we stimulated 3-dimensional (3D) ileum organoids with luminally relevant concentrations of butyrate and acetate. Butyrate has been reported to have epigenetic effects through inhibition of the activity of class I histone deacetylase activity, but we also showed that low levels of acetate display epigenetic potential possibly through histone H4 acetylation rather than H3 in the case of butyrate.

Recent studies have underlined the importance of vectorial secretion of proteins and expression of cell surface receptors on the intestinal epithelium. The 3D organoids form spheroids with the apical epithelial surface in the inner luminal compartment, making it laborious assay for molecular interactions on the apical side. The **third aim** (**Chapter 6**) was to develop an enhanced 2-dimensional (2D) model by enzymatically separating 3D organoids into single cells and plating onto tissue-culture treated plates or transwells. These organoids retained their heterotypic cellular differentiation and formed confluent monolayers amenable for luminal exposure. The model was first used to test the non-nutritional effects of conventional animal feed protein (soybean) and alternative protein sources (**Chapter 7**). The altered expression profiles by individual protein sources and their unique effects showed that the organoids can be used as model to evaluate feed-component interactions with the intestinal epithelium. The static characteristics of organoid monolayers do not fully recapitulate the intricate crosstalk of a renewing intestinal epithelium. In **Chapter 8**, we therefore optimized the organoid monolayer model to be used in scratch assays. These assays can be used to study epithelial wound healing and test the effects of protein fermentation metabolites on gap closure rate, cell migration and motility. Our **fourth aim** was to identify molecular effects of protein fermentation metabolites on the intestinal epithelium. In **Chapter 9**, we combined the 2D organoids and the scratch assay to model the effects of protein fermentation metabolites on epithelial renewal. From this we found that ammonia and hydrogen sulfide had distinct effects on epithelial barrier functioning, energy metabolism, and cell directionality.

The concluding chapter, **Chapter 10**, summarizes the thesis research chapters and discusses their scientific advancement in the field of PWD and protein fermentation, and the use of intestinal organoids to decipher the effects of metabolites on the intestinal epithelium and the molecular mechanism of action. This chapter also discusses future perspectives on piglet weaning, nutritional strategies, and advancement of intestinal organoid models to increase their physiological relevance.

Scriptie Samenvatting

Dit project maakte deel uit van een groter consortium gefinancierd door de Nederlandse Organisatie voor Wetenschappelijk Onderzoek (NWO) en DSM. Het consortium onderzocht de bijdrage van eiwitfermentatie aan de gezondheid en ziekte van landbouwhuisdieren. Het voornaamste doel van het consortium was het begrijpen van fundamentele aspecten van eiwitfermentatie en darmgezondheid, en het formuleren van vooruitzichten voor 'gezondere dieren door voedingsoplossingen' (HANS). Er heerst over het algemeen de opvatting dat metabolieten van eiwitfermentatie een negatief effect hebben op de darmintegriteit. Deze scriptie heeft tot doel de verbanden tussen diarree na het spenen (post weaning diarrhea, PWD) en fermentatiemetabolieten op te helderen en de directe interacties hiervan met het epitheel van het biggetje te onderzoeken.

Het **eerste doel** van deze scriptie was om de verbanden te onderzoeken tussen PWD, de bijdragende factoren vóór het begin van diarree, microbiota en fermentatiemetabolieten. Om dit te relateren aan de omstandigheden die in de praktijk zijn aangetroffen hebben wij in **Hoofdstuk 2** prospectieve monsters genomen van biggen op vier afzonderlijke boerderijen vóór en na het spenen. Eerdere studies onderzochten het effect van het voeren van diëten met een hoog of laag ruw eiwitgehalte op de concentratie van fermentatiemetabolieten, maar wij hebben onderzocht of de concentratie van fermentatiemetabolieten varieerde tussen boerderijen bij biggen die typische voedingsformules kregen, en of dit samenhangt met het voorkomen van PWD. Op het moment van diarree werd een toename van fermentatiemetabolieten waargenomen, wat de sterke associatieve verbanden met PWD benadrukt. Profilering van microbiota, metagenomische sequencing en qPCR op fecale DNA toonden de aanwezigheid aan van enterotoxigene *Escherichia coli* (ETEC) bij veel biggen met PWD, maar de waargenomen grote interindividuele variatie kan te wijten zijn aan een multifactoriële oorzaak van het begin van PWD. De resultaten geven ook aan dat eiwitfermentatie waarschijnlijk wordt uitgevoerd door pathogene bacteriën, zoals ETEC en *Fusobacterium spp*.

Om een beter begrip te krijgen van de effecten van (eiwit) fermentatiemetabolieten op het darmepitheel, hebben we een model op basis van stamcelorganoiden opgezet dat de ruimtelijke en heterotypische cellulaire samenstelling van het darmepitheel beter nabootst dan conventionele cellijnen. Ons **tweede doel** was om de robuustheid van het model te valideren voordat we het gingen gebruiken, door de lange termijn stabiliteit van de expressie van biologische pathways in darmorganoiden van varkens te evalueren en het behoud van darmsegment-specifieke genexpressie. In **Hoofdstuk 3** hebben we ontdekt dat dunne darm organoiden overeenkomsten vertonen met de genexpressiepatronen van hun

oorspronkelijke gastheer epitheel en stabiel blijven gedurende minstens 17 passages. Bovendien hebben we ook aangetoond dat de intrinsiek problematische mutaties die worden gevonden in IPEC-J2, een dunne darm cellijn van biggen die als niet-kwaadaardig wordt beschouwd, niet worden waargenomen in dunne darm organoiden. Bovendien duidt de gelokaliseerde expressie van spijsverteringsgenen in vergelijking met het ileum op het belang van weefselselectie voor vervolgonderzoek.

In **Hoofdstuk 4** hebben we een literatuuroverzicht geschreven over de effecten van korteketenvetzuren (SCFA's) op de fysiologie van de gastheer, waarbij we de veelzijdige rol ervan benadrukten in het signaleren via GPCR en de effecten op het epigenoom. Op basis hiervan waren we geïnteresseerd in het identificeren van de effecten van SCFA's op de organoiden van het distale ileum, het eerste darmsegment waar SCFA's worden geproduceerd. Daarom hebben we in **Hoofdstuk 5** driedimensionale (3D) ileum organoiden gestimuleerd met luminair relevante concentraties butyraat en acetaat. Er is gemeld dat butyraat epigenetische effecten heeft door remming van de activiteit van klasse I histone-deacetylase, maar we hebben ook aangetoond dat lage niveaus van acetaat epigenetisch potentieel vertonen, mogelijk door acetylering van histone H4 in plaats van H3, zoals het geval is bij butyraat.

Recente studies hebben het belang benadrukt van vectoriële secretie van eiwitten en expressie van celoppervlakreceptoren op het darmepitheel. De 3D-organoiden vormen sferoïden waarbij het apicale epitheeloppervlak zich bevindt in het binnenste lumencompartiment, waardoor het een arbeidsintensief proces is om moleculaire interacties aan de apicale zijde te bewerkstelligen. Het **derde doel** (**Hoofdstuk 6**) was om een verbeterd 2-dimensionaal (2D) model te ontwikkelen met behulp van enzymatische scheiding van 3D-organoiden tot enkele cellen en het uitzaaien op weefselkweekplaten of transwells. Deze organoiden behielden hun heterotypische cel differentiatie en vormden aaneengesloten monolagen die geschikt waren voor luminaal contact. Het model werd eerst gebruikt om de niet-voeding gerelateerde effecten van dierlijk voerproteïne (soja) en alternatieve eiwitbronnen te testen (**Hoofdstuk 7**). De gewijzigde expressieprofielen door individuele eiwitbronnen en hun unieke effecten toonden aan dat de organoiden kunnen worden gebruikt als model om de interacties van voedingscomponenten met het darmepitheel te evalueren.

De statische kenmerken van de ontwikkelde monolagen bootsen niet volledig de complexe interacties na van een vernieuwend darmepitheel. In **Hoofdstuk 8** hebben we daarom het monolaag model geoptimaliseerd voor gebruik in kras (of wond)-assays. Deze assays kunnen worden gebruikt om de genezing van epitheliale wonden te bestuderen en de effecten van fermentatiemetabolieten van eiwitten op sluitingssnelheid van openingen, cel dynamiek en beweeglijkheid te testen. Ons

vierde doel was om de moleculaire effecten van fermentatiemetabolieten van eiwitten op het darmepitheel te identificeren. In **Hoofdstuk 9** hebben we de 2D-organoiden en de kras-assay gecombineerd om de effecten van fermentatiemetabolieten van eiwitten op de vernieuwing van het epitheel te modelleren. Hieruit bleek dat ammoniak en waterstofsulfide verschillende effecten hadden op de barrièrefunctie van het epitheel, het energiemetabolisme en de richting van celgroei.

Het afsluitende hoofdstuk, **Hoofdstuk 10**, vat de onderzoek hoofdstukken van de scriptie samen en bespreekt hun wetenschappelijke vooruitgang op het gebied van PWD en eiwitfermentatie, en het gebruik van darmorganoiden om de effecten van metabolieten op het darmepitheel en de moleculaire werkingsmechanismen te ontrafelen. In dit hoofdstuk worden ook toekomstperspectieven besproken met betrekking tot het spenen van biggen, voedingsstrategieën en de ontwikkeling van darmorganoid-modellen om hun fysiologische relevantie te vergroten.

Acknowledgements

"I fly a starship, across the universe divide…"

What a journey. It has been a long, but rewarding set of years, of which I fondly look at the connections made, the alliances developed, and the people that were there for me. Within this section, I would like to express this gratitude in writing, but it remains difficult to put into words what you have all meant to me.

To start, I would like to express my deepest gratitude to my two promotors, **Jerry** Wells and **Hauke** Smidt. Two very different people with each a phenomenal love for science. Their invaluable support, guidance, and expertise throughout the whole process of completing this thesis. I highly appreciate their unwavering belief in my abilities as a young scientist and fueled my motivation to dig deeper every day. **Jerry**, when I think of you, I always remember the sheer love for science and discovery and the spark of scientific wonder when I brought back some new results. Your enthusiastic motivation is contagious and your subtle bouts of humor during our meetings a fond memory. **Hauke**, I admire your calmness and deep level of knowledge throughout my thesis. You were always quick in replying with feedback while publishing, making me think you work at least 25 hours in a day. Having both of you as supervisors helped me to appreciate my work and made me work hard at work worth doing.

That brings me to **Myrthe** and **Walter**, who put my feet back on the ground in piglet science and showed me that sampling diarrheic piglets is also very necessary. **Myrthe**, I always enjoyed our scientific discussions related to our project, which had to be preceded by a mandatory pre-meeting talking about anything else. I guess our meetings didn't involve talking about the projects much, but more about the herpetofauna of Wageningen and aspirations. I highly admire your tenacity and humor and I deeply appreciate all our interactions. **Walter**, you made me think about the context of my research and was always amazed if I showed any image related to organoids. Your dedication to my project and me personally is always appreciated.

The thesis was part of a larger TTW-DSM partnership that involved multiple universities throughout The Netherlands. Firstly, I would like to thank **Arie** for his never subsiding interest in my project and the wonder about organoids and its applications. I will always remember you as a kind person with a contagious laughter. Also, I would like to thank other members of the DSM committee, namely **Pim**, **Anna-Maria**, **Elodie**, **Estefania**, and **Britt**. Furthermore, I also enjoyed working with

an amazing group of fellow PhD's and PostDocs withing this project; **Anna**, **Joanna**, **Judith**, **Kim**, **Miranda**, **Myrthe**, **Rianne**, **Stefania**, and **Lonneke**. An additional thanks goes to **Lonneke** for our collaboration during the final animal trial, I admire your work ethic and practical knowledge. During this thesis, I also interacted many times with our collaborators from UMC Utrecht. I would like to specifically thank **Boudewijn** for all his input in my project, but foremost his input into my scientific thinking. You helped me tremendously in being critical towards research findings, and I appreciate that you were always open to lend a helping hand and mind, but also a fresh set of cynical humor.

Of course, it takes a village to raise a child; apparently it takes a chair group to raise a PhD. **Loes**, you are the engine that keeps us running smoothly. Every question, every task, nothing was too much to ask. I deeply appreciate all you have done for me, and I hope that with **Nienke** by your side the administrative powerhouse flourishes. Next up are my paranymphs, **Anja** and **Nico**. Your unwavering support during my thesis means the world. There was always room to help if I put effort in, and I cannot describe my gratitude in words. Therefore, I am honored to have you both to accompany me on stage during the defense. I would also like to deeply thank my fellow PhD and postdoctoral colleagues at the group; my original office mates, **Raka**, **Jori**, and **Marcela**, and later **Isabela** always made coming to work more enjoyable. **Raka**, you are the most kindhearted person I know, and I always enjoyed our conversations. Sorry that you were bothered by **Jori** and me so often. **Jori**, our mutual love for a diverse set of tv-shows often led to humorous moments in the office, hopefully we will share a mega-desk at some point, beltalowda. The occasional "AHK" in the office from **Marcela** startled us less as time moved by, and it was eerily quiet when you moved on from the group to become an astronaut. Sometimes we mimicked the sound, just to have you with us for a moment. **Isabela**, your kindness, and happiness radiated when you moved into our office. Meeting you at the PhD party and the following years made me realize you're a very special person, and you will be missed in the group. I will always fondly remember our office and I wish there was a way to know that we were in the good old times, before we actually left them. Furthermore, I would also like to thank my other PhD colleagues, **Berdien** and **Avis**, we started at the same time, and you are both two amazing people, **Blanca**, **Adria**, and **Adam**, my new office mates; you are a set of amazing people, and I look forward to the future. I would also like to thank **Alex**, good luck with finalizing your thesis! **Maria**, thank you for being in the office, you always light up the room and keep me updated, maruja! I would also like to thank **Simen** for the insightful bioinformatics talks, and **Aisha**, **Evelien**, **Hedi**-**Britt**, all the best for the

future! My next adventure involves working with **Maaike**; in this short time, you have already shown yourself to be a formidable researcher with good critical thinking, and I hope that your future of managing the people in Sprint is doable! Next, I would also like to thank **Simon**, the insightful conversations about artificial intelligence, dystopian futures, human consciousness, and scientific thinking were always a welcome part of the day. Also, the insightful conversations with **Soumya** about pigs, organoids, and omics were always amazing, and I am happy that we've built this friendship over the years. **Nuning**, my master thesis supervisor and later my friend. I always think about our time fondly and I am looking forward to seeing you in the near future.

I also want to dedicate a separate sentence to **Arabela**. ¡caracoles! Your work ethic and tenacity are an example for science, and I am proud of being your daily supervisor. Your kindness towards me and my children, and big heart are two of your best traits. Also, **Tiantong**, your kindhearted communication and willpower are commendable, and supervising you taught me many things, including some Chinese; 謝謝你為我做的一切. And last but not least, **Zhan**; during the last few years we built a friendship worth remembering, and I am looking forward to joining you when you've built a group back in China so we can rule all the science together! Of course, I would also like to thank the new PhDs in our office, to which I hope to work with in the future, **Zizhuang**, **Mohak**, **Oshin**, and **Gwen**.

Furthermore, I would like to thank the staff at HMI. **Joyce**, you started with us for an internship, and you have proven yourself to be a formidable addition to the lab. **Michiel**, I thoroughly enjoy our conversations about science, but mostly the jokes and juvenile interactions. Your down-to-earth mentality and scientific knowledge made you into one of the best scientists in our university, but I still picture the person emptying yoghurt cartons for a living. Moreover, **Jos**, **Peter**, **Maria**, **Sylvia**, **Aline**, and **Anda**, you are amazing people, and I am happy to be working with you in the lab and outside. A special thanks goes to **Linda**; during the beginning of my thesis, you helped me to get on track with my PhD and I always enjoyed our meetings. I always appreciate our conversations, albeit about sick children, tough projects, or just life. It's good to know that someone understands what we're going through. Also, **Ellen**, even though you have left the group you substantially helped me during my PhD. Without you I would not be here, and I am very thankful for that. Inmiddels heb ik zelf een aanhangwagen, dus moeten we in plaats daarvan elkaar maar tegenkomen op de kinderboerderij.

I would like to specifically thank the technicians at MIB, **Ineke**, **Merlijn**, **Laura**, and **Steven**. They not only contributed to my thesis in the lab, but they also helped in sampling on-farm. I will always remember when we were sampling a piglet and I looked back and saw the wide smile on **Ineke's** face thoroughly enjoying being out of the lab. **Hugo**, you were my counterpart from MIB, mirroring our positions between HMI and MIB. I always thoroughly enjoyed our interactions, and I am happy to call you my friend. On that note, I need to thank your wife, **Mirelle**. If not for her, you would have never been tamed. Attics overflowing with mushrooms, sheds full of lab equipment, and front laws strewn with mopeds. You are both wonderful people, and I am looking forward to meeting your upcoming baby.

During the thesis, I had the honor of supervising the most incredible set of students. The future of humanity sometimes looks bleak, but your contribution to science and your motivation to work outshines the dread. Therefore, I would like to thank you all, **Nalin**, **Panos**, **Fitri**, and **Joris** during the initial on-farm trials, **Marith**, **Eva**, **Veerle**, **Gijs**, **Xiaohui**, and **Maika** for their work in organoids, **Mandy** and **Gwen** for their work on the microbiology of my thesis, **Larissa**, **Lieke**, and **Sylvia** for their immense contribution to the second *in vivo* trial, and **Maika** again for her work on the Research Master Cluster. Moreover, I had the pleasure of collaborating with a large group of people outside my research domain. Firstly, I want to thank **David**, **Lieuwke**, **Robin**, **Louis**, **Bart**, and **Kitty** for showing me that other animals, namely horses, are also interesting for research. **David**, throughout my career you have always supported me in any way possible with sheer enthusiasm and nothing short of opportunity, and I look forward to working with you in the near future on equine organoids. I also look forward to finalizing multiple papers on pig digestion with **Sonja** and **Rik**, and I want to specifically thank **Henk** for all his help with histology.

Finalizing and doing my thesis would have never been possible without the unrelenting support of my family. Lieve **Nik**, het waren lange jaren maar we hebben het voor elkaar gekregen. Jouw toewijding en onwankelbaar vertrouwen hebben zo'n grote contributie gehad dat deze prestatie net zoveel de jouwe is als de mijne. We hebben tijdens de PhD twee prachtige kinderen gekregen. **Haley** en **Brenn**, papa is ontzettend trots in de persoontjes die jullie nu al zijn. Daarnaast veel liefde van mijn familie, **pap**, **mam**, **Henrieke** en **Gerald**, en **Dirk Jan** en **Lucinda**, maar ook mijn 'kouwe kant', **Roel**, **Leonie**, en **Tijn** en **Yari**; dank jullie voor wie jullie zijn en alle steun. En dan als laatste een bericht voor mijn oma; ja, school is nu voorbij.

"… and now I've reached the other side."

About the author

Bart van der Hee was born on October 23rd, 1990, in Zwammerdam, The Netherlands. As the son of a car mechanic and automotive family business, he started competing in national motor sports at an early age together with his brother, mainly oval car racing on tarmac and fields. After a short interlude studying Automotive Engineering, he quickly transitioned into studying Applied Biology at the HAS university of Applied Sciences (Dutch HBO) in Den Bosch. During this, he performed a 6-month internship at the Farm Animal Health department of Utrecht University studying osteochondrosis-induced gait problems in pigs. Moreover, he also performed a second 6-month internship at Landcare Research (Manaaki Whenua) in New Zealand studying the hepatic conversion of 4-vinylcyclohexine to its ovotoxicity-inducing diepoxide in brown rats and brushtail possums. These internships also resulted in the accreditation for article 12 (now 13f) WOD.

After graduating, he started a study Animal Sciences at Wageningen University in Wageningen for his master's degree. During his studies he specialized in Applied Zoology and Immunology with a major thesis at Human and Animal Physiology, studying the effects of nicotinamide riboside on adipocytes in mice, and a second major thesis at the Host-Microbe Interactomics group, studying the effects of *Faecalibacterium prausnitzii* on human intestinal health using cell lines. During his studies, he obtained his accreditation for article 9 WOD.

In 2016, just after graduating, he started his PhD research in the Host-Microbe Interactomics group in the PWDinPIGS project together with post-doctoral colleague Myrthe Gilbert. When this project ended during the pandemic, he switched to the post-doctoral project PIGSs to study the efficacy of *Streptococcus suis* vaccines in piglets. Last September he started his second post-doc in the SPRINT project to study the effects of plant protection products (PPP's) on the airway and intestine of pigs and humans.

A recurring theme during his studies and thesis is collaboration and the motivated drive to say yes. This has resulted in countless colleague interactions and network. In the future, he aims at continuing this form of interaction. He lives with his wife and two amazing children in Ede.

List of publications

Peer-reviewed Journals

Benis, N., J. M. Wells, M. A. Smits, S. K. Kar, **B. van der Hee**, Vapm Dos Santos, M. Suarez-Diez, and D. Schokker. 2019. 'High-level integration of murine intestinal transcriptomics data highlights the importance of the complement system in mucosal homeostasis', *Bmc Genomics*, 20: 1028.

Kar, S. K.*, **B. van der Hee***, L. M. P. Loonen, N. Taverne, J. J. Taverne-Thiele, D. Schokker, M. A. Smits, A. J. M. Jansman, and J. M. Wells. 2020. 'Effects of undigested protein-rich ingredients on polarised small intestinal organoid monolayers', *J Anim Sci Biotechnol*, 11: 51.

Noorman, L., M. S. Gilbert, **B. van der Hee**, S. de Vries, and W. J. J. Gerrits. 2023. 'Low sanitary housing conditions increase protein fermentation in piglets but do not aggravate the effects of protein fermentation on intestinal health', *Animal Feed Science and Technology*: 115669.

Shi, W., M. A. Hegeman, D. A. M. van Dartel, J. Tang, M. Suarez, H. Swarts, **B. van der Hee**, L. Arola, and J. Keijer. 2017. 'Effects of a wide range of dietary nicotinamide riboside (NR) concentrations on metabolic flexibility and white adipose tissue (WAT) of mice fed a mildly obesogenic diet', *Mol Nutr Food Res*, 61.

van der Hee, B., L. M. P. Loonen, N. Taverne, J. J. Taverne-Thiele, H. Smidt, and J. M. Wells. 2018. 'Optimized procedures for generating an enhanced, near physiological 2D culture system from porcine intestinal organoids', *Stem Cell Res*, 28: 165-71.

van der Hee, B., O. Madsen, J. Vervoort, H. Smidt, and J. M. Wells. 2020. 'Congruence of Transcription Programs in Adult Stem Cell-Derived Jejunum Organoids and Original Tissue During Long-Term Culture', *Front Cell Dev Biol*, 8: 375.

van der Hee, B., and J. M. Wells. 2021. 'Microbial Regulation of Host Physiology by Short-chain Fatty Acids', *Trends Microbiol*, 29: 700-12.

Wolthuis, J. C., S. Magnusdottir, E. Stigter, Y. F. Tang, J. Jans, M. Gilbert, **B. van der Hee**, P. Langhout, W. Gerrits, A. Kies, J. de Ridder, and S. van Mil. 2023. 'Multi-country metabolic signature discovery for chicken health classification', *Metabolomics*, 19: 9.

Zhang, H., N. van der Wielen, **B. van der Hee**, J. Wang, W. Hendriks, and M. Gilbert. 2020. 'Impact of Fermentable Protein, by Feeding High Protein Diets, on Microbial Composition, Microbial Catabolic Activity, Gut Health and beyond in Pigs', *Microorganisms*, 8.

Conference proceedings/Other

Gilbert, MS, L Noorman, **B. van der Hee**, and WJJ Gerrits. 2022a. 'O162 Feeding high indigestible protein and housing under low sanitary conditions increases post-weaning diarrhoea and reduces nitrogen retention in weaned piglets', *Animal-science proceedings*, 13: 444-45.

Gilbert, MS, **B. van der Hee**, and WJJ Gerrits. 2019. 'The role of protein fermentation metabolites in post-weaning diarrhoea in piglets.' in, *EAAP Scientific Series* (Wageningen Academic Publishers).

Gilbert, MS, **B. van der Hee**, M Gulersonmez, E Stigter, Arie Kies, and WJJ Gerrits. 2018. 'Post-weaning diarrhoea in piglets in practice is associated with protein fermentation, but specific protein fermentation metabolites contribute differently'.

Gilbert, Myrthe, Lonneke Noorman, **B. van der Hee**, and Walter Gerrits. 2022b. 'P194. Dietary indigestible protein increases post-weaning diar-rhoea in piglets irrespective of sanitary housing conditions', *Animal-science proceedings*, 13: 218.

Giuffra, Elisabetta, Hervé Acloque, Giorgia Egidy Maskos, Nico Taverne, JJ Taverne-Thiele, **B. van der Hee**, Linda MP Loonen, and Jerry M Wells. 2018. 'Generating 3D organoid-like structures from porcine induced pluripotent-like cells in vitro'.

Noorman, Lonneke, Sonja de Vries, Myrthe Gilbert, **B. van der Hee**, and Walter Gerrits. 2022. 'O9. Low sanitary housing conditions reduce ileal N digestibility and enhance the production of protein-derived metabolites in piglets', *Animal-science proceedings*, 13: 148.

Noorman, Lonneke, Sonja de Vries, **Bart van der Hee**, Myrthe Gilbert, and Walter Gerrits. 2022. 'P112. Influence of removing serosal and outer muscle layers on estimates of intestinal permeability in everted sac segments', *Animal-science proceedings*, 13: 191.

van der Hee, B. 2021. "Testing direct effects of antibiotic alternatives on the intestinal epithelium using intestinal organoids." In *5th International Conference on Responsible Use of Antibiotics in Animals: Towards Sustainable Solutions*.

van der Hee, B., LMP Loonen, N Taverne, JJ Taverne-Thiele, H Smidt, and JM Wells. 2019. "Organoids as models to study probiotics." In *IPC2019: International scientific conference on probiotics, prebiotics, gut microbiota, and health*.

van der Hee, B., David van Doorn, LMP Loonen, Kitty van der Moolen, H Smidt, and JM Wells. 2019. 'Development of equine intestinal organoid monolayers to study location-specific epithelial responses: Employing the self-replicative potential of stem cells to generate equine mini guts'.

van der Hee, B., MS Gilbert, Arie Kies, MM Fernandez Gutierrez, HJA de Vries, Nico Taverne, JJ Taverne-Thiele, GAM Heikamp-de Jong, Merlijn van Gaal, and WJJ Gerrits. 2020. "Post-weaning diarrhoea is associated with protein fermentation, alterations in intestinal microbiota, and host physiological parameters in piglets." In *WIAS Annual Conference 2020: Frontiers in Animal Sciences*, 29-29. WIAS.

van der Hee, B., Myrthe Gilbert, Ineke Heikamp-de Jong, Merlijn van Gaal, Boudewijn Burgering, Walter Gerrits, Jerry Wells, and Hauke Smidt. 2022. 'P148. Increased protein fermentation metabolites and pathogenic bacteria are linked to piglet post-weaning diarrhoea under practical conditions', *Animal-science proceedings*, 13: 203.

van der Hee, B., Myrthe Gilbert, Miranda van Triest, Boudewijn Burgering, Nico Taverne, Anja Taverne-Thiele, Hauke Smidt, Walter Gerrits, and Jerry Wells. 2022. 'P120. Generating piglet intestinal organoids to study the effects of luminal fermentation metabolites', *Animal-science proceedings*, 13: 194.

van der Hee, B., W Shi, MA Hegeman, and J Keijer. 2016. "Nicotinamide Riboside increases adipogenesis and could be a potential vitamin to counteract obesity related complications." In *Euroleague for Life Sciences (ELLS) Scientific Student Conference*.

Zhao, Tiantong, **Bart van der Hee**, Sylvia Brugman, P van Baarlen, and Jerry M Wells. 2023. "Crossing borders how Streptococcus suis invades the brain." In *WIAS Annual Conference 2023*, 32-32.

Completed Training and Supervision Plan

Bart van der Hee

Wageningen Institute of Animal Sciences

Education and Training	Info	Year	ECTS*
(A) The basic package			
WIAS Introduction Day	WIAS	2017	0.3
WGS Scientific Integrity	WGS	2020	0.6
Ethics and Animal Sciences	WGS	2021	0.8
(scientific) Integrity workshop ASG-WU	WUR	2021	0
WIAS Introduction course on personal effectiveness for your PhD	WIAS	2021	1.2
(B) Disciplinary competences			
Article 9 WOD	WUR	2016	3
The intestinal microbiome and diet in human and animal health	VLAG	2017	0.8
Literature review: Effects of SCFA on host physiology	WIAS	2020	6
Specialized Training Program on the Cytoflex flow cytometer	Beckman Coulter	2017	0.6
Training in Omnilog phenotyping	Biolog	2019	0.3
Introduction to R	VLAG	2017	0.6
(C) Professional competences			
High impact writing in science	WIAS	2017	1.3
Popular Scientific Writing	DSM	2017	1
Popular Scientific Presenting	DSM	2018	1
Career assessment	WGS	2020	0.3
Searching and organising literature	Library WUR	2020	0.6
Writing propositions for your PhD	WGS	2020	0
Last Stretch of the PhD programme	WGS	2020	0
Project and Time Management	WGS	2021	1.5
Introduction to LaTeX	PE&RC	2021	0.1
Benoemings Advies Commissie (BAC) new chair CBI-WUR	ASG - WUR	2020	2
Benoemings Advies Commissie (BAC) new chair EZO-WUR	ASG - WUR	2022	2
(D) Societal relevance			
Making Impact: Increasing the relevance of research through science-society interaction	WGS	2021	1
Societal impact of your research	WGS	2021	1.5

(E) Presentation skills				
Oral presentation, ELLS scientific conference	Germany		2016	0
Oral presentation, DSM Heidedagen	The Netherlands		2017	0
Oral presentation, DSM HANS meeting	The Netherlands		2017	0
Poster presentation, WIAS Annual Conference	The Netherlands		2018	0
Poster presentation, STW-DSM program 2	Germany		2018	0
Oral presentation, EEHNC conference	The Netherlands		2019	1
Oral presentation, IPC conference	Czech Republic		2019	1
Poster presentation, STW-DSM program 3	Germany		2020	0
Oral presentation, WIAS Annual Conference	The Netherlands		2020	1
Poster presentation, EMBL Organoids conference	Germany		2020	0
Oral presentation, Antibiotics in animals conference	Virtual (online)		2021	1
Poster presentation, poster 1 DPP conference	The Netherlands		2022	0
Poster presentation, poster 2 DPP conference	The Netherlands		2022	0
(F) Teaching competences				
Teaching assistant	HMI-50306		2016	0.9
			2017	0.6
			2018	0
			2019	0
Teaching assistant	HMI-30306		2017	0.5
			2018	0
			2019	0
Teaching assistant	ABG-30306		2018	0
			2019	0
Teaching assistant	HMI-20306		2020	0
Thesis supervision	MSc	8 Major	2017-2021	2
		2 Minor	2019	2
		1 Internship	2018	0
	MBO	1 Eindstage	2018	0
	Erasmus	1 Student	2018	0
	Research Master Cluster	1 Student	2020	0
			Total	**36.5**

**1 ECTS credit is equal to a studyload of approximately 28 hours*

Colophon

This research was funded by a research partnership between the Applied and Engineering Sciences Division of the Netherlands Organization for Scientific Research NWO (project number 14935), the Ministry of Economic Affairs, and DSM Nutritional Products. Financial support from Wageningen University, NWO, and the Host-Microbe Interactomics group for printing this thesis is gratefully acknowledged.

Layout: Bart van der Hee

Cover design and chapter illustrations: Bart van der Hee and Midjourney AI

Printing: ProefschriftMaken.nl